istituto nazionale di fisica nucleare
laboratori nazionali di frascati

2007
ANNUAL REPORT

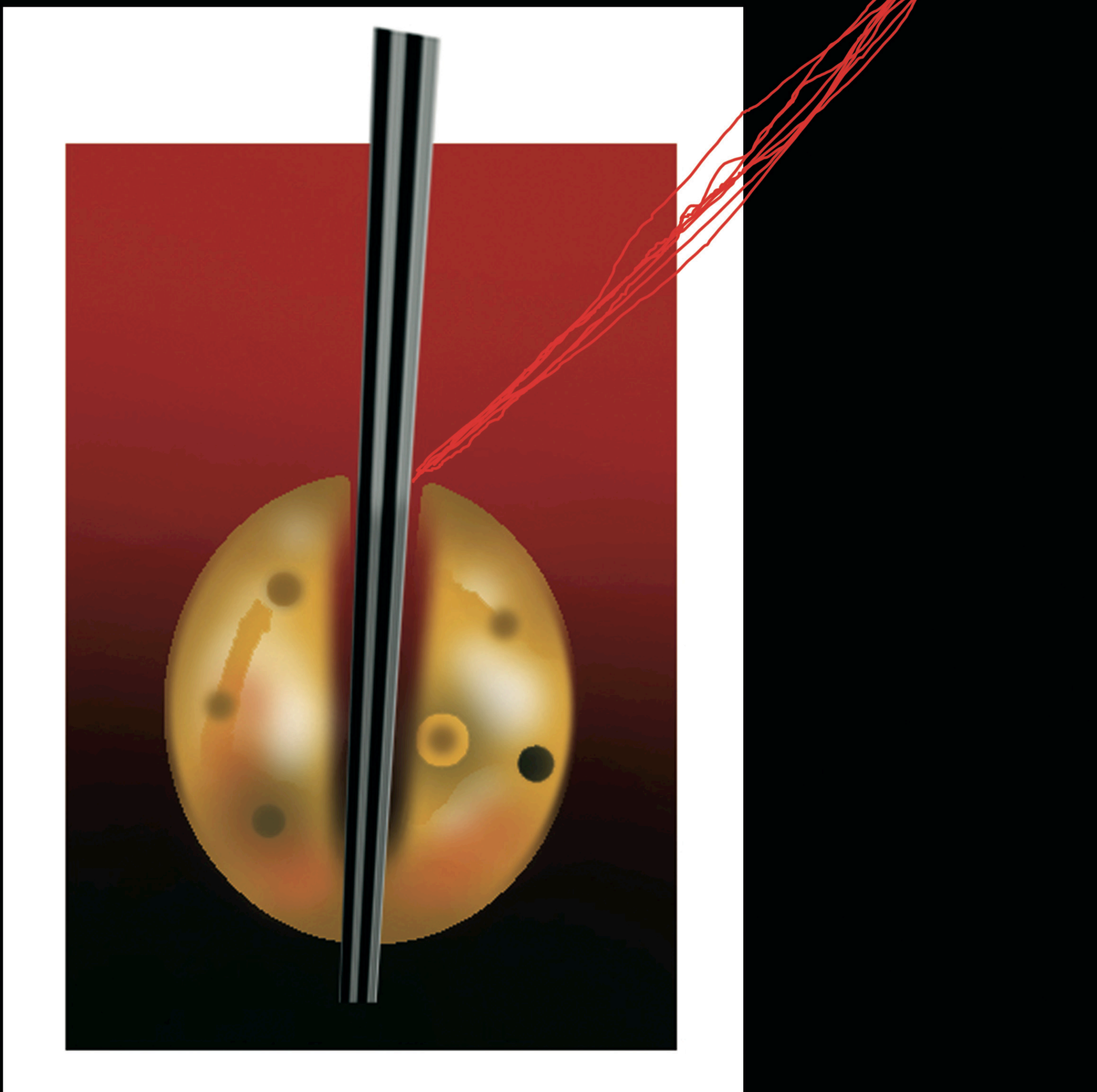

Cover: Evolving shapes

Cover artwork: *Claudio Federici*

istituto nazionale di fisica nucleare
laboratori nazionali di frascati

2007
ANNUAL REPORT

LNF-08/20 (IR)
September, 2008

Editor
Mario Antonelli

Technical Editor
Luigina Invidia

Published by
SIS-Pubblicazioni
P.O.Box 13 – I–00044 Frascati (Italia)

Available at   www.lnf.infn.it/rapatt

Mario Calvetti
LNF Director

Maria Curatolo
Head, Research Division (until August 2007)

Vitaliano Chiarella
Head, Research Division (since August 2007)

Pantaleo Raimondi
Scientific Head, Accelerator Division

Claudio Sanelli
Technical Head, Accelerator Division

LNF Scientific Coordinators

Riccardo De Sangro
Particle Physics

Marco Ricci
Astroparticle Physics

Pasquale Di Nezza
Nuclear Physics

Calogero Natoli
Theory and Phenomenology

Roberto Cimino
Techn. And Interdisciplinary Research

FOREWORD
Laboratori Nazionali di Frascati-Frascati National Laboratories (LNF)
Present and Future

1 Introduction

The Frascati National Laboratories (LNF), situated on a hill just south of Rome, is the largest laboratory of the Italian Institute of Nuclear Physics (INFN). The laboratory is organized into three substructures: the Accelerator Division, the Research Division and the Administration, for a total of about 380 staff members.

The Accelerator Division runs the DAΦNE accelerator complex, an $e^+ \; e^-$ storage ring, used to produce ϕ-mesons at a high rate. Three experiments, KLOE, FINUDA and SIDDHARTA, study the ϕ decays, the charged and neutral kaon decays, the kaonic nuclei, produced when a negative kaon is absorbed in a nucleus, and the properties of any other of the particles produced in the ϕ decay chain. A linear accelerator (the Linac) accelerates electrons and positrons to fill the storage rings. The very clean electron and positron beams, with variable energy in the interval between 50 MeV and 850 MeV, variable intensity from 1 to 1010 electrons per bunch, at a rate of 50 Hz, can be deflected into an experimental area, the Beam Test Facility (BTF), where a photon tagged beam, of variable energy, is also available. The BTF facility is continuously used by internal and external users. Last year, for example, the photon calorimeter of the AGILE satellite was calibrated using the energy tagged photon beam, and the properties of several detectors, used by the LHC experiments, were also measured. Experiments with cryogenic detectors, channelling of positron with undulated crystals for x ray production, and other experiments, are planned for the coming years. The Accelerator Division participates in the construction of the CNAO (Centro Nazionale di Adroterapia Oncologica), a 1.2 GeV proton synchrotron used for cancer therapy in Pavia. A free electron laser, named SPARC, is being assembled at the LNF, in collaboration with ENEA (the Italian National Agency for New Technologies, Energy and the Environment). The scientific goal of the SPARC project consists in producing 10 ps electron bunches, with emittance smaller then 2 mm mrad, able to induce the self amplified green synchrotron laser light in the magnetic undulator placed downstream the electron gun. A very intense LASER, able to produce 200 TW of 0.8 micron wave length for 10 fs (the Frascati Laser for Acceleration and Multidisciplinary Experiments, FLAME) is being assembled nearby the SPARC linac. The possibility to accelerate a bunch of electrons in the plasma waves produced by the light in a gaseous target will be explored. The proton synchrotron in Pavia (CNAO), the SPARC free electron laser and the FLAME laser will be operational by the end of the year 2008. Physicists and engineers of the Accelerator Division also participate in the research and development in the field of accelerator technology. The construction of CTF3, the CLIC Test Facility at CERN, the TTFII, the Tesla Test Facility at DESY, the work for the future Linear Collider and the study for a possible future Super B-factory as well, are part of our research program. The DAΦNE accelerator, which is continuously being improved, produces synchrotron radiation light used by many experimental groups. The very intense infrared light from a synchrotron source is available at DAΦNE. At the moment we have three lines running, the Infra Red line, the X ray line and the UV line, a second x-ray line is under construction. More than a hundred users, in the context of the European research funding TARI program, used this facility last year.

The Research Division is composed of physicists and engineers working in many experiments at the LNF, at CERN (ATLAS, LHCb, DIRAC), at FNAL (CDFII), at SLAC (BABAR), at JLAB (AIACE), at DESY (HERMES), in Grenoble (GRAAL), at the Gran Sasso National Laboratories LNGS (OPERA, ICARUS), at Cascina (VIRGO), in space borne experiments within the WIZARD program, and also, locally, in the search for gravitational waves with a cryogenic bar (NAUTILUS).

1.1 Short range future at LNF

In the spring of 2006 KLOE was removed from the DAΦNE ring and placed in the assembly hall, while the FINUDA detector has been placed on the machine. In the 2006-2007 run of DAΦNE, FINUDA has collected 1 ft^{-1} as expected, concluding seccesfully the data collection of the first phase of the FINUDA scientific program. DAΦNE is a beautiful opportunity to study machine physics at its cutting edge. Several possible modifications of the accelerator can be implemented to increase the luminosity. New technologies will be applied, like fast kickers, to increase the injection efficiencies, kickers that could be used for the ILC dumping rings, crab cavities, wigglers with shaped poles, to follow the particle trajectory in the alternating magnetic fields, and so on. An adequate fraction of the beam time will be dedicated to machine studies, because it is important to understand the machine limits, the new technologies and the new ideas. The LNF are also very active in the field of scientific communication. In fact, every year we have more than a thousand visitors, mainly students and teachers. Every autumn we organize a week long meeting, with lectures, discussions, visits to the labs, attended by more than 250 secondary school teachers of physics and philosophy. In the year 2005 our Scientific Information Services has organized 26 conferences.

1.2 Long range future - The LNF roadmap

The main research programs of the LNF, the CNAO, the SPARC, the FLAME projects, will either have ended or be in smooth running conditions by the end of 2008, similarly for the LNF groups that collaborate with the LHC experiments. We consider it very important to have a strong physics research program, to be pursued at Frascati beyond the year 2010. A major upgrade of the present accelerator is under evaluation, aiming at a machine able to deliver more than 50 fb^{-1} at the ϕ resonance, in 4 or 5 years of data taking, starting in 2011, and to operate with a centre of mass energy in the interval 1GeV - 2.5 GeV. Recently we have stimulated an intense effort to study the physics case of this new accelerator named DANAE. Five Letters of Intent on different research topics have recently been received and will be evaluated in the framework of this possible new future initiative. The letters of intent and the proposal for the new accelerator can be found at the following address http://www.lnf.infn.it/lnfadmin/direzione/roadmap.html. New collaborators for the experiments and the construction of a top class accelerator would be welcome at LNF.

Prof. Mario Calvetti
Director of LNF

ACKNOWLEDGMENTS

I want to thank all the authors that contributed to this report. A special acknowledgment goes to Luigina Invidia for her very pleasant and productive collaboration in the realization of this report. I would like also to thanks Claudio Federici for the excellent realization of the cover page, Stefano Bianco and Danilo Babusci for their help and suggestions.

Mario Antonelli
Editor

2007 ANNUAL REPORT
CONTENTS

COMMUNICATION AND OUTREACH

R. Centioni, V. Ferretti (art.15), S. Miozzi, L. Sabatini, S. Vannucci (Resp.)
Office of Education and Public Relations
Scientific Information Service

The "Laboratori Nazionali di Frascati dell'INFN" (INFN-LNF) provide basic education in Physics for the general public, students and teachers. The LNF Educational and Public Relation programmes are made possible by the enthusiastic involvement of the laboratory graduate students, postdocs, researchers, engineers and technicians. This report describes 2007 activity including special events organized for the European Researchers' Night 2007 and LNF 50° Anniversary concert.

1 Visiting LNF

`http : //www.lnf.infn.it/edu/`

LNF Guided Tours A well established tradition: for general public, students and teachers: **about 2800 people**, (120 volounteers) have received 144 groups.
A typical visit consists of:

- history of the laboratory;
- presentation of INFN-LNF activities on site and abroad;
- visit to the "en plein air museum";
- visit to experimental areas.

LNF Scientific Week and Open day: about 800 visitors.
Scientific Coordinator P. Gianotti. Since 1990 - Most of LNF employees are in action to present their research center, answer questions and care for their guests:

- guided tours;
- conferences and public lectures;
- scientific videos;
- exhibitions of students' projects;

2 Scientific Itineraries - Scienza Orienta and Frascati Scienza

The aim is to offer a more complete view of the scientific institutions operating in the area and improve the communication with the general public. In collaboration with:

- CNR Tor Vergata;
- ENEA Frascati;
- ESA-ESRIN Frascati;
- INAF Astronomical Observatory of Rome, Monte Porzio Catone;
- INAF/IASF;

- Frascati Scienza;
- Frascati and Castelli Romani Municipalities;
- International non-government organizations;
- University of Rome Tor Vergata.

3 Students' programme

`http://www.lnf.infn.it/edu/stagelnf/`

LNF Stages for high school students, Scientific Coordinators: D. Babusci, F. Bossi, P. Gianotti.
Goal: enable students to acquire the knowledge and understanding of INFN research activities.

- Winter stages, 9 days: 26 students with 12 tutors;
- EU Project Masterclasses 2007, 3 days: 38 students with 6 tutors;
- Summer stages, 2 weeks: 99 students with 37 tutors;
- Lectures at school by LNF researchers, 2-3 days: 596 students with 24 tutors.

Figure 1: *Students programme: EU Project Masterclasses 2007. (INFN-LNF Photo).*

Special Programme for Primary School: QUASAR

`http://www.lnf.infn.it/edu/quasar/`

Care of F. Murtas and B. Sciascia.
Age: 8 - 14.
First meeting with the children at their school to introduce the world of research and some concepts of modern physics. Then, visit to the Frascati National Laboratories by small groups. Total of children and teachers in visit: about 550.

4 High school teachers' programme

"Incontri di Fisica"

http : //www.lnf.infn.it/edu/incontri/

Organizing Committee: D. Babusci (chair), S. Bianco, M. Calvetti, P. Campana, L.E. Casano, R. Centioni, C.O. Curceanu, P. Di Nezza, V. Ferretti, S. Miozzi, L. Sabatini, S. Vannucci.

- Lectures for high-school science teachers and people involved in scientific research dissemination.
- Goal: stimulate teachers' professional training and provide an occasion for interactive and hands-on contact with the latest developments in physics.

Seventh edition (October 1-3, 2007): 199 participants and 59 LNF Tutors (researchers, engineers and technicians).

5 Online resources for theachers and students: Lezioni di Fisica, Live lectures by scientists

http : //www.lnf.infn.it/media/

Care of M. Calvetti, O. Ciaffoni, G. Di Giovanni.
E. Iacopini: "Simmetrie".
A. Masiero: "La freccia del tempo".

6 General public programme

Seminars

http : //www.lnf.infn.it/edu/seminaridivulgativi/

Upon request, LNF researchers gave seminars to high school students and the general public on:

- INFN Activities and Elementary Particles;
- Radioactivity;
- Gravitational waves;
- LHC;
- Modern Physics and Cosmology;
- Physics and Techonology for historic and artistic patrimony.

7 Events

European Researchers' Night 2007

`http : //www.lnf.infn.it/nottedellaricerca/`

2007 Project done in the framework of the European Researchers' Night on 28 September 2007. About 700 visitors at LNF. The key of the success was an intense and constructive collaboration between INFN, ENEA, ESA-ESRIN, Frascati Municipality, European Commission, Regione Lazio, Provincia di Roma, XI Comunitá Montana, Parco Regionale dei Castelli Romani, Grottaferrata Municipality, Monte Porzio Catone Municipality, Filas, Trenitalia. This collaboration allowed to present to the general public many different and complementary activities, in an informal way.

Organizing Committee: D. Babusci, G. Bernardi, S. Bertolucci, M. Calvetti, C.O. Curceanu, P. Di Nezza, A. Gallo, A. Fantoni, D. Maselli, G. Mazzitelli, F. Murtas, G. Pancheri, B. Sciascia, V. Tullio.

Project Coordinator: G. Mazzitelli.

An important feedback of the success of the event comes from the questionnaire (available on the web site http://www.infn.it/nottedellaricerca) addressed to investigate the achievement of the main purpose of the project and of the quality of the activities.

50° LNF Anniversary and Christmas Concert, Orchestra Papillon, LNF 17 December, 2007.

Figure 2: *50° LNF Anniversary and Christmas Concert December 17, 2007 (INFN-LNF Photo).*

Conferences

International conferences, workshops and schools hosted and/or organized by the LNF:

1. Les Rencontres de Physique, La Thuile, 4-10 March, 2007;
2. ILCDR07 - Dampig Rings R&D Meeting, LNF 5-7 March, 2007;
3. Meeting BABAR, LNF 29-30 March, 2007;
4. Commissione Scientifica Nazionale II, LNF 4-5 April, 2007;
5. Spring Institute, LNF 2 May/31 July, 2007;
6. Super B-Factory, LNF 4 May, 2007;
7. Observation of the universe from the moon, LNF 7 May, 2007;
8. Frascati Spring School "Bruno Touschek", LNF 14-18 May, 2007;
9. Kaon International Conference, LNF 21-25 May, 2007;
10. String Phenomenoloy 2007, LNF 4-8 June, 2007;
11. Channeling 2007, S. Pietroburgo (Russia), 11-15 June. 2007;
12. Commissione Scientifica Nazionale III, LNF 13 June, 2007;
13. School on Attractor Mechanism, LNF 18-22 June, 2007;
14. From Synchrotron to FEL radiation, LNF 18-20 June 2007:
15. Commissione Scientifica Nazionale I, LNF 25-26 June, 2007;
16. School on diffraction and low-x physics, Copanello di Staletti (Catanzaro) 1-15 July, 2007;
17. QCD in extreme conditions, LNF 6-8 August, 2007;
18. Collaboration meeting for european network Light Net, LNF 6-8 September, 2007;
19. Frontiers in FEL Physics and Related Topics, Elba Island, 8-14 September, 2007;
20. Commissione Scientifica Nazionale V, LNF 10-14 September, 2007;
21. Commissione Scientifica Nazionale I, LNF 17-21 September, 2007;
22. Commissione Scientifica Nazionale II, LNF 24-28 September, 2007;
23. Hadron Physics 2, LNF 28-30 September, 2007;
24. Incontri di Fisica 2008, LNF 1-3 October 2007;
25. XII International Conference on Hadron Spectroscopy - Hadron 07, LNF 8-13 October, 2007;

26. Nanotubes & Nanotechnology, Villa Mondragone (Monte Porzio Catone), 15-16 October, 2007;

27. Rich2007, Trieste, 15-20 October, 2007;

28. 3rd Annual EUROFEL Meeting, LNF 24-25 October, 2007;

29. CARE-HHH-APD IR'07 (Interaction Regions for the LHC Upgrade, DAFNE and SuperB), LNF 6-9 November, 2007;

30. Terzo convegno nazionale sulla fisica di ALICE Terzo convegno nazionale sulla fisica di ALICE, LNF 12-14 November, 2007;

31. International Review Committee for SuperB, LNF 12-13 November, 2007;

32. International Capillary Optics Workshop COW2007, LNF 19-21 November, 2007.

1 – Particle Physics

ATLAS

A. Annovi, M. Antonelli, M.M. Beretta, H. Bilokon, E. Capitolo (Tecn.), F. Cerutti, V. Chiarella, M. Curatolo, B. Esposito(Resp.), M.L. Ferrer, C. Gatti, S. Giovannella, K. Kordas, P.F. Laurelli, G. Maccarrone, A. Martini, W. Mei, S. Miscetti, G. Nicoletti, G. Pileggi (Tecn.), B. Ponzio(Tecn.), V. Russo(Tecn.), A. Sansoni, T. Vassilieva (Tecn.), S. Ventura (Dott.), E. Vilucchi

In collaboration with:
Servizio Progettazione Apparati Sperimentali:
C. Capoccia, S. Cerioni
Centro di Calcolo:
D. Maselli, C. Soprano

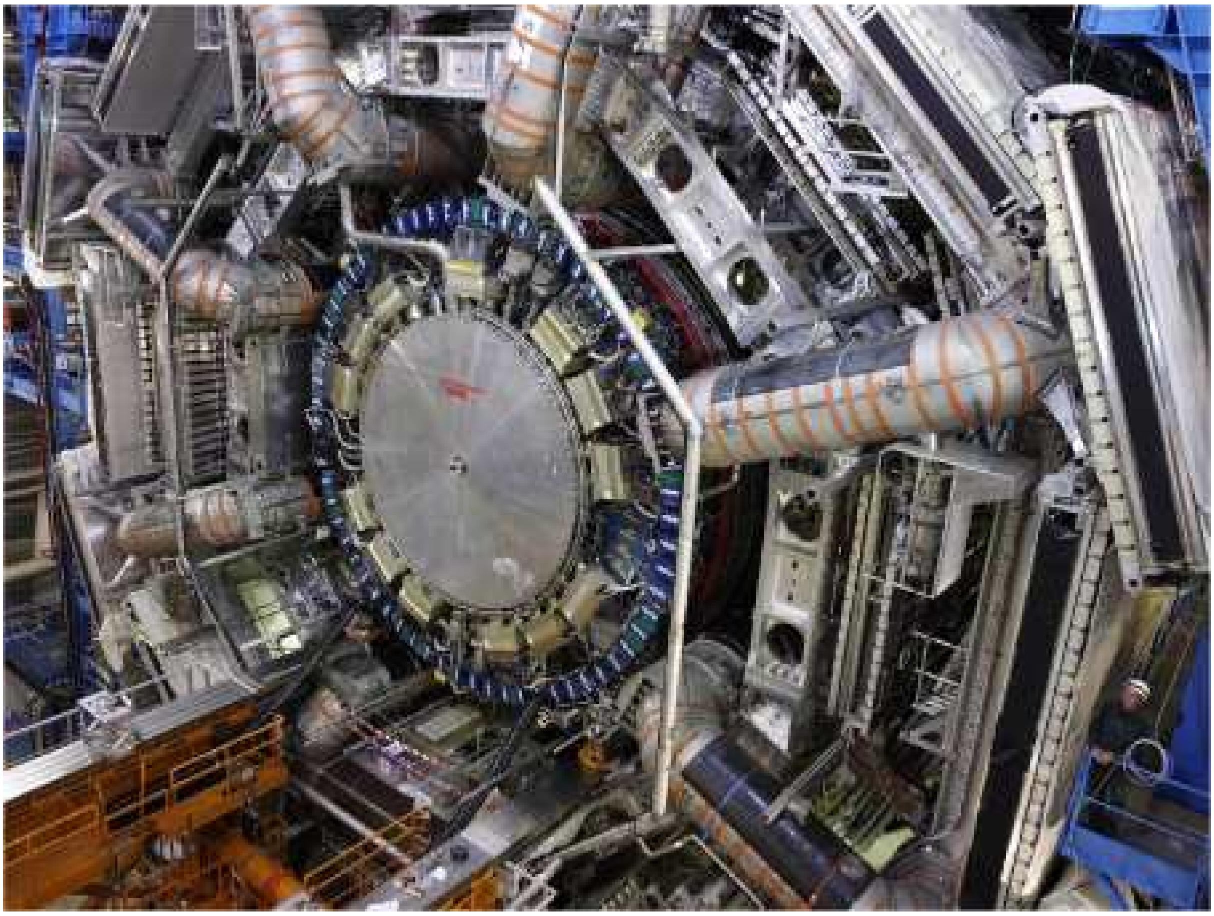

1 Introduction

The year 2007 was dedicated to the completion of the installation of the Atlas detector in the cavern,the commissioning of the detector, the DAQ, the trigger and to the preparation of the computing resources, the software, the analysis tools and algorithms, in view of the start of the LHC in summer 2008.

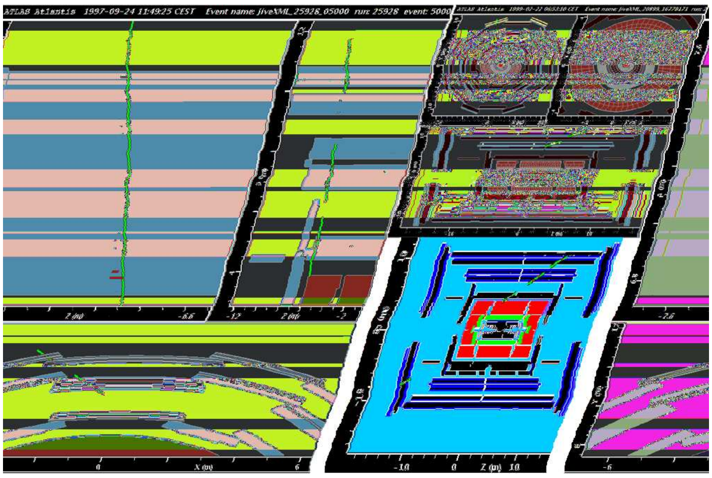

Figure 1: *Exemples of event display of cosmic muons taken during the commissioning runs.*

2 Muon Chamber installation

The totality (94) of the BML stations had been integrated with the RPC, or re-integrated after the RPC refurbishing operations, already at the end of 2006. A final cosmic ray test of the complete RPC-MDT stations at the BB5 stand was performed to declare them ready for installation in Atlas. The number of BML stations that had undergone in 2006 this cosmic ray final test was 76. In the first months of 2007 the rest of 18 BML stations have been tested in BB5. All the muon stations arrived at ATLAS after the cosmic ray certification at the BB5 stand were re-tested at SX1 (the surface area at the ATLAS point), before being downloaded in the pit and installed in the muon spectrometer. Each single chamber was connected to the low voltages, and then readout from the CSM board via an optical fiber by a standalone PC to check the whole functionality of the FEE mounted on the chamber. Tests of the HV system, of the gas-tightness and of the optical alignment parts were also performed. In the overall ATLAS schedule, the installation of the majority of the BML stations was scheduled in 2006 and a few of them in 2007, for reasons of detector accessibility. In 2007, 9 more muon stations of side A and 19 more muon stations of side C have been installed. Few stations (in sectors 11,13,15) are still not in the final position due to the necessity of maintaining the accessibility into ATLAS up to the last moment. Where possible all the alignment sensors have been tested and the optical lines for axial and projective alignment verified.

3 Commissioning and Cosmic data taking

The year 2007 has been characterized by the intense work for the commissioning of the stations in the pit. The aim is to test not only the functionality of the MDT chambers but the whole system (trigger, Detector Control System, data acquisition and online/offline monitoring). For the MDT, the chambers have been connected to the final services: gas, HV, LV, RO-fibers, DCS. Soon after the commissioning started sector by sector. It consists of some different steps. In the first step MDT chambers are made operational, power and the HV are switched on, DCS values are read-out and checked, the MDT read-out initialized. A local data taking with the MDT standalone using a random trigger is performed as soon as all chamber of a sector are operational. This allows us to know the single tube noise level. As soon as the relative RPC are ready the final step consists in a data taking with cosmic rays using the central Atlas DAQ system. At the end of 2007 12 MDT sectors (out of 16) had passed the first two steps and were ready for cosmic rays test which, for 6 of them has been successfully performed. The MDT system has always participated to the Atlas Milestone weeks dedicate to the integration of the various Atlas components in the global DAQ.

4 DAQ Commissioning

The activity on the Trigger and Data Acquisition (TDAQ) system has been focused, during the year 2007, on the following aspects:

1. Developments of the Event Building (EB) sub-system;
2. Technical runs for TDAQ commissioning, using an increasing number of PC's and network devices approaching the final configuration;

The Event Builder sub-system was running with minimal interventions during all the TDAQ and detectors commissioning activities. New facilities have been added in preparation to the new TDAQ-01-09-00 release to be built starting in 2008. This new facilities are related to (i) the definition and implementation of new functionalities in the interface versus the level-2 trigger, and (ii) the ability to build partial events when requested. The LNF group has been involved in the definition and implementations of both components.

A full event in ATLAS is foreseen to be about 1.5 MB, recorded at a rate of 100 to 200 Hz. In some cases the complete information of an ATLAS event is not needed as, for example, for the muon detector calibration events, where higher rates should be needed. In 2006, the new functionality of building *partial events*, based only on the data readout of a specific list of sub-detectors or specific readout drivers (ROBs), was programmed to be added to the ATLAS TDAQ system. The full definition and implementation was delayed during all 2007, waiting for important revisions in particular of the readout architecture and the event format.

5 LNF Tier-2 activity

The LNF Tier-2 computing farm is considered a proto-Tier-2 by INFN and is still in the process of getting officially approved. However, during 2007 it has worked at almost full efficiency providing computing power and data storage for official and private ATLAS simulation production campaigns.

The financial support received, both from central and local resources, made possible to expand the initial configuration.

- The computing power increased from 41 KSI2k to 80 KSI2k;
- The storage capability increased from 11.5 TB to 36 TB usable, corresponding to 47 TB raw.

At present the Tier-2 has a dedicated man-power equivalent to 3.5 FTE: 0.5 FTE from the Computing Service, responsible of maintenance and software installations, and 3 FTE from the ATLAS group, responsible of all ATLAS related interventions and users support. The computer farm provided by the LNF Computing Service is also available to local ATLAS users. To facilitate the users a parallel ATLAS software installation is maintained and a dedicated afs disk area of about 3 TB is available.

The plot Fig. 2 shows in red the Computing time available, obtained by multiplying the number of CPUs by 24 hours and integrating day by day during the year 2007. In blue the time used by the collaboration is presented. The overall efficiency in the usage of the Tier-2 by the virtual organization ATLAS was about 72%.

6 In-situ Data driven calibration

The first data collected at LHC will be important for the understanting of the detector response and for its calibration. The Frascati group is involved in this activity, in particular in the study

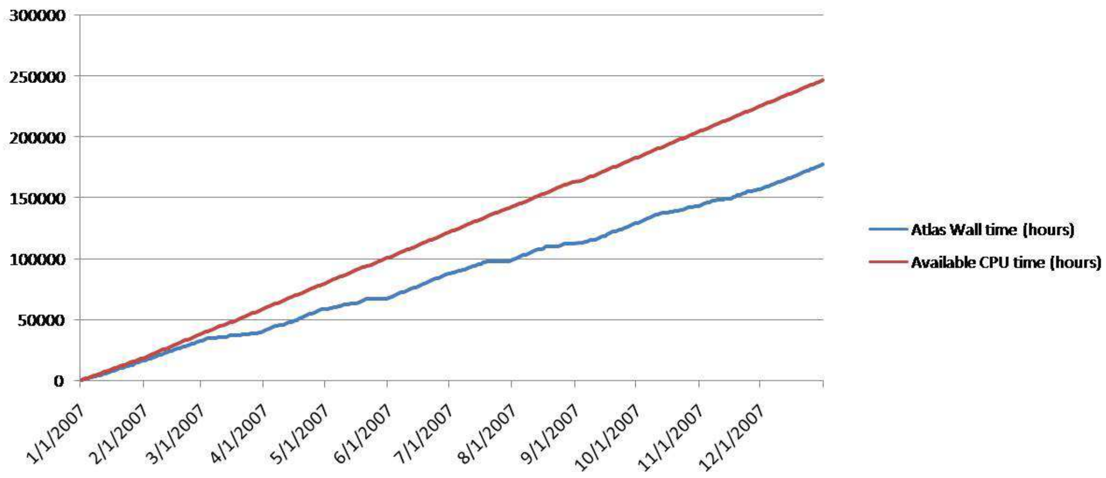

Figure 2: *Plot Tier-2*

of the performances of the muon spectrometer. Resonances such as J/ψ, Υ's, and the Z boson decaying to muon pair, are produced with large cross sections, about 50 nb, 10 nb, and 2 nb, respectively, with muon transverse momenta above the minimum trigger threshold of 4-5 GeV/c. Our effort is to exploit the large rate and known kinematics of these decays for a direct measurement of miscalibrations, misalignments, wrong maps of the magnetic field and of the material in the detector as well as inefficiencies of the trigger and precise-measurement chambers.

6.1 Performances with $Z \to \mu\mu$

The energy scale of the muon spectrometer can be estimated by measuring the invariant mass distribution of the resonances discussed above. The different mass ranges will help in disentangling various effects such as energy loss and magnetic field errors. Differences between the experimental widths in data and in the Monte Carlo will allow the determination of the real momentum resolution. We have divided a Monte Carlo sample of $Z \to \mu\mu$ events corresponding to an integrated luminosity of about 40 pb^{-1}, into two samples, to be used as a *data* sample and a Monte Carlo sample. The invariant mass distribution obtained from the *data* sample is then fit with the distribution obtained from the Monte Carlo sample, after appropriately changing the reconstructed momenta by means of two parameters that are determined by the fit procedure. The two parameters take into account the errors in the energy scale calibration and in the spectrometer resolution. An example of the fit is shown in the left panel of Fig. 3. We have verified that in this way it is possible to determine the energy scale and the spectrometer resolution at the permil level with about 20 pb^{-1} of integrated luminosity. We have checked the effect of large ($\sim$ 1mm) misalignments in the chamber positions. In this case, right panel of Fig. 3, the fit returns the correct value of the parameters but with larger errors. Infact, in presence of large errors in the description of the detector, the value of the momentum scale and resolution depend on the impact position in the spectrometer and have standard deviations of 1% and 10%, respectively.

In order to monitor the chamber calibration locally and to eventually correct it, we have divided the detector in about 360 projective towers, corresponding in first approximation to the physical detector towers. Imposing the Z mass constraint we estimate a new value for the muon momenta and compare it with the reconstructed one. The distribution of the residuals is shown in Fig. 4. On the left panel the estimated residuals are shown as a function of the relative momentum obtained using the Monte Carlo truth, for a sample of miscalibrated events. The correlation is well visible. On the right panel, we show the residuals estimated for positive muon as a function of those for the negative muons. The anti-correlation is due to errors in the sagitta measurement, while the correlated error is due to the wrong knowledge of the magnetic field. Exploiting these correlations, we can correct at momentum level and improve the final momentum resolution. Applying this

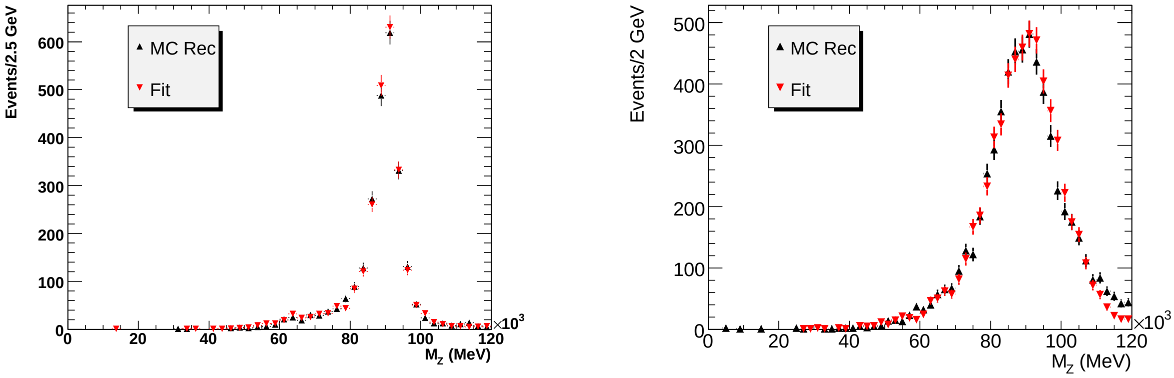

Figure 3: *Example of fit to the Z lineshape: (Left) with a well calibrated spectrometer; (right) with unknown misalignments as described in the text. The* data *is shown in black, while the MC fit is shown in red.*

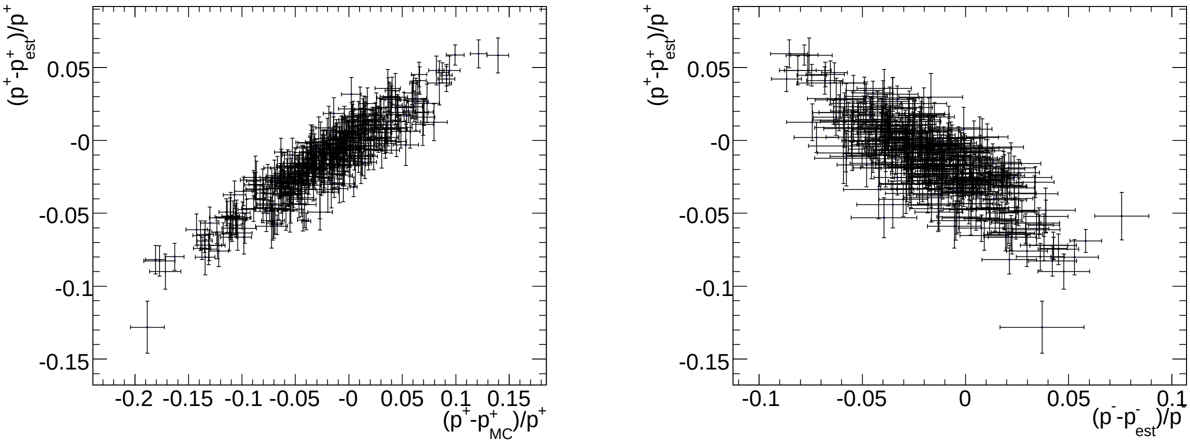

Figure 4: *Left: Estimated relative momentum residuals as a function of the one expected from MC truth information. Right: Estimated residuals for positive muons as a function of those for negative muons. Each point correspond to the average value obtained for each tower.*

procedure to a sample of about 80,000 reconstructed events with $80 < M_Z < 100$ GeV, the core-width of the Z lineshape improves from 7.4 GeV to 6 GeV, being 3.7 GeV the value expected with a well calibrated detector. Further understanding of the role played by chamber rotation is under investigation to improve the final correction.

6.2 Performances with $J/\psi \to \mu\mu$

J/ψ's are produced with a very large cross section and are complementary to the Z boson. We have analyzed a sample of about 50,000 $J/\psi \to \mu\mu$ with muon transverse-momentum above 4 and 6 GeV, corresponding to an integrated luminosity of about 1 pb^{-1}. Muons from J/ψ decay have low momentum, about 6 GeV on average. The momentum resolution is dominated by the fluctuations of the energy loss in the calorimeter. Muons lose about 3 GeV with a standard deviation of about 300 MeV. Therefore, they are very sensitive to any error in the description of the energy loss both in the simulation and in the reconstruction programs. In principle, the energy loss in the calorimeter can be studied by comparing the momentum measured in the inner detector with that measured inside the muon spectrometer. However, since any difference between inner and outer detectors could be due to miscalibrations and different momentum scales, we need an independent check based only on the muon spectrometer information. This can be done by reconstructing the decay vertex of the J/ψ at the interaction point and imposing the constraint of its mass. Eventually, we

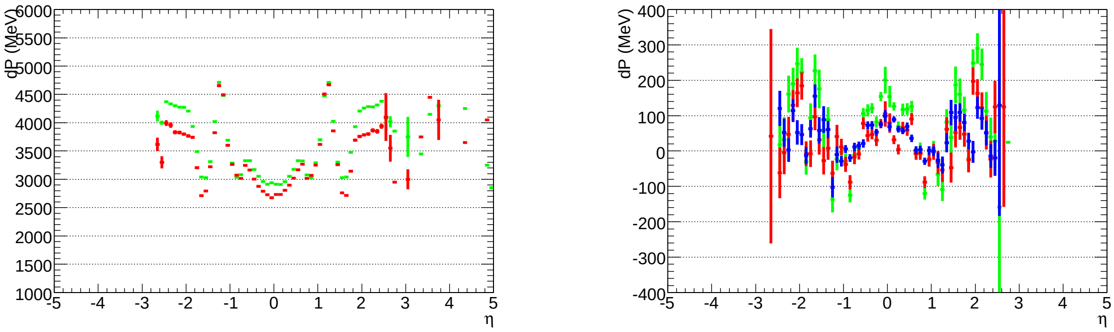

Figure 5: *Left: Mean energy loss as a function of the pseudorapidity for the reconstruction program (green) and for the Monte Carlo simulation (red). Right: Energy loss as a function of the pseudo-rapidity, obtained from the difference of reconstructed ad Monte Carlo momenta (green), momenta from kinematic fit and Monte Carlo (red), and from the difference of the momenta reconstructed ad estimated from the kinematic fit (blue).*

can impose also the beam position constraint. With the constraint from the vertex and the beam profile the invariant mass resolution improves from about 450 MeV to 180 MeV. As in the case of the Z decays, we use the new estimated momenta to check the residuals as a function of the entry position of the muons.

In Fig. 5 (left) we show the mean energy loss in the calorimeter used in the track reconstruction (green) and in the Monte Carlo simulation (red). The two energy losses are different for a well known problem, and it has been fixed. However, we can test our procedure and check if we are sensitive to errors of 5-10% in the energy loss parametrization. In the right panel, we show the difference between the reconstructed and the Monte Carlo momenta (green), the difference between the new estimated momenta and the Monte Carlo momenta (red), and the difference between the reconstructed and the new estimated momenta (blue). As we can see, the new estimated momenta are also affected by the wrong energy loss parameterization (red markers), but less than the reconstructed momenta. Infact, the difference between the two (blue markers) is still sensitive to the wrong parametrization, even if for a smaller amount. This difference can be used as a monitor of the reconstruction, and eventually for an iterative correction of it.

Using the same sample, we have investigated the possibility of measuring the tracking efficiency in the low p_T region. This region is important for the B physics program, but also for the correct estimate of the efficiency for decays such as $H \rightarrow 4\mu$. J/ψ decays are selected by requiring a muon completely reconstructed in the muon and inner chambers, and a track in the inner detector that satisfies with the muon track a two sigma cut on the J/ψ mass. The tag is enforced by requiring that the inner detector track has an energy loss in the calorimeter compatible with the loss of a muon. Once an event is selected, we determine the tracking efficiency by counting the fraction of events in which a muon is reconstructed in the outer spectrometer in correspondance of the inner detector track. At present, the calorimeter tag has been done only for the tile calorimeter in the barrel region. Several tools are available for extending this tag to the endcap region. In Fig. 6 we show the estimated efficiency using this method as a function of the transverse momentum, for the pseudorapidity region $-0.48 < \eta < 0$. The true Monte Carlo efficiency is also shown. The two plots refer to the case in which a cut is applied or not to the χ^2 of the track.

The main background is due to $b\bar{b}$ with a muon in the final state. In this events, the inner detector track is usually a pion with low p_T. Most of the events are rejected by requiring $p_T >$ 3 GeV and by the request on the energy loss in the calorimeter. The background level is few percent at the end of the selection.

7 Physics studies: search for $Z' \rightarrow \mu\mu$

Several models predict the existence of an extra boson decaying into two muons [1]. Such bosons, generically called Z', have been excluded in the mass range below $\sim$ 900 GeV. At the LHC, the

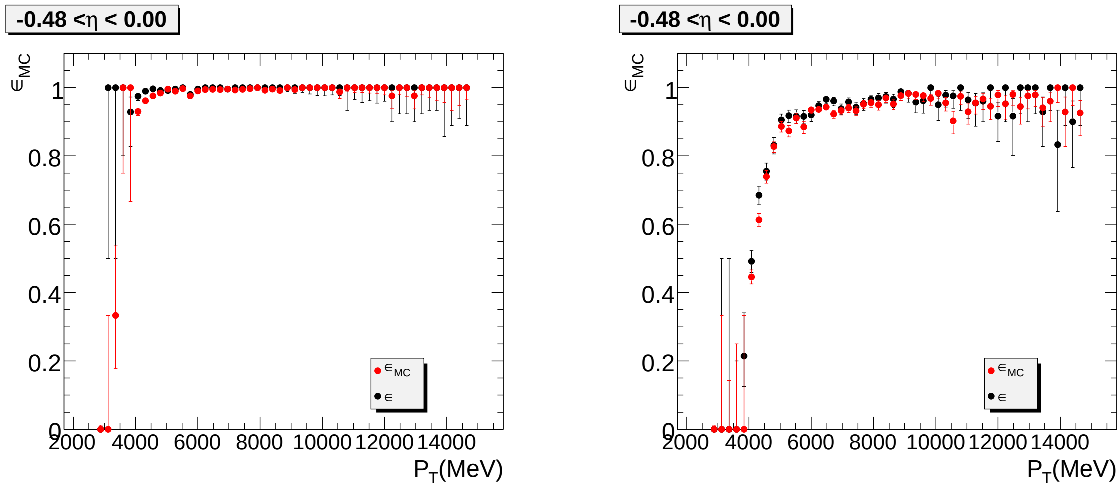

Figure 6: *Muon-track reconstruction efficiency as a function of the transverse momentum, for the pseudorapidity region $-0.48 < \eta < 0$. In the pictures are shown the true (red) and the estimated (black) efficiencies. The two plots refer to different requirements on the track quality: no cut (Left); cut on the track χ^2.*

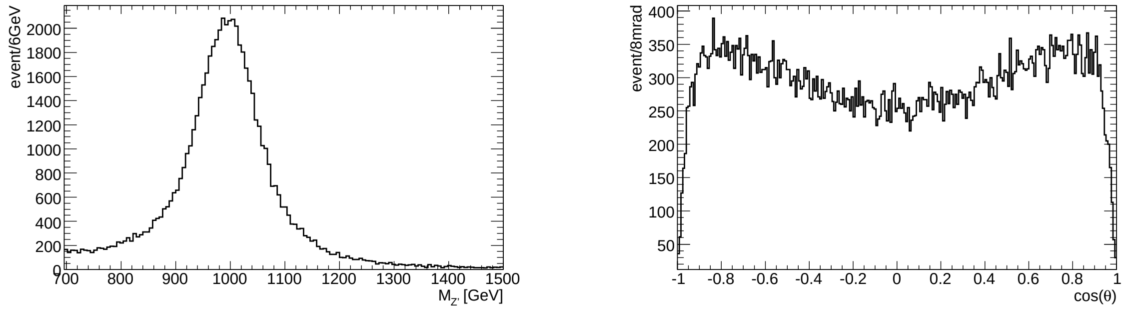

Figure 7: *Left: Invariant mass distribution for events simulated with the SSM model. Right: Angular distribution of the muon showing the typical spin-1 behavior.*

production cross section times branching ratio ranges from 20 to 80 fb for 1.5 TeV mass, and from 0.2 to 2 fb for 4 TeV mass, depending on the model, while the width is dominated by the experimental resolution. The main background is due to the Drell-Yan production of dimuon events, on the order of 1 fb/40GeV at 1.5 TeV. The reconstructed invariant mass spectrum is shown on the left panel Fig. 7, for events simulated in the SSM model with mass 1 TeV. The signal peak is well visible over the Drell-Yan tail. On the right panel we show the muon angular distribution, showing the typical spin-1 behavior. This last quantity will allow us to disantangle between several models.

Z' couplings can be studied also measuring the forward-backward asymmetry of the muons. However, since LHC is a symmetric p-p machine, the Z-axis versus is taken parallel the Z' momentum. The asymmetry as a function of the reconstructed invariant mass is shown in Fig. 8. A 20% variation is well visible in the region of the Z' peak.

A detailed study of the ATLAS discovery potential is ongoing for several models and several mass values. The minimal luminosity required to mesure the particle spin and asymmetry distribution must also be determined.

8 Tracking trigger upgrade

The trigger is a fundamental part of any experiment at hadron colliders needed to select on-line the low cross-section physics from the huge QCD background.

Experience at high luminosity hadron collider experiments shows that controlling trigger rates can be extremely challenging as the luminosity increases, physics goals change in response to new discoveries, and the detector ages. It is thus essential that the trigger system be flexible and robust,

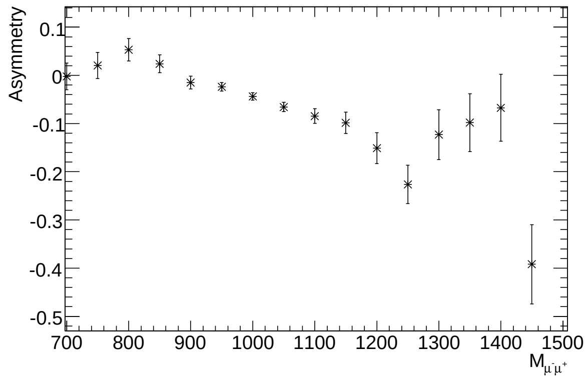

Figure 8: *Muon angular asymmetry as defined in the text as a function of the reconstructed invariant mass.*

and have redundancy and significant operating margin. Providing high quality track reconstruction over the full ATLAS Inner Detector by the start of processing in the level-2 computer farm can be an important element in achieving these goals.

With the goal to improve and make more robust the ALTAS trigger, the group joined the Fast-Track proposal for a hardware track finder for the ATLAS trigger. This is a proposal to build a hardware track finder (FTK) as an upgrade to the ATLAS trigger. It will provide global reconstruction of tracks above 1 GeV/c in the silicon detectors, with high quality helix parameters, by the beginning of level-2 trigger processing. FTK can be particularly important for the selection of 3rd-generation fermions (b and c background from QCD jets) which can be quickly rejected in level-2 if reconstructed tracks are available early. This R&D proposal is aimed at producing a full technical design report for FTK in the next year.

The Frascati's group is developing a hardware-implementable clustering algorithm for the pixel detector. The clustering for the pixel detector is one piece of Fast-Track that needs R&D from scratch. Clustering in the pixel detector is a non trivial computational problem because of the 2D nature of the pixel detectors and of the huge amount of data involved. The pixel detector's RODs deliver data with 120 S-link fibers each with a 1.2 Gbits bandwidth. The clustering algorithm must identify clusterized hits and calculate the center of the cluster.

During 2007 we implemented a first offline simulation of a first clustering algorithm. This algorithm will not necessarily be the final algorithm but is used as first reference for the clustering performances. The chosen algorithm is such that foreseen hardware implementation will achieve similar performances. The clustering simulation is now used as part of the full Fast-Track simulation to study the algorithm and study FTK performances as needed to prepare the project TDR.

On the hardware side, we started discussion of realistic algorithms to be implemented in hardware. Those algorithm must be fast, must have good clustering properties and must be implementable within reasonable time and cost. We have first candidate hardware based algorithms that should satisfy all the requirements. The next step will be the study of one specific hardware algorithm with the goal to proof the feasibility of its hardware implementation.

The Fast-Track proposal has been approved for R&D by the ATLAS experiment on February 2008.

References

1. T. Rizzo, arXiv:hep-ph/0610104.

BaBar

F. Anulli, R. Baldini Ferroli, A. Calcaterra, L. Daniello (Tecn.), R. de Sangro,
G. Finocchiaro, S. Pacetti, P. Patteri, I. Peruzzi (Resp.), M. Piccolo, M. Rama, A. Zallo

1 Introduction

BaBar is the experiment running at the SLAC asymmetric B-factory PEP-II; the physics program is centered on, but not limited to, the study of the *CP* violation in the decay of neutral B mesons. The B system is the best suited to study *CP* violation because the expected effects are large, appear in many final states and, most importantly, can often be directly related to the Standard Model parameters. The large data sample being collected has already allowed significant advances in a large number of topics in B, charm and tau lepton physics; all three angles of the Unitarity Triangle have been measured, direct *CP* violation has been observed in B decays, several new B decay modes have been measured, and new charmed states have been discovered. The highlight of the physics results obtained in 2007 was the discovery of the mixing phenomenon in the neutral D mesons system.

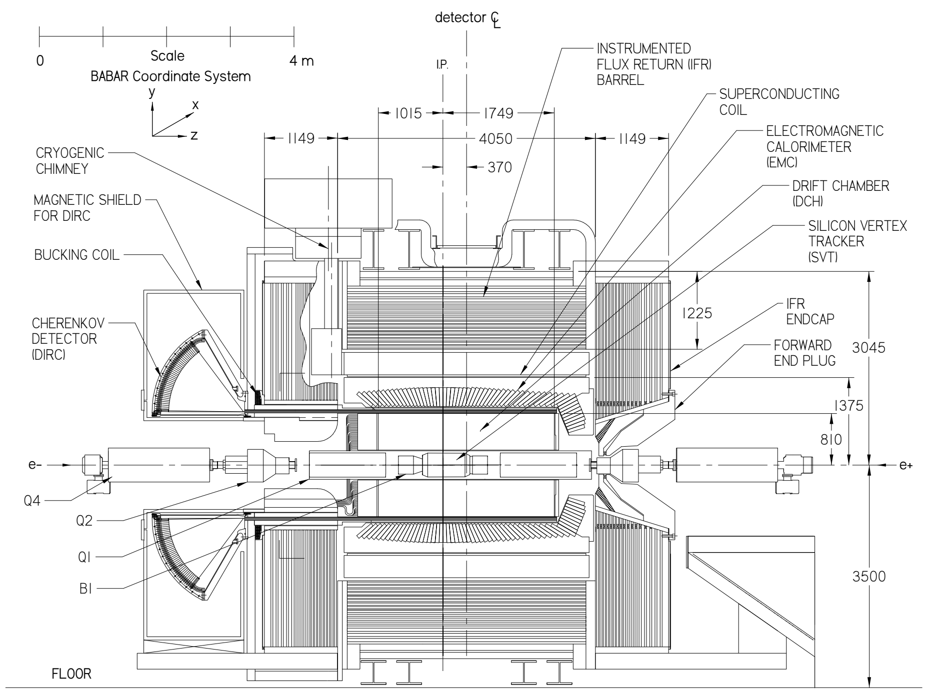

Figure 1: *Elevation view of the BaBar Detector.*

The PEP-II B factory is an asymmetric e^+e^- collider designed to operate at a center-of-mass energy of 10.58 GeV corresponding to the mass of the $\Upsilon(4S)$ resonance, which decays 50% in B^+B^- and 50% in $B^0\ \overline{B}^0$. In PEP-II the electron beam of 9.0 GeV collides head-on with the positron beam of 3.1 GeV resulting in a Lorentz boost ($\beta\gamma = 0.56$) to the $\Upsilon(4S)$ resonance, making possible the measurement of the time-dependent CP violation of the neutral B's.

The *BaBar* Collaboration includes about 540 physicists, with contributions from about 80 Institutions in 10 countries in North America, Europe, and Asia. Approximately half of the group are physicists from U.S. Universities and Laboratories, with the largest foreign contribution coming from Italy, with 12 INFN Institutions and more than 90 people.

The *BaBar* detector (fig. 1) has been designed primarily for *CP* violation studies, but it is also serving well for the other physics objectives of the experiment. The asymmetry of the beam energies is reflected in the detector design: the apparatus is centered 37 cm ahead of the collision point, along the direction of the high-energy beam, to increase forward acceptance. All services are placed on the opposite side of the detector, in order to minimize multiple scattering in the forward direction. The momentum of the charged tracks is obtained from the curvature in a solenoidal field of 1.5 T and is measured in a low mass Drift Chamber. Different species of hadrons are identified in the DIRC, a dedicated device of a novel kind, based on the detection of Čerenkov light. Excellent photon detection and electron identification is provided by a CsI crystals electromagnetic calorimeter. Muons and neutral hadrons are identified in the iron magnet's yoke, where a total thickness of 65 cm of Fe plates has been segmented in 18 slabs of graded thickness (from 2 to 10 cm) and instrumented with Resistive Plate Counters and Limited Streamer Tubes. This system, made of a 6-sided barrel, 2 endcaps and a double cylindrical layer inside the magnet coil, is called Instrumented Flux Return, or IFR. The final ingredient in the *CP* asymmetry measurements, the distance between the two decay vertices, is measured by a state of the art vertex detector, with five layers of double sided silicon sensors. It also provides standalone tracking for particles with low transverse momentum that cannot be measured reliably in the Drift Chamber alone.

2 Summary of 2006 activity

Data taking in 2006 continued until August 20, when the machine was shut down for maintenance and upgrade work. The Frascati group had an active part in the upgrade of the IFR: in 2004 two barrel sextants were upgraded with addition of copper plates in six of the gaps, to increase the amount of absorber, and instrumented with LST (Limited Streamer Tubes. In the Fall of 2006, the remaining 4 barrel sextants were similarly upgradated. A very productive analysis activity took place during the whole year, resulting in many pubblication and Conference contributions.

3 Activity

Data taking in 2007 continued with consistent high luminosity and excellent detector efficiency. The superb machine performance allowed a delivery of approximately $90 fb^{-1}$ in 2007, mostly at the energy of the Y(4S) resonance, bringing the total data sample recorded by *BaBar* to almost one half of an inverse attobarn. The integrated luminosity as function of time is reported in fig. 2.

Data analysis activity by *BaBar* in 2007 continued regularly, covering a very wide spectrum of measurements, like the angles of the Unitarity Triangle β, α, γ, branching ratios and CP-violation of rare B decays, $|V_{ub}|$, $|V_{cb}|$, the extensive study of charm and τ decays (*BaBar* is also a charm and τ factory), and the most extensive systematic study up to now of low-energy meson spectroscopy in the energy range between 1 and 4 GeV, possible at *BaBar* using the technique of Initial State Radiation (ISR). In 2007 *BaBar* discovered the existence of oscillations in the $D^0\overline{D}^0$ system, with mixing at the level expected in the SM. A total of 65 papers were published in the same year on major journals and Babar continued as a major contributor at all HEP Conferences In the next sections the analysis items which led to a publication in 2007 or beginning of 2008 and in which the Frascati group is more directly involved are shortly described.

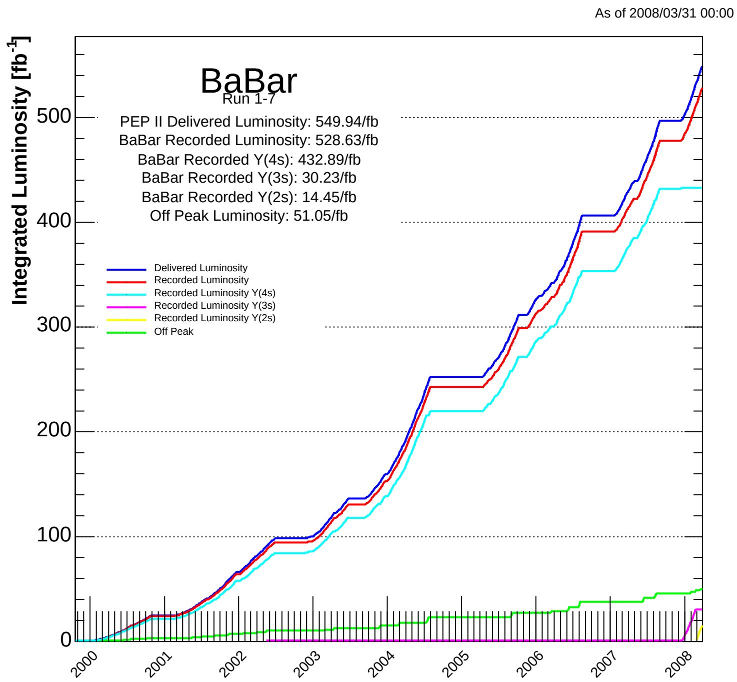

Figure 2: *BABAR integrated luminosity from the start of the data taking in 1999 till the end of 2007.*

4 Improved measurement of CP violation in neutral B decays to $(c\bar{c})K^{(*)0}$

In the Standard Model of particle physics CP violation is described as a consequence of a complex phase in the three-generation Cabibbo-Kobayashi-Maskawa (CKM) quark-mixing matrix. In this context, measurements of CP asymmetries in the proper-time distribution of neutral B decays to CP eigenstates containing a charmonium and K^0 meson provide a direct measurement of sin2β. The angle β is defined in terms of the CKM matrix elements V_{ij} as $\arg[-(V_{cd}V^*_{cb})/(V_{td}V^*_{tb})]$. At the $\Upsilon(4S)$ resonance, the CP asymmetry $\mathcal{A}_{CP} \equiv S_f \sin(\Delta m_d \Delta t) - C_f \cos(\Delta m_d \Delta t)$ is extracted from the distribution of the difference of the proper decay times Δt between the reconstructed B meson and the other B meson in the event (B_{tag}). The decay products of B_{tag} are used to identify its flavor (B^0 or $\overline{B}^0$) at its decay time. Here Δm_d is the mass difference determined from B^0-$\overline{B}^0$ oscillations.

Members of our group have contributed to the update of this flagship B-factory measurement with the new data. Since our previously published result we have added about 157×10^6 decays and applied an improved event reconstruction to the complete dataset of $(384 \pm 4) \times 10^6 \Upsilon(4S) \to B\overline{B}$ decays. We have also developed a new $\eta_c K^0_S$ event selection based on the Dalitz structure of the $\eta_c \to K^0_S K^+ \pi^-$ decay and we have performed a more detailed study of the CP properties of our background events, resulting in a reduced systematic error. The measurement has been published in [32]. The final results are $\sin 2\beta = 0.710 \pm 0.032\,(\text{stat}) \pm 0.018\,(\text{syst})$ and $|\lambda| = 0.952 \pm 0.022\,(\text{stat}) \pm 0.017\,(\text{syst})$, both in agreement within errors with the published results and with the theoretical estimates of the magnitudes of CKM matrix elements in the context of the Standard Model. The measured value of $|\lambda|$ is consistent with no direct CP violation with a significance of 1.72 standard deviations. We also reported the first individual measurements of sin2β and $|\lambda|$ for each of the decay modes within our *CP* sample, and of the $J/\psi K^0(K^0_S + K^0_L)$ sample.

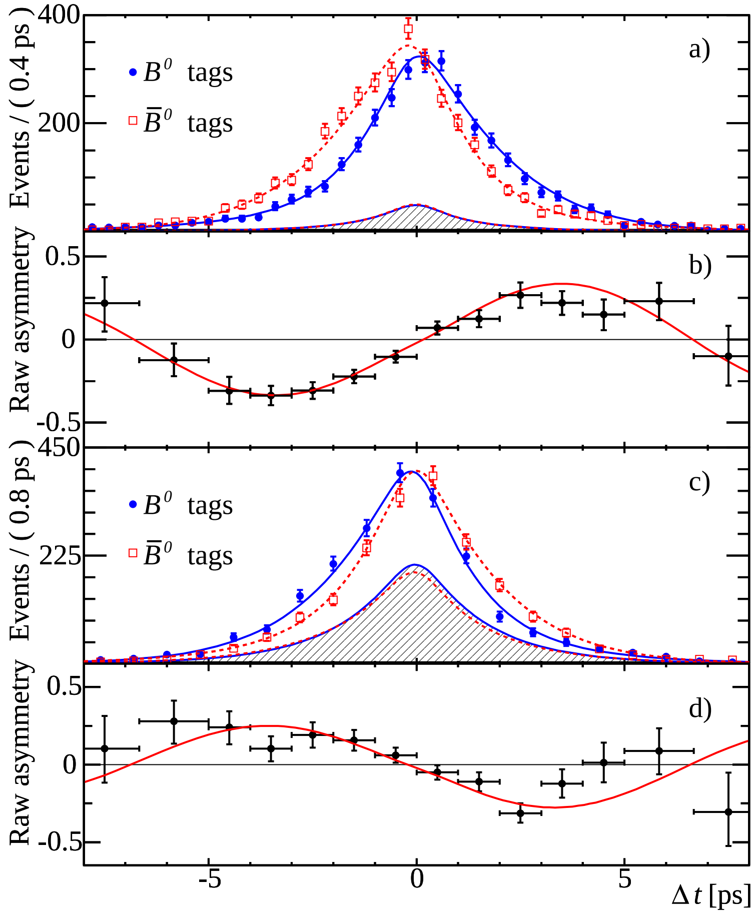

Figure 3: *a) Number of* $\eta_f = -1$ *candidates* ($J/\psi K^0_S$, $\psi(2S)K^0_S$, $\chi_{c1}K^0_S$, *and* $\eta_c K^0_S$) *in the signal region with a* B^0 *tag* (N_{B^0}) *and with a* $\overline{B}^0$ *tag* ($N_{\overline{B}^0}$), *and b) the raw asymmetry* $(N_{B^0} - N_{\overline{B}^0})/(N_{B^0} + N_{\overline{B}^0})$, *as functions of* Δt. *Figures c) and d) are the corresponding distributions for the* $\eta_f = +1$ *mode* $J/\psi K^0_L$. . *The solid (dashed) curves represent the fit projections in* Δt *for* B^0 ($\overline{B}^0$) *tags. The shaded regions represent the estimated background contributions.*

5 Measurement of the angle γ with $B^{\pm} \to D^{(*)0} K^{(*)\pm}$ decays

The measurement of the angle γ of the Unitarity Triangle (defined as the phase of V^*_{ub} in the Wolfenstein parametrization of V_{CKM}) has been performed through the decays $B^- \to D[\to f]K^-$ (and the *CP*-conjugated process), where f is a state accessible from both D^0 and $\bar{D}^0$. The rate of the process is the result of the interference of the amplitudes $A(B^- \to D^0 K^-)$ and $A(B^- \to$

$\bar{D}^0K^-$), the latter depending on V_{ub} and therefore on γ. Our group has contributed to the measurement of γ using the $B \to D^{(*)0}K^{(*)-}$ decays with $D^0 \to K^0_S h^+h^-$ ($h = \pi, K$). The analysis has been performed in two steps. First, the Dalitz plots of high-purity and high-statistics samples of flavour-tagged $D^0 \to K^0_S\pi^-\pi^+$ and $D^0 \to K^0_S K^-K^+$ were fit to determine their Dalitz models. Second, we have selected $B^\pm \to D^{(*)}K^{(*)\pm}$ decays with $D \to K^0_S h^-h^+$, whose Dalitz plots differ from the ones found in step 1 depending on the value of γ due to the aforementioned interference. The angle γ was therefore extracted through a fit to the Dalitz plot distributions of $D \to K^0_S\pi^-\pi^+$ and $D \to K^0_S K^-K^+$ of the $B^\pm \to D^{(*)}K^{(*)\pm}$ decays. On a data sample of 383×10^6 $B\bar{B}$ we have selected $B \to D^{(*)}K^{(*)}$ events and we have measured $\gamma = (76 \pm 22(stat) \pm 5(syst) \pm 5(model))^o$, where the third uncertainty comes from the model assumptions for the Dalitz plots of the flavour-tagged D^0's (Fig. 4). This result supersedes the preliminary measurement presented in 2006 and improves it in several ways. The addition of $B \to D^0K^*$, of $D^0 \to K^0_S K^-K^+$, and of 10% more data have dramatically reduced the statistical error from 41° to 22°. Furthermore the systematic error associated to the Dalitz models has decreased from 13° to 5°. The new result has been submitted to Phys. Rev. D in March 2008.

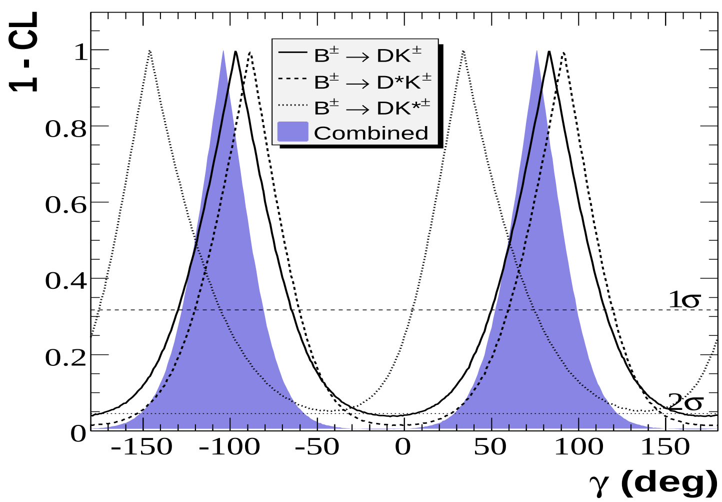

Figure 4: $\alpha = 1 - \mathrm{CL}$ *as a function of* γ *for* $B^- \to D^0K^-$, $B^- \to D^{*0}K^-$, *and* $B^- \to D^0K^*$ *decays separately, and their combination, including statistical and systematic uncertainties and their correlations. The dashed (upper) and dotted (lower) horizontal lines correspond to the one- and two-standard deviation intervals, respectively.*

6 Light hadron spectroscopy with initial state radiation events

Initial state radiation (ISR) events can be effectively used to measure e^+e^- annihilation at a high luminosity storage ring, such as the B-factory PEP-II. A wide mass range is accessible in a single experiment, contrary to the case of fixed energy colliders, which are optimized only in a limited energy region. In addition, the broad-band coverage may result also in greater control of systematic effects because only one experimental setup is involved.
Measurements of the main hadronic final states in the energy range between thresholds and 6 GeV have been carried out at BABAR.

Our group has carried out the study of the $KK\pi$ and $KK\eta$ final states in the energy region from threshold up to ~ 4.6 GeV [66]. The cross sections for the processes: $e^+e^- \to \gamma K^0_S K^\pm\pi^\mp$, $e^+e^- \to \gamma K^+K^-\pi^0$, $e^+e^- \to \gamma\phi\eta$ and $e^+e^- \to \gamma\phi\pi^0$ have been measured with an integrated luminosity of 232 fb^{-1}.
For the first time, from the Dalitz plot analysis of the $K^0_S K^\pm\pi^\mp$ final state, moduli and relative phase of the isoscalar and the isovector components of the $e^+e^- \to KK^*(892)$ cross section have been extracted.
The isospin components are described by means of isoscalar and isovector resonant contributions separately, while the relative phase and the other total cross sections, using suitable combinations of the same resonances.
Parameters of ϕ and ρ recurrences are measured, performing a global fit which exploits the interconnection among amplitudes, moduli and phases of the $K^0_S K^\pm\pi^\mp, K^+K^-\pi^0, \phi\eta$ final states. The dominant isoscalar component, characterized by a main contribution due to the $\phi(1680)$, shows also a significant signal around 2.1 GeV (mainly in the $\phi\eta$ channel), which is compatible with the structure already observed by *BABAR* in the $\phi f_0(980)$ final state. The isovector component is fully described by a broad ρ-like excited state.
The cross section for the OZI-forbidden process $e^+e^- \to \phi\pi^0$ has been also measured. This is a pure isospin-one final state, hence its amplitude can be described with only ρ-like recurrences. We found that the main contribution is due to a broad $\rho(1450)$, but there is also a narrower signal, around 1.9 GeV. This structure has properties compatible with the "dip" observed in multi-pionic final states by different experiments: DM2 at Orsay, E687 at Fermilab, and also *BABAR*.
The J/ψ branching fractions to $KK^*(892)$ and, for the first time, $\eta(K^+K^-)_{\text{non-resonant}}$ have been also measured. The results have been accepted for publication by Phys. Rev. D.

6.1 Unexpected threshold behavior in baryon-antibaryon cross sections [67]

Recent *BABAR* data on baryon-antibaryon cross sections show an unexpected threshold behavior. In particular the cross sections for $e^+e^- \to p\overline{p}$, $\Lambda\overline{\Lambda}$, $\Sigma^0\overline{\Sigma^0}$, and $\Lambda\overline{\Sigma^0}$ have monotonically decreasing behaviors starting from the threshold, where they take non vanishing values, up to about 4 GeV. Generally the baryon-antibaryon cross section should be zero at threshold due to the vanishing of the phase space. In the $p\overline{p}$ case the phase space vanishing is cancelled by the Coulomb correction. Moreover, using such a correction we get a unitary normalization for the common proton form factor at the production threshold. The same argument can not be used in the case of neutral baryons. We propose a simple method to extend the application of the Coulomb correction at the parton-level, hence also to the neutral baryons. In such a way, we obtain also for the Λ form factors the unitary normalization at threshold, while the other baryon form factors obey some U-spin symmetry relations.

7 Planned activity in 2008

The data taking will end on April 7, 2008; the physics program for the last 3 months include data taking at the Y(3S) resonance for a total of $30 fb^{-1}$. The collected data sample would increase the available data at this energy by an order of magnitude and provide physics opportunities ranging from spectroscopy and discovery of unobserved bottomonium states and transitions within the Standard Model, to searches for exotic physics including low mass Higgs boson and dark matter candidates.

8 The Super$B$ project

A conceptual design report of a next generation asymmetric-energy e^+e^- collider (Super$B$) capable of delivering 100 times the luminosity of the current B factories has recently been compiled [68]. This report discusses the physics motivation, detector, and accelerator designs for the next generation B factory at an e^+e^- collider.

8.0.1 R&D for the SuperB Drift Chamber

In 2007 the *BaBar* Frascati group has started coordinating the R&D activities towards the design and construction of the tracking detector for the Super$B$.

Since the *BaBar* drift chamber has performed excellently throughout the course of the experiment, we chose it as the baseline design for the Super$B$ tracking detector. However, at a luminosity of at least $10^{36}\,\mathrm{cm}^{-2}s^{-1}$ we expect the occupancy in the drift chamber volume to be considerably higher than in *BaBar*. The gas mixture and the cell shape need therefore to be optimized for faster operation. In contrast with the *BaBar* drift chamber, we envisage an all-Carbon Fiber structure to minimize the material in front of the outer detector components. The engineering of the front-end electronics also needs complete rework.

An accurate but reasonably fast simulation of the detector response to the physics and background-related processes is a necessary ingredient for the optimization studies, along with tests on drift chamber prototypes.

During 2007 we have started the simulation studies and designed a drift tube telescope to be used as an external tracker for a small drift chamber prototype.

9 Talks at conferences in 2007

- F. Anulli, "Time-like Form Factors", presented at the 7^{th} European Research Conference on "EM Int. with Nucleons and Nuclei", Milos Island, Greece, 10-15 September 2007.
- R. Baldini-Ferroli, "BaBar proton GE/GM and related physics", presented at the Exclusive Reactions at High Momentum Transfer, Jefferson Lab, Newport News, VA USA.
- S. Pacetti, Unmasking the Proton Form Factors, Panda experiment Workshop, March 8-9, 2007, Orsay, France.
- S. Pacetti, Nucleon time-like form factors: overview of the experimental data and possible analysis methods, Hard QCD with Antiproton at GSI-FAIR, July 16-20, 2007, Trento, Italy.
- S. Pacetti, "Extraction of Form factors in ISR processes at BaBar", presented at the 11^{th} Intern. Conf. on Meson-Nucleon Physics and the Struc. of the Nucleon, Forschungzentrum Juelich, Germany, 10-14 September 2007.
- S. Pacetti, Baryon form factors from initial state radiation processes and some phenomenological considerations, Nucleon Structure af FAIR, 15-16 October, 2007, Ferrara, Italy.
- M. Rama "Measurement of the angle gamma of the Unitarity Triangle: status and prospects" presented at the Joint Experimental-Theoretical Seminar, Fermilab, 25 May 2007.
- M. Rama, "Misura di gamma alle B-factories, stato e prospettive" presented at the *IV incontro sulla fisica del B*, Bologna, February 2007.
- M. Rama, "New Measurements of CKM Angles at BaBar and Belle", presented at the *XXI Rencontres de Physique de la Vallèe d'Aoste*, La Thuile, Italy, 4-10 March 2007.

10 *BaBar* publications in 2007

References

1. B. Aubert *et al.* "Study of e+e- −¿ Lambda anti-Lambda, Lambda anti-Sigma0, Sigma0 anti-Sigma0 using Initial State Radiation with BABAR," Phys. Rev. D **76** (2007) 092006

2. B. Aubert *et al.* "Improved Limits on the Lepton-Flavor Violating Decays tau- −¿ l-l+l-," Phys. Rev. Lett. **99** (2007) 251803

3. B. Aubert *et al.* "Measurements of the Branching Fractions of $B0-->K^*0K+K-$, $B0-->K^*0pi+K-$, $B0-->K*0K+pi-$, and $B0-->K*0pi+pi-$," Phys. Rev. D **76** (2007) 071104

4. B. Aubert *et al.* "The $e^+e^- \to 2(\pi^+\pi^-)\pi^0$, $2(\pi^+\pi^-)\eta$, $K^+K^-\pi^+\pi^-\pi^0$ and $K^+K^-\pi^+\pi^-\eta$ Cross Sections Measured with Initial-State Radiation," Phys. Rev. D **76** (2007) 092005

5. B. Aubert *et al.* Improved Measurement of Time-Dependent CP Asymmetries and the CP-Odd Fraction in the Decay B0-¿D*+D*-," Phys. Rev. D **76** (2007) 111102

6. B. Aubert *et al.* "Measurement of cos2beta in B0-¿D(*)h0 Decays with a Time-Dependent Dalitz Plot Analysis of D-¿KSpi+pi-," Phys. Rev. Lett. **99** (2007) 231802

7. B. Aubert *et al.* "Search for the decay B+ -¿ K+ tau-/+ mu+/-," Phys. Rev. Lett. **99** (2007) 201801

8. B. Aubert *et al.* "Observation of the Decay B+ −¿ K+K-pi+," Phys. Rev. Lett. **99** (2007) 221801

9. B. Aubert *et al.* "Search for $b-->u$ transitions in $B-->[K+pi-pi0]_DK-$," Phys. Rev. D **76** (2007) 111101

10. B. Aubert *et al.* "Evidence for charged B meson decays to a1(1260)+/- pi0 and a1(1260)0 pi+/-," Phys. Rev. Lett. **99** (2007) 261801

11. B. Aubert *et al.* "Observation of B-meson decays to b_1 pi and b_1 K," Phys. Rev. Lett. **99** (2007) 241803

12. B. Aubert *et al.* "Measurement of the $tau---->K-pi0nu_{tau}$ Branching Fraction," Phys. Rev. D **76** (2007) 051104

13. B. Aubert *et al.* "Study of B0 -¿ pi0 pi0, B -¿ pi pi0, and B -¿ K pi0 Decays, and Isospin Analysis of B -¿ pipi Decays," Phys. Rev. D **76** (2007) 091102

14. B. Aubert *et al.* "Evidence for the B0-¿ppbarK*0 and $B+->eta_cK*+$ decays and Study of the Decay Dynamics of B Meson Decays into ppbarh Final States," Phys. Rev. D **76** (2007) 092004

15. B. Aubert *et al.* "Search for Prompt Production of χ_c and X(3872) in e^+e^- Annihilations," Phys. Rev. D **76** (2007) 071102

16. B. Aubert *et al.* Branching fraction and CP-violation charge asymmetry measurements for B-meson decays to eta K+-, etapi+-, eta'K, eta'pi+-, omega K, and omegapi+-," Phys. Rev. D **76** (2007) 031103

17. B. Aubert *et al.* “Measurements of CP-Violating Asymmetries in the Decay B0–¿ K+K-K0,” Phys. Rev. Lett. **99** (2007) 161802

18. B. Aubert *et al.* “Search for the decay B+ -¿ Kbar*0(892) K+,” Phys. Rev. D **76** (2007) 071103

19. B. Aubert *et al.* “A Study of B0 to rho+rho- Decays and Constraints on the CKM Angle alpha,” Phys. Rev. D **76** (2007) 052007

20. B. Aubert *et al.* “A search for B+ –¿ tau+ nu,” Phys. Rev. D **76** (2007) 052002

21. B. Aubert *et al.* “Measurement of $\boldsymbol{CP}$-Violating Asymmetries in $\boldsymbol{B^0 \to D^{(*)\pm} D^{\mp}}$,” Phys. Rev. Lett. **99** (2007) 071801

22. B. Aubert *et al.* “Search for D0 - anti-D0 mixing using doubly flavor tagged semileptonic decay modes,” Phys. Rev. D **76** (2007) 014018

23. B. Aubert *et al.* “Search for B0 –¿ Phi (K+ pi-) decays with large K+ pi- invariant mass,” Phys. Rev. D **76** (2007) 051103

24. B. Aubert *et al.* “Amplitude Analysis of the decay $\boldsymbol{D^0 - -> K^- K^+ pi^0}$,” Phys. Rev. D **76** (2007) 011102

25. B. Aubert *et al.* “Branching fraction and charge asymmetry measurements in B –¿ J/psi pi pi decays,” Phys. Rev. D **76** (2007) 031101

26. B. Aubert *et al.* “Measurement of decay amplitudes of B $\longrightarrow$ J / psi K*, psi(2S K*, and chi(c1) K* with an angular analysis,” Phys. Rev. D **76** (2007) 031102

27. B. Aubert *et al.* “The $\boldsymbol{e^+e^- \to K^+K^-\pi^+\pi^-}$, $\boldsymbol{K^+K^-\pi^0\pi^0}$ and $\boldsymbol{K^+K^-K^+K^-}$ Cross Sections Measured with Initial-State Radiation,” Phys. Rev. D **76** (2007) 012008

28. B. Aubert *et al.* “Search for neutral B-meson decays to a0 pi, a0 K, eta rho0, and eta f0,” Phys. Rev. D **75** (2007) 111102

29. B. Aubert *et al.* “Measurement of CP violation parameters with a Dalitz plot analysis of B+- –¿ D(pi+ pi- pi0) K+-,” Phys. Rev. Lett. **99** (2007) 251801

30. B. Aubert *et al.* “Production and decay of Omega/c0,” Phys. Rev. Lett. **99** (2007) 062001

31. B. Aubert *et al.* “Measurement of the relative branching fractions of anti-B –¿ D / D* / D** l- anti-nu/l decays in events with a fully reconstructed B meson,” Phys. Rev. D **76** (2007) 051101

32. B. Aubert *et al.* “Improved Measurement of CP Violation in Neutral B Decays to c cbar s,” Phys. Rev. Lett. **99** (2007) 171803

33. B. Aubert *et al.* “Evidence for D0 - anti-D0 mixing,” Phys. Rev. Lett. **98** (2007) 211802

34. B. Aubert *et al.* “Measurement of the time-dependent CP asymmetry in B0 –¿ D(*)0(CP) h0 decays,” Phys. Rev. Lett. **99** (2007) 081801

35. B. Aubert *et al.* “Search for the rare decay B to pi l+ l-,” Phys. Rev. Lett. **99** (2007) 051801

36. B. Aubert *et al.* “Observation of CP violation in B0 –¿ K+ pi- and B0 –¿ pi+ pi-,” Phys. Rev. Lett. **99** (2007) 021603

37. B. Aubert *et al.* “Measurement of CP-violating asymmetries in B0 –¿ (rho pi)0 using a time-dependent Dalitz plot analysis,” Phys. Rev. D **76** (2007) 012004

38. B. Aubert *et al.* “Measurement of CP Asymmetries in B0 –¿ K0S K0S K0S Decays,” Phys. Rev. D **76** (2007) 091101

39. B. Aubert *et al.* “Observation of B+ –¿ rho+ K0 and measurement of its branching fraction and charge asymmetry,” Phys. Rev. D **76** (2007) 011103

40. B. Aubert *et al.* “Measurement of CP asymmetry in B0 –¿ K0(S) pi0 pi0 decays,” Phys. Rev. D **76** (2007) 071101

41. B. Aubert *et al.* “Measurement of the B+- –¿ rho+- pi0 branching fraction and direct CP asymmetry,” Phys. Rev. D **75** (2007) 091103

42. B. Aubert *et al.* “Measurements of CP-violating asymmetries in B0 –¿ a1(1260)+- pi-+ decays,” Phys. Rev. Lett. **98** (2007) 181803

43. B. Aubert *et al.* “Evidence for B0 –¿ rho0 rho0 decay and implications for the CKM angle alpha,” Phys. Rev. Lett. **98** (2007) 111801

44. B. Aubert *et al.* “Measurement of the B0 –¿ pi- l+ nu form-factor shape and branching fraction, and determination of —V(ub)— with a loose neutrino reconstruction technique,” Phys. Rev. Lett. **98** (2007) 091801

45. B. Aubert *et al.* “Branching fraction measurements of B+ –¿ rho+ gamma, B0 –¿ rho0 gamma, and B0 –¿ omega gamma,” Phys. Rev. Lett. **98** (2007) 151802

46. B. Aubert *et al.* “Measurement of B decays to Phi K gamma,” Phys. Rev. D **75** (2007) 051102

47. B. Aubert *et al.* “Evidence for the rare decay B+ –¿ D/s+ pi0,” Phys. Rev. Lett. **98** (2007) 171801

48. B. Aubert *et al.* “Vector - tensor and vector - vector decay amplitude analysis of B0 –¿ Phi K*0,” Phys. Rev. Lett. **98** (2007) 051801

49. B. Aubert *et al.* “Search for lepton flavor violating decays tau+- –¿ l+- pi0, l+- eta, l+- eta’,” Phys. Rev. Lett. **98** (2007) 061803

50. B. Aubert *et al.* “Evidence of a broad structure at an invariant mass of 4.32-GeV/c**2 in the reaction e+ e- –¿ pi+ pi- psi(2S) measured at BaBar,” Phys. Rev. Lett. **98** (2007) 212001

51. B. Aubert *et al.* “Branching fraction measurement of anti-B0 –¿ D(*)+ pi-, B- –¿ D(*)0 pi- and isospin analysis of anti-B –¿ D(*) pi decays,” Phys. Rev. D **75** (2007) 031101

52. B. Aubert *et al.* “Observation of CP violation in B0 –¿ eta’ K0 decays,” Phys. Rev. Lett. **98** (2007) 031801

53. B. Aubert *et al.* “Inclusive Lambda/c production in e+ e- annihilations at s**(1/2) = 10.54-GeV and in Upsilon(4S) decays,” Phys. Rev. D **75** (2007) 012003

54. B. Aubert *et al.* “Measurement of the CP asymmetry and branching fraction of B0 –¿ rho0 K0,” Phys. Rev. Lett. **98** (2007) 051803

55. B. Aubert *et al.* “Improved Measurements of the Branching Fractions for B0 –¿ pi+pi- and B0 –¿ K+pi-, and a Search fro B0 –¿ K+K-,” Phys. Rev. D **75** (2007) 012008

56. B. Aubert *et al.* “Observation of B –¿ eta’ K* and evidence for B+ –¿ eta’ rho+,” Phys. Rev. Lett. **98** (2007) 051802

57. B. Aubert *et al.* "Measurement of the pseudoscalar decay constant f(D/s) using charm-tagged events in e+ e- collisions at s**(1/2) = 10.58-GeV," Phys. Rev. Lett. **98** (2007) 141801

58. B. Aubert *et al.* "Study of the exclusive initial-state radiation production of the D anti-D system," Phys. Rev. D **76** (2007) 111105

59. B. Aubert *et al.* "Measurement of the q**2 dependence of the hadronic form factor in D0 –¿ K- e+ nu/e decays," Phys. Rev. D **76** (2007) 052005

60. B. Aubert *et al.* "Search for the reactions e+ e- –¿ mu+ tau- and e+ e- –¿ e+ tau-," Phys. Rev. D **75** (2007) 031103

61. B. Aubert *et al.* "Study of inclusive B- and anti-B0 decays to flavor-tagged D, D/s and Lambda/c+," Phys. Rev. D **75** (2007) 072002

62. B. Aubert *et al.* "Observation of decays B0 –¿ D/s(*)+ pi- and B0 –¿ D/s(*)- K+," Phys. Rev. Lett. **98** (2007) 081801

63. B. Aubert *et al.* "Observation of a charmed baryon decaying to D0 p at a mass near 2.94-GeV/c**2," Phys. Rev. Lett. **98** (2007) 012001

64. B. Aubert *et al.* "Measurements of Lambda/c+ branching fractions of Cabibbo-suppressed decay modes involving Lambda and Sigma0," Phys. Rev. D **75** (2007) 052002

65. B. Aubert *et al.* "Measurement of branching fractions and mass spectra of B –¿ K pi pi gamma," Phys. Rev. Lett. **98** (2007) 211804

66. B. Aubert *et al.* [BaBar Collaboration], arXiv:0710.4451 [hep-ex] accepted by Phys. Rev. D.

67. R. Baldini, S. Pacetti and A. Zallo, arXiv:0711.1725 [hep-ph].

68. Conceptual Design Report of Super$\boldsymbol{B}$: A High-Luminosity Asymmetric $\boldsymbol{e^+e^-}$ Super Flavour Factory; arXiv:0709.0451v2 [hep-ex].

CDF

A. Annovi (Art. 36), M. Cordelli (Resp.), P. Giromini,
F. Happacher (Art. 23), S. Torre (Ass.)

1 Introduction

The Tevatron, with a $p\bar{p}$ collision energy of 1.96 TeV in the center of mass system, is running with a record instantaneous luminosity, L, delivered to the experiments of 315×10^{30} $cm^{-2}s^{-1}$ ($vs.$ $\sim 10^{31}$ of Run I). At the end of year 2007, the Tevatron has delivered to the experiments ~ 2500 pb^{-1}; CDF experiment has collected on tape ~ 3500 pb^{-1} (see Figure 1); during the whole Run I we collected ~ 109 pb^{-1}. The instantaneous luminosity is still increasing during the first months of data taking of the year 2008 and we plan to integrate 6-8 pb^{-1} by the end of 2009.

The CDF group of Frascati has built the central hadronic calorimeter (the iron-scintillator based calorimeter in the central and end-wall region, CHA and WHA) and is responsible for the hardware maintenance and for the energy scale calibration.

Since year 2005 we are also responsible of the Silicon Vertex Trigger operations.

The analysis interest of the Frascati group focuses on the measurements of b quark production cross sections. Indeed, the bottom quark production at the Fermilab Tevatron has been called one of the few instances in which experimental results appear to challenge the ability of perturbative QCD to accurately predict absolute rates in hadronic collisions. We are repeating the most significant b quark cross section measurements from Run I in order to clarify the current situation.

2 Calibration of the central hadron calorimeter

The Frascati group plays a leading role in the calibration of the central hadron calorimeters, CHA/WHA.

For the WHA calorimeter the original Run I ^{137}Cs Sources system is fully working and therefore it can be used to set the absolute energy scale for all the towers; we have taken two ^{137}Cs Source runs during 2007 and we have accordingly computed a set of Linear Energy Response:

$$LER = \frac{^{137}Cs(test - beam)e^{-\Delta t/\tau}}{^{137}Cs(today)}$$

that have been downloaded in the front end electronics to correct the raw ADMEM counts. This system effectively probes the behavior of the calorimeter since the source runs in front of the inner scintillator plane of the wedges thus irradiating few of the scintillator/absorber layers of the calorimeter. In this way we monitor aging phenomena of the scintillator together with PM gain variations.

We calibrate the CHA calorimeter looking at the energy deposition of Minimum Ionizing Particles (i.e. muons from J/Ψ decays).

We briefly recall the procedure to set the absolute calorimeter energy scale using Mip's. Looking at μ's from the ~ 81 pb^{-1} dimuon trigger sample collected in Run Ib, we determined the necessary statistics to determine the peaks of μ's hadronic energy, HadE, distributions with enough precision per every CHA tower. With a statistics of ~ 40 pb^{-1} we find that the tower by tower peak is determined with a precision of $\sim 1.5\%$. The LER's correction factors are derived

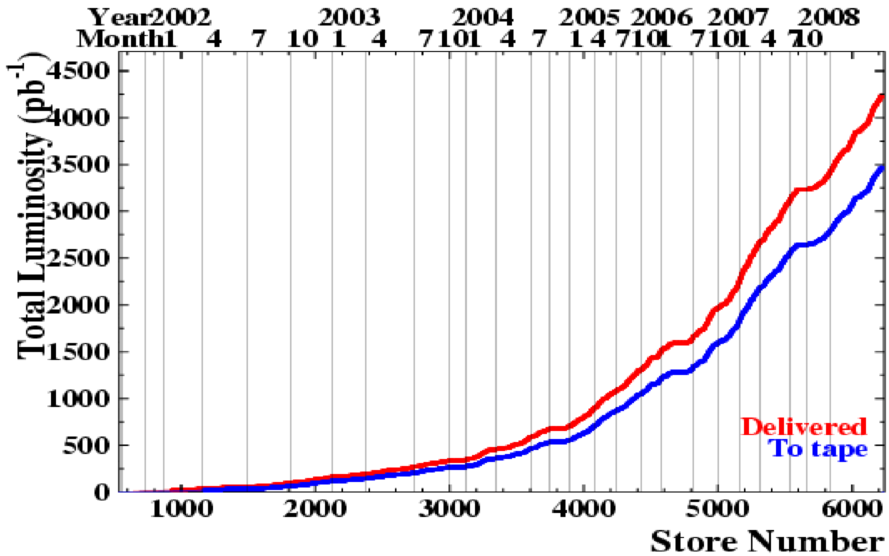

Figure 1: *Integrated Luminosity vs time*

comparing tower by tower the HadE deposition for Run I and Run II mips every 30-40 pb^{-1} of data; the LER at a given time time t are defined as the previous set of LER (t-1) multiplied by the observed ratio of the Mip's at a time t and in Run I:

$$LER(t) = LER^{t-1} \times \frac{MIP(RunI)}{MIP(t)}$$

We look at Mip's peaks response every $\sim$ 100 pb^{-1} and the typical response shows a tiny 1.5% gain variations on average and few channels that drift more than 5%.

The laser system represents a quick tool to follow the trend of the PM's gains. We have continuously acquired laser runs since year 2003 to monitor the gain variations of each photomultiplier; the CHA is stable within $\sim$ 2%.

2.1 ONLINE-OFFLINE energy scale calibration

At CDF with the current luminosity the data are being processed through the OFFLINE reconstruction every couple of months. Before producing the fully reconstructed events from the raw information of the detector we first produce small dedicated calibration samples to derive the calibrations constants for all the sub detectors. Every 6-8 weeks we run an executable called CalibExe which produces all the data ntuples for different data sets, including the dimuon trigger data sample where we reconstruct J/Ψ events; then the various calibrators use these samples to derive the calibrations. We made all this procedure automatic during the year 2006.

Usually for the Hadron calorimeters we produce two set of calibrations: ONLINE calibrations are directly downloaded in the ADMEM electronics and are intended to correct the energy response for data that have to be acquired afterward; the OFFLINE calibrations attempts to propagate back to the data already acquired the needed corrections. The calibration constants are then filled in appropriate ORACLE data base tables called CHALINERESPONSE and CHAOFFLER. To validate the OFFLINE calibrations, the same data sets are reconstructed again picking the right calibration tables for every run range they have been produced for and the calibrators have to repeat their analysis to check that the calibrations are correct.

With this procedure the calorimeter response is kept constant at $\sim 2\%$ level over the running period.

3 SVT

During 2007 we have been responsible of the Silicon Vertex Trigger operations.

The Silicon Vertex Trigger (SVT) is part of the L2 trigger of CDF II. The SVT reconstructs tracks by associating Silicon hits to Central Tracker (COT) tracks reconstructed by the L1 trigger. By using the hits in the silicon, SVT is able to measure the impact parameter of the tracks so that this information can be used by the L2 to select data enriched of heavy flavor decays. Data collected using the SVT processor made possible the first measurement of the B_s mixing.

In order to optimize the maintenance we continue to improved the online and offline monitoring allowing for a better understanding of the problems and a quicker reaction when they appear during data taking.

4 Studies of b quark cross section

4.1 Status of the Tevatron measurements

The bottom quark production at the Fermilab Tevatron has been called one of the few instances in which experimental results appear to challenge the ability of perturbative QCD to accurately predict absolute rates in hadronic collisions. In general, the data are underestimated by the exact next-to-leading-order (NLO) QCD prediction. The most recent measurement from the Tevatron is however in very good agreement with an improved QCD calculation (FONLL), and has prompted a number of studies suggesting that the apparent discrepancy has been resolved with incremental improvements of the measurements and predictions. The increase of the cross-section predicted by FONLL with respect to original NLO calculatiuons, which results into a better agreement with data, is mostly coming from new structure functions and fragmentation functions that have been computed at next-to-leading-order, in order to match the perturbative order of the FONLL calculation. The measured single b-quark cross-section is also in agreement with the prediction of LL shower MC, with an *ad hoc* tuning.

Because of the experimental difficulty inherent to each result, we reviewed all measurements of the single b cross section performed at the Tevatron, and then compared their average to the standard and to the improved QCD predictions. We have also compared the cross sections for producing both b and $\bar{b}$ quarks - centrally and above a given transverse momentum cut - to theoretical predictions. The single b-quark cross section is inferred from the measurement of the production rate as a function of the transverse momentum, p_T, of: B hadrons; or some of their decay products (leptons or ψ mesons); or jets produced by the hadronization of b quarks. Most of the Tevatron measurements correspond to b quarks produced centrally (rapidity $|y^b| \leq 1$) and with $p_T \geq 6$ GeV/c (up to $p_T \simeq 100$ GeV/c). We have performed a consistency check of all available data. For that purpose, we use the value of the single b-quark cross section extracted from the data and integrated from the p_T threshold of each experiment. We determined the ratio R of

channel	R for $p_T^{\min}$ (GeV/c) =					
	6	$8-10$	$12-15$	$19-21$	$\simeq 29$	$\simeq 40$
$J/\psi K^+$		$4.0 \pm 15\%$	(3.4)			
$J/\psi K^+$		$2.9 \pm 23\%$	(1.9)			
$\mu\, X$				$2.5 \pm 26\%$	(1.9)	
$e\, X$			$2.4 \pm 27\%$			
eD^0				$2.1 \pm 34\%$		
$J/\psi\, X$		$4.0 \pm 10\%$	(3.4)			
$J/\psi\, X$		$3.1 \pm 9\%$	(2.7)			
$\mu\, X$	$2.1 \pm 27\%$		(1.7)			
$\mu\, X$	$2.5 \pm 25\%$		(3.5)			
b jets (μ)				$2.4 \pm 20\%$		(2.0)

Table 1: Ratio R of measured single b cross sections to a prediction based on the exact NLO calculation .

each measurement to the same theoretical prediction. We have then evaluated the average R and its dispersion. As benchmark prediction of the b-quark parton-level cross section we choose the exact NLO calculation implemented with old but consistent sets of parton distribution functions (PDF), since it has been used in most published works, convoluted with the Peterson fragmentation function; B-hadron decay are modeled with the QQ Monte Carlo generator program.

There are 10 measurements of the single b cross section performed by the CDF and DØ collaborations at the Tevatron. The ratios of these measurements to the standard theory are summarized in Table 1.

Using the measurements listed in Table 1, we derive an average ratio of the data to the standard theory that is $< R >= 2.8$; the RMS deviation of the 10 measurements in Table 1 is 0.7 It has to be noticed that all the measurement involving the J/Ψ reconstruction, experimentally the cleanest, are consistently much higher than the ones based on the detection of a semileptonic decay.

The new measurement of the $B^+ \to J/\Psi(\to \mu^+\mu^-)K^+$ differential cross section (see next paragraph) carried on by the Frascati group finds a ratio R with the theory of 2.80 ± 0.24, somehow closer to the average of all measurements.

Leading-order (LO) and higher-than-LO terms are sources of b and $\bar{b}$ quarks with quite different topological structure. The production of events with both a b and $\bar{b}$ quark with $p_T \geq$ 6 GeV/c and $|y| \leq 1$ is dominated by LO diagrams and the parton-level cross sections predicted by the exact NLO calculation is comparable to that predicted by LL Monte Carlo generators.

R_{2b}, the ratio of $\sigma_{b\bar{b}}$ measured at the Tevatron to the exact NLO prediction, $\simeq 1$ would imply that the parton-level cross section predicted by LL generators (NLO) is correct and that the contribution of higher-than-LO terms has to be a factor of two larger than in the present NLO or FONLL prediction. If the ratio R_{2b} is much larger than one, then the agreement between the observed single b cross section and the prediction of LL Monte Carlo generators is fortuitous and agreement with the data may be found by using harder fragmentation functions as in the FONLL calculation.

We review five measurements, listed in Table 2, and derive a value of $< R_{2b} >= 1.8$ with a 0.8

channel	R_{2b} for $p_T^{\rm min}$ (GeV/c) =			
	$6-7$	10	15	$\simeq 20$
$b+\bar{b}$ jets			$1.2 \pm 25\%$	
$b+\bar{b}$ jets				$1.0 \pm 32\%$
$\mu + b$ jet		$1.5 \pm 10\%$		
$\mu^+ + \mu^-$	$3.0 \pm 20\%$			
$\mu^+ + \mu^-$	$2.3 \pm 33\%$			

Table 2: Ratio R_{2b} of $\sigma_{b\bar{b}}$, the observed cross section for producing both b and $\bar{b}$ quarks, centrally and above a given $p_T^{\rm min}$ threshold, to the exact NLO prediction.

RMS deviation. Such a large RMS deviation indicates that the experimental results are inconsistent among themselves. Additional measurements are certainly needed to clarify the experimental situation.

4.2 $B^+ \to J/\Psi(\to \mu^+\mu^-)K^+$

We have repeated the Run I analysis that measures the B^+ differential cross section as a function of p_T, reconstructing the decay $B^+ \to J/\Psi(\to \mu^+\mu^-)K^+$. We search for $B^\pm \to J/\psi K^\pm$ candidates in the data set selected by the $J/\psi \to \mu^+\mu^-$ trigger. We search for J/ψ candidates by using pairs of muons, reconstructed in the CMU detector, with opposite charge, and $p_T \geq 2$ GeV/c. The invariant mass of a muon pair is evaluated by constraining the two muon tracks to originate from a common point in three-dimensional space (vertex constrain) in order to improve the mass resolution. All muon pairs with invariant mass in the range $3.05-3.15$ GeV/c^2 are considered J/ψ candidates. If a J/ψ candidate is found, we search for $B^\pm$ mesons by considering all charged particle tracks in the event as possible kaon candidates. The invariant mass of the μ^+ μ^- $K^\pm$ system is evaluated constraining the corresponding tracks to have a common origin while the μ^+ μ^- invariant mass is constrained to the value of 3096.9 GeV/c^2. In fig. 2 we show the comparison of the recent RUN II CDF b cross section result with the FONLL theoretical predictions.

To measure the B^+ differential cross section as a function of p_T, we divide the sample of $B^\pm$ candidates into five p_T bins: $6-9$, $9-12$, $12-15$, $15-25$, and ≥ 25 GeV/c. In each p_T bin, we fit the invariant mass distribution of the B^+ candidates with a binned maximum likelihood method to determine the number of B^+ mesons. We use a first order polynomial function to model the combinatorial background and gaussian function to model the B^+ signal. All fits return a B^+ mass of 5279.0 ± 0.5 MeV in agreement with the PDG value.

The detector acceptance is calculated with a Monte Carlo simulation based on the NLO calculation. The $B^\pm$ decay is modeled with the EVTGEN Monte Carlo program. The detector response to the generated $B^\pm$ decay prongs is modeled with the CDF II detector simulation that in turn is based on the GEANT Monte Carlo program.

The differential cross section $d\sigma/dp_T$ is calculated as

$$\frac{d\sigma(B^+)}{dp_T} = \frac{N/2}{\Delta p_T \times \mathcal{L} \times \mathcal{A}_{\rm corr} \times BR} \tag{1}$$

where N is the number of $B^\pm$ mesons determined from the likelihood fit to the invariant mass distribution of the J/ψ $K^\pm$ candidates in each p_T bin. The factor 1/2 accounts for the fact that both B^+ and B^- mesons are used and assumes C invariance at production. Δp_T is the

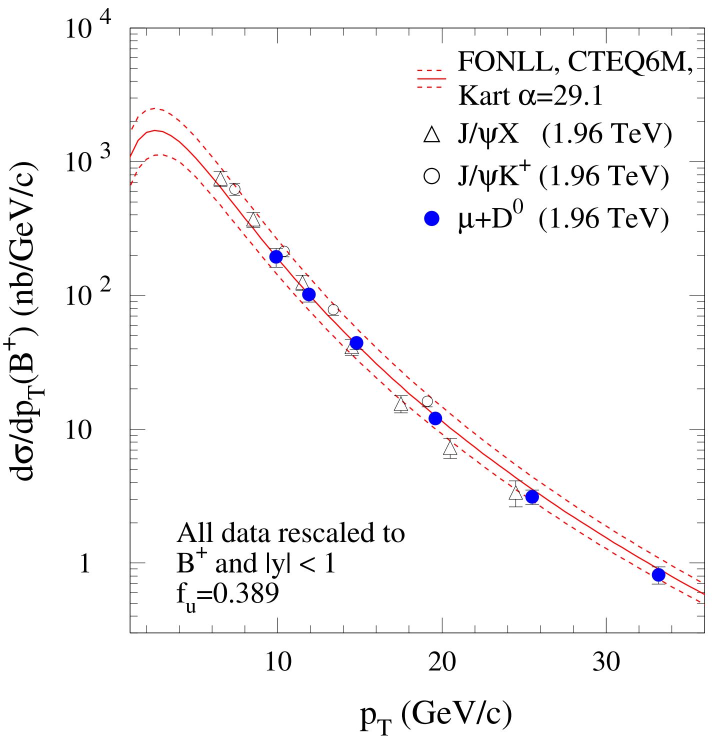

Figure 2: *Comparison of the CDF b cross section results with the FONLL theory as a function of the B hadron* p_T.

bin width and $\mathcal{A}_{\rm corr}$ is the geometric and kinematic acceptance that includes trigger and tracking efficiencies measured with the data. The integrated luminosity of the data set is $\mathcal{L} = 739 \pm 44$ pb$^-1$. The branching ratio $BR = (5.98 \pm 0.22) \times 10^{-5}$ is derived from the branching fractions $BR(B^\pm \to J/\psi\ K^\pm) = (1.008 \pm 0.035) \times 10^{-3}$ and $BR(J/\psi \to \mu^+\ \mu^-) = (5.93 \pm 0.06) \times 10^{-2}$.

The B^+ total cross section is $\sigma_{B^+}(p_T \geq 6.0\ \text{GeV/c}, |y| < 1) = 2.78 \pm 0.24\ \mu$b, where the 8.6% error is the sum in quadrature of the 6% error on the integrated luminosity, the 3.7% uncertainty of the $B^+ \to J/\psi\ K^+$ and $J/\psi \to \mu^+\ \mu^-$ branching fractions, the 2.5% uncertainty of the acceptance calculation, and the 4.4% statistical error.

This analysis has been published on Phys.Rev.D75:012010,2007.

4.3 $b\bar{b}$ correlation

Another analysis in progress is the study of the so called $b\bar{b}$ correlation. This study is a new measurement of $\sigma_{b\bar{b}}$ that uses dimuons arising from from $b\bar{b}$ production. At the Tevatron, dimuon events result from decays of heavy quark pairs ($b\bar{b}$ and $c\bar{c}$), the Drell-Yan process, charmonium and bottomonium decays, and decays of π and K mesons. Background to dilepton events also comes from the misidentification of π or K mesons. We make use of the precision tracking provided by the CDF silicon microvertex detector to evaluate the fractions of leptons due to long-lived b- and c-hadron decays, and to the other background contributions.

The method used to determine the $b\bar{b}$ and $c\bar{c}$ content of the data is to fit the observed impact parameter distribution of the muon pairs with the expected impact parameter distributions of leptons from various sources. After data selection, the main sources of reconstructed muons are semileptonic decays of bottom and charmed hadrons, and prompt decays of onia and Drell-Yan

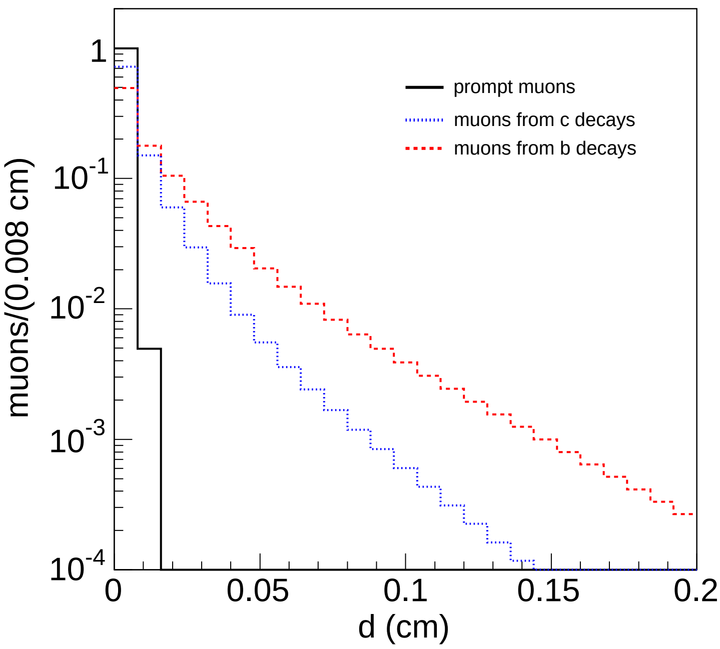

Figure 3: *Impact parameter distributions of muons coming from b- and c-hadron decays (simulation) and of prompt muons (data). Distributions are normalized to unit area.*

production.

Herwig Monte Carlo simulations are used to model the impact parameter distributions for leptons from b- and c-hadron decays. The impact parameter distribution of leptons from prompt sources such as quarkonia decays and Drell-Yan production is derived using muons from $\Upsilon(1S)$ decays. In Fig. 3 we show the one-dimensional impact parameter distribution for muon pairs from different sources. Fig. 4 shows the breakdown of the result of the fit to the data with the various sources of dimuon events.

For muons with $p_T \geq 3$ GeV/c and $|\eta| \leq 0.7$, that are produced by b and $\bar{b}$ quarks with $p_T \geq 2$ GeV/c and $|y| \leq 1.3$, we measure $\sigma_{b\to\mu,\bar{b}\to\mu} = 1549 \pm 133$ pb. The NLO prediction is $\sigma_{b\to\mu,\bar{b}\to\mu} = 1293 \pm 201$ pb. The ratio of the data to the NLO prediction is 1.20 ± 0.21.

This analysis is submitted for publication to Phys. Rev. D.

4.4 Search for dimuon resonances

This work repeats the study performed by the Frascati group in RUN I, published in G. Apollinari *et al.*, Phys. Rev. D **72**, 092003 (2005), that found an excess of events in the 7.2 GeV/c^2 region of the dimuon invariant mass distribution as shown in Fig. 5. We take advantage of a higher statistics data sample that corresponds to an integrated luminosity of 630 pb^{-1} collected with the CDF II detector after may 2006. At that time, the CDF II trigger system has been upgraded and is capable of acquiring events containing muon pairs with invariant mass larger than 6 GeV/c^2 with a kinematical acceptance comparable to that of the Run I trigger system. As in G. Apollinari *et al.*, Phys. Rev. D **72**, we limit our search for narrow resonances to the mass region above 6.3 GeV/c^2 at which the kinematical acceptance becomes independent of the $\mathcal{E}$-candidate transverse momentum.

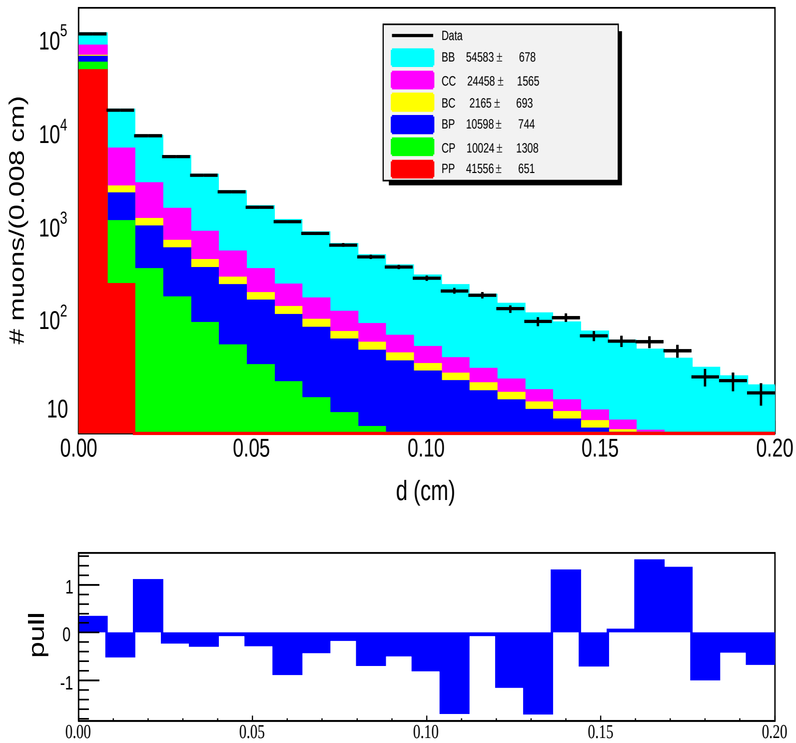

Figure 4: *For each contribution the impact parameter distribution of muon pairs is compared to the fit result (histogram).*

We use a fifth order polynomial to model the continuum in the invariant mass region $6-12$ GeV/c^2 and Gaussian functions to model the Υ contributions. The best fit returns 50286 ± 257 $\Upsilon(1S)$ mesons over a background of 13976 events in the region $9.3 \leq M_{\mu^+\mu^-} \leq 9.55$ GeV/c^2. To search for the existence of narrrow $\mathcal{E}$ states we add a Gaussian term to the likelihood function and fit the data in the $6-9.1$ GeV/c^2 mass interval. Fig. 6 shows the results of this fit where no excess is found.

This analysis is being reviewed by the collaboration.

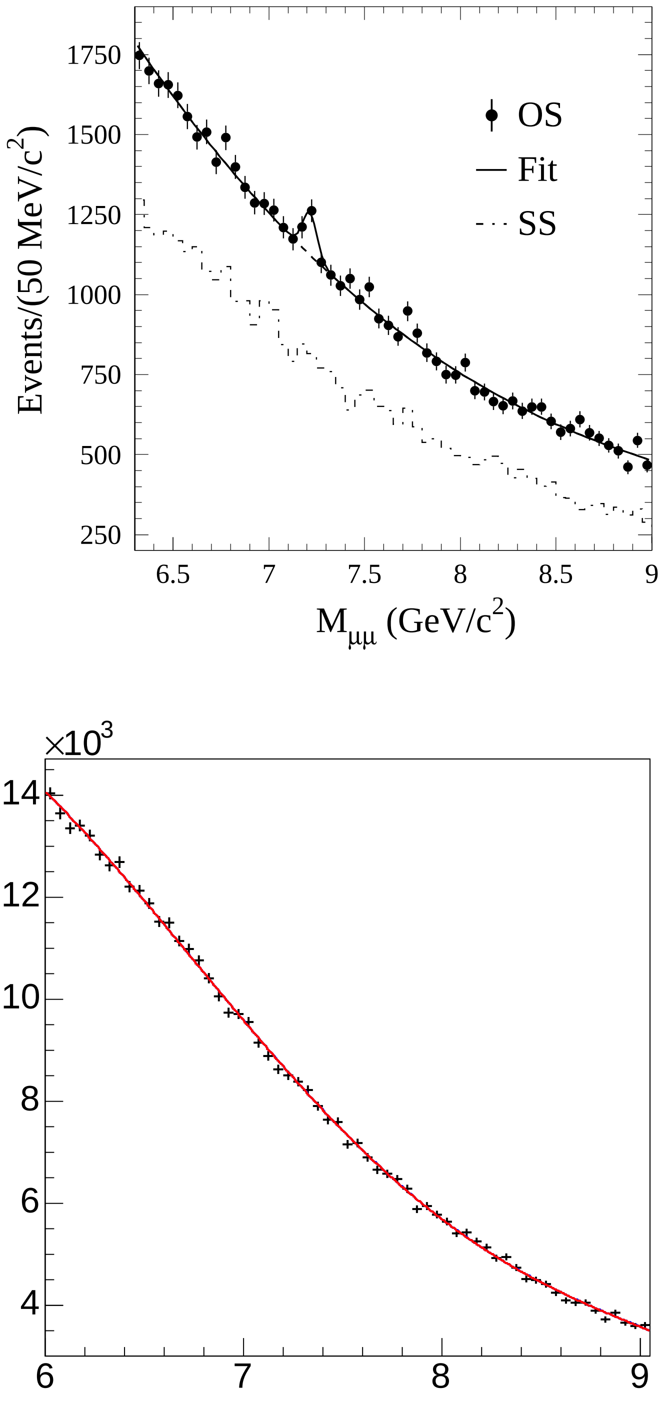

Figure 6: *Run II result of the dimuon resonance search.*

Conferences 2007

- A. Annovi, **"Measurement of Heavy Quark cross-sections at CDF"** *Presented at International Europhysics Conference on High Energy Physics (EPS-HEP2007), Manchester, England, 19-25 Jul 2007*

Publications 2007

1. T. Aaltonen *et al.* [CDF Collaboration], arXiv:0712.3273 [hep-ex].
2. J. Adelman *et al.* [CDF Collaboration], Nucl. Instrum. Meth. A **572**, 361 (2007).
3. T. Aaltonen *et al.* [CDF Collaboration], arXiv:0712.2534 [hep-ex].
4. T. Aaltonen *et al.* [CDF Collaboration], Phys. Rev. Lett. **100**, 161802 (2008) [arXiv:0712.2397 [hep-ex]].
5. T. Aaltonen *et al.* [CDF collaboration], Phys. Rev. Lett. **100**, 121803 (2008) [arXiv:0712.2348 [hep-ex]].
6. T. Aaltonen *et al.* [CDF Collaboration], Phys. Rev. Lett. **100**, 121802 (2008) [arXiv:0712.1567 [hep-ex]].
7. T. Aaltonen *et al.* [CDF Collaboration], Phys. Rev. Lett. **100**, 101802 (2008) [arXiv:0712.1708 [hep-ex]].
8. T. Aaltonen *et al.* [CDF Collaboration], Phys. Rev. Lett. **100**, 182002 (2008) [arXiv:0712.1506 [hep-ex]].
9. T. Aaltonen *et al.* [CDF Collaboration], arXiv:0712.1311 [hep-ex].
10. T. Aaltonen *et al.* [CDF Run II Collaboration], Phys. Rev. D **77**, 052004 (2008) [arXiv:0712.0604 [hep-ex]].
11. T. Aaltonen *et al.* [CDF Collaboration], Phys. Rev. D **77**, 011108 (2008) [arXiv:0711.4044 [hep-ex]].
12. T. Aaltonen *et al.* [CDF - Run II Collaboration], Phys. Rev. Lett. **100**, 102001 (2008) [arXiv:0711.3717 [hep-ex]].
13. T. Aaltonen *et al.* [CDF Collaboration], Phys. Rev. D **77**, 052002 (2008) [arXiv:0711.3161 [hep-ex]].
14. T. Aaltonen *et al.* [CDF Collaboration], Phys. Rev. Lett. **100**, 091803 (2008) [arXiv:0711.2901 [hep-ex]].
15. A. Annovi [CDF Collaboration], Nucl. Phys. Proc. Suppl. **170**, 283 (2007).
16. T. Aaltonen *et al.* [CDF Collaboration], Phys. Rev. D **77**, 051102 (2008) [arXiv:0710.5335 [hep-ex]].
17. T. Aaltonen *et al.* [CDF Collaboration], Phys. Rev. Lett. **100**, 041801 (2008) [arXiv:0710.4363 [hep-ex]].

18. T. Aaltonen *et al.* [CDF Collaboration], Phys. Rev. Lett. **100**, 082001 (2008) [arXiv:0710.4199 [hep-ex]].

19. T. Aaltonen *et al.* [CDF Collaboration], Phys. Rev. Lett. **100**, 071801 (2008) [arXiv:0710.4112 [hep-ex]].

20. T. Aaltonen *et al.* [CDF Collaboration], Phys. Rev. Lett. **100**, 062005 (2008) [arXiv:0710.4037 [hep-ex]].

21. T. Aaltonen *et al.* [CDF Run II Collaboration], arXiv:0710.1895 [hep-ex].

22. A. Annovi [CDF Collaboration], arXiv:0709.4572 [hep-ex].

23. T. Aaltonen *et al.* [CDF Collaboration], arXiv:0709.0705 [hep-ex].

24. T. Aaltonen *et al.* [CDF Collaboration], arXiv:0708.3642 [hep-ex].

25. T. Aaltonen *et al.* [CDF Collaboration], Phys. Rev. D **76**, 072010 (2007) [arXiv:0707.2567 [hep-ex]].

26. T. Aaltonen *et al.* [CDF Collaboration], Phys. Rev. Lett. **99**, 171802 (2007) [arXiv:0707.2524 [hep-ex]].

27. T. Aaltonen *et al.* [CDF Collaboration], Phys. Rev. Lett. **99**, 242002 (2007) [arXiv:0707.2374 [hep-ex]].

28. T. Aaltonen *et al.* [CDF Collaboration], Phys. Rev. Lett. **99**, 191806 (2007) [arXiv:0707.2362 [hep-ex]].

29. T. Aaltonen *et al.* [CDF Collaboration], Phys. Rev. Lett. **99**, 171801 (2007) [arXiv:0707.2294 [hep-ex]].

30. T. Aaltonen *et al.* [CDF Collaboration], Phys. Rev. Lett. **99**, 052002 (2007) [arXiv:0707.0589 [hep-ex]].

31. T. Aaltonen *et al.* [CDF Collaboration], Phys. Rev. Lett. **99**, 151801 (2007) [arXiv:0707.0085 [hep-ex]].

32. A. Cerri *et al.*,

33. T. Aaltonen *et al.* [CDF Collaboration], Phys. Rev. Lett. **99**, 202001 (2007) [arXiv:0706.3868 [hep-ex]].

34. T. Aaltonen *et al.* [CDF Collaboration], Phys. Rev. D **76**, 072009 (2007) [arXiv:0706.3790 [hep-ex]].

35. T. Aaltonen *et al.* [CDF Collaboration], Phys. Rev. D **76**, 072006 (2007) [arXiv:0706.3264 [hep-ex]].

36. T. Aaltonen *et al.* [CDF Collaboration], arXiv:0706.2832 [hep-ex].

37. T. Aaltonen *et al.* [CDF Collaboration], Phys. Rev. D **76**, 111103 (2007) [arXiv:0705.2247 [hep-ex]].

38. T. Aaltonen *et al.* [CDF Collaboration], Phys. Rev. D **75**, 111103 (2007) [arXiv:0705.1594 [hep-ex]].

39. A. Abulencia *et al.* [CDF Collaboration], Phys. Rev. Lett. **99**, 121801 (2007) [arXiv:0704.0760 [hep-ex]].

40. A. Abulencia *et al.* [CDF Collaboration], Phys. Rev. Lett. **99**, 132001 (2007) [arXiv:0704.0638 [hep-ex]].

41. A. Abulencia *et al.* [CDF Collaboration], Phys. Rev. Lett. **99**, 182002 (2007) [arXiv:hep-ex/0703045].

42. A. Abulencia *et al.* [CDF Run II Collaboration], Phys. Rev. Lett. **98**, 232001 (2007) [arXiv:hep-ex/0703028].

43. A. Abulencia *et al.* [CDF Collaboration], Phys. Rev. Lett. **98**, 221803 (2007) [arXiv:hep-ex/0702051].

44. A. Abulencia *et al.* [CDF Collaboration], Phys. Rev. Lett. **98**, 251801 (2007) [arXiv:hep-ex/0702037].

45. A. Abulencia *et al.* [CDF Run II Collaboration], Phys. Rev. D **75**, 112001 (2007) [arXiv:hep-ex/0702029].

46. A. Abulencia *et al.* [CDF Collaboration], Phys. Rev. Lett. **98**, 161801 (2007) [arXiv:hep-ex/0702027].

47. A. Abulencia *et al.* [CDF - Run II Collaboration], Phys. Rev. D **75**, 092006 (2007) [Erratum-ibid. D **75**, 119901 (2007)] [arXiv:hep-ex/0701051].

48. A. Abulencia *et al.* [CDF Collaboration], Phys. Rev. Lett. **98**, 131804 (2007) [arXiv:0706.4448 [hep-ex]].

CMS

L. Benussi, M. Bertani, S. Bianco (Resp.), M.A. Caponero (Ass.)
S. Colafranceschi (Laur.), D. Donisi (Dott.), F.L. Fabbri (Ass.)
F. Felli (Ass.), M. Giardoni, T. Greci (Laur.), B. Ortenzi (Tecn.), M. Pallotta(Ass.), A. Paolozzi (Ass.)
L. Passamonti (Tecn.), C. Pucci (Dott.), G. Saviano (Ass.)

In collaboration with:
D. Pierluigi, B. Ponzio, A. Russo

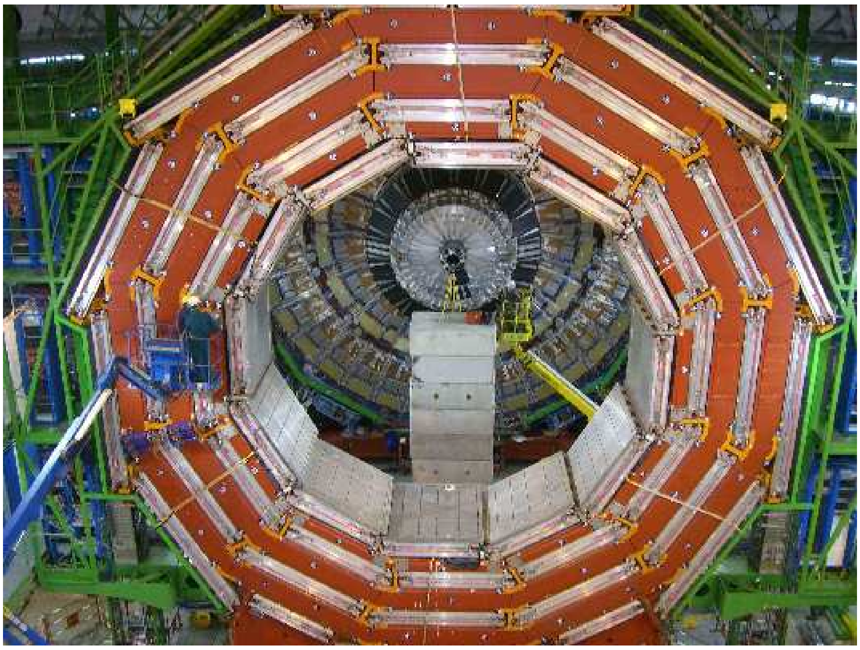

1 The CMS Experiment and the RPC Muon Detector

The Compact Muon Solenoid (CMS) experiment [1] will search for the missing block of Nature - the Higgs boson - and for new exotic elementary particles that are predicted by theory and by cosmological observations. During 2007 CMS has been powered and commissioned with cosmic rays. Completely assembled and debugged each five wheels and endcap pplates were lowered to the experimental cavern.

The CMS detector uses Resistive Plate Chambers (RPC) as muon detectors, coupled to Drift Tubes in the barrel region, and to Cathode Strip Chambers in the endcaps. Resistive Plate Chambers (RPC) detectors are widely used in HEP experiments for muon detection and triggering at high-energy, high-luminosity hadron colliders, in astroparticle physics experiments for the detection of extended air showers, as well as in medical and imaging applications. While gain and efficiency stability are always a must, in the case of RPC detectors in high-rate experiments which use freon-based gas mixtures, utmost care has to be paid also for the possible presence of gas contaminants. RPC counters [2] are fast, efficient and economical charged particles detectors, well-suited for operation in high magnetic field. The elementary component is a gap, a gas volume enclosed between two resistive plates. Resistive plates are made of bakelite, coated with linseed oil for surface uniformity. Gas mix used is 96.2% $C_2H_2F_4$ / 3.5% Iso-C_4H_{10} / 0.3% SF_6, with a 45% relative humidity. Signal pulses are picked up by readout strips. In CMS, RPC counters are operated in avalanche mode to sustain high-rate operation, with the streamer suppressed by the addition of SF_6 gas in the mixture.

2 Activity of the CMS Frascati group in 2007

The Frascati group has joined CMS in the RPC muon detectors at the end of year 2005. Frascati is responsible for the Gas Gain Monitoring system, RPC materials studies, and the test of the Closed Loop recirculation system at ISR for characterization of gas purifiers.

2.1 The CMS Closed Loop Gas System

Because of high costs and huge volumes of the freon-based gas mix used, CMS will use a recirculation (Closed Loop) gas system developed by the CERN gas group. The Closed Loop is a critical component of RPC. CMS has accumulated experience on its use and performances during the test at the Gamma Irradiation Facility at CERN in 2001 [3], and currently at the ISR where chambers are tested in CL prior to installation. At the GIF facility we observed substancial production of HF, linearly correlated with the signal current.

In the Closed Loop (CL) system, purifiers are the crucial component. Purifiers were determined after tests at the GIF in order to minimize the unknown contaminants which showed as spurious peaks besides the known gas mix components. Three filters were selected: 5A molecular sieve, Cu/Cu-Zn, Ni/Al_2O_3. A small scale CL system is currently in use at the ISR test station, where RPC chambers are tested at CERN prior to installation in the CMS detector.

A measurement campaign [4] on purifiers is in progress, using chemical, SEM/EDS (Scanning Electron Microscopy/Energy Dispersive Spectroscopy), XRD (x-ray Diffrattometry) analyses. Preliminary results show evidence of metal elements released by purifiers, and heavy HF production.

2.2 Gas Gain Monitoring System

The gas gain monitoring system will monitor the RPC working point faster and more precisely than what one could get by using the CMS RPC system, and provide a warning in case of shifts caused by the gas mixture changes. The system is designed to monitor efficiency and charge continuously in one-hour cycles with a 1% precision. The system is composed of three subsystem of RPC single gaps, readout by 45cm x 45cm pads in a cosmic ray telescope located in the SGX5 gas building. Each subsystem is flushed with a different gas. The Reference subsystem is flushed with fresh open loop gas mixture. The MonitorOut subsystem is flushed with CL gas downstream of CMS RPCs. The MonitorIn subsystem is flushed with CL gas upstream of CMS RPCs. Each subsystem is composed of three gaps, whose high voltage is set to the standard working point voltage at the efficiency knee, and to 200V above and below the knee respectively. Each cosmic ray track therefore provides completely correlated pulses in the three subsystems, allowing one to study the differential response of gaps and by disentangling any effect due to changes in the gas mixture. In case a working point change is detected, an alarm condition is released and the gas quality monitoring system will verify what the change of work point is due to.

The system was built and operated in Frascati, and during 2007 it was shipped to CERN and installed at the ISR Closed Loop system.

3 Activity planned for 2008

The CMS Frascati group is performing a detailed and complete analysis campaign since early tests at the GIF in 2001, to guarantee high-purity gas mixture for a reliable operation of the detector. A lot of work is being spent into the full understanding of the chemistry of purifiers in CL gas system. During 2008 tests at ISR will be improved by the use of a better gas sampling scheme which will allow the full characterization of contaminants. Gas gain monitoring chambers will be studied and characterized at the ISR Close Loop system prior to installation on the CMS detector. Physics analysis will also be started with emphasys on dimuon pairs for both high- and low-pt channels.

References

1. CMS Collaboration home page is /cms.cern.ch/.
2. M. Abbrescia et al., Nucl. Instr. And Meth. A533 (2994) 102-106; M.Abbrescia et al., Nucl. Instr. And Meth. A515 (2993) 342-347.
3. M.Abbrescia et al., HF production in CMS Resistive Plate Chambers, submitted to NIM, presented by R.Guida at the RPC Conference, Seoul (Korea) 2005.
4. M.Abbrescia et al., Proposal for a systematic study of the CERN closed loop gas system used by the RPC muon detectors in CMS, Frascati preprint LNF-06/26(IR).
5. M. Abbrescia *et al.*, “Gas analysis and monitoring systems for the RPC detector of CMS at LHC,” arXiv:physics/0701014.

KLOE

The KLOE-LNF Collaboration

A. Antonelli, M. Antonelli, D. Babusci, G. Bencivenni, S. Bertolucci,
C. Bloise(Resp.), F. Bossi, P. Campana, G. Capon, T. Capussela AR),
P. Ciambrone, E. De Lucia (Art.23), P. de Simone, D. Domenici(AR),
M. Dreucci (Art.2222), G. Felici, C. Gatti (art.36), S. Giovannella, G. Lanfranchi,
J. Lee-Franzini (AS), M. Martini (Ass)*, S. Miscetti, M. Moulson, S. Müller (Art.2222),
F. Murtas, M. Palutan, V. Patera (Ass.)*, D. Pietreanu, P. Santangelo, T. Spadaro,
G. Venanzoni, R. Versaci (Ass)*, B. Sciascia (Art.23), A. Sciubba (Ass.)*,

**Also Dipartimento di Energetica, "La Sapienza" University, Rome*

The KLOE-LNF Technical Staff

M. Anelli, M. Carletti, G. Fortugno, R. Rosellini, F. Sborzacchi

1 Overview

The efforts of the Collaboration were focused on data analysis and on the supporting activities to ensure data reprocessing, production of large samples of simulated data, and a smooth, continuous running of the the computing farm and data handling systems.

In year 2007 the KLOE data analysis has resulted in several precision measurements, in the kaon sector and on radiative ϕ decays.

We presented in May new results on kaon physics, namely:

- the measurement of the absolute semileptonic branching ratios of charged kaons;
- two independent measurements of the lifetime of charged kaons;
- the measurement of the parameters describing the form factor dependence on the momentum transfer, with $K_{\mu 3}$ decays of neutral kaons;
- the update of the analysis of the QM-interference in the process $\phi \to K_S K_L \to \pi^+\pi^-\pi^+\pi^-$;
- the measurements of the branching ratios BR($K_S \to \gamma\gamma$) and BR($K_S \to e^+e^-$), based on the entire data sample of 2.5 fb^{-1};
- the results of the analysis of the radiative decay, $K_L \to \pi e \nu \gamma$, giving also a first measurement of the photon direct-emission (DE) contribution to the process;
- the preliminary result of the analysis of the K_{e2} channel.

The absolute measurement of the $K_{\pi 2}$ branching ratio has been presented to the EPS-HEP Conference, in July. We have also prepared one review paper on the unitarity test of the CKM matrix, whose experimental inputs from KLOE constitute a consistent and redundant framework.

With the analysis of the entire data sample we were able to reach a stringent upper limit (1.8 10^{-8}) on the branching ratio $\phi \to K_S K_S \gamma$, very close to the lowest expected value from several models describing the radiative coupling of the ϕ meson to neutral kaons.

We have published the analysis of the radiative ϕ decays, $\phi \to \pi^0\pi^0\gamma$, the paper on the $\eta - \eta'$ mixing, and the precision measurements of the η and kaon masses.

The study of the isosping-violating $\eta \to 3\pi$ decays has shown experimental evidence for the relations among the Dalitz-plot distributions of the $\eta \to \pi^+\pi^-\pi^0$ and the $\eta \to \pi^0\pi^0\pi^0$, as predicted in the framework of Chiral Perturbation Theory, ChPT.

We have presented the preliminary measurement of the branching ratio of the $\eta \to \pi^+\pi^-e^+e^-$ decay, based on the selection of 700 signal events, in October.

The following sections, 2 and 3, are devoted to the discussion of the results obtained with kaons, and on the other processes accessible at the ϕ factory.

We have progressed in the study of the KLOE detector upgrades in view of the continuation of the experimental program at higher luminosity. In particular, we have

- realized a full-scale prototype of the inner tracker,
- studied possible upgrades of the calorimeter readout,
- realized a prototype of the gamma-gamma tagger,
- made a proposal for a crystal calorimeter to detect small-angle photons and for a new system to instrument the quadrupoles.

We have presented the proposal for resuming the data taking in year 2009. At that time, the KLOE apparatus with minimal upgrades, required to operate a fully-efficient detector, will be ready (phase-0). This phase will be followed by the installation of the detector upgrades (phase 1), mostly for improving the tracking and clustering capabilities of the experiment in view of a longer data taking campaign, aiming for 50 fb^{-1} of integrated luminosity.

2 Results in Kaon physics

2.1 Measurement of the scalar Form-Factor slope for $K_L \to \pi\mu\nu$

The semileptonic kaon decay still provides the best process for the measurement of $|V_{\rm us}|$, because only the vector part of the weak current contributes to the matrix element $\langle\, \pi\,|J_\alpha|\, K\,\rangle$. In general,

$$\langle\, \pi\,|J_\alpha|\, K\,\rangle = f_+(t)(P+p)_\alpha + f_-(t)(P-p)_\alpha,$$

where P and p are the kaon and pion four-momenta, respectively, and $t = (P-p)^2$. The form factors (FF) f_+ and f_- appear because pions and kaons are not point-like particles, and reflect both SU(2) and SU(3) breaking. Introducing the scalar FF $f_0(t)$, the matrix element above is written as

$$\langle\pi(p)|\bar{u}\gamma_\alpha s|K(P)\rangle = f(0)\left((P+p)_\alpha\,\tilde{f}_+(t) + (P-p)_\alpha\left(\tilde{f}_0(t)\frac{\Delta_{K\pi}}{t} - \tilde{f}_+(t)\frac{\Delta_{K\pi}}{t}\right)\right), \tag{1}$$

with $\Delta_{K\pi} = m_K^2 - m_\pi^2$. The f_+ and f_0 FFs must have the same value at $t = 0$. We have therefore factored out a term $f(0)$. The functions $\tilde{f}_+(t)$ and $\tilde{f}_0(t)$ are both 1 at $t = 0$. The scalar form factor $\tilde{f}_0(t)$ is only relevant for $K_{\mu 3}$ decays. The behaviour of the reduced FFs $\tilde{f}_+(t)$ and $\tilde{f}_0(t)$ as a function of t can be measured from the decay spectra. Following the approach of Ref. [1], based on dispersion relation, we fit the data with the following parameterization:

$$\tilde{f}_{+,0}(t) = 1 + \lambda_{+,0}\frac{t}{m^2} + \frac{\lambda_{+,0}^2 + p_2}{2}\left(\frac{t}{m^2}\right)^2 + \frac{\lambda_{+,0}^3 + 3p_2\lambda_{+,0} + p_3}{6}\left(\frac{t}{m^2}\right)^3, \tag{2}$$

with $p_2 \sim 5 \times 10^{-4}$ and $p_3 \sim 3 \times 10^{-5}$, as evaluated from $K - \pi$ scattering data. The measurement of the vector and scalar form-factor slopes using $K_L \to \pi\mu\nu$ decays has been published by KLOE in year 2007 [2]. At KLOE energies, clean and efficient π/μ separation is much more difficult to obtain than good π/e separation. However, the form-factor slopes can be obtained from fits to the distribution of the neutrino energy E_ν, rather than to the distribution in t. E_ν is simply the missing momentum in the $K_L \to \pi\mu\nu$ decay evaluated in the K_L rest frame, and does not require any π/μ identification. A price is paid in statistical sensitivity, 2–3 times worst with respect to the case of a t-spectrum fit. This is partly recovered, by combined fit with $K_L \to \pi e\nu$ events. The E_ν spectrum, obtained with a sample of 1.8 million $K_L \to \pi\mu\nu$ decays, is shown in fig. 1. Finally, we obtain:

$$\begin{aligned} \lambda_+ &= (25.7 \pm 0.4_{\text{stat}} \pm 0.4_{\text{syst}} \pm 0.2_{\text{param}}) \times 10^{-3} \\ \lambda_0 &= (14.0 \pm 1.6_{\text{stat}} \pm 1.3_{\text{syst}} \pm 0.2_{\text{param}}) \times 10^{-3} \end{aligned} \tag{3}$$

with $\chi^2/\text{dof} = 2.6/3$ and a total correlation coefficient of -0.26, and where uncertainties from the choice of parameterization for the vector and scalar FFs are explicitily given. Using our slopes, we are able to compute the phase space integrals for semileptonic kaon decays with $\sim 0.25\%$ and $\sim 0.5\%$ accuracy for K_{e3} and $K_{\mu 3}$ decays, respectively.

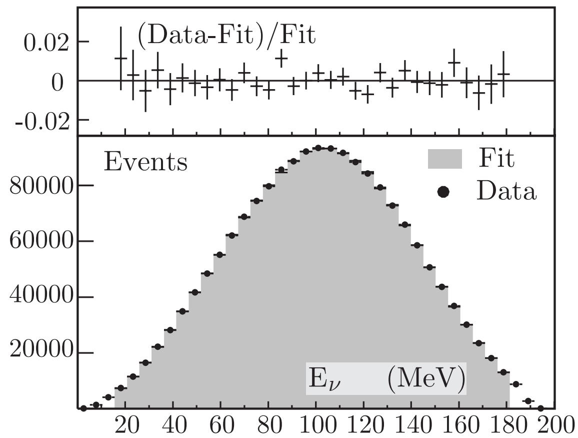

Figure 1: Residuals of the fit (top plot) and E_ν distribution for data events superimposed on the fit result (bottom plot).

2.2 Measurement of BR($K_L \to \pi e \nu \gamma$)

Two different processes contribute to photon emission in kaon decays: inner bremsstrahlung (IB) and direct emission (DE). DE is radiation from intermediate hadronic states and is sensitive to hadron structure. The relevant kinematic variables for the study of radiation in K_{l3} decays are E^*_γ, the energy of the radiated photon, and θ^*_γ, its angle with respect to the lepton momentum in the kaon rest frame. The IB amplitude diverges for $E^*_\gamma \to 0$. For K_{e3}, with $m_e \approx 0$, the IB spectrum in θ^*_γ is peaked near zero as well. The IB and DE amplitudes interfere. The contribution to the width from IB-DE interference is 1% or less of the purely IB contribution; the purely DE contribution is negligible. To disentangle the IB and DE components, we measure the double differential spectrum $d^2\Gamma/dE^*_\gamma d\theta^*_\gamma$ and compare the result with expectations from Monte Carlo (MC) generators. In the ChPT treatment of Ref. [3], the photon spectrum is approximated by

$$\frac{d\Gamma}{dE^*_\gamma} \simeq \frac{d\Gamma_{\rm IB}}{dE^*_\gamma} + \langle X \rangle f(E^*_\gamma). \tag{4}$$

The DE contributions are summarized in the function $f(E^*_\gamma)$, which represents the deviation from a pure IB spectrum. All information on the strength of the DE terms is contained in the parameter $\langle X \rangle$. Theoretical predictions on this parameter suffer by large uncertainties, due to the poor knowledge of ChPT low-energy constants. In contrast, a fit to the E^*_γ-θ^*_γ spectrum allows us to measure for the first time a value for $\langle X \rangle$. From the fit, we extract also

$$R \equiv \frac{\Gamma(K_{e3\gamma}; E^*_\gamma > 30\,\text{MeV}, \theta^*_\gamma > 20°)}{K_{e3(\gamma)}}. \tag{5}$$

The value of this ratio has been computed at $\mathcal{O}(p^6)$ in ChPT, leading to the prediction [4] $R = (0.963 \pm 0.006\langle X \rangle \pm 0.010) \times 10^{-2}$.

The (E^*_γ, θ^*_γ) distribution obtained from data has been fit using the sum of four independently normalized MC distributions: the distributions for $K_{e3\gamma}$ events from IB satisfying (not satisfying) the kinematic cuts $E^*_\gamma > 30\,\text{MeV}$ and $\theta^*_\gamma > 20°$, the distribution corresponding to the function $f(E^*_\gamma)$, and the physical background from $K_L \to \pi^+\pi^-$ and $K_L \to \pi\mu\nu$ events. Using a sample of 9 000 $K_{e3\gamma}$ events, and 3.5 million $K_{e3(\gamma)}$ for normalization, we find [5]:

$$\begin{aligned} R &= (0.924 \pm 0.023_{\rm stat} \pm 0.016_{\rm syst}) \times 10^{-2} \\ \langle X \rangle &= 2.3 \pm 1.3_{\rm stat} \pm 1.4_{\rm syst}. \end{aligned} \tag{6}$$

The dependence of R on $\langle X \rangle$, predicted by ChPT, can be used to further constrain the possible values of R and $\langle X \rangle$ from our measurement. The constraint is applied via a fit, which gives $R = (0.944 \pm 0.014) \times 10^{-2}$ and $\langle X \rangle = -2.8 \pm 1.8$, with $\chi^2/\text{ndf} = 0.64/1$ ($P = 42\%$).

2.3 Measurement of BR($K_S \to \gamma\gamma$)

A precise measurement of the $K_S \to \gamma\gamma$ decay rate is an important test of ChPT predictions. The decay amplitude of $K_S \to \gamma\gamma$ has been evaluated at leading order in ChPT [6], $\mathcal{O}(p^4)$, providing a precise estimate of BR($K_S \to \gamma\gamma$) $= 2.1 \times 10^{-6}$, with 3% uncertainty. This estimate is $\sim 30\%$ lower with respect to the latest determination from NA48 [7], thus suggesting relevant contributions from higher order terms.

We measured the $K_S \to \gamma\gamma$ rate using 1.9 fb^{-1} of integrated luminosity. A MC background sample of comparable statistics and a large MC signal sample (equivalent to $\sim$ 50 fb^{-1}) have been used in the analysis. Using the tag from K$_L$ interactions in the calorimeter (K-crash tag), we select $\sim$ 700 million events, out of which $\sim$ 1900 are $K_S \to \gamma\gamma$ decays.

The signal is selected by requiring exactly two prompt photons, with an efficiency of $\sim$ 83%. After photon counting, the background composition is dominated by $K_S \to 2\pi^0$, with two undetected photons by the electromagentic calorimeter, EMC. This background is strongly reduced, with negligible signal loss, by vetoing the events with a signal from the quadrupole instrumentation, QCAL, in coincidence, within a 5 ns window, with the beam crossing time (the event-T_0). Further background reduction is obtained by performing a kinematic fit to the event in the signal hypothesis, using as constraints the total 4-momentum conservation, the kaon mass, and the light velocity for determining the photon time-of-flight (ToF). After this cut, we count signal events by fitting the 2-D distribution of photon invariant mass, $M_{\gamma\gamma}$, and opening angle in the K_S center of mass, $\theta^*_{\gamma\gamma}$, using MC-predicted shapes for both, signal, and residual background. We count $N(\gamma\gamma) = 711 \pm 35$ signal events out of 2740 events, with $\chi^2/\text{dof} = 854/826$ corresponding to a probability P(χ^2) $\sim$ 24%. In fig. 2 the observed distributions of $\cos\theta^*_{\gamma\gamma}$ and $M_{\gamma\gamma}$ are compared with the simulated signal and background shapes as weighted by the fit results. To get the BR($K_S \to \gamma\gamma$), signal events

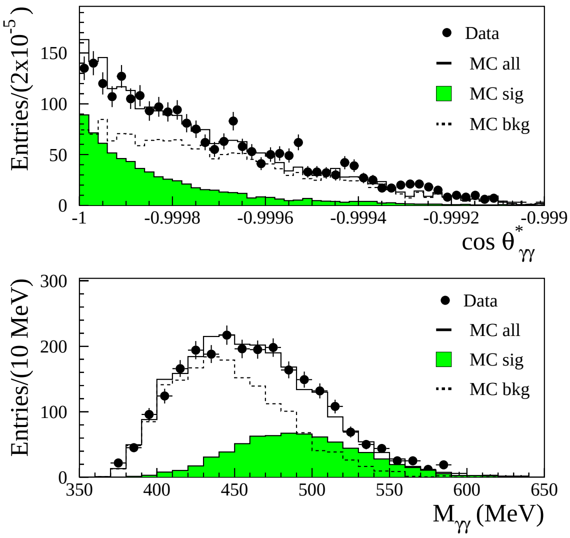

Figure 2: Distributions of cos$\theta^*_{\gamma\gamma}$ (top) and $M_{\gamma\gamma}$ (bottom) at the end of the analysis chain; black points are data, solid line is the sum of MC signal and background shapes as weighted by the fit.

are normalized to the number of $K_S \to 2\pi^0$ decays observed in the same data sample. Finally, we obtain [8)]

$$\text{BR}(K_S \to \gamma\gamma) = (2.26 \pm 0.12_{\text{stat}} \pm 0.06_{\text{syst}}) \times 10^{-6}, \tag{7}$$

which differs by 3σ from the previous best determination. Our result is also consistent with $\mathcal{O}(p^4)$ ChPT prediction.

2.4 Direct search of $K_S \to e^+e^-$

This decay is a flavour-changing neutral current process, suppressed in the SM, with an amplitude dominated by two-photon intermediate state. Using ChPT to $\mathcal{O}(p^4)$, one obtains BR($K_S \to e^+e^-$) $\sim 2\times10^{-14}$ [9]. A value significantly higher could indicate new physics. Prior to KLOE, the best experimental limit on this decay was set by CPLEAR, BR($K_S \to e^+e^-$) $\leq 1.4\times10^{-7}$ at 90% CL [10].

We performed a search for the $K_S \to e^+e^-$ decay using 1.9 fb^{-1} of integrated luminosity. A MC background sample of comparable statistics and a large MC signal sample have been also used in the analysis. After K-crash tag, we search for the signal by requiring two tracks of opposite charge originating near the collider interaction region (IP). The two tracks are required to have an invariant mass M_{ee}, evaluated in the electron hypothesis, in a $\sim$ 20 MeV window around the nominal K_S mass. This cut is particularly effective on $K_S \to \pi^+\pi^-$ events, which peak at $M_{ee} \sim 409$ MeV. After the cut, the background is dominated by $K_S \to \pi^+\pi^-$ with at least one pion wrongly reconstructed, and by $\phi \to \pi^+\pi^-\pi^0$ events. The K_S events are strongly reduced by cutting on the track momentum in the K_S rest frame, which is expected to be $\sim$ 206 MeV for $K_S \to \pi^+\pi^-$ decays. To reject $\phi \to \pi^+\pi^-\pi^0$ events we use instead $|\vec{p}_{miss}| = |\vec{p}_\phi - \vec{p}_{K_S} - \vec{p}_{K_L}|$, where K_S and K_L momenta are evaluated from the charged tracks and from the K-crash tag, respectively. The value of $|\vec{p}_{miss}|$ peaks at zero for the signal, within the experimental resolution of few MeV and it spreads towards higher values for $\phi \to \pi^+\pi^-\pi^0$ events. The residual background, both from $K_S \to \pi^+\pi^-$ and $\phi \to \pi^+\pi^-\pi^0$ decays, is rejected identifying the two electrons by ToF, and by using the properties of the associated calorimetric cluster. The reliability of the MC background simulation is checked after each step of the selection on the invariant mass sidebands. At the end of the analysis chain, no events are found in the signal box; the background estimate is also compatible with zero. The upper limit on the number of signal events is therefore $N_{ee} = 2.3$ at 90% CL. The signal selection efficiency, after tagging, is $\sim$ 47%. Such performance, in terms of exceptional background rejection ($> 10^8$) with an acceptable signal efficiency, has been achieved thanks to the very good momentum resolution of our drift chamber, DC. To obtain an upper limit for the BR($K_S \to e^+e^-$), we normalize N_{ee} to the $K_S \to \pi^+\pi^-$ decays observed in the same data sample. Finally, we obtain [11]

$$\mathrm{BR}(K_S \to e^+e^-) \leq 9.3 \times 10^{-9} \quad \text{at}\, 90\%\, \text{CL}, \tag{8}$$

which represents a factor of $\sim$ 15 improvement with respect to the best previous limit.

2.5 The absolute branching ratio $K^\pm \to \pi^\pm\pi^0$

The importance to measure the BR($K^+ \to \pi^+\pi^0(\gamma)$) is twofold: i) the most recent measurement BR($K^+ \to \pi^+\pi^0(\gamma)$)=0.2118$\pm$0.0028 [12] dates back to 1972, and the information on the treatment of radiative corrections is incomplete, and ii) this BR is fundamental for BR(K_{l3}) measurements normalized to BR($K_{\pi2}$) [13] [14], used to measure the CKM matrix element V$_{us}$ [15].

At KLOE, we measure the absolute BR($K_{\pi2}(\gamma)$) tagging with both $K^-_{\mu2}$ and $K^-_{\pi2}$ decays. The selection of $K^+_{\pi2}(\gamma)$ decays uses DC information only. The K^+ track and its decay vertex are selected in the fiducial volume , $40 < R_V < 150$ cm, $|z| < 150$ cm. Loose cuts on the momentum of the charged secondary track in the kaon rest frame, p^*, and on the momentum difference between the kaon and the charged secondary track are applied to reject $K \to 3\pi$ decays and $K^{\pm}$ split tracks.

The signal count is then extracted from the fit of the p^* distribution in the window starting from p^*_{cut}=180 MeV/c (see figure 3). This spectrum exhibits two peaks, the first at about 236 MeV/c from $K^+_{\mu 2}$ decays and the second at about 205 MeV/c from the signal $K^+_{\pi 2}$ decays. Lower p^* values are due to three-body decays. The fit to the p^* distribution is done using the following

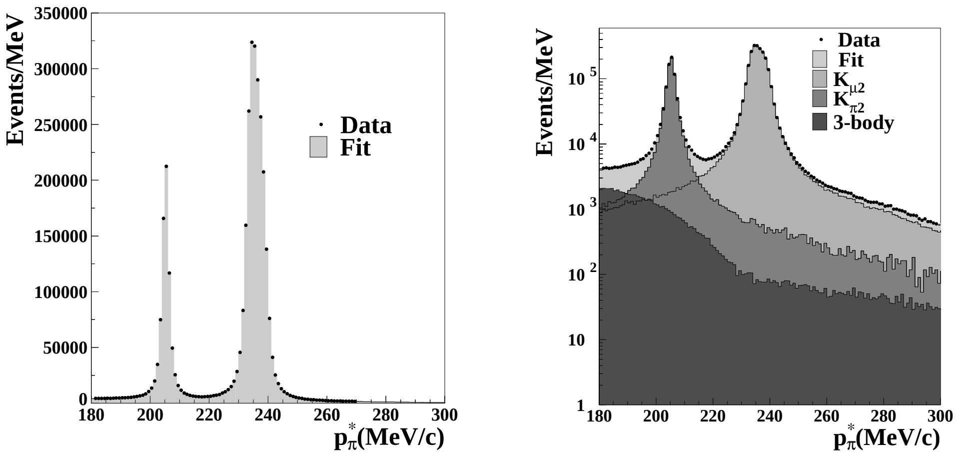

Figure 3: Fit of the p^* distribution. Left: black dots are Data and grey histogram is the fit output. Right: the three contributions used to fit the Data are shown: $K_{\mu 2}$, $K_{\pi 2}$ and *three-body* decays.

three contributions: $K_{\mu 2}$, $K_{\pi 2}$ and three-body decays. For $K_{\mu 2}$ and $K_{\pi 2}$ components we use shapes obtained from data control samples selected using EMC information only. For the contribution from three-body decays we use the MC-smeared distribution. Figure 3 left shows the result of the fit of the p^* distribution performed on the $K^-_{\mu 2}$-tagged data sample. The right panel shows the three contributions: $K_{\pi 2}$, $K_{\mu 2}$ and three-body decays. The reconstruction and selection efficiency has been evaluated with data from a control sample selected using EMC information only, to avoid any correlation with the DC-driven sample selection. The final efficiency evaluation is related to the charged kaon lifetime $\tau_{\pm}$ via the geometrical acceptance. The weighted average, accounting for correlations, of the absolute branching ratios obtained using events tagged by $K^-_{\mu 2}$ and $K^-_{\pi 2}$ decays is a measurement to 4.6 per mil accuracy [16]:

$$BR(K^+ \to \pi^+ \pi^0 (\gamma)) = 0.2065 \pm 0.0005_{\rm stat} \pm 0.0008_{\rm syst}. \tag{9}$$

The value reported is shifted by -1.3% with respect to the PDG06 fit value [17] and has a 20% better fractional accuracy.

2.6 V_{us} and lepton universality with KLOE data

During the last years, we measured most decay branching ratios of K_S and K_L [18] [19] [20]. We published this year a new measurement of $K^{\pm}$ semileptonic decay branching ratios [21]. We're close to complete the work on $K^{\pm}$ two-body decays described in the previous section by submitting the new measurement of BR($K^+ \to \pi^+ \pi^0$), having published already in 2006 the BR($K^+ \to \mu\nu$) [22].

We have also measured the K_L lifetime [23] and we recently published a new measurement of the $K^\pm$ lifetime [24]. Finally, the shape of the form factors of the semileptonic decays have been measured for both K_{e3} [25] and $K_{\mu 3}$ decays [2], as discussed in sect. 2.1. The above results provide the basis for the determination of the CKM parameter $V_{\rm us}$, and a test of the unitary of the quark flavor matrix. We also test the lepton universality in K_{l3} decays and place bounds on new physics using measurements of $V_{\rm us}$ from K_{l2} and K_{l3} decays. A well organized compendium of all of our data has been recently published [26]. We summarize here the main results.

Using our determinations of the kaon semileptonic decay rates, we obtained the values of $f_+(0)\,V_{us}$ for K_{Le3}, $K_{L\mu 3}$, K_{Se3}, $K^\pm_{e3}$, and $K^\pm_{\mu 3}$ decay modes, as shown in fig. 4. It is worth noting that the only external experimental input to this analysis is the K_S lifetime. The five different

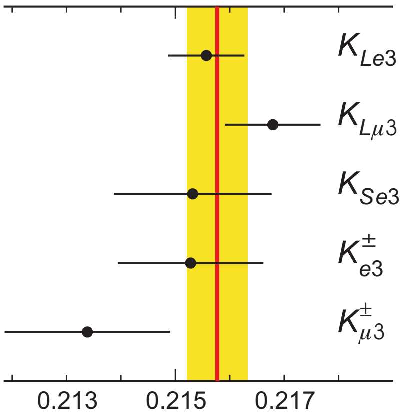

Figure 4: KLOE results for $f_+(0)\,V_{us}$.

determinations have been averaged, taking into account all known correlations. We find

$$f_+(0)\,V_{us} = 0.2157 \pm 0.0006, \tag{10}$$

with $\chi^2/\mathrm{ndf} = 7.0/4$ (13%).

The comparison of the values of $f_+(0)\,V_{us}$ for K_{e3} and $K_{\mu 3}$ modes provides a test of lepton universality. Specifically,

$$r_{\mu e} = \frac{(f_+(0)\,V_{us})^2_{\mu 3,exp}}{(f_+(0)\,V_{us})^2_{e3,exp}} = \frac{\Gamma_{\mu 3}}{\Gamma_{e3}}\,\frac{I_{e3}(1+\delta_{Ke})^2}{I_{\mu 3}(1+\delta_{K\mu})^2}, \tag{11}$$

where δ_{Kl} is a correction due to $SU(2)$ breaking and photon radiation. The ratio $r_{\mu e}$ is equal to the ratio g_μ^2/g_e^2, with g_ℓ the coupling strength at the $W \to \ell\nu$ vertex. In the SM, $r_{\mu e} = 1$. Averaging charged and neutral modes, we find

$$r_{\mu e} = 1.000 \pm 0.008. \tag{12}$$

This has to be compared with the sensitivity obtained in $\pi \to \ell\nu$ decays, $(r_{\mu e})_\pi = 1.0042(33)$, and in τ leptonic decays, $(r_{\mu e})_\tau = 1.000(4)$ [17].

Lattice evaluations of $f_+(0)$ are rapidly improving in precision. For example, the RBC and UKQCD Collaborations have recently obtained $f_+(0) = 0.9644(49)$ from a lattice calculation with $2 + 1$ flavors of dynamical domain-wall fermions [27]. Using their value of $f_+(0)$, with our determination of $f_+(0)\,V_{us}$, with 2.8 per mill fractional accuracy, we obtain $V_{\rm us} = 0.2237(13)$.

The availability of precise lattice evaluations for the pion- and kaon-decay constants f_π and f_K allows to use a relation between $\Gamma(K_{\mu2})/\Gamma(\pi_{\mu2})$ and $|V_{\rm us}|^2\,/\,|V_{\rm ud}|^2$, with the advantage that lattice-scale uncertainties and radiative corrections largely cancel out in the ratio [28]. From our measurements of $\mathrm{BR}(K_{\mu2})$ and $\tau_\pm$, and using $\Gamma(\pi_{\mu2})$ from [17], we evaluate:

$$V_{us}/V_{ud} \times f_K/f_\pi = 0.2766 \pm 0.0009. \tag{13}$$

Using the recent lattice determination of f_K/f_π from the HPQCD/UKQCD collaboration, $f_K/f_\pi = 1.189(7)$ [29], we finally obtain $V_{\rm us}/V_{\rm ud} = 0.2326 \pm 0.0015$. To test the unitarity of the quark mixing

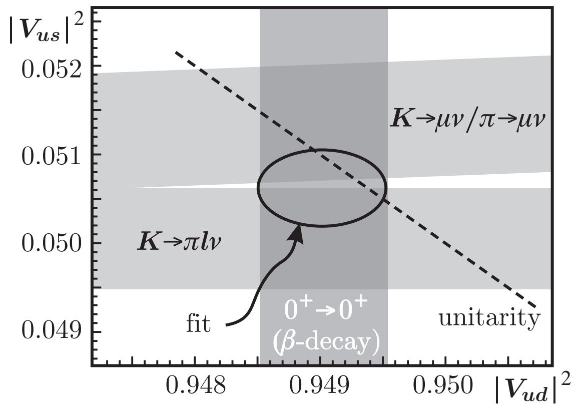

Figure 5: KLOE results for $|V_{\rm us}|^2$ and $|V_{\rm us}/V_{\rm ud}|^2$, together with $|V_{\rm ud}|^2$ from β-decay measurements. The ellipse is the 1σ contour from the fit. The unitarity constraint is illustrated by the dashed line.

matrix, we combine all the information from our measurements on $K_{\mu2}$, K_{e3}, $K_{\mu3}$, together with superallowed $0^+ \to 0^+$ nuclear β decays (fig. 5). The best estimate of $|V_{\rm us}|^2$ and $|V_{\rm ud}|^2$ can be obtained from a fit to our results $V_{\rm us} = 0.2237(13)$ and $V_{\rm us}/V_{\rm ud} = 0.2326(15)$, together with $V_{\rm ud} = 0.97418(26)$ [30]. The fit gives $|V_{\rm us}|^2 = 0.0506(4)$ and $|V_{\rm ud}|^2 = 0.9490(5)$, with $\chi^2/\mathrm{ndf} = 2.34/1$ (13%) and a correlation coefficient of 3%. The values obtained confirm the unitarity of the CKM quark mixing matrix as applied to the first row. We find

$$|V_{\rm us}|^2 + |V_{\rm ud}|^2 - 1 = -0.0004 \pm 0.0007 \quad (\sim 0.6\sigma). \tag{14}$$

A particularly interesting observable is the ratio of the $V_{\rm us}$ values obtained from helicity suppressed and helicity allowed modes: $R_{\ell 23} = |V_{\rm us}(K_{\ell 2})/V_{\rm us}(K_{\ell 3}) \times V_{ud}(0^+ \to 0^+)/V_{ud}(\pi_{\mu2})|$. This ratio, which is equal to 1 in the SM, would be affected by the presence of scalar density or extra right-handed currents. A scalar current due to a charged Higgs H^+ exchange is expected to lower the value of $R_{\ell 23}$, which becomes [31]:

$$R_{\ell 23} = \left| 1 - \frac{m_{K^+}^2}{m_{H^+}^2}\left(1 - \frac{m_{\pi^+}^2}{m_{K^+}^2}\right)\frac{\tan^2\beta}{1 + 0.01\tan\beta} \right|, \tag{15}$$

with $\tan\beta$ the ratio of the two Higgs vacuum expectation values in the MSSM. In addition, in this scenario both, $0^+ \to 0^+$ nuclear beta decays, and $K_{\ell 3}$, are not affected and the unitarity constraint for this modes can be applied. To evaluate $R_{\ell 23}$, we fit our experimental data on $K_{\mu 2}$ and $K_{\ell 3}$ decays, using as external inputs the most recent lattice determinations of $f_+(0)$ and f_K/f_π, and the value of V_{ud} from [30]. We obtain

$$R_{\ell 23} = 1.008 \pm 0.008, \tag{16}$$

which is one σ above the SM prediction. This measurement can be used to set bounds on the charged Higgs mass m_{H^+} and $\tan\beta$. Figure6 shows the region excluded at 95% CL in the $m_{H^+} - \tan\beta$ plane. The measurement of $\mathrm{BR}(B \to \tau\nu)$ [32] can also be used to set bounds in the $m_{H^+} - \tan\beta$ plane, which are also shown in fig. 6. While the $B \to \tau\nu$ can exclude quite an extensive region of this plane, there is an uncovered region corresponding to the change of sign of the correction. This region is fully covered by our result.

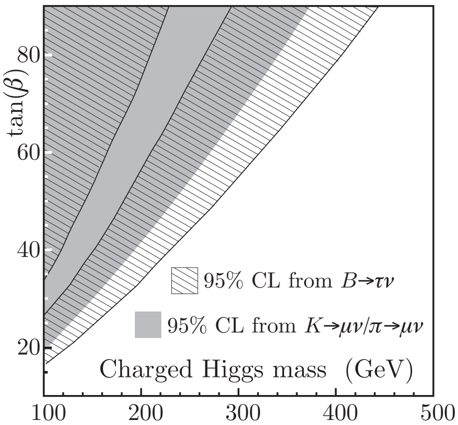

Figure 6: Excluded region in the $m_{H^+} - \tan\beta$ plane by the measurement $R_{\ell 23}$; the region excluded by $B \to \tau\nu$ is also indicated.

2.7 Measurement of $\Gamma(K \to e\nu)/\Gamma(K \to \mu\nu)$

A particularly sensitive probe of new physics in leptonic kaon decays is the ratio

$$R_K = \frac{\Gamma(K^\pm \to e^\pm \nu_e)}{\Gamma(K^\pm \to \mu^\pm \nu_\mu)} \tag{17}$$

This observable is predicted to 0.04% accuracy within the SM [33], while R_K deviations from SM prediction can reach $\sim 1\%$ in the MSSM scenario, and in particular should be dominated by lepton-flavor violating contributions with τ-neutrinos emitted [34]. The current official world average on R_K has a relative error of $\simeq 6\%$, but a series of new preliminary results by NA48/2 and KLOE are improving the knowledge on R_K.

At KLOE, we measure R_K performing a "direct search" for $K^\pm \to e^\pm \nu_e$ and $K^\pm \to \mu^\pm \nu_\mu$ decays without tagging, to keep the statistical uncertainty on the number of $K^\pm \to e^\pm \nu_e$ below 1%.

The presence of a one-prong decay vertex in the DC volume with a secondary charged decay track with relatively high momentum ($180 \div 270$ MeV) is required. To distinguish $K^{\pm} \to e^{\pm}\nu_e$ and $K^{\pm} \to \mu^{\pm}\nu_{\mu}$ decays from the background we use the lepton mass $M^2_{\rm lep}$ obtained from the momenta of the kaon and the charged decay particle, assuming zero neutrino mass. This provides a clean identification of the $K^{\pm} \to \mu^{\pm}\nu_{\mu}$ sample, while to improve background rejection in selecting $K^{\pm} \to e^{\pm}\nu_e$ decays we use also information from the EMC. The particle identification (PID) is based on E/p distributions and cluster shape, in particular on the spread of the energy deposits in the EMC planes $E_{\rm R.M.S.}$. The number of signal events is extracted from a likelihood fit to the two-dimensional $E_{\rm R.M.S.}$ vs $M^2_{\rm lep}$ distribution, using MC shapes for signal and background. The MC shapes for $K \to l\nu(\gamma)$ include radiative contributions.

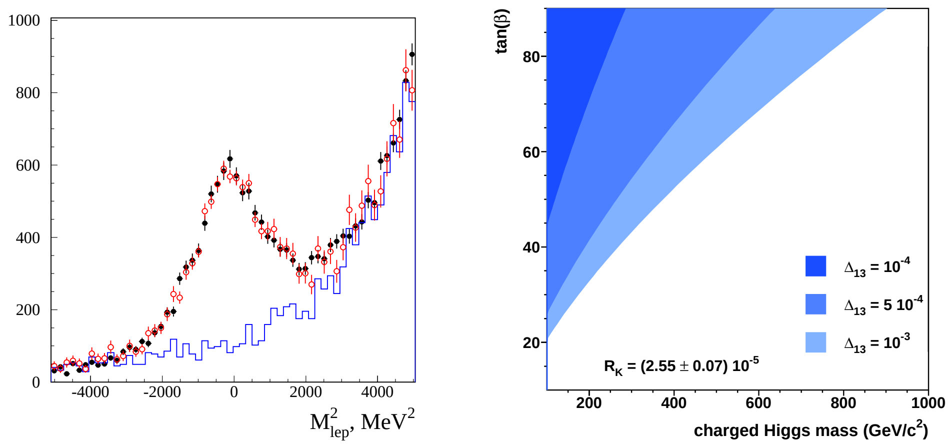

Figure 7: Left: Distribution of the squared lepton mass of the charged secondary track $M^2_{\rm lep}$: filled dots are data, open dots the result from the maximum-likelihood fit. Right: Exclusion limits at 95% CL on $\tan\beta$ and charged Higgs mass $m_{H^{\pm}}$ for different values of Δ_{13}.

The projection of the fit result on the $M^2_{\rm lep}$-axes is compared to data in figure 7 left. The number of $K^{\pm} \to \mu^{\pm}\nu_{\mu}$ events in the same data set is extracted from a similar fit to the $M^2_{\rm lep}$ distribution, where no PID cuts are applied. The fraction of background events under the muon peak is estimated from MC to be less than one per mil. Our preliminary result is [35]:

$$R_K = (2.55 \pm 0.05 \pm 0.05) \times 10^{-5}. \tag{18}$$

This value is compatible within errors with the very precise SM prediction. In the supersimmetric framework of Ref. [34] this result implies significant constraints in the $m_{H^+} - \tan\beta$ plane (see figure 7 right). The constraints depend on the lepton flavour violating (LFV) coupling Δ_{13}, whose natural values lie below 10^{-3}.
Our preliminary measurement is based on $\simeq 1.7$ fb^{-1}. Adding the remaining event statistics and improving the selection efficiency we aim to reduce the error to the 1% level.

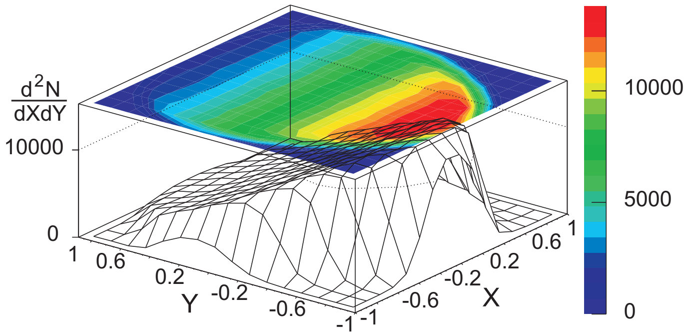

Figure 8: Dalitz plot density for $\eta \to \pi^+\pi^-\pi^0$ events.

3 Results in hadronic physics

3.1 Study of the $\eta \to 3\pi$ decays

The $\eta \to \pi\pi\pi$ decay violates iso-spin invariance. Electromagnetic contributions to the process are very small and the decay is dominantly induced by strong interactions, via u, d mass difference. The $\eta \to 3\pi$ decay is therefore an ideal laboratory for testing ChPT.

We have studied both $\pi^+\pi^-\pi^0$ [36)] and $\pi^0\pi^0\pi^0$ [37)] final states using ~ 450 pb^{-1} collected at the ϕ peak. The η mesons are tagged by detecting the monochromatic recoil photon ($E_{\gamma\,\rm rec} = 363$ MeV) of the $\phi \to \eta\gamma$ decay. A constrained kinematic fit is performed imposing 4-momentum conservation and light velocity for each photon, significantly improving the photon energy resolution. After background rejection the residual contamination is at the level of few per mil.

The conventional Dalitz plot variables for the $\pi^+\pi^-\pi^0$ final state are $X \propto (T_+ - T_-)$ and $Y \propto T_0$, where T is the kinetic energy of the pions. The measured distribution is parametrized as: $|A(X,Y)|^2 = 1 + aY + bY^2 + cX + dX^2 + eXY + fY^3 + \ldots$. Any odd power of X in $A(X,Y)$ implies violation of charge conjugation. The Dalitz plot density is shown in Fig. 8. After background subtraction we remain with $1.34 \cdot 10^6$ events. The fit is then performed including all cubic terms. As expected from C-invariance, c and e are consistent with zero. The other non-null parameters are:

$$
\begin{aligned}
a &= -1.090 \pm 0.005\,(\text{stat.})\ ^{+0.008}_{-0.019}\ (\text{syst.}) \\
b &= 0.124 \pm 0.006\,(\text{stat.})\ \pm 0.010\,(\text{syst.}) \\
d &= 0.057 \pm 0.006\,(\text{stat.})\ ^{+0.007}_{-0.016}\ (\text{syst.}) \\
f &= 0.14\ \ \pm 0.01\ \ (\text{stat.})\ \pm 0.02\ (\text{syst.})
\end{aligned}
$$

Our fit raises several points unexpected from previous, low statistics analyses: (i) the fitted value for the quadratic slope in Y is almost one half of simple Current Algebra predictions ($b = a^2/4$), indicating that higher order corrections are necessary; (ii) the quadratic term in X and the cubic term in Y are unambiguously different from zero.

We have also fitted the Dalitz plot with a different parametrization of the event density which takes into account π-π rescattering in the final state. Since strong interactions are expected to mix the two isospin $I = 1$ final states of the $\eta \to 3\pi$ decay, it is possible to introduce a unique rescattering matrix R which mixes the corresponding I=1 decay amplitudes [38]. Thus, we have made a fit using the alternative parametrization of the Dalitz plot density distribution, from which it is possible to extract also the slope α, describing the Dalitz plot density of the $\eta \to \pi^0\pi^0\pi^0$ decay, $|A(z)|^2 \propto 1 + 2\,\alpha\, z$, where z is related to the three pion energies in the η rest frame. The result is $\alpha = -0.038\ \pm 0.002$.

While the polynomial fit of the Dalitz plot density gives valuable information on the matrix element, integrated asymmetries are very sensitive in assessing the possible presence of C violation in amplitudes of given ΔI. In particular, left-right asymmetry tests C violation with no specific ΔI constraint, quadrant asymmetry tests C violation for $\Delta I = 2$ and sextant asymmetry tests C violation for $\Delta I = 1$ [39]. All of them are consistent with zero at 10^{-3} level, thus improving existent evaluations obtained combining different experiments [17]:

$$
\begin{aligned}
A_{\rm LR} &= (+0.09 \pm 0.10\,(\text{stat.})\,^{+0.09}_{-0.14}\,(\text{syst.})\,) \times 10^{-2} \\
A_{\rm Q} &= (-0.05 \pm 0.10\,(\text{stat.})\,^{+0.03}_{-0.05}\,(\text{syst.})\,) \times 10^{-2} \\
A_{\rm S} &= (+0.08 \pm 0.10\,(\text{stat.})\,^{+0.08}_{-0.13}\,(\text{syst.})\,) \times 10^{-2}
\end{aligned}
$$

In the analysis of $\eta \to \pi^0\pi^0\pi^0$ decay, photons are paired to form π^0's after kinematically constraining the total four-momentum to M_ϕ to improve the energy resolution. Three samples, with different efficiency (30.3%, 13.6% and 4.3%) and purity on photon pairing (75.4%, 92.0% and 97.6% respectively), have been analyzed. Results are consistent within errors. The preliminary value obtained is $\alpha = -0.027 \pm 0.004_{\rm stat} \pm 0.006_{\rm syst}$. The comparison of results from samples with different photon-pairing purity and from several fit ranges has been used to determine the error. This measurement is in agreement with current best measurement from Crystal Ball [40], with the KLOE measurement from $\eta \to \pi^+\pi^-\pi^0$ and with theoretical evaluations based on chiral unitarity approach [41].

3.2 The measurement of the branching ratio $\eta \to \pi^+\pi^-e^+e^-$

There are several theoretical reasons to study the $\eta \to \pi^+\ \pi^-\ e^+\ e^-$ decay. First, by using the virtual photon it is possible to probe the structure of the η meson in the time-like region of four momentum transfer square, q^2, which is equal to the invariant mass squared of the lepton pair [42]. One may also compare the predictions of the branching ratio value based on Vector Meson Dominance model, and ChPT [43] [44] [45] [46]. Moreover, it would be possible to study CP violation beyond the prediction of the Standard Model [47]. CPV can be introduced by a flavor-conserving, CP violating, four-quark operators involving two strange quarks together with combinations of other light quarks. It can be experimentally tested by measuring the angular asymmetry between pions and electrons decay planes.

The samples used in this analysis are: 622 pb^{-1} from 2004-2005 data taking; Montecarlo signal and background equivalent to 46 $\times$ 10^3 pb^{-1} and 1723 pb^{-1}, respectively.

The algorithm for the selection of the η meson decay in four charged particles requires: 1) four tracks coming from the interaction point, IP; the fiducial volume around the IP is a cylinder having radius R = 4 cm and height h = 20 cm; 2) at least one neutral cluster having energy $E_{cl} \geq 250$

MeV; 3) zero neutral clusters having energy in the range $50 \leq E_{cl} \leq 250$ MeV. A neutral cluster is defined as an energy deposit in the calorimeter without any associated track, having a polar angle in the range $(23°, 157°)$ and a time compatible with photons (i.e.: $|t_{cl} - r_{cl}/c| < min(5\ \sigma_t,\ 2\ ns)$). It can happen that the track of a particle is poorly reconstructed and splits in two. A dedicated algorithm has been developed to recover broken tracks: for each pair of tracks, the four possible inward-outward combinations (i.e.: FirstHit-FH, FH-LastHit LH-FH, LH-LH) are considered. If any combination satisfies both the checks on the differences of the momenta: $\Delta p_T < 4.5$ MeV and $\Delta p_z < 3.0$ MeV the two tracks are considered as coming from the same particle. The track having the largest distance to the IP is flagged as broken and discarded. The candidate tracks are ordered according to their momentum (separately per charge). The first is classified as pion and the second as electron. Four candidate tracks are required, two positive and two negative.

The main backgrounds after event selection are $\phi \to \pi^+\pi^-\pi^0$, other $\phi \to \eta\gamma$ decays and $\phi \to K^+K^-$. The first ($\phi \to \pi^+\pi^-\pi^0$) simulates the signal when the π^0 undergoes a Dalitz decay or a photon converts in a e^+e^- pair. It is also useful to notice that in $\eta \to \pi^+\pi^-\gamma$ events, with photon conversion, the invariant mass of the four tracks reproduces to η mass peak. Backgrounds are reduced cutting on the sum of the momenta of the two particles classified as pions ($S2p = |\vec{p}(\mathrm{p}_1^+)|\ +\ |\vec{p}(\mathrm{p}_1^-)|$) and on the sum of the momenta of the four selected tracks ($S4p = \sum_1^4 |\vec{p}_i|$). It is required that: $270 < S2p < 470\ MeV$ and $450 < S4p < 600\ MeV$. After this cuts the background over signal ratios (B/S) is reduced by two order of magnitude and is $\mathcal{O}(1)$.

For the selected events it is possible to reconstruct the invariant mass of the four tracks according to the mass hypothesis previously defined. To improve the resolution on the track momenta and on the energy of the neutral cluster a kinematic fit is performed imposing the four-momentum conservation and the cluster timing.

To evaluate the number of signal events we use the MC shapes to fit the data spectrum. We have used as reference the fit of the spectrum in the range [400:700] MeV, with 3 MeV per bin, and three MC shapes to fit the data, corresponding to signal, other η decays and non-η backgrounds. We have chosen this background shape parametrization to minimize correlations among shapes.

We have performed several fits with different background parametrization, obtaining stable results. They are stable also with respect to the choice of the fit range and of the bin size.

The fit of the distribution of the reconstructed invariant mass of the four tracks, constrained by kinematic fit, is shown in figure 9. The peak of the signal corresponding to the η mass is evident. The small background contribution peaked at the η mass is due to $\eta \to \pi^+\pi^-\gamma$ events with photon conversion into an electron-positron pair. A dedicated study to reject this background is in progress [1].

We have found $N_{events} = 733 \pm 62$ events, with $\chi^2/dof = 92/97$, corresponding to a χ^2 probability $P(\chi^2) = 0.61$.

The preliminary value of the branching ratio has been obtained using the formula: $BR = N_{events}/(\sigma_\phi \cdot BR(\phi \to \eta\gamma) \cdot \mathcal{L} \cdot \epsilon)$ where σ_ϕ is the cross section of the process $e^+e^- \to \phi$ and $\mathcal{L}$ is

[1]The branching ratio of the $\eta \to \pi^+\pi^-\gamma$ decay used in this analysis is the one reported by the PDG 2002 [48]. Recently the CLEO collaboration has published a new measurement [49] which is 15% lower: $BR(\eta \to \pi^+\pi^-\gamma) = (3.96 \pm 0.14 \pm 0.14) \times 10^{-2}$. This value would lead to an increase of our preliminary result on the BR($\eta \to \pi^+\ \pi^-\ e^+\ e^-$).

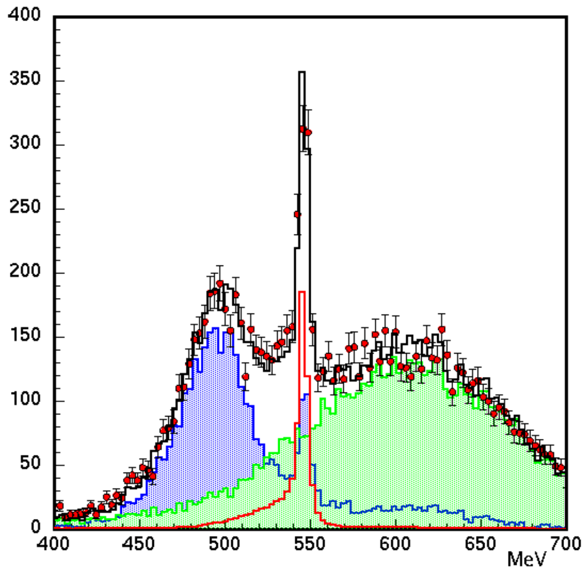

Figure 9: Fit to the invariant mass of the four selected tracks after background rejection. Red dots: data. Solid line: total MC. MC signal: red. Other $\phi \to \eta\gamma$ decays: blue. Other sources of background: green.

the luminosity of the data sample used for the measurement. The selection efficiency of our signal, ϵ, is evaluated by MC: $\epsilon = 0.1175(5)$. A correction to the efficiency, accounting for Data/MC discrepancies, is under evaluation. Based on previous studies done on 2001-2002 data, $\Delta\epsilon/\epsilon$ is expected of the order of 5-10%.
The preliminary value for the branching ratio is:

$$BR(\eta \ \to \ \pi^+ \ \pi^- \ e^+ \ e^-) = (24 \pm 2_{Fit} \pm 4_{Syst.}) \times 10^{-5} \tag{19}$$

where the systematic error accounts for the uncertainty on the efficiency and on the background rejection. A preliminary MC study on the asymmetry in the decay plane distribution shows that the cuts used in the analysis do not introduce any relevant distortion on the asymmetry shape.

3.3 Study of the process $e^+e^- \to \omega\pi^0$

In the energy region of few tens of MeV around M_ϕ, the $\omega\pi^0$ production cross section is largely dominated by the non-resonant processes $e^+e^- \to \rho/\rho'$. However, in a region closer to M_ϕ, a contribution from the OZI and G-parity violating decay $\phi \to \omega\pi^0$ is expected. This strongly suppressed decay can be observed only through the interference pattern with the previous reaction, which shows up as a dip in the production cross section as a function of the center of mass energy ($\sqrt{s}$). The interference scheme depends on the final state used in the analysis. For the $\pi^+\pi^-\pi^0\pi^0$ channel only the already mentioned processes are present while for $\pi^0\pi^0\gamma$ there are

Table 1: Fit results for the $e^+e^- \to \pi^+\pi^-\pi^0\pi^0$ and $e^+e^- \to \pi^0\pi^0\gamma$ cross sections.

Parameter	4π channel	$\pi\pi\gamma$ channel
σ_0 (nb)	8.12 ± 0.14	0.776 ± 0.012
$\mathrm{Re}(Z)$	0.097 ± 0.012	0.013 ± 0.013
$\mathrm{Im}(Z)$	-0.133 ± 0.009	-0.155 ± 0.007
σ' (nb/MeV)	0.072 ± 0.008	0.0079 ± 0.0006
χ^2/N_{df}, $P(\chi^2)$	13.4/13 (42%)	12.8/15 (62%)

also contributions from $\phi \to f_0(980)\gamma$ and $\phi \to \rho\pi^0$ which modify the $\sqrt{s}$ behaviour.

The dependence of the cross section on the center of mass energy can be parametrized in the form [50]:

$$\sigma(\sqrt{s}) = \sigma_{NR}(\sqrt{s}) \cdot \left| 1 - Z \frac{M_\phi \Gamma_\phi}{D_\phi} \right|^2 \tag{20}$$

where $\sigma_{NR}(\sqrt{s})$ is the bare cross section for the non-resonant process, Z is a complex interference parameter while M_ϕ, Γ_ϕ and D_ϕ are the mass, the width and the inverse propagator of the ϕ meson, respectively. Since in the considered center of mass energy range the non-resonant cross section increases almost linearly, we assume a simple linear dependence:

$$\sigma_{NR}(\sqrt{s}) = \sigma_0 + \sigma'(\sqrt{s} - M_\phi) \tag{21}$$

The analysis has been performed on ~ 600 pb^{-1} at center of mass energies between 1000 and 1030 MeV. For both final states used in this analysis ($\pi^+\pi^-\pi^0\pi^0$ and $\pi^0\pi^0\gamma$) data are filtered by selecting events with the expected signature. After performing a kinematic fit which improves the energy resolution of photons, specific cuts for background rejection are applied. The measured values of visible cross section are then fitted using as free perameters σ_0^i, $\mathrm{Re}(Z_i)$, $\mathrm{Im}(Z_i)$ and σ_i', where i is the 4π or $\pi\pi\gamma$ final state. In Fig. 10 data points with the superimposed fit function are shown for both channels. The preliminary values for the extracted parameters are reported in Tab. 1.

From the two previous measurements, taking into account the phase space difference between the two decays [50], we obtain: $\Gamma(\omega \to \pi^0\gamma)/\Gamma(\omega \to \pi^+\pi^-\pi^0) = 0.0934 \pm 0.0021$. Since these two final states correspond to $\sim 98\%$ of the ω decay channels, this ratio and the sum of the existing BR measurements on the remaining rarer decays [17] are used to extract the main ω branching fractions imposing the unitarity:

$$BR(\omega \to \pi^+\pi^-\pi^0) = (89.94 \pm 0.23)\% \tag{22}$$

$$BR(\omega \to \pi^0\gamma) = (8.40 \pm 0.19)\% \tag{23}$$

with a correlation of 82%. Comparison between our evaluation and the values reported by PDG [17] is shown in Fig. 10.

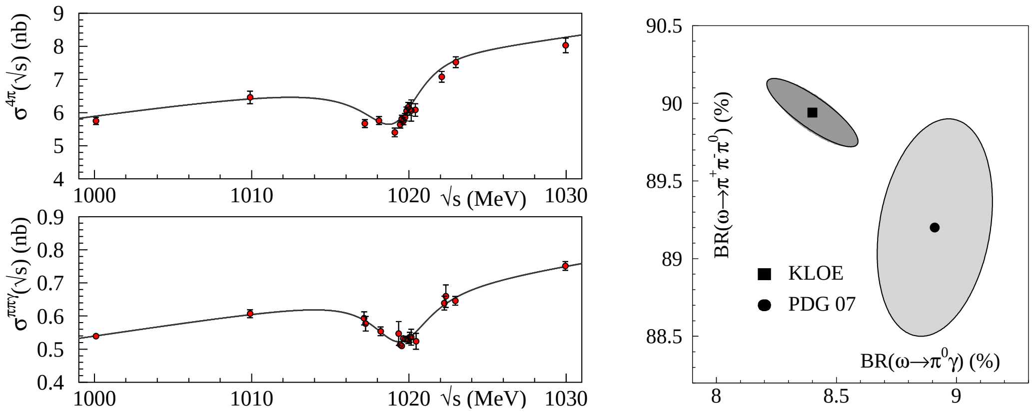

Figure 10: Fit results for the $e^+e^- \to \pi^+\pi^-\pi^0\pi^0$ (top-left) and $e^+e^- \to \pi^0\pi^0\gamma$ (bottom-left) channels. Black dots are data, solid line is the resulting fit function. Right: branching fraction for the two main ω decay channels. The square is the KLOE fit result, while the dot is the PDG constrained fit result. The shaded regions are the 68% C.L.

Using the parameters obtained from the $\pi^+\pi^-\pi^0\pi^0$ analysis, the Γ_{ee} measurement from KLOE [51] for the evaluation of σ_ϕ, and our value for $BR(\omega \to \pi^+\pi^-\pi^0)$, we extract:

$$BR(\phi \to \omega\pi^0) = (5.63 \pm 0.70) \times 10^{-5}, \tag{24}$$

in agreement and with better accuracy with respect to what obtained by the SND experiment ($5.2^{+1.3}_{-1.1} \times 10^{-5}$) [50].

3.4 The measurement of the hadronic cross section

In year 2007, the analyses of the hadronic cross section measurement from KLOE data were further improved. The improvement on our published analysis [52], normalising $\pi^+\pi^-$ events to the Bhabha sample, yielded a preliminary result on $a_\mu^{\pi\pi}$, the low-energy contribution of the hadronic vacuum polarization to the anomalous momentum of the muon. The preliminary result, in the range between 0.35 and 0.95 GeV^2, presented at the 2007 Europhysics Conference in Manchester [53]:

$$a_\mu^{\pi\pi}(0.35, 0.95) = (386.3 \pm 0.6_{stat} \pm 3.9_{syst}) \times 10^{-10},$$

is in perfect agreement with our published result (updated in trigger efficiency and Bhabha reference cross section [54])and with the recent results from SND and CMD2 experiments at Novosibirsk [55].

Work is in progress to finalize this analysis, evaluating all of the systematic uncertainties from event selection, reconstruction and from the theoretical inputs to extract $a_\mu^{\pi\pi}$(s) from the process $e^+e^- \to \pi^+\pi^-\gamma$.

A second analysis, selecting muons from $e^+e^- \to \mu^+\mu^-\gamma(\gamma)$ to extract the pion form factor from the ratio $\frac{d\sigma(e^+e^-\to\pi^+\pi^-\gamma(\gamma))}{ds'} / \frac{d\sigma(e^+e^-\to\mu^+\mu^-\gamma(\gamma))}{ds'}$ still suffers from incomplete understanding of reconstruction and pion contamination of the muon sample. A considerable amount of work has been dedicated to evaluate the muon selection efficiency from independent control samples.

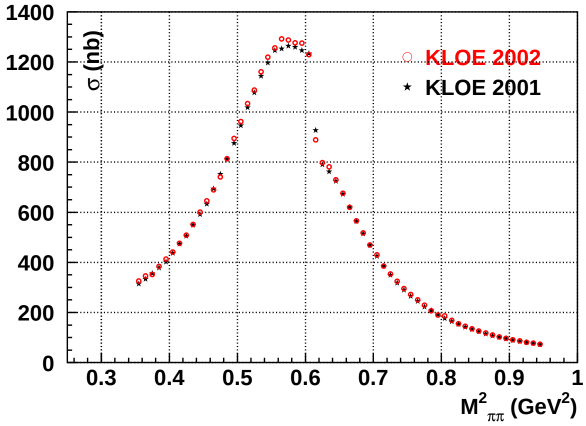

Figure 11: $\sigma_{\pi\pi}$ measured in 2001 (updated for the trigger correction and for the new theoretical Bhabha cross section); and $\sigma_{\pi\pi}$ measured in 2002.

We have organized at LNF the Second Meeting of the Working Group on Radiative Corrections and MC Generators for Low Energies, which brought together theorists and experimentalists to discuss current status and decide the plans for the improvement of the low-energy MC generators. As an outcome of the meeting, a precise comparison of different MC generators used to simulate Bhabha events for the luminosity measurement was performed, and an accuracy on the level of few per mill was found.

4 KLOE papers in year 2007

1. *F. Ambrosino et al.*, "Dalitz plot analysis of $e^+e^- \to \pi^0\pi^0\gamma$ events at $\sqrt{s} \simeq M_\phi$ with the KLOE detector, Eur. Phys. J. **C49** (2007) 2.

2. *F. Ambrosino et al.*, "Measurement of the $K_L \to \pi\mu\nu$ form factor parameters with the KLOE detector", J. High Energy Phys. **12** (2007) 105.

3. *F. Ambrosino et al.*, "Measurement of the pseudoscalar mixing angle and eta' gluonium content with the KLOE detector", Phys. Lett **B648** (2007) 4.

4. *F. Ambrosino et al.*, Precise measurements of the eta meson and the neutral kaon masses with the KLOE detector", J. High Energy Phys.**12** (2007) 073.

5. *F. Ambrosino et al.*, Measurement of the $K_L \to \pi\mu\nu$ form factor parameters with the KLOE detector, J. High Energy Phys. **12** (2007) 105.

6. *F. Ambrosino et al.*, Measurement of the charged kaon lifetime with the KLOE detector, J. High Energy Phys. **01** (2008) 073.

7. *F. Ambrosino et al.*, Measurement of the absolute branching ratios for semileptonic $K^\pm$ decays with the KLOE detector, J. High Energy Phys. **02** (2008) 098.

8. *F. Ambrosino et al.*, V_{us} and lepton universality from kaon decays with the KLOE detector, J. High Energy Phys. **04** (2008) 059.

5 Public notes in year 2007

1. F. Ambrosino, T. Capussela, F. Perfetto " Dynamics of $\eta \to \pi^+\pi^-\pi^0$ " KLOE Note 215, May 2007.

2. M. Antonelli, M. Dreucci, C. Gatti "Measurement of the radiative K0e3 branching ratio and Direct Emission contribution in semileptonic decay $K_L \to \pi e \nu(\gamma)$ ", KLOE Note 216, October 2007.

6 Contributions to Conferences and Seminars

1. *M. Dreucci* , "KLOE Results on neutral kaons", WIN07, Kolkata, Jan 15-20, 2007.

2. *P. de Simone* , "Recent KLOE results", Les Rencontres de Physique de la Vallee d'Aoste, La Thuile, Mar 4-10, 2007.

3. *R. Versaci* , "Observation of the $\eta \to \pi^+\pi^-e^+e^-$ at KLOE", Workshop of the EtaMesonNet, Peniscola, May 10-11, 2007.

4. *B. Sciascia*, "KLOE measurement of the charged kaon absolute semileptonic branching ratios", KAON07, Frascati, May 21-25, 2007.

5. *C. Gatti*, "KLOE measurement of the scalar form factor slope for $K_L \to \pi l \nu$ decays", KAON07, Frascati, May 21-25, 2007.

6. *M. Palutan*, "Experimental Review on Vus extraction from Kaon decays", invited talk, KAON07, Frascati, May 21-25, 2007.

7. *M. Dreucci*, "Measurement of the radiative $K0_{e3}$ branching ratio and Direct Emission contribution in semileptonic decays $K_L \to \pi e \nu(\gamma)$", KAON07, Frascati, May 21-25, 2007.

8. *M. Martini*, "KLOE measurements of the BR($K_S \to \gamma\gamma$) and direct search for $K_S \to e^+e^-$", KAON07, Frascati, May 21-25, 2007.

9. *M. Martini*, "Recent KLOE results on rare processes", EPS-HEP07, Manchester, July 19-25, 2007.

10. *E. De Lucia*, "Vus determination from KLOE", EPS-HEP07, Manchester, July 19-25, 2007.

11. *T. Spadaro*, "Tests of lepton universality at KLOE", EPS-HEP07, Manchester, July 19-25, 2007.

12. *S. Mueller*, "Evaluation of $a_\mu(\pi\pi)$ between 0.35 and 0.95 GeV^2 with data from the KLOE detector", EPS-HEP07, Manchester, July 19-25, 2007.

13. *S. Giovannella*, "Light Meson Spectroscopy", Invited Talk at Lepton-Photon 07, Daegu, Aug 13-18, 2007.

14. *M. Antonelli*, "Precision tests of Standard Model with Kaons", Invited Talk at Lepton-Photon 07, Daegu, Aug 13-18, 2007.
15. *S. Miscetti* "The Flavour of KLOE ... with a byte of hadrons", Invited Seminar at CERN, September 4, 2007.
16. *P. de Simone* "Precision Kaon and Hadronic Physics with KLOE", Invited Seminar at SLAC, October 30, 2007.
17. *R. Versaci*, "Observation of the $\eta \to \pi^+\pi^-e^+e^-$ decay at KLOE", Hadron07, Frascati, Oct 8-13, 2007.
18. *M. Martini*, "KLOE recent results on KS/KL decays", Hadron07, Frascati, Oct 8-13, 2007.
19. *D. Domenici*, "The upgrade of the KLOE detector: KLOE2", Hadron07, Frascati, Oct 8-13, 2007.

References

1. V. Bernard, M. Oertel, E. Passemar and J. Stern, Phys. Lett. B **638** (2006) 480
2. F. Ambrosino *et al.*, KLOE Collab., JHEP **12** (2007) 105.
3. J. Gasser *et al.*, Eur. Phys. J. C40 (2005) 205.
4. B. Kubis, private communication.
5. F. Ambrosino *et al.*, (KLOE Collab.), arXiv:0707.4634 (2007), submitted to EPJC.
6. G. D'Ambrosio and D. Espriu, Phys. Lett. B175 (1986) 237.
7. J.R. Batley *et al.*, NA48 Collab., Phys. Lett. B551 (2003).
8. F. Ambrosino *et al.* (KLOE Collab.), arXiv:0707.3933 (2007), submitted to JHEP.
9. G. Ecker and A. Pich, Nucl. Phys. B366 (1991) 189.
10. A. Angelopoulos *et al.*, CPLEAR Collab., Phys. Lett. B413 (1997) 232.
11. F. Ambrosino *et al.* (KLOE Collab.), arXiv:0707.2687 (2007).
12. I.H. Chiang *et al.*, Phys. Rev. D **6**, 1254 (1972).
13. The NA48/2 Collaboration, Eur. Phys. J. C **50** 329 (2007).
14. V.I. Romanovsky *et al.*, arXiv:0704.2052.
15. M.Antonelli *et al.*, arXiv:0801.1817.
16. F. Ambrosino *et al.*, (KLOE Collab.), arXiv:0707.2654 (Jul 2007).
17. W. M. Yao *et al.*, JP **G 33** (2006) and 2007 partial update for 2008 edition [*http://pdg.web.cern.ch/pdg*]

18. F. Ambrosino *et al.*, KLOE Collab., Eur.Phys.J. C 48 (2006) 767.

19. F. Ambrosino *et al.*, KLOE Collab., Phys. Lett. B636 (2006) 173.

20. F. Ambrosino *et al.*, KLOE Collab., Phys. Lett. B632 (2006) 43.

21. F. Ambrosino *et al.*, J. High Energy Phys. **02** (2008) 098.

22. F. Ambrosino *et al.*, KLOE Collab., Phys. Lett. B632 (2006) 76.

23. F. Ambrosino *et al.*, KLOE Collab., Phys. Lett. B626 (2005) 15.

24. F. Ambrosino *et al.*, KLOE Collab., J. High Energy Phys. **01** (2008) 073.

25. F. Ambrosino, *et al.*, KLOE Collab., Phys. Lett. B 636 (2006) 166.

26. F. Ambrosino *et al.*, KLOE Collab., J. High Energy Phys. **04** (2008) 059.

27. RBC/UKQCD Collaboration, P.A. Boyle, *et al.* arXiv:0710.5136, 2007.

28. W. Marciano *Phys. Rev. Lett.* **93** (2004) 231803.

29. HPQCD/UKQCD Collaboration, E. Follana, *et al.* arXiv:0706.1726, 2007.

30. I.S. Towner and J.C. Hardy, arXiv:0710.3181, 2007.

31. G. Isidori and P. Paradisi, Phys. Lett. B 639 (2006) 499.

32. Belle Collaboration, K. Ikado, *et al.* Phys. Rev. Lett. **97**, 251802 (2006); BaBar Collaboration, B. Aubert, *et al.* arXiv:0705.1820, 2007.

33. M.Finkemeier, Phys. Lett. B **387**, 391 (1996).

34. A.Masiero, P.Paradisi, and R.Petronzio, Phys. Rev. D **74** 011701 (2006).

35. F. Ambrosino *et al.*, (KLOE Collab.), PoS(KAON)050 (May 2007).

36. KLOE Collaboration, F. Ambrosino *et al.*, arXiv:0801.2642.

37. KLOE Collaboration, F. Ambrosino *et al.*, arXiv:0707.4137.

38. G. D'Ambrosio, G. Isidori, Int. J. Mod. Phys. A 13 (1998) 1.

39. J. G. Layter *et al.*, Phys. Rev. Lett. 29 (1972) 316.

40. W. B. Tippens *et al.*, CRYSTAL BALL Collaboration, Phys. Rev. Lett. 87 (2001) 192001.

41. B. Borasoy and R. Nissler, Eur. Phys. J. A 26 (2005) 383.

42. L. G. Landsberg, Phys. Rept. **128** (1985) 301.

43. Jarlskog, C., & Pilkuhn, H., Nucl. Phys. B **1** (1967) 264.

44. A. Faessler, C. Fuchs and M. I. Krivoruchenko, Phys. Rev. C **61** (2000) 035206

45. C. Picciotto and S. Richardson, Phys. Rev. D **48** (1993) 3395.

46. B. Borasoy and R. Nissler, arXiv:0705.0954 [hep-ph].

47. D. N. Gao, Mod. Phys. Lett. A **17** (2002) 1583

48. K. Hagiwara *et al.*, Phys. Rev. D **66** (2002) 010001

49. A. Lopez *et al.* [CLEO Collaboration], Phys. Rev. Lett. **99** (2007) 122001

50. V.M. Aulchenko *et al.*, JETP **90** (2000) 927.

51. F. Ambrosino *et al.* [KLOE Collaboration], PL **B608** (2005) 199.

52. A. Aloisio *et al.*, KLOE Collab., Phys. Lett. B 606 (2005), 12

53. S. E. Müller (for the KLOE Coll.), to apppear in the 'Proceedings of the 2007 Europhysics Conference in Manchester', JoP Conference Series

54. C. M. Carloni-Calame *et al.*, Nucl. Phys. B 758 (2006), 227

55. R. R. Akhmetshin *et al.*, CMD-2 Coll., Phys. Lett. B 648 (2007), 28

LHCb

M. Alfonsi (Dott.), M. Anelli (Tecn.), G. Bencivenni, P. Campana, G. Capon,
M. Carletti (Tecn.), P. Ciambrone, E. Dané (Ass. Ric.), P. de Simone,
A. Di Virgilio (Tecn.), C. Forti, G. Lanfranchi, F. Murtas, M. Pistilli (Tecn.),
M. Poli Lener (Ass. Ric.), R. Rosellini (Tecn.), G. Sabatino (Dott.), M. Santoni (Tecn.),
A. Saputi, A. Sarti (Art. 23), A. Sciubba (Resp.Ass.), S. Valeri (Tecn.), A. Zossi (Tecn.)

In collaboration with:
A. Battisti
In collaboration with the "SSCR":
M. Arpaia, G. Bisogni, A. Cassará, E. Iacuessa, U. Martini

In collaboration with the "Servizio di Elettronica e Automazione":
A. Balla, G. Corradi, G. Felici, M. Gatta, G. Papalino

1 Introduction

The LNF group of LHCb operates on the **muon sub-detector** [1, 2] with responsibilities on detectors (MWPC and GEM), electronics and mechanics.

The mechanical structure of stations M2-M5 (downstream the calorimeters) was completed in 2006 allowing for the installation of the detector in 2007. The station M1 (between RICH2 and calorimeters) is being installed at beginning of 2008.

The M2-M5 installation started in 2006: chambers, gas lines, signal and service cables (LV, HV), have been installed, as well as the MWPC chambers in 2007.

The detector production started in autumn 2003: the MWPC production ended in November 2006, while the GEM production was completed by may 2007. The electronics production started in 2006; the installation of power supplies, HV, LV modules, patch panels, Intermediate Boards (IB) and Off Detector Electronics (ODE) modules was completed in 2007 for the M2-M5 stations.

The installation of the M1 off-detector electronics will start after the tests on cabling connectivity. The M1 installation will be mostly achieved in 2008, while the complete commissioning will end later since the LHC schedule will interrupt the installation works in the experimental area.

2 Multiwire Proportional Chambers

The LNF group of LHCb has the responsibility for the construction of $\sim 1/4$ of the MWPCs of the muon detector. Depending on the position inside the detector, there are different chamber dimensions with different readout: anode pads, cathode pads, anode & cathode pads.

We designed, collaborating with the Ferrara group, all the details of 10 different chambers types (with active dimensions ranging from 29×35 cm^2 to 31×151 cm^2). With these characteristics 292 chambers have been assembled and tested in LNF. The same design is applied to the remaining 1170 chambers that have been built in Ferrara, Firenze, CERN and S.Petersbourg (PNPI).

The MWPC chambers of the LHCb muon detector must fulfill stringent requirements on time response: for triggering purpose $\sim 99\%$ minimum efficiency must be exploited in 20 ns. Each chamber is constituted by four layers assembled as two independent double-gaps with hardwired-OR of the readout. In each 5 mm gap there are 30 microns gold-plated tungsten wires stretched at about 65 grams with a pitch of 2 mm.

2.1 Construction of the MWPCs

During 2007, we have completed the production of all the M2-M5 chambers (except some additional spare chambers) and done most of the M1 chamber production. We have built 59 MWPC chambers for region M1R3 and 61 for M1R4. The M1R3 and M1R4 were assembled in INFN-Firenze and in LNF. The M1R2 were done at CERN.

The detectors for the inner region R1 of station M1 are GEMs, designed and built in INFN-Cagliari and in LNF. The status report on construction and tests of these detectors can be found in Section 3.

2.2 Installation of the MWPCs in the experiment

In 2007 we have completed the installation of the MWPCs of the M2-M5 stations. Only $\sim 1\%$ of the chambers have not been installed because they are being built in PNPI site, together with some additional spare chambers. Below, we briefly describe the main steps of the chamber commissioning, before and after the installation on the support wall.

2.3 Chamber commissioning

All the INFN chambers, sent from LNF to CERN, are tested again in the lab before being installed in the experiment. The commissioning foresees four steps :

- check of gas tightness ;
- high voltage conditioning (check on dark current) ;
- check of electronics behavior (dead channels, noise, etc.) ;
- measurement of cosmic ray rate as a function of high voltage.

This procedure has been applied, in 2007, to all the chambers of different type and readout (M5R4, M5R3, M3R3, M1R4 and M1R3), that have been (or will be) installed on the muon walls on access side of stations M2 to M5 and on the whole station M1.

2.3.1 Measurement of gas tightness

To test the gas tightness, each chamber is inflated, using N_2 gas at an overpressure of 5 mbar: the pressure drop ΔP, with respect to a reference chamber of the same size and geometry that is known to be gas tight, is measured as a function of time. The requirement is that ΔP should be less than 2 mbar/hour. All the chambers tested so far in the lab at CERN (before installation in the experiment) were gas tight. In few cases (less than 5%) it was necessary to improve the sealing of the chambers to achieve the requirements.

2.3.2 *HV training*

Each gas-tight chamber is flushed with nominal gas mixture (40/55/5 $Ar/CO_2/CF_4$) for several hours before starting the HV training. Each chamber is slowly conditioned, with an automated procedure, raising the HV in steps of 100 V, starting from 2.0 kV. The target voltage, for a successful conditioning, is 2.85 kV (well above the operational value): the chamber passes the test if it draws a negligible (<10 nA) dark current at this voltage. All the chambers tested so far did pass the HV training test.

2.3.3 *FEE tests*

Each chamber, according to its type, is read out with several FE boards and we tested:

- that the I2C chain, connecting the various FEBs was working properly ;
- that the internal and external counters on each FEB were giving the same results ;
- if there were noisy/dead channels ;
- if the electronics readout was performing uniformly a counting scan on all the channels at 2.7 kV with the nominal gas mixture.

Using those tests it has been possible to fix connection problems (came up after chamber transportation), cross check noise measurements made at CERN with those made in LNF and fix or replace faulty Front End Boards.

Chambers were also retested in the pit after the installation on the wall. So far, all the installed chambers fulfill the requirements:

- no dead channel, no short circuits ;
- I2C line properly working ;
- ACQ and interal counters consistency ;
- low noise: all channels <1kHz with 8(14)fC threshold for the positive(negative) FE boards.

Figure 1 shows the values of the noise measured for M5R4, M5R3, M5R2, M4R4, M4R3, M4R2, M3R3 and M2R3 chambers respectively, for an 8fC threshold.

2.3.4 *Measurement of cosmic ray rate*

In order to ensure the proper uniformity of the electronics and chamber response we measured the cosmic ray rate as a function of the high voltage: a plateau curve was obtained for each chamber (or group of channels) and disuniformities between different FEBs could be identified and fixed.

As an example, in figure 2, we show the result of an M5R4 chamber: the left plot shows the counting rate in 100s, while the right plot shows the acquisition performed at 2500 V. The counting rate, shown in figure 2(a), has the expected behaviour: a plateau around 2.5 kV (operational voltage) with the expected rate value (i.e. 3 Hz, calculated using the pad area). The acquisitions done at different voltages show a good uniformity: figure 2(b) shows that at 2.5 kV the fluctuations inside each FEB are below 10% and the fluctuations with respect to the chamber average below 20% (fulfilling the requirements).

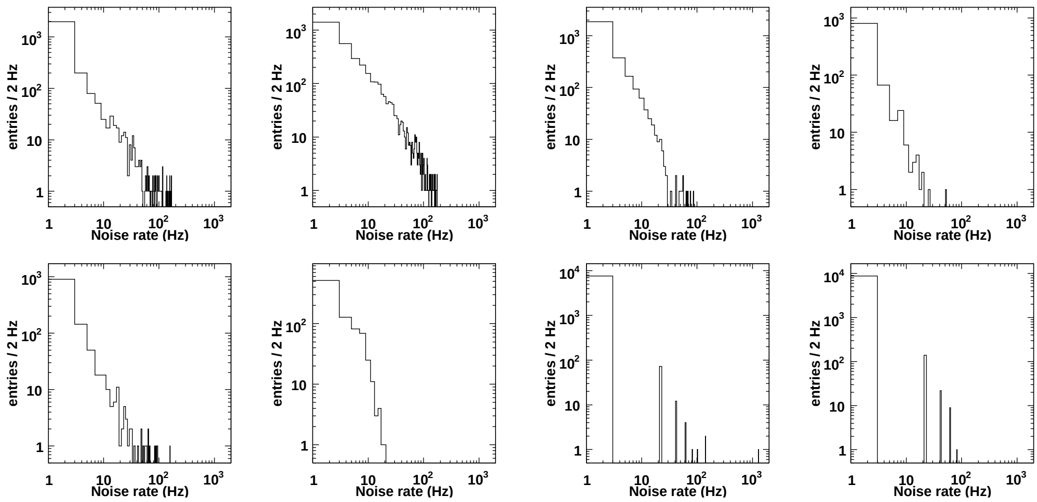

Figure 1: Noise rate values (8 fC threshold) measured from FE boards of M5R4, M5R3, M5R2 and M4R4 chambers (left) and of M4R3, M4R2, M3R3 and M2R3 chambers (right).

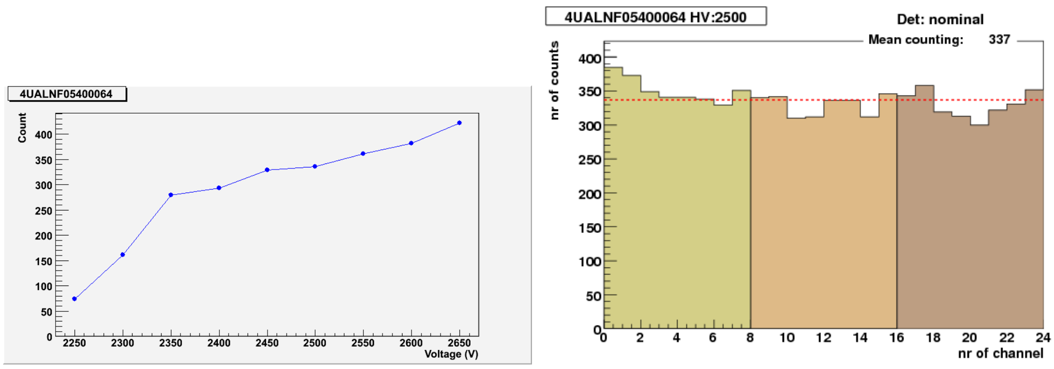

Figure 2: Cosmics acquisition of an M5R4 chamber. Figure (a), on the left, shows the results of the acquisition as a function of the applied HV: the plateau around the operational voltage (2.5 kV) can be seen and the expected rate (3 Hz) is found. Figure (b), on the right, shows the detailed acquisition done at 2.5 kV: the uniformity of the various FEBs is tested and found within the requirements.

2.4 Chamber alignment

Once the chambers are installed on the support wall in the experiment, we repeat once more the tests on gas leakage and on electronics noise. Morevoer, we perform the chamber spatial alignment.

During 2007, much work has been done for the chamber alignment, after installation on the support walls.

Each wall is made of several (5 to 6) panels in Aluminum honeycomb. The panels were glued and riveted together and lifted up one by one, until the whole wall was completed. The walls were dressed with balconies (to handle the chambers) and cable clamps. The design of the walls and of the lifting system was realized in LNF. Tests of resistance to load were performed in LNF using a prototype wall.

The walls were dressed with guides, allowing to close the structure inside the iron filters in a safe way.

The alignment of each wall was measured after assembly. First, we checked the wall planarity. Then, the relative alignment of the walls between them. We plan to verify as soon as possible the alignment of the walls with respect to the beam.

After the installation of the chambers on the wall, each chamber have been aligned with respect to some reference points on the top and the sides of the wall.

3 Triple GEM detectors

The innermost part (regions R1, ~ 0.6 m^2 area) of the first muon station (M1) of the LHCb experiment will be equipped with a detector based on Gas Electron Multiplier (GEM) technology. The responsability of a such detector is shared between LNF and INFN Cagliari. In M1R1 region each detector is composed by two triple-GEM chambers logically OR-ed pad by pad (10×25 mm^2 large) and the requirements are [1]: a rate capability of ~ 500 kHz/cm^2, an efficiency of $\sim 96\%$ in a 20 ns time window and a pad cluster size, i.e. the number of adjacent deetctor pads fired when a track crosses the detector, less than 1.2 for such pad size. In addition the detector must tolerate, without damages or large performance losses, an integrated charge of ~ 0.88 C/cm^2 in 10 years of operation at a gain of $\sim 6\times10^3$ and an average particle flux of 184 kHz/cm^2, for an average machine luminosity of 2×10^{32} $cm^{-2}s^{-1}$.
The GEM [6] consists of a thin (50 μm) kapton foil, copper clad on each side, chemically perforated in order to obtain a high density of holes having bi-conical structure, with external (internal) diameter of 70 μm (50 μm) and a pitch of 140 μm. In safe condition, gains up to 10^4 are reachable using multiple structures, realized assembling more than one GEM at close distance one to each other.
After a long period of R&D, spent to qualify the GEMs as detectors suitable for the harsh environment around the beam pipe of LHCb, we chose to operate the detector with the $Ar/CO_2/CF_4$(45/15/40) gas mixture with an overall gain of $\sim$6000.
In the 2005 the triple-GEM detectors were officially approved by LHC Committee to equip the M1R1 region of the Muon apparatus [7].

In December 2006 the construction and the quality tests of 12 + 6 spare chambers (for the LNF production site) has been completed. The first couples of chambers have been fully instrumented with 24 FEE boards based on CARIOCA-GEM chip. The performances of the detector have been measured in September 2006 at the LNF-BTF beam and at the CERN-SPS beam, confirming the results obtained during the R&D phase [8].

In the 2007 the group was mainly involved in the calibration of the CARDIAC-GEM boards, the instrumentation of the chambers with the FEE and LV boards and HV filters and the tests of the fully equipped detectors.

About 300 FEE boards have been calibrated with a dedicated facility in order to equalize the discriminator threshold of all channels. The equalization has been performed injecting ~ 4, 5 and 6 fC delta signals in each channel of FEE board through a capacity of 20 pF. The efficiency curves ("S-curves") have been measured by scanning the front-end threshold. The threshold values, which allow to reach the 50% of the "S-curves", define the channel linearity.
In Fig. 3 is shown the "S-curves" and the linearity for the first channel of a FEE board.

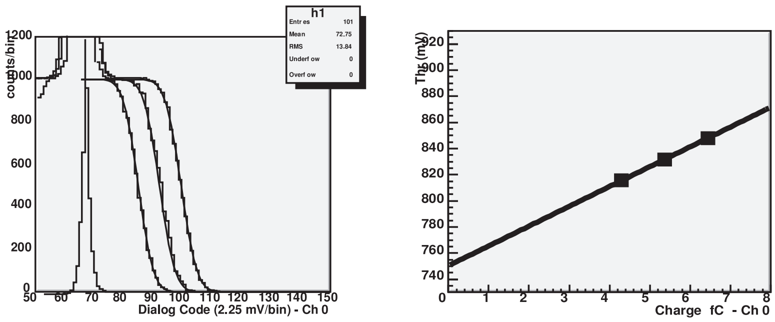

Figure 3: "S-curves" and linearity of the first channel of a CARDIAC-GEM board when are injected 4, 5 and 6 fC delta signals.

In the linearity plot, the y axis intercept defines the minimum charge integrated by the single channel, while the slope of the straight line defines the sensitivity of such channel. The minimum detectable charge (~ 1.5 fC) and the sensitivity (~ 15 mV/fC) distributions of a CARDIAC-GEM board are shown in Fig. 4.

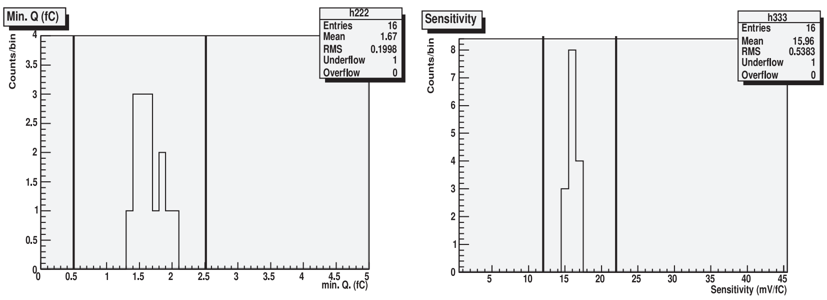

Figure 4: Minimum charge and sensitivity distributions of a CARDIAC-GEM board. The vertical lines indicate the region in which a FEE board is validated.

The instrumentation procedure of M1R1 detectors has been defined in each single step:

- two chambers that pass quality checks (see the activity report of the 2006 for details), are coupled through the four reference pins with the cathodes faced one to each other;
- two HV filters are located between the FEE boards and the detector edges. The filters togheter with a radiation hard RADIAL HV connector are plugged on the corresponding cathode panels;

- CARDIAC-GEM boards, previously calibrated, are installed along the detector perimeter and closed with the faraday cage;
- the low voltage and LVDS signal distribution card is laid on the detector back-plane;
- the I^2C card is fixed on the faraday cage.

The instrumentation phase has been completed by the end of May 2007 (Fig. 5).

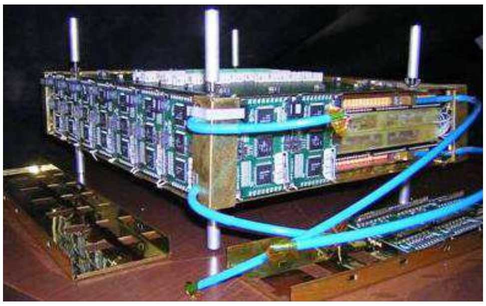

Figure 5: Picture of a M1R1 triple-GEM detector with HV filters, the FEE boards and the distribution card.

All instrumented detectors have been preliminary tested with cosmic rays at LNF and successively at CERN before the installation on the Muon apparatus. Fig. 6(a) shows the noise rate as a function of the FEE threshold at a gain of 4000. The plateau of the curve is due to the expected cosmic rays rate on the detector area (480 cm^2), while the increase of the noise below the threshold of 3 fC is given by some noisy channels.
The uniformity response has been performed with an external scintillator trigger requiring by means the DIALOG the logical AND of the channels in order to eliminate the random noise. Fig. 6(b) shows the cosmic rays rate per 2.5 cm^2 pad area at a gain of 4000 and a FEE threshold of 3 fC.

Tests and checks have been completed by the end of August 2007 and the detectors are ready to be installed in the M1 station (Fig. 7).

In the last part of the year the integration of the detectors in the tight space around the beam pipe has been studied in detail, taking into account all the problems correlated with the cabling and the gas piping required for the operation.
The installation of the gas pipes, the HV and LV, the LVDS and the I^2C cabling will start in January 2007 and will be completed by the end of March 2008.
The installation of detectors is foreseen to start in April 2008, the commissioning phase will follow soon and will be concluded before the first LHC run.

4 Electronics

The LHCb muon trigger architecture relays on 1248 Trigger Sectors (TS) built by the first stages of the front-end electronic chain. About 122,112 physical channels are merged to generate

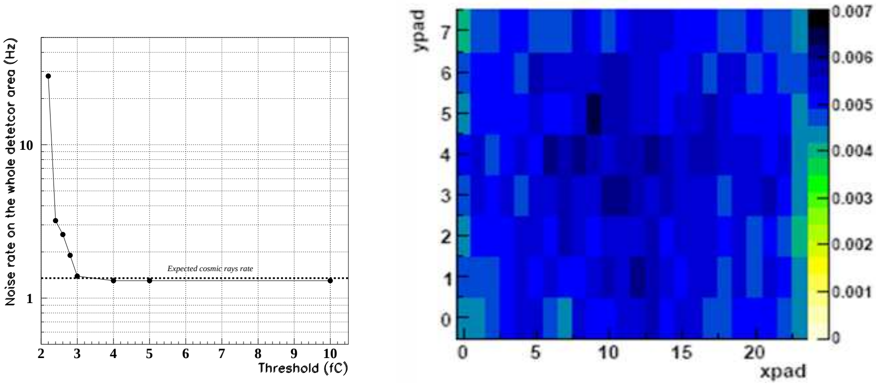

(a) Noise rate on the whole detector area as a function of the FEE threshold. The ~ 1 Hz horizontal line indicates the expected cosmic rays rate on 480 cm^2 detector area.

(b) Cosmic rays rate per pad area (2.5 cm^2) at a FEE threshold of 3 fC obtained with an external scintillator trigger [11].

Figure 6: Cosmic rays tests on a M1R1 detector fully instrumented at a gain of 4000.

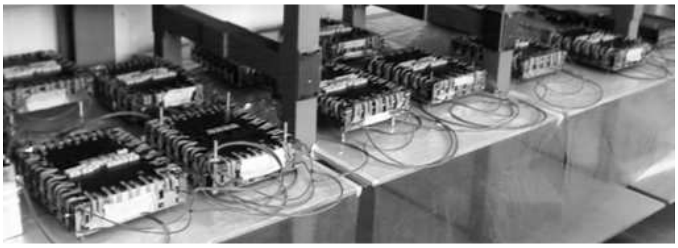

Figure 7: The GEM detectors at the CERN laboratory.

about 26,000 logical channels both in the chamber front-end and in the Intermediate Boards (IB) system and the logical channels are grouped in Trigger Sector in the Off Detector Electronics (ODE) system.

The last two item (IB and ODE systems) are under LNF responsability both for thr project and the production.

The IB system is made of:

- 168 active boards (IB) to generate the logical channels. Each IB board can manage up to 192 LVDS input signals and 60 LVDS output signals. To minimize the number of boards (because the chamber/TS geometries we have 5 different IB I/O configurations) the logic functions have been implemented using programmable devices with 5 different versions of firmware. That choice allowed us to design a single PCB to match the whole detector geometry. The use of anti-fuse technology for programmable devices (ACTEL devices) gives also an intrinsic robustness in moderate radiation environment (like the levels foreseen near the LHCb detector).

- 168 passive Transition Board (TB) to re-arrange in the right way the input signals that are in the same logical channel.

- 12 custom backplanes to interconnect IB and TB boards and to distribute low voltages (+2.5V and + 3.3V) to the IB boards.

During the 2007 the mass production (IB + TB + backplane) has been completed and all the boards tested. A custom test board for IB mapping verification and time skew measurements has been realized and all the IB of the stations M2-M5 have been installed.

The ODE system is made of:

- 152 active boards (ODE). Each ODE board can manage up to 192 LVDS input signals and provide optical interfaces with the trigger system, DAQ system and TFC(time and fast control) system. In the ODE board, the logical channels are synchronized to the bunch crossing, arranged to implement the required TS, and, finally, sent to the Level-0 (L0) trigger logic through 12 parallel optical links at 1,6 Gbit/s. The ODE board also provides a measure of signal arrival times (1.5 ns time resolution) and implements L0-pipelines and DAQ interface via a single 1.6 Gbit/s optical link. The board receives and decodes the syncronization signal and command from TFC via optical receiver and communicates with the ECS (experimental control system) via CANbus interface.

  Because the huge number of input channels per board (192 LVDS) and the very strict requirements on timing performances for optical link connections (less than 100 ps peak to peak on clock jitter) the design of this board has been very challenging. Besides the board has been implemented using radiation tolerant components, while critical components (anti-fuse and flash based FPGA) have been qualified (vs radiation) at the Louvain La Neuve irradiation facility and the firmware has been implemented using triple redundancy technique.

- 152 passive Transition Board (TB) to re-arrange in the right way the input logical channels that are in the same TS. Due to high number of TS topologies, 7 different layouts of TB have been realized.

- 12 custom backplanes to interconnect ODE and TB boards and to distribute low voltages (+2.5V, + 3.3V and +5V) to the ODE boards.

During the 2007 the mass production (ODE + TB + backplane) has been completed and all the boards tested. For the test a custom VME optical receiver board with Bit Error Rate capability has been realized to fully qualified the ODE boards. All the ODE of the stations M2-M5 have been installed and a 192 channels DISPLAY board has been developed to check the signal integrity.

Beside the LNF electronics Workshop has also developed:

- 14 Low Voltage distribution boxes for M1. The box receives 12 high-current low voltage channels (4V/50A) and splits each input channel in 32 low voltage output (4V/1.5A) with overload protection;

- 14 Low voltage systems for the GEM detector. Each system generates 8 low voltage outputs with remote sense for the front end electronics of a double triple gem detector;
- 28 High Voltage filters for the GEM detector. Each filter manages and distributes 7 high voltage lines of a triple gem detector;
- 1 HV power supply system for the GEM detector. The system have 24 modules and each module uses a novel custom architecture that allows to generates 7 high voltage channels connectable in series.

Finally the LNF Electronic Workshop supplies services to the detector setup (chamber/readout installation).

5 Installation of the Muon Station M1

The year 2007 has been dedicated to the preparation of the installation of M1 Muon Station.
The chambers produced in the Ferrara, Florence and Frascati assembly sites have been transferred to the Frascati Gran Sasso Hall where they have been equipped with Faraday Cages, HV supply lines and LV cards, together with FEE electronics.

A total of 60 M1R3 (see Fig. 8) and 200 M1R4 have been prepared and tested for gas tightness, trained with HV and measured for the noise level. This set of chambers has been sent to CERN in three different shipments during the year. Upon arrival at CERN, the same batch of detectors is being tested again, to check for possible defects arose during transport. None of these chambers showed non-conformities. The testing procedure will continue during the first months of 2008.

The LHCb-Gem groups in Cagliari and Frascati have performed the same kind of activity for M1R1 detectors. The mounting of the Faraday Cages and of LV, HV and FEE electronics has been completed during 2007 and afterwards the GEMs have been successfully tested at CERN at the end of the year and are ready to be installed.

The preparation of all the material related to the electronics and to the services for M1 has been completed in 2007. Racks, crates, HV system, LV supply, ODE and TB boards, long cables to the barracks, cables for the detectors, etc. are ready and shipped to CERN.

The installation of electronic boards in the crates will start in early 2008. This part of the work has been realized under the supervision of Frascati, with the support of the LNF Electronics Group.

A huge effort has been put in the preparation of the mechanics of the M1 Station. This station, being inserted between the RICH2 and the Preshower detectors, has very little room (some 40 cm) for the installation and deserves special attention to the mechanical issues. Moreover, the station has to comply with as small as possible material budget (being in front of the calorimeters) and to face the presence of approximately 40% of the total amount of electronic channels of the whole Muon detector. The high electronics density on one hand requires air-cooling, on the other

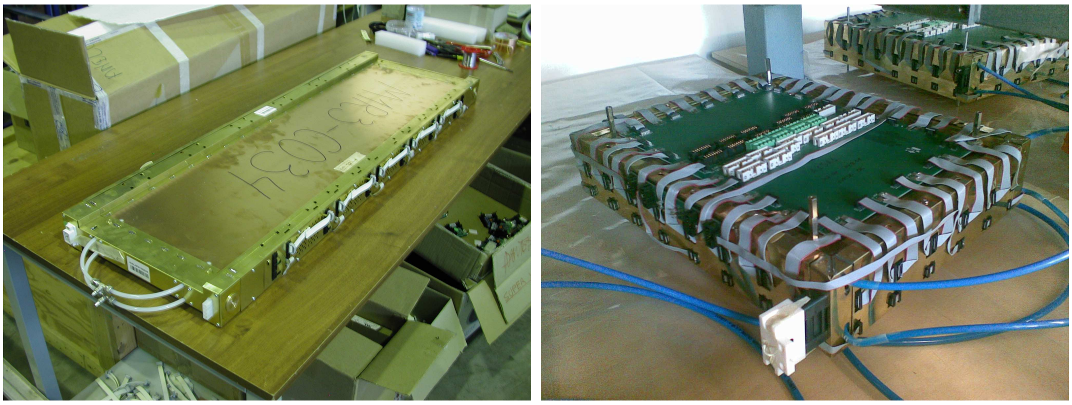

Figure 8: M1R3 - MWPC (left) and M1R1 - GEM (right) detectors

hand the large amount of cables (approximately 1,200) that must be movable together with the station, makes the whole project a real challenge.

Figure 9: Layout of the M1 station

The layout of the station is shown in Fig. 9. To reduce the material budget, the wall (approx 10x5 m2, divided in two parts) has been built with very light aeronautical aluminium honeycomb panels (made by Cospal company). The panels holding the chambers have been made mobile, attaching them to a chariot hold by a support beam at approximately 7 m height. The wall was subdivided into smaller units, so to make possible their assembly in the pit. All the mechanics of M1 is under the responsibility of LHCb-Frascati group and a team from the LNF Workshop has installed the two walls during the summer 2007, and will continue the job of mechanics installation in 2008.

An important item of the project has been the design of the moving system for the cable chain, its support, the mechanical system to attach the chambers to the wall, and the exact routing of all services (LV, Gas, HV, signal and control cables). Again, the work has been particularly difficult due to the limited space available and the constraints mentioned above. Part of this work is still in progress, and it will be completed in the first months of 2008.

As soon as the wall has been assembled and preliminary aligned, a team of technicians from various LHCb Muon-INFN groups have started the cabling of the Gas and LV lines. The plan is to complete the installation of the cable chain and of its moving system by spring 2008 and then start the cabling of services on the wall. The whole services installation should be completed by the end of April. Again, this part of the installation is under responsibility of Frascati and is done with the help of technicians from LHCb Muon-INFN sections.

After that, the installation, alignment and debug of the chambers can start. As of today, it is not clear if the LHC schedule will allow having a complete M1 at the very start-up of the machine. Should not be the case, the completion of M1 will be done during the winter 2008 shutdown. The absence of M1 will not degrade the data taking of 2008 (if any), as the run is considered preliminary for the whole detector.

6 Software and analysis work

The software activities in 2007 were mainly focused on the physics that LHCb can do with the first data.

The analysis of B→hh decays, started in 2006, has been continued in 2007: the performances of the analysis strategy have been assessed on refined MC production, the sensitivities on CKM angle gamma have been crosschecked with a new fit strategy and the simultaneous approach has been developed. So far the B→hh analysis is one of the most advanced and complete in LHCb: selections, performances and systematic studies have been reported in a public LHCb note [12] that will be used as a supporting document for the CERN yellow report of the Flavour in the LHC Era workshop report.

The first years physics will be dominated by muon channels: in particular the $b \to J/\Psi X$ channels ($B_d \to J/\Psi(\mu\mu)K_S$ golden channel for the $\sin(2\beta)$ measurement, $B_s \to J\Psi(\mu\mu)\Phi)$ golden channel for ϕ_s measurement, $B^{\pm} \to J/\Psi(\mu\mu)K^{\pm}$ and $B_d \to J/\Psi(\mu\mu)K^*$ control channels for tagging and proper time calibration) and the very rare channel $B_s \to \mu^+\mu^-$.

The Frascati group is involved in all the physics items listed above and in the related software activities, as explained in detail below.

- **Development of the Muon identification procedure and methods to calibrate it with the first data**

The Muon identification procedure in LHCb is beeing developped by LNF in collaboration with a group from Rio de Janeiro. The procedure is based on the energy released in the calorimeter and on the hits position in the muon chambers.

Monte Carlo simulations show that we can reach an efficiency of identification for muons of $\sim 95\%$ and a misidentification rate for hadrons of $\sim 3\%$ for tracks with momentum down to 3 GeV/c. This procedure will be calibrated with data by using pure samples of muons and hadrons selected without using the Muon System.

Several samples will be used depending on the luminosity delivered:

1. muons from prompt $J/\Psi(1S) \rightarrow \mu^+\mu^-$ selected by using kinematics and MIP peaks in the electromagnetic and hadron calorimeters. With $\sim 10^9$ minimum bias events (which corresponds to ~ 100 seconds of running at nominal luminosity) we should have $\sim 10^4$ events with $J/\Psi(1S) \rightarrow \mu^+\mu^-$ reconstructed and selected. The same procedure will be applied to J/Ψ from b decays (a factor ~ 100 less abundant with respect to J/Psi prompt) as soon as the luminosity will increase.
2. hadrons from $\Lambda(1115) \rightarrow \pi p$ and prompt $K_s \rightarrow \pi^+\pi^-$ decays: these channels are quite abundant since the very beginning (in 10^9 minimum bias events we have several millions of events reconstructed and selected) and very easy to be selected given the very long lifetimes of K_S ($\tau = 89$ ps) and Λ ($\tau = 263$ ps) and the two body decay kinematics. In particular the simultaneous use of protons and pions will allow to separate in the muon misidentification rate the contribution of decays in flight from punch-through and combinatorics.
3. hadrons from the $D^{*\pm}(2010) \rightarrow D^0(K^\pm\pi\mp)\pi^\pm$ decays: the over-constrained chain of the D^* decay will give kaons and pions of high purity that will be used both for the muon misID rate evaluation and for RICH calibration.

This study has been included in the report given to the Commissione Nazionale 1 in the September 2007 (Conference Talks n.1).

- **Unified selection of $B_d \rightarrow J/\Psi K_S$, $B_s \rightarrow J/\Psi\Phi$, $B^\pm \rightarrow J/PsiK^\pm$ and $B_d \rightarrow J/PsiK^*$ channels**:

The Frascati group is developing in collaboration with the group of INFN Milano Bicocca and a French group from Marseille a unified selection for the four decay channels listed above. The idea, with respect to other selections currently present in the Collaboration, is to develop a selection as much similar as possible among signal and control channels in order to minimize the systematics: in fact if the channels cover the same phase space it is safer to transfer the efficiencies values, the tagging dilution and the proper time resolution from the control to the signal channels. Moreover the selection is lifetime unbiased in order to avoid dangerous acceptance corrections in the measurement of time-dependent CP asymmetries. The work is being worked out. A talk related to this issue has been presented in the italian Workshop *IV Incontro sulla Fisica del B*, Bologna, February 2007 (Conference Talks n.3).

- **Measurement of the very rare $B_s \to \mu^+\mu^-$ decay**:

  The $B_s \to \mu^+\mu^-$ is a Flavour Changing Neutral Current decay with a very small BR in the Standard Model, $BR = (3.4 \pm 0.5) \times 10^{-9}$. However, new physics contributions can enhance significantly this value: for example in the MSSM the BR is proportial to $\tan^6 \beta$, being $\tan \beta$ the ratio of the vacuum expectation values of the two neutral and CP-even Higgs. The actual limit from CDF Collaboration, $BR < 47 \times 10^{-9}$@90% CL, is still a factor $\sim$14 above the SM predictions.

  The analysis strategy for the measurement of the $BR(B_S \to \mu^+\mu^-)$ is beeing designed by a mixed group of researchers from CERN, University of Barcelona, University of Santiago de Compostela, NIKHEF and INFN-LNF. In particular, the LNF group is taking care of the part of the analysis related with the Muon identification and misidentification capability and therefore with the critical issue of the control of the backgrounds.

  Monte Carlo simulations show that the LHCb potential to perform this measurement is very high: LHCb can bring down the present CDF limit to 5×10^{-9}@90% CL with only 0.5 fb^{-1} of integrated luminosity.

  Results about the LHCb potential in measuring this BR have been reported in Commissione Nazionale 1 (November 2007) (Conference Talks n.3) and to an International Conference (Conference Talks n.4).

7 List of Conference Talks by LNF Authors in Year 2007

- G. Lanfranchi, *Start-up Strategy of LHCb experiment*, Talk given in Commissione Nazionale 1, Laboratori Nazionali di Frascati, September 17th, 2007.

- G. Lanfranchi, *Time dependent decay asymmetries at LHCb*, IV Incontro sulla Fisica del B, Bologna, 13-24 February, 2007.

- G. Lanfranchi, *LHCb potential for the search of the decay* $B_s \to \mu^+\mu^-$, Talk given in Commissione Nazionale 1, November 2007.

- G. Lanfranchi, *Search for the* $B_s \to \mu^+\mu^-$ *decay at LHCb*, Lake Louise Winter Institute (Alberta, Canada), 19-24 February, 2007.

- M. Alfonsi *et al.*, "Status of the triple GEM Muon chambers for the LHCb experiment", presented at the 11th Vienna Conference on Instrumentation, Vienna (Austria), February 19-24, 2007.

- M. Alfonsi *et al.*, "GEM detectors activity at the Laboratori Nazionali di Frascati of INFN", presented at the 10th ICATPP Conference on Astroparticle, Particle, Space, Detectorsand Medical Applications, Villa Olmo, Como (Italy), October 8-12, 2007.

- M. Alfonsi *et al.*, "The commissioning of the GEM detector for the Muon Apparatus of the LHCb experiment", presented at the Nuclear Science Symposium and Medical Imaging Conference, Honolulu, Hawaii (U.S.A.), October 27 - November 3, 2007.

References

1. LHCb Collaboration, "LHCb: muon system technical design report", CERN LHCC MUON 2001-010, LHCb TDR 4, 28 May 2001.

2. LHCb Collaboration, "LHCb: Addendum to muon system technical design report", CERN LHCC MUON 2003-002, LHCb TDR 4 Addendum 1, 15 January 2003.

3. M. Anelli *et al.* "Quality tests of the LHCb muon chambers at the LNF production site ", Poster presented at the IEEE 2004 (Rome, Italy, October 16-22, 2004), and submitted to Transaction on Nuclear Science.

4. D.Pinci and A.Sarti, "Production and test of the LHCb Muon Chambers", presented at Hadron Collider Physics Symposium (HCP05), Les Diablerets, Switzerland July 4-9, 2005.

5. M. Anelli *et al.*, "Test of a MWPC for the LHCb Muon System at the Gamma Irradiation Facility at CERN", Public Note LHCb MUON-2005-003. `http://cdsweb.cern.ch/search.py?recid=815058&ln=en`

6. F. Sauli, Nucl. Instrum. Meth. **A386** (1997) 531.

7. LHCb Collaboration, "LHCb: Second addendum to muon system technical design report", CERN LHCC MUON 2005-012, LHCb TDR 4 Addendum 2, 9 April 2005.

8. M. Alfonsi *et al.*, Nucl. Instrum. Meth. **A581** (207) 283.

9. M. Alfonsi *et al.*, presented at Puerto Rico 2005 IEEE conference (Oct. 23-29) and submitted to Transaction on Nuclear Science.

10. A. Balla *et al.*, Muon Off-Detector electronics: The IB system, LHCb note, LHCb 2003-023.

11. W. Bonivento *et al.*, Test with cosmics of the GEM chambers for the LHCb muon system produced in Cagliari, LHCb Note 2007-110.

12. A. Carbone,J. Nardulli, S. Pennazzi, **A. Sarti**, V. Vagnoni, "Charmless charged two-body B decays at LHCb", CERN-LHCB-2007-059

P326

A. Antonelli (Resp.), P. Cooper (Osp.), B. Dulach (Tecn.), G. Maccarrone,
M. Moulson, M. Raggi (Ass. Ric.), T. Spadaro

1 The P326 Experiment

The branching ratio (BR) for the decay $K^+ \to \pi^+ \nu\bar{\nu}$ can be related to the value of the CKM matrix element V_{td} with minimal theoretical uncertainty, providing a sensitive probe of the flavor sector of the Standard Model. The measured value of the BR is $1.47^{+1.30}_{-0.89} \times 10^{-10}$ on the basis of three detected events [1]. P326, an experiment at the CERN SPS, has been proposed with the goal of detecting $\sim$100 $K^+ \to \pi^+ \nu\bar{\nu}$ decays with a S/B ratio of 10:1 [2]. The experimental layout is illustrated in Fig. 1.

The experiment will make use of a 75 GeV unseparated positive secondary beam. The total beam rate is 800 MHz, providing $\sim$50 MHz of K^+'s. The decay volume begins 102 m downstream of the production target. 10 MHz of kaon decays are observed in the 120-m long vacuum decay region. Ring-shaped large-angle photon vetoes are placed at 12 stations along the decay region and provide full coverage for decay photons with 8.5 mrad $< \theta <$ 50 mrad. The last 35 m of the decay region hosts a dipole spectrometer with four straw-tracker stations operated in vacuum. The NA48 liquid krypton calorimeter [3] is used to veto high-energy photons at small angle. Additional detectors further downstream extend the coverage of the photon veto system (e.g. for particles traveling in the beam pipe).

The experiment must be able to reject background from, e.g., $K^+ \to \pi^+\pi^0$ decays at the level of 10^{12}. Kinematic cuts on the K^+ and π^+ tracks provide a factor of 10^4 and ensure 40 GeV of electromagnetic energy in the photon vetoes; this energy must then be detected with an inefficiency of $\leq 10^{-8}$. For the large-angle photon vetoes, the maximum tolerable detection inefficiency for photons with energies as low as 200 MeV is 10^{-4}. In addition, the large-angle vetoes must have good energy and time resolution and must be compatible with operation in vacuum.

In 2007, the main involvement of the LNF P326 group was in the development and testing of prototype photon veto detectors, in order to guide the choice of technologies to be used in the experiment. In addition, the group participated in the summer/fall 2007 run of NA62, a P326 precursor in which the NA48 apparatus was used to collect data for a measurement of $R_K \equiv \Gamma(K_{e2})/\Gamma(K_{\mu 2})$. LNF group members played a significant operational role in data taking and continue to be centrally involved in data analysis.

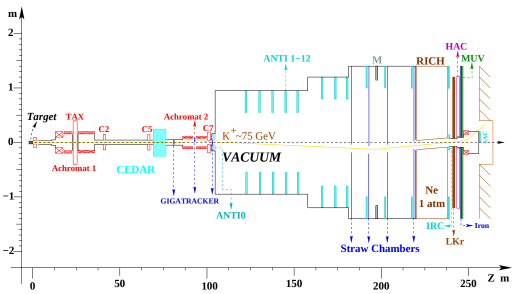

Figure 1: The P326 experimental layout.

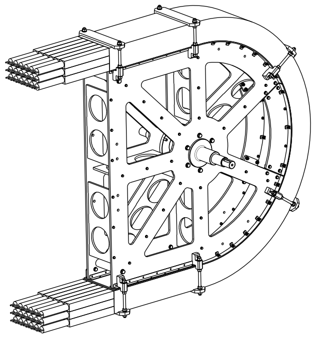

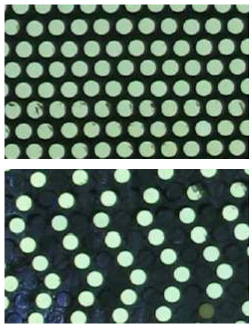

Figure 2: Left: Schematic diagram of the fiber prototype attached to construction saddle. Right: Photographs of fiber fill patterns in the (top) first four and (bottom) last two cells in longitudinal depth.

2 Large-Angle Photon Vetoes

Two designs were initially considered for the construction of the veto detectors. One consists of a sandwich of lead sheets and scintillating tiles with WLS-fiber readout. An example of such a detector, using 80 layers of 1-mm thick lead sheets and 5-mm thick scintillating tiles, had been designed for the (now canceled) CKM experiment at Fermilab. Tests of a prototype at Jefferson Lab had showed that the inefficiency of the detector for 1.2 GeV electrons was at most 3×10^{-6} [4]. An alternative solution is based on the design of the KLOE calorimeter [5], and consists of 1-mm diameter scintillating fibers sandwiched between 0.5-mm thick lead foils. The fibers are arranged orthogonal to the direction of particle incidence and are read out at both ends. Two U-shaped modules form a veto station. This solution offers advantages in terms of hermeticity, position resolution, and time resolution. Since a prototype based on the tile design had already been tested, we chose to construct and test a prototype fiber module. We obtained the CKM prototype on loan for further testing and comparison.

2.1 Construction of the fiber prototype

One U-shaped module was constructed at Frascati in fall 2006 (Fig. 2, left). The inner radius (60 cm) and length (310 cm along the inner face) of the prototype are identical to the specified values for one of the upstream veto stations in the actual experiment. The prototype has a radial thickness of 12.5 cm, corresponding to 35% of the specified value for one of the upstream stations. This thickness was chosen to reduce prototyping costs; it is sufficient for transverse containment of low-energy electron showers incident half-way between the inner and outer edges of the module.

For construction of the prototype, we designed the steel and aluminum support structure, or "saddle," seen in Fig. 2 (left). The lead foils were grooved using a rolling machine built for the construction of the KLOE calorimeter [5]. With the curved surface of the saddle upwards, a foil was draped over the saddle, the surface of the foil was painted with optical cement, and fibers were laid into the grooves. The fibers were then painted with optical cement, and the next foil was draped on top, providing the bottom surface of the next layer. The desired radial thickness was obtained by stacking 99 layers. The ends of the module were then milled and fitted with 4.2×4.2 cm^2 lucite light guides terminating in Winston-cone concentrators. This determines the segmentation of the module in the plane transverse to the fibers—there are three readout cells in the radial direction and six cells in depth. Light from the fibers is read-out by Hamamatsu R6427 28-mm photomultiplier tubes (PMTs) coupled to the light guides with optical grease.

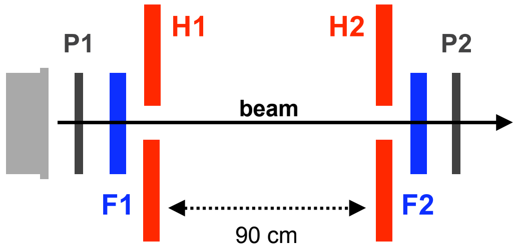

Figure 3: Schematic diagram of the beam tagging system, comprising two paddles for single-electron event selection (F1, F2), two hole counters for trajectory definition (H1, H2), and two beam-profile monitors for alignment (P1, P2).

In the region covered by the first four cells in depth, every groove in the lead is occupied by a scintillating fiber. In the region covered by the last two cells, the scintillating fibers in alternating grooves are replaced by lead wire. This reduces the number of scintillating fibers by 17% and increases the thickness of the module in radiation lengths. The resulting fill pattern is illustrated in Fig. 2 (right). The first four cells in depth contain lead, fiber, and glue in the proportions 42:48:10 by volume, for a thickness of $13X_0$. For the last two cells, the proportions are 66:24:10, for a thickness of $10X_0$.

2.2 Other prototypes

As described in Sec. 2, the prototype lead/scintillating-tile photon veto detector constructed for the CKM experiment was obtained on loan from Fermilab for testing and comparison. This detector is fully described in Ref. 4.

In addition, 3800 modules from the central part of the OPAL electromagnetic calorimeter barrel [6] recently became available for use in P326. These modules consist of blocks of SF57 lead glass with an asymmetric, truncated square-pyramid shape. The front and rear faces of the blocks measure about 10×10 cm^2 and 11×11 cm^2, respectively; the blocks are 37 cm long. The modules are read out at the back side by Hamamatsu R2238 76-mm PMTs, coupled via 4-cm cylindrical light guides of SF57. There are obvious practical advantages to basing the P326 large-angle photon veto system on existing hardware; the collaboration is actively seeking to understand whether these Cerenkov radiators are suitable. For most of our beam tests, we used a tower of four lead-glass blocks, with the beam centrally incident on the side face of the first module. In this configuration, the stack was $\sim$40 cm ($27X_0$) deep.

2.3 Prototype tests at the LNF Beam-Test Facility

The fiber prototype was first tested at the BTF during two-week runs in March and April 2007. During the April run, the tile prototype was also tested. These runs served primarily to debug the prototypes and optimize the tagging system.

The telescope of scintillation counters used to tag single-electron events is schematically illustrated in Fig. 3. F1 and F2 are scintillator paddles of area 60×85 mm^2; H1 and H2 are larger paddles with 14-mm diameter holes in the center. All paddles are 10 mm thick. The tagging criterion for single-electron events used in the efficiency studies was $\mathrm{F1} \cdot \overline{\mathrm{H1}} \cdot \overline{\mathrm{H2}} \cdot \mathrm{F2}$, where F1 and F2 refer to charge signals on the paddle counters consistent with passage of a single electron, and $\overline{\mathrm{H1}}$ and $\overline{\mathrm{H2}}$ refer to null signals on the hole counters. Acceptable beam trajectories were thus defined by the two 14-mm diameter holes separated by 90 cm. The tagging system was mounted on a rigid support structure allowing fine and reproducible positioning of all counters in the horizontal

Prototype	Beam energy [MeV]	Tagged events
Fiber (KLOE)	203	70k
	350	210k
	483	370k
Tile (CKM)	203	65k
	350	220k
	483	370k
Lead glass (OPAL)	203	25k
	483	90k

Table 1: Statistics Collected During the Summer 2007 BTF Run

and vertical coordinates. We designed and constructed the support structure and refurbished all four trigger counters for the June-July 2007 run.

The bulk of our data were collected during a 25-day run during June-July 2007. For the fiber and tile prototypes, data were taken at beam energies of 203, 350, and 483 MeV. For the lead-glass detectors, data were taken at beam energies of 203 and 483 MeV. Table 2.3 summarizes the data collected. In tests of the tile prototype at Jefferson Lab, data were taken at beam energies of 500, 800, and 1200 MeV. Our tests thus extend to significantly lower beam energies the experimental knowledge of the detection efficiency for this prototype.

In addition to the data samples listed in Table 2.3, for each detector, smaller samples were also collected in a variety of configurations with the beam incident at different points and/or at different angles.

The BTF hosts an apparatus for producing a tagged photon beam, originally developed for testing the AGILE satellite gamma-ray telescope [7]. While the tagged photon beam has been used with some success for energy calibration, e.g., of the AGILE satellite, at present, background levels in the photon beam are prohibitive for sensitive efficiency measurements. This background consists of photons from showering on upstream beam elements by particles from the attenuating target. This was the basis for our decision to use the electron beam to test the prototypes.

2.4 Results obtained with the fiber prototype

2.4.1 Energy and time resolution

To obtain the energy resolution, we perform Gaussian fits to the single-electron peak after run-by-run energy scale calibration is applied. In Fig. 4 (left), we plot the relative energy resolution, σ_E/E_{meas}, as a function of E_{beam}, for the measurements from each side of the prototype and for the combined measurement. The curves in Fig. 4 show the results of fits to the form

$$\frac{\sigma_E}{E} = \frac{p_1}{\sqrt{E}\,(\text{GeV})} \oplus p_2.$$

Using the information from both sides of the prototype, we find $p_1 = 5.1\%$ and $p_2 = 4.4\%$. The coefficient obtained for the stochastic term (p_1) is in reasonable agreement with expectation from our preliminary Monte Carlo studies and from experience with the KLOE calorimeter.

For the tests described here, the beam was incident at the midpoint of the fibers; we therefore have independent time measurements from each side of each cell. The time measurements for sides

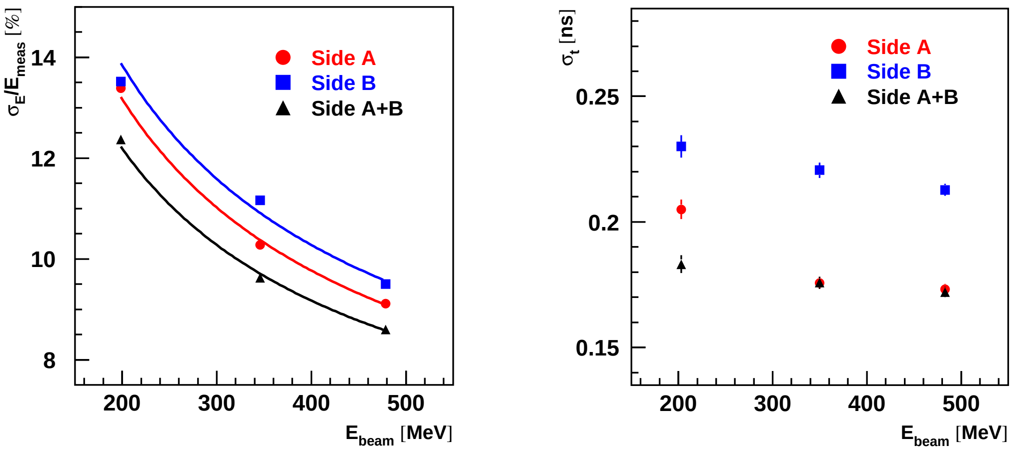

Figure 4: Energy (left) and time (right) resolution for the fiber prototype at $E_{\mathrm{beam}} = 203$, 350, and 483 MeV.

A and B, t_{A} and t_{B}, and the combined time measurement $t_{\mathrm{A+B}}$, are taken to be the energy-weighted averages of the time measurements for the corresponding group of cells. The event time reference is provided by the tagging system: $t_{\mathrm{tag}} \equiv (t_{\mathrm{F1}} + t_{\mathrm{F2}})/2$, where F1 and F2 are the trigger paddles described in Sec. 2.3. The time resolution of the tagging system is found to be $\sigma_{\mathrm{tag}} \approx 147$ ps and stable for points with different E_{beam}.

Our results on the time resolution are still preliminary. They are plotted in Fig. 4 (right) as a function of E_{beam}. For the point at 483 MeV, the resolution for the combined measurement is $\sigma_{\mathrm{A+B}} = 172$ ps, of which 158 ps is due to the common-mode fluctuation in the time measurements from each side.

2.4.2 Efficiency

Our measurements of the detection efficiency are summarized in Fig. 5. For each beam energy, the panel on the left shows the energy distribution for all collected events (open histogram) and for fully-tagged events (shaded) histogram. The one- and two-electron peaks are clearly visible in the distribution for all events; application of the tagging criterion reduces the contribution from multiple-electron events to a level negligible for our purposes.

We consider a fully-tagged single-electron event to be undetected if the measured energy is below a threshold value of $E_{\mathrm{thr}} = 50$ MeV. At $E_{\mathrm{beam}} = 203$ MeV, we find five such events out of 68 829 total tagged events; at $E_{\mathrm{beam}} = 350$ MeV, we find three out of 207 385; and at 483 MeV, we find one out of 371 633. We thus quote inefficiencies of $7.3^{+4.1}_{-3.3} \times 10^{-5}$, $1.4^{+1.1}_{-0.9} \times 10^{-5}$, and $2.7^{+4.7}_{-1.7} \times 10^{-6}$, respectively, where the asymmetric uncertainties represent 68.27% unified confidence intervals [8]. We assume that no undetected events are due to false tags.

The choice of threshold $E_{\mathrm{thr}} = 50$ MeV is reasonable but arbitrary. For each beam energy, we obtain the inefficiency as a function of threshold from the normalized cumulative energy distribution for fully-tagged events. The results are presented in the right panels of Fig. 5. One again, the shaded bands indicate 68.27% unified confidence intervals, and we assume that there are no false tags. For $E_{\mathrm{beam}} = 203$ MeV, the inefficiency remains at the level of a few per mil even for thresholds as high as 100 MeV.

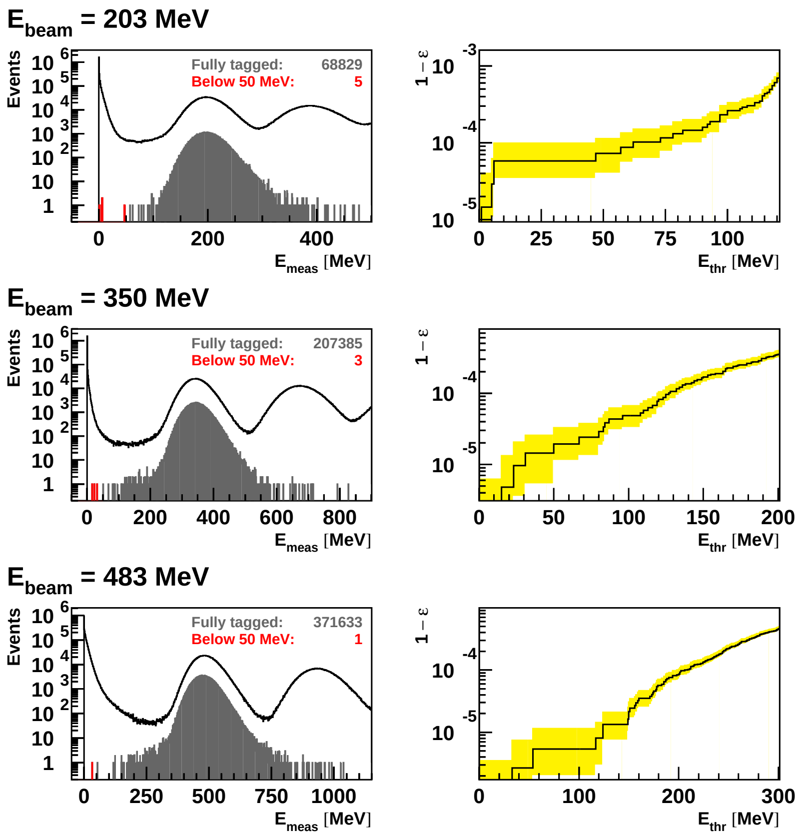

Figure 5: Measurements of detection efficiency for electrons with $E_{\mathrm{beam}} = 203$, 350, and 483 MeV. Left: Measured energy distributions for all events (open histograms) and for fully tagged events (shaded histograms). Right: Inefficiency as a function of E_{thr}.

2.4.3 Comparison with other prototypes

The analysis of the data from the tile and lead-glass detectors is not yet complete, in particular with respect to the final, run-dependent energy calibrations. Nevertheless, we believe that our preliminary results on the detection efficiencies for these prototypes are sufficiently stable to provide meaningful comparison with the results obtained with the fiber prototype. The results obtained for the inefficiency with $E_{\mathrm{thr}} = 50$ MeV for all three prototypes are summarized in Fig. 6. The efficiency for detection of low-energy electrons is seen to be similar for all three technologies tested. However, the detection efficiency for photons may be worse, whether because of punch-through, or because of a high intrinsic inefficiency for the detection of photonuclear interactions [9, 10].

Since there is a significant practical advantage to basing the P326 photon vetoes on existing hardware, our focus for the near-term future will be on investigation of the OPAL lead-glass modules as an appropriate technology on which to base the P326 low-energy photon vetoes.

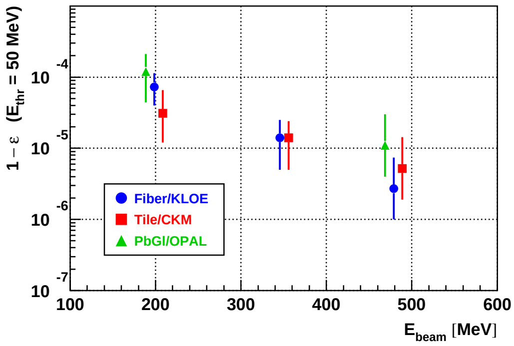

Figure 6: Comparison of detection efficiencies for each of the three prototypes, for 203, 350, and 483 MeV electrons with $E_{\rm thr} = 50$ MeV. Results obtained with the CKM tile prototype and OPAL lead-glass modules are preliminary.

3 NA62 and the Measurement of R_K

3.1 The ratio $K_{e2}/K_{\mu 2}$

Despite poor knowledge of the meson decay constants, ratios of leptonic decay rates of pseudoscalar mesons such as $R_K \equiv \Gamma(K_{e2})/\Gamma(K_{\mu 2})$ can be predicted with high accuracy within a given model, and have been considered to be stringent tests of the $V - A$ structure of the weak interaction and of lepton universality. By convention, the definition of R_K includes the contribution of inner bremsstrahlung (IB) to the radiative $K_{l2\gamma}$ width, while the structure-dependent processes are considered as background. The Standard Model prediction is [11]:

$$R_K^{\rm SM} = \left(\frac{m_e}{m_\mu}\right)^2 \left(\frac{M_K^2 - m_e^2}{M_K^2 - m_\mu^2}\right)^2 (1 + \delta R_{\rm QED}) = (2.477 \pm 0.001) \cdot 10^{-5} \quad (1)$$

where $\delta R_{\rm QED} = -3.6\%$ is a correction due to the contributions to the $K_{l2\gamma}$ width from IB and virtual photon processes. A recent theoretical study [12] points out that lepton-flavor violating effects arising in supersymmetric extensions of the Standard Model can induce sizable violations of $\mu - e$ universality, shifting the value of R_K by as much as a few percent, without contradicting any other presently known experimental constraints. The K_{e2} decay rate is particularly sensitive to new physics because the Standard Model contribution is helicity suppressed. The 2006 world average [13] is determined by experiments performed in the 1970s; the relative error on this average ($\delta R_K/R_K = 4.5\%$) is too large to allow tests of the Standard Model. Inclusion in the average of the recent preliminary results from the NA48/2 and KLOE collaborations leads to a new value of $R_K^{2007} = (2.457 \pm 0.032) \cdot 10^{-5}$ [14], with a precision of $\delta R_K/R_K = 1.3\%$.

3.2 The NA62 experimental program in 2007

In 2007, NA62 running took place from the beginning of June to 11 November. The K_{e2} physics run took place from 23 June to 22 October. More than 110 000 events were collected, as illustrated in Fig. 7, together with various smaller data samples to allow detailed systematic studies. The running period from 22 October to 11 November was dedicated to the in-beam testing of straw tracker and ring-imaging Cerenkov counter prototypes for use with the P326 apparatus.

The Frascati P326 group contributed significantly to the success of the 2007 NA62 run. Group members participated in data taking for a significant fraction of the running period, and provided on-call support for the hodoscope readout electronics. As run coordinators for five weeks

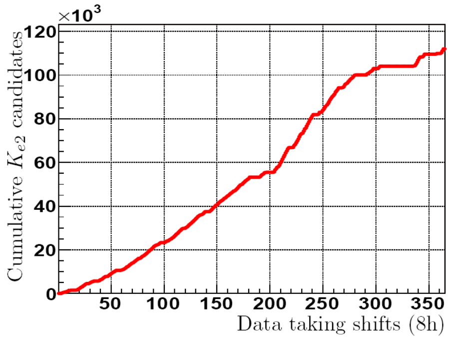

Figure 7: Cumulative distribution of the number of K_{e2} candidates recorded by NA62 in 2007.

of the 18-week run, LNF group members were directly responsible for the operational aspects of the experiment. The running period coordinated by LNF group members included K_{e2} data collection, the collection of samples for systematic studies, and the entire straw tracker beam test.

LNF group members are currently playing a central role in the analysis of the K_{e2} data. At the collaboration level, the analysis effort is being conducted by two independent groups to ensure redundancy and tighter systematic control. Frascati group members form the core of one of these two analysis groups. A preliminary result for R_K is expected during the first half of 2008.

4 2007 Conference Talks by LNF Authors

- M. Moulson, "A prototype large-angle photon veto detector for the P326 experiment at CERN," IEEE Nuclear Science Symposium, Honolulu HI, USA, 29 October 2007.

References

1. E949 Collaboration, V. Anisimovsky, *et al.*, *Phys. Rev. Lett.*, vol. 93, p. 031801, 2004.
2. G. Anelli *et al.*, CERN, Geneva, Tech. Rep. CERN/SPSC 2005-013, 2005.
3. NA48 Collaboration, V. Fanti, *et al.*, *Nucl. Instrum. Meth. A*, vol. 574, p. 433, 2007.
4. E. Ramberg, P. Cooper, and R. Tschirhart, *IEEE Trans. Nucl. Sci.*, vol. 51, p. 2201, 2004.
5. M. Adinolfi *et al.*, *Nucl. Instrum. Meth. A*, vol. 482, p. 364, 2002.
6. OPAL Collaboration, K. Ahmet, *et al.*, *Nucl. Instrum. Meth. A*, vol. 305, p. 275, 1991.
7. S. Hasan *et al.*, in *Proc. 9^{th} ICATPP Conf. on Astroparticle, Particle, Space Physics, Detectors, and Medical Physics Applications*, Como, Italy, Oct. 2005.
8. G. Feldman and R. Cousins, *Phys. Rev. D*, vol. 57, p. 3873, 1998.
9. S. Ajimura *et al.*, *Nucl. Instrum. Meth. A*, vol. 435, p. 408, 1999.
10. S. Ajimura *et al.*, *Nucl. Instrum. Meth. A*, vol. 552, p. 263, 2005.
11. V. Cirigliano and I. Rosell, *Phys. Rev. Lett.*, vol. 99, p. 231801, 2007.
12. A. Masiero, P. Paradisi and R. Petronzio, *Phys. Rev. D*, vol. 74, p. 011701, 2006.
13. Particle Data Group, W. M. Yao *et al.*, *J. Phys. G*, vol. 33, p. 1, 2006.
14. The FlaviaNet Kaon Working Group, `arXiv:0801.1817`, 2008.

STUDY OF SCINTILLATION TILE DETECTORS READOUT VIA SILICON/PHOTOMULTIPLIER DEVICES

A. Calcaterra (Resp.), L. Daniello (Tecn.), R. de Sangro, G. Finocchiaro,
P. Patteri, M. Piccolo, M. Rama

1 Introduction and motivation for this study

Silicon photomultipliers [1], often called "SiPM" in literature, are semiconductor photon detectors built from a square matrix of avalanche photodiodes (APD's) on a common silicon substrate. The side of each single APD square microcell can vary in length from 20 to 100 μm. Every microcell -or pixel- acts like a capacitor holding a given charge, and releases this entire charge when a photoelecton created in the cell reaches an active region inside the pixel, initiating a Geiger-like discharge. Pixel charges then build up again in a small time (25–250 ns). Although individual pixels are intrinsically digital, the SiPM behaves more like an analog device, because its signal is the sum of signals from all pixels discharged at the same time.

The PILC-LNF group is one of two groups started in 2007 (the second one based in Rm1) in the context of the "Proposal for ILC" initiative, with the intent to develop complete detectors of a size suitable for ILC calorimetry, and to study their performance with cosmic rays and beam tests. We give here a brief account of both activities.

2 Results at the Beam Test Facility in Frascati

The Beam Test Facility exploits, by means of a transfer line, the DAΦNE ϕ-factory LINAC, and is optimized for the production of electron and positron bunches in a wide range of multiplicities, down to single-electron. The beam profile from the BTF has typical vertical and horizontal dispersions of $\sigma_v = 2$ mm and $\sigma_h \leq$5–10 mm, with some additional, wider halo in the horizontal plane, where the bending magnets act. The BTF equipment includes a Pb-glass calorimeter, having dimensions 10 by 10 cm^2 by $\sim 20X_0$, to be placed downstream the user setup, read by a PM gated at every beam pulse. The beam pulse is totally absorbed in the calorimeter, and the integrated signal from the PM measures the particle multiplicity in a beam pulse.

The counters used at the BTF were 3, differing only for the scintillating material and the MPPC type:

- for counter "1", a scintillation tile made of St. Gobain BC-400 (blu-scintillating material, equivalent to Nuclear Enterprises NE-102), coupled to the MPPC using a green fiber of thickness 1 mm, inserted into a groove machined along the tile center. The MPPC had 1600 pixels arranged in a square matrix of 1 by 1 mm, and the pixel pitch was 25 μm.
- for counter "2", a scintillation tile made of green-scintillating material, similar to Scionix EJ260, coupled to the MPPC analogously to counter "1". The MPPC had 400 pixels arranged in a square matrix of 1 by 1 mm, and the pixel pitch was 50 μm.
- for counter "3", a scintillation tile like counter "1", directly coupled to the MPPC without any fiber. The MPPC was like the one in counter "2".

Fig. 1(left) shows the pedestal-subtracted charge spectra (in pC) for counters 2 (top) and 3 biased at 69.5 V, about 1 V above the MPPC breakdown voltage; they both have a 400-pixels MPPC, but differ by the type of scintillator, and the type of coupling (see above). Exactly 1

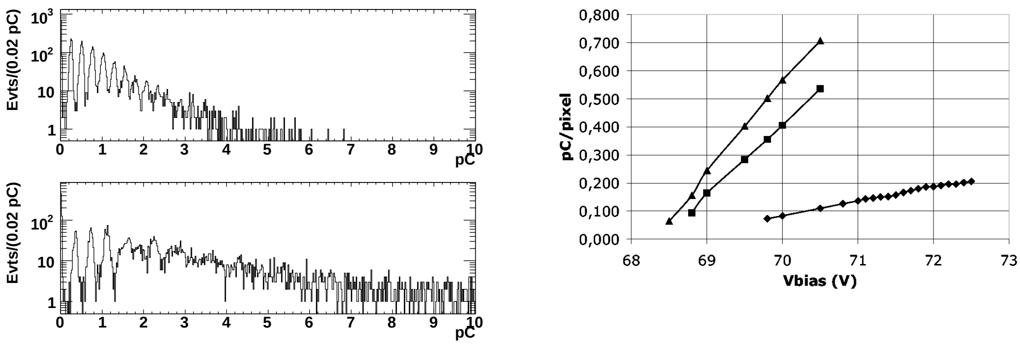

Figure 1: Left: charge spectra (pC) for counters 2 (top plot) and 3 ($V_{bias} = 69.5$ V for both); right: gains for the three counters studied.

particle per beam pulse has been requested here. The contribution from events having 2 particles per pulse is estimated at $\sim 5\%$.

Both spectra have a very narrow peak at 0, barely visible in the picture, and a series of equally-spaced peaks, due to events firing 1, 2, 3, and more pixels in the MPPC's. The RMS noise, estimated by fitting with a Gaussian the peak at 0 pC is 2–3 fC and the gain, measured by fitting the peak pitch, is $\sim 1.6 \times 10^6$ for counter 2 and $\sim 2.2 \times 10^6$ for counter 3. In fact, the peaks from counter 3 are visually more widely spaced than those from counter 2.

Since the preamplifiers for all counters were equal, and all 3 channels of electronics identical, the gain difference indicates that the working points for the 2 MPPCs were actually different: the scintillator material and the coupling geometry would have rather affected the peak populations, creating a bigger or smaller "average number of peaks".

Counter 3 (lower plot in Fig. 1(left)) is affected, from ~ 0.150 pC on, by considerable widening of the peaks, making the measurement of the number of pixels impossible; this effect does not seem attributable to electronics noise, because the width of the peak at 0 pC (not visible in Fig. 1) is about the same as for counter 2 (upper plot).

A measurement of the gain for all 3 MPPC's as a function of the biasing tension V_{bias} is shown in Fig. 1(right); the data shown are for counter 1(diamonds), 2(squares) and 3(triangles). From the comparison, the 1600-pixels MPPC needs a higher V_{bias} to obtain the same gain as the others, that are moreover not identical. Counter 2 needs a higher V_{bias} than counter 1, for the same gain.

We measured the efficiency of counters 2 and 3 by plotting the signal from counter 2 along the horizontal axis of Fig. 2(left) and the signal from counter 3 vertically.

Cutting slightly above the pedestal ($\sim 4\sigma$'s) for one of the two, due to the very close proximity of the 2 scintillating tiles, we evaluate the efficiency of the other one as the ratio of above-pedestal signals to the total for the events left by the former cut. These proximity-defined efficiencies are of $(84 \pm 1)\%$ and $(92 \pm 1)\%$ for counters 2 and 3 respectively. We attribute the difference in efficiencies to the different working point of the 2 MPPC's, that were identically biased at 69.5 V.

In Fig. 2(right) one may see the charge spectrum in pC for counter 1, biased at 72.0 V. At first sight, the pixel structure is less visible than for counters 2 and 3, but it is still present, as shown in the inset, that displays on an expanded scale the region close to the pedestal.

Dividing the data in Fig. 2(right) by the gain, one gets the histogram shown in the top left part of Fig. 3, where the charge axis is now in "pixel" units. Repeating this procedure for events

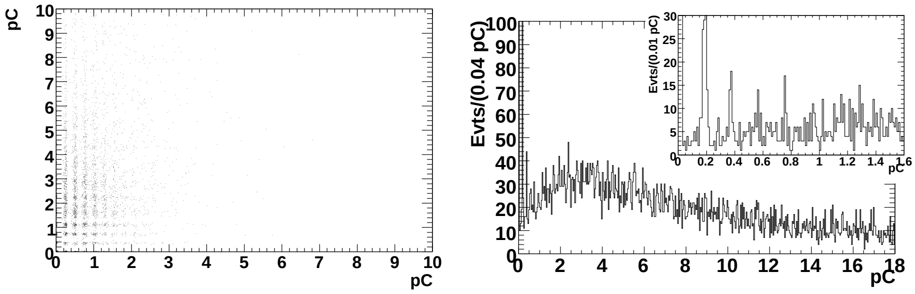

Figure 2: Left: integrated charge from counter 2 (horizontal axis) and 3; right: charge spectrum in pC for counter 1. In the inset, on an expanded scale, the pedestal region.

selected in the 2- and 3-particle region one obtains the top right and bottom left plots in Fig. 3.

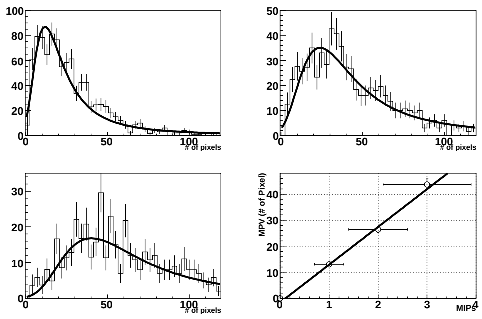

Figure 3: Linearity of counter 1 readings. The two upper plots and the bottom left one show charge spectra in units of "pixels" and the curves are fits to the Landau distribution. In the bottom right plot we see the MPV's of the Landau distributions plotted against the number of MIP's in the beam pulses.

Fitting the data to Landau distributions we obtain the Most Probable Values (MPV's) plotted in the bottom right part of Fig. 3. The fitted line is a measurement of the most probable number of pixels fired in the MPPC of counter 1 as a function of the number of MIPs in the beam pulses. The points lie very close to the line: the fitted number of pixels per MIP is 14, and the extrapolated line passes close to the origin.

3 First results from the cosmic ray test

Our equipment is also set up to take data with cosmic rays, the trigger being given by the coincidence of two scintillators. After the test at the BTF discussed in the previous sections, the RPC-based tracker has been optimized to yield slightly better efficiency and spatial resolution $\mathcal{O}(1)$ mm; a temperature probe was also integrated in the DAQ system. The electronic noise is slightly worse (~ 20 fC vs. 10 fC) than at the BTF test, due to reduced shielding of the experimental hall. This figure, however, is still adequate with respect to the typical charge of 300 fC in an MPPC pixel.

Using the RPC tracker we can define a fiducial region were cosmic muons should impinge on the MPPC's; the charge profiles as function of the track impact point on the scintillator tiles are shown in the left plot of Fig. 4. We studied the gain of our devices by fitting the pixel charge at different biasing voltages and temperatures. The gain variation with temperature for a particular biasing voltage in MPPC n.2 is shown in the middle plot of Fig. 4. The right plot of the same figure shows the gain as a function of V_{bias}, for temperatures T= $26-28°$.

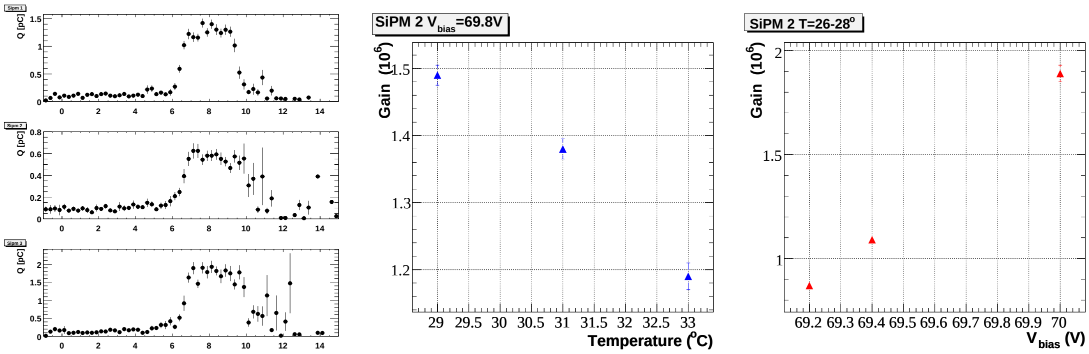

Figure 4: Left: charge amplitude profile in the three counters as functions of the impact points predicted by the tracker; center: gain variation as a function of operating temperature in counter 2 for $V_{bias} = 69.8\,\mathrm{V}$; right: gain variation as a function of V_{bias} for T= $26-28°$.

4 Foreseen activity in 2008

These results, although still in an initial stage, encourage us to proceed with the study of the performance of scintillation counters employing an MPPC as detection element.

We plan to increase in 2008 the number of studied counters by an order of magnitude, and take more data at the BTF and in cosmic rays, where the small rate may be offset by continuous data taking. We intend to perform an accurate measurement of the variation of MPPC's gain as a function of T.

5 Conference Talks by LNF Authors in 2007

1. A. Calcaterra, Beam test of scintillation tiles with MPPC readout, 2007 International Linear Collider Workshop, DESY
2. G. Finocchiaro, Study with cosmics and test-beam particles of scintillation tile detectors read out via Silicon Photomultiplier devices, 10^{th} ICATPP Conference, Villa Olmo 2007

6 Publications

1. A. Calcaterra *et al*, Proc. 8^{th} Int. Conf. Phys.on Large Scale Applications and Radiation Hardness of Semiconductor Detectors, Florence 2007, subm. to Nucl. Instr. and Meth.

References

1. B. Dolgoshein et al., Nucl. Instr. and Meth. A563,368(2006), and references therein.

2 – Astroparticle Physics

BENE_DTZ

F. Terranova

BENE-INFN is a study group closely related to the European initiative BENE (Beams for European Neutrino Experiments). The latter is aimed at developing novel sources for high intensity neutrino beams and is focused on the conceptual design of Superbeams, Beta Beams and Neutrino factories. In 2007, the outcome of the International Scoping Study for these future facilities has been delivered [1]. LNF contributed particularly on future applications of OPERA-like detectors [1], i.e. hybrid emulsion cloud chambers with and without magnetic field, as a far detector to exploit the $\nu_e \rightarrow \nu_\tau$ transitions ("silver channel") at the Neutrino Factories. Further activities focused on the combination of accelerator data from Beta Beams with natural sources (atmospheric neutrinos) to improve the sensitivity to the neutrino mass hierarchy (sign of Δm^2_{32}) and on sterile neutrinos after MiniBoone [2].

List of Conference Talks by LNF Authors in Year 2007

1. F. Terranova "High Density Detectors to exploit the technology of the Beta Beams", 21st International Workshop on Weak Interactions and Neutrinos (WIN07), Kolkata, India, January 15-20, 2007
2. F. Terranova, "Neutrino hierarchy from CP-blind observables with high density magnetized detectors", 9th International Workshop On Neutrino Factories, Superbeams and Betabeams, Okayama University, Japan, August 6-11, 2007,

References

1. T. Abe *et al.*, "Detectors and flux instrumentation for future neutrino facilities," arXiv:0712.4129 [physics.ins-det], 2007.
2. A. Donini, M. Maltoni, D. Meloni, P. Migliozzi and F. Terranova, JHEP **0712**, 013 (2007).

LARES

A. Boni (Bors.), C. Cantone (Bors.), S. Dell'Agnello (Resp.), G.O. Delle Monache, M. A. Franceschi, M. Garattini (Bors.), N. Intaglietta (Tecn.), M. Maiello (Bors.), M. Martini (Bors.), R. Tauraso (Ass.), C. Prosperi (Bors.)

1 Introduction

Gravity can be studied in detail in Near Earth Orbits (NEO) using laser-ranged test masses tracked with 1 cm accuracy by ILRS. The two LAGEOS satellites have been used to measure frame dragging (a truly rotational effect predicted by GR) with a 10% error [1]. A new mission and an optimized, second generation satellite, LARES (I. Ciufolini PI), is in preparation to reach an accuracy of 1% or less on frame dragging, to measure some PPN parameters, to test the $1/r^2$ law in very weak field and, possibly, to test select models of unified theories (using the perigee). This requiresa full thermal analysis of the laser ranging performace of the test mass and an accurate knowledge of the asymmetric thermal thursts acting on the test mass due to the radiation emitted by Sun and Earth.

The LAGEOS and LARES three-satellite experiment was approved by INFN at the end of 2007, while the LARES space mission was approved by ASI in the beginning of 2008. LARES will be launched with the first flight of the new European rocket, VEGA. The following is the announcement posted on www.asi.it around mid February 2008. "Nella seduta del 7 febbraio 2008, il Consiglio di Amministrazione dell'ASI ha approvato in via definitiva il finanziamento industriale di LARES, il satellite che volera' con il primo lancio del nuovo vettore europeo VEGA, previsto entro la fine del 2008. LARES, che verra' costruito da Carlo Gavazzi Space SpA, e' un satellite completamente passivo, in tungsteno, che ospita retro-riflettori grazie ai quali il suo spostamento sara' seguito via laser da terra. Il suo obiettivo scientifico e' misurare con unaccuratezza dell'ordine dell'1% l'effetto Lense-Thirring, cioe' lo spostamento dall'orbita newtoniana che, secondo la Teoria della Relativa' Generale, subisce un satellite in orbita a causa della rotazione terrestre. Attualmente l'accuratezza di questa misura e' dell'ordine del 10% . LARES e' stato progettato in collaborazione con l'INFN e il suo principal investigator e' Ignazio Ciufolini, dell'Universita' di Lecce.

2 Thermal and Laser Ranging Characterization of Laser Retro-reflector Arrays

Starting from 2004 INFN invested resources and manpower to build and start the operation of a *Satellite Laser Ranging* (SLR) Characterization Facility (SCF) for Near Earth Orbits (NEOs) in Frascati, near Rome, dedicated to the space calibration of the thermal properties and the laser ranging response of laser retro-reflector arrays (LRAs) [2].

Its initial purpose was to perform the full space-climatic, thermo-vacuum characterization of LAGEOS cube corner retro-reflectors (CCRs) to study the asymmetric thermal thrusts (TTs) acting on LAGEOS due to the varying environmental conditions. This characterization has never been done before and has become necessary because TTs are the most significant non-gravitational perturbations (NGPs) for measurements of Gravitation and Space Geodesy. Moreover, due to the relentless improvements of the accuracy of SLR and of the Earth gravitational models (EGMs), soon NGP, SLR and EGM uncertainties will have a comparable effect on the overall error budget.

The effect of TTs on LAGEOS orbits is driven by the value of τ_{CCR}, the thermal relaxation time of its CCRs, which has never been measured before. τ_{CCR} estimates in the literature vary from 2,000 sec to 7,000 sec (by 350%!) and are comparable with the duration of the eclipse in the

Earth shadow (4,400 sec max) and the orbital period (13,300 sec). The SCF has been designed to measure τ_{CCR} at 10% accuracy. This will make the error on the Lense-Thirring effect due to TTs negligible (permil level) with respect to the ultimate LARES and LAGEOS three-satellite experiment goals for frame dragging. Simulations studies indicate that measuring τ_{CCR} at 10% relative statistical accuracy with the SCF requires a temperature uncertainty of 0.5 to 1 K, which is a moderate experimental constraint.

The modular and evolutionary design of the SCF turned out to be well suited to characterize also the optical SLR performance of *any* LRA in NEOs, at GNSS altitudes [3] and on the Moon [4]. In fact, the operational experience of the ILRS (International Laser Ranging Service) has shown that LRAs optical performance is affected by climatic changes. The latter include transitions of the satellite between the Sun illumination and the Earth shadow and vice versa. For LAGEOS and for LARES, which share the same type of fused silica CCR, these eclipses are influenced by the thermal variations defined by τ_{CCR}, because the CCR index of refraction varies linearly with temperature around 300K.

At the end of 2006 an *engineering* prototype of LAGEOS (the **sector**, built in 1992) was sent to LNF by NASA-GSFC for SCF testing. In the same year a flight model of a GPS-2 LRA was also sent to LNF by the University of Maryland to be SCF-tested. The latter array is the third and last original array (the **GPS3**) manufactured by IPIE of Russia to be deployed on one of the next GPS-2 satellites to be launched. These loans were the result of a close cooperation of INFN with ILRS and international partners in the US and in Russia.

Complete thermal tests have been performed in 2006 and 2007 with a LAGEOS 3×3 LRA built at LNF (the **matrix**). The first integrated, concurrent thermal and laser-ranging characterizations ("SCF-Test") have been performed successfully in 2007 with a prototype GLONASS CCR nominally identical to those deployed on the GPS3, Giove-A and Giove-B. Data analysis is in progress. A preliminary SCF-Test of the sector has also been done.

3 SCF Apparatus

A schematic view of the SCF is shown in fig. 1. The size of the steel cryostat is approximately 2 m length by 0.9 m diameter. The inner copper shield is painted with the Aeroglaze Z306 black paint (0.95 emissivity and low out-gassing properties) and is kept at T = 77 K with liquid nitrogen. When the SCF is cold, the vacuum is typically in the 10^{-6} mbar range. A positioning system at the top of the cryostat (show in fig. 5) holds the prototype in front of the Earth infrared Simulator (ES, inside the SCF), of the Solar Simulator (SS) and of the IR camera (the latter are both located outside the SCF). The prototype can also be rotated at 90° in front of interrogating laser-ranging beams.

The SS beam enters through a quartz window (37 cm diameter, 4 cm thickness), transparent to the solar radiation up to 3000 nm. A side Germanium window at 45o wrt the SS beam allows for the acquisition of *thermograms* of the LRA with an infrared (IR) digital camera (both during the ES/SS illumination and the laser interrogation phases). The SS (from www.ts-space.co.uk) provides a 40 cm diameter beam with close spectral match to the AM0 standard of 1 solar constant in space (1366.1 W/m^2) in the range 400-1800 nm (see fig. 2). The uniformity is about ± 5% over an area of 35 cm diameter. The spectrum is formed from a metal halide (HMI) arc lamp (UV-V; 6 KW), together with a quartz halogen, tungsten filament lamp (Red-IR; 12 KW). The SCF spectrum is also in reasonable agreement with the AM0 over λ = 1500 - 3000 nm. The absolute scale of the SS intensity is established by exposing the SS beam to a reference device, the *solarimeter*, which is a standard www.epply.com thermopile (calibrated blackbody), accurate and stable over 5+ years to ±2%.

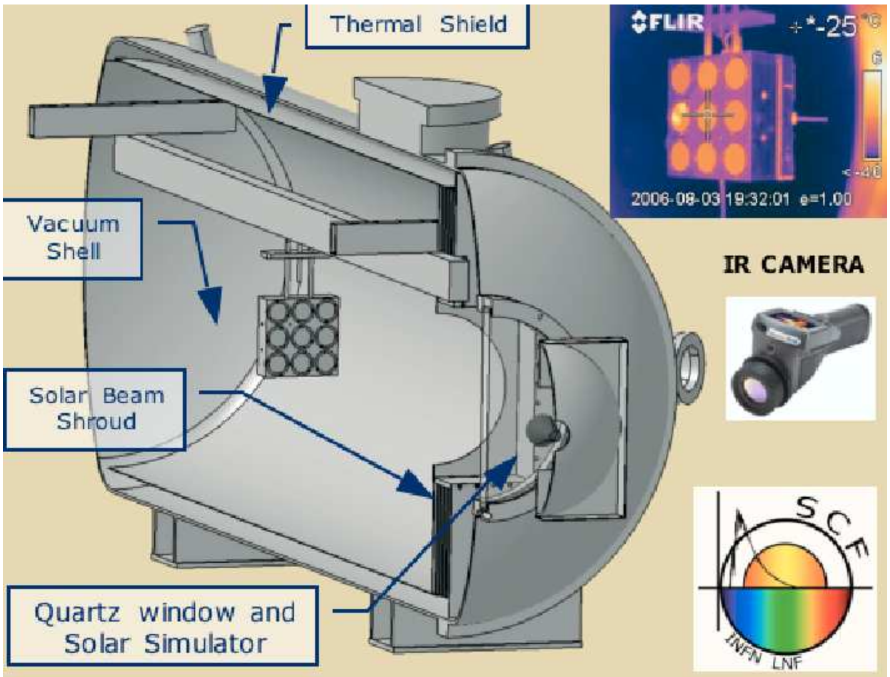

Figure 1: The SCF with the LAGEOS matrix built at LNF. A temperature photo taken with the IR camera and the IR camera are shown at the right. Bottom right is the SCF logo.

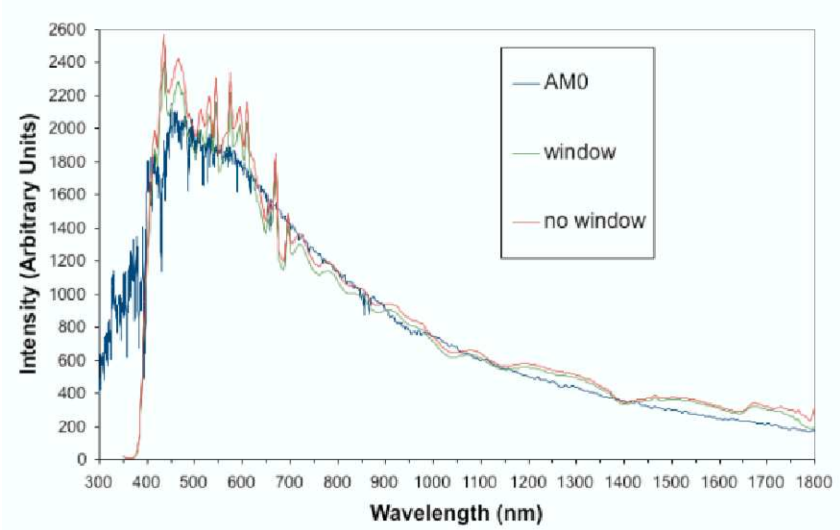

Figure 2: SS spectrum of the SCF with and without quartz window, compared to the AM0.

The ES is a 30 cm diameter disk painted with Aeroglaze Z306, kept at the appropriate temperature (260-280 K) and distance from the satellite prototype, in order to provide the CCRs with the same Earth viewing angle in orbit (60° for LAGEOS). The temperature DAQ consists of an IR camera for non-invasive, high spatial granularity measurements (FLIR ThermaCAMs EX320/SC640, 320×240/640×480 pixels) and class-A PT100 probes with 4-wire readout. The PT100s are used to calibrate the IR cameras. They are also used below 250/230K, outside the working ranges of the IR cameras.

SCF photos taken during a preliminary SCF-Test of the LAGEOS sector are shown in fig. 3. On the side note the left IR camera window, the central window for laser measurements and the right spare window. The SS beam enters from the front through the AM0 window. The specs of the LASER window are: fused silica material; 150 mm diameter, 37 mm thickness, surface quality

= 10-5 scratch-dig, deformations of the transmitted wavefront ¡ $\lambda/20$, anti-reflective coating on both sides (reflectivity = 0.2% for λ = 532 nm and 632.8 nm).

Each CCR will be first exposed to the SS and ES. Then, the CCR will be rotated at 90° in front of the LASER window to acquire its FFDP. Thermograms will be taken at any time.

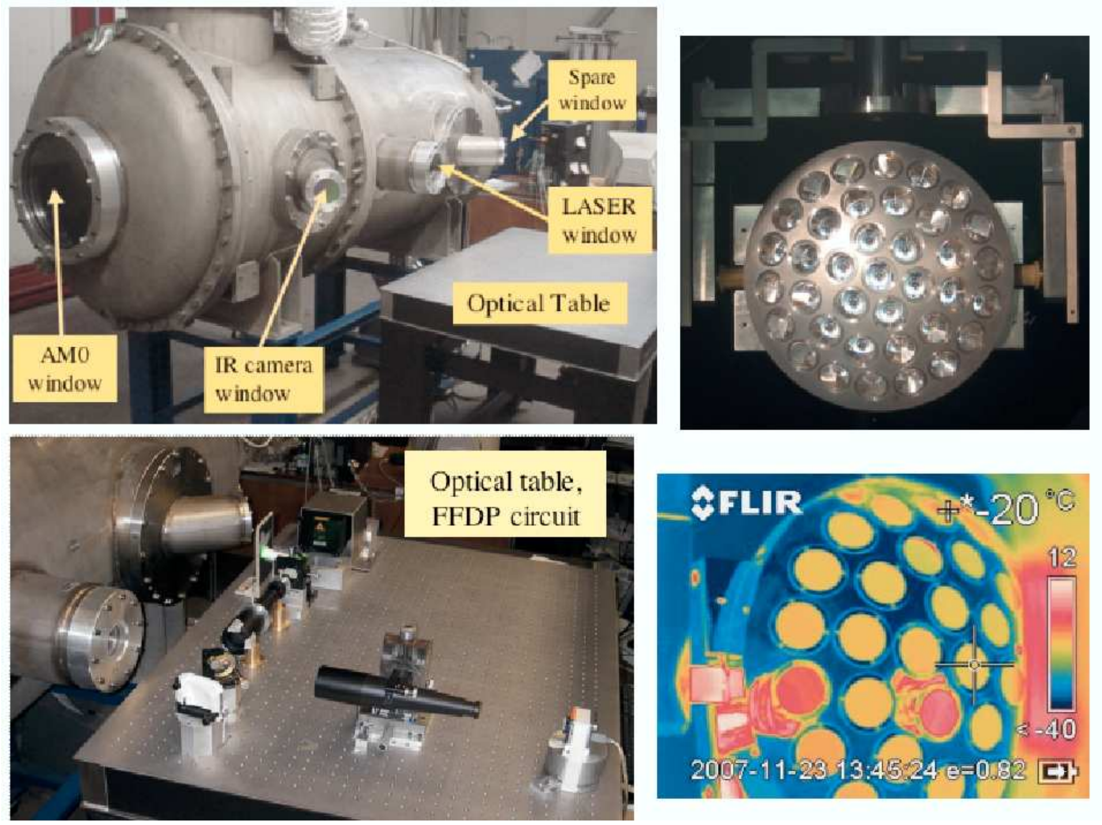

Figure 3: Top left: SCF windows. Bottom left: optical table for FFDP tests. Top right: the sector mounted inside the SCF on the rotation/tilt system. Bottom right: the sector in the SCF as seen by the IR camera (the CCR with cross-hairs on top is under FFDP measurement).

4 Measurements of Far Field Diffraction Patterns (FFDPs)

The basic *acceptance* test of laser ranging performance is the measurement of the absolute angular size and absolute intensity of single-CCR FFDPs with linearly polarized CW lasers. The optical circuit for CCR FFDP measurements is shown in fig. 4. The laser beam profiler (by Spiricon) uses a 2 MPixel CCD camera (by PtGrey), readout via Firewire by a PC. FFDPs are acquired both with the CCR at STP (ie, in isothermal conditions), or with the CCR in the SCF, concurrently to thermal tests. Figure 3 also shows measured and simulated FFDPs of a LAGEOS-type CCR with zero dihedral angle offsets (DAO) taken at STP. Optical flats with known reflectivity are used as normalization to determine the absolute intensity of the CCR laser return. The absolute angular scale of the circuit is calibrated with the double-slit method to test the consistency of each CCR FFDP with its nominal DAO. The latter are strictly related to the satellite velocity aberration, which is in turn determined by its orbital altitude.

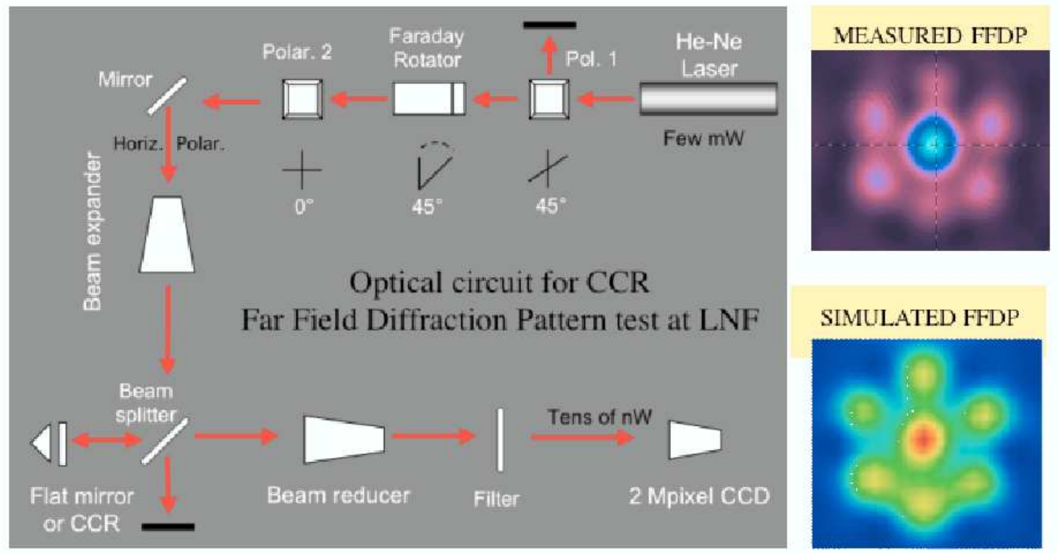

Figure 4: FFDP optical circuit (left) and FFDPs measured for a LAGEOS sector CCR w/zero DAO (top right) and simulated with CODEV (bottom right). Note that LAGEOS (LARES) CCRs have three DAO = +1.25 (+1.5) 0.5 arcsec.

5 Software Simulation Suite

SCF measurements are also modeled with thermal and optical simulations done with:

- Autocad Inventor (solid modeling) and ANSYS (FEM analysis).
- For satellite thermal analysis we adopted since 2005 a specialized suite by C&Rtech, used by several space agencies and industries: (i) Thermal Desktop, the CAD-based geometric thermal modeler, (ii) RadCad, the radiation analysis module, (iii) Sinda-Fluint, the solver and orbital simulator (TRS). TRS can handle satellites with up to 20000 FEM nodes and a generic satellite spin and orbit configuration. It also provides the thermal inputs and orbital motions of the Sun, Earth, Moon and other planets of the solar system.
- Optical design and analysis software: CODEV, by ORA. Note that TRS has built-in provisions for integration with CODEV. With ORA we are developing CCR dn/dT functionality in CODEV to perform an integrated thermal and optical analysis of CCRs in space and in the SCF.

6 "SCF-Test" of LAGEOS and LARES

The SCF-Test consists of the integrated thermal and optical measurements described below, performed on LAGEOS and LARES matrix LRAs, on the LAGEOS sector and on the full LARES satellite. The SCF-Test is innovative and it was not performed for LAGEOS I and II. The SCF-Test is the outcome of in-depth discussions with expert SLR users and the ILRS.

- Hold the average temperature of the matrix or sector (W-alloy for LARES, Al for LAGEOS), T_M, to the expected value, TAVG. Then, estimate with SCF data and TRS models:
  1) IR emissivity and Solar absorptivity of the CCRs, of their external retainer rings, of the external satellite metal surface and of the internal surface of the cavity
  2) τ_{CCR} and $\tau_{METAL-RING}$ (thermal relaxation time of the CCR and of its external retainer ring)
  3) surface temperature distribution (ie, thermal forces, TTs)
  4) temperature difference between the CCR outer face and the CCR corner inside the cavity. Repeat the above for TM different from TAVG, in the appropriate range.
- Measure CCR FFDPs in the SCF (this is done previously also at STP).
- Repeat the above for different Sun illumination conditions:
  1) transition from SS turned off to on and vice versa (ie, Earth shadow)
  2) varying incidence angles of the Sun illumination
  3) different times along the thermal relaxation curve.
- Tune the TRS models to the SCF data for *static* climatic conditions, in which the SS and ES are turned on and off alternatively.
- Use validated TRS and CODEV simulations to model the satellite behaviour for generic orbit and spin configurations.
- Full satellite calibrations. The test mass will be kept thermally floating in the SCF, with a highly insulating support by the pole or the equator. With continuous rotation around the vertical axis we will estimate the absolute value of the LARES core temperature in space and test the effect of satellite spin on TTs, τ_{CCR}, $\tau_{METAL-RING}$ and FFDPs. This will also be done in a static, zero spin configuration.

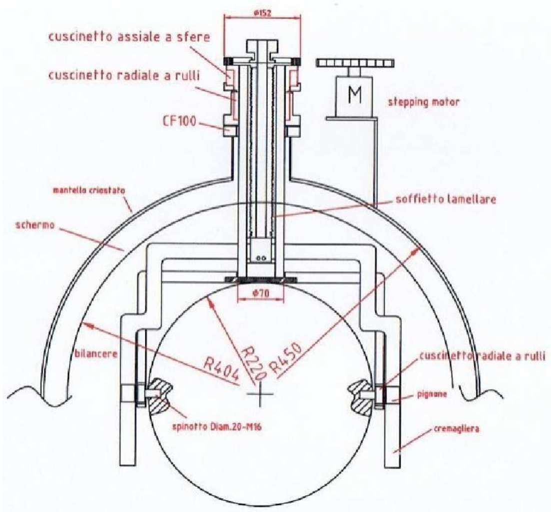

Figure 5: Sketch of LAGEOS sector or full LARES on the SCF rotation+tilt positioning system, which can support a weight of 750 Kg. Shown is the maximum radius for a W-alloy test mass.

7 Talks by LARES-LNF Collaborators

- S. Dell'Agnello, "SCF-Test of LAGEOS and GLONASS Retro-Reflectors", ILRS Conf., Sep. 2007, Grasse, France.
- A. Boni, "The INFN-LNF SCF", 10th ICATPP, Int. Conf.on Astropart. and Part. Phys., Oct. 2007, Como, Italy.
- C. Cantone, "The INFN-LNF SCF", XIX Congresso Nazionale AIDAA, Sept. 2007, Forli, Italy.

References

1. I. Ciufolini, E. C. Pavlis, Nature, Vol. **431**, 21 October 2004.
2. A. Bosco, C. Cantone, S. Dell'Agnello, G. O. Delle Monache, et al, *Probing Gravity in NEOs with High-Accuracy Laser-Ranged Test Masses*, Int. Jou. Mod. Phys. D, Vol. 16, N. 11 (2007) 1-15.
3. S. Dell'Agnello, R. Vittori, G. O. Delle Monache, et al, *ETRUSCO: Extra Terrestrial Ranging to Unified Satellite COnstellations*, INFN-LNF Report LNF-07/8(IR).
4. D. G. Currie, S. Dell'Agnello, G. O. Delle Monache, R. Vittori, et al, *MoonLIGHT: Moon Laser Instrumentation for General relativity High-accuracy Tests*, INFN-LNF Reports LNF-06/28(IR), approved Proposal to NASA; LNF-07/02(IR), study financed by ASI.

NEMO

Marco Cordelli, Agnese Martini, Luciano Trasatti (Resp), Roberto Habel

1 Activity

The NEMO collaboration aims at building a 1 km3 Cerenkov neutrino detector in the Mediterranean Sea. During the year 2007 the collaboration concentrated on running and analyzing the data from Phase 1, the 4 floor detector that was deployed in december 2006 at the Catania test site. The LNF group gave its contribution to this enterprise in the development of the console human interface software, in collaboration with the LNS group. The console software has been developed using LabVIEW as the interface between the database and the operators.

Moreover, we continued the development of NERONE, an instrument designed and built at the LNF to measure the attenuation length of light in water at 3500 m depth. Unfortunately the cruise that was scheduled for october to test the instrument was cancelled due to ship problems, and the final test had to be postponed to the spring of 2008. During 2007 several improvements have been done to the laser projection unit and to the detector assembly. In 2008 the instrument was deployed successfully.

OPERA

F. Bersani Greggio (Ass.), A. Cazes (Ass.Ric.), V. Chiarella, C. Di Troia (Ass.),
B. Dulach, G. Felici, A. Franceschi, F. Grianti (Ass.), A. Gambarara (Tecn.),
A. Mengucci (Tecn.), T. Napolitano (Art.23), A. Paoloni (Art.36),
M. Spinetti, F. Terranova (Resp.), T. Tonto (Tecn.), M. Ventura (Tecn.), L. Votano

in collaboration with

LNF-SEA: A. Balla, G. Corradi, U. Denni, A. Frani, M. Gatta, G. Paoluzzi, G. Papalino
LNF-SPAS: A. Cecchetti, D. Orecchini
LNF-SSCR: G. Catitti, A. Ceccarelli, N. Intaglietta, A. Tiburzi
LNF Divisione acceleratori: C. Fusco, F. Iungo, L. Pellegrino, C. Sanelli

1 The experiment

OPERA [1] has been designed to provide a very straightforward evidence for $\nu_\mu \rightarrow \nu_\tau$ oscillations in the parameter region indicated by Super-Kamiokande as the explanation of the zenith dependence of the atmospheric neutrino deficit. It is a long baseline experiment located at the Gran Sasso Laboratory (LNGS) and exploiting the CNGS neutrino beam from the CERN SPS. The detector is based on a massive lead/nuclear emulsion target. The target is made up of emulsion sheets interleaved with 1 mm lead plates and packed into removable "bricks" (56 plates per brick). The bricks are located in a vertical support structure making up a "wall". These bricks are produced in situ by a "brick assembly machine" (BAM) located near the OPERA experimental Hall; they are inserted into the wall support structure by a dedicated robot (BMS). Nuclear emulsions are used as high resolution tracking devices for the direct observation of the decay of the τ leptons produced in ν_τ charged current interactions. Electronic detectors positioned after each wall locate the events in the emulsions. They are made up of extruded plastic scintillator strips read out by wavelength-shifting fibers coupled with photodetectors at both ends. Magnetized iron spectrometers measure charge and momentum of muons. Each spectrometer consists of a dipolar magnet made of two iron walls interleaved with pairs of precision trackers. The particle trajectories are measured by these trackers, consisting of vertical drift tube planes. Resistive Plate Chambers (RPC) with inclined strips, called XPC, are combined with the precision trackers to provide unambiguous track reconstruction in space. Moreover, planes of RPCs are inserted between the magnet iron plates. They allow a coarse tracking inside the magnet to identify muons and ease track matching between the precision trackers. They also provide a measurement of the tail of the hadronic energy leaking from the target and of the range of muons which stop in the iron. A block of 31 walls+scintillator planes, followed by one magnetic spectrometer constitutes a "super-module". OPERA is made up of two supermodules (SM) located in the Hall C of LNGS (see Fig. 1). At the time of writing 72% of the bricks have been produced. The total amount that will be available by the end of the production (summer 2008) is ∼150000 corresponding to a target mass of about 1.3 kton. This amount is 30% smaller than the original design, the reduction being mainly due to funding cuts

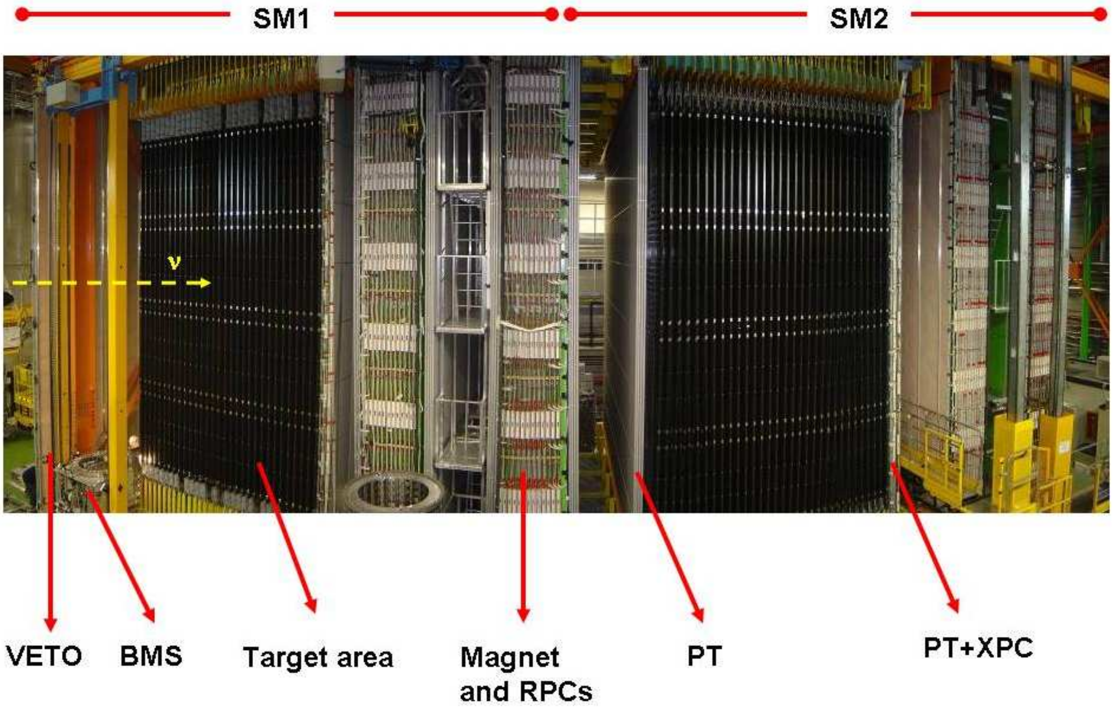

Figure 1: A fish-eye view of the OPERA experiment (summer 2007). The upper red horizontal lines indicate the position of the two identical supermodules (SM1 and SM2). The "target area" is made up of planes of walls filled with lead-emulsion bricks interleaved with planes of plastic scintillators (TT): the black covers visible in the photograph are the end-caps of the TT. Arrows show also the position of the VETO planes, the drift tubes (PT) followed by the XPC, the magnets and the RPC installed among the magnet slabs. The Brick Manipulator System (BMS) is also visible. The direction of incoming neutrinos from CERN is indicated by the yellow arrow.

for the emulsion purchase in Japan.

OPERA is able to observe the ν_τ signal with an impressively low background level. The direct and unambiguous observation of $\nu_\mu \rightarrow \nu_\tau$ appearance will constitute a milestone in the study of neutrino oscillations. Moreover, OPERA has some sensitivity to the sub-dominant $\nu_\mu \leftrightarrow \nu_e$ oscillations in the region indicated by the atmospheric neutrino experiments. It has been shown [2] that the CNGS beam optimized for ν_τ appearance, will improve significantly (about a factor of three) the current limit of CHOOZ.

Opera is an international collaboration (Belgium, China, Croatia, France, Germany, Israel, Italy, Japan, Russia, Switzerland, and Turkey) and the INFN groups involved are Bari, Bologna, LNF, LNGS (Gran Sasso), Naples, Padova, Rome and Salerno. The Technical Coordinator of the experiment (M. Spinetti), the Chairperson of the Collaboration Board (L. Votano) and two of the OPERA project leaders (A. Franceschi for the wall construction and F. Terranova for the magnets) are LNF researchers.

2 Overview of the OPERA activities in 2007

The 2006 OPERA physics run was stopped prematurely due to a failure in the cooling system of one of the two horns ("reflector") in the CNGS beamline at CERN. In 2007 the system has been repaired and a full overview of the cooling plant and of the strip-line distributing the current to the horns has been carried out. The commissioning of the beam was completed in September and OPERA was able to take data in October. During this high intensity run, however, a new failure has appeared in the beamline. It was traced back to the inappropriate shielding of the electronics for the control of the ventilation system. The data taking was, therefore, stopped the 22th of October. Further investigation showed that, due to a mistake in the design, many components have been located in areas where the neutron fluence was expected to be too high. In response to this, the CERN management and INFN setup a task force to re-design the shielding system, preventing radiation damage of the beamline components during the operation of CNGS at nominal intensity. The corresponding interventions are in progress and CNGS is expected to restart in June 2008. Also the brick production of OPERA was slower than foreseen (see Sec. 3.5) and during the short October run only 60000 brick were installed. In spite of this, CNGS accumulated 0.8 10^{18} protons-on-target: OPERA observed 38 events in its bricks ("internal events") and 355 events in the surrounding material. The first OPERA event in a lead-emulsion brick is shown in Fig. 2. Therefore, the 2007 run allowed to accomplish vertex location and event characterization in the emulsions and validated for the first time the full OPERA analysis chain.

3 Activities in Frascati

The Frascati group has been responsible for the design and construction of the dipolar magnets and the general support structure for the subdetectors. It shares responsibility with INFN Padova and LNGS for the construction and running of the bakelite RPC planes. Frascati and Naples also designed and prototyped the wall support structures housing the lead/emulsion bricks and LNF was responsible for their production and installation. Moreover, the group contributes to software development and to the analyses aimed at assessing the performance of the experiment after the completion of the CNGS programme. LNF is also involved in the construction of the Brick Assembly Machine (BAM) and will contribute to the emulsion scanning with two dedicated microscopes located in Frascati. Finally, since 2007 LNF follows the brick handling of OPERA, i.e. the operation chain that goes from the extraction of the brick after an interaction has occurred up to the emulsion development.

3.1 OPERA General layout

The OPERA general support structure is a project by LNF-SPAS and external firms and it has been mounted in parallel with the electronic subdetectors and the brick walls between 2003 and 2006 [3]. The project has been completed in 2006 and, during 2007, only auxiliary installations have been added. The most important one is a support floor that ease the access rock-side to the OPERA magnets and targets. The structure has been designed by LNF-SPAS; construction and mounting has been carried out by external firms under the supervision of LNF. Moreover,

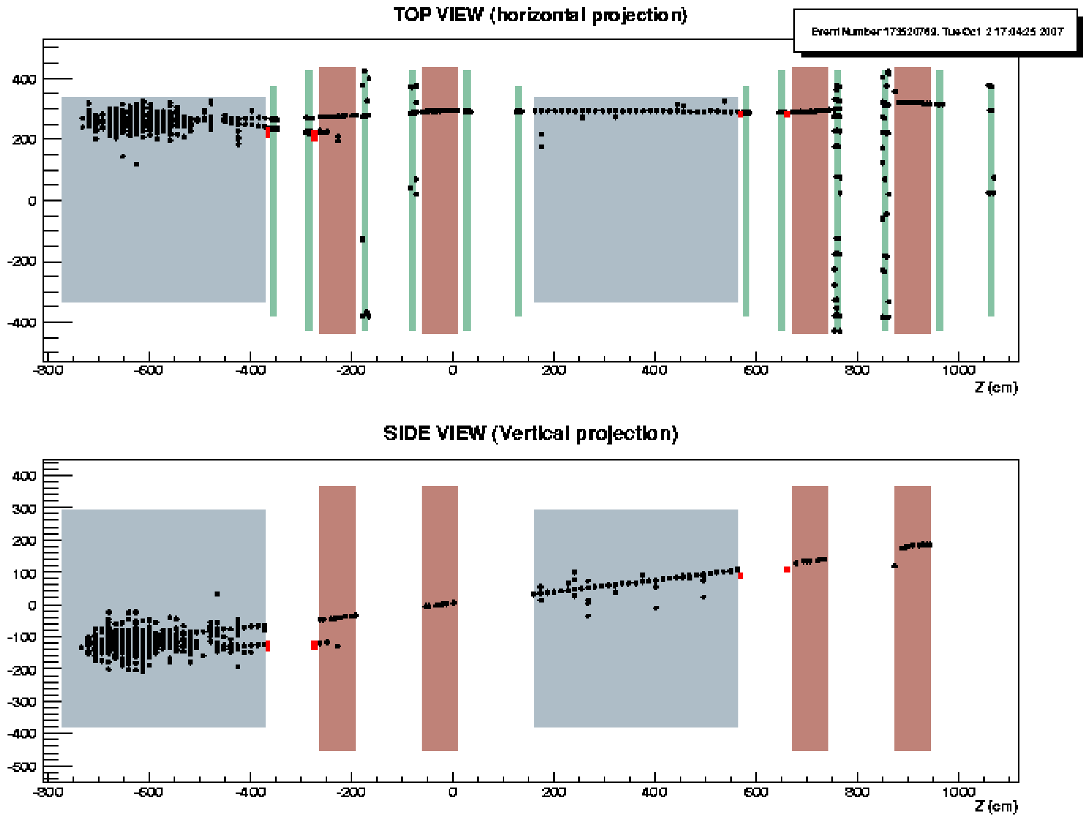

Figure 2: The first OPERA internal event (2^{nd} October 2007): a ν_μ charged-current interaction in one of the lead-emulsion brick.

LNF-SPAS followed the installation of the remaining pathways to access the TT and drift tube electronics in the second supermodule.

In winter 2007, the filling with bricks of the first supermodule has been completed and the loading station feeding the BMS has been moved from SM1 to SM2. This operation required mechanical interventions, realignment and re-optimization of the BMS operations. The interventions have been done in November for the BMS running corridor-side and in Dicember for the BMS running rock-side. It has been coordinated by LNF-SPAS and IN2P3-Annecy in collaboration with external firms.

3.2 Magnets

The OPERA magnets and their infrastructures have been commissioned in spring 2006 and were fully operative since the first CNGS run [4, 5, 6]. In 2007 most of the activities have been devoted to the completion of the slow control. A set of hard-wired alarms have been installed to allow for automatic ramp-down of the magnet power supplies (PS) in the occurrence of failures at the cooling system. Moreover, an overall Alarm Manager has been developed and tested: it supervises the clients of all temperature problems both in the magnets and in the cooling circuits, the status, currents and voltages of the PS and signal anomalies to on-call experts and on-site operators. This Manager is interfaced with the RPC/Magnet database (Postgres) and exchanges information with the OPERA DAQ through CORBA. Finally, two additional heat exchangers have been installed along the upper part of the bottom coil in both magnets.

During the 2007 physics runs the magnets were operated continuously. The livetime in the presence of neutrino beam has been 100% for both of them. Unwilled ramp-down have been reported only during power cuts (after the completion of the brick production, all services will be put under UPS). Since in 2007 the power supplies were permanently on without interruptions for several weeks, long term thermal tests have been carried out. It has been demonstrated that the coils reach thermal equilibrium in about 30 hours and the overall spectrometer, including the iron bulk, reaches equilibrium after ~ 5 days. The temperature increase of the OPERA Precision Trackers and the RPC never exceeded 1.5 degree.

In 2008, the standalone OPERA cooling system will be interfaced with the water circuits of LNGS through a dedicated heat exchanger; an automatic refill system for demineralized water will also be installed. Moreover, work is in progress to improve the accessibility of the Alarm Manager with emphasis on the development of web interfaces to the database and the alarms, and the commissioning of an automatic alerting system based on GPRS cards.

3.3 Resistive Plate Chambers

As mentioned above, for each of the two OPERA spectrometers 22 RPC planes have been installed. They are placed in the 2 cm gaps between the iron slabs of the magnet and equipped with horizontal and vertical readout strips. Two additional RPC layers with inclined read-out strips (called XPCs) are placed upstream the magnet along the beam direction. A short description of the read-out electronics can be found in [3]. The OPERA RPCs are operated at 5.8 kV with the gas mixture $Ar/C_2H_2F_4/i-C_4H_{10}/SF_6 = 75.4/20.0/4.0/0.6$ [7]. Signals coming from horizontal and vertical strips are discriminated at 40 mV.

The XPC layers and 7 out of 22 RPC layers in each spectrometer are instrumented with dedicated Timing Boards (TBs). The Timing Boards are 16 channel positive discriminators, plugged on the read-out strip panels, performing the OR of the discriminated signal. Up to 14 TBs, corresponding to a whole RPC and one half XPC layer, are managed by one OPE board, performing the global OR of the connected TBs; OR signals from OPE boards are used to generate the trigger signal for the drift tubes. OPERA Timing Boards are operated at 15 mV, well below the threshold employed for the RPC read-out. Each spectrometer is served by 153 timing boards and 11 OPE boards. Since the timing board signals themselves are read out by means of TDCs, they can be used for time-of-flight measurements, exploiting the good time resolution obtainable with streamer operated RPCs.

The commissioning of the drift tubes and of their trigger was completed during the cosmic runs of march and july 2007. The full RPC system ran smoothly during these and the following CNGS beam runs, with almost no dead-time.

Typical tracking resolution values for the RPCs are around 1.4 cm. The average cluster sizes are about 2.4 strips in the bending projection and 1.4 strips in the other projection. The average efficiency of each RPC layer has been measured to be 95%, due to geometric inefficiency; XPCs have slightly lower efficiencies because of the not-ideal adherence between the read-out strips and the chambers. Counting rates between 1 and 2 kHz/layer have been observed with operating currents around 500 nA for each RPC row (3 chambers, corresponding to a sensitive area of 9 m^2). The operating currents are measured by means of precise custom nano-amperometers, designed by the LNF-SEA and described in [8]. These performances are consistent with those observed during the 2006 runs and reported in [3].

The time resolution of OPERA RPCs has been estimated on 2007 data using the time difference between two consecutive layers, applying corrections for the muon time-of-flight and the signal propagation along the read-out strips. A gaussian fit is then performed and the correponding σ is divided by $\sqrt{2}$. The estimated time resolution is around 3 (4) ns for RPC (XPC) layers, as shown in figure 3. These values are within the required specifications for ensuring a space resolution of $\sim 300\ \mu$m in the drift tubes.

3.4 Wall support structure

The wall support structure ("walls") is made of thin stainless steel vertical bands welded to light horizontal trays where the bricks are positioned with a precision of one millimeter. The structure is suspended through rods and joints from the general support structure and tensioned from the bottom through a spring system. The walls were installed in parallel with the plastic scintillators. This project has been under the responsibility of LNF-SSCR and was successfully completed in 2006 [3]. In 2007 only maintenance operations (see Sec. 3.7), fixing of damaged parts and alignment updates during the filling phase have been carried out.

3.5 Brick Assembly Machine

In 2007, the Brick Assembling Machine project had to face major difficulties during the startup of the mass production. In response to this, LNF increased substantially its involvement in this enterprise. The mechanical properties of the input material for the brick (mainly the new Ca-

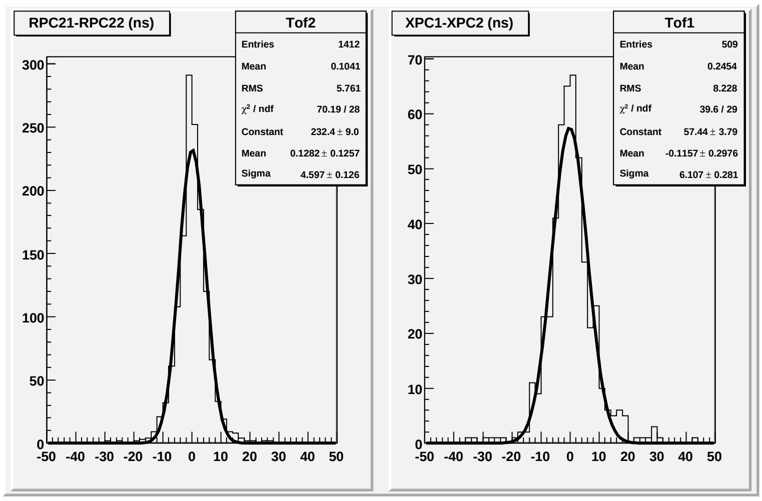

Figure 3: Arrival time difference between RPC21 and RPC22 (plot at left), and between XPC1 and XPC2 (plot at right) in the first spectrometer. The values in the histograms have been corrected for the propagation along the read-out strips and the muon time-of-flight. To estimate the time resolution, the σ estimated with the gaussian fit must be divided by $\sqrt{2}$.

Pb alloy and the emulsions) have turned out to be significantly different with respect to early expectations. At the time of the commissioning and delivery at LNGS, the BAM piling stations were inadequate to handle these materials and the production rate was extremely slow. In 2007 all the 5 piling stations have been re-optimized by the firm in charge of the construction of the BAM (Tecnocut snc) in collaboration with INFN-Naples, LNGS and LNF-SSCR. Several changes have also been done in the system handling the lead boxes and, particularly, in the wrapping system after the lead-emulsion piling phase. In March 2007 the average production was 60 brick/day and it increased steadily up to 650-700 brick/day in October. Thanks to these efforts, OPERA was able to complete the first supermodule in November 2007. At present production rate, the full detector is expected to be ready by summer 2008. Up to the completion of the OPERA target, LNF is also responsible for the organization and management of the production shifts, the maintenance of the BAM database and its interface with the OPERA central database.

3.6 The LNF scanning station

Emulsion layers are made of gel with interspersed AgBr crystals; in the case of OPERA, two such layers, each 40 μm thick are poured on a 200 μm plastic base. A particle crossing an emulsion layer ionises the medium, leaving a sequence of “sensitized” sites. After development, these sites are turned into silver grains, with a linear dimension of about 0.6 μm. About 30 grains every 100 μm are left by a minimum ionizing particle.

Nuclear emulsions are analyzed by means of optical microscopes: adjusting the focal plane of the objective lens through the whole emulsion thickness allows to obtain an optical tomography of each field of view, in order to reconstruct 3D tracks. A detailed description of the automatic microscopes developed for OPERA can be found in Ref. [9].

During 2006, two microscopes have been installed in Frascati. In 2007 one of this has been commissioned and aligned. The scanning laboratory is now fully instrumented with the handling system for the oil, the air conditioning and remote climate control station. It is expected to start nominal scanning procedures by the end of 2008.

3.7 Brick handling

During nominal CNGS operation, about 20 neutrino interactions per day occur in the OPERA target and several candidate bricks are tagged as containing the corresponding primary vertex. These predictions are validated scanning preliminarily a pair of detachable emulsions ("changeable sheets", CS). If confirmed, the corresponding brick is extracted, aligned using an X-ray machine and sent to the emulsion development facility located on surface. All the operations of CS and brick handling require dedicated tools and personnel running synchronously with the CNGS data taking. LNF is responsible of the coordination of these tasks and provides most of the tools for brick handling. In particular, in 2007 LNF-SPAS started the design of the unloading station and defined the procedure aimed at delivering the extracted bricks from the BMS to the X-ray marking area. The full operation chain is planned to be operative by summer 2008. Some brick handling tasks have also been planned during the filling phase of the target: they include cleaning and maintenance of the walls, delivery of the temporary containers of the bricks ("drums") from the BAM to the BMS loading stations and the above-mentioned displacement of the stations after the completion of SM1 (see Sec.3.1). These tasks have been coordinated by LNF-SPAS and LNF-SSCR in collaboration with external firms; they will continue until the completion of SM2 (summer 2008).

3.8 Software and analysis

In the last two years LNF has given major contributions to the online and offline software and analysis tools; LNF (A. Cazes) is currently responsible for the reconstruction of the electronic detector data, both at the level of single digit (calibration, alignment, etc...), in collaboration with the sub-detectors experts (INFN-Padova, Strasbourg, Hamburg), and at the level of the global event reconstruction. We provided crucial tools for the CNGS run: the online event display, the definition and implementation of the data format for the electronic detectors. Furthermore, we colaborated with the Lyon group to provide muon predictions extrapolated at the locations of the emulsion bricks [10]. In 2007 the brick finding strategy has been finally tested with real CNGS data: this allowed a re-optimization and validation of the pattern recognition and track finding strategy that acts as an input for the brick finding algorithms. Several improvements have also been achieved in the 3D reconstruction of tracks and a new algorithms for tracking in the occurrence of cosmic events have been developed (INFN-LNF, INFN-Bo, Hamburg). Finally, LNF contributes to the development of the spectrometer slow control (SC) and the interface (through CORBA protocol) with the overall OPERA DAQ/SC system.

4 List of Conference Talks by LNF Authors in Year 2007

1. A. Paoloni "The OPERA experiment", Four-Seas-Conference, Iasi, Romania, 29 May - 3 June 2007.

2. M. Spinetti, “OPERA”, Workshop on Next Generation Nucleon Decay and Neutrino Detectors 2007, Act City, Hamamatsu, Japan, 2-5 October 2007
3. F. Terranova “First results from OPERA/CNGS”, 21st International Workshop on Weak Interactions and Neutrinos (WIN07), Kolkata, India, January 15-20, 2007
4. A. Cazes, "OPERA, Première Données", Plenary meeting of the french GDR Neutrino. CENBG-Bordeaux (France), October 25-26, 2007.

References

1. M. Guler *et al.*, OPERA proposal, CERN/SPSC 2000-028, SPSC/P318, LNGS P25/2000.
2. M. Komatsu, P. Migliozzi, F. Terranova, J. Phys. **G29**, 443 (2003); P. Migliozzi, F. Terranova, Phys. Lett. **B563**, 73 (2003).
3. See “LNF 2006 Annual Report”, M. Antonelli ed., LNF-07/10 (IR), p.87; “LNF 2005 Annual report”, E. Nardi ed., LNF-06/10 (IR), p.78; “LNF 2004 Annual Report”, E. Nardi ed., LNF-05/5 (IR), p.70; “LNF 2003 Annual Report”, S.Dell’Agnello ed., LNF-04/08 (IR), p.64.
4. A. Cazes *et al.*, JINST **2**, T03001 (2007).
5. R. Adinolfi Falcone *et al.* Nucl. Phys.Proc.Suppl. **B172**, 165 , (2007).
6. A. Candela, G. Felici, F. Terranova, “The Opera power distribution system”, LNF-07/7 (NT), 2007.
7. A. Mengucci, A. Paoloni, M. Spinetti, L. Votano, Nucl. Instrum. Meth., **A583**, 264 (2007).
8. M. Bazzi *et al.*, Nucl. Instrum. Meth., **A580**, 1441 (2007).
9. N. Armenise *et al.*, Nucl. Inst. Meth. **A551**, 261 (2005).
10. R. Acquafredda *et al.* [OPERA Collaboration], New J. Phys. **8**, 303 (2006).

RAP

M. Iannarelli (Tecn.), R. Lenci (Tecn.), C. Ligi (Art.23), A. Marini (Resp. Naz.),
G. Mazzitelli, G. Modestino, G. Pizzella (Ass.), L. Quintieri (Art.23),
F. Ronga (Resp.), E. Turri (Tecn.), S.M. Vinko (Bors.)

1 Aim and description of the experiment

The primary scope of the experiment RAP is to measure the longitudinal vibrations of cylindrical test masses, that are impinged by the electrons provided by the DAΦNE Beam Test Facility (BTF) and to investigate if the mechanism of the particle energy loss conversion into mechanical energy depends on the conduction state of the bar.
The experiment was motivated by the fact that the gravitational wave antenna Nautilus has detected high energy cosmic rays at a rate higher than expected when the bar was operated at $T = 0.14$ K, that is in the superconductive (s) state. On the contrary, the observed rate of high energy cosmic rays was in agreement with expectations when the bar was operated at $T = 1.5$ K, that is in the normal (n) state.
The oscillations of a bar caused by interacting high energy particles have been described by models [1, 2, 3] that account for the excitations of the longitudinal modes of vibration due to pressure sources related to the energy lost by particles in the interaction. For a thin cylinder in the n state, if a particle normally impinges on the middle point of the generatrix then the maximum amplitude of the first longitudinal mode of oscillation (FLMO) is given by [1]:

$$B_0^n = \frac{2\alpha^n LW}{\pi c_V^n M} \, , \tag{1}$$

where L and M are the cylinder length and mass, W is the total energy lost by the particle in the cylinder, α^n and c_V^n are respectively the linear thermal expansion coefficient and the specific heat at constant volume of the material in the n state. B_0 is related to the pressure source due to thermal effects. The expected FLMO maximum amplitude is given by $X_{exp} = B_0^n(1+\epsilon)$, where ϵ is estimated by a montecarlo simulation, which takes into account the solutions at the 2nd order for the modes of oscillation of a cylinder, the transverse dimension of the beam at the impact point and the angles with the cylinder axis of the secondary particles generated in the bar. To evaluate B_0 at different temperatures and for each beam pulse, α and c_V are computed by interpolating data available on the literature, while W is given by $N_e \times \Delta E$. The number of electrons per pulse, N_e, is measured by the BTF beam monitor facility, while the average energy lost by each electron in the interaction, ΔE, is estimated by the montecarlo simulation. In order to assess the models, X is compared with the values of the measured FLMO maximum amplitude, which is given by $X_{meas} = V_{meas}/(G\lambda)$, where λ is the electro-mechanical conversion factor of the piezoelectric transducers (Pz), G is the amplifier gain and V_{meas} is the maximum amplitude of the signal component at the FLMO frequency, which is obtained by Fast Fourier Transform algorithms

applied to the digitized Pz signals. Two ways of comparing data and expectations are possible when the bar is in the s state. In the first mode data are compared against $X_{exp} = B_0^s(1+\epsilon)$, where B_0^s is given by (1) using α^s and c_V^s. The second way [2, 3] takes into account two pressure sources: one due to $s-n$ transitions in small regions centered around the particle tracks and the other due to thermal effects in these regions now in the n state. Therefore X_{exp} is given by $X_{tr} + X_n$, where X_{tr} is a function of the specific volume and enthalpy variations in the $s-n$ transition.
The experimental setup (*viz.* the beam, the test masses, the suspension system, the cryogenic and vacuum system, the mechanical structure hosting the cryostat, the readout and the data acquisition system) is described in [4, 6]. In particular two test masses have been used: one made of AL5056, the same material of NAUTILUS, which has a critical temperature $T_c \sim 0.9\ K$, and one made of Nb ($T_c \sim 9\ K$).
INFN and Physics Department Università di Roma Tor Vergata and Kamerlingh Onnes Laboratory, Leiden University (The Netherlands) are participating Institutions to the experiment.

2 Short summary of the 2006 activities

Two lines of activity were performed in the year: *a*) the commissioning of the dilution refrigerator, needed to cool the AL5056 bar at temperatures below 1 K where the material is in the s state and *b*) the completion of the analysis of the data taken with the Nb bar.

a) The manufacturer completed the shipment of the dilution refrigerator components on January, 2006. The assembly of the refrigerator inside the cryostat required the $ex-novo$ realization of parts and the first cooling at LHe temperature occurred on September, revealing leaks in the cryogenic system. The completion of the commissioning was planned for Spring 2007.

b) The data collected in the year 2005 with the Nb bar were fully analyzed and the results were published [5]. A good agreement was found among observed and expected values for Nb in n state. For Nb in s state a linear dependence of X_{meas} on the measured energy deposited by the beam pulses as well as oscillation amplitudes smaller than those expected for the n state were observed. Moreover, a possible agreement with the predictions of the models taking into account local transitions was found. The conclusion was that the amplitude of oscillations due to the energy released by particles impinging on the bar depends on the state of conduction and that a final investigation on the AL5056 bar cooled at temperatures below 1 K was needed, since the amplitude is expected larger for aluminum in the s state.

3 Activities in the year 2007

The activities have been focussed on (a) the preparation of the cryogenic system for the measurements on the AL5056 at the BTF and (b) the measurement execution at $T < 1$ K.

a) The setup of the dilution refrigerator and of the ancillary equipments was completed in spring. A malfunction of the heat exchanger between the Still and the Mixing chamber was detected during the characterization phase. As data taking at BTF get near, a temporary solution was found by running the refrigerator in ^{3}He evaporation mode ($T_{min} \sim 0.5$ K).

b) Data taking on the AL5056 bar was successfully performed at BTF in an interval ranging from room temperature down to 0.5 K. Fig.1 (left) shows the measured values of FLMO maximum amplitudes (X) normalized to the total energy lost per beam pulse (W) at $T < 1.3$ K: for $T > 0.9$ K data agree with the expectations for the n state, the onset of the s state effects appears at $T < 0.9$ K and at $T < 0.7$ K the amplitude is larger than in the n state. This fact gives a qualitative explanation of the cosmic ray observation made by NAUTILUS operating in s state. Fig.1 (right) shows the averages of the FLMO maximum amplitudes normalized to the total energy lost per beam pulse as a function of T after the grouping in four classes of deposited energy: a possible dependence of the average normalized amplitudes on the deposited energy appears; the figure also shows the same quantity as derived by the analysis of the cosmic ray events detected by NAUTILUS operating in s state, which is compatible with the data of RAP.

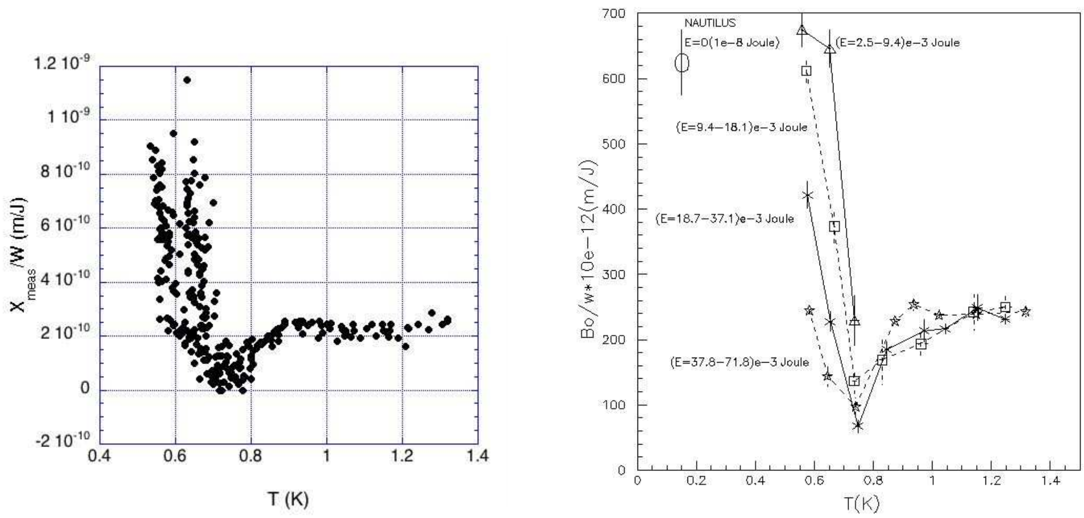

Figure 1: *AL5056 - Left: FLMO maximum amplitudes (X) normalized to the total energy lost per beam pulse (W) vs. temperature (T). Right: Averages of the FLMO maximum amplitudes (X) normalized to the total energy lost per beam pulse (W) vs. temperature (T); see text.*

4 Planned activities for the year 2008

The activities will be aimed at performing the measurements at BTF at temperatures below 0.5 K, in order to explore the region in which NAUTILUS was operated.

5 List of Conference Talks by LNF Authors in the Year 2007

- S.M. Vinko, "The RAP experiment: acoustic detection of particles in Niobium and Aluminum bars", SIF, Pisa - September 26, 2007.

References

1. A.M. Grassi Strini *et al.*, J. Appl. Phys. **51**, 948 (1980).
2. A.M. Allega and N. Cabibbo, Lett. Nuovo Cim. **38**, 263 (1983).
3. C. Bernard *et al.*, Nucl. Phys. B **242**, 93 (1984).
4. B. Buonomo *et al.*, Astropart. Phys., **24**, 65 (2005).
5. M. Bassan *et al.*, Europhys. Lett. **76**(6), 987 (2006).
6. C. Ligi and S. M. Vinko, LNF - 07 / 4(IR) (2007).
7. M. Bassan *et al.*, Nucl. Phys. B (Proc. Suppl.), **172**, 219 (2007).

ROG

G. Giordano (Resp.), M. Iannarelli (Tecn.), R. Lenci (Tecn.),
A. Marini, G. Modestino, G.P. Murtas (Ass.), G. Pizzella (Ass.),
L. Quintieri (Art. 23), F. Ronga (Resp.), E. Turri(Tecn.)

Collaboration with: LNGS, INFN Genova,
University of Rome La Sapienza and INFN Roma 1,
University of Rome Tor Vergata and INFN Roma 2,
Geneva University

1 Introduction

The ROG group is currently operating two cryogenic gravitational wave (GW) bar detectors: EXPLORER (at CERN) and NAUTILUS (in Frascati). The main goal of this search is the direct detection of the GW's that could be emitted by astrophysical sources (such as Supernovae or Coalescent Binaries). Such detection would be of enormous interest for general relativity and astrophysics.

Both detectors consist of an aluminum cylindrical bar having a mass of $\simeq 2.3$ tons, with a capacitive resonant transducer mounted on one of the bar faces. They are contained in a vacuum cryostat, cooled at cryogenic temperatures ($\simeq 3$ K) to reduce thermal noise, and are isolated from seismic and acoustic disturbances.

The capacitive transducer is coupled to a very low noise superconducting amplifier (d.c. SQUID) whose output is acquired by a VME ADC board, sampled at 5 kHz.

A GW signal would excite the mechanical resonant modes of the bar-transducer system. When searching for impulsive signals, the data are filtered with an adaptive filter matched to a delta-like signal. This search for bursts is suitable for any transient GW which shows a nearly flat Fourier spectrum at the two resonance frequencies of each detector.

Both EXPLORER and NAUTILUS have been kept in continuous observational mode since 2003, with a duty cycle between 80 and 90%, mainly limited by the necessary periodic cryogenic operations.

The LNF group has major responsibilities in the maintenance and running of NAUTILUS (including the production of liquid Helium), in the maintenance, upgrading and running of the cosmic ray detectors, in the development of a new nearly quantum limited signal read-out, in the data acquisition and in many items of data analysis.

2 NAUTILUS and EXPLORER

The ultra-cryogenic detector NAUTILUS is operating at the INFN Frascati National Laboratory since December 1995. It is equipped with a cosmic ray detector based on a streamer tube assembly.

The present data taking started in 2003, with a new bar tuned at 935 Hz, where a pulsar, remnant of the SN1987A, is supposed to emit GW's, with a more sensitive readout chain (the same as for EXPLORER), and a new suspension cable, to provide a more stable position setting. At present, the temperature of the bar is 3.5 K and the resulting strain noise (the minimum detectable spectral density) is $\tilde{h} \simeq 1 \div 2 \cdot 10^{-21}\ /\sqrt{Hz}$ around 935 Hz, and $\tilde{h} \leq 10^{-20}\ /\sqrt{Hz}$ over about 30 Hz. The noise temperature is less than 2 mK, corresponding to an adimensional amplitude of GW bursts $h = 3.4 \cdot 10^{-19}$.

NAUTILUS is the only resonant detector capable of reaching a temperature as low as 0.1 K, being equipped with a ^{3}He-^{4}He dilution refrigerator. This ultra-cryogenic operational mode would result in a better sensitivity but also in a decrease of the duty cycle. Up to now, we decided to give the priority to the observational time and so we keep the standard operation at 3 K.

The EXPLORER antenna is located at CERN and is very similar to NAUTILUS, but can operate only down to 2.6 Kelvin. Also the duty cycle of EXPLORER is very high (of the order of 90%) and the noise temperature of the order of 2 mK, with a strain sensitivity $\tilde{h} \simeq 2 \div 3 \cdot 10^{-21} \ /\sqrt{Hz}$ around the two resonances at 904 Hz and 927 Hz, and $\tilde{h} \leq 10^{-20} \ /\sqrt{Hz}$ over about 30 Hz. Also EXPLORER is equipped with a cosmic ray detector, based on a set of long plastic scintillators.

The read-out systems installed in 2001 on EXPLORER and in 2003 on NAUTILUS, obtained a larger bandwidth and consequently improved the time resolution (now less than 10 ms), as it is also been checked with the events due to cosmic ray showers.

3 Read-out developments

The read-out of all the resonant-mass GW detectors is based on an electromechanical transducer (capacitive or inductive) and a d.c. SQUID amplifier.

In most practical applications the sensitivity of a SQUID with a standard electronics is usually good enough. However GW detectors require the highest possible sensitivity of a d.c. SQUID. In this case the standard read-out may not be the best solution, because the overall sensitivity can be limited by the room-temperature preamplifier noise. With this standard setup the typical energy resolution measured by the detector is about $20000\hbar$.

The sensitivity of a resonant-mass detector is limited by three sources of noise which, referred to the output are: the narrowband thermal noise, due to the input wideband brownian motion of the resonant masses, which appears at the output after passing through the mechanical transfer function of the system; the wideband amplifier noise, which appears directly at the output and the narrowband back-action noise, originated from the back-energy flow from the amplifier, which excites the resonant masses.

The useful bandwidth of such detectors is by no means limited to the very narrow width of the high Q mechanical resonance. Rather, it is the amplifier noise that limits the bandwidth. The lowest spectral noise is found in the frequency region where the narrowband (thermal plus back action) noises dominate the amplifier noise, and there the noise level is the sum of the two. As a consequence, any reduction in the amplifier noise and/or increase in transducer coupling, increases the antenna bandwidth.

In the last years, it has been shown that a double-SQUID system can reach quantum limit energy resolution and that a double-SQUID system can be arranged in a stable configuration when connected to a high-Q resonant circuit. The double-SQUID amplifier of the ROG Collaboration is made of a sensor d.c. SQUID, developed by the Institute of Photonic and Nanotechnologies of CNR, while the preamplifier SQUID is a commercial Quantum Design d.c. SQUID. The performances of the device are very good: with open input and open loop it exhibited energy resolutions equal to $28\hbar$ at 4.2 K and $5.5\hbar$ at 0.9 K.

With this new device, the expected NAUTILUS sensitivity at 0.1 K is around $3 \cdot 10^{-22}\mathrm{Hz}^{-1/2}$ and the bandwidth, at the level of $10^{-21}\mathrm{Hz}^{-1/2}$, is about 35 Hz. The noise temperature of the detector should be around 7μK corresponding to a sensitivity to 1 ms bursts $h = 2.1 \cdot 10^{-20}$.

An even better type of d.c. SQUID has recently been produced by CNR and is currently under test.

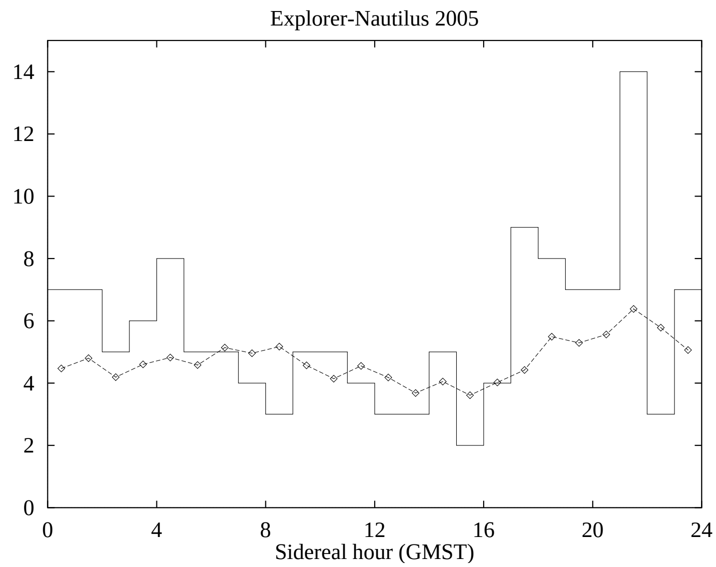

Figure 1: Explorer-Nautilus coincidences in 2005. Number of coincidence and average accidentals as a function of sidereal hour.

4 Data analysis

In the last years a continuos effort has been payed in improving the data analysis system already present and in testing independent algorithms and new methods. As a result of these, still going, efforts we were able to improve the accuracy in the reconstruction of both the amplitude and time characteristic of the signals. At the same time, we performed detailed studies of the detectors response to other class of signals than the simple delta-like burst previously considered. All this was done also with a particular eye on the perspective of performing joint analyses with the interferometric type of GW detectors.

4.1 EXPLORER-NAUTILUS coincidences

We continued to study all possible wide-band noises that can result in a candidate event and also, through simulations and software injections of signals, to find the event characteristics (e.g. length vs. amplitude) that an event due to a real excitation must have. All this aims to reduce the number of candidate events, but, being this study not yet finalized, we decided to maintain the same analysis conditions used in 2003 and 2004, namely a threshold at 19.5 in energy signal to noise ratio and a coincidence window fixed at 30 ms.

In 2005 we had a total overlap of 182.1 days of good data periods for both Explorer and Nautilus. The average number of accidentals, estimated as usual with realtive shifs in time between the Explorer and Nautilus events, was 113.51, the true coincidences were 136. Fig.1 shows the distribution of coincidences and accidentals as a function of the sidereal time.

We notice that in 2005 the sidereal time distributions show some differences between coincidences and accidentals, but the main feature is the significant difference between the numbers of true coincidences and accidentals, 136 against an expected value of 113.51, a fluctuation of probability about 0.022.

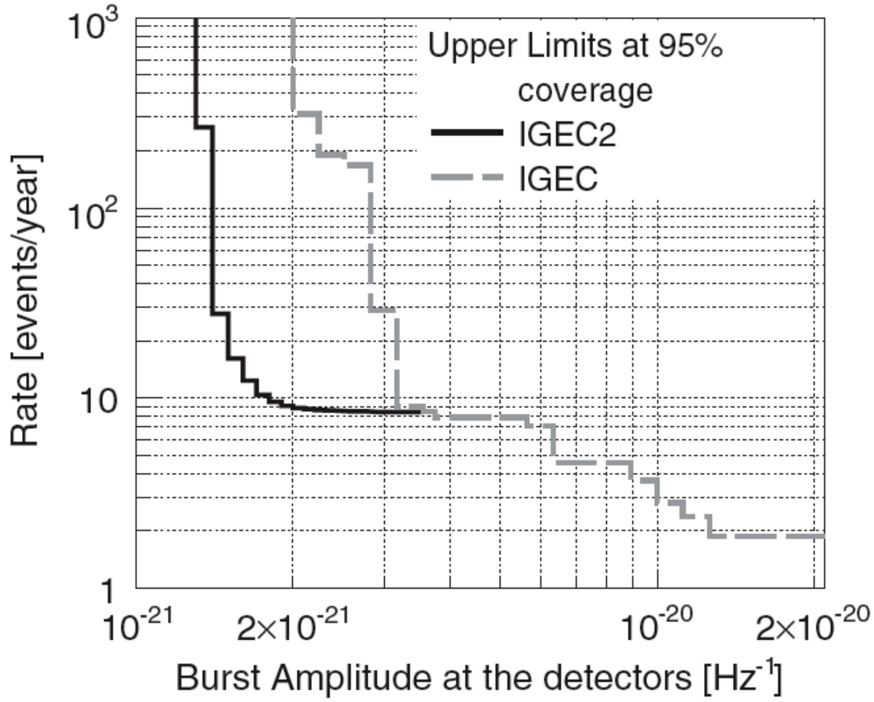

Figure 2: Upper limit at 95% on the rate of detectable GW events as a function of the threshold in amplitude used in the search.

4.2 IGEC-2 collaboration

The bar detectors distributed worldwide operated for a few years (1997-2000) as a network, giving for the first time significant upper limits to the yearly rate of GW burst events in the Galaxy. In 2003 and 2004 EXPLORER and NAUTILUS have been the only two detectors in data taking over long time periods. Since 2005 both Auriga at LNL and Allegro at the Lousiana State University restarted regular operation, so the former IGEC collaboration was restarted, under a new agreement (IGEC-2) between the 4 bar detectors.

The network of resonant bar detectors of gravitational waves resumed coordinated observations within the International Gravitational Event Collaboration (IGEC-2). Four detectors are taking part in this Collaboration: ALLEGRO, AURIGA, EXPLORER and NAUTILUS. We present here the results of the search for gravitational wave bursts over 6 months during 2005, when IGEC-2 was the only gravitational wave observatory in operation. The implemented network data analysis is based on a time coincidence search among AURIGA, EXPLORER and NAUTILUS; ALLEGRO data was reserved for follow-up studies. The network amplitude sensitivity to bursts improved by a factor of 3 over the 1997-2000 IGEC observations; the wider sensitive band also allowed the analysis to be tuned over a larger class of waveforms. Given the higher single-detector duty factors, the analysis was based on threefold coincidence, to ensure the identification of any single candidate of gravitational waves with high statistical confidence. The false detection rate was as low as 1 per century. No candidates were found.

The search for coincidences among ALLEGRO, AURIGA, EXPLORER and NAUTILUS has

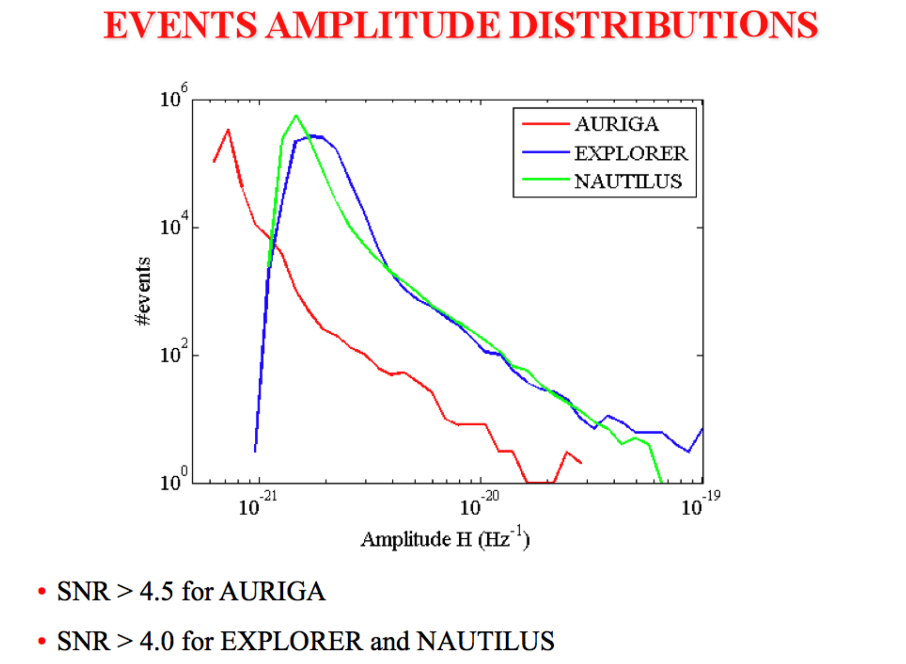

Figure 3: Events amplitude distribution for AURIGA, EXPLORER and NAUTILUS in 2006.

Table 1: Number of days with detectors in simultaneous operation.

# detector	days
no detector	0.9
only one	19.9
only two	140.8
three	249.4

continued with the data obtained in 2006. The final result is not available yet. We show in the fig.3 the distribution of the events which shall be used for the coincidence search and in the Table 1 the number of days of operation.

4.3 Collaborations between resonant bars and interferometers

A first joint data analysis between all the INFN GW detectors (AURIGA, EXPLORER, NAUTILUS and VIRGO) has been performed for the period of the VIRGO C7 run (September 2005). Since the period was really short (VIRGO could provide only less than 1 day of good data), the analysis has addressed more methodological than scientific issues. The efficiency of each detector separately, and then of the network, was extensively studied through a large number of software injections of damped sinusoid signals with 11 different carrier frequencies or damping times. The detailed knowledge of the efficiency as a function of time has been employed in the study of possible optimized ways for the selection of vetoes and thresholds. A publication concerning the results obtained is currently in preparation.

An agreement between LIGO and all the groups forming the IGEC collaboration (Allegro, Auriga and ROG) is being established. Likely, this agreement will conceive the common analysis of about 1÷2 months of data, that is the period of the LIGO S5 run, started in November 2004 and still going, when only one of the LIGO interforemeters was in operation. In such periods, LIGO cannot hope to perform any detection by itself and so the addition of the IGEC bar detectors will retrieve these periods.

4.4 Other type of analyses

- Cosmic Rays - The study of the response of our detectors to cosmic ray showers continues to demonstrate experimentally the actual capability to detect very small mechanical excitations of the bars. While the study of the timig characteristics of the larger events produced by the rare very high density showers allows us a real measure of the accuracy in the time reconstruction, the study of the much more numerous cases of low density showers, performed with a cumulative-type analysis, constitutes an independent cross-check of the amplitude response calibration.

- Search for monochromatic signals -

The search for periodic gravitational wave signals is a stimulating challenge for data analists because of the considerable amount of computing time required. For blind searches, i.e. without any a priori knowledge about the source, a fully coherent analysis can not handle more than a few days of data because of the steep dependence of the size of the parameter space on the frequency resolution. In the past, data from the Explorer 1991 run have been coherently studied by means of the F statistics method which led to and an upper limit of $h = 10^{-22}$ in the narrow band 921.00-921.76 Hz.

In the work published in 2007, the simple technique of adding power spectra has been applied to the most sensitive 40Hz band of the 2005 run of the Explorer bar, resulting in a further improvement on the best upper limit on h, which is set to $3 \cdot 10^{-23}$ at 920.14Hz.

- Search triggered by astrophysical events - The analysis of our detectors data at the time of a large number of Gamma-ray bursts allowed us to set upper limits on the amplitude of possible GW signals associated to them. This kind of study is continuing and actually has been extended to detailed analysis of the data collected in coincidence with some rare astrophysical events, like the giant flares happened 1998 and 2004.

- SN1987A revisited - The measurements made with the neutrino detectors during the supernova SN1987A are revisited. It is shown that, while the LSD detector observed just one burst at $2^h 52^{min} 36.8^{sec}$ U.T., the Kamiokande data show a possible second burst, in addition to the well known burst at $7^h 35^{min} 33.7^{sec}$ U.T.

This second burst consists of a cluster of seven pulses, well above background, during 6.2 seconds at $7^h 54^{min} 22.2^{sec}$ U.T., with an imitation rate of several hundreds years. These observations imply a long duration of the collapse.

5 ROG publications in 2007

1. P. Astone *et al* “All-sky incoherent search for periodic signals with Explorer 2005 data.” e-Print: arXiv:0708.4367 [gr-qc]

2. P. Astone *et al* “Results of the IGEC-2 search for gravitational wave bursts during 2005” Phys.Rev. **D76** 102001 (2007)

3. P Galeotti and G. Pizzella “SN1987A revisited after 20 Years: May the supernova bang more than once?” *Venice 2007, Neutrino telescopes* 27-32, e-Print: arXiv:0706.2235 [gr-qc]

WIZARD

G.Basini, F.Bongiorno (Ass.), L.Bongiorno (Bors.),
G.Mazzenga (Tecn.), M.Ricci (Resp.)

Participant Institutions:

ITALY: INFN Bari, LNF, Firenze, Napoli, Roma Tor Vergata, Trieste;
CNR Ist. Fisica Applicata "Nello Carrara" Firenze;
ASI (Italian Space agency);
Electronic Engineering Department, University of Roma 2 "Tor Vergata";
RUSSIA: MePhi Moscow;
FIAN Lebedev Moscow;
IOFFE St Petersburg;
TsSKB-Progress Samara;
SWEDEN: KTH Stockholm;
GERMANY: Siegen University;
USA: NASA Goddard Space Flight Center;
New Mexico State University.

1 Experimental Program and Scientific Objectives

The WIZARD experimental program is devoted to the extensive study of cosmic ray spectra (particles, antiparticles, isotopes, abundances and search for antimatter) in several energy ranges achievable through different instruments on board stratosferic balloons and long duration satellite missions. WIZARD is an International Collaboration between several Universities and Research Institutions from Russia, Sweden, Germany, USA togheter with the Space Agencies NASA, RSA (Russia), SNSB (Sweden), DLR (Germany) and ASI. The experimental activities have been and are carried out through three main programs:

- Stratospheric Balloon flights;
- Satellite missions NINA-1 and NINA-2;
- Satellite mission PAMELA.

We refer to previous editions of this report for the descrition of the activities related to the balloon flights and to the two NINA missions.

1.1 The satellite mission PAMELA

PAMELA is a cosmic ray space experiment installed on board a Russian satellite (Resurs-DK1) which has been successfully launched on June 15th, 2006 from the cosmodrome of Baikonur, Kazakhstan, by a Soyuz TM2 rocket. Fig. 1 shows the lift-off of the rocket.

The satellite is due to fly for at least 3 years in a low altitude, elliptic orbit (350-610 km) with an inclination of 70.0 degrees. The PAMELA telescope consists of a magnetic spectrometer composed of a permanent magnet coupled to a silicon tracker, an electromagnetic silicon-tungsten calorimeter, a time-of-flight system, an anticoincidence system, a shower tail catcher scintillator

Figure 1: *Lift-off of the Soyuz rocket from the Baikonur cosmodrome.*

and a neutron detecto wn in fig.2 and a photo
of the completed Fligh

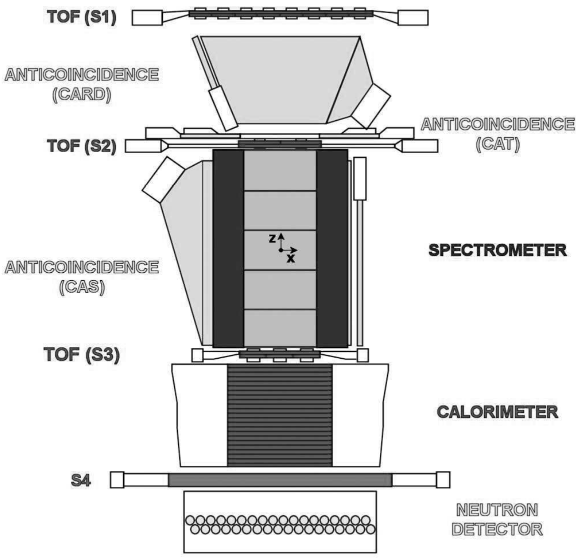

Figure 2: *Sketch of the flight detectors the PAMELA telescope.*

The total height of PAMELA is $\sim$ 130 cm, the mass is 470 kg and the power consumption is 355 W.

The observational objectives of the PAMELA experiment are to measure the spectra of antiprotons, positrons and nuclei over an extended range of energies, to search for antimatter and for indirect signatures of dark matter and to study cosmic ray fluxes over a portion of the Solar cycle.

The main scientific goals can be schematically listed as the following:

a) measurement of the antiproton spectrum in the energy range 80 MeV-190 GeV;
b) measurement of the positron spectrum in the energy range 50 MeV-270 GeV;
c) measurement of the electron spectrum in the energy range 50 MeV-400 GeV;
d) measurement of the proton spectrum in the energy range 80 MeV-700 GeV;
e) measurement of the electron+positron spectrum up to 2 TeV;

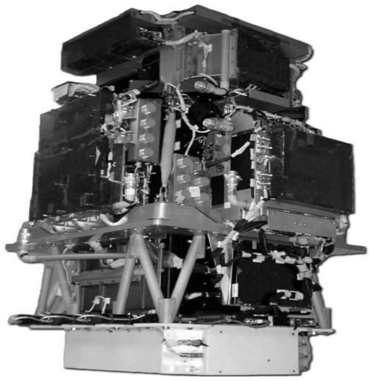

Figure 3: *The PAMELA Flight Model.*

f) measurement of light nuclei spectra (up to Z=6) at energies 100 MeV/n - 200 GeV/n;
g) search for antinuclei with a sensitivity better than 10^{-7} in the $\overline{He}/He$ ratio (95% C.L.).

Additional objectives are:
Long-term monitoring of the solar modulation of cosmic rays;
Measurements of Energetic Particles from the Sun;
High-energy Particles in the Earth magnetosphere and Jovian electrons.

So far, the satellite and the PAMELA instrument are functioning nominally and the overall performance of the detectors is fairly good. Every day, an average of 14 GBytes of data are transmitted to the main Receiving Station NTsOMZ located in Moscow. Then, alla data are transferred through high-speed networks to CNAF, Bologna and to the participating institutions of the PAMELA International Collaboration where preliminary analysis of data has started. PAMELA, at present, after 650 days of continuous data taking, has collected some 9 TByte of data corresponding to about 1 billion events. A sample of events gathered in flight is displayed in figs. 4-7 where a 18 GeV electron, a 70 GeV positron, a 35 GeV interacting proton and a 11.6 GeV interacting antiproton are shown, respectively.

Activity in the year 2007 has covered the following items:

Mission control (shifts at NTSOMZ ground station, Moscow)
Continuos data taking
Data analysis - setup of working groups
Presentation of preliminary results at several conferences
Additional beam test at CERN SPS of the PAMELA technological detectors

2 Activity of the LNF group during year 2007

The LNF WIZARD group has been fully involved in all the previous balloon and present satellite programs. During the year 2007 the activity for the PAMELA experiment has been carried on as follows:
Shifts for mission control at NTSOMZ ground station, Moscow
Data analysis, preliminar phase
Responsibility of the beam test at CERN SPS (trigger, beam counters, general organization)

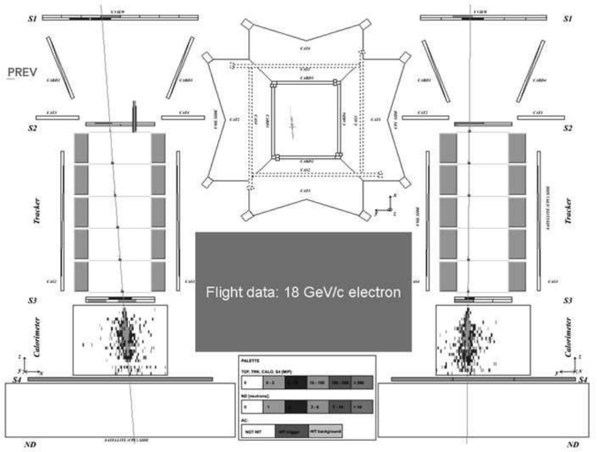

Figure 4: *Display of an in-flight 18 GeV electron*

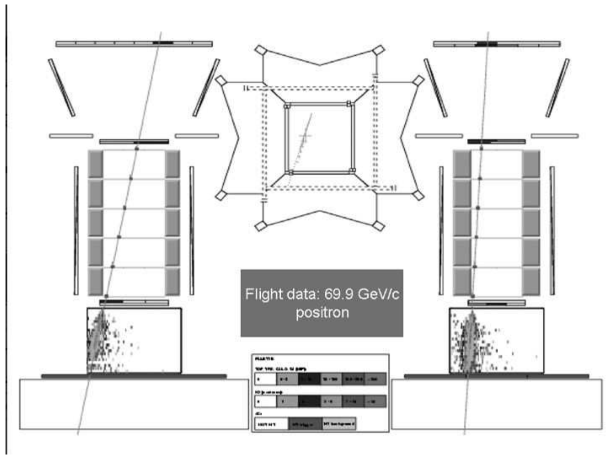

Figure 5: *Display of an in-flight 69.9 GeV positron*

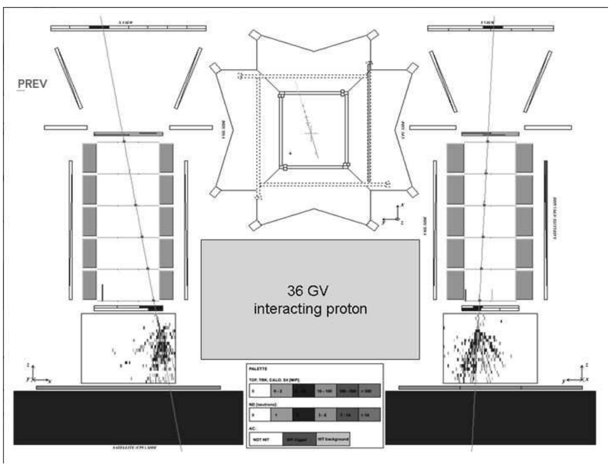

Figure 6: *Display of an in-flight 35 GeV interacting proton*

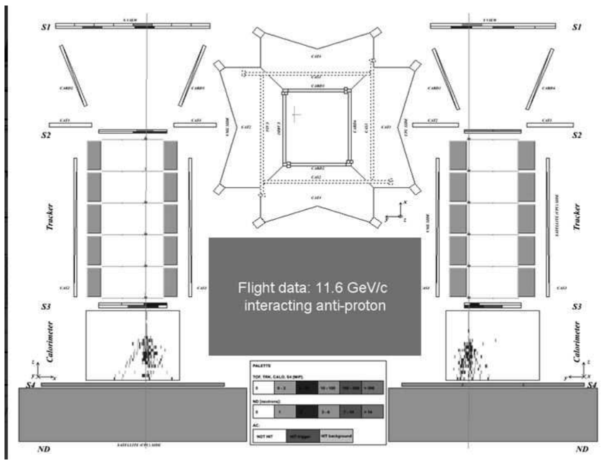

Figure 7: *Display of an in-flight 11.6 GeV interacting antiproton*

3 Planned activity in 2008

- Shifts at NTsOMZ ground control center for the monitoring of the mission and data transmission to ground.
- Continuation of data analysis, presentation to Conferences and publication of first results.
- Beam tests of detectors of the Technological/Engineering Model at GSI/Darmstadt (nuclei).

4 A selection of Publications in 2007

1. P. Picozza *et al.*,"PAMELA - A Payload for Antimatter Matter Exploration and Light-nuclei Astrophysics ", Astrop. Phys.**27**, 296 (2007)
2. O. Adriani *et al.*,"The Pamela Experiment Ready for Flight", Nucl. Instr. and Meth. **A572**, 471 (2007)
3. M. Casolino *et al.*,"The PAMELA storage and control unit", Nucl. Instr. and Meth. **A572**, 349 (2007)
4. L. Bonechi *et al.*,"Status of the PAMELA silicon tracker", Nucl. Instr. and Meth. **A570**, 281 (2007)
5. S. Orsi *et al.*,"A Second Level Trigger for the PAMELA Satellite Experiment", Astrop. Phys.**25**, 296 (2007)
6. M. Casolino *et al.*,"Data processing and distribution in the PAMELA experiment", Nucl. Instr. and Meth. **A572**, 351 (2007)

References

1. P. Picozza *et al.*, "PAMELA - A Payload for Antimatter Matter Exploration and Light-nuclei Astrophysics ", Astrop. Phys.**27**, 296 (2007)
2. O. Adriani *et al.*,"The Pamela Experiment Ready for Flight", Nucl. Instr. and Meth. **A572**, 471 (2007)

3 – Nuclear Physics

AIACE

M. Aghasyan (Bors. PD), E. De Sanctis, M. Mirazita (Art. 36),
J. de Oliveira Echeimberg (Dott.), A. Orlandi (Tech.), S. A. Pereira (Ass.),
W. Pesci (Tech.), E. Polli, F. Ronchetti (Art. 23), P. Rossi (Resp. Naz.), A. Viticchié (Tech.)

1 Introduction

AIACE stands for Attività Italiana A CEbaf: it is the collaboration of the INFN groups of Frascati and Genova. They participate into the physics program carried on by the CLAS collaboration, at the 6 GeV Continuous Electron Beam Accelerator Facility (CEBAF) at the Jefferson Laboratory (JLab). The CLAS collaboration counts about 150 physicists from 36 Institutions from seven Countries. Its scientific program is focused on the precision study of the structure of the nucleon and the nature of the strong interaction.

CEBAF will increase its beam energy from currently 6 GeV to 12 GeV by 2014. This requires the upgrade of the CLAS detector, called CLAS12.

In the period covered by this report, the Frascati AIACE group has continued to work in the 6 GeV program and has started its partecipation to the 12 GeV one. Concerning the current activity with the 6 GeV beam, the group has performed the analysis of strangeness photoproduction reactions and single pion photoproduction reaction. Moreover, it has started to study the Transverse Momentum parton Distribution functions (TMDs). As for the 12 GeV upgrade program, the group has centered its activity in the central detector project for CLAS12.

2 Experimental Activity at CLAS

2.1 Strangeness photoproduction

An important key in the study of the structure of the nucleon is to understand its spectrum of excited states. Mapping out this spectrum will provide insight into the underlying degrees of freedom of the nucleon. However, due to the non-perturbative nature of QCD at these energies, this task is challenging. Recent symmetric quark model calculations predict more states than have been seen experimentally [1]. Because most of our present knowledge of baryon resonances comes from reactions involving pions in the initial and/or final states, a possible explanation could be that pionic coupling to the intermediate missing N^* or Δ^* states is weak. This suggests a search for these hadronic states in strangeness production reactions. Beyond different coupling constants (e.g. g_{KNY} vs $g_{\pi NN}$), the study of the exclusive production of $K\Lambda$ and $K\Sigma$ final states has the advantage that the higher masses of the kaon and hyperons, compared to their non-strange counterparts, kinematically favor a two-body decays mode for resonances with masses near 2 GeV, a situation that is experimentally advantageous.

The photoproduction data collected for the pentaquark search on a deuteron target (G10 experiment) have been used by the Frascati group to analyze the $\gamma p(n) \to K^+\Lambda(n)$ and $\gamma n(p) \to K^+\Sigma^-(p)$ reactions in the invariant mass range from 1.54 to 2.76 GeV. These data are very suitable for measuring cross sections on bound proton and neutron.

2.1.1 Λ photoproduction

We will extract the differential cross section for the $\gamma p(n) \rightarrow K^+\Lambda(n)$ reaction from threshold up to 3.5 GeV. For the analysis a kinematic fitting code has been developed. Also an event generator to be used to calculate the CLAS detector acceptance has been set.

In order to test procedures and programs for the cross section extraction on the bound nucleon, we have first extracted the cross section of the $\gamma p \rightarrow K^+\Lambda$ reaction on free proton. For this measurement we have used an hydrogen target.

The $\gamma p \rightarrow K^+\Lambda$ photoproduction on free proton has been studied by CLAS [2] and SAPHIR [3] from threshold ($E_\gamma^{th} = 0.911$ GeV) up to 2.5 GeV. The CLAS σ_{tot} data have shown a prominent peak centered near 1.9 GeV which doesn't resemble a simple single Lorentzian, reflecting the expectation that several resonant structures are present in this mass range. Because this result differs from the SAPHIR one, namely the SAPHIR σ_{tot} is smaller than the CLAS result by a factor of close to 3/4, it is very important to have other measurements to confirm this possible resonance structure. Moreover, the study of the $\gamma p(n) \rightarrow K^+\Lambda(n)$ reaction on a proton bound in the deuteron nucleus can provide interesting information on several aspects apart from the study of the baryon resonance spectrum: *1)* since the free cross section is known, it can be used as a benchmark to test methodes to extract cross sections on bound nucleons; *2)* to test models for Final State Interaction; *3)* to extract elementary hadron-hadron cross sections not otherwise measurable; *4)* to study the propagation of exotic hadrons in nuclear matter.

The analysis of the $\gamma p \rightarrow K^+\Lambda$ has been completed and the obtained results (see Fig. 1) are in good agreement with the published data, giving us confidence on our analysis procedure.

2.1.2 Σ photoproduction

In the period covered by this report, the analysis of the $\gamma n(p) \rightarrow K^+\Sigma^-(p)$ reaction has been almost completed. The preliminary $\gamma n(p) \rightarrow K^+\Sigma^-(p)$ differential cross section has been measured using tagged photons in the energy range 1.0-3.6 GeV and at kaon center-of-mass angles between 10^o and 140^o in 10^o step. In this exclusive measurement, K^+ and π^- and n from Σ decay, are detected by the CLAS while the spectator proton is identified as missing particle, $p = MM(K^+\pi^-n)$ with the additional cut that the missing momentum should be less than 0.25 GeV/c (the proton doesn't partecipate to the reaction so its momentum is only due to the Fermi motion). The Σ^- in the $\gamma n \rightarrow K^+\pi^-nX$ is identified calculating the invariant mass of pion and neutron.

The key point of this analysis is the correct identification of the K^+ and the neutron. Being this the first analysis with a neutron detected in the CLAS, a detailed study of the neutron detection and of the electomagnetic calorimeter neutron timing calibration, have been undertaken.

After the channel identification and the background subtraction, a Monte Carlo simulation has been used to evaluate the event detection efficiency allowing the extraction of the corrected event yield. The preliminary results of the obtained event normalized yield are shown in Fig. 2.

2.2 **Single pion photoproduction reactions**

The interplay between the nucleonic and partonic pictures of the strong interaction represents one of the major issues in contemporary nuclear physics. Although standard nuclear models are successful in describing the interactions between hadrons at large distances, and QCD accounts well for the quark interactions at short distances, the physics connecting the two regimes remains unclear. In fact, the classical nucleonic description must break down once the probing distances become comparable to those separating the quarks. The challenge is to study this transition region by looking for the onset of some experimentally accessible phenomena naturally predicted by perturbative QCD. Exclusive processes are essential probes to accomplish this aim.

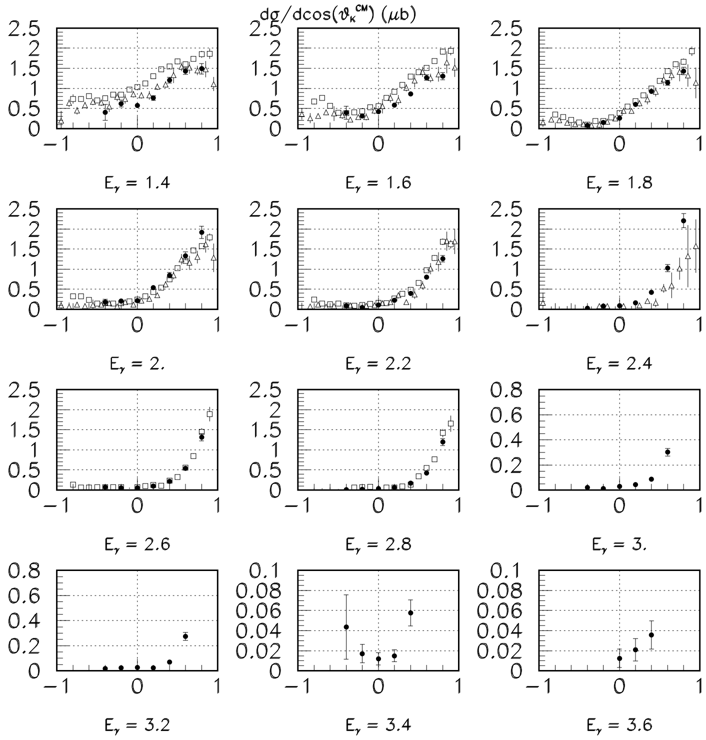

Figure 1: Differential cross section of the $\gamma p \to K^+\Lambda$ reaction (full circles) compare with SAPHIR (empty triangles) and previuos CLAS data (empty squares) for the twelve photon energy bins.

The simplest signature of the partonic picture is the validity of the constituent counting rule (CCR) for high-energy exclusive reactions [4)]. CCR predicts the energy dependence of the differential cross section at fixed center-of-mass angle for an exclusive two-body reaction at high energy and large momentum transfer as: $d\sigma/dt = h(\theta_{cm})/s^{n-2}$, where s (total energy in the center-of-mass frame) and t (momentum transfer squared) are the Mandelstam variables and n is the total number of elementary fields in the initial and final states, while $h(\theta_{cm})$ depends on details of the dynamics of the process.

The CCR scaling behavior has been investigate for the first time on the $\gamma n \to \pi^- p$ from a deuterium target at $\theta_{cm} = 50°, 70°$ and $90°$ [5)]. The results at $\theta_{cm} = 70°, 90°$ exibit a global CCR scaling behaviour at the expected transverse momentum ($\sim 1.2\ GeV/c$), and in addition, an enhancement in the scaled differential cross section at $\theta_{cm} = 90°$ below the scaling region, and at center-of-mass energy ranging approximately from 1.8 GeV to 2.5 GeV.

The aim of studying the $\gamma n \to \pi^- p$ using the G10 data, is to investigate this behavior in much finer photon energy bins and for a wide angular range and to study the angular dependence of the scaling behavior. In the period covered by this report the analysis has been completed. The differential cross section has been extracted in the angular range between 50° and 115° (in 5° steps) and in the photon energy range between 0.8 and 3.6 GeV (in 50 MeV steps). Results confirm the previous observation of a broad resonance structure around a center of mass energy of 2.1 GeV at $\theta_{cm}^{\pi^-} = 90°$ in the scaled differential cross section. They also show a center of mass angular dependence of the invariant mass of the observed new resonance structure. The scaling region is reached at backward angles (between 70 and 110 degrees) at transverse momenta of $\sim$ 1.1 GeV/c,

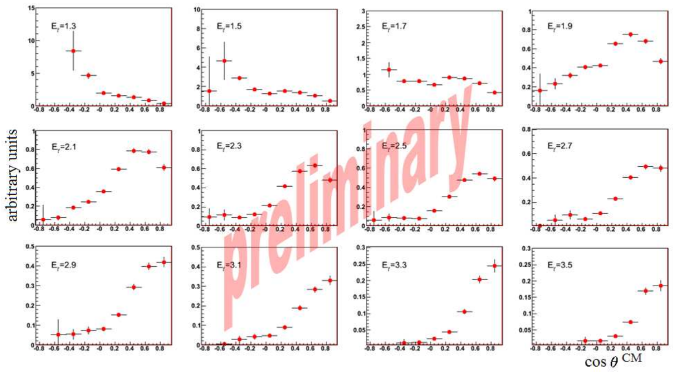

Figure 2: Preliminary normalized yield for the $\gamma n(p) \rightarrow K^+\Sigma^-(p)$ reaction.

while in more forward angles higher photon energies need to reach the scaling region.

2.3 Transverse momentum parton distribution functions (TMDs)

The spin structure of the nucleon has been of particular interest since the EMC [6] measurements, subsequently confirmed by a number of other experiments [7, 8, 9, 10, 11, 12], implied that the helicity of the constituent quarks account for only a fraction of the nucleon spin. Possible interpretations of this result include significant polarization of either the strange sea (negatively polarized) or gluons (positively polarized) and the contribution of the orbital momentum of quarks. The semi-inclusive deep inelastic scattering (SIDIS) experiments, when a hadron is detected in coincidence with the scattered lepton provide access to spin-orbit correlations. Observables are spin azimuthal asymmetries, and in particular single spin azimuthal asymmetries (SSAs), of the detected hadron, which are due to the correlation between the quark transverse momentum and the spin of the quark/nucleon. Knowledge of SSAs provide access to a list of novel distribution functions, the Transverse Momentum Dependent distribution functions (TMDs) which contain information on the parton transverse momentum.

TMDs studies are one of the primary goal of experiments at JLab 12 GeV but their investigation has already started with the 6 GeV beam using unpolarized, longitudinally and transversely polarized target. During the reporting period the Frascati group has worked on the proposal to study transverse spin effects in SIDIS at 6 GeV with an HD-Ice transversely polarized target.

3 Experimental Activity for CLAS12

The group will partecipate to the JLab 12 GeV program in Hall B. This requires an upgrade of the CLAS detector, called CLAS12. It consists of a two-part detector : a forward spectrometer and a Central Detector. The Central Detector is essentially a recoil detector which will detect particles at large angles and lower energies. It consists of three sub-detectors: a Tracker (CT), a Time-of-Flight (CTOF) and a Calorimeter and Neutron Detector. The effort to design and build this detector is lead and mainly carried by European groups.

During the reporting period the group has started to work on the Neutron Detector and on the Time-of-Flight. The physics motivation for a neutron detector is to measure DVCS on the neutron, with a deuterium target. This reaction is the most sensitive one to the GPD E. The knowledge of the GPDs E and H (the latter accessible through DVCS on the proton) can allow one to extract the orbital angular momentum of the quarks, via the Ji's sum rule. A study to investigate the different option for the construction of a neutron detector ("spaghetti" calorimeter, plastic scintillator, ecc.) is in progress.

For the Time-of-Flight detector studies are underway for suitable and efficient light guides to collect signals of scintillator counters in tight geometry and high magnetic field (the Central Detector is surrounded by a solenoid magnet producing a magnetic field of 5 T). Moreover, the CLAS12 physics program requires timing at the 50 ps level for particle ID in the Central Detector region. This will allow p/K separation up to 0.6 GeV/c and π/p separation up to 1.25 GeV/c Simulations have started to study the signal at the CTOF PMT and its time response to minimum ionizing particles.

4 List of Publications

1. Quark-Hadron Duality in spin structure functions g_1^p and g_1^d.
   P.E. Bosted *et al.* and CLAS collaboration, Phys. Rev. C75 (2007), 035203.

2. Separated structure functions for the exclusive electroproduction of $K^+\Lambda$ and $K^+\Sigma^0$ final states.
   P. Ambrozewicz *et al.* and CLAS collaboration, Phys. Rev. C75 (2007), 045203.

3. First measurement of beam-recoil observables C_X and C_Z in hyperon photoproduction.
   R. Bradford *et al.* and CLAS collaboration, Phys. Rev. C75 (2007), 035205.

4. Cross section for the $\gamma p \to K^{*0}\Sigma^+$ at $E_\gamma = 1.7 - 3.0$ GeV.
   I. Hleiqawi *et al.* and CLAS collaboration, Phys. Rev. C75 (2007), 042201.

5. Experimental study of exclusive 2H(e,e'p)n reaction mechanism at High Q^2.
   K.Sh. Egiyan *et al.* and CLAS collaboration, Phys. Rev. Lett. 98 (2007), 262502.

6. Q^2 dependence of the $S_{11}(1535)$ photocoupling and evidence for a P-wave resonance in η electroproduction.
   H. Denizli *et al.* and CLAS collaboration, Phys. Rev. C76 (2007), 015204.

7. Cascade Production in the Reaction $\gamma p \to K^+K^+X$ and $\gamma p \to K^+K^+\pi^-X$.
   L. Guo *et al.* and CLAS collaboration, Phys. Rev. C76 (2007), 025208.

8. ρ^0 photoproduction on the proton for photon energies from 0.675 to 2.875 GeV.
   M. Dugger *et al.* and CLAS collaboration, Phys. Rev. C76 (2007), 025211.

9. Coherent ϕ meson mhotoproduction from the deuteron at low energies.
   T. Mibe *et al.* and CLAS collaboration, Phys. Rev. C76 (2007), 052202.

10. Search for medium modifications of the ρ meson.
    R. Nasseripour *et al.* and CLAS collaboration, Phys. Rev. Lett. 99 (2007), 262302.

11. Transverse spin effects in SIDIS at 6 GeV with transversely polarized target using the CLAS Detector.
    H. Avakian *et al.*, http://www.jlab.org/ rossi/PAC33/*sidis_transverse_6GeV.pdf*.

5 Presentation at Conferences, Workshops, Seminars

1. *Study of the $\gamma n(p) \to K^+\Sigma^-(p)$ reaction at Jefferson Lab*
   Sergio Anefalos Pereira - "XLV International Winter Meeting on nuclear physics" - Bormio (Italy) January 15-21, 2007.

2. *The DANTE project at DAFNE*
Patrizia Rossi - Invited talk at the "PANDA EM Working Group Workshop" - Orsay (France), March 8-9, 2007.

3. *Pentaquark search at CLAS*
Patrizia Rossi - Invited talk at "DIS 2007" - Munchen (Germany), April 16-20, 2007.

4. *Physics with CLAS @ Jefferson Lab*
Patrizia Rossi - Invited talk at the "IXth International School-Seminar the actual problems of microworld physics," - Gomel (Belarus) July 23-August 3, 2007.

5. *Measurement of the $\gamma n(p) \rightarrow K^+\Sigma^-(p)$ reaction at Jefferson Lab*
Sergio Anefalos Pereira - "7th European Research Conference on Electromagnetic Interactions with Nucleons and Nuclei (EINN)" - Milos (Greece) September 10-15, 2007.

6. *GPDs measurements at CLAS: a tomography of the nucleon*
M. Mirazita - "SIF Conference", - Pisa (Italy), September 24-29, 2007.

7. *Transversity and SIDIS at CLAS*
Patrizia Rossi - Invited talk at "HADRON 07" - Frascati (Italy), October 8-13, 2007.

8. *Measurement of the $\gamma n(p) \rightarrow K^+\Sigma^-(p)$ reaction at Jefferson Lab*
Sergio Anefalos Pereira - "HADRON 07" - Frascati (Italy), October 8-13, 2007.

9. *The Jefferson Laboratory and the physics program in Hall B: present and future*
Patrizia Rossi - Seminar at the " Universidade Estadua de Santa Cruz" - Ilheus (Brazil) October 24, 2007.

10. *Simulation of the timing response of a scintillator*
M. Mirazita - "CLAS12 meeting", - Genova (Italy), December 19-20, 2007.

References

1. S. Capstick and W. Roberts, Phys.Rev. **D58**, 74011 (1998).
2. CLAS Collaboration, R. Bradfort *et al*, Phys. Rev. **C 73**, 035202 (2006).
3. K. H. Glander *et al.*, Eur. Phys. J. **A19**, 251 (2004).
4. S.J. Brodsky and G.R. Farrar, Phys. Rev. Lett. **31**, 1153 (1973); Phys. Rev. D **11**, 1309 (1975); V. Matveev *et al.*, Nuovo Cimento Lett. **7**, 719 (1973). **70**, 014005 (2004).
5. L. Y. Zhu *et al.*, Phys. Rev. Lett. **91**, 022003 (2003); L. Y. Zhu *et al.* Phys Rev. C, **71**, 044603 (2005).
6. J. Ashman *et al*, Phys. Lett. **B206**, 364 (1988).
7. D. Adams *et al*, Phys. Rev. **D56**, 5330 (1997).
8. K. Abe *et al*, Phys. Rev. **D58**, 112003 (1998).
9. P. Anthony *et al*, Phys. Lett. **B458**, 529 (1999).
10. K. Ackerstaff *et al*, Phys. Lett. **B464**, 123 (1999).
11. A. Airapetian*et al*, Phys. Rev. **D71**, 012003 (2005).
12. R. Fatemi *et al*, Phys. Rev. Lett. **91**, 222002 (2003).

ALICE

N. Bianchi (Resp. Loc.), G.P. Capitani, A. Casanova (Ass.), G. Conesa (Ass.), P. Di Nezza, A. Fantoni, D. Hasch (Ass.), V. Muccifora, A. Orlandi (Tecn.), W. Pesci (Tecn.), F. Ronchetti (Ass.), A. Viticchié (Tecn.)

1 Introduction

ALICE is an experiment at CERN which involves about 1000 physicists from more than 100 Institutions from several Countries. Italy participates with 12 groups and more than 150 physicists. The Frascati group is participating to the electromagnetic calorimeter project, which will complete the ALICE detector capabilities for measuring the entire range of physics observables in heavy ion interactions. Jet quenching, the interaction of energetic partons with dense matter, has been shown at RHIC to provide a broad range of unique and sensitive probes of the hot QCD medium. Jet quenching will play an important role in the LHC heavy ion physics program. The EMCal enables ALICE to explore the physics of jet quenching in detail, over the large kinematic range provided by the LHC. The EMCal will provide fast triggers (level 0 and 1) for photons, electrons, and jets. The choice of a large acceptance, moderate resolution electromagnetic calorimeter provides a cost-effective pathway into jet physics in ALICE. The EMCal increases electromagnetic calorimeter coverage of ALICE by nearly an order of magnitude. It provides a fast and efficient trigger for hard jets, photons and electrons, allowing ALICE to exploit fully the luminosity of the LHC. The EMCal also measures the neutral energy component of jets, enabling full jet reconstruction in all collision systems, from proton.proton to Pb.Pb. The combination of the EMCal, the excellent ALICE charged tracking capabilities, and the modest ALICE magnetic field strength, is a preferred configuration for jet reconstruction in the high background environment of heavy ion collisions, allowing detailed optimization of background rejection while preserving the crucial jet quenching signals at moderate transverse momentum. The EMCal in ALICE in conjunction with the TPC has good jet energy resolution in Pb.Pb collisions, and excellent sensitivity to the full range of jet quenching effects available at the LHC.

2 The EMCal Project

The EMCal is a large Pb-scintillator sampling calorimeter with cylindrical geometry, located adjacent to the ALICE magnet coil at a radius of ~ 4.5 meters from the beam line. Its coverage in phase space is $-0.7 < \eta < 0.7$ and $\Delta\phi = 107^o$, positioned approximately opposite in azimuth to the high precision but low acceptance ALICE Photon Spectrometer (PHOS) calorimeter. The EMCal is segmented into 12672 projective towers. The chosen technology is a layered Pb-scintillator sampling calorimeter with a longitudinal pitch of 1.44 mm Pb and 1.76 mm scintillator. Wavelength shifting readout fibers are configured in a Shashlik geometry and are coupled to an Avalanche Photodiode (APD) sensor. The EMCal is composed by 11 Super Modules which represent the basic structural unit of the detector. Each full size super module is assembled from 12x24=288 modules arranged in 24 strip modules 12x1 modules each. Each module contains a 2x2=4 independent towers built up from 76 alternating layers of 1.44 mm Pb (Pure Pb-standard mill spec.) and 77 layers of 1.76 mm polystyrene base, injection molded scintillator (BASF143E + 1.5of 50% Anthracene. White, acid free, bond paper serves as a diffuse reflector on the scintillator surfaces and, in addition, provides the required degree of static friction between the calorimeter layers. The scintillator edges are treated with a TiO_2 loaded reflector to improve the transverse optical uniformity within a single tower. Each scintillator edge also receives an over-coating of black paint to provide tower to tower optical isolation better than 99%. All modules in the calorimeter are mechanically and dimensionally identical. The front face dimensions of the towers are 6x6cm^2 resulting in individual tower acceptance of $\Delta\eta x \Delta\phi \sim 0.014x0.014$.

The Pb-scintillator stack in a module is secured in place by the static friction between individual layers under the load of an internal pressure of $2kg/cm^2$. The module is closed by a skin of 150 μm thick stainless steel on all four transverse surfaces. Flanges are welded to the ends of the stainless steel skin (straps) to permit secure attachment to the front and rear plates of the module. This thin stainless skin plus the optical treatment of the scintillator edges is the only inert material between the active tower volumes. The internal pressure in the module is stabilized against thermal effects, mechanical relaxation and long term flow of the Pb and/or polystyrene by a customized array of 5 non-linear spring sets (Belleville washers) per module. In this way, each module is a self supporting unit with a stable mechanical lifetime of more than 20 years with a large safety factor on the final compressing force. This compressed module design allows the detector to be completely supported from its rear surface.

An array of 12 modules in the ϕ direction and a strong back (which links them) form an EMCal strip module. Like the individual module, the strip module is a self supporting unit. The super module is made from 24 strip modules mounted in th η direction. The strong back, an aluminum beam, which integrates the modules into the strip module, functions as the mechanical support for modules and a stiff structural element of the super module structure. It provides protection for the optical fibers, structural mount for the light guide, APD and charge sensitive preamplifier housing and a light tight enclosure for these elements.

The interface between the super module crate and the EMCal support structure is achieved with a set of rails mounted on the inner surface of the EMCal support structure and rollers fitted to carriages mounted on super module crates. Each super module slides into its resting place inside the ALICE L3 magnet on two U-shaped aluminum rails. This system allows installation of super modules as needed during the annual LHC shutdown period until the full EMCal is in place

3 Experimental activity of the LNF group in 2007

During the year 2007 the project of the Calorimeter has been finalized. In particular the Frascati group has provided the final 3D design of all the components of the module (front plate, back plate, compression plate, scintillator tile, paper sheet, lead tile, strap, black shroud). The module assembling stations have been designed and constructed in the Frascati mechanical workshop. Four assembling stations have been realized, two of them will remain in Frascati while the other two will be send to Catania and Nantes, respectively. The assembling procedure has been optimized and tested. The modules are realized by piling up scintillator tiles, lead tiles and paper sheet along movable guiding rods. The correct location of the tiles during the assembly is ensured by the lateral presence of tool-plates machined and displaced with high accuracy. After the modules will stay under load compression for about 2 days. Several module prototypes have been realized and all the components have been measured carefully with a 4μm CMM machine in order to verify the matching with tolerances and specifications.

A sputtering chamber for the aluminization of the WLS fibers has been designed and constructed. The chamber is able to reach a vacuum of about 10^{-7} and is equipped by an Aluminum target, a magnetron, a thickness monitor and vacuum gauge. several tests have been performed to optimize the deposition time and the thickness of the Aluminum on the fiber bundle. All the tools needed for the cutting, the gluing and the polishing of the fibers have been also realized.

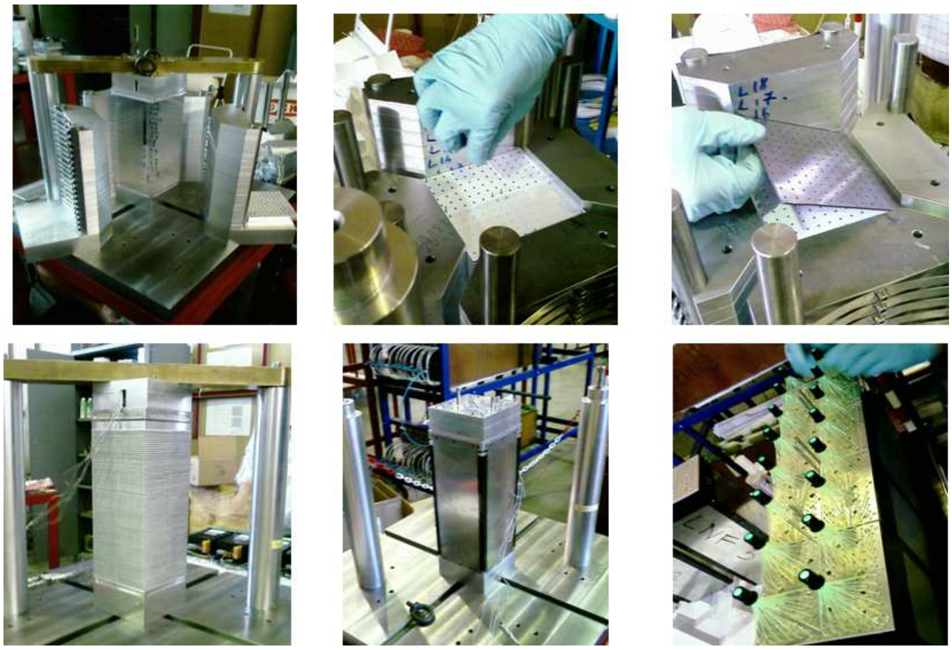

Figure 1: Various steps in module assembly. From upper-left to lower-right: 1-the assembly station; 2-scintillator tile insertion; 3-lead tile insertion; 4-stacking complete; 5-final module; 6-mini-strip module with WLS inserted.

4 Test Beam Measurement

During a period of 5 weeks in September/October 2007 EMCAL modules have been tested using the electron and pion beams of the CERN SPS and PS beam-lines. The test utilized a stacked 4x4 array of EMCAL modules (8x8 towers) of final design equipped with the final electronic readout chain.

The goals of the test beam measurements were:

-determine the ultimate energy resolution;

-investigate linearity and uniformity of the energy response;

-determine the position resolution;

-study the energy dependence of the response to electrons and hadrons to determine the particle identification capabilities of the EMCAL by shower shape analysis;

The readout of the front end electronics used the official ALICE DAQ (DATE) readout system. The test beam data files are stored on the grid CASTOR storage system. They offer the opportunity to test the AliRoot cluster reconstruction software with real data and to develop within the AliRoot environment the calibration tools needed for data taking.

The experiment took place at the SPS H6 and PS T10 secondary beam-lines. The SPS H6 provided clean electron and pion beams in the momentum range 5-100 GeV and with a resolution of about $\delta p/p \sim 1.3\%$. The PS T10 delivered a mixed beam of hadrons and electrons in the momentum range 0.5-6.5 GeV. The modules were located on a movable platform that allowed for position scans in horizontal and vertical directions over the whole array surface. Part of the data were taken with tilted configurations of the modules. A pair of scintillator paddles in front of the EMCAL modules were used for the beam definition trigger and timing. At the SPS, a

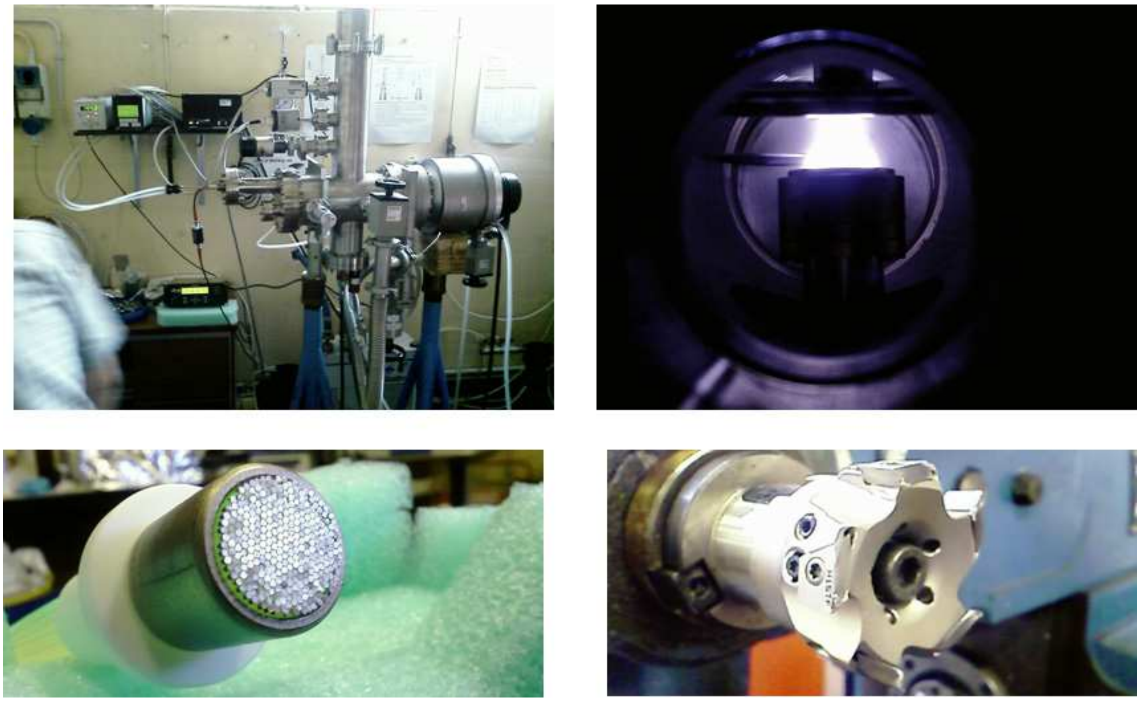

Figure 2: Various steps in WLS fiber work. From upper-left to lower-right: 1-the sputtering station; 2-plasma formation during the sputtering process; 3-WLS bundle after aluminization; 4-WLS cutting tool.

set of MWPCs located in front of the EMCAL modules served as a reference tool for position measurements. No particle identification detectors were available but the purity of the beams is supposed to be $\sim 99\%$ for electrons. At the PS, electrons and pions were separated up to momenta of 5.5 GeV using the information from a threshold Cherenkov.

Data were taken for gain matching with a scan through all module and all tower centers using a 80 GeV electron beam at SPS. Additional surface scans were performed on tower and module boundaries. Energy scans in the momentum range 5-100 GeV were performed at several different locations. The goal of this surface and momentum scans with electrons was to determine the energy and position resolution and to investigate uniformity and linearity of the response. In addition, detailed position and angle of incident scans were performed with 5-60 GeV electrons with modified geometries (tilted and with tower offsets) to investigate the uniformity of the response for different incident locations corresponding to the super module as installed in ALICE. A hadron beam of 100 GeV was used for detailed position scans and at several different positions energy scans in the range of 40-100 GeV were performed. The goal of these measurements was a study of the shower shape of the response to electrons and hadrons in order to investigate the particle identification capabilities of the EMCAL. In addition, the hadron beam data allow for relative tower-by-tower calibrations using the MIP peak. With the data taken at the PS the energy range was extended down to 0.5 GeV. Energy scans were performed in the range 0.5-3 GeV at several positions. In order to bridge to the SPS data, few runs were taken with energies of 5.5 GeV and 6.5 GeV. In order to provide clean data for resolution estimates, the information from the Cherenkov was used to 'trigger' electrons.

For nearly all runs, in parallel to the beam data, also the signals from a LED pulser was registered. The LED system serves to track time and temperature dependent effects in order to set up a gain monitoring and correction system. In addition, temperature sensors were mounted on the top and bottom of each strip unit, for a total of 8 sensors which were continuously read out. Temperature variations of typically 2° C over 8h at the SPS and of 3-4 ° C over 8h at the PS were observed.

The analysis of the data collected is still going on. However, even with very preliminary calibrations the first results demonstrate a satisfactory performance of the EMCAL modules in term of the energy resolution ($\delta E/E$) as function of the incident beam energy. No unfolding of the beam momentum resolution is performed for these data.

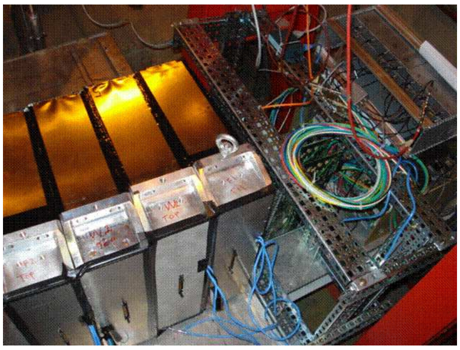

Figure 3: Test beam set-up.

5 Forward Calorimetry

After the shutdown of HERA, the HERMES calorimeter has been dismantled. Half of it has been moved to CERN with the idea of using it as a possible forward calorimeter in ALICE. The 420 blocks are radiation-resistant F101 lead glass blocks, each of them has an area of 9x9 cm^2 and a length of 50 cm, which corresponds at about 18 radiation length. The blocks are polished, wrapped with 0.051 mm thick aluminized mylar foil, and covered with a 0.127 mm thick tedlar foil to provide light isolation. Each block is coupled to a 7.62 cm Philips XP3461 PMT by a silicon glue (SILGARD 184) with refractive index of 1.41. a μ-metal magnetic shield surrounds the PMT. A surrounding aluminum tube houses the μ-metal and provides the light seal. It is fixed to a flange that is glued to the surface of the lead glass. This flange is made of titanium, matching the thermal expansion coefficient of F101. The performance of a 3x3 array of counters are described by an energy resolution that can be parameterized as $\sigma(E)/E$ [%] $= (5.1 \pm 1.1)/\sqrt(E]GeV]) + (1.5 \pm 0.5)$ and a spatial resolution of the impact point of about 0.7 cm.

A forward physics in ALICE will allow to study the physics at high gluon density, where the gluon saturation can be described in the framework of a Color Glass Condensate and will allow also a test of pQCD predictions in case of pp interactions, by looking the forward particle production. Moreover it will be possible to have many interesting physics like jets, jets quenching, Cronin effect, shadowing, γ tagging of the jets, limit fragmentation and a lots more. At low x Bjorken values, the gluon density is large and increases very strongly as $x \rightarrow 0$. For the unitary principle it can't grow indefinitely and a saturation must appear at high density, in a forward rapidity when gluons start to overlap. Studying the pseudorapidity (η) dependence of particle production it will be possible to probe the parton distributions at different x. Particle productions at forward rapidities probes

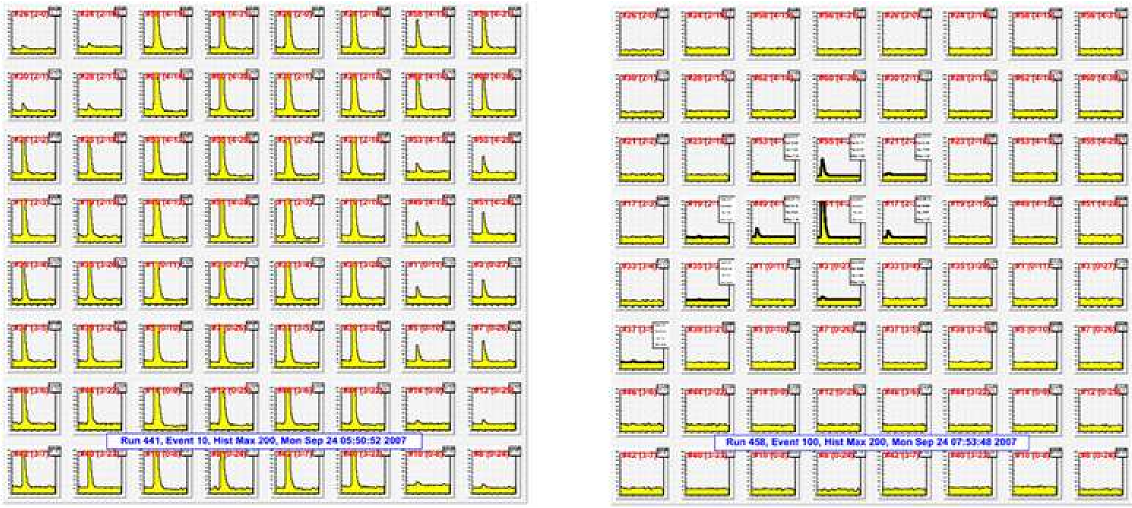

Figure 4: Event display of the 64 towers during the test beam. Left: Led calibration events. Right : beam events in central tower.

partons at smaller x scale. A study at different pseudorapidities has been done at RHIC in 2004, where going from the mid-rapidity η=0 to forward-rapidity η=3.2 a Cronin-like enhancement at η=0 and a suppression of the hadron yields at η=3.2 have been found. Saturation effect should increase with the thickness of nuclear material traversed by the incoming probe, and indeed a greater suppression for more central collision has been seen. Forward measurements at the LHC are a very promising playground for testing the new regime at small-x where the effects of large gluon densities become crucial.

A detailed study must be done for exploring the feasibility of a forward calorimeter in ALICE and eventually the use of the half wall of the HERMES calorimeter. The place where the calorimeter can be installed is after the PMD, the Photon Multiplicity Detector.

6 Software development

6.1 Code tuning

The cluster reconstruction in EMCal needs different reconstruction parameterization as a function of the particle multiplicity environment. The clustering algorithm works in the following way (very schematically), first it takes a cell above a given energy threshold, CellMinThres, then constructs the cluster summing all the cells around this cell and finally it accepts the cluster if the summed cell energy is above another energy threshold, ClusterMinThres. The parameters in the code were set for low particle environment (p-p collisions at $s^{1/2}$ = 14 TeV) and are 10 MeV and 100 MeV, respectively. In case of high particle environment (central PbPb collision at $s^{1/2}$ = 5.5A TeV) these thresholds are clearly not working because we have several low energy particles contributing to the same cluster, changing significantly the reconstructed energy and position of high energy clusters in which we are interested. In order to have a reasonable energy and position resolution the two parameters mentioned above must be changed. In order to set these parameters in high particle multiplicity environment, we studied systematically the change in the

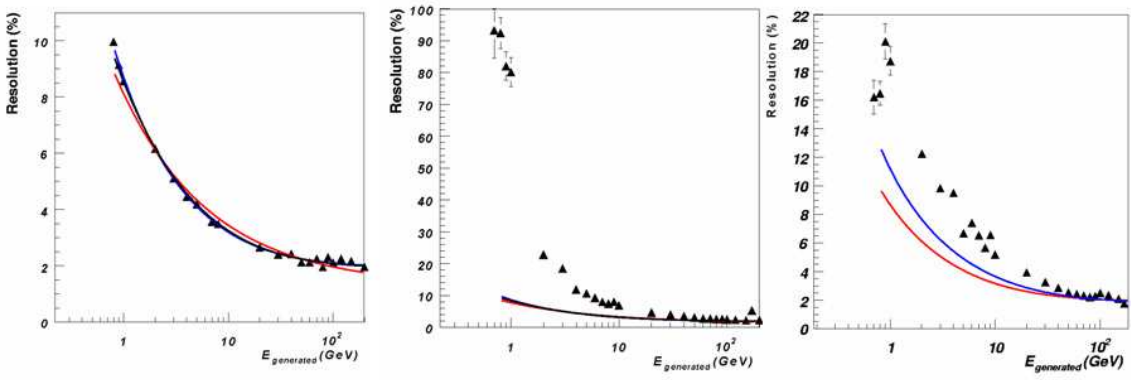

Figure 5: Photon energy resolution in EMCal. Left plot: for low particle multiplicity with ClusterMinThres = 100 MeV and CellMinThres=10 MeV. Middle plot: for high particle multiplicity with ClusterMinThres = 100 MeV and CellMinThres=10 MeV. Middle plot: for high particle multiplicity with ClusterMinThres = 0.5 GeV and CellMinThres=0.45 GeV. Lines are fits to the ideal case with low particle environment.

resolution of high energy photons merged in high particle environment for different parameters and set the ones which gave the best resolutions. We found that a minimum cell energy of 0.45 GeV and a minimum cluster energy of 0.5 GeV were the best solutions which anyway are worse than in low particle environment.

Until this moment we used fixed parameters, hard-coded in the software, independently of the particle environment. After this study it was clear that we needed different set of parameters as a function of the particle environment. We developed a code that would enable to change these parameters at will without having to modify the code. The reconstruction parameters, and other parameter that may change with the particle environment (PID and track matching for example) will be stored on the GRID in the OCDB (offline condition data base) and once we know the running conditions the parameters can be accessed with this new code which we developed and is available for the collaboration in SVN.

6.2 Calorimeter information stored for analysis

The official format for the data stored on the grid to be used for the analysis are the ESDs (event summary data) and a refined compressed version more oriented for final analysis, the AODs (analysis oriented data). Due to the limited storage resources for all the LHC experiments we have to reduce the amount of the information from the detectors that can be stored for analysis in ESDs. The main class dealing the cluster information is called AliESDCaloCluster which reads/creates a branch of data with the calorimeter clusters information, being this information the cluster energy, position, different shower shape parameters, track-matching, distance to dead channel, PID and some few information of the cells generating the clusters (energy, time and position) but not all the cells are considered. A new calorimeter dedicated data branch managed by the class AliESDCaloCells was also added and implemented. This last class will be used to store all the cell information, crucial for jet background studies and for cluster calibration. The difference between the AODs and ESDs is that the amount of data should be reduced. Also AOD will be produced when there is an event with some trigger for the physics that we want to study. All this is available for the collaboration in SVN.

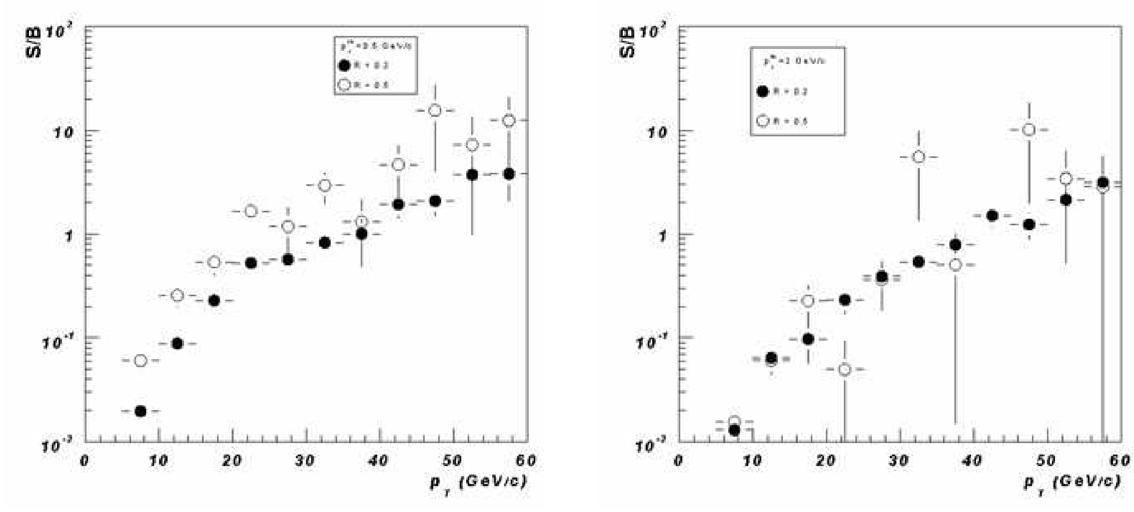

Figure 6: Ratio signal to background where the signal are isolated direct photons and the background are π^0. Left plot: pp collisions at 14 TeV. Right plot: PbPb collisions at 5.5 TeV.

6.3 Gamma and gamma correlations analysis frame code

The analysis of the data will be done within an analysis frame developed by the ALICE core offline team. It is optimized for the analysis in the GRID and CAF. We implemented different possibilities of photon analysis and correlations which are published and available of all the collaboration in SVN. This analysis code does:

- Direct photon analysis: Gets the clusters in the calorimeters and checks if the cluster is identified as photons by the identification software based in shower shape analysis. Then it checks if it is isolated, looking inside a cone around the identified photon if there is any other high energy particle, if it is isolated, this cluster is taken since it is a direct photon and creates different histograms with the final results (p_T and ϕ distributions for example).
- Correlation analysis between direct photons and hadrons or jets: This analysis takes as input the direct photons found by the previous analysis and correlates them with hadrons or previously reconstructed jets in the opposite side. The final output are correlation or fragmentation function histograms.

This code is constantly evolving adding new cases, and also producing AODs from ESDs.

7 Data generation and Analysis

There will be different sources of photons in pp and PbPb collisions. We are specially interested in direct prompt photons since they are produced in the early stage of the collision associated to a back-to-back jet, with almost the same energy. The photon will not be modified by the medium but the jet will be modified, the particle distribution in the jet will change, less high energy particles and more low energy particles due to the jet-quenching effect. Measuring the gamma we have a direct measurement of the jet energy and direction which measurement is challenging in heavy ion collisions, specially for jet energies smaller than 40 GeV. Such direct photons can be identified versus other photon sources because they have the property of being produced isolated. We investigated the measurement of such photons with EMCal with the isolation cut method: we construct a cone around the photon candidate and look the particles inside it, if there are no particles in the cone with pT larger than a given threshold, then the photon is isolated. Another approach is if sum of the particles inside the cone is larger than a given threshold then the candidate is not isolated. In order to perform this study we generated PYTHIA events, pp collisions at 14 TeV and 5.5 TeV. Two kind of events, one set of gamma-jet events containing our signal, and another one with jet-jet events, which contain our main background, π^0 and fragmentation photons. We performed first this study at the generator level due to the lack of time for a full analysis with particle transport in the materials of the detector. Such analysis is being done in 2008. We also mimicked the heavy ion collision merging the pp PYTHIA collisions at 5.5 TeV with HIJING simulations at 5.5 TeV.

We found that the isolation cut method is feasible, rejecting well the π^0 sources for energies larger than 20 GeV in pp collisions with a cone size of 0.4-0.5 and a p_T threshold of 0.5-1 GeV. In PbPb collisions the measurement is feasible for energies larger than 40 GeV (no quenching considered) with a cone size of 0.2 and a p_T threshold of 2 GeV. Note that the background will be suppressed also with the help of shower shape analysis, so that the final results will improve. Also note that in PbPb we have not yet considered the quenching which will decrease the high pT background particle yield. We also checked the rejection of PYTHIA fragmentation photons and we observed that we could not reject more than 50% of them with the isolation cut method.

8 Outlook

9 Conferences and Papers by LNF Authors in Year 2007

9.1 Conference Talks

1. N. Bianchi, Jet Physics in ALICE, XXX RTFNB, Aguas de Lindoia, 02-06 September 2007
2. N. Bianchi, Jet quenching at ALICE, XI Workshop on Nuclear Physics, Havana, 05-08 February 2007
3. D. Hasch, Results from the EMCal test beam, III Convegno Italiano sulla Fisica di ALICE, Frascati 12-14 November 07
4. G. Conesa Balbastre, Direct photon and jet physics with the ALICE calorimeters, III Convegno Italiano sulla Fisica di ALICE, Frascati, 12-14 November 2007
5. G. Conesa Balbastre, Photon-jet/hadron correlations in ALICE, Workshop on High p_T physics at LHC, Jyvaskyla, 23-27 March 2007

9.2 Conference organization and advisory

1. N. Bianchi, (Advisor) XI Workshop on Nuclear Physics, Havana, 05-08 February 2007
2. N. Bianchi, P. Di Nezza, A. Fantoni, F. Ronchetti, (Organizers) III Convegno Italiano sulla Fisica di ALICE, 12-14 November 2007 Frascati
3. N. Bianchi, P. Di Nezza, A. Fantoni, F. Ronchetti, (Organizers) 1^{st} EMCal International Collaboration Meeting, 12-14 March 2007 Frascati

9.3 Publications

1. Direct photon detection in PbPb collisions in the ALICE experiment at LHC, Nucl. Phys. A 782 (2007) 356

FINUDA

The Finuda-LNF Collaboration
L. Benussi (Art. 23), M. Bertani (resp.), S. Bianco, M. A. Caponero (Ass.), F. L. Fabbri
P. Gianotti, M. Giardoni, V. Lucherini, E. Pace, M. Pallotta (Ass.), S. Tomassini,
L. Passamonti (Tecn.), D. Pierluigi (Art. 15), F. Pompili (Art 36), A. Russo (Art. 15)

1 Introduction

FINUDA is the experiment devoted to hypernuclear physics studies at DAΦNE. Hypernuclei are nuclear systems in which one or more nucleons are replaced by a hyperon. This feature adds explicit strangeness to the nuclear system allowing to study, in a more general environment, the baryon-baryon interaction. FINUDA produces hypernuclei via the reaction:

$$K^- + ^A Z \rightarrow ^A_\Lambda Z + \pi^- \tag{1}$$

stopping K^- from $\phi(1020)$ decay almost at rest into thin ($\sim$ 0.2 g cm^{-2})nuclear targets. The spectroscopy of the hypernuclear levels produced is performed by measuring the momentum of the outgoing π^-. The products of the sub-sequent decay of the Λ bound to the nucleus can be detected by FINUDA, allowing to investigate simultaneously the decay mechanisms of hypernuclei.

The hypernuclear research program includes also Neutron-rich hypernuclei, systems with a large N/Z ratio, which could give more information on baryon-baryon interaction, and on the importance of the ΛNN force related to the "coherent $\Lambda - \Sigma$ coupling" in connection with nuclear astrophysics implications [1]. The search for neutron rich Λ hypernuclei is carried out by studying the reaction:

$$K^-_{stop} + ^A Z \rightarrow ^A_\Lambda (Z-2) + \pi^+ \tag{2}$$

By measuring the momentum of the outgoing π^+, it is possible to determine the energy level of the hypernucleus that could be formed.

The unique combination of the clean K^- source (DAΦNE) and the very transparent and complete detector optimized for the study of the interactions of Kaons in thin nuclear targets (FINUDA) has allowed the study of new items, not foreseen in the original proposal, such as a study of the ^{7}Li(K$^+$, K^0) reaction close to threshold [2] and topics related to the possible existence of Deeply Bound Kaon States (DBKS). The interest in such an item was triggered by a theoretical suggestion by Akaishi and Yamazaki [3] about possible aggregates of few nucleons strongly bound by a K^- and with a narrow width. These systems should have a density even ten times larger than the usual nuclear matter one, with a potential great impact on the comprehension of the origin and structure of the neutron stars.

The FINUDA Collaboration consists of about 60 physicists coming from LNF, several INFN sections and Italian universities (Bari, Brescia, Pavia, Torino, Trieste) plus foreign researchers from Canada, the University of Victoria, Vancouver; from Japan, the KEK laboratory of Tsukuba, RIKEN and the University ok Tokyo; from South Korea, the Seoul National University, from Russia, the Joint Institute for Nuclear Research of Dubna and from Iran, the S. Beheshty University of Teheran.

2 FINUDA activity in 2007

The activity of the LNF FINUDA group during 2007 has been devoted to the following main tasks:

1. The completion of the data taking started on November 20, 2006 and ended on June 6, 2007 with the collection of a total integrated luminosity of 966 pb^{-1};

2. Drift times calibration for the straw tube detector and data quality monitoring through Bhabha scattering and μ^+ from K^+ decay;

3. The analysis of the data collected in the first data taking as well as of the new set of data to produce scientific results.

Lets recall that in the first (engineering+data) data taking (December 2003-March 2004), a total of 250 pb^{-1} (190 for physics) were collected with a set of eight targets: 2 ^{6}Li, ^{7}Li, 3 ^{12}C, ^{27}Al and ^{51}V. No measurements on medium A targets were performed before and FINUDA showed that reaction (1) has a reasonable capture rate for p-shell nuclei only, and the analysis was focused mostly on light Hypernuclei.

The targets installed for the 2006-2007 data taking were: 2 ^{6}Li, 2 ^{7}Li, 2 ^{9}Be, D_2O, and ^{13}C.

The LNF FINUDA group oversaw all the data taking activities, having as run coordinator Dr. V. Lucherini, and had the responsibility for the data taking quality insurance.

The group had the coordination of the analysis of the (K^+, K^0) interaction at low energy and of the hypernuclear spectroscopy studies. It has moreover performed a detailed study of the relevant DAFNE parameters (luminosity, c.m. energy, boost, etc.) as monitored online and offline by FINUDA [4].

3 Summary of 2006-2007 Data Taking

During the 2006-2007 data taking, the average daily luminosity delivered to FINUDA was 7 pb^{-1} (improving with time since the beginning of the run), the peak daily luminosity reached by the machine was 9.4 pb^{-1}. The total collected integrated luminosity was 966 pb^{-1}.

Table 1 shows the amount of data collected by FINUDA during the full running time, according to the applied trigger, and reports, for comparison, the statistics collected in 2003-2004 with the same trigger conditions.

		2006-2007	2003-2004
Total collected luminosity		966 pb^{-1}	220 pb^{-1}
HYPE type triggers		210×10^6	29.7×10^6
BHABHA type triggers		32.8×10^6	7.5×10^6
cosmic ray data	B=0 T	8.8×10^6	5.5×10^6
	B=1 T	3.7×10^6	1.8×10^6

Table 1: Statistics collected in the 2006-07 data taking, compared to the 2003-2004 data taking (running since Dec. 1, 2003 to Mar. 23, 2004).

4 Hypernuclear physics results

4.1 Spectroscopy of Λ-hypernuclei

The target array used in the 2006-2007 run was composed by two ^{6}Li and two ^{7}Li targets, already present in the 2003-2004 run, plus four new ones, namely two ^{9}Be, one ^{13}C and one D_2O. The latter were expected to deliver interesting results about the spectroscopy of new hypernuclear species, the former ones were used to increase the already available statistics for the study of non-mesonic weak decays of hyperfragments produced from the ^{6}Li target and for the spectroscopy of the $^7_\Lambda$Li hypernucleus.

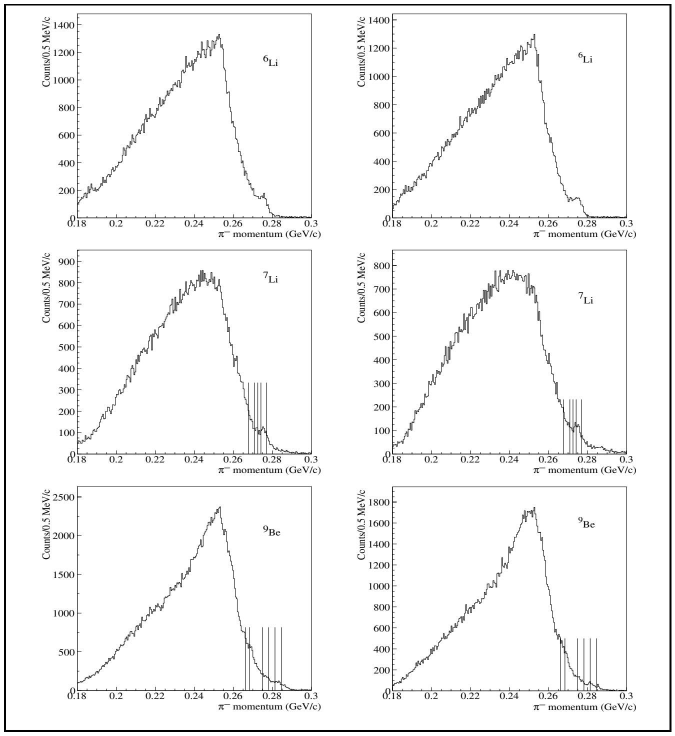

Figure 1: π^- inclusive momentum spectra for events with K^- stopping in ^{6}Li (top line), ^{7}Li (center line), and ^{9}Be (bottom line). Long, high resolution (four points) and forward tracks selected. The lines correspond to the momentum values for the formation of hypernuclear species (when possible).

An overview of the inclusive π^- momentum spectra from each of the eight targets is reported in Fig. 1 (for ^{6}Li, ^{7}Li and ^{9}Be targets) and Fig. 2 (^{13}C and ^{16}O targets). The tracks were selected to achieve the best available resolution: four points well fitted tracks, forward heading, with K^- vertex correctly reconstructed in the target volume. We can see that the quality and population of the spectra out of homologous targets is comparable, in spite of finer alignments still to be fulfilled.

The two spectra from ^{6}Li have a comparable shape to what we got in the first run, with a bump beyond 275 MeV/c, corresponding to the threshold for the formation of the $^5_\Lambda$He hyperfragment, in which the unstable $^6_\Lambda$Li decays by proton emission. These data are mainly useful for non-mesonic weak decay studies, as described afterwards.

In spite of the huge statistics collected by two targets, the π^- spectra from ^{9}Be targets (last line in Fig. 1) show just feeble signals where the hypernuclear levels were expected, in the 268–285 MeV/c region, mainly in the form of small knees (except for a hint corresponding to the production of the ground state). The estimated capture rate for these states is some 10^{-4}/K$^-_{stop}$: probably the real rate is even lower, and our sensitivity is not enough to disentangle them. It is interesting however to note the steepness of the rising left side, which is peculiar and similar for the ^{9}Be and ^{6}Li targets, while it rises much more softly for all the other ones. This feature deserves a detailed study: it might be related to the α-cluster substructures present in the two nuclei (namely, $(\alpha\alpha n)$ in ^{9}Be, (αd) in ^{6}Li).

Clear signals for the formation of $^{13}_\Lambda$C hypernuclear levels emerge corresponding to the expected momenta for the ground and first excited states – some of them are overlapping and cannot

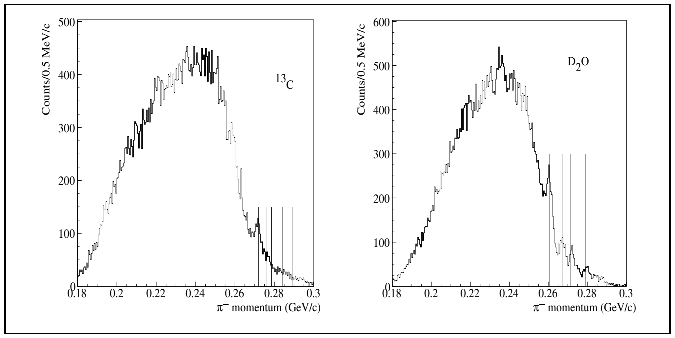

Figure 2: π^- inclusive momentum spectra for events with K^- stopping in ^{13}C (left) and ^{16}O (right). Long, high resolution (four points) and forward tracks selected. The lines correspond to the momentum values for the formation of hypernuclear species.

be disentangled yet with the present resolution, but a clear indication of the most populated one at 272 MeV/c, which is expected to be produced with a capture rate of about $7 \times 10^{-4}/\mathrm{K}^-_{stop}$, is present in the spectrum. From a single target, about 100 events have been collected in the most populated peak.

The signals out of the deuterated water target are very interesting as well. For the $^{16}_{\Lambda}$O hypernucleus signals are expected in the momentum spectrum at 279.20, 271.50, 267.01 and 260.44 MeV/c. All the four levels are visible in the experimental spectrum, in spite of just one target available. With the events in the ground state peak, interesting coincidence studies can be done on $^{16}_{\Lambda}$O non-mesonic weak decays.

4.2 Non Mesonic Weak Decays

The importance of the Non Mesonic Weak Decay (NMWD) of hypernuclei was recognized since the early days of hypernuclear physics [5)]. It is the most spectacular example of nuclear medium modification and it gives information on the four baryon weak process $\Lambda N \rightarrow NN$, with possble hints also on the ΛNN interaction. Nevertheless the process of NMWD of hypernuclei has been scarcely studied on the experimental side for a few decades due to experimental difficulties. Indeed it is not only mandatory to identify hypernuclei in their ground states but also to detect and measure the energy of the emitted protons and neutrons. Moreover there has been a long standing "puzzle" concerning the Γ_n/Γ_p ratio. The values reported by the former experiments, even though with large errors, were close to or larger than 1, whereas the simple one-pion exchange model with ΔI=1/2 rule foresaw values one order of magnitude lower.

In Ref. [6)], the FINUDA results for the energy spectra of the protons from the non mesonic weak decay of $^{5}_{\Lambda}$He, $^{7}_{\Lambda}$Li and $^{12}_{\Lambda}$C hypernuclei are presented (fig. 3). In particular the proton spectrum following the weak decay of $^{7}_{\Lambda}$Li has never been studied before. In FINUDA the thin targets permits to lower the threshold on the proton energy spectrum down to 15MeV, the lowest energy ever. The spectra show a similar shape, *i.e.* a peak around 80 MeV, corresponding to about a half the Q-value for the free $\Lambda p \rightarrow np$ weak reaction, with a low energy rise, due to the final state interactions (FSI) and/or to two nucleon induced weak decays. A comparison of the FINUDA with the theoretical calculation [7)] for $^{5}_{\Lambda}$He and with the previous measurement by Okada [8)] indicates that there is a disagreement between the two experiments and between experiment and theory. A further increase in statistics would help the comparison with theoretical calculations.

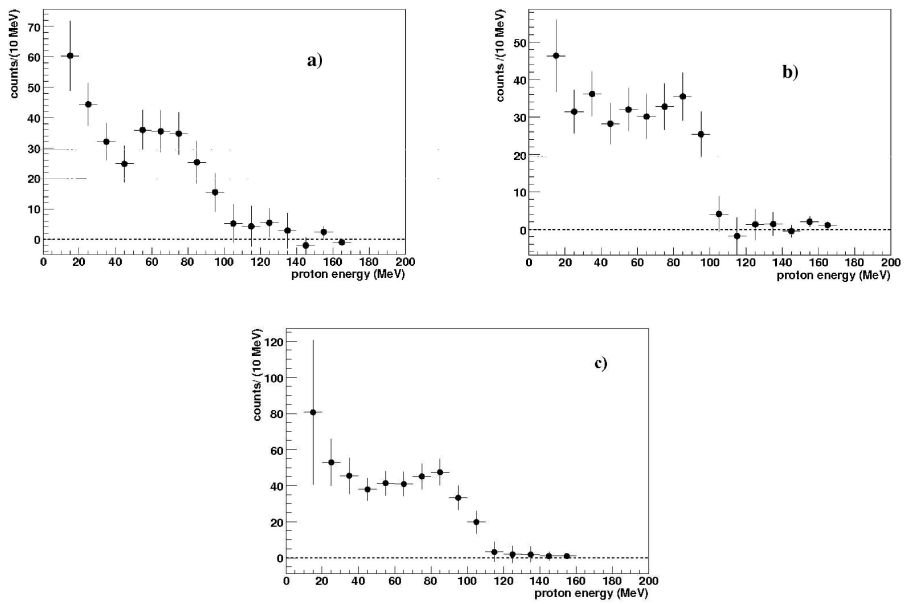

Figure 3: Proton energy spectrum after the background subtraction from NMWD of a)$^{5}_{\Lambda}$He, b) $^{7}_{\Lambda}$Li and c)$^{12}_{\Lambda}$C.

4.3 Neutron-rich Λ-hypernuclei

The observation of the large N/Z ratio neutron-rich hypernuclei can provide information on the "glue-like" role of the Λ and on the baryon-baryon interaction. In FINUDA the search for neutron rich Λ hypernuclei is been carried out by studying the reaction (2). For $^{6}_{\Lambda}$H and $^{7}_{\Lambda}$H the momentum of the outgoing π^+ is expected to be $\sim$ 252 and 246 MeV/c respectively.

From the first data set FINUDA looked to the inclusive π^+ spectrum from ^{6}Li, ^{7}Li and ^{12}C targets which shows no evidences for the formation of Λ bound states. The upper limits for the production rates have been evaluated [9]. With the 2006-2007 data, the increase in statistics on $^{6}_{\Lambda}$H and $^{7}_{\Lambda}$H will allow the use of more stringet cut to reduce background, and new neutron-rich hypernuclear system can be studied: $^{9}_{\Lambda}$He, $^{13}_{\Lambda}$Be, and $^{16}_{\Lambda}$C. The new analysis on this subject is in progress [10].

5 Nuclear bound kaonic systems

The detector characteristics have turned out to be excellent to give clear results on a topic that has became of extreme interest in the last years. In fact, the existence of kaon-nucleon bound systems is highly debated. The main features of $\bar{K}N$ and $\bar{K}A$ interactions don't foresee clearly detectable levels since the expected binding energies are around 10-30 MeV, and the widths of 80-100 MeV exclude the possibility of an experimental observation. Nevertheless, a different approach of recent theoretical works by Akaishi and Yamazaki [3] shows the possibility that $\bar{K}N$ interaction, under certain conditions, could became strongly attractive allowing the formation of kaon-multinucleon systems with a binding energy varying from 86 MeV to 113 MeV, depending on the target nucleus, and with widths of 20-40 MeV. These Authors also suggest that the presence of a K^- inside the nucleus should enhance the binding energy of the system increasing the density several times that of the ordinary nuclei. These aggregates should be formed with higher probabilities when the kaon interacts with light nuclei.

5.1 Λp coincidence analysis

The first paper published by FINUDA on the evidence of a Deeply Bound K$^-$-Nuclear States observed in the $(K^- pp)$ system [11], riding the tide of the first observations in agreement wih Akaishi-Yamazaki model, needs an urgent confirmation with the data collected recently, as in the following years several criticisms raised [12] in that it was claimed that the data could to be simply explained by FSI effects. A way to disprove this interpretation would be the observation of the same signal in different targets, where the FSI effect should act differently, more sizeably in heavier nuclear media. For this reason a new analysis is under way following the same exclusive approach as in Ref. [11], now possible target by target. At the same time, the problem has also been attacked in a different way (resorting to inclusive spectra), in order to cross-check possible biasing effects. Fig. 4 shows a comparison between the analysis published in Ref. [11] and the new data, selected according to the same criteria and according to the target where the K^- stops.

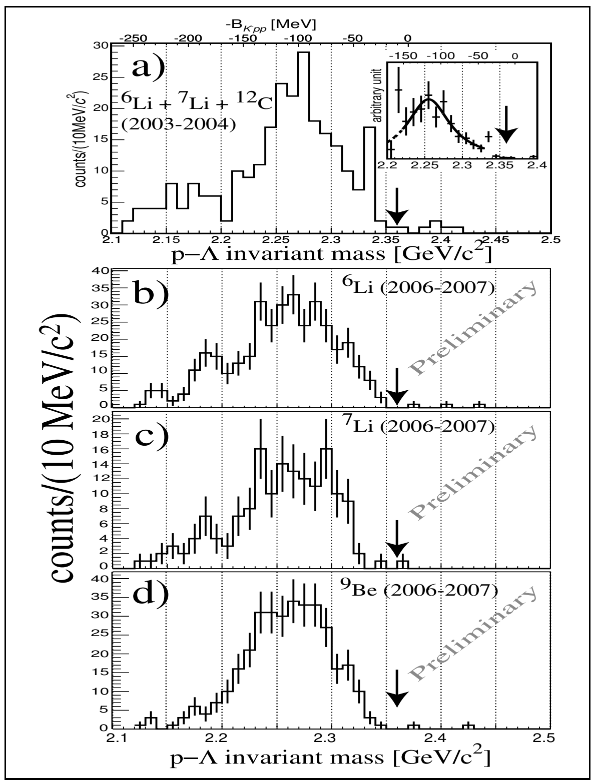

Figure 4: Acceptance not-corrected (Λp) invariant mass distributions for: a) 2003-2004 data, all light targets ($2\times{}^6$Li, $1\times{}^7$Li and 3×12C) (in the inset the acceptance corrected and fitted spectrum is shown [11]); b) 2006-2007 data, $2\times{}^6$Li targets; c) 2006-2007 data, $2\times{}^7$Li targets; d) 2006-2007 data, $2\times{}^9$Be targets. The arrows mark the $(K^- pp)$ threshold.

We recall that in this analysis long (four points reconstructed) proton tracks, a pion track reconstructed with at least three points and Λ identification were required; then an angular cut between the selected Λ and the recoiling proton was applied, asking for a back-to-back correlation. The amount of events entering the invariant mass (Λp) spectrum was about 200, cumulating the events with the K^- stop point in ^{6}Li, ^{7}Li, and ^{12}C targets (6 targets overall). Fig. 4a) shows the spectrum obtained with 2003-2004 data, not corrected for acceptance. This spectrum has to be compared to what we get in the 2006-2007 data taking from each target (further analysis currently underway) b) ^{6}Li (356 events), c) ^{7}Li (157 events), d) ^{9}Be (340 events). The shape of the spectra, though not corrected for acceptance yet, is similar enough to indicate a probably common mechanism effective in all targets to produce an aggregate at a mass lower than the (K^-pp) threshold (indicated in the Figure with arrows).

An exclusive analysis is also being carried as a cross check, the results at the moment are in agreement with the first statement that the signal on the (Λp) events is generated by a kaon-nuclear bound system.

5.2 Λd correlations

In the FINUDA paper [13] the invariant mass spectrum of the (Λd) system following the capture of K^-_{stop} in ^{6}Li and ^{12}C nuclei was shown: a seemingly "bound" structure could be seen in the case of ^{6}Li (fig.5). The presence of such a system produced in light nuclei would be a nice confirmation of a genuine bond, since in this case the FSI contribution should be largely reduced as compared to systems decaying in nucleons.

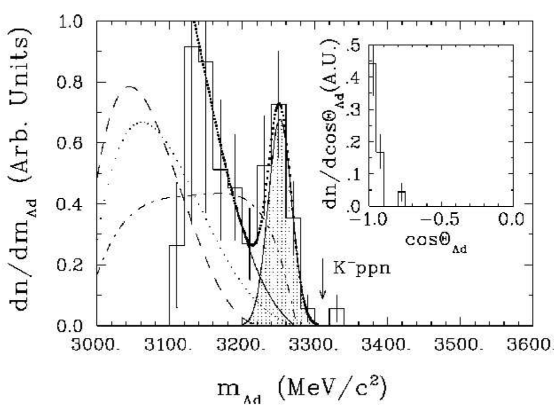

Figure 5: Invariant mass distribution of the (Λd) system for events from the ^{6}Li(K^-_{stop}, Λd)$3N$ reaction, solid line histogram; superimposed are the results of phase space simulations of several channels: dashed line $[\Lambda d]nnp$, dotted line $[\Lambda d]nd$, dot-dashed line $[\Lambda d]t$. The bold dotted-line is a fit of the experimental data with a Gaussian function and a linear combination of the above mentioned absorption reactions; the solid curve shows the contribution of the simulated background only

The enhancement on the right part of the spectrum was interpreted as due to a K^--nuclear aggregate with a mass of 3125 MeV/c^2 and a width $\Gamma = 37$ MeV, recoiling against a (nd) pair, in which the deuteron plays as a spectator and the neutron carries away all the excess kinetic energy.

The 2006-2007 data analysis is in progress [10] still confirming the first observation from the two ^{6}Li targets while the signal from heavier targets is broader than what is observed in ^{6}Li, in agreement with its absence in the ^{12}C data of 2003-2004, that is probably due to the dominant FSI contribution in systems with many nucleons.

6 Study of the (K^+,K^0) reaction on medium-light nuclei close to threshold

The inelastic charge exchange reaction (K^+,K^0) on ^{7}Li has been experimentally investigated close to threshold with FINUDA spectrometer by searching for K^0_S decay. It is the first time that this process has been studied at such low momentum. An upper limit of 2.0 mb (at 95% confidence level) has been measured for the total cross section [2].

In this analysis, events originated from the K^+ interactions with the FINUDA targets were selected. Such events are collected using the same trigger of the Hypernuclear data taking. Almost all the K^+ entering the FINUDA targets are brought to rest and then decay.

The elementary reaction $K^+ + n \rightarrow K^0_S + p$ can occur inside the nuclei of the FINUDA targets. Indeed, the elementary process cannot be studied experimentally on free neutrons and existing data were thus obtained mainly on deuterium targets. This means that the effective threshold of the reaction (*i.e.* the minimum kaon momentum value) increases with respect to that of the elementary one (63.8 MeV/c), depending on the selected nucleus. The K$^+$ produced by DAΦNE have a maximum momentum of $\approx$ 130 MeV/c for kaons whose direction is parallel to the outward boost. After crossing the beam pipe and the FINUDA inner detectors, they reach the targets in slots 4 and 5 mainly with momenta $\approx$ 100 MeV. This means that the reaction under study can be below threshold on several nuclei. Moreover, due to the low momentum of the K$^+$, also the Coulomb barrier plays a role in the probability of K^+ interaction on nuclei, that it is expected to increase with the Z of the target nucleus. As a result, in the FINUDA first run, the reaction was accessible only to the ^{7}Li target, while in the second one, it was possible on the ^{7}Li, the ^{13}C and the ^{2}H of ^{2}H$_2$O targets.

The main source of background is the K^+ decay at rest into π^+, π^0. It produces, with a rather high BR of $\approx$21%, π^+, π^0 pairs whose topologies and momenta are similar to those of the π^+, π^- pairs from K^0_S decay. The π^0 decays immediately, mainly into $\gamma\gamma$. One of the γ rays can be emitted in the same direction of the π^0, and by crossing the target material it can create an e^+e^- pair. If the e$^-$ is also forward emitted, the topology and momentum of this event are similar to those from the $K^0_S \rightarrow \pi^+\pi^-$ decay.

The presence of this background has been proven in Ref. [2] both by a Monte Carlo simulation and experimentally. At the momenta involved, FINUDA cannot discriminate between an e^- and a π^-, hence this background is very insidious. The possible contamination from this reaction was studied with the Monte Carlo program. A number of $K^+ \rightarrow \pi^+\pi^0$ decays comparable with the experimentally measured number of stopped K$^+$ was generated, and the distributions in relative angle and invariant mass of the resulting π^+e^- events in the hypothesis they represent $\pi^+\pi^-$ pairs was examined. From this study it is possible to define, at 95% confidence level, a background free region in the relative angle versus invariant mass distribution between 176 and 180 degrees and between 494 and 502 MeV/c^2, respectively.

From the analysis of the first set of FINUDA data, in which the reaction (K^+, K^0) was accessible only to the ^{7}Li target, no event was found. The effective integrated luminosity for ^{7}Li target in the first FINUDA run was 8.71$\times$10^{27} cm^{-2}, hence with the related collected statistics we achieved a sensitivity of $\approx$1 mb per event. Table 2 shows the effective integrated luminosity for each target above threshold of the second FINUDA run and the expected events considering a 1 mb cross section.

The result of the first FINUDA run indicates that the cross section near threshold for ^{7}Li(K$^+$,K^0)^{7}Be is less than 2 mb with a probability of $\approx$95%. No previous measurements of this cross section exist on whichever nuclei, deuterons included. A compilation of the existing cross

Table 2: *Effective integrated luminosity per each target above threshold of the second FINUDA run and expected events per $\sigma_{K^0_S}$ 1 mb.*

Nuclear target	Eff. $\int \mathcal{L}$ (cm^{-2})	Expected Events / 1 mb
^{7}Li (slot 3)	1.13617×10^{29}	~ 13.6
^{1}3C (slot 4)	1.42054×10^{29}	~ 17
^{7}Li (slot 5)	1.66538×10^{29}	~ 12
^{2}H (slot 6)	2.81157×10^{28}	~ 5

section data and the calculations up to 800 MeV/c K^+ laboratory momenta are shown in Fig.6. The experimental data were extracted from measurements on deuterium or on heavier nuclei. As one can see, in the low momentum region, the available data or calculations are very old and go down to a minimum momentum twice bigger than that accessible to FINUDA.

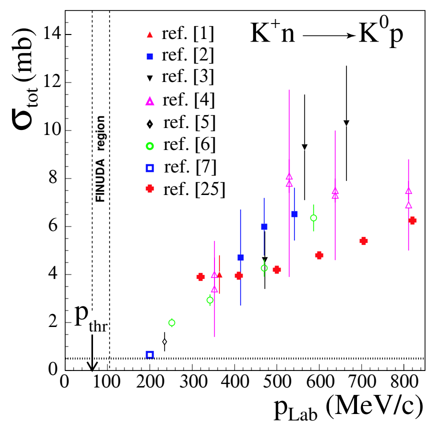

Figure 6: *Existing data and calculations of the total cross section of the elementary charge exchange reaction $K^+ + n \rightarrow K^0 + p$ below 800 MeV/c K^+ laboratory momentum. The momentum threshold and the region explored by FINUDA are also indicated. The horizontal dotted line shows the 0.5 mb cross section level for the elementary process [see Ref [2]].*

In conclusion the FINUDA result confirms, for the first time experimentally, a smooth and rather low cross section on nuclei (at least for ^{7}Li) in this momentum region.

7 List of 2007 FINUDA publications

1. M. Agnello *et al.*, " Experimental study of the (K^+, K^0) interactions on ^7Li close to threshold.", Phys.Lett.B649, 25-30, 2007;

2. M. Agnello *et al.*, " DAFNE monitored by FINUDA. ", Nucl.Ins.Meth.A570, 205-215, 2007;

3. M. Agnello *et al.*," The $A(K^-_{stop}, \Lambda d)A'$ reaction, a tool to observe $[\bar{K}NNN]$ clusters ", Eur.Phys.J.A33:283-286, 2007;

4. M. Agnello *et al.*, " Correlated Λd pairs from the $K^-_{stop}A \rightarrow \Lambda dA' reaction$", Phys.Lett.B654, 80-86, 2007;

5. M. Agnello *et al.*, " Study of the proton weak decay of ${}^{12}_{\Lambda}$C(g.s.) with FINUDA ", Eur.Phys.J.A33:251-254, 2007;
6. M. Agnello *et al.*," Measurement with high resolution of the proton spectra from non-mesonic weak decay of ${}^{5}_{\Lambda}$He, ${}^{7}_{\Lambda}$Li AND ${}^{12}_{\Lambda}$C", Frascati Physics Series Vol. XLVI, 2007;
7. M. Agnello *et al.*," Study of the (K^+,K^0) reaction on medium light nuclei close to threshold", Frascati Physics Series Vol. XLVI, 2007.
8. FINUDA Offline Group, " Status Report on FINUDA Data Analysis", October 2007, document prepared for the 35th LNF Scientific Committee

8 Conference presentations by LNF collaborators

1. L. Benussi, "FINUDA status report ", invited talk presented at XCIII Congresso Nazionale della Societa' Italiana di Fisica, Pisa, September 2007;
2. M. Bertani, "Recent Results on Nuclear Kaon Clusters from FINUDA", invited talk presented at 20th European Few Body Conference Pisa, September 2007;
3. L. Benussi, " Experimental study of the (K^+, K^0)interactions on ^7Li at FINUDA, poster presented at INPC 2007 International Nuclear Physics Conference, Tokio, June 2007.

References

1. Y. Yamamoto *et al.*, Nucl. Phys. A **691** (2001), 432c.
2. M. Agnello *et al.*, Phys.Lett.B **649** (2007),25 ; M. Agnello *et al.*," Study of the (K^+,K^0) reaction on medium light nuclei close to threshold", Frascati Physics Series Vol. XLVI (2007);
3. Y. Akaishi, T. Yamazaki, Phys. Rev. C **65** (2002), 044005; T. Yamazaki, Y. Akaishi, Nucl. Phys. B**535** (2002), 70; Y. Akaishi *et al.*, nucl-th/0501040;
4. M. Agnello *et al.*, Nucl.Instrum.Meth.A**570**(2007), 205;
5. W. Cheston and H. Primakoff, Phys. Rev. **92** (1953),1537;
6. M. Agnello *et al.*," Measurement with high resolution of the proton spectra from non-mesonic weak decay of ${}^{5}_{\Lambda}$He, ${}^{7}_{\Lambda}$Li AND ${}^{12}_{\Lambda}$C", Frascati Physics Series Vol. XLVI, 2007; M. Agnello *et al.*, Eur.Phys.J.A**33**(2007), 286;
7. G. Garbarino, A. Parreno and A. Ramos, Phys. Rev. C **69** (2004) 054603;
8. S. Okada *et al.*, Phys. Lett. B **597** (2004), 249;
9. M. Agnello *et al.*, Phys. Lett. B **640** (2006), 145;
10. FINUDA Offline Group, Status Report on FINUDA Data Analysis, October 2007, document prepared for the 35th LNF Scientific Committee;
11. M. Agnello *et al.*, Nucl. Phys A**775**(2006), 35;
12. V. Magas *et al.*, *Phys. Rev.* C**7**4 (2006), 0205206;
13. FINUDA Collaboration, M. Agnello *et al.*, *Phys. Lett.* B **654** (2007), 80.

GRAAL

D. Babusci, P. Levi Sandri (Resp.), D. Pietreanu.

1 Introduction

The Graal experiment aims at a more detailed knowledge of the baryon spectrum via the precise measurement of cross sections and polarisation observables in photo-induced reactions on the nucleon.

The use of the electromagnetic probe and of it's polarisation, coupled to large acceptance detectors with cylindrical symmetry and high efficiency in the detection of all final state particles, is the technique chosen in many laboratories to perform the ambitious program of a full determination of the scattering amplitude of a given photonuclear reaction. Such determination requires, for each reaction channel, the measurement of the cross section, of the three single polarisation observables and of four appropriately chosen double polarisation observables.

The Graal esperiment is performed in collaboration between 6 INFN Sections (Roma2, LNF, Catania-LNS, Roma1, Genova and Torino), LPSC-Grenoble and INR-Moscow. The Frascati group is responsible of running and maintaining the $\Delta E/\Delta x$ scintillator barrel detector, the Montecarlo simulation program LAGGEN, the off-line reconstruction of events in the BGO calorimeter, the data analysis for coherent η photoproduction off the deuteron and contributes to the data analysis of π^0 and η photoproduction from the neutron bound in a deuteron in the quasi-free kinematics regime.

2 The Graal Beam and the Lagranγe apparatus

The Graal facility provides a polarised and tagged photon beam by the backward Compton scattering of laser light on the high energy electrons circulating in the ESRF storage ring [1]. Using the UV line (350 nm) of an Ar-Ion laser we have produced a gamma-ray beam with an energy from 550 to 1550 MeV. Its polarisation is 0.98 at the maximum photon energy and the energy resolution has been measured to be 16 MeV (FWHM).

The Lagranγe detector is formed by a central part surrounding the target and a forward part. Particles leaving the target at angles from 25^o to 155^o are detected by two cylindrical wire chambers with cathode readout, a barrel made of 32 strips of plastic scintillator parallel to the beam axis, used to determine the $\Delta E/\Delta x$ of charged particles, and the BGO rugby-ball made of 480 crystals of BGO scintillator.

The BGO ball is made of crystals of pyramidal shape with trapezoidal basis which are 21 radiation lengths long (24 cm). This calorimeter has an excellent energy resolution for photons [2], a good response to protons [3], a high detection efficiency for neutrons [4] and is very stable in time due to a continuous monitoring and to the calibration slow control system [5].

Particles moving at angles smaller than 25^o encounter two plane wire chambers, (xy and uv) two walls of plastic scintillator bars, 3 cm thick, located at 3 m from the target point, that provide a measurement of the time-of-flight for charged particles (700 ps FWHM resolution) followed by a shower wall made by a sandwich of four layers of lead and plastic scintillators, 4 cm thick, that provides a full coverage of the solid angle for photon detection (with 95 percent efficiency) and a 20 percent efficiency for neutron detection [6].

The beam intensity is continuously monitored by a flux monitor, composed by three thin plastic scintillators and by a lead/scintillating fibre detector that measures energy and flux [7].

3 2007 activity

During the year 2007 the Graal experiment has collected data to improve the upper bound to the anysotropy of the speed of light. A new DAQ system allows to measure the Compton edge of the gamma-ray spectrum on-line every minute improving by a factor 50 with respect to the previous situation. The data analysis was continued for the photoproduction of π^0 and η mesons off the neutron and was concluded for the simutaneous photoproduction of π^0 and η from the proton and for the double π^0 photoproduction off the neutro.

3.0.1 Hydrogen target

The data analysis activity was mainly focused upon the study of strangeness photoproduction. The reactions $\gamma + p \rightarrow K^+ + \Lambda$ and $\gamma + p \rightarrow K^+ + \Sigma^0$ where analysed and the beam asymmetry and recoil polarisation were extracted for both reactions.

The result is the more extended data base for strangness photoproduction that includes, for the Λ channel, 66 data points in the beam asymmetry and 66 data points in the recoil polarisation while for the Σ^0 channels the points produced were 42 (beam asymmetry) and 8 (recoil polarisation). In the case of the Σ^0 channel, these are the very first data available in literature.

The data were compared to the most recent theoretic approaches allowing for a better determination of some resonance parameters and strengthening the need for a new D_{13} state around 1900 MeV.

The simultaneous photoproduction of π^0 and η on the proton was measured and the beam asymmetry was derived for the first time.

Also the total photoabsorbtion cross-section for Hydrogen was measured and compared to the existing data. In the second and third resonance region this is the first measurement for long time and confirms the existing data though introducing some small differences that can have impirtant consequences for the study of resonance propagation inside nuclei.

3.0.2 Deuterium target

The deuteron was used at Graal as a target of quasi-free neutrons in order to bring in complementary information and towards a full multipole analysis including the isospin structure.

The data analysis was focused on the π^0 and η photoproduction for which reactions a large data base was produced in recent years by Graal. As a first step, data for free and quasi free protons were compared and found quite consistent allowing, as far as the beam asymmetry is concerned, to extract the neutron asymmetry from the deuteron target.

4 Activity in 2008 and conclusions

The Graal experiment started data taking in 1997. It was run both with the green laser line giving rise to a photon beam of maximum energy of 1100 MeV and with UV multi-line with the corresponding gamma-ray beam of 1550 Mev maximum energy. The typical intensity was $2 \cdot 10^6\, s^{-1}$ for the UV line and $5 \cdot 10^6\, s^{-1}$ for the green line, reaching the design intensity. The detector was found very stable during the eight years of operation, with only minor maintenance problems.

Proton and deuteron targets of different lenghts were used and asymmetry data and cross sections have been produced for η, π^0, π^+, $2\pi^0$ and and ω photoproduction channels providing, for these reactions, the most extended and coherent data base available until now. Also the strangness photoproduction from the proton with $K^+\Lambda$ and $K^+\Sigma^0$ final states has been analysed and the final results are being published. The total photoabsorption cross section has been measured and will be published soon. The analysis of the Compton process on the proton, and of all the mentioned photoreactions on the quasi-free neutron of the deuteron target are underway.

During the year 2008 Graal will conclude the data taking. The BGO calorimeter will be moved to the B1 photon beamline of the ELSA stretcher in Bonn where the experimental studies initiated at GRAAL will be continued and extended to higher energies.

5 Recent pubblications

1. Polarization observable measurements for $\gamma p \to K^+\Lambda$ and $\gamma p \to K^+\Sigma^0$ for energies up to 1.5 GeV.
   Eur. Phys. J A31, 79, 2007.

2. Meson photoproduction on the nucleon with polarized photons.
   Eur. Phys. J A31, 441, 2007.

3. Measurement of η photoproduction on the proton from threshold to 1500 MeV.
   Eur. Phys. J A33, 169, 2007.

4. Meson photoproduction on the neutron at GRAAL.
   Int. J. Mod. Phys. 22, 341, 2007.

5. Double π^0 photoproduction on the neutron at GRAAL.
   Phys. Lett. B651, 108, 2007.

6. Measurement of Total Photoabsorption Cross Section on Proton in 600 - 1500 MeV Energy Region at the GRAAL.
   Phys. Atom. Nucl. 71, 75, 2008.

7. Simultaneous photoproduction of η and π^0 mesons on the proton.
   Phys. Rev. Lett. 100, 052003, 1008.

References

1. Graal Collaboration, Nucl. Phys. A622, (1997) 110c.
2. P. Levi Sandri *et al.* Nucl. Inst. and Meth. in Phys. Research A370, (1996), 396.
3. A. Zucchiatti *et al.*, Nucl. Inst. and Meth. in Phys. Research A321, (1992), 219.
4. O. Bartalini *et al.*, to be published in Nucl. Instr. and Meth. in Phys. Research A
5. F. Ghio *et al.*, Nucl. Inst. and Meth. in Phys. Research A404, (1998), 71.
6. V. Kouznetsov *et al.*, Nucl. Instr. and Meth. in Phys. Research A487 (2002), 396.
7. V. Bellini *et al.*, Nucl. Inst. and Meth. in Phys. Research A386, (1997), 254.
8. arXiv:hep-ph/0512136v1 (12/12/2005).

HERMES

E. Avetisyan (Ass.), N. Bianchi, G.P. Capitani, E. De Sanctis, P. Di Nezza
A. Fantoni (Resp. and Resp. Naz.), C. Hadjidakis (Ass. Ric.), D. Hasch (Art.23), V. Muccifora,
A. Orlandi (Tecn.), W. Pesci (Tecn.), E. Polli, A.R. Reolon, A. Viticchié (Tecn.)

1 Introduction

HERMES (HERa MEasurement of Spin) is an experiment at DESY mainly dedicated to study the spin structure of the nucleon. Nucleons (protons and neutrons) are the basic ingredients of the matter of the known universe and their most important quantum number is the spin 1/2. The nucleon is a composite object which can be described in terms of moving quarks of different flavors (up, down and strange) in different configurations (valence and sea) and gluons. Up to year 2000, HERMES collected data with a longitudinally polarized positron beam of 27.5 GeV on longitudinally polarized H, D and ^{3}He internal gas targets. From these runs HERMES provided the most accurate and complete data set for the polarized structure function g_1 and allowed for the first time a direct flavor decomposition of the nucleon spin. The use of a tensor polarised deuteron gas target with only a negligible residual vector polarization enabled the first measurement of the tensor asymmetry A^d_{zz} and of the tensor structure function b^d_1. Runs on several unpolarized nuclear gas targets have been also collected.
In the years 2002-2005 data HERMES has taken data with a transversely polarized hydrogen target. The azimuthal asymmetries are evaluated in two dimensions (ϕ and ϕ_S) and the amplitudes for the Collins and Sivers mechanism were extracted simultaneously.
HERMES has measured also longitudinal double spin asymmetries as a function of transverse momentum p_T using charged inclusive hadrons from electroproduction off a deuterium target.
In the last two yeasr of operation (2006 and 2007) HERMES has taken data with the Recoil Detector installed and no polarisation of the target, with the aim of providing new results in the exciting field of hard exclusive production of mesons and real photons with positron and electron beams. Moreover, as previously done, unpolarized hydrogen and deuterium runs at high density have been also collected for studying nuclear effects.
HERMES ended the data taking at the end of June 2007, due to the HERA shutdown.
During the second half of 2007, the HERMES spectrometer has been completely dismantled, as scheduled.

2 The LNF HERMES group

HERMES is a Collaboration of about 180 physicists from 31 Institutions from 12 Countries. Italy participates with 4 groups and more than 30 physicists from Bari, Ferrara, Frascati and Rome. A Frascati physicist (A. Fantoni) has been the Run Coordinator and also the Deputy Spokesperson. The Frascati group is responsible for the electromagnetic calorimeter and has participated in the project and in the construction of two dual RICH detectors. It has been involved in the project and in the construction of Photon Detector, a part of the new Recoil Detector, installed at the end of 2005. A Frascati physicist (C. Hadjidakis) has the responsibility of the analysis working groups of azimuthal asymmetries in semi-inclusive processes and of the pseudoscalar meson exclusive production. A Frascati physicist (P. Di Nezza) has the responsibility of the nuclear physics analysis working group. Frascati physicists are involved in the analysis of many other physics processes. In addition they are playing a major role in the physics paper draftings and in the editorial process being the leading authors of about one third of the HERMES Collaboration physics publications. Two Frascati physicists (P. Di Nezza and D. Hasch) are part of the HERMES Editorial Board.

3 Experimental activity of the LNF group in 2007

3.1 Calorimeter and TOF

In the period of data taking 2006-2007 with Recoil detector, one of the most important physics goals of HERMES is the investigation of the properties of the Deeply Virtual Compton Scattering (DVCS), a process where a virtual photon is transforming to a real one. For the detection of real photons the HERMES electromagnetic calorimeter, consisting of 840 lead-glass blocks, is used. It's basic purposes are the first level trigger on leptons and offline separation of charged hadrons from leptons by comparing their momentum from the energy of the electromagnetic showers deposited in the clusters of the calorimeter. In addition it allows to measure the energy and the angle of single photons from DVCS as well as double photons from π^0 and η meson decays. The responsibility for the calorimeter required the online monitoring of the status of the detector for the whole period of data taking. During 2007 all the data collected in the past has been reprocessed with recalibration of many detectors, including the calorimeter.
A precise energy and position reconstruction of electromagnetic showers allowed to separate leptons and hadrons with high efficiency by comparing their energy with momentum measured in the tracking system. An improved method of the energy reconstruction accounting for the losses in the preshower lead layer allowed to improve the resolution of the measured energy by $\sim$25%.
HERMES has two sets of scintillator hodoscope paddles which were mainly designed for charge particle triggering and lepton/hadron separation. The second one is also working as a preshower detector. Nevertheless, it turned out that they can be used also as a time-of-flight system to distinguish different hadron types from each other by their mass extracted from speed and momentum. A method was therefore developed to allow a nice separation of pions from protons in the momentum range of 0.6-3 GeV/c with total efficiency of 98% and pion contamination in proton sample of less then 5%. This momentum range is complementary to the one provided by the HERMES dual RICH detector.

3.2 Recoil detector

The recent proof of factorization for exclusive processes and their interpretation in terms of Generalized Parton Distributions to describe the nucleon structure, suggested the detailed investigation of these processes in which a fast meson or a photon is emitted in the forward direction while the slow nucleon is recoiling intact at large angle. Several exclusive processes have been already investigated by HERMES with the missing mass technique. To better identify these processes, a compact Recoil Detector has been constructed and installed around the target in autumn 2005. It consists of three part: an inner Silicon Detector inside the beam vacuum (SD), a SciFi (Scintillating Fibre - SFT) Detector that is situated concentrically outside the beam pipe and an outer Photon Detector that is made of scintillator blocks, with the purpose to reconstruct the paths of protons involved in DVCS reactions from a hydrogen target cell located at the center of the detector. The Frascati group has built the Photon Detector (PD), used to detect photons from the π^0 decay. It consists of three layers of scintillating strips with a WLS fiber system readout. Multi-anode photomultipliers are used with specially designed fan-in/preamplifiers to ensure capable transmittance of the signal. The Photon detector has been assembled in Frascati, transported to DESY and tested with cosmic rays with different trigger configurations. The cosmic rays have been used to test the full readout of the detector, using the Photon Detector as a trigger and a stand-alone tracking system, since the magnet was not included in the test. The reconstruction algorithm, the event display and the wire maps were developed, ensuring effective data acquisition, data processing and interpretation for standard HERMES software analysis tools. The Recoil Detector has been aligned in 2007: the fiber positions of the SFT have been measured in a test beam, the alignment has been optimized using cosmic rays, the SSD and PD have been aligned with respect to SFT and the Recoil HERMES Forward Spectrometer will be aligned by the $e - p$ elastic scattering process. The statistics collected with the Recoil Detector is larger than that one from pre-Recoil data taking. With the Recoil Detector, Deeply Virtual Compton Scattering events can be directly measured and the background rejected; the pre-Recoil results can be refined once the background processes are measured.

3.3 Technical software

LNF members were main responsible for Particle Identification (PID). In particular they worked on the maintenance and code development of the PID library function, on the PID calibration, on the new data productions of 2004, 2005, 2006, and 2007 on the flux corrections to PID for different physics analysis.
The LNF group acted also as HERMES Linux administrator and represented HERMES on DESY Linux user meeting, where user requirements and future strategy for Linux support were discussed. HERMES has a powerful Linux-based PC-farm with 2 workgroups servers, 5 fileservers, 50 batch nodes for various types of analysis and 3 dedicated dCache pools. Several new powerful nodes were purchased to replace the master application server and the interactive workgroups servers, based on Intel Quad Core Xeon CPUs. The computer farm was upgraded to a newer operating system - Scientific Linux v.3.0.8 to allow better consistency with world standards and future participation in GRID computing. A suitable Linux distribution for this cluster has been set up to meet the growing demands of the users on data analysis and Monte-Carlo productions. The maintenance of the computers is provided through SNMP protocol plugged through an SMS gateway, which allows immediate knowledge in case of failures. In addition, there are about 40 desktop PCs acting as terminals for users and about 20 notebook computers for working use.

4 Data analysis and physics results of the LNF group in 2007

4.1 Inclusive spin structure functions

The final results on the polarised structure function g_1 have been already shown in the Activity Report of 2006 and they have been published in Phys. Rev. D 75 (2007), 012007.

4.2 Hadronization in semi-inclusive deep inelastic scattering

A series of semi-inclusive deep-inelastic scattering measurements on deuterium, helium, neon, kripton, and xenon target has been performed in order to study hadronization. Hadron multiplicities on nucleus A relative to those on deuteron, R_A^h, are presented for various hadrons (π^+, π^-, π^0, K^+, K^-, p, and $\bar{p}$) as a function of the virtual-photon energy ν, the fraction z of this energy transferred to the hadron, the photon virtuality Q^2, and the hadron transverse momentum squared p_t^2.
The analysis of the complete data set of the SIDIS data on He, Ne, Kr, Xe allowed for the first time: a multidimensional analysis of the hadron multiplicity ratio as shown in Fig. 1; the study of the Cronin effect in SIDIS for identified hadrons as shown in Fig. 2; the study of the mass number dependence of the hadron attenuation. All these measurements are fundamental to clarify the underlying mechanisms of the hadronization process. The analysis has been completed and the results published in Nucl. Phys. B 780 (2007), 1.
The data reveal a systematic decrease of R_A^h with the mass number A for each hadron type h. Furthermore, R_A^h increases (decreases) with increasing values of ν (z), increases slightly with increasing Q^2, and is almost independent of p_t^2. For pions two-dimensional distributions indicate that the dependences of R_A^π on ν and z can largely be described as a dependence on a single variable L_c, which is a combination of ν and z. The dependence on L_c suggests in which kinematic

conditions partonic and hadronic mechanisms maybe dominant. The behaviour of R_A^π at large p_t^2 constitutes tentative evidence for a partonic energy loss mechanism. A-dependence of R_A^h is investigated as a function of ν, z and L_c, showing an approximately form as A^α with $\alpha \approx$0.5-0.6. A full theoretical description of hadronization in nuclei in one consisten framewok, including partonic and hadronic (absorption plus rescattering) mechanisms is badly needed. Clearly it will be a challenge for any theoretical model that is developed to describe these data for the various hadrons and nuclei as a function of all kinematic variables, but it is successful, this combination of data and theoretical interpretation will contribute essentially to the understanding of non-perturbative QCD at normal, and thence higher densities.

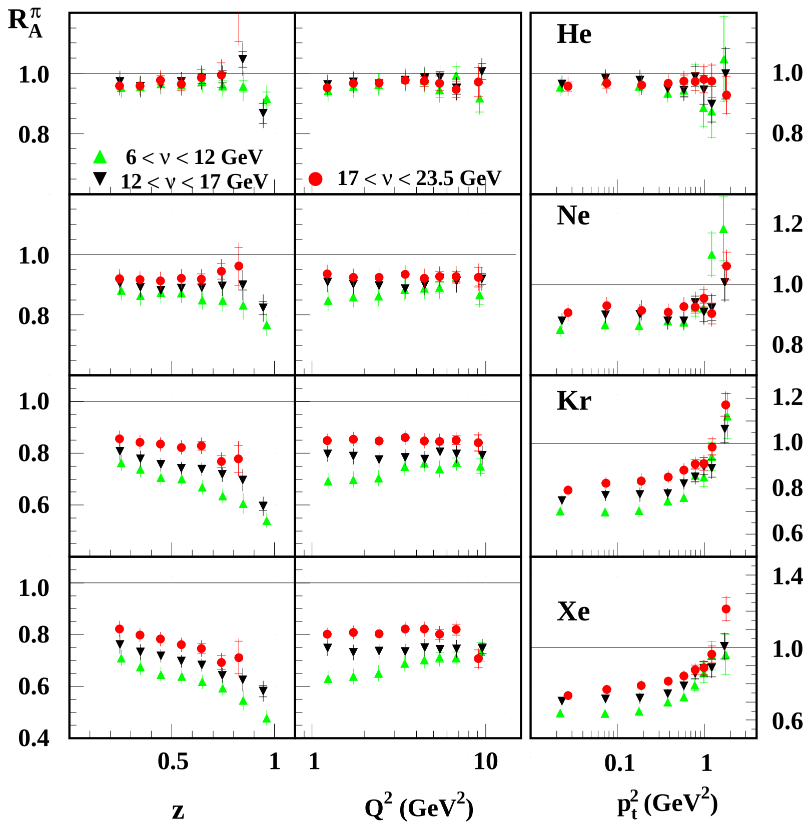

Figure 1: *Values of R_A^h for charged pions for three ν ranges.*

4.3 Transverse momentum broadening of hadron production in semi-inclusive deep inelastic scattering on nuclei

Measurements performed up to now of semi-inclusive production of hadrons in deep-inelastic scattering off nuclei have provided precious information about the space-time development of the hadronization process Lately, by these measurements, HERMES is studying p_t-broadening, defined as $\Delta < p_t^2 >^h = < p_t^2 >_A^h - < p_t^2 >_D^h$ that is also strongly related to the interpretation of high-p$_t$ hadron production in heavy ion collisions. The first direct measurement of p_t-broadening in deep inelastic scattering as a function ν, z, Q^2 and A for pions and positive charged kaons has been performed. These measurements provide strong constraints on the space-time development

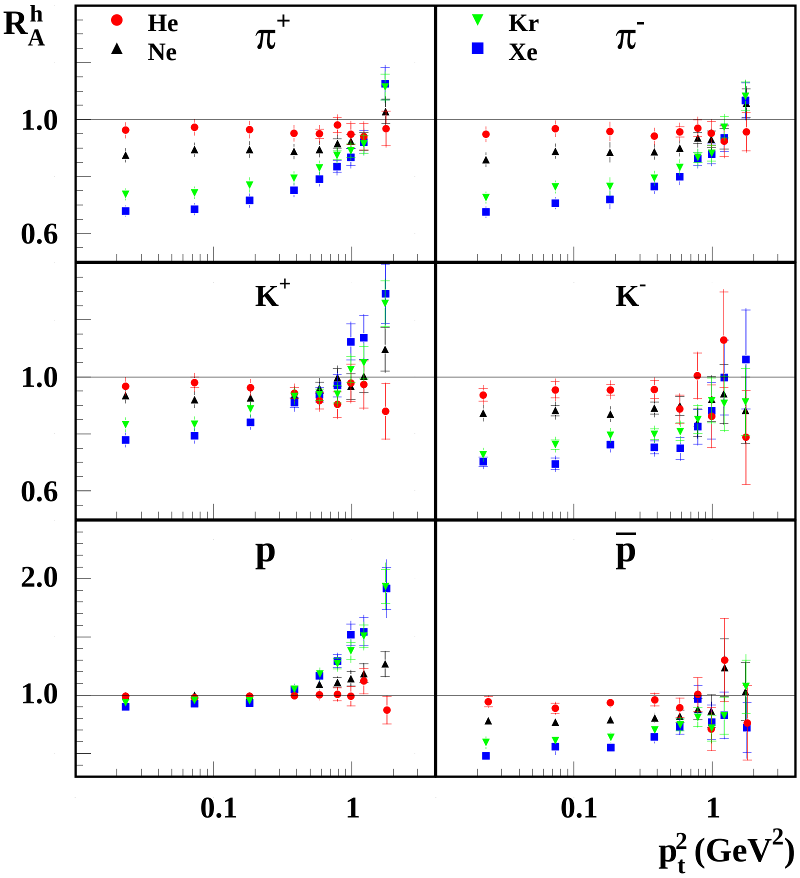

Figure 2: *Values of R_A^h for positively (left panel) and negatively (right panel) charged hadrons as a function of p_t^2.*

of the hadronization process as well as on the parton energy loss in cold nuclear matter. By using some of the theoretical models validated by the multidimensional analysis of the HERMES attenuation data, it has been clarified that the p_t-broadening becomes consistent with zero as $z \to 1$: a detected hadron with a z value close to 1 didn't loose its energy in any kind of interaction or reaction process. The ν dependence of p_t-broadening shows a behavior pointing toward long production time, meaning the pre-hadron is mainly formed outside the nucleus. Results are shown in Fig. 3.

4.4 Exclusive production of single pion

The interest in the hard exclusive electroproduction of mesons has grown since a QCD factorization theorem was proved in the case of longitudinal photon at large Q^2. The amplitude for such reactions can be factorized into a hard lepton scattering part and two soft parts which parametrize the produced meson by a distribution amplitude and the target nucleon by four Generalized Parton Distributions (GPDs). In case of exclusive electroproduction of pion, the reaction provides essential information of the largely unknown space-like form factor and of the polarized GPDs ($\tilde{H}$ and $\tilde{E}$). Fig. 4 shows the t' dependence of the differential cross section for four Q^2 bins. As Q^2

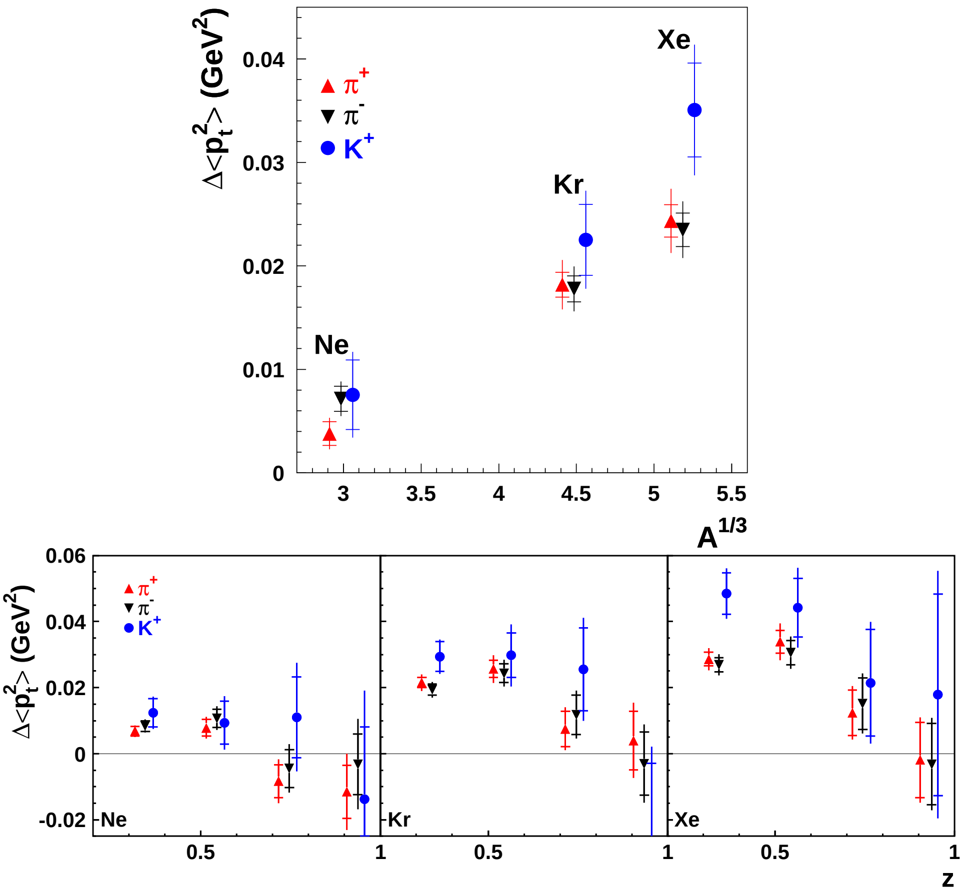

Figure 3: *Top: p_t-broadening as a function of the atomic number $A^{1/3}$ for several hadron types. The inner (outer) error bars represent the statistical (total) uncertainties and are added in quadrature. Bottom: The z dependence of p_t-broadening for different hadron types produced on Ne, Kr, and Xe targets. The inner (outer) error bars represent the statistical (total) uncertainties and are added in quadrature.*

is closely related to x_B (due to the Hermes acceptance as well as the upper limit on the pion momentum) low values of Q^2 correspond to low values of x_B. The dashed-dotted lines in Fig. 4 show the leading-order calculations of the longitudinal part computed using the VGG (Vanderhagen, Guidal, Guichon) GPD model. The GPD $\widetilde{E}$ is considered to be dominated by the $t-$channel pion-pole and the pseudoscalar contribution to the cross section is parametrized in terms of the pion electromagnetic form factor F_π. A Regge-inspired t' dependence is used for $\widetilde{E}$. The GPD $\widetilde{H}$ is neglected here as $\widetilde{E}$ is expected to dominate the cross section at low $-t'$. The solid lines include the power corrections due to the intrinsic transverse momentum of the partons and due to the soft-overlap contribution, the latter being dominant. While the leading-order calculation strongly underestimates the data, the calculations including power corrections agree with the data for $-t' < 0.3$ GeV^2 for the four Q^2 bins. As the GPD model requires $-t'$ to be much smaller than Q^2, the calculations are not expected to describe the full t' range. Furthermore, at larger $-t'$, the data may receive a significant contribution from the transverse part of the cross section, which is

not described by the GPD model.
Both the transverse and longitudinal parts of the cross section were computed using a Regge model from Laget, where pion production is described by the exchange of π and ρ Regge trajectories. In this formalism, the meson-nucleon coupling constants are fixed by pion photoproduction data. The dashed (dotted) lines in Fig. 4 show the total (longitudinal) cross section computed using the Regge model. In this model the transverse part of the cross section is estimated to represent from 6% to 8% of the total cross section at $-t' = 0.07$ GeV^2 and from 15% to 25% of the total cross section integrated over t', confirming the expected suppression of the transverse to the longitudinal part of the cross section. The total cross section computed by the Regge model describes well the t' dependence of the differential cross section (dashed line on Fig. 4) and the Q^2 dependence of the cross section integrated over t'. The model calculations give also a good description of the magnitude of the data except at low $-t'$ for $Q^2 < 3$ GeV^2, where the calculations overestimate the data up to 70%.
The Frascati group was responsible for the full analysis and for the paper, published in Phys. Lett. B 659 (2007), 486.

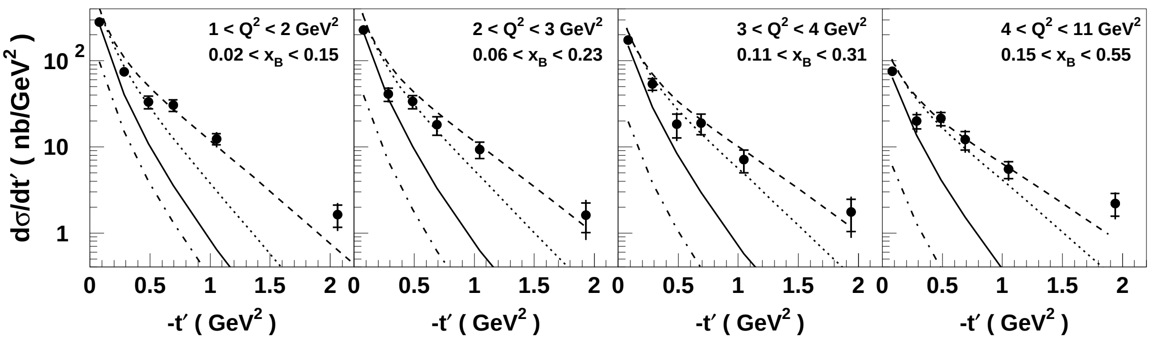

Figure 4: *Differential cross section for exclusive π^+ production by virtual photons as a function of $-t'$ for four Q^2 bins. The inner bars represent the statistical uncertainty and the outer error bars the quadratic sum of statistical and systematic uncertainty. The curves represent calculations based on GPD and on Regge models.*

4.5 Single-spin asymmetry A_{UT} for exclusive ρ^0 production, with L/T separation

Measurements of exclusive leptoproduction of mesons provide new information about the structure of the nucleon via the relation of this class of processes with the GPDs. The quantum number of the produced meson determine the sensitivity to different GPDs. In particular, longitudinally polarised vector mesons are sensitive to the GPDs H and E. It has been shown by Ji that the second moment of these GPDs are related to the contribution J^q of the total angular momentum of quarks to the nucleon spin $\lim_{t\to 0} \int_0^1 x\,(H_q(x,\xi,t) + E_q(x,\xi,t))\,dx = J_q$. Since the contribution of the quark spin to the nucleon has been measured through polarised DIS, measurements of J^q would provide a way to determine the unknown contribution of the orbital angular momentum of quarks to the nucleon spin.
The transverse target-spin asymmetry in exclusive leptoproduction of longitudinally polarised ρ^0, induced by longitudinally polarised virtual photons, is linearly dependent on the GPD E. Due to this property the asymmetry is in particular an observable sensitive to J^q.
In order to distinguish vector mesons with longitudinal polarisation use can be made of the fact that the polarisation state of the vector meson is reflected in its decay angular distribution. Preliminary

results have been obtained for the transverse target-spin asymmetry in exclusive ρ^0 leptoproduction. By including the ρ^0 deacay angular distribution in the asymmetry extraction procedure the contribution for longitudinally and transversely polarised ρ^0 mesons could be separated. Results are shown in the left panel of Fig. 5.
The LNF Hermes group plays the leading role in the coordination of this analysis and is active in the committee for the publication of these data.

4.6 Measurement of azimuthal asymmetries with respect to both beam charge and transverse target polarisation in exclusive electroproduction of real photons

In the context of the rapid theoretical developments of the last decade, usual Parton Distribution Functions (PDFs) have been conceptually subsumed within the broader framework of Generalized Parton Distributions (GPDs), which also describe elastic form factors and amplitudes for hard-exclusive reactions leaving the target nucleon intact. Strong interest in the formalism of GPDs and their experimental constraint has emerged after moments of certain GPDs were found to relate directly to the total (including orbital) angular momenta carried by partons in the nucleon, via the Ji relation, which has been a hot topic since decades, and is still unknown. Among all presently practical hard exclusive probes, the Deeply Virtual Compton Scattering (DVCS) process, i.e., the hard exclusive leptoproduction of a real photon (e.g., $\gamma^* N \to \gamma N'$), appears to have the most reliable interpretation in terms of GPDs. While at HERMES kinematics this process is intrinsically indistinguishable from the Bethe-Heitler (BH) process, in which the photon is radiated from the lepton before or after the interaction with the quark, the interference of these two processes provides valuable information about GPDs through various azimuthal amplitudes. The unique conditions at HERA and HERMES allow the extraction of all possible combinations of asymmetry amplitudes, e.g. beam-charge and beam-spin as well as longitudinal and transverse target spin. In 2007, the combined analysis of the beam-charge and transverse target spin asymmetries (BCA and TTSA, respectively) was finalized using the advanced maximum likelyhood method and reported in a paper, submitted to JHEP in early 2008.
Transverse target-spin azimuthal asymmetries in electroproduction of real photons are measured for the first time, and for both beam charges. A combined fit of this data set separates for the first time the azimuthal harmonics of the squared DVCS amplitude and the interference term BH-DVCS. The extracted charge asymmetry of the interference term is much more precise than previously published results, and constrains models for Generalized Parton Distributions. By comparing GPD-model calculations with extracted azimuthal asymmetry amplitudes associated with both beam charge and transverse-target polarisation, a model-dependent constraint on the total angular momenta carried by u and d-quarks in the nucleon is obtained as $J_u + J_d/2.8 = 0.49 \pm 0.17(\exp_{\mathrm{tot}})$ using a double-distribution GPD model, and $J_u + J_d/2.8 = -0.02 \pm 0.27(\exp_{\mathrm{tot}})$ using the dual-parameterisation model, as summarized in Fig. 5 right. Thus, such data have the potential to provide quantitative information about the spin content of the nucleon when GPD models become available that fully describe all existing DVCS data. Members of the Frascati group were actively involved in the full chain of the data and MC analysis as well as in the paper drafting process.

4.7 Nuclear DVCS

Deeply virtual compton scattering (DVCS), e.g. the hard exclusive leptoproduction of a real photon ($ep \to e'p'\gamma$), appears to be the theoretically cleanest access to GPDs. Hermes has a broad program for measuring several different observables in DVCS on a proton as well as on heavier targets. Results have been obtained for the measurement of cross section asymmetries w.r.t. the beam spin, the beam charge and the target spin. Extracting beam-charge asymmetries, that allow the separation of the interference and the dvcs^2 terms, is a unique feature of the HERA experiments.

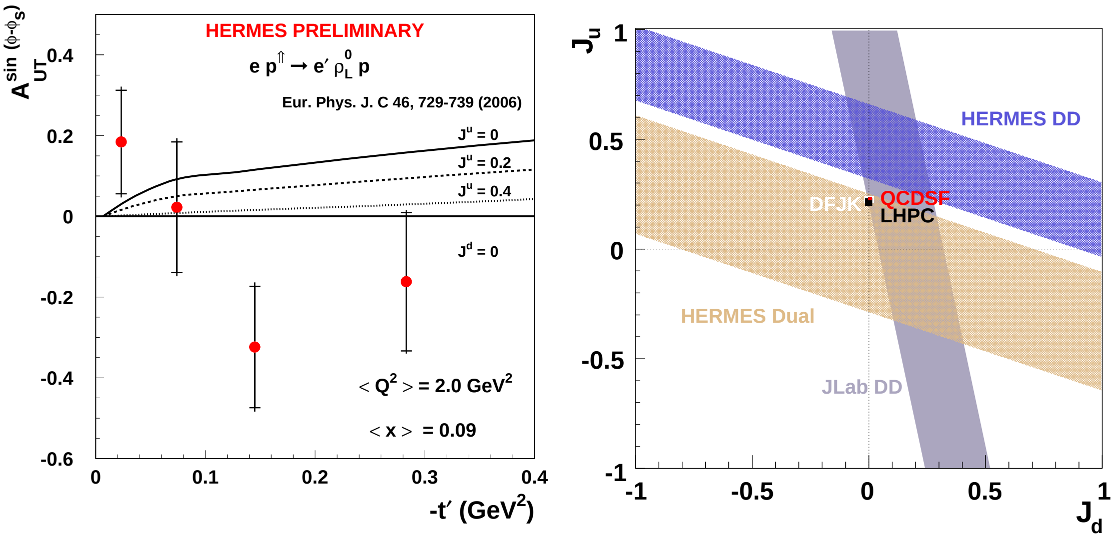

Figure 5: *Left: Sivers moments for exclusive production of longitudinally-polarized* ρ^0 *from a transversely polarized hydrogen target vs* $-t'$*, compared with a GPD calculation. Right: Model-dependent constraints on u-quark total angular momentum* J_u *vs d-quark total angular momentum* J_d*, obtained by comparing DVCS experimental results and theoretical calculations.*

The transverse target-spin asymmetry has been measured for the first time by HERMES. It is particularly sensitive (just as this asymmetry in exclusive ρ^0 production as mentioned above) to the GPD E and therefore an indispensable observable for gaining information on the total angular momentum of quarks. In fact, a first, model dependent, extraction of the total angular momentum for u and d quarks has been presented in DESY-07-225. The prospects for these measurements at HERMES have been significantly enhanced with the installation of a Recoil detector in the early 2006.

Moreover, HERMES has collected a unique data set using heavier nuclear targets allowing to study nuclear GPDs. Specifically for nuclear targets, GPDs of nuclei give an access to the spacial distribution of energy, pressure, angular momentum and shear forces in nuclei. Therefore, studies of nuclear GPDs address the problem of the origin of nuclear forces from the first principles. Studies of nuclear GPDs serve as a guide (and a cross check) for microscopic models of nuclear structure better than nuclear PDFs.

In experimental studies of DVCS on nuclear targets, the important issue is the interplay between the coherent (nucleus is intact) and incoherent (nucleus breaks up or excites) contributions to the measured cross section. The two contributions have a very distinct dependence on the momentum transfer t: the coherent contribution has a fast t-dependence proportional to the nuclear form factor squared; the incoherent contribution has a slow t-dependence proportional to the nucleon form factor squared. At small values of the momentum transfer t, nuclear break-up is unlikely and the DVCS process is predominantly coherent. At large t, the target nucleus break-up and DVCS takes place on individual uncorrelated nucleons.

First preliminary results of the DVCS beam-spin asymmetry as a function of the atomic number have been presented for coherent and the incoherent enriched samples. This analysis has been significantly improved in 2007 by combining data for H, D, Kr and Xe taken with both electrons and positrons. This way also the beam-charge asymmetry could be extracted and the interference and DVCS^2 terms of beam-spin asymmetries be separated. The LNF Hermes group plays the leading role in the coordination of these new studies and serves as author for the publication of the results for nuclear DVCS.

5 Outlook

The data taking with Recoil Detector has been successfull, new precision data on hard exclusive reactions have been collected and will be analyzed, providing results on the exciting and new field of hard exclusive production of mesons and real photons with positron and electron beams. DVCS can be directly measured and the background rejected; pre-recoil results will be refined once the background processes are measured.
The analysis of data with a transversely polarized hydrogen target has been completed and will be finalized soon, provide a demonstration of a new tool for studying the transverse structure of the nucleon.
The ongoing physics analysis and the phenomenological investigations will be completed.

6 Conferences by LNF Authors in Year 2007

6.1 List of Conference Talks

1. E. Avetisyan, "Overview of Exclusive Physics at HERMES" Advanced Studies Institute on Symmetries and Spin (SPIN-Praha2007), Prage, Czech Republic, July 2007.
2. N. Bianchi, "Determination of the Gluon Polarization at HERMES, 6th Circum Pan Pacific Symposium on High Energy Spin Physics (PACSPIN07), Vancouver, Canada, July 2007.
3. N. Bianchi, "Nuclear Effects in Hadron Production" International Workshop on Quantum Chromodynamics Theory and Experiment (QCD@Work2007), Martina Franca, Italy, June 2007.
4. E. De Sanctis, "Transversity: the role of transverse spin effects" I3 Hadron Physics Meeting, Laboratori Nazionali di Frascati, Italy, May 2007.
5. E. De Sanctis, "TMD Network Project", Workshop on Trnasverse momentum, spin and position distributions of partons in hadrons, ECT* Trento, Italy, June 2007.
6. E. De Sanctis, "Networking project TMD-net", I3 Hadron Physics Meeting, Laboratori Nazionali di Frascati, Italy, September 2007.
7. P. Di Nezza, "Medium modification of fragmentation function" (invited talk), XI International Conference on Nuclear Physics WONP2007), Havana, Cuba, February 2007.
8. P. Di Nezza, "Nuclear Attenuation and p_t broadening DIS at HERMES", EPS International Europhysics Conference in High Energy Physics (EPS-HEP2007), Manchester, United Kingdom, July 2007.
9. A. Fantoni, "Spin Physics at HERMES: recent results" (invited talk), International Conference on Hadron Structure (HS07), Modra-Harmonia, Slovakia, September 2007.
10. C. Hadjidakis, "Spin Physics from HERMES" (invited talk), Gordon Research Conference on Nuclear Physics, Newport, USA, July 2007.
11. D. Hasch, "Summary of the Spin physics session - experimental part", 15th International Workshop on Deep Inelastic Scattering on QCD (DIS 2007), Munich, Germany, April 2007.

12. D. Hasch, “Polarised deep-inelastic scattering - experimental overview”, ECT* workshop on hard QCD with antiprotons at GSI FAIR, Trento, Italy, July 2007.
13. D. Hasch, ”Transverse Spin Structure of the Nucleon”, 7th Research Conference on Electromagnetic Interactions with Nucleons and Nuclei (EINN2007), Milos, Greece, September 2007.
14. D. Hasch, Spinstruktur des Nukleons 0 elektromagnetische Sonden bei hohen Energien”, Annual Meeting of the Committee for Hadron and Nuclear Physics, GSI-Darmstadt, Germany, October 2007.
15. D. Hasch, “Exclusive processes at HERMES”, Journees GDR Nucleon - Extracting GPDs, Ecole Polytechnique Paris, France, November 2007
16. V. Muccifora, “Latest Results from HERMES on the Nuclear Dependence of Pion, Kaon, and Proton Formation”, International Conference on the Structure and Interactions of the Photons, Paris, France, July 2007.

6.2 Conference organization and advisory, Projects, Seminars, Lectures, Editors

1. E. Avetisyan, Seminar “What do we know about the nucleon spin”, Tokyo, Japan, March 2007
2. N. Bianchi, Editor of The European Physical Journal A
3. N. Bianchi, International Advisor Committee of BARYONS07 International Conference, Seoul, Korea, June 2007
4. E. De Sanctis, Convener of HERMES-LNF TARI at DESY
5. E. De Sanctis, Convener of Studio di effetti di spin trasverso nel nucleone, PRIN 2006-2008 project of the MIUR
6. E. De Sanctis, Convener of N7-Transversity: Exploring the unknown transverse spin structure of the nucleon, Project of the I3-HP program of the European Commission
7. E. De Sanctis, Member of HERMES Nominating Committee
8. P. Di Nezza, Member of HERMES Editorial Board
9. P. Di Nezza, Convener of Hadron Structure Session at XI International Conference on Hadron Spectroscopy, Laboratori Nazionali di Frascati, Italy, October 2007
10. P. Di Nezza, Organizer of the XII LNF Spring School in Nuclear and Subnuclear and Astroparticle Physics, Laboratori Nazionali di Frascati, Italy, May 2007
11. P. Di Nezza, Organizer of the XI International Conference on Hadron Spectroscopy, Laboratori Nazionali di Frascati, Italy, October 2007
12. P. Di Nezza, Editor of Proceedings of the XI International Conference on Hadron Spectroscopy, Laboratori Nazionali di Frascati, Italy, October 2007
13. D. Hasch, Member of HERMES Editorial Board
14. D. Hasch, Member of the committee for the DESY thesis award

15. D. Hasch, Convener of the Spin Physics Session at the 15th International Workshop on Deep Inelastic Scattering and QCD (DIS 2007)
16. D. Hasch, Organizer (Chair) of the ECT* Workshop on Transverse Momentum, Spin, and Position Distributions of Partons in Hadrons, Trento, Italy, June 2007
17. D. Hasch, Seminar "The spin of the nucleon from the HERMES point of view", LPSC Grenoble, France, March 2007
18. D. Hasch, Seminar "The spin of the nucleon from the HERMES point of view", IPN Orsay, France, March 2007
19. D. Hasch, Lecture Series "Transverse Spin Phenomena in DIS - experiments", CLXVII Course of the Enrico Fermi School on "Strangeness and Spin in Fundamental Physics", Varenna, June 2007
20. D. Hasch, Seminar "The spin of the nucleon from the HERMES point of view", Gutenberg-University of Mainz, Germany, November 2007

7 Publications of LNF Authors in Year 2007

1. A. Airapetian *et al.*, "The Beam-Charge Azimuthal Asymmetry and Deeply Virtual Compton Scattering", Phys. Rev. **D**75, 011103 (R) (2007).
2. A. Airapetian *et al.*, "Precise Determination of the Spin Structure Function g_1 of the Proton, Deuteron and Neutron", Phys. Rev. **D**75, 012007 (2007).
3. A. Airapetian *et al.*, "Beam-Spin Asymmetries in the Azimuthal Distribution of Pion Electroproduction", Phys. Lett. **B**648, 164 (2007).
4. A. Airapetian *et al.*, "Hadronization in Semi-inclusive Deep Inelastic Scattering on Nuclei", Nucl. Phys. **B**780, 1 (2007).
5. A. Airapetian *et al.*, "Transverse Polarization of Λ and $\bar{\Lambda}$ Hyperons in Quasi-Real Photon Nucleon Scattering at HERMES", Phys. Rev. **D**76, 092008 (2007).
6. A. Airapetian *et al.*, "Cross sections for hard exclusive electroproduction of π^+ mesons on a hydrogen target, Phys. Lett. **B** in print, arXiv: 0707.0222.
7. N. Bianchi, "Review on DIS electroproduction on nuclei" Nucl. Phys. **A**782 , 150 (2007).
8. N. Bianchi, "Nuclear modification of two-hadron correlations from HERMES" Nucl. Phys. **A**783 , 93c (2007).
9. N. Bianchi, "Nuclear effect in hadron production", AIP Conference Proceedings 964, 188 (2007).
10. A. Fantoni, "The spin puzzle: recent results from the HERMES experiment", Intern. Journ. of Modern Physics **A**22, 249 (2007).
11. A. Fantoni, "Measurement of polarised distribution functions at HERMES", Nucl. Phys. **B** Proc. Suppl. 174, 43 (2007).
12. D. Hasch, "Spin Physics at HERMES", AIP Conference Proceedings 915, 307 (2007)
13. D. Boer, D. Hasch, G. Mallot, "Spin Physics: Session Summary", arXiv 0707.1259, published in "Munich 2007, Deep Inelastic Scattering" 267-282

$\overline{\text{P}}$ANDA - $\bar{\text{p}}$ Annihilation at Darmstadt

B. Dulach, P. Gianotti (Resp. Naz.), M. Giardoni, C. Guaraldo, O.N. Hartmann (Art. 23),
M. Iliescu (Art. 23), V. Lucherini, D. Orecchini (Tecn.), E. Pace,
L. Passamonti (Tecn.), D. Sirghi (Art. 2222),

1 Introduction

$\overline{\text{P}}$ANDA is one of the biggest future experiments in nuclear and hadron physics that will be carried out at the new Facility for Antiproton and Ion Research (FAIR). It is dedicated to study annihilations of antiprotons on nucleons and nuclei up to a maximum center-of-mass energy in $\bar{p}p$ of 5.5 GeV. Presently, the $\overline{\text{P}}$ANDA collaboration consists of 400 physicists from 17 countries spreada all over the world. The Italian groups involved are: Torino, University, Politecnico and INFN, Trieste, University and INFN, Genova INFN, Pavia, University and INFN, Ferrara, University and INFN, Frascati INFN laboratory, Catania, University and INFN. The LNF group is involved in the design and construction of the central tracker of the $\overline{\text{P}}$ANDA detector.

2 $\overline{\text{P}}$ANDA experiment

A new facility for hadronic physics is under construction in Germany. It consists of a major upgrade of the presently running GSI accelerator complex of Darmstadt [1]. An intense, high momentum

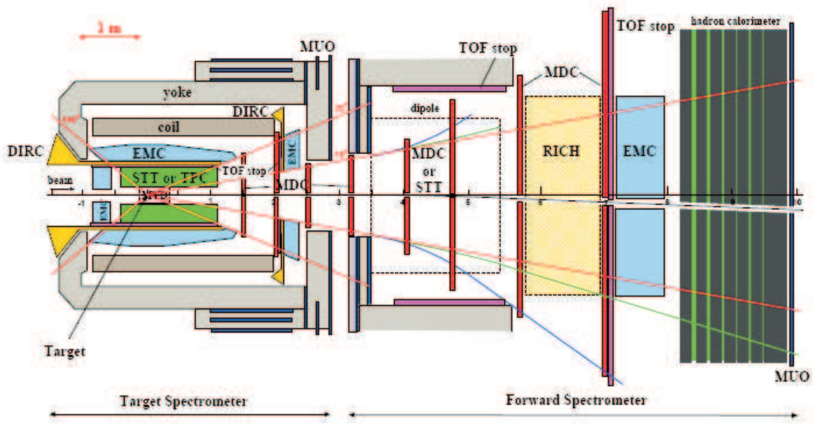

Figure 1: *A schematic view of the $\overline{\text{P}}$ANDA detector. The different components are: DIRC (Detection of Internally Reflected Cherenkov light), EMC (Electromagnetic Calorimeter), STT (Straw Tube Tracker), TPC (Time Projection Chamber), MVD (Micro Vertex Detector), MDC (Mini Drift Chamber), MUO (Muon Detector), RICH (Ring Imaging Cherenkov counter), TOF (Time-Of-Flight detector).*

resolution antiproton beam, with momenta between 1.5 and 15 GeV/c, will be available at the High Energy Storage Ring (HESR), and the experimental activity will be carried out using a general purpose detector $\overline{\text{P}}$ANDA that will be build surrounding an internal target station installed in

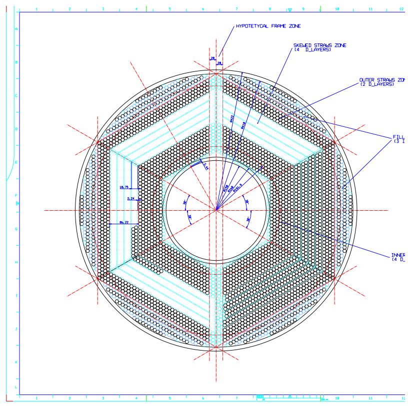

Figure 2: *A possible layout for the STT. Details are in the text.*

one of the two straight sections of the storage ring. Fig. 1 shows a schematic drawing of the $\overline{\mathrm{P}}$ANDA dedector. It is designed as a large acceptance multi-purpose detector consisting of two distinct parts: a solenoidal spectrometer, surrunding the interaction target region, and a forward spectrometer to cover the solid angle between 5 and 22 degrees.

3 The $\overline{\mathbf{P}}$ANDA Central Tracker

The $\overline{\mathrm{P}}$ANDA Central Tracker has to satisfy the following requirements:

- almost full solid angle coverage;
- momentum resolution $\delta p/p \sim 1.5\%$;
- low material budget $X/X_0 \sim$ few %;
- good spatial resolution $\sigma_{r,\phi} = 150$, μm, $\sigma_z =$ few mm.

This detector will be placed around the Micro Vertex Detector (MVD) at a radial distance from the interaction point between 15 and 42 cm. Along the beam axis the allowed space is 150 cm. Presently, for this detector, two options are under discussion: a Straw Tube Tracker (STT) and a Time Projection Chamber (TPC). The LNF $\overline{\mathrm{P}}$ANDA group, having experience in straw tubes, is involved in the realization of the STT.

3.1 Straw tube detector layout

The overall $\overline{\mathrm{P}}$ANDA tracking volume will be divided in two half by the target pipe, therefore the detector will consist of two identical semi-chambers. In the hypotesis of a straw tube tracker, each one will be made of aluminized mylar straw tubes, diameter 10 mm, length 150 cm, thickness 30 μm, arranged in planar double layers. Inside a double layer the tubes are glued together and operated with an Ar+CO_2 gas mixture with an over-pressure of 1 bar. This solution will help to avoid strong support structures and will keep the detector design modular and simple. To measure also particle z coordinate, some layers will be mounted with a skew angle of few degrees with respect to the beam axis.

Figure 2 shows a possible layout for the STT. There are 4 internal duoble-layers parallel to the beam axis, then 4 double-layers mounted with an opposite skew angle, and finaly 2 other layers

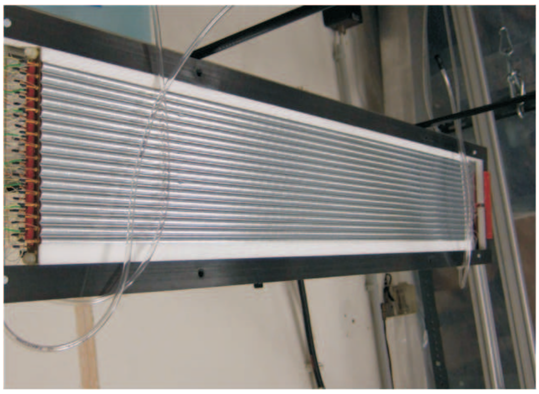

Figure 3: *Prototype of a straw tube double layer.*

parallel to the beam axis. To fill up the cylindrical volume, the remaining region houses smaller tube layers. The activity of the LNF $\overline{\text{P}}$ANDA group during 2007 has been devoted to the definition and the design of the STT. In particular we mainly concentrate in the design of the mechanical support structure.

4 List of publications

1. O. N. Hartmann, "Hadron properties in the nuclear medium the panda program with pA reactions", Int. J. Mod. Phys. A 22-2-3 (2007).
2. P. Gianotti, "New physics and technical challenges of PANDA", Eur. Phys. Jour. A31 (2007) 679-683.

5 Conference presentations

1. P. Gianotti, "Hadron Physics", invited talk at the ,FAIR Kick-Off International Symposium on the Physics at FAIR, November the 7th 2007, Darmstadt, Germnay.
2. P. Gianotti, "Hadronic Physics with PANDA at FAIR", invited talk at the 11th international Baryons Conference (baryon07),11-15 June 2007, Seoul, South Korea.

References

1. http://www.gsi.de/fair/
2. http://www.gsi.de/panda/
3. PANDA Letter of Intent, 2004; PANDA Technical Progress Report, 2005.

SIDDHARTA

M. Bazzi (Art. 23), M. Bragadireanu (Bors. UE), M. Catitti (Ass. Ric.),
C. Curceanu Petrascu (Co-Resp. Naz.), C. Guaraldo (Co-Resp. Naz.), M. Iliescu (Art. 2222),
P. Levi Sandri, V. Lucherini, F. Lucibello (Tecn.),
D. Pietreanu (Bors. PD), A. Romero Vidal (Bors PD), A. Scordo (Dott.), D. Sirghi (Art. 2222),
F. Sirghi (Bors. UE), D. Tagnani (Bors.), O. Vazquez Doce (Bors. PD)

1 The SIDDHARTA scientific program

The objective of the SIDDHARTA (Silicon Drift Detector for Hadronic Atom Research by Timing Application) experiment is to continue, to deepen and enlarge the successful scientific line, initiated by the DEAR experiment in performing precision measurements of X-ray transitions in exotic (kaonic) atoms at DAΦNE.

The eV precise determination of the shift and width of the $1s$ level with respect to the purely electromagnetic calculated values, in kaonic hydrogen and kaonic deuterium, generated by the presence of the strong interaction, through the measurement of the X-ray transitions to this level, will allow the first precise experimental determination of the isospin dependent antikaon-nucleon scattering lengths.

The shift ϵ and the width Γ of the $1s$ state of kaonic hydrogen are related to the real and imaginary part of the complex s-wave scattering length, a_{K^-p}, through the Deser formula (in the isospin limit):

$$\epsilon + i\Gamma/2 = 2\alpha^3\mu^2 a_{K^-p} = (412\ eV\ fm^{-1}) \cdot a_{K^-p} \tag{1}$$

where α is the fine structure constant and μ the reduced mass of the K^-p system. In the isospin limit, i.e. in the absence of the electromagnetic interaction and at $m_d = m_u$, a_{K^-p} can be expressed directly in terms of the scattering lengths for isospin I=0 and I=1:

$$a_{K^-p} = \frac{1}{2}(a_0 + a_1) \tag{2}$$

A similar relation applies to the case of kaonic deuterium and to the corresponding scattering length a_{K^-d}:

$$\epsilon + i\Gamma/2 = 2\alpha^3\mu^2 a_{K^-d} = (601\ eV\ fm^{-1}) \cdot a_{K^-d} \tag{3}$$

An accurate determination of the K$^-$N isospin dependent scattering lengths will place strong constraints on the low-energy K$^-$N dynamics, which, in turn, constraints the SU(3) description of chiral symmetry breaking in systems containing the strange quark.

The DEAR measurement on kaonic hydrogen, performed in 2002 (Phys. Rev. Lett 94 (2005), 212302), has already triggered an increased activity of the theoretical groups working in the low-energy kaon-nucleon interaction field, as well as in more general non-perturbative QCD.

The SIDDHARTA experiment aims to improve the precision obtained by DEAR by an order of magnitude and to perform the first measurement ever of kaonic deuterium. Other measurements (kaonic helium, sigmonic atoms, precise determination of the charged kaon mass) are as well considered in the scientific program.

2 The SIDDHARTA experiment features

SIDDHARTA represents a new phase in the study of kaonic atoms at DAΦNE. The DEAR precision was limited by a signal/background ratio of about 1/70. In order to significantly improve this ratio a breakthrough was necessary. An accurate study of the background sources present at DAΦNE was re-done. The background includes two main sources:

- synchronous background: coming together with the K^- - related to K^- interaction in the setup materials and also to the ϕ-decay process; it can be defined hadronic background;
- asynchronous background: final products of electromagnetic showers in the machine pipe and in the setup materials originated by particles lost from primary circulating beams either due to the interaction of particles in the same bunch (Touschek effect) or due to the interaction with the residual gas.

Accurate studies performed by DEAR showed that the main background source in DAΦNE is of the second type, which shows the way to reduce it. A fast trigger correlated to the negative kaon entrance in the target would cut the main part of the asynchronous background.

While DEAR used for the X rays detection the CCD (Charge Coupled Device) detectors - excellent X-ray detectors, with very good energy resolution (about 140 eV FWHM at 6 keV), but having the drawback of being non-triggerable devices (since the read-out time per device is at the level of 10 s), a recently developed device, which preserves all good features of CCDs (energy resolution, stability and linearity) but additionally is triggerable - i.e. fast (at the level of 1μs) was implemented. This new detector is represented by large area Silicon Drift Detector (SDD), specially designed for spectroscopic application. The development of the new 1 cm^2 SDD device is partially performed in the framework of an European Joint Research Activity (JRA10) within the FP6 program, the HadronPhysics I3.

Successful tests of SDD prototypes were performed in 2003, 2004, 2005 and 2007 at the Beam Test Facility of Frascati (BTF), in realistic (i.e. DEAR-like) conditions and in the laboratory. The results of these tests were very encouraging: a trigger rejection factor of $5 \cdot 10^{-5}$ was measured. Extrapolated to SIDDHARTA conditions, this number translates into a S/B ratio in the region of interest about 20/1 for same background situation as in DEAR. By triggering the SDDs, the asynchronous e.m. background (mainly due to Touschek effect) can therefore be eliminated.

3 Activities in 2007

In what follows, we present the main 2007 SIDDHARTA activities performed at LNF.

3.1 Beam Test Facility (BTF) trigger test of the final SIDDHARTA SDD detectors

A setup containing 3x1cm^2 final type SDDs, together with a prototype of the final readout electronics and a final stabilized power supply module was tested at the BTF facility in the period 19 March - 1 April 2007, with very positive results. The following measurements were performed:

- energy resolution of the SDD chips in the experimental hall; a value of 250 eV (FWHM) was obtained, showing the importance of the grounding and a proper filtering of the noise for the final setup installation (in laboratory, were grounding loops were carefully checked, the resolution was 150 eV);
- linearity of the SDD answer: the SDD answer is linear to better than 0.3%; in laboratory the value of linearity was checked to better than 0.1% - meaning a systematic error at the level of eV;

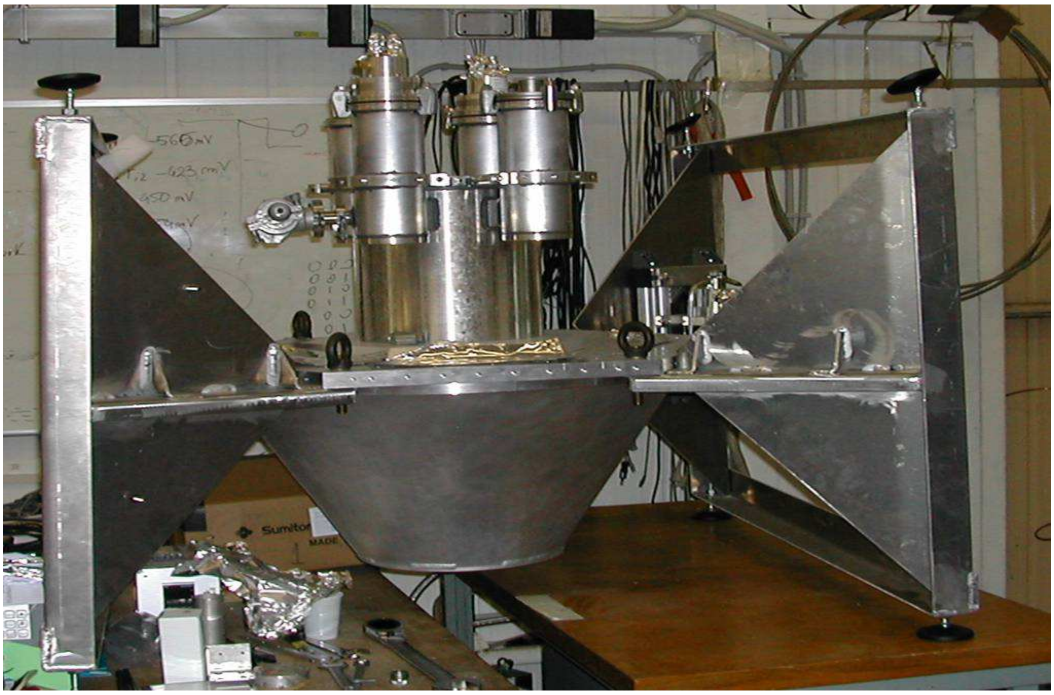

Figure 1: *SIDDHARTA setup in the laboratory - during mounting.*

- trigger performance: a trigger signal, coming from a system of scintillators (similar to the one to be used by SIDDHARTA) placed along the BTF beam, was giving the signal to SDD system; radioactive Sr and Fe sources were used to create an asynchronous background. For a total incident rate of about 900 Hz on the 3 SDD chips, with the trigger rate (given by BTF beam structure) of 48 Hz, the rejection factor was measured to be 15 x 10−5, confirming the feasibility of the SIDDHARTA experiment.

More infos can be found in the SIDDHARTA Technical Note IR-9, 19 June 2007.

3.2 Preparation of the final SIDDHARTA setup

All components of the final setup were built during the 2007 (mechanics, electronics, power supplies, DAQ). The setup is presently being mounted in the SIDDHARTA laboratory, being ready for installation in 2008 (Fig. 1).

3.3 DAY1 - SIDDHARTA setup

In its early phase of measurements on the new upgraded DAΦNE, SIDDHARTA will install a reduced setup, the so-called DAY1 setup - much more easy to handle, containing a cryogenic target filled with nitrogen (or helium) and a number of 12 SDD chips (Fig. 2) This setup was installed on DAΦNE in March 2008 (Fig. 3) and is presently taking data in order to : understand background and trigger performance; help DAΦNE in the optmization phase; optimize degrader and prepare the conditions for the final setup installation.

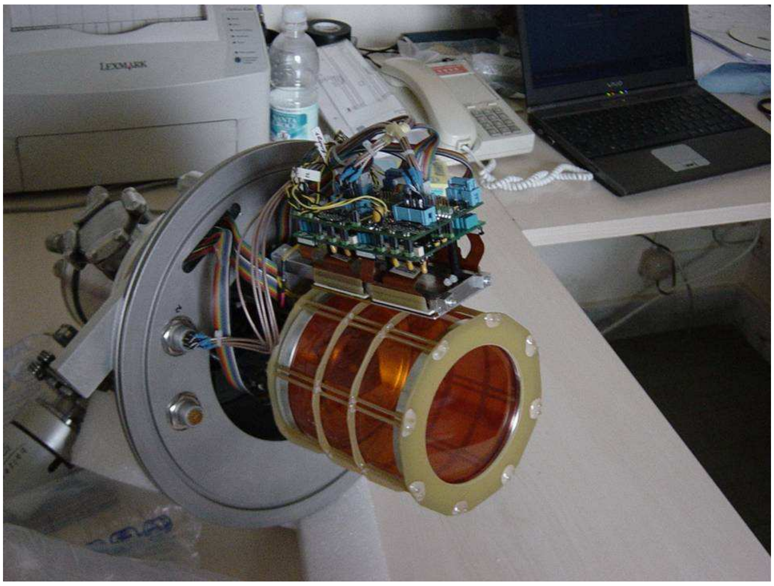

Figure 2: *DAY1 - SIDDHARTA setup - detail*

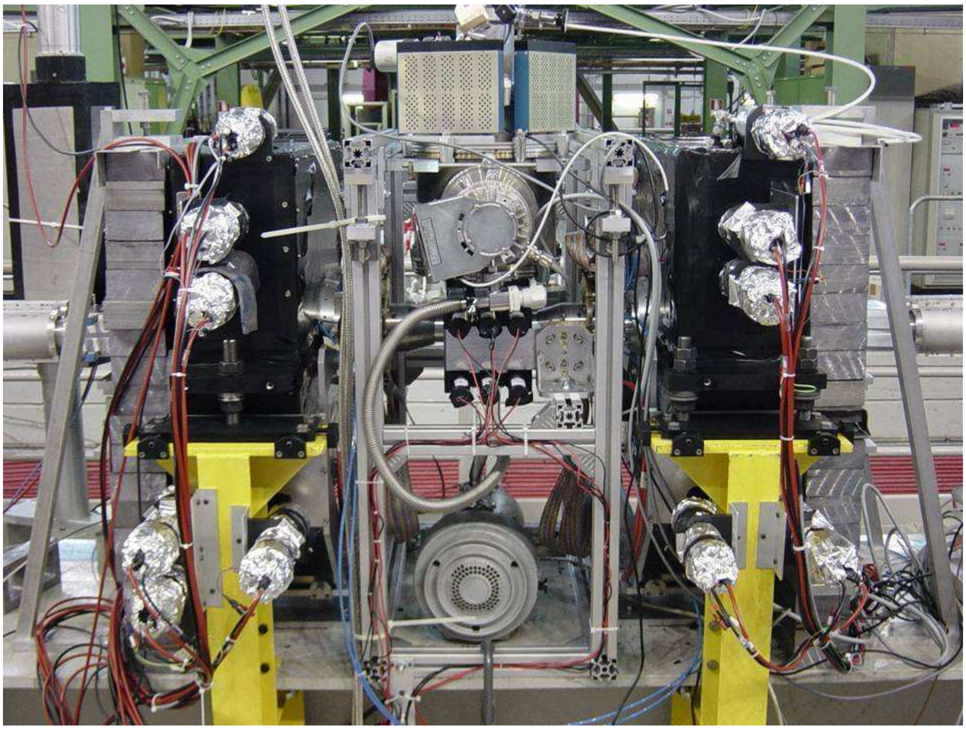

Figure 3: *DAY1 - SIDDHARTA setup mounted on DAΦNE*

4 Activities in 2008

The LNF group main activities in SIDDHARTA for 2008 are the following ones:

- data taking with DAY1 SIDDHARTA setup: optimization of performances (trigger, background, degrader);
- measurement of kaonic nitrogen (helium) with DAY1 setup;
- as soon as DAΦNE's performances, measured by DAY1, are the ones required for final setup installation (see Scientific Committee SIDDHARTA presentation of November 2007), install the final setup;
- measurement of kaonic hydrogen;
- measurement of kaonic deuterium;
- data analyses and Monte Carlo simulations.

5 Publications 2007

5.1 List of Conference Talks given by LNF Authors in Year 2007:

1. C. Curceanu (Petrascu), "Atoms/Nuclei measurements at DAΦNE: SIDDHARTA and AMADEUS experiments", talk at the Chiral Symmetry in Hadron and Nuclear Physics - CHIRAL07, 13 - 16 November, 2007, Osaka (Japan).
2. F. Sirghi, "Kaonic Atom measurements at DAFNE", talk at the Frascati Spring School "Bruno Touschek" in Nuclear and Subnuclear and Astroparticle Physics, May 14th-18th, 2007, Frascati (Italy).
3. C. Curceanu, "Kaonic atoms experimental studies at DAΦNE", talk at the 11th International Conference on Meson-Nucleon Physics and the Structure of the Nucleon (MENU07, 10-14 September 2007, Juelich (Germany).
4. C. Curceanu, "L'esperimento SIDDHARTA a DAFNE", talk at the XCIII Congresso Nazionale Societa' Italiana di Fisica, Pisa 24-29 Settembre 2007.

5.2 Papers and Proceedings

1. J. Zmeskal *et al.*, "Experimental studies on kaonic atoms at DAΦNE", Nucl. Phys. **A790** (2007) 663.
2. C. Curceanu *et al.*,"Precision measurements of kaonic atoms at DAFNE and future perspectives", Eur. Phys. J. **A31** (2007) 537.
3. M. Cargnelli *et al.*, "Kaonic hydrogen X-rays experiments at DAFNE", Canadian Journal of hysics **85** (2007) 479.
4. V. Lucherini *et al.*, "Hadronic atoms physics at DAFNE", Int. J. of Modern Phys. **A22** (2007) 221.
5. M. Cargnelli *et al.*, "Kaonic X-ray experiments at DAFNE using SIDDHARTA", Proceedings of KAON07 Conference, 21 - 25 May 2007, Frascati (Italy).

6. J. Marton *et al.*, “New precision measurements of the strong interaction in kaonic hydrogen”, Proceedings of the International Conference of Muon Catalyzed Fusion 2007, 18 - 21 June 2007, Dubna, Russia.

7. J. Marton *et al.*, “New precision measurements of the strong interaction in kaonic hydrogen”, Proceedings of the European Few Body 2007 Conference, 10 - 15 October 2007, Pisa (Italy).

8. J. Marton *et al.*, “Precision X-ray measurements on kaonic atoms at LNF”, Proceedings of the XLV International Winter meeting on Nuclear Physics, 14 - 21 January 2007, Bormio (Italy).

9. T. Ishiwatari *et al.*, “Silicon Drift Detectors for the kaonic atom X-ray measurements in the SIDDHARTA experiment”, Nucl. Instrum. Meth **A581** (2007) 326.

10. T. Ishiwatari *et al.*, “The SIDDHARTA experiment: Kaonic Hydrogen and Deuterium X-Ray Spectroscopy””, 9th International Workshop on Meson Production, Proceedings of XII International Conference on Hadron Spectroscopy - HADRON07, 8 - 13 October 2007, Frascati (Italy).

VIP

S. Bartalucci, S. Bertolucci, M. Catitti (Ass. Ric.), C. Curceanu Petrascu (Resp. Naz.), S. Di Matteo (Art. 23), C. Guaraldo, M. Iliescu (Art. 2222), F. Lucibello (Tecn.), D. Pietreanu (Bors. PD), D. Sirghi (Art. 2222), F. Sirghi (Bors. UE), L. Sperandio (Dott.), O. Vazquez Doce (Bors. PD)

1 The VIP scientific case and the experimental method

The Pauli exclusion principle (PEP), which plays a fundamental role in our understanding of many physical and chemical phenomena, from the periodic table of elements, to the electric conductivity in metals, to the degeneracy pressure (which makes white dwarfs and neutron stars stable), is a consequence of the spin-statistics connection. Although the principle has been spectacularly confirmed by the number and accuracy of its predictions, its foundation lies deep in the structure of quantum field theory and has defied all attempts to produce a simple proof. Given its basic standing in quantum theory, it seems appropriate to carry out precise tests of the PEP validity and, indeed, mainly in the last 15-20 years, several experiments have been performed to search for possible small violations. The indistinguishability and the symmetrization (or antisymmetrization) of the wave-function should be then checked independently for each particle, and accurate tests were and are being done.

The VIP (VIolation of the Pauli Exclusion Principle) experiment, an international Collaboration among 6 Institutions of 4 countries, has the goal to improve the limit on the probability of the violation of the PEP for electrons, (P $< 1.7 \times 10^{-26}$ established by E. Ramberg e G. A. Snow: *Experimental limit on a small violation of the Pauli principle*, Phys. Lett. **B 238** (1990) 438) by three-four orders of magnitude (P $< 10^{-39 \div -30}$), exploring a region where new theories might allow for a possible PEP violation.

The experimental method consists in the introduction of new electrons into a copper strip, by circulating a current, and in the search for X-rays resulting from the forbidden radiative transition that occurs if one of the new electrons is captured by a copper atom and cascades down to the 1s state already filled by two electrons with opposite spins. The energy of this transition would differ from the normal K_α transition by about 300 eV (7.729 keV instead of 8.040 keV) providing an unambiguous signal of the PEP violation. The measurement alternates periods without current in the copper strip, in order to evaluate the X-ray background in conditions where no PEP violating transitions are expected to occur, with periods in which current flows in the conductor, thus providing "fresh" electrons, which might possibly violate PEP. The rather straightforward analysis consists on the evaluation of the statistical significance of the normalized subtraction of the two spectra in the region of interest.

The experiment is being performed at the LNGS underground Laboratories, where the X-ray background, generated by cosmic rays and natural radioactivity, is reduced.

2 The VIP experimental setup

The VIP setup was built in 2005, starting from the DEAR setup, reutilizing the CCD (Charge Coupled Devices) X-ray detectors, and consists of a copper cylinder, 4.5 cm in radius, 50 μm thick, 8.8 cm high, surrounded by 16 equally spaced CCDs of type 55.

The CCDs are at a distance of 2.3 cm from the copper cylinder, grouped in units of two chips vertically positioned. The setup is enclosed in a vacuum chamber, and the CCDs are cooled to about 165 K by the use of a cryogenic system.

The DAQ alternates periods in which a 40 A current is circulated inside the copper target with periods without current, referred as background.

VIP was installed and is taking data at the LNGS Laboratory since Spring 2006.

3 Activities in 2007

During 2007 the VIP experiment was in continuous data taking, alternating periods of "signal" (I=40 A) with periods without signal (I=0 A). Data analyses were performed (energy calibration, sum of spectra, subtraction of background) and the probability of violation of PEP for electrons obtained (upper limit).

A new result, improving the previously published VIP result (S. Bartalucci *et al.*, "New experimental limit on the Pauli exclusion principle violation by electrons", Phys. Lett. B641 (2006) 18-22) by about an order of magnitude was obtained:

$$\frac{\beta^2}{2} < 6 \times 10^{-29} \qquad at \quad 99.7\% \quad CL. \tag{1}$$

We have thus improved the limit obtained by Ramberg and Snow by a factor about 300, representing the new world's best limit at present.

The new result was object of the Ph. D. Thesis of Laura Sperandio (presented in February 2008 at Tor Vergata University) and object of publicatons (see publications' list).

4 Activities in 2008

In 2008 the VIP setup will continue the data taking at LNGS, alternating periods of DAQ with current with periods of DAQ without current. Periodical energy calibrations, using an X-ray tube which activates foils of Ti and Zr placed inside the setup, will be performed.

The data analyses will go on in parallel with the DAQ.

The aim is to reach a limit on PEP violation by the end of 2008 in the limit of 10^{-29} - 10^{-30}.

In parallel, the feasibility of an upgrading of VIP by using new X-ray triggerable detectors (Silicon Drift Detectors) is being put forward and experimental tests are in progress.

5 Publications 2007

5.1 List of Conference Talks given by LNF Authors in Year 2007:

1. D. Sirghi, "The VIP experiment: New experimental limit on the Pauli exclusion principle violation by electrons", talk at the XII LNF Spring School in Nuclear, Subnuclear and Astroparticle Physics, INFN National Laboratories in Frascati, Italy, 14-18 of May, 2007.

2. D. Pietreanu, "Search for the Pauli Exckusion Principle violation for electrons: the VIP experiment"", at The Photons, Atoms and Qubits Conference 2007 (PAQ07), 2 - 5 October 2007, London (UK).

3. C. Curceanu, "High precision test of the Pauli Exclusion Principle using X-ray Spectroscopy", at the Vienna Symposium on the Foundation of Modern Physics, 7 - 10 July 2007, Vienna (Austria).

4. L. Sperandio, "The VIP experiment", talk at XCIII Congresso Nazionale SIF, Pisa, 24-29 September 2007.

5.2 Papers and Proceedings

1. S. Bartalucci *et al.*, “The VIP (Violation of the Pauli Exclusion Principle) experiment”, Int. Quantum, Inf. **5** (2007) 299.

2. E. Milotti *et al.*, “VIP: an experiment to search for a violation of the Pauli Exclusion Principle”, Int. J. of Modern Phys. **A22** (2007) 242.

3. S. Bartalucci *et al.*,“Experimental search for a violation of the Pauli Exclusion Principle for electrons”, AIP Conf. Proceedings **889** (2007) 390.

4. S. Bartalucci *et al.*, “New experimental limit on Pauli Exclusion Principle violation by electrons (VIP experiment)”, Journal of Phys., Conference Series **67** (2007) 012033.

5. J. Marton *et al.*, “A new high sensitivity test of the Pauili exclusion principle”, Proceedings of the 1st AFI Symposium, From Vacuum to the Universe, 19 - 20 October (2007), Innsbruck (Austria).

6. J. Marton *et al.*, “High Sensitivity Test of the Pauli Exclusion Principle using X-ray spectroscopy: VIP Experiment”, talk at IQOQI, 21 May 2007, Vienna (Austria).

4 – Theory and Phenomenology

FA51: Fisica Astroparticellare

D. Aristizabal Sierra (Bors.), E. Nardi (Resp.)

1 Description of the 2007 activity

During 2007 the main research activities of the IS FA51-LNF focused on the study of the mechanism of leptogenesis as a way to generate the observed Cosmic baryon asymmetry.

The effects of the lepton asymmetries generated in the decays of the heaviest seesaw neutrinos was investigated in ref. [1].

In ref. [2] we have computed the CP asymmetries in scattering processes, that represents a new source of CP asymmetry that must be added to the usual source from the heavy right handed neutrinos decays. All the corresponding effects have been included in the Boltzmann Equations and analyzed in great detail.

In ref. [3] we have investigated the possible effects on the leptogenesis mechanism of the presence of a new scale, possibly related to the breaking of a flavor symmetry. This scale is assumed to lie in-between the lepton number breaking scale and the electroweak scale. Interesting new effects have been found, among which the possibility of generating the baryon asymmetry through a lepton number conserving (but lepton flavor violating) CP asymmetry. Thus, the Cosmic baryon asymmetry could arise exclusively as a result of lepton flavor dynamics. In addition, we have also found that the presence of a flavor symmetry breaking scale allows to lower the leptogenesis scale down to a few TeV.

The proceedings of two review talks on leptogenesis [Moriond (March 2007) [4] and 6th-SILAFAE (November 2006) [5] also appeared in 2007.

An invited review article on leptogenesis, to be published in Physics Reports, has been prepared throughout the year 2007, and was submitted to the arXives in early 2008 [6].

Other issues, different from leptogenesis, have also been the object of research activities:

The generation of neutrino masses in leptoquarks models has been investigated in [7]. Special attention was put in identifying possible signatures of these models at the LHC.

A long lasting study of higher order contributions to the charged fermion mass operators, in models based on the GUT-flavor symmetry $SU(5) \times U(1)$, was carried out throughout 2007 and appeared in ref. [8]. Among various interesting results, it was found that in these models b-τ Yukawa unification is generally preserved, while for the two lighter families, the mass degeneracies for the leptons and quarks belonging to the same $SU(5)$ representation is always lifted, in agreement with observations.

In ref. [9] novel signals of Higgs decays in supersymmetric models without R-parity were analyzed, and it was suggested that in the context of these models the Higgs may be efficiently observed at the LHC through its decay -via two neutralinos- into final states containing missing energy and isolated charged leptons.

References

1. **"The importance of $\mathbf{N_2}$ leptogenesis"**
G. Engelhard, Y. Grossman, E. Nardi (INFN) and Y. Nir
Phys. Rev. Lett. **99**, 081802 (2007) [arXiv:hep-ph/0612187].

2. **"CP violation in scatterings, three body processes and the Boltzmann equations for leptogenesis"**
E. Nardi (INFN), J. Racker and E. Roulet
JHEP **0709**, 090 (2007) [arXiv:0707.0378 [hep-ph]].

3. **"Variations on leptogenesis"**
D. Aristizabal Sierra, M. Losada and E. Nardi (INFN)
Phys. Lett. B659, 328 (2008) [arXiv:0705.1489 [hep-ph]].

4. **"Leptogenesis"**
Sacha Davidson, Enrico Nardi (INFN) and Yosef Nir .
e-Print: arXiv:0802.2962 [hep-ph]. To be published in Physics Reports.

5. **"Recent Issues in Leptogenesis"**
E. Nardi (INFN)
arXiv:0706.0487 [hep-ph]
Proceedings of the 42nd Rencontres de Moriond on Electroweak interactions and Unified theories, La Thuile, Italy, 10-17 Mar 2007
[`http://events.lal.in2p3.fr/Moriond/Images/EW2007-Book.pdf`].

6. **"Topics in leptogenesis"**
E. Nardi (INFN)
AIP Conf. Proc. **917**, 82 (2007) [arXiv:hep-ph/0702033]
Also in *Puerto Vallarta, Particles and fields* 82-89
Proceedings of 12th Mexican School on Particles and Fields and 6th Latin American Symposium on High Energy Physics (VI- Silafae/XII-MSPF), Puerto Vallarta, Mexico, 1-8 Nov 2006.

7. **"Leptoquarks: Neutrino masses and accelerator phenomenology"**
D. Aristizabal Sierra (INFN), M. Hirsch and S. G. Kovalenko,
Phys. Rev. D77:055011, (2008) [arXiv:0710.5699 [hep-ph]].

8. **"Fermion mass hierarchy and non-hierarchical mass ratios in SU(5) x $\mathbf{U(1)_F}$"**
L. F. Duque, D. A. Gutierrez, E. Nardi (INFN) and J. Norena,
arXiv:0804.2865 [hep-ph].

9. **"Novel Higgs decay signals in R-parity violating models"**
D. Aristizabal Sierra (INFN), W. Porod, D. Restrepo and C. E. Yaguna,
arXiv:0804.1907 [hep-ph].

LF21: PHENOMENOLOGY OF ELEMENTARY PARTICLE INTERACTIONS AT COLLIDERS

A. Achilli (Laur.), D. Cocolicchio (Ass. PZ), V. Del Duca (Ass.),
G. Isidori (Resp. Loc.), O. Leitner (Bors. Stran.),F. Mescia (Art. 23),
M. Nicolaci (Dott.), S. Pacetti (Bors. Centro Fermi), G. Pancheri (Senior Ass., Resp. Naz.),
O. Shekhovtsova (Bors. Stran.)

1 Summary of the project

The research topics investigated by this project can be divided into the following areas:

- Flavour physics, precision tests and physics beyond the Standard Model (F. Mescia, G. Isidori, M. Nicolaci),
- Light flavour spectroscopy and τ-physics (O. Leitner)
- Hadronic Form Factors and meson spectroscopy (S. Pacetti)
- Hadronic cross-sections (A. Achilli, G. Pancheri and O. Shekhovtsova)
- QCD and the Higgs boson at the LHC (V. Del Duca)

The activity of the phenomenology group at Frascati can be seen in detail at the site

`http://www.lnf.infn.it/theory/pheno2.html`

In the following we shall briefly describe all the different projects undertaken by the above participants.

2 Flavour physics, precision tests, and physics beyond the Standard Model

One of the strategies to obtain additional clues about the nature of New Physics (NP) is by means of precision tests of the Standard Model (SM) at low energies. These are particularly interesting in: i) electroweak processes calculable with high precision, where even tiny deviations from the SM can be detected; ii) processes which are not mediated by tree-level SM amplitudes, where the relative effect of NP contributions can be enhanced. Up to now there is no clear evidence for deviations from the SM in both type of processes, and this leads to significant constraints in building realistic extensions of the SM. For instance, realistic models must possesses a highly non-generic flavour structure. These constraints are particularly severe for NP models with new degrees of freedom around the TeV scale, as required by a natural stabilisation the $SU(2)_L \times U(1)_Y \to U(1)_Q$ spontaneous symmetry breaking. The attempt to clarify this problem, both at the phenomenological level (with the help of precision data on rare decays) and at a more fundamental level (with the help of new symmetry principles), is one of the main activity of our group.

A closely related subject –which is also one of the primary research objectives of our group– is a better understanding of the SM itself, fixing his fundamental couplings (quark masses, CKM angles, non-perturbative condensates, . . .) by means of precise calculations within the framework of effective field theories and Lattice QCD.

Within this general scenario, last year we have performed a series of works on:

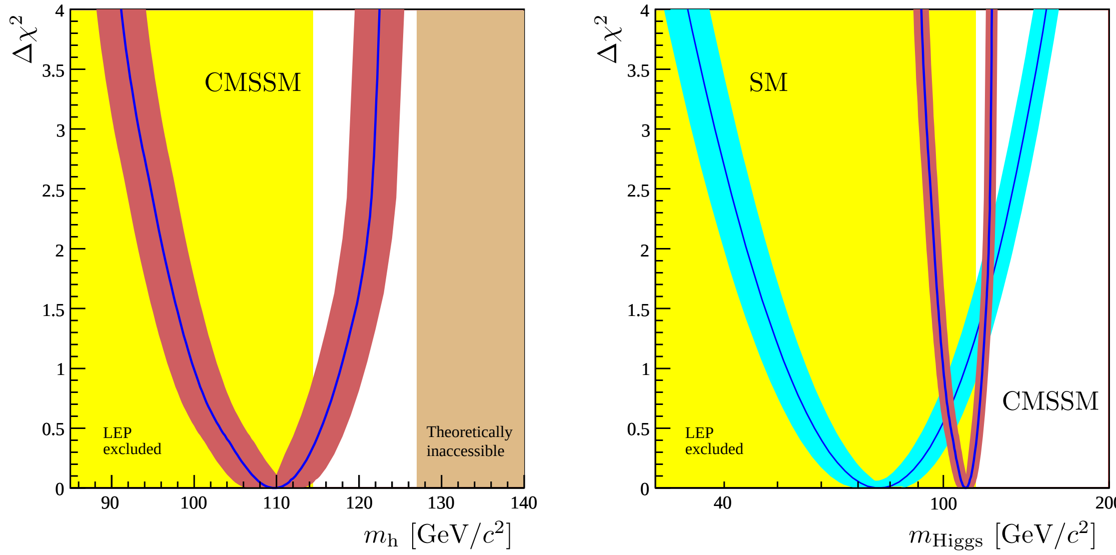

Figure 1: Left: Scan of the lightest Higgs boson mass versus $\Delta\chi^2 = \chi^2 - \chi^2_{\rm min}$. The curve is the result of a CMSSM fit using all of the available constraints, except the limit on $m_{\rm h}$. The red (dark gray) band represents the total theoretical uncertainty. Right: Scan of the Higgs boson mass versus $\Delta\chi^2$ for the SM (blue/light gray), as determined by the LEP Electroweak WG using all available electroweak constraints, and for comparison, with the CMSSM scan superimposed (red/dark gray). The blue band represents the total theoretical uncertainty.

Supersymmetry and Higgs-boson mass.

Motivated by recent progress in consistently and rigorously calculating electroweak precision observables and flavour related observables, we have performed a global analysis of the Constrained Minimal Supersymmetric Standard Model (CMSSM), taking into account electroweak precision data, flavour physics observables and the abundance of Cold Dark Matter. [1] The model is found to be consistent with data and the lightest Higgs boson mass in predicted to be $m_h^{\rm CMSSM} = 110^{+8}_{-10}({\rm exp.}) \pm 3({\rm theo.}){\rm GeV}/c^2$ (see Fig. 1).

Heavier values of the Higgs mass are found in a different version of the MSSM, namely the MFV-large $\tan\beta$ sscenario, which is also well motivated and consistent with present data. [2]

We have also refined and updated the metastability constraints on the Higgs boson mass which hold within the SM, [3] assuming a scale of new physics very high (around the Planck mass). Interestingly, we find that present best-fit ranges of the top and Higgs masses mostly lie in the narrow metastable region.

Leptogenesis in models with MFV.

Minimal Flavor Violation (MFV) is an attractive approach to solve the flavour problem assuming that the Yukawa couplings are the only irreducible sources of flavour symmetry breaking also beyond the SM. We have investigated the viability of leptogenesis in models respecting the MFV hypothesis in the lepton sector (i.e. models with three heavy right-handed neutrinos, where the charged-lepton and the neutrino Yukawa couplings are the only irreducible sources of lepton-flavour symmetry breaking). We have shown that in this framework a specific type of resonant leptogenesis can generate the observed matter-antimatter asymmetry. [4]

Kaon physics.

We have extended our previous studies of rare K decays and precision tests of the SM in the K system. [5, 6, 7, 8] Most notably, the matrix elements relevant to rare K decays have been related to those measured in K_{l3} using Chiral Perturbation Theory, beyond the lowest order. [5] As a result, the non-parametric errors for $B(K \to \pi\nu\bar{\nu})$ and for the direct CP-violating contributions to $B(K_L \to \pi^0\ell^+\ell^-)$ are now completely dominated by those on the short-distance physics. We have also derived analytical expressions for the electromagnetic correction factors relevant to the distortion of Dalitz-plot distributions of $K \to 3\pi$ decays. [8]

Lattice QCD.

We have explored different strategies to extract the D-meson semileptonic decay form factors from the Green functions computed in QCD numerically on the lattice. [9] We have found that strategies based on the use of double ratios of 3-point correlation functions, lead to an appreciable reduction of systematic uncertainties. This is an important step in reducing the overall uncertainty in the lattice QCD results for the D-decay form factors which are needed to determine the CKM entries $|V_{cd}|$ and $|V_{cs}|$.

3 Light flavour spectroscopy and τ-physics

This part of the project is aimed at analysing three open-questions, mainly inlight flavour physics: the search for T-observable, the prediction of τ-decay and the understanding of the quark structure in scalar mesons. Within the Standard Model framework, one has obtained promissing results as shortly described below:

Time Reversal effect

Calculations of the angular distributions, which represent real physical observables, as well as branching ratios of the process $\Lambda_b \to \Lambda V$ with $\Lambda \to P\pi$ and V into lepton lepton or V into hadron hadron have been performed by using the helicity formalism and stressing on the correlations which arise among the final decay products. A first computation of the asymmetry parameter, α_{As}, in Λ_b decays into Λ V has been performed as well as the longitudinal polarization of the vector meson, which is shown to be dominant [10].

Tau decay

In order to study the phenomenology of light flavor mesons below 1 GeV, one needs a framework which includes in a well defined manner the lowest nonets of pseudo scalar and vector mesons: the hidden local symmetry model, HLS. In our approach, we proposed to have a framework giving simultaneously an account of the partial decay width of light meson decays of the pion form factor in e+e- data and in tau decay. In our approach, we made a prediction of the tau decay 2 pion spectrum which can be compared with the existing measurements.

Scalar mesons

A phenomenological analysis of the scalar meson $f_0(980)$ was performed, which makes use of experimental D branching ratios. With a relativistic quark model formalism, in which the transition form factors are calculated for time like momenta, and electroweak D decay amplitudes calculated in QCD factorization, one can extract informations on the structure of the meson $f_0(980)$ in terms of the quark-antiquark pairs as well as on the mixing angle theta between strange and non strange components. The electroweak transition form factors are computed using triangle diagrams within the constituent quark model in CLFD [11, 12, 13].

4 Hadronic form factors - S. Pacetti

Two-photon contribution in $e^+e^- \to p\overline{p}$ [14)]

The two-photon exchange contribution in the space-like process $e^-p \to e^-p$ appears as one of the best candidates to explain the observed discrepancy in the data on the ratio G_E^p/G_M^p achieved by means of the Rosenbluth formula (SLAC) and those obtained using the recoil polarization technique (Jefferson Lab). Such a two-photon contribution should be equally important in the time-like process $e^+e^- \to p\overline{p}$. Moreover, in that case, the main one-photon and the further two-photon contribution have opposite C parity, hence the latter should manifest itself in a asymmetry "forward-backward" in the $\cos\theta$ angular distribution (θ is the proton scattering angle in the center of mass frame).

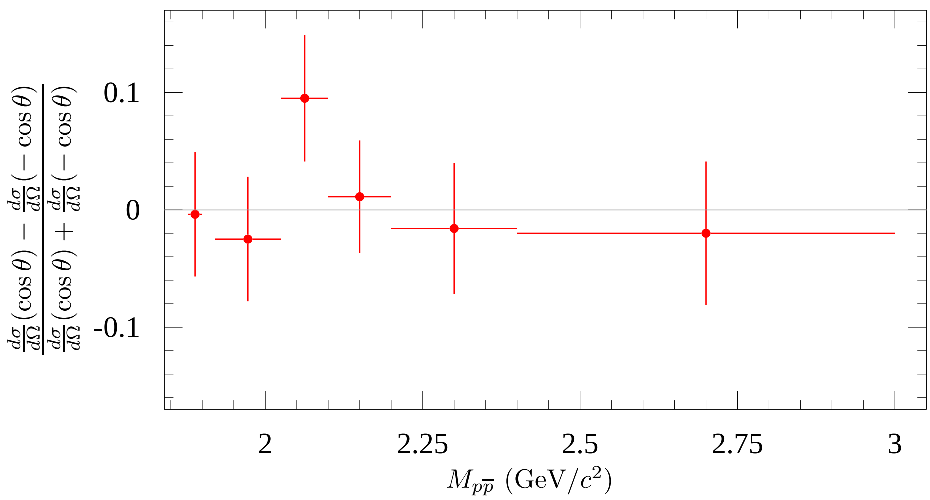

Figure 2: "Forward-backward" asymmetry as a function of the center of mass energy in $e^+e^- \to p\overline{p}$.

Exploiting the *BABAR* data on $e^+e^- \to p\overline{p}$, obtained with the initial state radiation technique, we have estimated this asymmetry in six energy bins, from the threshold $2M_P$ up to about 2.8 GeV/c^2 (fig. 2). The obtained mean value is compatible with zero at a 2% level. In light of this result we may conclude that the *BABAR* data do not give any relevant information on the two-photon exchange contribution.

Unexpected threshold behavior in baryon-antibaryon cross sections [15)]

Recent *BABAR* data on baryon-antibaryon cross sections show an unexpected threshold behavior. In particular the cross sections for $e^+e^- \to p\overline{p}$, $\Lambda\overline{\Lambda}$ (see fig. 3), $\Sigma^0\overline{\Sigma^0}$, and $\Lambda\overline{\Sigma^0}$ have monotonically decreasing behaviors starting from the threshold, where they take non vanishing values, up to about 4 GeV. Generally the baryon-antibaryon cross section should be zero at threshold due to the vanishing of the phase space. In the $p\overline{p}$ case the phase space vanishing is cancelled by the Coulomb correction. Moreover, using such a correction we get a unitary normalization for the common proton form factor at the production threshold. The same argument can not be used in the case of neutral baryons. We propose a simple method to extend the application of the Coulomb correction at the parton-level, hence also to the neutral baryons. In such a way, we obtain also for the Λ form factors the unitary normalization at threshold, while the other baryon form factors obey some U-spin symmetry relations.

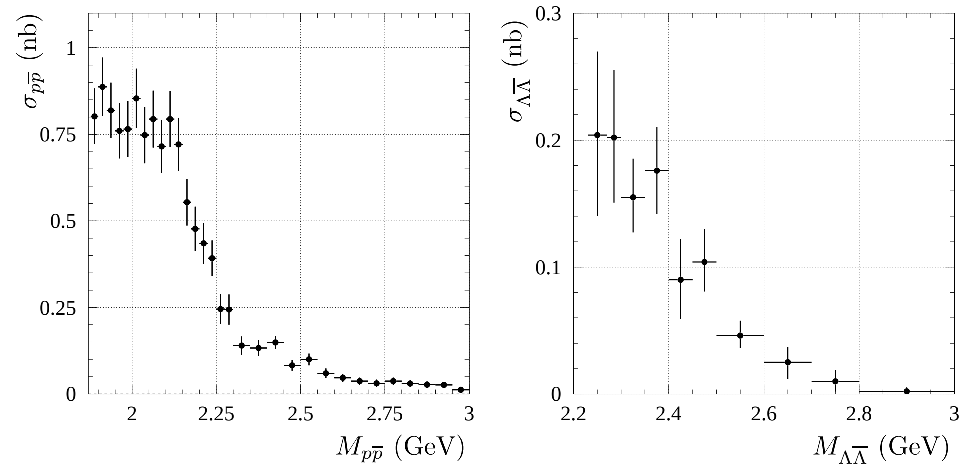

Figure 3: The $p\overline{p}$ (left) and $\Lambda\overline{\Lambda}$ (right) cross sections measured by the *BABAR* Collaboration.

Study of the reaction $e^+e^- \to KK\pi$ [16]

In the *BABAR* Collaboration, using the initial state radiation technique, we have analyzed the processes $e^+e^- \to K_S K^\pm \pi^\mp$ and $e^+e^- \to K^\pm K^\mp \pi^0$, that contribute to the most general reaction $e^+e^- \to KK^*(890)$. The $KK^*(890)$ transition form factor is just the object of our study. The analysis of the high-statistics $K_S K^\pm \pi^\mp$ Dalitz plot allows, for the first time, the extraction of the isoscalar and isovector components of the transition form factor, as well as of their relative phase. The two isospin components have been fit with isoscalar and isovector resonances separately, the same structures have been used to describe also the $K^\pm K^\mp \pi^0$ and $\phi\eta$ cross sections.

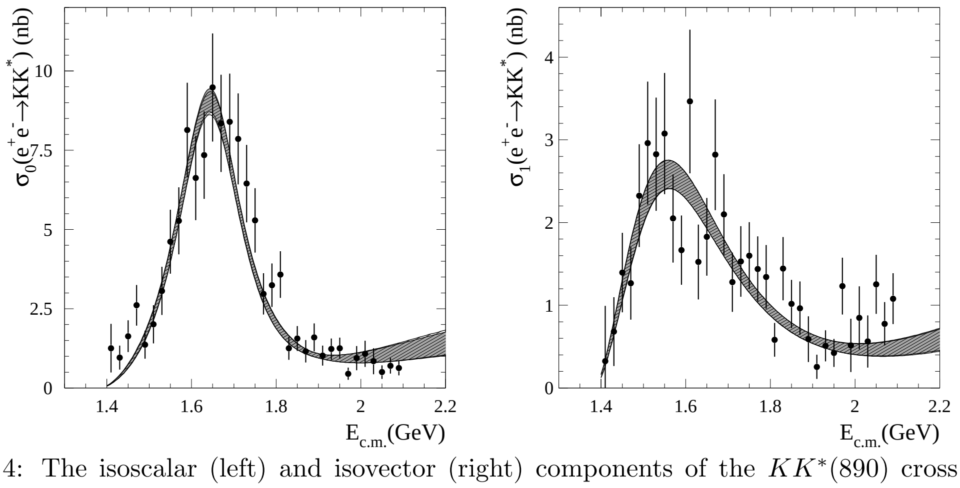

Figure 4: The isoscalar (left) and isovector (right) components of the $KK^*(890)$ cross section measured by the *BABAR* Collaboration with fit (gray band) superimposed.

Finally, we study the OZI-suppressed process $e^+e^- \to \phi\pi^0$. This is a pure isospin-one final state, hence we describe the cross section and corresponding transition form factor with only ρ-like recurrences. We found that the main contribution is due to a broad $\rho(1450)$, but there is also a narrower signal, around 1.9 GeV/c^2. This structure has properties compatible with the "dip" already observed, in multi-pionic final states, from different experiments: DM2 at Orsay, E687 at Fermilab, and also *BABAR*.

5 Hadronic cross-sections

Hadronic cross-sections were studied in two different type of processes and different energy ranges, namely at DAΦNE, and at high energy colliders in reactions of the type $A + B \to X$ where A, B could be a proton or an antiproton or a photon, with emphasis on the role played by soft gluons on the saturation of the Froissart bound

Future prospects at DAΦNE

The process $e^+e^- \to e^+e^-\gamma\gamma$ has been studied in the context of the proposed upgrade of DAΦNE, both in energy and luminosity [17]. The possibility that KLOE, in the low energy DAΦNE run, has the concrete opportunity to find (or disprove) a resonant σ in the cleanest possible channel has been shown. Other interesting physics processes to explore have been the transition form factors of the low lying pseudoscalar mesons: in this context, the interest of this measurement with regard to the theoretical determination of the light-by-light contribution to the hadronic contribution to $g-2$ of the muon has been discussed.

Final State Radiation effects at DAPHNE

Final state radiation in the process e+e- into two charged pions is being studied as a possibility to test a pion-photon interaction model near two-pion threshold. A Monte Carlo event generator FEVA that simulates the process $e^+e^- \to \pi^+\pi^-\gamma$ and $e^+e^- \to \pi^0\pi^0\gamma$ for the DAΦNE accelerator setup has been developed. The applied formalism is quite general and consistent with all symmetries of the strong and EM interactions [18, 19, 20].

The study of the reactions of electron-positron annihilation into a final state consisting of two pseudoscalar mesons and a photon, allows one to have information on the hadron–photon interaction in the low-energy region. These reactions allow also to test the properties of the scalar mesons $a_0(980)$ $(I^G(J^{PC}) = 1^-(0^{++}))$ and $f_0(980)$, $f_0(600) \equiv \sigma$ $(I^G(J^{PC}) = 0^+(0^{++}))$. Most studies deal with charged pions production, i.e. the reaction $e^+e^- \to \pi^+\pi^-\gamma$. From threshold upto a given collider beam energy, this type of the reactions is explored at the Φ-factory in Frascati ($s = 4E^2 = m_\phi^2$),the B-factory PEP-2 at SLAC ($s = m^2_{\Upsilon(4s)}$), and KEKB at KEK ($s = m^2_{\Upsilon(4s)}$) using the method of radiative return,Originally, the radiative return method was proposed in order to acess c.m. energy lower than the e^+e^- c.m. energy, and thus allow scanning the hadronic cross section ($\sigma(e^+e^- \to \pi^+\pi^-)$) even at machines operating at a fixed c.m. energy, namely at a resonance peak. The method would measure the cross section of the process $e^+e^- \to \pi^+\pi^- + \gamma$, where the photon is emitted from the initial state (the (ISR) process), i.e. by the electron or positron. The method thus is essentially based on the assumption on the dominance of the initial photon radiation from the electron or positron and allows one to study the pion electromagnetic form factor $F_\pi^{em}(p^2)$ at the reduced energy $p^2 < s$. In the case of the neutral final states ($\pi^0\pi^0\gamma$) despite the smaller size of the cross section, in comparison with the charged case, the process may give a cleaner information on the models describing pion-photon interaction.

We have written the Monte Carlo event generator FEVA that simulates the process $e^+e^- \to \pi^+\pi^-\gamma$ and $e^+e^- \to \pi^0\pi^0\gamma$ for the DAΦNE accelerator setup. The applied formalism is applicable at values of the CM energy $\sqrt{s}$ not only at the ϕ-resonance but in a wider region of energies from the threshold upto $s = m_\phi^2$. The previous version of FEVA was described in [18], where the Bremsstrahlung process (both in the framework of Resonance Perturbation Theory and scalarQED) and the ϕ direct decay (only f_0 parameterization) were considered. The current version of FEVA [20] includes in addition the double resonance contribution and a more sophisticated parameterization for the ϕ direct decay. Also the channel $e^+e^- \to \pi^0\pi^0\gamma$ has been added.

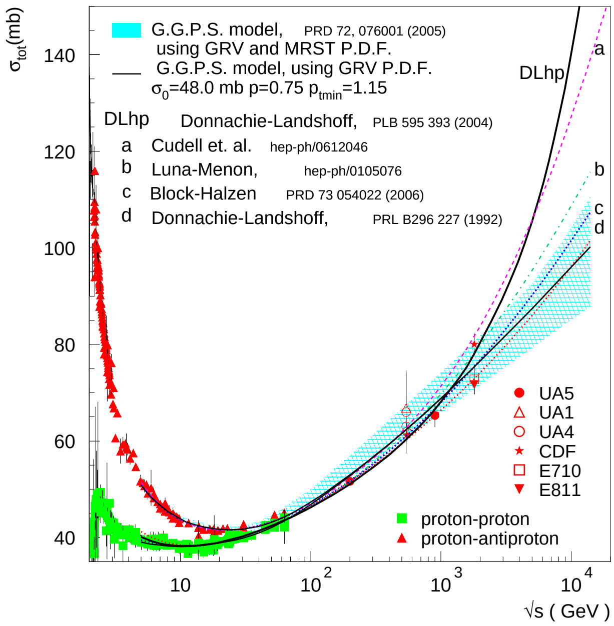

Figure 5: The Bloch-Nordsieck model results for pp and $p\bar{p}$ total cross-sections are compared with data and other model predictions.

Total cross-sections and the Froissart bound

A model for total cross-sections based on the complementarity between QCD mini-jets contributions and soft gluon resummation has been applied to study minimum bias effects in high energy hadronic collisions. Among these processes, we have studied in particular the energy behaviour of total cross-sections and Survival Probability of Large Rapidity Gaps. The calculation of the total cross-section proceeds through an eikonal formulalism where QCD mini-jets drive the rise at high energy and soft gluon emission from the initial state dampens it. This model, labelled after Bloch-Nordsieck (BN) resummation type effects in QCD, puts central emphasis on the infrared behaviour of the strong coupling constant for which the following ansätz has been formulated:

$$\alpha_s(Q^2) \rightarrow \frac{1}{Q^{2p}} \qquad as \quad Q^2 \rightarrow 0 \tag{1}$$

with $1/2 < p < 1$ for convergence of the infrared integral and analyticity requirements. It has been seen that the results of such a model allow for an asymptotic behaviour of proton-proton and proton-antiproton total cross-section in compliance with saturation of the Froissart bound [21]. These results are shown in Fig.5, where our model has been compared to present data and other results in the literature. In particular we notice that our model does not agree with all those with an explicit hard Pomeron exchange. The model can also be applied to photon processes and some results have been presented at Photon 2007 Workshop in Paris, in july 2007. Our conclusion, for the time being, is that this Eikinal mini-jet Model with Bloch-Nordsieck resummation describes photon-photon LEP scattering data better than other models based on factorization. More work to assess these findings is under progress.

6 QCD and the Higgs boson at the LHC-V. Del Duca

This project is focused on Higgs studies and the strong interactions in the Standard Model (SM). Its research goals are:

i) to evaluate accurately signals and backgrounds for Higgs boson production at the LHC;

ii) to develop advanced techniques to improve the precision of the calculation of scattering cross sections at high momentum transfer Q^2.

Higgs Boson Production in Hadronic Collisions

At the LHC, the Higgs boson will be produced mostly via gluon fusion, with the Higgs boson interacting with the gluons via a top-quark loop. This production mode is known at next-to-leading-order (NLO) accuracy in the strong coupling constant α_S for finite values of the top-quark mass m_t, and at next-to-next-to-leading-order (NNLO) accuracy in the limit $m_t \to \infty$. The latter, though, generates spurious logarithms $\ln(\hat{s}/m_H^2)$, which are not present when the full m_t dependence is taken into account. Higgs production via gluon fusion has been considered for finite values of m_t in the limit of high parton centre-of-mass energy $\hat{s}$ [22], which allows us to improve upon the NNLO calculation mentioned above.

The second largest Higgs production mode is via vector boson fusion (VBF). Besides providing a clean discovery channel, this allows for the study of the coupling of the Higgs boson to the electro-weak gauge sector. To enhance Higgs production via VBF over the one via gluon fusion, it is convenient to produce the Higgs boson in association with two jets far apart in rapidity. In a realistic simulation, the final-state partons shower and hadronise. Thus more than two jets usually appear in the final state. Such a final state has been considered through a matrix-element Monte Carlo generator in Ref. [23].

Higher-Order Corrections to Scattering Cross Sections at high Q^2

In the quest to discover New Physics signals, typically covered by the huge SM backgrounds, the precise experimental measurements at the Tevatron and at the LHC require theoretical calculations which are at least as precise. In some instances, like in the inclusive production of the Higgs boson via gluon fusion mentioned above, the desired accuracy is achieved only at NNLO in α_S. Thus, a general algorithm to compute jet cross sections at NNLO is being implemented.

7 List of Conference Talks by LF21 Participants in Year 2007

1. V. Del Duca, Higgs the missing link of the Standard Model, Workshop "Physics for Large and Small Scale", Nha Trang, Vietnam, 2007.

2. V. Del Duca, Higgs production in association with jets at the LHC, 3^{rd} Hera and LHC Workshop, DESY, Hamburg, Germany, 2007.

3. V. Del Duca, Higgs production in association with jets at the LHC, XLII Rencontres de Moriond, La Thuile, Italy 2007.

4. G. Isidori, Flavour Physics: Now and in the LHC era, 23rd International Symposium on Lepton-Photon Interactions (LP07), Daegu, Korea, 13-18 Aug 2007.

5. G. Isidori, Large tan(beta) effects in flavour physics, 15th International Conference on Supersymmetry (SUSY2007), Karlsruhe, Germany, July 26 - August 1, 2007.

6. G. Isidori, Conference summary, Kaon International Conference (KAON'07), Frascati, Italy, 21-25 May 2007.
7. G. Isidori, Supersymmetric effects in favour physics, Supersymmetry at LHC: Theoretical and Experimental Perspectives, Cairo, Egypt, 11-14 March 2007.
8. G. Isidori, Rare Kaon decays within and beyond the SM, 6th KEK Topical Conference: Frontiers in Particle Physics, KEK, Japan, 6-8 Fb 2007.
9. G. Pancheri, LHC Predictions for total cross-sections from the eikonal mini-jet model and the Froissart Bound, XLII Rencontres de Moriond, La Thuile, Italy, 17-24 March 2007.
10. G. Pancheri, QCD predictions for total cross-sections and the Froissart bound, IX Workshop on Perturbative QCD, Paris, France, June 4-8, 2007.
11. G. Pancheri, Minijets, soft gluon resummation and photon cross-sections, Photon 2007, Paris, France, 9-13 July 2007.
12. G. Pancheri, Large rapidity gaps survival probabilities LHC, International Symposium on Multiple Dynamics (ISMD07), Berkeley, California, 4-9 August 2007.
13. G. Pancheri, QCD Contributions to the Froissart bound for the total cross-section, Hadron Structure (HS07), Modra-Harmonia, Slovak Republik, september 3-9 2007.
14. G. Pancheri, Total cross-sections and rapidity gaps survival probability at LHC, XII Conference on Hadron Spectroscopy, Frascati, 4-10 september 2007
15. G. Pancheri, QCD issues in photon-photon total cross-section : why we need a photon collider, International Workshop on Laser-Electron Interactions, Hiroshima, Japan, 10-14 december 2007
16. S. Pacetti, Unmasking the Proton Form Factors, Panda experiment Workshop, March 8-9, 2007, Orsay, France.
17. S. Pacetti, Nucleon time-like form factors: overview of the experimental data and possible analysis methods, Hard QCD with Antiproton at GSI-FAIR, July 16-20, 2007, Trento, Italy.
18. S. Pacetti, Extraction of Baryon Form Factors from Initial State Radiation Processes at *BABAR*, International Conference on Meson-Nucleon Physics and the Structure of the Nucleon, September 10-14, 2007, Juelich, Germany.
19. S. Pacetti, Baryon form factors from initial state radiation processes and some phenomenological considerations, Nucleon Structure af FAIR, 15-16 October, 2007, Ferrara, Italy.
20. S. Pacetti, Charmed Particles Production in $e^+e^- \to c\bar{c}$ at 10.6 GeV, Workshop on parton fragmentation processes in the vacuum and in the medium, February 25-29, 2008, ECT* Trento, Italy.
21. S. Pacetti, Initial state radiation at *BABAR*, Workshop on parton fragmentation processes in the vacuum and in the medium, February 25-29, 2008, ECT* Trento, Italy.
22. S. Pacetti, Mesoni leggeri e fattori di forma del nucleone a *BABAR*, Mini-Workshop sulle prospettive di fisica adronica al Jefferson Lab e in altri laboratori, February 27-28, 2008, Genova, Italy.

8 Publications of the year 2007

References

1. O. Buchmueller *et al.*, *Prediction for the Lightest Higgs Boson Mass in the CMSSM using Indirect Experimental Constraints,* Phys. Lett. B **657** (2007) 87 [arXiv:0707.3447 [hep-ph]].

2. G. Isidori, F. Mescia, P. Paradisi and D. Temes, *Flavour physics at large* $\tan\beta$ *with a Bino-like LSP,* Phys. Rev. D **75** (2007) 115019 [arXiv:hep-ph/0703035].

3. G. Isidori, V. S. Rychkov, A. Strumia and N. Tetradis, *Gravitational corrections to Standard Model vacuum decay,* Phys. Rev. D **77** (2008) 025034 [arXiv:0712.0242 [hep-ph]].

4. V. Cirigliano, A. De Simone, G. Isidori, I. Masina and A. Riotto, *Quantum Resonant Leptogenesis and Minimal Lepton Flavour Violation,* JCAP **0801** (2008) 004 [arXiv:0711.0778 [hep-ph]].

5. F. Mescia and C. Smith, *Improved estimates of rare K decay matrix-elements from* K_{l3} *decays,* Phys. Rev. D **76** (2007) 034017 [arXiv:0705.2025 [hep-ph]].

6. F. Mescia, *Precision tests with Kl3 and Kl2 decays,* arXiv:0710.5620 [hep-ph].

7. G. Isidori, *Soft-photon corrections in multi-body meson decays,* Eur. Phys. J. C **53** (2008) 567 [arXiv:0709.2439 [hep-ph]].

8. G. Isidori, *KAON 2007: Conference Summary,* arXiv:0709.2438 [hep-ph].

9. D. Becirevic, B. Haas and F. Mescia, *Semileptonic D-decays and Lattice QCD,* PoS(LATTICE 2007)355. arXiv:0710.1741 [hep-lat].

10. O. Leitner, B. Loiseau, B. El-Bennich, J.P. Dedonder, *Form factors in B to f0(980) and D to f0(980) transitions from dispersion relations*, Int. J. Mod. Phys. **A22**, 641, 2007.

11. O. Leitner, B. Loiseau, B. El-Bennich, J.P. Dedonder, *Scalar meson properties from D-meson decays*, Nucl. Phys. **A790**, 510, (2007).

12. O. Leitner, B. Loiseau, B. El-Bennich, J.P. Dedonder, *Resonances and weak interactions in* $D^+ \to \pi^+\pi^-\pi^+$ *decays*, Int. J. Mod. Phys. **E16**, 2876, 2007.

13. O. Leitner, B. Loiseau, B. El-Bennich, J.P. Dedonder, *Pseudoscalar-scalar transition form-factors in covariant light front dynamics*, World Scientific, vol II, 984, 2007.

14. E. Tomasi-Gustafsson, E. A. Kuraev, S. Bakmaev and S. Pacetti, Phys. Lett. B **659**, 197 (2008) [arXiv:0710.0454 [hep-ph]].

15. R. Baldini, S. Pacetti and A. Zallo, arXiv:0711.1725 [hep-ph].

16. B. Aubert *et al.* [BaBar Collaboration], arXiv:0710.4451 [hep-ex] to be published in Phys. Rev. D.

17. F. Ambrosino *et al.*, *Prospects for* e^+e^- *physics at Frascati between the* ϕ *and the* Ψ, Eur.Phys.J. **C50**, 729.

18. G. Pancheri, O. Shekhovtsova, G. Venanzoni, *Tests of the final-state radiation model at DAPHNE near* $\pi^+ pi^-$ *threshold*, Eur.Phys.J. **A31**, 458 (2007).

19. G. Pancheri, O. Shekhovtsova, *A problem of final state radiation in the process* $e^+e^- \to \pi^+\pi^-\gamma$ *near the threshold* G. Venanzoni, Acta Pol. Phys. **38** (2007) 2999.

20. G. Pancheri, O. Shekhovtsova, G. Venanzoni, *Final state radiation and a possibility to test a pion-photon interaction model near two-pion threshold*, JETP **133** (2008) 544, [arXiv: 0706.3027].

21. A. Achilli, R.M. Godbole, I. Grau, G. Pancheri and Y.N. Srivastava, *LHC predictions for total cross-sections from the eikonal mini-jet model and the Froissart bound*, 2007 QCD and High Energy Hadronic Interactions, Proc. XLII Rencontres de Moriond, (eds. E. Auge', B. Pietrzyk and J. Tran Than Van, La Thuile, March 2007), pag. 321 (World Scientific, Singapore, 2008).

22. S. Marzani, R. D. Ball, V. Del Duca, S. Forte and A. Vicini, *Higgs production via gluon-gluon fusion with finite top mass beyond next-to-leading order*, arXiv:0801.2544 [hep-ph].

23. V. Del Duca, '*Monte Carlo studies of jet activities in Higgs production in association with 2 jets at the LHC*, Proc. 42nd Rencontres de Moriond, La Thuile 2007.

INIZIATIVA SPECIFICA LF61:
Low-dimensional systems and spin-Hall effect

S. Bellucci (Resp. Naz.), M. Cini (Ass.), F. Corrente (Dott.), G. Iovane (Ass.),
P. Onorato (Borsista PD), E. Perfetto (Borsista PD), N. Pugno (Ass.), R. Raimondi (Ass)

1 External collaborating Institutions:

Univ. Roma La Sapienza, Univ. Roma Tor Vergata, IHEP-Protvino (Russia), Univ. Pune, India, Burnham Institute (La Jolla, CA, USA), ILL (Grenoble, France).

2 Research Activity

Our research activity has pursued the objective to study the characteristic behavior of Luttinger Liquids and, in particular how this becomes influenced from the dimensions and the doping in the Carbon Nanotubes (CNs). An important contribution to the research in the field of transport in CNs has been related to the most general Crossover between the regime of the Luttinger Liquid and the regime of Coulomb Blockade (CB) that characterizes the system to low temperature. Such a study, based on the microscopical structure of nanotubes, has been further developed also in relation to the effects of the magnetic field on the CNs of large radii. In this field we have begun to further develop our analysis in the perspective to inquire the possible presence of a Quantum Hall Regime in the CN with multiple walls. For what concerns Superconductivity in CNs, recently the case of the ultrasmall nanotubes was analyzed, discussing if the superconductive behavior can be attributed to a purely electronic effect, that is not assisted by phonons. In this sense, two different approaches have been put to comparison, one connected to the Luttinger Liquid, the other, that emphasizes the role of the lattice and the short-range terms of the interaction, developed starting from the Hubbard model. Subsequently the model has been generalized with the scope to explain the superconductive behavior of Multi Walled CNs, in order to construct a quite general theory, suitable to explain the occurring of Superconductivity in the Nanotubes under opportune conditions. The extension of this study with the aim of supplying a unique interpretation of all the phenomenology that regards the superconductivity in CNs is in progress, as a further objective of the research.

3 List of Conference Talks by LNF Authors in Year 2006

1. P. Onorato, Per qualche “senso” in piu’... esempi di impiego di sensori nell’ambito del Progetto Lauree Scientifiche, Convegno SIF Pisa, Italy 24-25.9.2007.
2. F. Corrente, Polarizzazione delle correnti di spin in nanostrutture a bassa dimensionalita’. Pubbicato su: Spin currents polarization in low-dimensional nanojunctions Il Nuovo Cimento DOI 10.1393/ncb/i2007-10404-9, Convegno SIF Pisa, Italy 24-25.9.2007.

References

1. Spin hall accumulation in ballistic nanojunctions, S. Bellucci and P. Onorato EUROPEAN PHYSICAL JOURNAL B Volume: 59 Issue: 1 Pages: 35-40 Published: SEP 2007

2. Quantum Hall effect in carbon nanotubes and curved graphene strips Perfetto, E., Gonzalez, J., Guinea, F., Bellucci, S., Onorato, P. PHYSICAL REVIEW B Volume: 76 Issue: 12 Article Number: 125430 Published: SEP 2007

3. Size dependent superconductivity in small-diameter carbon nanotubes S. Bellucci, M. Cini, P. Onorato, E. Perfetto PHYSICA C-SUPERCONDUCTIVITY AND ITS APPLICATIONS Volume: 460 Pages: 1057-1058 Part: Part 2 Published: SEP 1 2007

4. Josephson currents in correlated nanoscopic models S. Bellucci, M. Cini, P. Onorato, E. Perfetto PHYSICA C-SUPERCONDUCTIVITY AND ITS APPLICATIONS Volume: 460 Pages: 1313-1314 Part: Part 2 Published: SEP 1 2007

5. The influence of dimensionality on superconductivity in carbon nanotubes S. Bellucci, M. Cini, P. Onorato, E. Perfetto JOURNAL OF PHYSICS-CONDENSED MATTER Volume: 19 Issue: 39 Article Number: 395016 Published: OCT 3 2007

6. Magnetic field effects in carbon nanotubes S. Bellucci, J. Gonzalez, J. Guinea, P. Onorato, E. Perfetto JOURNAL OF PHYSICS-CONDENSED MATTER Volume: 19 Issue: 39 Article Number: 395017 Published: OCT 3 2007

7. Spin separation in a T ballistic nanojunction due to lateral-confinement-induced spin-orbit coupling, S. Bellucci, F. Carillo and P. Onorato JOURNAL OF PHYSICS-CONDENSED MATTER Volume: 19 Issue: 39 Article Number: 395018 Published: OCT 3 2007

8. Spin Hall effect and spin filtering in ballistic nanojunctions S. Bellucci, F. Corrente and P. Onorato JOURNAL OF PHYSICS-CONDENSED MATTER Volume: 19 Issue: 39 Article Number: 395019 Published: OCT 3 2007

9. Filtering of spin currents based on a ballistic ring S. Bellucci and P. Onorato JOURNAL OF PHYSICS-CONDENSED MATTER Volume: 19 Issue: 39 Article Number: 395020 Published: OCT 3 2007

10. Spin Hall effect and spin-orbit coupling in ballistic nanojunctions S. Bellucci and P. Onorato PHYSICAL REVIEW B Volume: 75 Issue: 23 Article Number: 235326 Published: JUN 2007

INIZIATIVA SPECIFICA MI12

S. Bellucci (Resp.), S. Ferrara (Ass.), E. Latini (Dott.), S. Krivonos (osp.),
A. Marrani (bors. PD), V. Ohanyan (osp.), A. Shcherbakov (dott.),
C. Sochichiu (bors. PD), A. Sutulin (osp.), A. Yeranyan (bors. PD)

1 Research Activity

Supersymmetric field theories, supergravity, attractor mechanism, black holes, superstrings and M-theory.

We investigated the properties of black hole attractors in supergravity theories. We continued the study of supersymmetric mechanics models. We studied dilatations in N=4 SYM theories. We also investigated higher spin theories.

Active collaborations include: JINR-Dubna, Russia Tomsk Univ. Russia Univ. Hannover, Germany Turin Polytechnic, Italy CERN, Switzerland Annecy, LAPTH, France Valencia U., Spain

We also organized so far three Schools with the participation of fair amount of collaborators, both as lecturers and as students: 1) Winter School on Supersymmetric Mechanics Frascati (Italy), 7 - 12 March 2005; 2) Winter School on Attractor Mechanism Frascati (Italy), 20 - 24 March 2006; 3) School on Attractor Mechanism SAM2007, 18 - 22 June 2007- INFN-Laboratori Nazionali di Frascati, Via E. Fermi 40, Frascati, Italy http://www.lnf.infn.it/conference/sam2007

We published the Proceedings of the first School as Lecture Notes in Physics, Springer-Verlag Berlin Heidelberg 2006, two volumes, edited by S. Bellucci: as Lecture Notes in Physics Vol. 698, Supersymmetric Mechanics - Vol. 1: Supersymmetry, Noncommutativity and Matrix Models (ISBN: 3-540-33313-4), and Lecture Notes in Physics Vol. 701, Supersymmetric Mechanics - Vol. 2: The Attractor Mechanism and Space Time Singularities (ISBN: 3-540-34156-0). The third volume containing the lecture notes of the School SAM2006, will appear soon with the title: Supersymmetric Mechanics - Vol. 3: Attractors and Black Holes in Supersymmetric Gravity.

We participate as a main node to the Project MRTN-CT-2004-005104 Constituents, Fundamental Forces and Symmetries of the Universe (Short title: ForcesUniverse), a Marie Curie Research Training Network supported by the European Community's Sixth Framework Programme. The network contract was started on 1st November 2004 with duration of 48 months.

Within this network a Workshop was organized at IFIC Valencia , Spain, 1-5 October 2007, with S. Ferrara 's invited talk on black hole attractors.

Another important and related event has been String phenomenology in Frascati 4-8 June 2007, with invited talks by S. Ferrara and S. Bellucci on N¿2 attractors and N=2 attractors respectively.

We coordinate an INTAS project "Extended supersymmetry, strings and noncommutativity in field theory", involving a consortium of 12 international Institutions, with duration of 30 months starting Nov. 2006, until October 2009.

2 List of Conference Talks by LNF Authors in Year 2006

1. S. Ferrara, Extremal black-holes and attractors in D=4 and D=5 supergravity, School on Attractor Mechanism SAM 2007, 18 - 22 June 2007, Frascati (Roma) Italy
2. S. Ferrara, Black attractors, IFIC Valencia, Spain, 01/10 - 05/10 2007.

3. S. Bellucci, N=2 Attractors, String Phenomenology, Frascati, Italy, 04/06 - 08/06 2007.
4. S. Ferrara, N>2 Attractors, String Phenomenology, Frascati, Italy, 04/06 - 08/06 2007.

References

1. Title: N=4 supersymmetric McIntosh-Cisneros-Zwanziger-Kepler systems on S-3 Author(s): Bellucci S, Krivonos S, Ohanyan V Source: PHYSICAL REVIEW D Volume: 76 Issue: 10 Article Number: 105023 Published: NOV 2007
2. Title: Attractors with vanishing central charge Author(s): Bellucci S, Marrani A, Orazi E, et al. Source: PHYSICS LETTERS B Volume: 655 Issue: 3-4 Pages: 185-195 Published: NOV 1 2007
3. Title: N=8 supersymmetric mechanics on the sphere S-3 Author(s): Bellucci S, Krivonos S, Sutulin A Source: PHYSICAL REVIEW D Volume: 76 Issue: 6 Article Number: 065017 Published: SEP 2007
4. Title: Generic N=4 supersymmetric hyper-Kahler sigma models in D=1 Author(s): Bellucci S, Krivonos S, Shcherbakov A Source: PHYSICS LETTERS B Volume: 645 Issue: 2-3 Pages: 299-302 Published: FEB 8 2007
5. Title: E-6 and the bipartite entanglement of three qutrits Author(s): Duff MJ, Ferrara S Source: PHYSICAL REVIEW D Volume: 76 Issue: 12 Article Number: 124023 Published: DEC 2007
6. Title: 4d/5d correspondence for the black hole potential and its critical points Author(s): Ceresole A, Ferrara S, Marrani A Source: CLASSICAL AND QUANTUM GRAVITY Volume: 24 Issue: 22 Pages: 5651-5666 Published: NOV 21 2007
7. Title: N=8 non-BPS attractors, fixed scalars and magic supergravities Author(s): Ferrara S, Marrani A Source: NUCLEAR PHYSICS B Volume: 788 Issue: 1-2 Pages: 63-88 Published: JAN 7 2008
8. Title: On the supergravity formulation of mirror symmetry in generalized Calabi-Yau manifolds Author(s): D'Auria R, Ferrara S, Trigiante M Source: NUCLEAR PHYSICS B Volume: 780 Issue: 1-2 Pages: 28-39 Published: SEP 24 2007
9. Title: On the moduli space of non-BPS attractors for N=2 symmetric manifolds Author(s): Ferrara S, Marrani A Source: PHYSICS LETTERS B Volume: 652 Issue: 2-3 Pages: 111-117 Published: AUG 23 2007
10. Title: E-7 and the tripartite entanglement of seven qubits Author(s): Duff MJ, Ferrara S Source: PHYSICAL REVIEW D Volume: 76 Issue: 2 Article Number: 025018 Published: JUL 2007
11. Title: Black-hole attractions in N=1 supergravity Author(s): Andrianopoli L, D'Auria R, Ferrara S, et al. Source: JOURNAL OF HIGH ENERGY PHYSICS Issue: 7 Article Number: 019 Published: JUL 2007
12. Title: Critical points of the Black-Hole potential for homogeneous special geometries Author(s): D'Auria R, Trigiante M, Ferrara S Source: JOURNAL OF HIGH ENERGY PHYSICS Issue: 3 Article Number: 097 Published: MAR 2007

13. Title: On dilatation operator for a renormalizable theory Author(s): Sochichiu C Source: JOURNAL OF HIGH ENERGY PHYSICS Issue: 9 Article Number: 025 Published: SEP 2007

14. Title: Dilatation operator or Hamiltonian? Author(s): Sochichiu C Source: FORTSCHRITTE DER PHYSIK-PROGRESS OF PHYSICS Volume: 55 Issue: 5-7 Pages: 816-820 Published: MAY-JUL 2007

15. Title: Statistical mechanics for dilatations in N=4 super-Yang-Mills theory Author(s): Sochichiu C Source: NUCLEAR PHYSICS B Volume: 767 Issue: 3 Pages: 352-384 Published: APR 9 2007

16. Title: Higher spin fields from a worldline perspective Author(s): Bastianelli F, Corradini O, Latini E Source: JOURNAL OF HIGH ENERGY PHYSICS Issue: 2 Article Number: 072 Published: FEB 2007

Iniziativa specifica PI11

F. Palumbo (Resp.)

Recently a new bosonization method has been used to derive, at zero fermion density, an effective action for relativistic field theories whose partition function is dominated by fermionic composites [1], chiral mesons in the case of QCD. This approach shares two important features with variational methods: the restriction to the subspace of the composites, and the determination of their structure functions by a variational calculation. But unlike standard variational methods it treats excited states at the same time and on the same footing as the ground state.

I extended [2] this method including states of nonvanishing fermion (baryon) number and derived an effective action for QCD at finite temperature and baryon density. I tested the result on a four-fermion interaction model.

References

1. Composite boson dominance in relativistic field theories, S. Caracciolo , V. Laliena and F. Palumbo, JHEP 0702:034,2007; e-Print: hep-lat/0611012

2. A semi-variational approach to QCD at finite temperature and baryon density, F.Palumbo, [ArXiv: hep-lat//0702001]

Iniziativa specifica PI31

F. Palumbo (Resp.)

I recently proposed a general approach to bosonization of Fermi systems which conserves all symmetries, including fermion number conservation, and is valid for arbitray fermion-fermion interactions and structure functions of the composite bosons. The resulting Hamiltonian, however, was studied only in the case of smooth structure functions of the composite bosons and complete bosonization, namely absence of unpaired fermions. I remove these limitations.

I get a Hamiltonian valid for arbitrary structure functions, showing that it yields exactly the results of the BCS theory of superconductivity and of the pairing model of atomic nuclei in the form of the quasichemical equilibrium theory /citePalu.

Then I extend the formalism including odd systems and excitations involving unpaired fermions [2].

References

1. Composite boson dominance in many-fermion systems, F.Palumbo, Eur.Phys.J. B56 (2007)335
2. Composite bosons and quasiparticles in a number conserving approach, F. Palumbo Proceedings of 9th International Spring Seminar on Nuclear Physics: Changing Facets of Nuclear Structure, Vico Equense, Italy, 20-24 Ma 2007; e-Print: arXiv:0711.4911 [nucl-th]

5 – Technological and Interdisciplinary Research

3+L (TIME RESOLVED POSITRON LIGHT EMISSION)

Alessandro Drago (Resp.Naz., Primo Tecnologo), Alessio Bocci (Bors.),
A. Marcelli (Primo Ricercatore), Mariangela Cestelli Guidi (Art.23),
Alberto Clozza (Primo Tecnologo), Antonio Grilli (Tecn.), Rossano Sorchetti (Tecn.)

1 Introduction

Goal of the experiment, other participating UUOO of INFN, commitments of the LNF group: To the purpose to set up a real time beam diagnostics on the positron ring of the DAΦNE collider, a new experiment named 3+L (Time Resolved Positron Light Emission) has been funded by the Vth Committee of the Istituto Nazionale di Fisica Nucleare and in 2007 has started the installation on the only available bending magnet exit port of the positron ring of DAΦNE [1]. One of the main expected results of the project is the detection of the time resolved positron signal with photoconductive and photovoltaic uncooled fast IR detectors [2]. The aim of this experiment is to improve accelerator diagnostics, i.e. to acquire the longitudinal and transverse bunch-by-bunch measurements in order to increase both the stored current in the e^+ ring and the collider luminosity. The participating group is located at the LNF, no other UUOO are involved.

2 Activity

During 2007 a dedicated SR exit port has been set up on the positron ring. The exit port includes a compact front-end with a small UHV Al chamber with an infrared window that allows the extraction of the light emitted by positrons. Inside the HV front-end chamber a gold-coated mirror deflects the photon beam by 90 degree towards a large ZnSe window installed on a CF100 flange that allows transmission of the mid-IR emission. After the window an optical system working in air and remotely controlled has been designed to focus radiation towards the detectors. An ion pump has been installed to achieve a high vacuum ($< 10^{-9}$ mbar) in the front-end and a vacuum sensor has been installed to read the pressure inside the camera. A beam stopper is also available after the metallic gate valve of the front-end and it is controlled from the DAΦNE control room. A pc has been installed in the DAΦNE hall to control remotely the status of the system, e.g., the vacuum pressure, and in the future for the acquisition of data from different detectors. A photograph of the front-end showing the ZnSe window is shown in Fig. 1, while in Fig. 2 the e^+ beam light, acquired by a webcam, is shown.

Figure 1: Photograph of the bending magnet exit port with a ZnSe window installed on the DAΦNE positron ring.

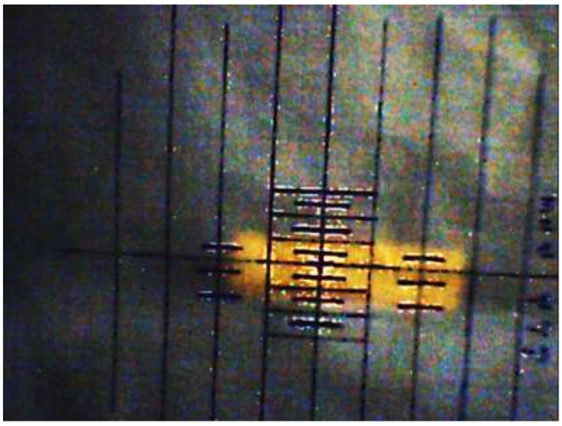

Figure 2: Photograph of the DAΦNE synchrotron light coming from the positron ring.

The design of the optical system started with both ray tracing and wave simulations of the IR source performed at the wavelength of 10.6μ which corresponds to the best working point of the fast mid-IR detectors that we will use for bunch diagnostics. In particular, the vertical and horizontal intensity distributions of the IR synchrotron radiation source have been simulated with the SRW software package [3]. The fast IR photo-detectors are manufactured by VIGO System S.A. These devices are photoconductive and photovoltaic detectors based on HgCdTe heterostructures fabricated on GaAs substrates operating at room temperature and optimized at 10.6m of wavelength. Preliminary time resolved measurements of the synchrotron light emitted by e- bunches have been carried out to measure and monitor the longitudinal bunch length of the electron bunches. With these compact photo-detectors, we indeed characterized the emission of single e- bunches using the light available at SINBAD, the IR beamline installed on the e- ring of DAΦNE [4,5]. In these experiments, the IR signal has been amplified by a MITEK amplifier with 2.5 GHz of bandwidth and 40 dB of gain. As an example, the measurement of three adjacent electron bunches is showed in Fig. 3. The measured structure indicates a rise time and a fall time of the signal emitted by these electrons bunches of about 560 ps and 600 ps, respectively.

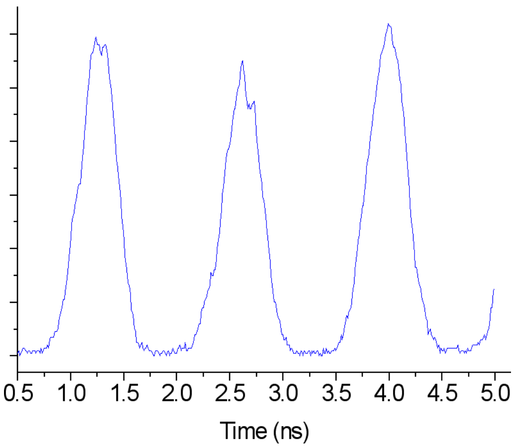

Figure 3: Photograph of the DAΦNE synchrotron light coming from the positron ring.

3 Short outline of the foreseen 2008 activity

The optical system will be optimized to focus the IR photon beam on the photo-detectors. The system will be set-up and aligned on top of an optical table installed near the exit port. Step motors controlled by an RS232 serial port will be used to tune the alignment of the optical components and detectors. The signal will be acquired remotely by a 6 GHz bandwidth scope also remotely controlled by a GPIB interface connected to the pc. A software package based on LabView routine has been developed to collect data during the year 2008.

Experiments with new IR detectors are planned in the next future using the electron beam emission, while the first tests with positron light are planned after the installation and test of the optical system necessary to focus the IR photon beam. Among the planned experiments, tests will be performed using faster photovoltaic IR detectors trying to improve the time-resolution of the bunch structure. The 3+L apparatus, when available could allow a simultaneous monitor of the electron and positron emission and, as a consequence, could be successfully used to improve DAΦNE diagnostics, i.e., identify and characterize bunch instabilities and/or increase the current in the e+ ring. The project includes also feasibility tests of fast imaging. To this purpose a compact infrared array detector has been developed in collaboration with the high-tech Polish company VIGO System S.A. This array detector is an uncooled IR photoconductive detector that consists of 2x32 pixels with a pitch of about 50x50 micron2 and a response time per pixel of about 500 ps. The bonding of the array has been performed on an pcb (printed circuit board) at the Department of Astronomy and Space Science of the University of Florence. First tests of the array with fast electronics are planned in the attempt to achieve a bunch by bunch imaging of the source and in order to monitor transverse bunch instabilities.

4 References

1. A. Bocci, M. Cestelli Guidi, A. Clozza, A. Drago, A. Grilli, A. Marcelli, A. Raco, R. Sorchetti, M. Piccinini, E. Pace and J. Piotrowski, Proceedings 8th European Workshop on Beam Diagnostics and Instrumentation for Particle Accelerators, 20-23 May 2007, Mestre (VE).

2. J. Piotrowski and A. Piotrowski, Proc. SPIE 5957 (2005) 117.

3. O. Chubar and P. Elleaume, Proceedings EPAC98 1998, p.1177-1179.

4. A. Bocci, A. Marcelli, E. Pace, A. Drago, M. Piccinini, M. Cestelli Guidi, A. De Sio, D. Sali, P. Morini and J. Piotrowski, NIM-A **580**, 190 (2007).

5. M. Cestelli Guidi et al., J. Opt. Soc. Am. **A22** (2005) 2810.

ALTCRISS

L. Bongiorno (Bors.), M.A. Franceschi, G. Mazzenga (Tecn.), M.Ricci (Resp.), B.Spataro

Participant Institutions:

ITALY: INFN LNF, Firenze, Roma Tor Vergata, Trieste; University of Genova
GERMANY: SIS (Darmstadt)
RUSSIA: MePhi, IBMP, RKK "Energia" (Moscow)
SWEDEN: KTH (Stockholm)
ESA European Astronaut Center

1 Introduction

The ALTCRISS experiment (Alteino Long Term monitoring of Cosmic Rays on the International Space Station) - previously named SI-RAD - is a continuation of the activities carried out for the experiments SIEYE1 and SIEYE2 on board the Russian Space Station MIR and for the experiments SIEYE3/ALTEINO on board the International Space Station (ISS) in the years 1995-2002 [1) 2) 3) 4) 5)].

The experimental task of the ALTCRISS experiment (approved by ESA) is to develop a detector to be placed on the external part of the ISS. The detector will be used to monitor cosmic rays and radiation environment in Low Earth Orbit. Long (Solar modulation) and short (coronal mass ejections, orbit dependence) of the particle flux and the dose absorbed by the astronauts will be monitored. In addition, data will be compared with measurements taken inside the ISS with ALTEA (see below) and ALTEINO detectors to validate radiation transport and dose estimation codes. At the same time, the investigation, with a more sophisticated instrument, of the "Light Flashes" phenomenon [6)], will be conducted to improve and refine the results obtained with the previous SIEYE experiments.

To meet these goals, a precursor mission in space with a high performance cosmic ray detector, LAZIO/SIRAD [7)], has been accomplished to measure and identify all particles traversing the detector separating nuclei from electrons/positrons, in the energy range ~ 10 to $\sim 100 MeV$. LAZIO/SIRAD has been launched in April 2005 on a Soyuz rocket and placed aboard the ISS by the italian astronaut Roberto Vittori. We refer to the previous Annual Report LNF 2005 for details on this mission [8)].

Moreover, in July 2006, the ALTEA experiment [9)], launched with the Space Shuttle Discovery, has been placed on board the ISS by the Swedish astronaut Christoph Fuglesang and has started taking data one month later.

The preparation of the next ALTCRISS extended mission is advancing towards the completion of the full flight instrument consisting of a 16-plane tower of double-sided silicon detectors (8x8 cm^2 area) equipped with trigger and anticoincidence counters. The total weight is about 15 kg and the total power consumption should not exceed 30 W. The hardware set-up is accomplished through three steps by the construction of a laboratory prototype model, an engineering model and the final flight, space qualified model.

The activity in 2007 has been focused on the development of the following systems of the engineering model:

- Trigger system.

- Development of Silicon Photomultiplier (SI-PM) technology for space applications and test of different SI-PM configurations at the LNF-BTF beam.
- Completion of a highly integrated silicon board (16 cm x 16 cm).
- Production and test of a low-power, low-mass Digital Processing Unit (DPU).

Moreover, activities dedicated to measurement sessions on board ISS have been performed as follows:

- Completition of data taking during expedition 14, with return of material with Soyuz 13-S (21-4-2007).
- Expedition 15 data taking: Progress M-60 launch (21-10-2007) and return (Soyuz 14-S, 21-10-2007).
- Launch of material with Soyuz 15-S (10-10-2007).
- Data acquisition in various orientation and shielding materials in the crew cabins, the service module and the docking compartment.
- Data acquisition with ALTEA in the US Lab.

In 2008, the planned activity includes the completion of the engineering ALTCRISS unit and the set-up of the flight configuration equipped with autotrigger capabilities for heavy nuclei and a trigger for crossing protons and nuclei. The interface with the ISS Space Station will be realized with an intermediate CPU to manage the telecommands from ground and the download of the data. Beam tests at the LNF-BTF, GSI/Darmstadt and other facilities are also planned together with the continuation of the R&D on the SI-PM technology.

2 Activity of the LNF group

The LNF group has taken the responsibility of the design, construction and test of the mechanical structures and interfaces of the three models of the detector also contributing to the integration of the mechanical support for the DAQ. This activity is carried out with the support and the participation of the LNF Service of Development and Costruction of Detectors (SSCR). The activity in 2007 has been mainly devoted to the completion of the mechanical support of the engineering model and to the interfaces of the front-end and DAQ with the detector. These systems are being developed for the final space-qualified flight configuration in the year 2008. The LNF group participates as well in the beam test activities at the above mentioned facilities having the responsibility of the beam trigger counters.

3 Selection of publications in 2007

1. M. Casolino *et al.*,“ The Sileye-Altcriss experiment on board the International Space Station”, Nucl. Instr. Meth. **572**, 235 (2007).
2. M. Casolino *et al.*,“ The Sirad experiment on board the International Space Station”, Nucl. Instr. Meth. **572**, 233 (2007).
3. D. Badoni *et al.*,“Silicon photomultipliers: On ground characterizations and modelling for use in front-end electronics aimed to space-borne experiments”, Nucl. Instr. Meth. **572**, 402 (2007).

References

1. V.Bidoli *et al.*,“In-flight performances of SilEye-2 Experiment and cosmic ray abundances inside space station MIR”; Journal of Physics G: Nuclear and Particle Physics **27**, 2051(2001).

2. S.Avdeev *et al.*,“Eye light flashes on the Mir Space Station”; Acta Astronautica, **50**, 511 (2002).

3. M.Casolino *et al.*,“The Sileye/3-Alteino experiment on board the International Space Station”; Nucl.Phys. **113B**, 88 (2002).

4. V.Bidoli *et al.*, “Dual origin of light flashes in space”, Nature **422**, 680 (2003).

5. P.Maponi *et al.*,“A syncitium model for the interpretation of the phenomenon of anomalous light flashes occurring in the human eye during space missions”, Nuovo Cim., **116B**, 1173 (2001).

6. G. Horneck, “Radiobiological experiments in space: a review”, Nucl. Tracks Radiat. Meas., **20**, 185 (1992).

7. F.Altamura *et al.*,“Preliminary results from the LAZIO-Sirad experiment on board the International Space Station”, Proc. XXIX ICRC, Pune (2005), SH35 p.101.

8. “LNF 2005 Annual Report”, LNF-06/10 (IR), March 2006.

9. L.Narici *et al.*,“ALTEA: Anomalous long term effects in astronauts. A probe on the influence of cosmic radiation and microgravity on the central nervous system during long flights”, Adv. Space Res. **31**, 141 (2003).

DIAFF
Deuterium Induced Anomalous Fission Fusion

F. Celani (Resp. Naz.), A. Spallone (Ass.), E. Righi (Ass.), G. Trenta (Ass.)
A. Marmigi, V. Andreassi, G. Cappuccio (Ass.), D. Hampai (Ass.), A. Marcelli

Collaboration with Companies/Universities:
ISCMNS (International Society of Condensed Matter Nulear Science, Rome Group, 5 Researchers);
STMicroelectronics (Cornaredo and Catania sites, 2 Researchers);
CSM SpA (Centro Sviluppo Materiali, Castel Romano, 2 Researchers, 2 Technicians);
ORIM Spa (Macerata, 1 Researcher, 1 Technician);
Pirelli Labs (Milan, 3 Researchers);
INFN and University of Lecce (2 Researchers);
Osaka University (2 Researchers);
Mitsubishi Heavy Industries (Yokohama, 2 Researchers)

1 Argument and location of the experiments; International organization of all theoretical and experimental activities

The DIAFF (**D**euterium **I**nduced **A**nomalous **F**ission **F**usion) experiment is devoted to study the anomalies (of thermal and/or nuclear origin) that sometimes are detected in Deuterium-Metal systems, especially when the D/Metal ratio is quite large (at least locally) and the system is forced to some *non-equilibrium condition*.

See the Activity Reports of previous years of DIAFF, FREETHAI, FREEDOM experiments for further details. The experiment is located, mainly, at Frascati National Laboratories. Some tests are also performed at Perugia INFN and University sites (Hydrogen, Deuterium absorption on Pd and Pd alloy) by a very high resolution and stability Sievert apparatus. Specific tests are made, at Lecce INFN and University, using films of Pd, H_2 or D_2 gas loaded that were "fired" by pulsed excimer Laser. Some of the materials for the experiment are prepared at: ORIM SpA (Macerata), STMicroelectronics (Cornaredo and Catania), Centro Sviluppo Materiali (Castel Romano). Some of the reproducibility tests were made both at Pirelli Labs (Milan) and Universities in Japan.
* Since over 6 years such kind of studies, both theoretical and experimental, are organised in the framework of the "Condensed Matter Nuclear Scienc". It was founded a Scientific International Society (the ISCMNS), registered according to the U.K. laws. F. Celani was elected, on October 2007, the Vice-President.

2 Activities

Main activities during 2007 at LNF were:

a) The construction of a true differential, high pressure (0-100bar) and temperature (350°C), reactor made in SS and insulated from environment (thermal power loss of 15W at 320°C measured inside the 12 cm^3 crucible chamber and 60bar pressure of Deuterium gas, see Fig. 1);

b) The developing of nanoparticles based on nanometric (mean diameter of holes is, nominally, 5.8nm) gamma Alumina "filled" with soluble salts of Pd and Sr.

Figure 1:

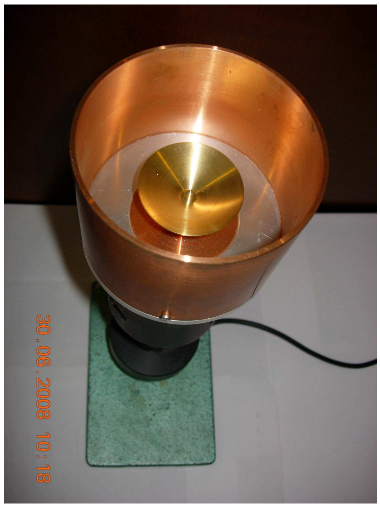

Figure 2:

c) The deep re-analysis of a specific experiment (performed on 2005) based on the use of very thin (diameter 50micron) and long (60cm) Pd wire that underwent specific surface treatments (nanometric material developed at LNF, patenting) located in a large (volume 5l) pressurised (10bar) SS chamber under H_2 gas and large (up to 40000A/cm^2) DC electromigration current.

d) The systematic work on performances of alkaline and alkaline-earth elements from the point of view of H/Pd overloading by electrochemical methods.

e) In order to build nano-particles also by hybrid approaches, it was designed and build a really innovative, very compact (external, overall, diameter of the spinner of only 10cm), electro-mechanical device able to perform, at the same time, ultra fast cooling of liquid (high temperature, up to now 800°C) metals and/or alloys and "atomisation" of the resulting amorphous compound (Fig. 2). For sake of comparison, the usual industrial spinner for high temperature materials are operated at a maximum speed of 3000rpm: our system can operate, continuously, from 1000 up to 33000rpm. Moreover, they needed water or even LN2 cooling; our system is self cooled by proper air fan inside the chamber. Preliminary tests, using middle-temperature alloys, were positive. We are evaluating about an INFN patent.

3 Activity at STMicroelectronics and Lecce University

In the framework of applying the, unexpected, "transmutation" effect on some specific natural material (e.g. Sr→ Mo, Cs→ Pr, Ba→Sm) also to radioactive one, (cfr. World Scientific, ISBN 981-256-901-4, pp. 289-292; also at: http://www.lnf.infn.it/sis/preprint), it was very recently developed by STMicroelectronics, our collaborator in the research, an innovative multilayer (nano-sized) material (Sr (or Cs)-Pd-CaO-Pd)) on nano-porous Silicon that, according to the project, will have a permissible flow rate of Deuterium about 1000 times larger than the original device developed by Y. Iwamura at Mitsubishi Heavy Industries (see the report LNF-06-19(P) for further details). If the "transmutation" rate will increase of the some amount as permeation rate, the device can be used, at the end, for recovering some of most dangerous radioactive wastes among fission products of any Nuclear Power Plant (^{90}Sr, ^{135}Cs, ^{137}Cs). Work in progress about step 1: under test the increasing of D_2 flow rate by a factor 1000 and stability versus temperature-pressure variations (i.e.

aging cycles). In short, there were made some progress about the construction of the innovative nanometric filter of pure silicon. Such filter is developed, and fully paid, by STMicroelectronics; the experimental activity started on January 2006. Some of the measurements are made also at Lecce University where sub-micrometric Palladium is deposited by Laser ablation procedures. Up to now, the results were promising: were filed several patents by STMicrolectronics both on some aspects of filter construction and on the nano-filter itself. Some of the results, without disclosure of patent sensitive information, were presented during the Annual Congress of Italian Physical Society held at Pisa on September 2007 (see publication list).

4 Joint activity with University-INFN of Perugia

It was continued the activity performed at INFN and University of Perugia where is located a very accurate Sievert apparatus for measuring the H/Pd ratio on Pd wires and/or powders. The Perugia apparatus is optimised for pressure of 0-1.2bar absolute and very large temperature range (from liquid nitrogen up to 900°C). Some of the results obtained were shown during the Annual Congress of Italian Physical Society (see publication list).

5 Nano-particles in CMNS studies

The procedures to load the D inside Pd are based on electrolysis (in very special conditions, LNF team is Internationally recognised as a specialist) and D_2 gas (using specifically activated and stabilised Pd surfaces). Recently used large amounts (up to 10g) of Pd nanoparticles: same of that were fully home made at LNF, using nanoporous Alumina filled by Pd and Sr soluble salts that underwent high temperatures, in proper atmospheres, calcinations cycles.
* The main reason to use nano-particles arises because, recently (November 2005), it was demonstrated by Academician Yoshiaki Arata (Osaka University) that specific nano-particles of Pd, dispersed in a Zirconia's matrix, are able to absorb D_2 gas at extremely large values (D/Pd=2.5-4) at room temperature and pressures of 10-100bar. Such material, after absorption of ultra-pure Deuterium, put in an isoperibolic type calorimeter, shows quite large temperature gain (recently up to 70°C), after that some threshold temperature (about 140°C) is overcome. The Arata's procedure to make Pd-ZrO_2 is quite complicated/expensive and is based mainly on metallurgical methods at high temperatures (>1700°C), under Ar atmosphere and ultra fast quenching (about 1000000K/sec): the MELT-SPINNING procedure. In alternative to such approach, we are studying:

a) more simple procedures based on direct chemical synthesis;

b) even other hybrid approaches using both nanopowders and thin Pd wires "painted" by nanomaterials properly stabilised against both the strong reducing proprieties and embrittlement effects of Hydrogen and/or Deuterium, specially at high temperatures and pressures (like in our experiments).

Considering the difficulties to produce the nano-materials (like Arata type) during 2007, in particular, after construction and calibration of the "TRUE DIFFERENTIAL REACTOR" made in SS, they were tested, at first and as starting point, "nanomaterials" that were allowable from the chemical research market: Palladium_Black at High Surface Area produced by Aldrich. We discovered the very strong effect, from the point of view of Deuterium/Palladium ratio and generation of anomalous thermal effects, due to the "BATCH" of production. We argued, comparing different batches, that some of key factors were: Pd nanoparticles dimensions (as small as better);

presence of some deleterious elements like S (it decreases the performance of Pd). Later, we concentrated on the fabrication, by chemical-physical route and fully in the LNF Laboratories, of Pd nanoparticles that filled the nano-holes of a specific gamma Alumina.

6 External constrains to the experimental activities and effect on publications

Because very severe budget limitation (only 9kEuro during the year 2007 obtained by INFN in respect to a well-documented request of about 120kEuro) we were not able to pay external Laboratories for High Resolution Transmission Electro Microscope (HR-TEM) systematic analysis of the nano-material produced. Such analysis, although expensive (about 1000 Euro each), is the ONLY that assures (by direct visual observation) about the proper dimension of nanoparticles (10-20nm seem the optimal one according to the experiments of Academician Yoshiaki Arata). In short, we can only argue about Pd dimensions by indirect measurements using XRPD (X Ray Powder Diffraction) instrument allowable at LNF: Rietvield analysis method. About analysis, in addition, complementary ones are needed, before and after each experiment: SEM (Scanning Electron Microscopy with micro-elemental analysis), ICP-MS (Inductively Coupled Plasma-Mass Spectrometry).

Although the, before quoted, and scientifically unjustified, budget limitations, using the only approach left in our hand, i.e. try construction/synthesis (in the dark!) and test materials with pressurised (and expensive) Deuterium, some of these materials give noticeable results. Obviously the procedures of synthesize and test, without HR-TEM analysis, is extremely time consuming and the progresses are very slow. According to us, it is quite mysterious the rational to, intentionally, slow-down such quite important experiments!

* The most of the results with nanoparticles were presented during respectively an International Conference in Russia (July 2007) and International Workshop in Italy (October 2007). In both case the papers were INVITED (clear "label" of high quality). The 2 papers are allowable also as preprint of Frascati Report LNF at the following address:
http://www.lnf.infn.it/sis/preprint/pdf/getfile.php?filename=LNF-07-18(P).pdf
http://www.lnf.infn.it/sis/preprint/pdf/getfile.php?filename=LNF-08-11(P).pdf

* The other activities (i.e. re-analysis of a old experiment by Pd wire-Hydrogen atmosphere; systematic study about the effect of alkaline and alkaline heart elements on Hydrogen loading by electrolytic methods) were presented, as contributed and poster papers, in the International Workshop held in Italy on October 2007. The 2 papers are allowable also as preprint of INFN-LNF at the following address: http://www.lnf.infn.it/sis/preprint/pdf/getfile.php?filename=LNF-08-09(P).pdf http://www.lnf.infn.it/sis/preprint/pdf/getfile.php?filename=LNF-08-10(P).pdf

7 List of publications

1. F. Celani *et al.,* "High Temperature Deuterium Absorption in Palladium Nano-Particles". Invited Paper at ICCF13, June 24-July 2, 2007, Sochi (Russia). Publishing by World Scientific (2008). Also at Frascati Report -LNF 07/18(P).

2. F. Celani *et al.,* "Palladio, in matrice nanoporosa, per indurre anomalie termiche in sistemi pressurizzati con deuterio ad alta pressione". Presented at XCIII Congress of Italian Physical Society; Pisa, September 24-29, 2007; Pg 30.

3. F. Celani *et al.,* "International trial on the reproducibility of large temperature gain, in Pd (nanoparticles)ZrO_2 system, under high-temperature pressurised deuterium". Presented at XCIII Congress of Italian Physical Society; Pisa, September 24-29, 2007; Pg. 63.

4. U. Mastromatteo, ..., F. Celani, "High flow rate permeation membrane, on porous silicon, for hydrogen filtering devices". Presented at XCIII Congress of Italian Physical Society; Pisa, September 24-29, 2007; Pg. 142.

5. F. Celani *et al.,* "Studio del iper-assorbimento di idrogeno, in materiali nanostrutturati in superficie e/o bulk, tramite misure Sievert al variare della temperatura". Presented at XCIII Congress of Italian Physical Society; Pisa, September 24-29, 2007; Pg. 212.

6. F. Celani *et al.,* "High temperature Experiments, by differential reactor, on Deuterium Absorbed by HSA Pd_black or γAl_2O_3-Pd-$Sr(NO_3)_2$ nanopowder". Invited Paper at 8^{th} International Workshop on Anomalies in Hydrogen/Deuterium Loaded Metals, October 13-18, 2007, Catania (Italy). Publishing by World Scientific (2008). Also at LNF 08/11 (P).

7. A. Spallone, A. Marmigi, F. Celani, P. Marini, V. di Stefano , "A review of experimental studies about Hydrogen over-loading within Palladium wires (H/Pd $\geq$1)".
Presented at 8th International Workshop on Anomalies in Hydrogen/Deuterium Loaded Metals, October 13-18, 2007, Catania (Italy), publishing by World Scientific (2008). Also at Frascati Report-LNF 08/10 (P).

8. A. Marmigi, A Spallone, F. Celani, P. Marini, V. di Stefano, "Anomalous heat generation by surface oxidized Pd wires in a Hydrogen Atmosphere". Presented at 8^{th} International Workshop on Anomalies in Hydrogen/Deuterium Loaded Metals, October 13-18, 2007, Catania (Italy). Publishing by World Scientific (2008). Also at Frascati Report-LNF 08/9 (P).

ETRUSCO

G. Bellettini, (Ass.), A. Boni (Bors.), C. Cantone (Bors.), S. Dell'Agnello (Resp.),
G. O. Delle Monache, M. Garattini (Bors.), N. Intaglietta (Tecn.), M. Martini (Bors.),
R. Tauraso (Ass.), R. Vittori (Ass.)

1 Introduction

A Space Climatic Facility (SCF) has been built at INFN-LNF (Frascati, Italy) in 2006. The SCF is described in detail in ref. [1]) and [2]). The initial purpose of the SCF was to study the non-gravitational perturbations on the LAGEOS and LARES satellites, used for precision Space Geodesy measurements and tests of General Relativity.

The modular and evolutionary design of the SCF turned out to be well suited to characterize the thermal and laser-ranging performance of cube-corner retro-reflector (CCR) arrays deployed on GNSS[1] constellations, like the existing US GPS-2, the imminent European GALILEO and the future GPS-3. The integration of satellite laser ranging (SLR) with the standard microwave ranging (MWR) to improve the satellite navigation capabilites has become another SCF goal.

With minor upgrades, the SCF can also test the laser-ranging performance of spherical test masses in the outer Solar System for DSGP (Deep Space Gravity Probe), which is a satellite formation of an active spacecraft and a few masses laser-tracked by the active spacecraft. DSGP is being conceived to accurately study the Pioneer effect (ie, deviations from the $1/r^2$ gravity force law) and to perform important (inter)planetary science investigations. For this purpose, the groups of INFN-LNF, Rome-Tor Vergata, plus R. Vittori[2] in 2006 proposed to INFN a new experiment, ETRUSCO (Extra Terrestrial Ranging to Unified Satellite COnstellations). ETRUSCO was approved by INFN in October 2006, with the recommentation to focus the activity on GNSS applications. The R&D for DSGP will be reconsidered at a later stage. We describe the first preliminary thermal measurements on a *flight* model of CCR array to be deployed soon on the GPS-2 constellation and the upgrade of the SCF to perform simultaneous thermal and laser-ranging tests.

2 Extra Terrestrial Ranging to Unified Satellite COnstellations

A space-climatic characterization of the detailed thermal properties and of the laser ranging response of the GALILEO CCR arrays will strongly enhance the integration ("unification") of SLR with MWR. For each CCR fo the array, the characterization will include the measurement of the thermo-optical parameters (emissivity and reflectivity), the thermal relaxation time and the variation of the laser far field diffraction pattern in a realistic space environment. This will be done with the arrays inside the SCF, exposed to simulators of the Sun and Earth illuminations. Since SLR gives a fundamental contribution to the definition of the Earth center of mass and of the absolute scale of length, this test program will improve the accuracy and long-term stability of the determination of the GALIELO orbits. The ultimate satellite positioning accuracy that can be reached is less than 1 cm. This in turn will propagate to the final end used on the Earth and all civil and commercial services provided by GALILEO will benefit from it. Since the large-scale deployment of SLR on GALILEO will be a world-first in GNSS, it is of the utmost importance that a full-fledged space-climatic characterization is performed. The experience of SLR with GPS-2 (two satellites) and GLONASS was a test more than a mission critical deployment. Over several years, these few satellites have indicated how crucial the proposed characterization is and how difficult it is to model climatic effects without experimental measurements. A third CCR array exists,

[1]Global Navigation Satellite System.

[2]Italian Air Force and European Astronaut Corps.

which will be deployed soon on a satellite of current GPS-2 constellation. This array is property of the University of Maryland (UMD, College Park, MD, USA) and is now at INFN-LNF for space climatic tests, following a special agreement with NASA-GSFC, IRLS[3] and UMD (C. O. Alley, D. G. Currie). Testing this third array is very important because the previous identical versions of the arrays when tracked with lasers show significant periods of low light returns. Climatic tests and simulations are important to assure that no failures occur in GALILEO, in the long term and with a large multiplicity of satellites. The Frascati SCF offers the unique possibility to understand in detail the effects of the severe space environment on the many years of expected lifetime of the CCR arrays of GALILEO. In addition, the proposed test program can help keep GALILEO competitive with the next generation of GPS-3 (about 2011-2012), which might take advantage of proposed innovative retro-reflectors, like the hollow type, as opposed to the traditional solid, fused-silica reflectors used by GLONASS, GPS-2 and GALILEO.

3 The "GPS3" Array

This so-called GPS3 array is identical to the ones installed on the GPS-35 and GPS-36 satellites in orbit. The three arrays have been manufactured in Russia. Mechanical drawings for its correct modelling have been provided courtesy of V. P. Vasiliev of the Russian IPIE (Institute for Precision Instrument Engineering of the Federal Space Agency of Russia, Moscow). Since this is a *flight* model, in 2006 it was decided not to start with a full test in the harsh SCF environment. Figure 1 shows a photo of the GPS3 and the warm-up and cool-down curve of a central retro-reflector, measured with a digital infrared camera. This preliminary test was conducted with the Solar simulator as the main thermal load, at 75% of its nominal intensity. A space-climatic test in the SCF will follow in 2007, under the supervision of D. G. Currie of UMD.

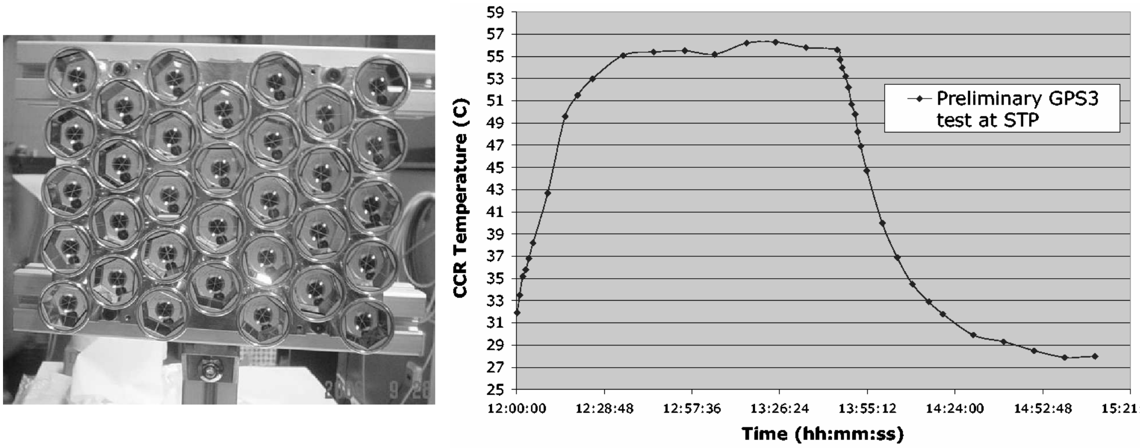

Figure 1: Left: the GPS3. Right: warm-up and cooldown curve of the GPS3 at STP.

4 Far Field Diffraction Pattern (FFDP) Measurement

The most basic test of the SLR performance, is the measurement of FFDPs. The optical circuit for FFDP measurements with CCRs is shown in fig. 2. The laser beam profiler (by Spiricon) uses a PtGrey CCD 2 MPix camera, readout via Firewire by a PC. These tests are currently done in STP conditions to check the optical instrumentation, but final tests will be performed with the

[3]International Laser Ranging Service

CCR array in the SCF. Figure 3 shows a preliminary measurement of an FFDP of a flat mirror, in place of the CCR. Optical flats like this with known reflectivity will be used as a normalization to determine the absolute intensity of the SLR return to Earth from the CCR under test.

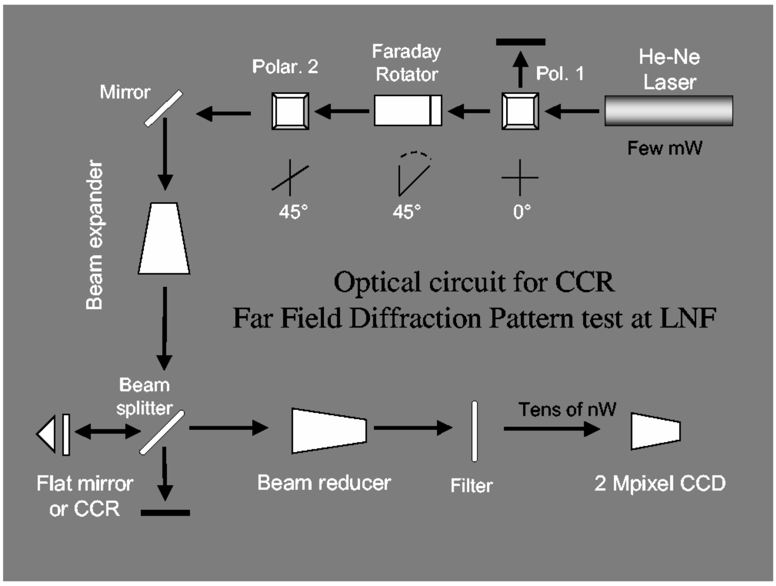

Figure 2: Scheme of the optical circuit for the FFDP measurement at LNF.

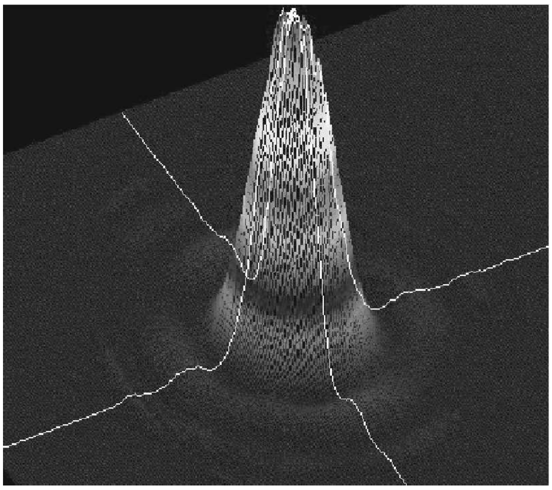

Figure 3: Preliminary FFPD measured for a flat optical mirror.

5 SCF Upgrade

The upgraded SCF is shown in the top view of fig. 4: the existing left window for the IR camera, the new central window for FFDPs and the new right spare window. The side view of fig. 4 shows the sketch of the LARES satellite ($\phi = 32$ cm) and of a GALILEO CCR array (~ 53 cm $\times$ 43 cm).

Each CCR will be first exposed to the Sun and the Earth simulators and its thermogram taken. Then, the CCR will be moved in front of the *central* window to take its FFPD.

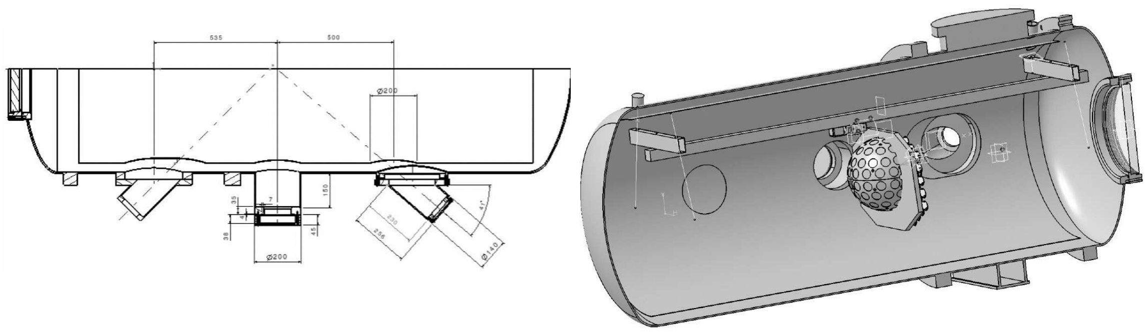

Figure 4: Upgraded SCF. Left: top view (Sun enters left). Right: side view (Sun enters right).

SCF measurements are complemented by simulations done with commercial software [3] [1].
1) Autocad INVENTOR for mechanical drawings and ANSYS for Finite Element. Meshing is done with great detail and in a complete *parametric* way for model portability, modularity and debugging.
2) Space-climatic simulations are handled by THERMAL DESKTOP (geometric thermal modeler) + RADCAD (radiation analysis) + SINDA-Fluint (solver) + orbital simulator, by $C\&R - Tech$ (`www.crtech.com`). This consists of thermal modelization coupled to satellite attitude and orbital motion in the whole Solar System. Models are tuned to the SCF data.
3) CODEV, by Optical Research Associates (`www.opticalres.com`) to analyze the FFDPs.

Talks in 2006 by ETRUSCO Collaborators

C. Cantone, Experimental Gravity in Space GGI Workshop, Florence, Italy, Sep. 2006.
G. O. Delle Monache, Int. Laser Ranging Service Conference, Canberra, Australia, Oct. 2006.

6 Conclusions

In September 2006 the SCF has become a permanent, small-size, experimental apparatus of INFN-LNF. During the last two years the collaboration of LNF with ILRS has been very fruitful. The current upgrade of the SCF, consisting of the integration of the thermal and the laser-ranging tests has been funded by INFN, and by LNF, explicitly for GNSS studies. An additional, dedicated optical table can thus be operated next to the SCF, when alternating among exposure to the heat simulators, IR thermography and laser ranging. At the end of 2006, LNF has become member of the "Signal Processing" Working Group of the IRLS.

References

1. LNF Report LNF-06-24(P); to be published on Int. Jour. Mod. Phys. D.

2. G. Bellettini et al, LNF Report LNF-06-26(IR).

3. A. Bosco, Thesis, Univ. of Rome Tor Vergata, 2006, LNF Report LNF-06/32(T).

FLUKA2

M. Carboni, M. Pelliccioni (Resp.), V. Patera (Ass.), S. Villari (Ass.)

1 Report year 2007

The calculation of the fluence-to-effective dose conversion coefficients for mono-energetic neutrons of energy up to 10 GeV have been in progess. New values have been determined for the rotational irradiation of human body. The work has been currently interrupted awaiting for ICRP directives to clarify some dosimetric rules and the Fluka developers to add a new neutron library for the code.

The FLUKA code has been widely engaged to study the radiation problems of the CNAO (i.e. shield penetrations, air activation, etc.).

2 List of Publications 2007

1. Battistoni, G.; Brugger, M., Cerutti, F.; Fasso', A.; Ferrari, A.; Muraro, S., Pelliccioni, M.; Ranft, J., Roesler S., Sala, P. R.; Vlachoudis, V. Overview of the FLUKA code and examples of use for radiation detectors. Coimbra Proceedings.
2. Beck, P., Latocha, M., Dorman, L., Pelliccioni, M. and Rollet, S., Measurements and simulations of the radiation exposure to aircraft crew workplaces due to cosmic radiation in the atmosphere, Radiat. Prot. Dosim, 2007.
3. Battistoni, G.; Cerutti, F.; Empl, A.; Fasso', A.; Ferrari, A.; Gadioli, E.;Garzelli, M.V.; Muraro, S.; Pelliccioni, M.; Pinsky, L.S.; Ranft, J., Roesler S.; Sala, P. R.; Villari, S. Hadronic models for cosmic ray physics: the FLUKA code. Invited talk at the ISVHECRI.
4. Ballarini, F. and 29 others, The physics of the FLUKA code: recent developments, Advance in Space Research, 40 (2007) 1339-1349.
5. Bassler, N. and 17 others, Fragmentation in human tissue from cancer therapy to space missions, paper presented at NUFRA2007, 26 Sept. 2007.

GIAF

L. Ficcadenti (Art. 2222), D. Alesini (Art. 2222), R. Boni (D.T.), A. Gallo (P.T.)
F. Marcellini (T.), M. Migliorati (R.U.), A. Mostacci (R.U.), B. Spataro (D.T.) (Resp.)
M. Ferrario (P.R.), V. Fusco(Art.23), M. Esposito (Ass.U.), L. Palumbo (P.O.),
J. Rosenzweig (P.O.)

1 Aim of the experiment

The aim of GIAF group is related to the design, realization and measurements of a hybrid standing wave (SW) traveling wave (TW) gun operating at 2.856 GHz. Two different structures have been analyzed, both devices are a 1.6-cell cavity in the standing wave part operating on a π-mode followed by a 5-cell cavity in the traveling wave part operating on a $2\pi/2$-mode, the first one has been realized in aluminum and measured at UCLA and the second one has been realized in copper and measured at LNF. Both hybrid gun have been designed with the HFSS and SUPERFISH codes. Prototype for both the structures have been successfully characterized.

2 UCLA aluminum prototype

The picture of the aluminum prototype realized at UCLA is reported in Fig. 1, the design of the structure, the cavity dimensions and parameters is reported on [1], [2], [3] and [4].

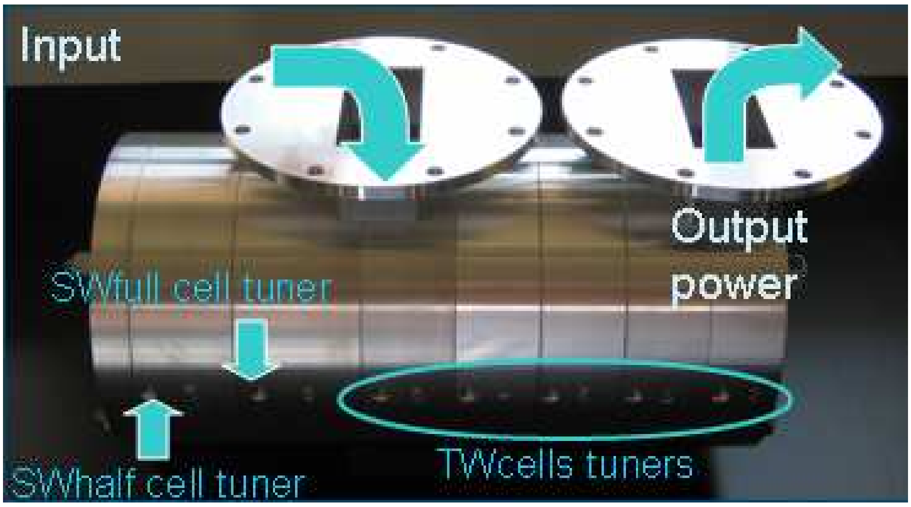

Figure 1: *Aluminum prototype.*

The reflection coefficient measured from the input power port superimposed with the simulation results is reported in Fig. 2 a), there is a very good agreement between them. In Fig. 2 b) we have reported the on axis accelerating field obtained with HFSS simulation code with 1W of input power, from this plot it is possible to see that to reach about 40 MV/m of peak electric field are required about 10 MW of input power. With the bead pull technique we have measured the electric field on axis. After an appropriate tuning procedure, we have obtained a good flatness of the electric field in the SW part of the gun at the right frequency of 2.856 GHz. The measured field is reported in Fig. 3. The field in the SW part is smaller than the field in the TW part because in this aluminum prototype there is a mechanical structural problem between the SW and TW part, where there is a substantial power loss. This problem has been resolved in the LNF copper prototype of the same device.

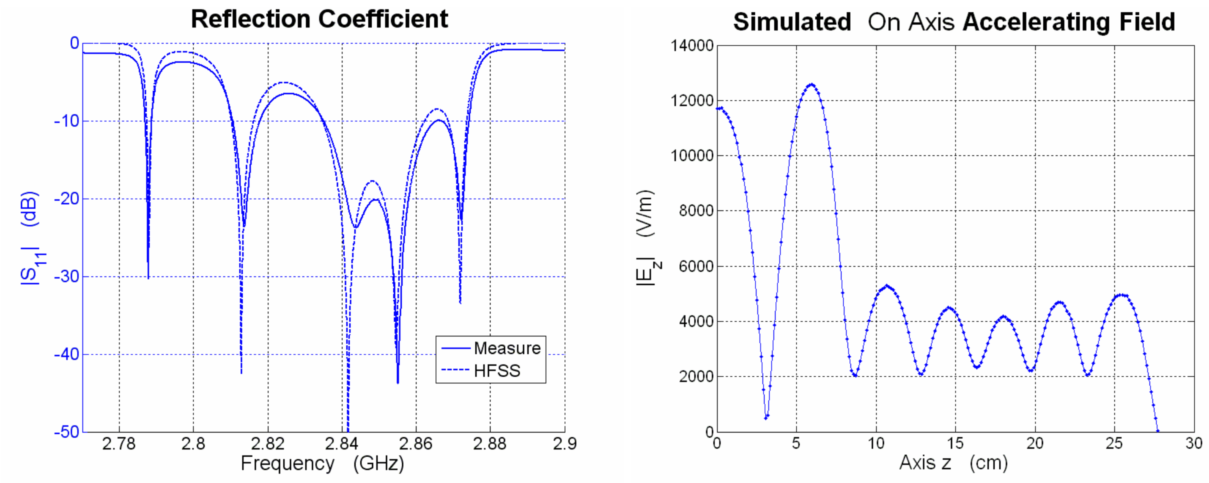

a) *b)*

Figure 2: *a)Input port reflection coefficient, b) On axis longitudinal electric field obteined with HFSS.*

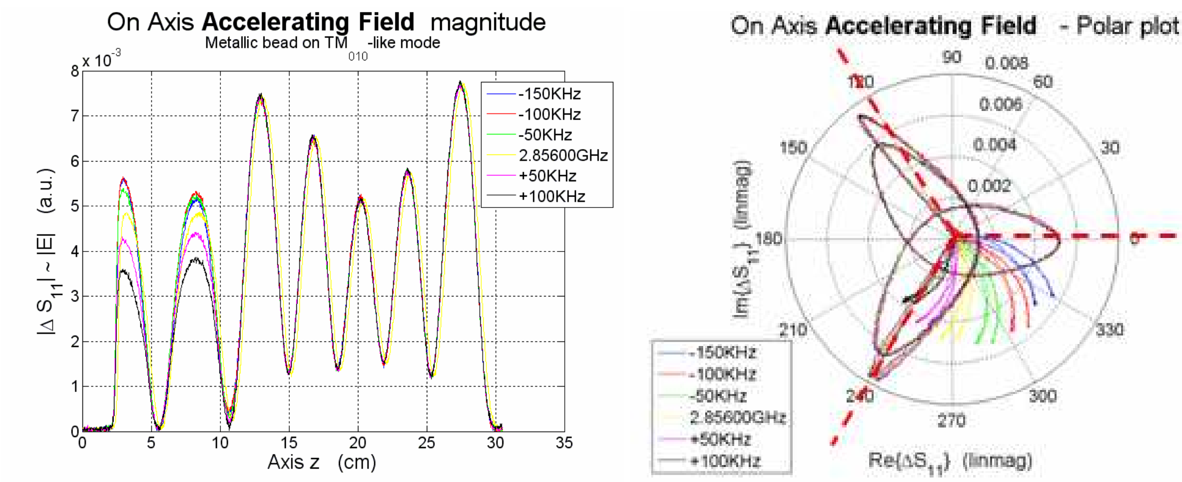

a) *b)*

Figure 3: *Measured on axis electric field at different frequency around the SW part resonant frequency, after an appropriate tuning procedure.*

3 LNF copper prototype

The picture of the aluminum prototype realized at LNF-INFN is reported in Fig. 4. The device is assembled using four copper rods. In the half cell of the SW part has been introduced a little probe to measure the quality factor of the π-mode.

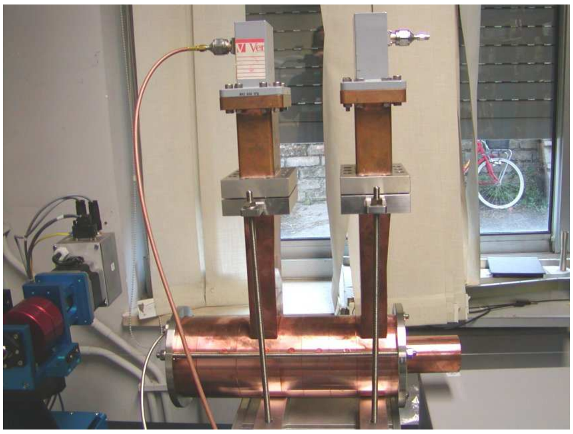

Figure 4: *Copper prototype.*

The reflection coefficient measured from the input port and the transmission coefficient between the small half SW cell probe and the input port are reported in Fig. 5 a) and Fig. 5 b) respectively. The unloaded quality factor of the operating π-mode is 12600.

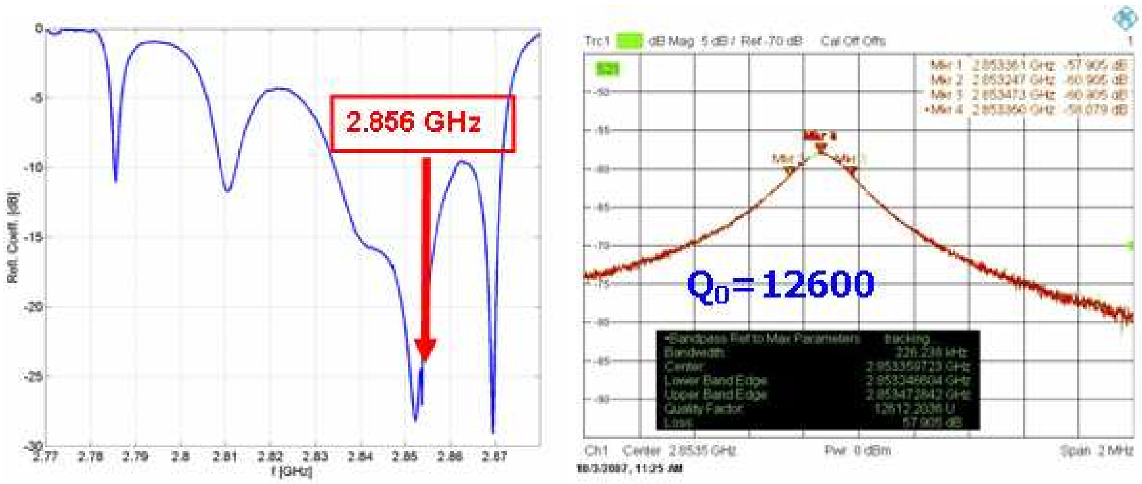

a) *b)*

Figure 5: *a) Input port reflection coefficient, b)Trasmission coefficient between the input port and the small lateral probe..*

The measured longitudinal electric field on axis, compared with the one of the HFSS simulation is reported in Fig. 6, where it is possible to see a very good agreement in amplitude and phase with the simulation results.

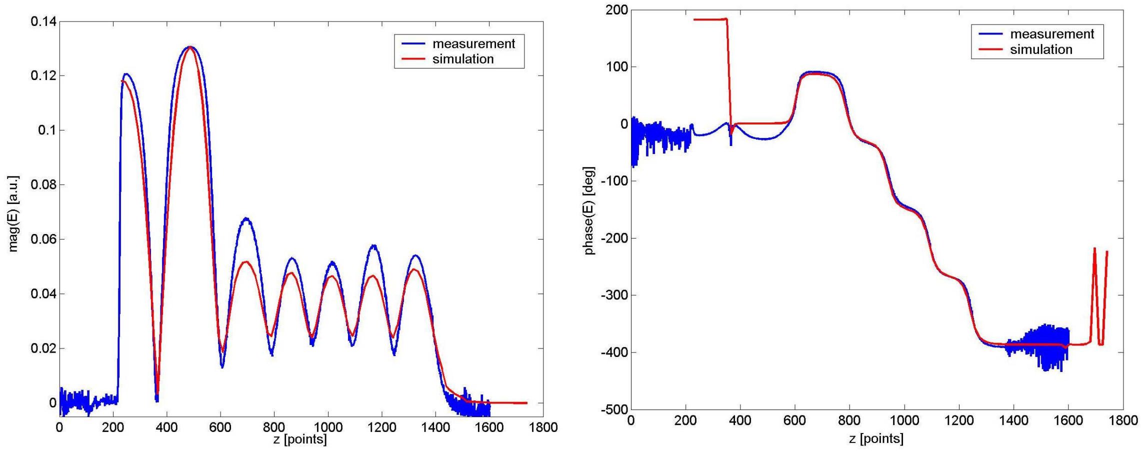

a) b)

Figure 6: *Amplitude and phase of the on axis longitudinal electric field.*

4 Activity 2008

The next steps will be a more detailed e.m. characterization of the copper hybrid gun first and after the brazing and electroforming procedures. We will measure the on axis field with proper calibrated perturbing object to obtain the right unit of measurements. In particular the behavior of the thermal stress will be investigated in detail with simulations and by comparing the results with dedicated measurements. As a final work, high power test will be made, too.

References

1. D. Alesini, L. Ficcadenti *et al.*, "The Design of a Hybrid Photoinjector for High Brightness Beam Applications", presentato ad EPAC 2006, Edimnburgh, Scotland.

2. B.D. O'Shea, A. Boni, A. Fukasawa, J. Rosenzweig, D. Alesini, M. Ferrario, B. Spataro, L. Ficcadenti, A. Mostacci, L. Palumbo, "Measurement of the UCLA/URLS/INFN Hybrid gun", presentato a PAC07, Albuquerque, New Mexico, USA.

3. B. O'Shea, J. Rosenzweig, A. Boni, A. Fukasawa, D. Alesini, M. Ferrario, B. Spataro, L. Ficcadenti, A. Mostacci, L. Palumbo, "RF Design of the UCLA/INFN Hybrid SW/TW Photoinjector", http://pbpl.physics.ucla.edu, presentato al 12th Advanced Accelerator Concepts Workshop (AAC 2006), Lake Geneva, Wisconsin, Jul 2006.

4. J. Rosenzweig, D. Alesini, A. Boni, M. Ferrario, L. Ficcadenti, A. Fukasawa, A. Mostacci, B. O'Shea, L. Palumbo, B. Spataro, V. Fusco, "Beam Dynamics in a Hybrid Standing Wave-Travelling Wave Photoinjector", presentato al 12th Advanced Accelerator Concepts Workshop (AAC 2006), Lake Geneva, Wisconsin, Jul 2006.

KLONE: KLOe calorimeter Neutron Efficiency

S. Bertolucci, A. Ferrari, M. Iliescu,
M. Martini(AR), S. Miscetti(Resp.Naz.), B. Sciascia, F. Sirghi

1 Measurement of detection efficiency to neutrons at 21, 46 and 174 MeV

As shown in the 2006 LNF activity report, the detection efficiency of etherogeneous calorimeters with high sampling to low energy neutrons is much larger than what expected if the signal was due only to the equivalent scintillator thickness in the calorimeter. The first measurement with the lead-scintillating fiber KLOE calorimeter prototype has been carried out at the "The Svedberg Laboratory" (TSL) high energy neutron facility. A first measurement with a neutron beam at 174 MeV was carried out in October 2006 while a second one at lower energies (21 and 46 MeV) took place in the same experimental facility in June 2007.

The prototype is composed of $\sim$ 200 layers of 1 mm diameter blue scifi glued inside grooved lead layers of 0.5 mm thickness The readout consists of four planes for the first 16.8 cm calorimeter thickness. Each plane is subdivided in 3 columns along the horizontal coordinate originating cells of 4.2×4.2 cm^2 area. The calorimeter was positioned with fibers running vertically, the lower (upper) end is called side A (B). We use the discriminated signals of the calorimeter analog sums, SA and SB, to make the trigger as $SA \cdot SB$. A reference counter for efficiency, of transversal dimensions 10×20 cm^2, was built with a 5 cm thick bulk of NE110 organic scintillator. When running with the beam, the scintillator was positioned with its longest dimension along the horizontal coordinate. To trigger on the scintillator, the PM signals, $S1$ and $S2$, were discriminated and a coincidence, $S1 \cdot S2$, formed. The neutron beam was shaped by a cilindrical collimator of 2 cm diameter at 3 m distance from the neutron source. We positioned the calorimeter from 5 to 6 m distance from the source to grant full beam acceptance. Neutron flux rate of 1.5 to 6 kHz/cm^2 were required to make negligible the probability of double neutrons/triggered event. Beam intensity was monitored by a calibrated beam Ionization Chamber (ICM) positioned just in front of the collimator exit. The trigger signal was phase locked with the cyclotron RF replica.

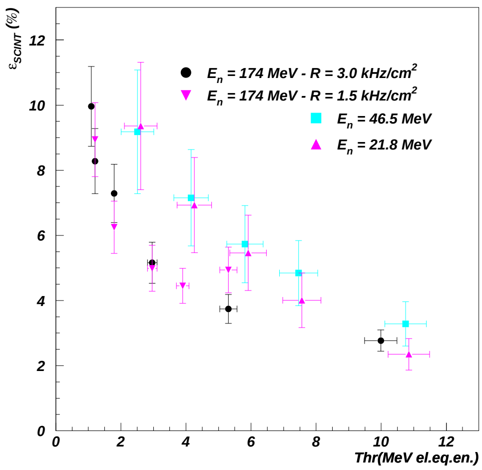

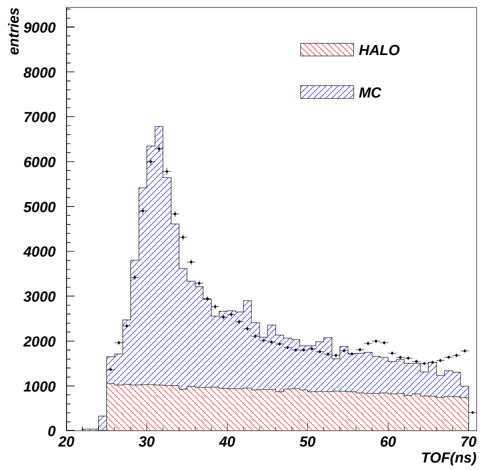

Figure 1: *(Left-plot) Scintillator detection efficiency for data taken at 21, 46 and 174 MeV. (Right plot) TOF distribution for the central cell in the first calorimeter plane: data (black points), MC simulated signal and halo contribution as estimated by calorimeter lateral cells.*

The preliminary detector efficiency to the overall neutron spectrum , ϵ_D, is determined as the ratio of the counted detector rate with the neutron beam rate estimated by the ICM assuming full acceptance and no background contamination. The dependence of the efficiency on the applied threshold in MeV for the reference scintillator is shown in Fig.1(left). A good agreement with the thumb rule of 1%/cm of scintillator thickness is observed. While the scintillator covers a small solid angle, the calorimeter coverage is much more extended and we carefully analized data to quantify the eventual presence of halo neutrons surrounding the beam core. This seems to be indeed the case. In Fig.1.right, the comparison of the TOF distribution between a FLUKA simulated signal at 174 MeV and data asks for a halo contribution as large as 30% of the total rate. We therefore corrected, in a conservative way, the calorimeter detection efficiency of such an amount. Similar comparisons are in progress also for data at 21 and 46 MeV. However a first correction for this data-set has been obtained by an independent halo measurement from the TSL beam experts and already applied. After this halo-correction, the neutron detection efficiency for the calorimeter are shown in Fig. 2.left (right) for the 174 (21,46) MeV beam as a function of the trigger threshold in MeV. These *almost final* results show that at 174 MeV, with the lowest trigger threshold of 3 MeV, the neutron detection efficiency of the calorimeter ranges from 28 % to 33 %. This corresponds to a sizeable enhancement with respect to the expected 8% based on the equivalent amount of scintillator only.

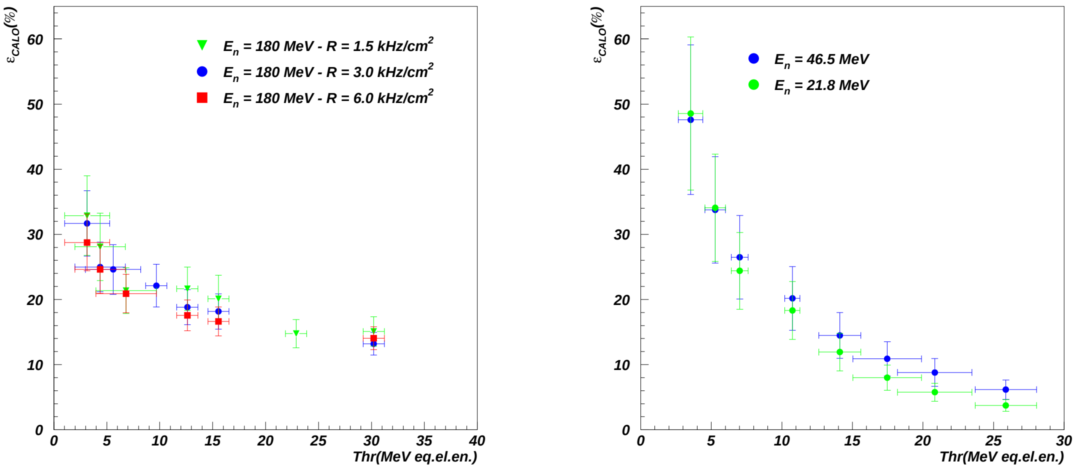

Figure 2: *(Left-plot) Calorimeter detection efficiency at 174 MeV and (right-plot) at 21, 46 MeV.*

FLUKA has been used for a detailed simulation of the calorimeter structure and of the TSL experimental beam-line. The primary reason for the observed efficiency enhancement appears to be the huge inelastic production of neutrons on the lead planes. The high sampling frequency of the calorimeter appears also to be a crucial point in the efficiency enhancement. By weightingthe efficiency curve with the neutron spectrum and correcting for the lowest trigger threshold, the overall efficiency turns to be 35 40% at 174 MeV , in reasonable agreement with the measured integrated value.

Results of this set of measurements have been shown at international instrumentation conferences such as VCI07 [1], SCINT-2007 and the 10th ICATPP conference.

References

1. M. Anelli et al., NIM **A 581**, 368-372 (2007).

MARIMBO

G. Celentano (Ass.), A. Della Corte (Ass.), U. Gambardella (Resp.)

1 Purposes of the project

The *MARIMBO* experiment, devoted to study the applications of superconducting wires and tapes made of magnesium diboride MgB_2, had a one year shift due to AS-G delay in manufacturing the dipole. This fact allowed also to benefit of the new tape technology which made available 1600 m long pieces of MgB_2 tapes with improved transport properties. The racetrack has finally wound and successfully tested in AS-G (see web page http://www.ge.infn.it/∼musenich/marimbo.html). Three INFN sections are involved: Genova (group leader), Milano, and LNF, in collaboration with AS-G SpA, Genova.

2 The Frascati group activity

The Frascati group, made of LNF and ENEA Frascati researchers, in 2007 carried out two activities: the bending effect on MgB_2 tapes, and have tested a MgB_2 coil made by using a double pancake technique by Ansaldo-CRIS, Naples.

2.1 Stress induced by bending

The critical current dependence as a function of induced mechanical stress has been analyzed. We tested the Columbus tape, which is going to be used in the racetrack coil and in the test coil manufactured by Ansaldo CRIS, against subsequent bending around a fixed circumference. The suggested minimum bending diameter for this tape was 100 mm, but nothing was specified about the numbers of bending which can be performed without damaging the cable. This occurrence may happen during a winding process, e.g. back winding for recover a position, or during the cable insulation. Experiments were thus performed with the well known tape available from Columbus, previously tested several times. The tape, 15 cm long, was bended one time on the surface of a cylinder having a radius of 50 mm, and after its plastic deformation it was deformed back to the

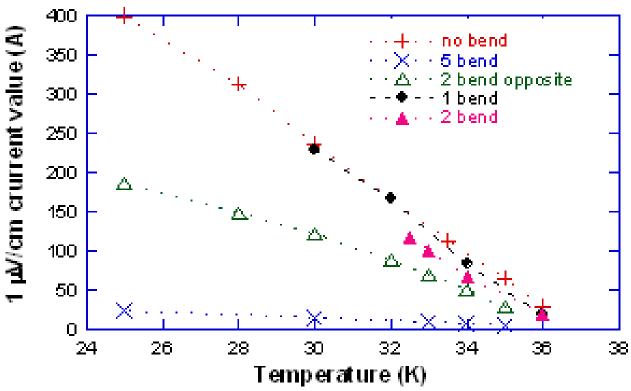

Figure 1: *Critical current of the Columbus multifilamentary MgB_2 tape as a function of the temperature in tapes which had different numbers of bending process.*

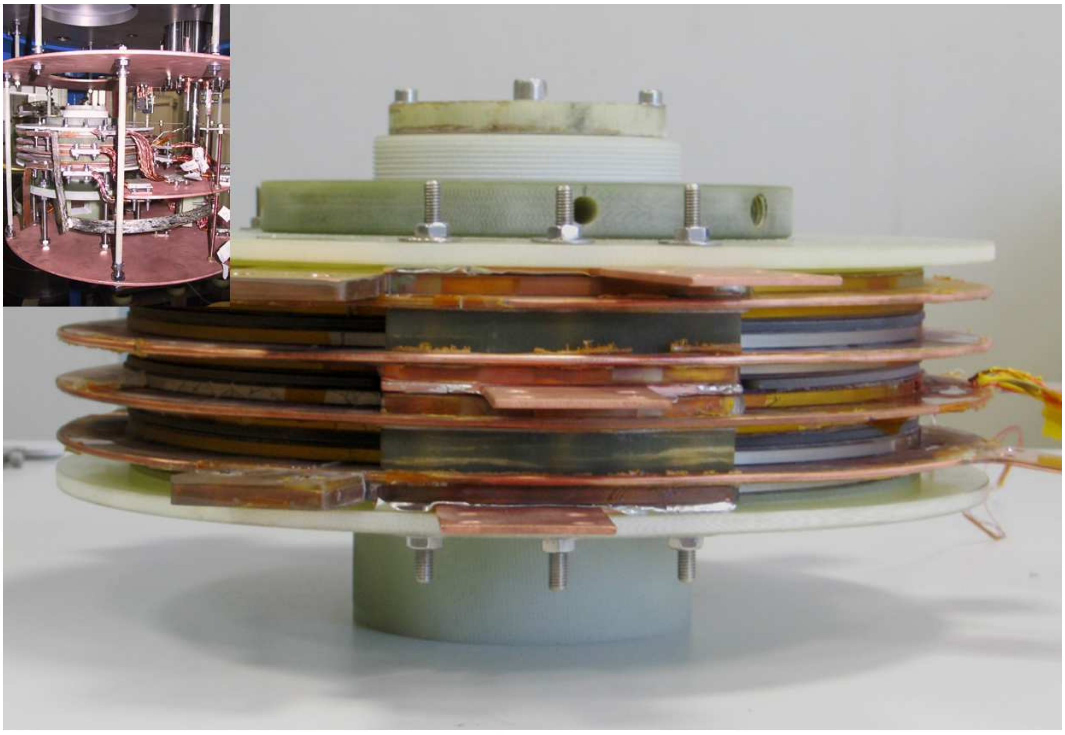

Figure 2: *Double pancake coil wound using the Columbus multifilamentary MgB_2 tape.*

previous straight geometry. Then the critical current has been measured as usual. We repeated the procedure with multiple bending and in one case also with two subsequent bendings in opposite directions. The results are reported in Figure 1, where it is clear the degradation of the critical current when more than one bending is performed. These results suggested us to put a special care when manufacturing a coil, avoiding either spring roll between spun and mandrel, and back winding during the manufacturing.

2.2 Energization, stability, and quench propagation in a test coil

In this work [1)] we analyzed a short coil realized superimposing four double pancake windings to form a single coil with a 100 mm bore. We used 400 m of the Cu-stabilized, 14 filaments, MgB_2 tape manufactured by Columbus SpA, Genova, taken from a 1.6 *km* length production. This magnet was designed to be used in a cryogen-free environment, thus each pancake is assembled on a copper disk for proper conduction cooling. In Figure 2 it is shown the coil assembly and in the inset the complete experimental setup in the cryocooler chamber. The maximum coil current at low temperature is limited by the two HTS (BSCCO type) current leads, designed for 150 A at 77K. Being the warmest side of the HTS lead connected to the cryocooler 1st stage (T$\approx$80K) we limited the bias current to $\approx$120A. This induced a 0.67 T field strength measured in the centre ($\sim$1T on the tape edge), well above the design value. A set of 8 thermometers provided a complete temperature maps in the experiment. The cool down time was $\sim$24h to reach a magnet temperature of 9 K. For testing we heated up the magnet by means of heaters with temperature controllers. Protection diodes, connected on the warm side of the current leads, and additional software control to shut down the power supply, allowed to safely operate and test the magnet.

The energization of the magnet, whose inductance was 80 mH, took place at 20 K with a constant ramp rate of 1A/s up to 120 A. Once the target value was reached twice, we started the

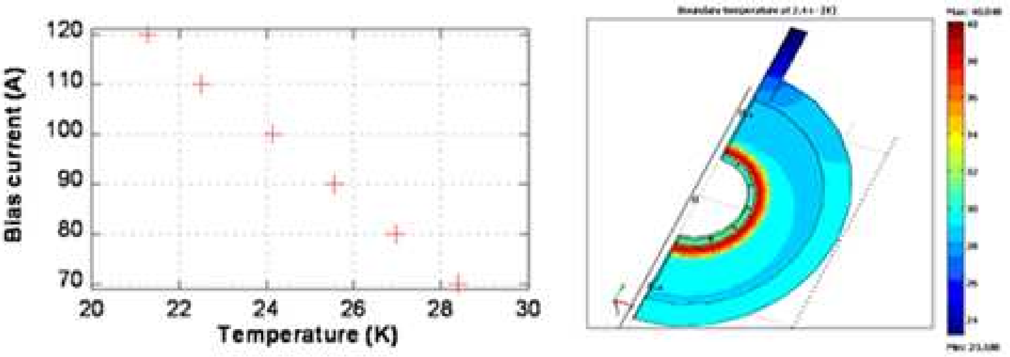

Figure 3: *Coil quench current as a function of the coil temperature (left); FEA of the central pancake temperature 2.5 s after a quench when a the bias is 70 A and the temperature is 28.5 K (right).*

quench tests increasing the temperature. In Figure 3 the maximum current before quench as a function of the temperature is reported (left), and the FEA computation of the central pancake temperature 2.5 s after a quench with the bias of 70 A and the temperature of 28.5 K.

In conclusion the MARIMBO project, further than fulfilling its targets, achieved relevant results. Following the MgB_2 tape developments, still in progress, we were able to test some interesting applications of MgB_2 tapes.

References

1. V. Cavaliere, A. Matrone, G. Masullo, R. Quarantiello A. Saggese, S. Pace, U. Gambardella, "Normal Zone Propagation in a MgB_2 Conduction Cooled Test Magnet", IEEE Applied Superconductivity (2008) to be published.

2. C.Tarantini, M.R.Cimberle, U.Gambardella, E.Lehmann, P.Manfrinetti, A. Palenzona, M.Putti, C.Ferdeghini, "Magnetization decays in neutron irradiated MgB_2 bulk", Journal of Applied Physics (2008) to be published.

3. U. Gambardella, A. Saggese, P. Sessa, A. Guarino, S. Pace, G. Masullo, A. Matrone, E. Petrillo, R. Quarantiello, "Stability Measurements in Multi-Filamentary MgB_2 Tapes", IEEE Applied Superconductivity **17**, 2937 (2007).

4. C. Tarantini, H. U. Aebersold, C. Bernini, V. Braccini, C. Ferdeghini, U. Gambardella, E. Lehmann, P. Manfrinetti, A. Palenzona, I. Pallecchi, M. Vignolo, M. Putti, "Nuclear irradiation on MgB_2", Physica C: Superconductivity **463-465**, 211 (2007).

5. E. Perini, S. Ginocchio, G. Giunchi, U. Gambardella, S. Pace, A. Matrone, R. Quarantiello, V. Cavaliere, and T. Cavallin, "The Magnetic Characterization of a MgB_2 Superconducting Hollow Cylinder at Variable Temperatures up to T_c", IEEE Applied Superconductivity **17**, 2730 (2007).

MICRO X

S.B. Dabagov (Resp. Naz., Resp. - Art. 23), G. Cappuccio (Ass.), G. Cibin (Osp.), A. Esposito, V. Guglielmotti (Osp.), D. Hampai (Ass.), A. Longoni (Ass.), V. Sessa (Ass.)

Collaboration:	Italy	INFN - LNF, Frascati
		Politecnico e INFN, Milano Bicocca
		Univ. "Tor Vergata", Roma
	Russia	RAS P.N. Lebedev Physical Institute, Moscow
		Institute for Roentgen Optics, Moscow
	Belorussia	Institute of Applied Physics Problems, Minsk
	Germany	Unisantis Europe GmbH, Georgsmarienhuitte

1 Introduction

The aim of "MicroX" project is to study and realize a pototype of X-ray microscope based on polycapillary optics in combination with a compound refractive lens, and to develop a unified theory of X-ray propagation in ultra narrow guides.

2 Activities in 2007

2.1 Experimental

In the first year of the MicroX project, we studied and realized a new scheme for X-ray microscope using polycapillary lens. The first prototype of a transmission imaging microscope, Fig. 1, was realized at LNF; it is composed by an X-ray source (Oxford), a polycapillary half-lens (Unisantis) and two detectors, a scintillator and a CCD camera (Photonic Science).

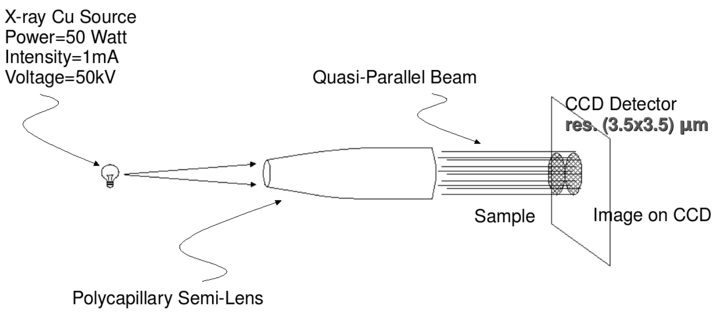

Figure 1: A scheme of the transmission imaging by means of polycapillary lens. Polycapillary half-lens provides a rather small beam divergence, improving in such a way the image contrast resolution.

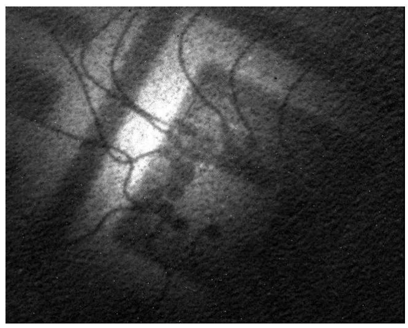

Figure 2: High resolution image of a gold wire ($\sim$25 μm). The image is taken at the detector position of $\sim$23 cm from the optics.

For this prototype our choice for a half-lens was postulated by the possibility to get a very small blurring effect due to rather small radiation divergence behind the optics (without taking into account diffraction effects on sample edges, i.e. far away from the wave zone, as well as multiple scattering radiation in matter). As known, for any kind of the lenses there is a residual divergence responsible for the final resolution. To obtain a quasi parallel X-ray beam we have used a half-lens manufactured by Unisantis Europe GmbH. This optics was first characterized in order to determine precisely both the focal distance from the entrance and the residual divergence at the lens exit.

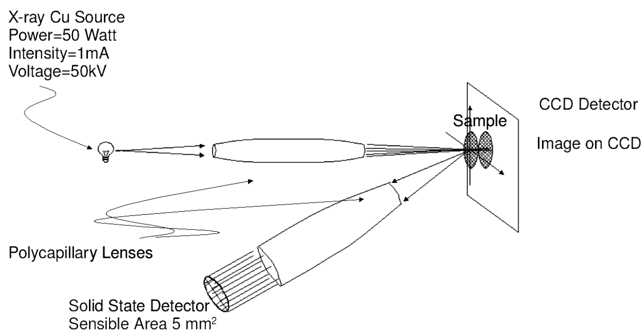

Figure 3: A scheme of XRF experiment in confocal geometry.

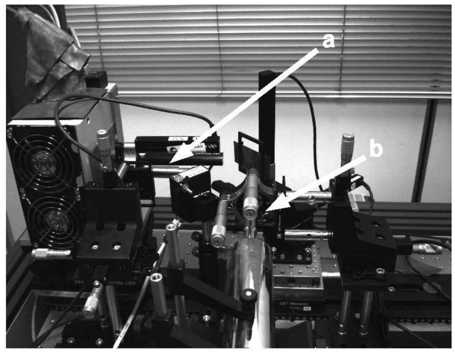

Figure 4: Picture of the experimental setup. The polycapillary lens positions are shown by the marks **a** and **b**.

Since the beam is not perfectly parallel behind the lens, an intensity maximum was detected at about 43 cm from the lens exit; however, the physical divergence at FWHM was about 1.5 mrad with the transmission efficiency of $\sim$60%. A polycapillary half-lens with the focal distance at the entrance about 48.5 mm was used with the Cu K_α source at 12 kV and 0.11 mA.

For evaluating the highest resolution available, a gold standard mesh 1000 (19 μm hole and 6 μm bar widths) was used. The images were registered at various sample-lens distances (the image of a gold $\sim$25 μm wire is presented in Fig. 2). It is notable that due to the very small residual beam divergence, all the registered images are practically similar: the detected widths of the bars are less than two pixels, i.e. $\sim$7 μm.

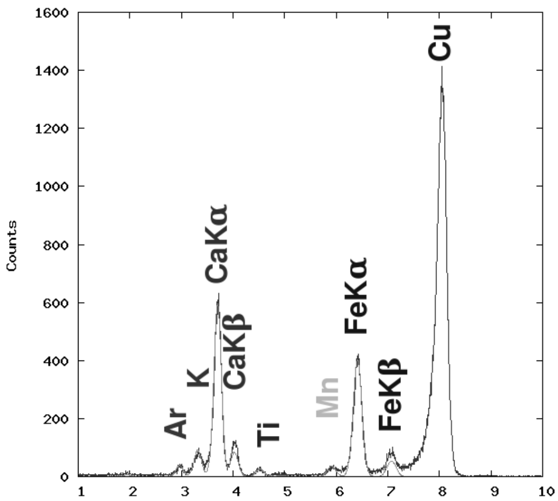

Figure 5: X-ray fluorescence spectra of a neolithic human bone. The Ar, K, Ca K_α and Ca K_α, Ti, Mn, Fe K_α and Fe K_α peaks are clearly resolved. The sample was in powder for an XRD measurement, and all the measurements were performed with a Ni filter.

Many works were presented in the last years, showing advantages of so-called "confocal" optical configuration: its peculiar property enables a table-top micro-fluorescence mapping simultaneously with imaging (Fig. 3). In our case, inserting a second polycapillary lens in the imaging layout allowed the express elemental analysis to be performed simultaneously with the micro-imaging (Fig. 4). For XRF measurements a SDD detector designed at Politecnico di Milano was used; it is characterized by 5 mm^2 effective detection area and 140 eV energy resolution. Fig. 5

shows an XRF spectrum of a neolithic human bone examined within confocal geometry proposed; the spectrum reveals the Ar, K, Ca K_α and Ca K_α, Ti, Mn, Fe K_α and Fe K_α peaks that is in rather good agreement with the data of XRD analysis of the sample. In order to increase the signal at the detector, we are going in the future to substitute the primary half-lens with a full one with a focus spot size of ~100x100 μm.

In our optical laboratory we have developed a procedure for complete characterization of the optics: determination of the focusing and shaping efficiencies as well as determination of the transmission, flux gain, divergence etc. behind the optical elements. Our experimental facility together with the developed ray tracing code (PolyCAD) allows us to study and test any kind of polycapillary optical systems; moreover, starting from the setup parameters we are able to conceive a suitable lens for a specific experiment. Using this procedure, by the agreement with Unisantis, we characterized several novel polycapillary optical samples.

2.2 Theoretical

During the first year of the project we have studied the fine features of X-ray propagation both in ultra-narrow collimators and at glancing reflection from a smooth surface; we have shown that all the processes can be described within the unified theory of trapped radiation propagation: *surface channeling in micro-guides* and *bulk channeling in submicron/nano-guides*.

We have shown that at the center of a any nano-guide *the flux peaking of X radiation*, i.e. the increase in radiation intensity at the center of a guide, should take place (Fig. 6). This feature is a proper channeling effect that can be explained only by the modal regime of radiation propagation, and may find interesting applications for the purposes of extreme focusing (under the diffraction limit).

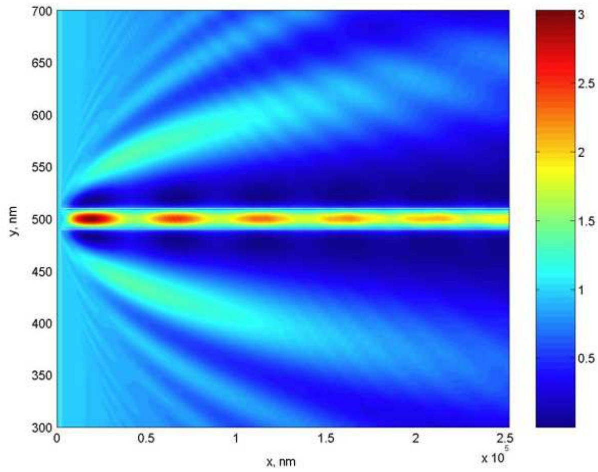

Figure 6: Radiation redistribution for a nano-guide of 20 nm gap size ($\lambda = 1$ Å, the guide thickness is about two radiation absorption length, $\lambda_\perp = 40$ nm for glass). The main portion of radiation flux is concentrated in the cladding; however, due to strong flux peaking effect, the intensity maxima are revealed at the guide center.

Analysis of X radiation propagation through the guides of various sizes and shapes has shown that the main criterion defining the character of radiation transmission is the ratio between the transverse wavelength of radiation and the effective size of a guide, i.e. $\lambda_\perp/d \equiv \vartheta_d/\vartheta_c$, in other words, the ratio between the diffraction and Fresnel angles. When this ratio is rather small, i.e. when the number of bound states is large, the ray optics approximation is valid. In turn, when $\lambda_\perp \simeq d$, a few modes will be formed in a quantum well; and just a single mode - for $\lambda_\perp \gg d$.

3 Activity in 2008

In 2008 we are going to study various schemes for novel X-ray microscopy measurements. The main purpose is to check the efficiency for using polycapillary optical elements in combination with either compound refractive lenses or Fresnel zone plates in order to develop a laboratory X-ray microscope, and, finally, to design a table-top prototype for high resolution X-ray microscopy.

4 Conferences, Seminars

1. S.B. Dabagov, "On extreme X-ray focusing", *Invited lecture to Workshop "Advances in AFM studies"*, Jan. 11-12, 2007, Marseille, France.
2. S.B. Dabagov, "Micro- and nano-optics as condenser for crystalline undulator radiation", *Oral report to PECU workshop*, Feb. 1-2, 2007, Frankfurt, Germany.
3. S.B. Dabagov, "Capillary optics for micro-focusing", *Oral report to Workshop on X-Ray Powerful Laboratory Sources for AFM*, Apr. 12, 2007, Pisa, Italy.
4. S.B. Dabagov, "Polycapillary optics: from micro- down to nanofocusing", *Invited lecture to Sattelite Meeting of Micro Area Analysis by X-ray in Laboratory*, Sept. 15-16, 2007, Osaka, Japan.
5. S.B. Dabagov, "On X-ray waveguiding: Channeling formalism", *Invited talk to ICXOM 2007 - Int Conf on X-Ray Optics and Microanalysis*, Sept. 17-21, 2007, Kyoto, Japan.
6. D. Hampai, "X-ray microfocusing by capillary optics", *Oral report to ICXOM 2007 - Int Conf on X-Ray Optics and Microanalysis*, Sept. 17-21, 2007, Kyoto, Japan.
7. S.B. Dabagov, "X-ray and neutron micro- and nano-guiding", *Invited talk to RREPS'07 - VII Int Sym "Radiation from Relativistic Electrons in Periodic Structures"*, Sept. 24-28, 2007, Prague, Czech Republic.
8. S.B. Dabagov, "Novel powerful X sources: from crystal undulators to capillary waveguides", *Lecture at Dept. of Physics*, University of Cagliari, Nov. 29, 2007.

References

1. S.B. Dabagov, Guest Editor, Special issue: The 18th International Congress on X-Ray Optics and Microanalysis ("ICXOM 2005", Frascati, September 25-30, 2005) *Spectrochimica Acta* **B62 (6/7)** (2007).
2. S.B. Dabagov, Editor, "Channeling 2006", Proceeding of the International Conference on Charged and Neutral Particles Channeling Phenomena (Frascati, July 3-7, 2006), *Proc. SPIE* **6634** (2007).
3. S.B. Dabagov, and H. Uberall, *Nucl.Instr.Meth.* **A580**, 756 (2007).
4. I. Bukreeva, A. Popov, D. Pelliccia, A. Cedola, S.B. Dabagov, and S. Lagomarsino, *Phys.Rev.Lett.* **97**, 184801 (2006).
5. S.B. Dabagov, and H. Uberall, *Nucl.Instr.Meth.* **B267** (2008) (in press).
6. D. Hampai, S. B. Dabagov, G. Cappuccio and G. Cibin, *Spectrochimica Acta* **B62**, 608 (2007).
7. G. Cappuccio, S. B. Dabagov, D. Hampai, Yu. I. Dudchik and F. F. Komarov, *Proc. SPIE* **6634**, 6634M (2007).
8. V. Rossi Albertini, B. Paci, A. Generosi, S.B. Dabagov, O. Mikhin, and M.A. Kumakhov, *Spectrochimica Acta* **B62 (11)**, 1203 (2007).
9. D. Hampai, G. Cappuccio, G. Cibin, S. B. Dabagov e V. Sessa, *Proc. SPIE* **6634**, 6634N (2007).
10. D. Hampai, G. Cappuccio, G. Cibin, S. B. Dabagov, and V. Sessa, *Nucl.Inst.Meth.* **A580**, 85 (2007).
11. S.B. Dabagov, M. Ferrario, L. Palumbo, and L. Serafini, in the book *The Physics and Applications of High Brightness Electron Beams*, L. Palumbo, J. Rosenzweig, L. Serafini, Eds., World Scientific Publishing, 2007, 602-631.
12. A. Babaev, and S.B. Dabagov, *Preprint* **LNF-07/23 (IR)**, November 5, 2007.
13. S.B. Dabagov, M. Ferrario, L. Palumbo, and L. Serafini, *Intern. Journal of Modern Physics* **A22 (23)**, 4280 (2007).

NEXT

S. Bellucci (Resp. Naz.), Balasubramanian C. (osp.), F. Corrente (Dott.), G. De Bellis (Laur.), G. Di Paolo (Laur.), A. Grilli (Tecn.), A. Marcelli, F. Micciulla (Laur.), R. Pastore (bors., specializ.), A. Petrucci (bors., specializ.), A. Raco (Tecn.), M. Regi(Ass.),I. Sacco (Laur.), A. Tiberia (bors., specializ.)

1 External collaborating Institutions:

Univ. Roma La Sapienza, Univ. Roma Tor Vergata, IHEP-Protvino (Russia), Univ. Pune, India, Burnham Institute (La Jolla, CA, USA), ILL (Grenoble, France).

2 Relevant results achieved:

We continue to develop the realization and field emission characterization of cold cathods based on carbon nanotubes for application to new electron and x-ray sources for medical diagnostics and electron guns. Carbon nanotubes (CNT) were synthesized by DC thermal plasma method. After optimizing the synthesis parameters like the pressure, current etc., the synthesized product, especially the anodic deposit, was characterized by electron microscopies like Scanning Electron and Transmission Electron microscopies. The morphology of the product was ascertained to be multiwalled carbon nanotubes in large ratio. The diameters of these nanotubes were of the order of 30 50 nm and the lengths extending upto a micron and sometimes even 2 or 3 microns.

We studied the field current emitted from the carbon nanotubes, that is important for applications to vacuum sensors, electronic guns and sources of X-ray beams of high brightness, based on pointlike emitters. The CNTs were deposited on a metal stub which acted as the cathode. Care was taken to ensure complete covering of the stub to remove any possibility of emission from the metallic stub itself. The emission studies were performed in a stainless steel chamber under a dynamic vacuum in the range of 10-8 torr. The field emitted current was detected using a phosphor coated ITO (Indium tin oxide) glass. The phosphorus coating also helped in imaging the tips of the nanotubes. This was crucial in estimating accurately the emitting area and thus the field enhancement factor. The I-V curves for the field emission were recorded for various distances between the electrodes.

Moreover we have measured the issued current for the obtained champions using the methods and the different conditions of synthesis, benchmarking the performances in terms of density of emitted current, the activation field, etc, of our samples against those available commercially. We optimized procedures of purification of the samples using strong acids, thermal oxidation, sonication.

We studied the electrical, mechanical and thermal properties of nanocomposite materials based on carbon nanotubes and epoxy resins, for the realization of screening protective devices for sensitive electronic equipment against the effect of electromagnetic interference. We characterized the cellular toxicity of carbon nanotubes.

A relevant national interest project PRIN 2006 (Medical Sciences, coordinated by E. Bergamaschi, Univ. Parma, Italy) approved by the Ministry of University and Research (MiUR) has been running throughout the year 2007. Within the framework of this project, we characterized the toxicity of carbon nanotubes, in collaboration with the INFN Servizio Medicina del Lavoro and SELEX SI. Indeed, a project on NMP materials regarding our collaboration on nanotoxicity with the Finmeccanica nanotechnology group coordinated by C. Falessi (SELEX-SI, Roma, Italy), was recently approved by the Ministry of Defense (Segredifesa).

Moreover, we obtained important results in the study of the channeling of particle beams through aligned arrays of carbon nanotubes.

3 List of Conference Talks by LNF Authors in Year 2006

1. S. Bellucci, "Aluminium nitride nanotubes: synthesis, characterizations, properties", DMM 2007: The International Workshop on Dynamics of Molecules and Materials, Grenoble, France, 31/01 - 02/02, 2007.
2. A. Tiberia, "Comparative Field Emission Studies of as-produced CNTs vis--vis commercially obtained SWCNT", Nanoscience and Nanotechnology 2007, Monte Porzio Catone (RM), 15-16 October 2007.
3. S. Bellucci, "Nanotoxicity and Nanomedicine", Nanoweek 2007, Verona (Italy) 15-20 January 2007.
4. S. Bellucci, "Screening Electromagnetic Interference Effect using Nanocomposites", EUPOC 2007 - Europolymer Conference, Gargnano (BS), Italy, 27 May - 1 June 2007.
5. S. Bellucci, "Screening Electromagnetic Interference Effect using Nanocomposites", Nano Metrology 2007, Turin, Italy, 14-15 June 2007.
6. C. Balasubramanian, "XANES studies of aluminium nitride nanostructures with synchrotron radiation", From Synchrotron to FEL Radiation: new opportunities for science in Frascati, INFN-LNF, Italy, 18-20 June 2007.

References

1. Soldatov A, Yalovega G, Smolentsev G, Kravtsova A, Lamoen D, Balasubramanian C, Marcelli A, Cinque G, Bellucci S, ALN nanoparticles XANES analysis: Local atomic and electronic structure, NUCL INSTRUM METH PHYS RES A, 575-1-2, (2007).
2. Bellucci S, Bolesta I, Guidi MC, Karbovnyk I, Lesivciv V, Micciulla F, Pastore R, Popov AI, Velgosh S, Cadmium clusters in CdI2 layered crystals: the influence on the optical properties, J PHYS-CONDENS MATTER, 19-39, 395015 (2007).
3. Bellucci S, Balasubramanian C, Micciulla F, Rinaldi G, CNT composites for aerospace applications, J EXP NANOSCI, 2-3, (2007).
4. De Nicola M, Gattia DM, Bellucci S, De Bellis G, Micciulla F, Pastore R, Tiberia A, Cerella C, D'Alessio M, Antisari MV, Marazzi R, Traversa E, Magrini A, Bergamaschi A, Ghibelli L, Effect of different carbon nanotubes on cell viability and proliferation, J PHYS-CONDENS MATTER, 19-39, 395013 (2007).
5. Zhukovskii YF, Pugno N, Popov AI, Balasubramanian C, Bellucci S, Influence of F centres on structural and electronic properties of AlN single-walled nanotubes, J PHYS-CONDENS MATTER, 19-39, 395021 (2007).
6. Bellucci S, Popov AI, Balasubramanian C, Cinque G, Marcelli A, Karbovnyk I, Savchyn V, Krutyak N, Luminescence, vibrational and XANES studies of AlN nanomaterials, RADIAT MEAS, 42-4-5, (2007).

7. Bolesta I, Velgosh S, Datsiuk Y, Karbovnyk I, Lesivtsiv V, Kulay T, Popov AI, Bellucci S, Guidi AC, Marcelli A, Piccinini A, Optical, infrared and electron-microscopy studies of (Cd-i)(n) metallic clusters..., RADIAT MEAS, 42-4-5, (2007).

8. Bellucci S, Biryukov VM, Possibility of crystal extraction and collimation in the sub-GeV range, PHYS REV SPEC TOP-ACCEL BEAMS, 10-1, 013501 (2007).

9. Bellucci S, Balasubramanian C, Micciulla F, Tiberia A, Study of field emission of multiwalled C nanotubes synthesized by arc discharge, J PHYS-CONDENS MATTER, 19-39, 395014 (2007).

10. Ramoni R, Bellucci S, Grycznyski I, Grycznyski Z, Grolli S, Staiano M, De Bellis G, Micciulla F, Pastore R, Tiberia A, Conti V, Merli E, Varriale A, Rossi M, D'Auria S, The protein scaffold of the lipocalin odorant-binding protein is suitable for the detection of explosive components, J PHYS-CONDENS MATTER, 19-39, 395012 (2007).

NUVOLA
Study of the vacuum chamber surface electronic properties influencing electron cloud phenomena

A. Balerna, M. Biagini, M. Boscolo, R. Cimino (Resp.), M. Commisso, A. Drago,
T. Demma, S. Guiducci, L. Palumbo. C. Vaccarezza, M. Zobov (INFN, LNF)
P. Barone, A. Bonanno , D. Grosso, M. Minniti, P. Riccardi, A. Oliva, F. Xu, (Uni. Calabria)

1 Activity

The NUVOLA experiment is devoted to the study of the potentially detrimental effects on accelerator performances of the formation of an e-cloud in the accelerator vacuum pipe. The study had different finalities and has been tackled with five different side-activities and approaches: a) Determine Experimental Secondary electron Yield (its energy and angular distribution) as a function of material and material status; b) Determine Experimental Photo-electron Yield (its energy and angular distribution) as a function of material and material status; c) construction of an experimental photon irradiation test facility to study in details the photon scrubbing process; d) construction and characterization of a Low Energy detector to be operated in the DAΦNE ring to directly measure the actual energy of the electrons forming the cloud; e) use of simulation programs to compare results and the impact of the newly determined parameters.
In 2007 we followed the five activities which represents the complementary goals of our project. In this report we see them in details.
We continued the experimental work to determine Secondary electron Yields as a function of material and material status. In the Surface Science laboratory of the university of Cosenza, we focussed on the angular dependence of electron stimulated secondary emission. Such studies have been presented in the international conference of IVC17 [1] where we analysed experiments of electron bombardment (200 eV impact energy) on representative samples of the real Cu surface used in the Large Hadron Collider (LHC) Beam Screen. In this context, energy distribution of emitted electrons have been measured as a function of the incidence angle of impinging electrons. The spectrum of emitted electrons is analyzed by dividing it into three energy regions, conventionally termed reflected, rediffused and true-secondary electrons. We observe that, for fixed electron impact energy, these three components of the spectrum show different angular dependences. The reported data might have implications into simulation codes of the electron cloud effect.
In the Frascati laboratory, we continued studying the scrubbing efficiency of electrons as a function of their energy. In fact, recently built and planned accelerators, base their ability to reach design parameters, on the capability to reduce Secondary Electron Yield (SEY) during commissioning, hence mitigating the potentially detrimental effects of e-cloud driven machine limitations. This SEY reduction (called "scrubbing"), which has been systematically observed and measured in accelerators and in laboratory experiments, is due to the fact that electrons produced during electron cloud formation hit the vacuum chamber wall, modifying its surface properties and reducing its SEY. This mechanism allows to obtain low enough SEY values to minimise any disturbing effects of the electron cloud to the beam. In all the available literature "Scrubbing" has been studied only as a function of impinging electron dose given in $[N^o e^- \ t(s) \ A(mm^2)]$. In reality SEY modi-

fications are only studied in literature by bombarding surfaces with 300-500 eV electrons, but no scrubbing dependence on the bombarding electron energy has ever been discussed. The actual energy of the electrons of the cloud hitting the wall in real accelerators has never been measured accurately, while simulations predict very low electron energies (below 50 eV). For this reason and given the peculiar behaviour observed for low energy electrons [2)], we decided to study this dependence accurately.
We are continuing constructing the beamline extracting a photon beam from DAFNE storage ring to analyse in details the obviously present but not -well studied phenomenon of photon- scrubbing. The experimental set-up has been designed and ordered. [3)] This set-up will give LNF the possibility to be the only Laboratory able to study SEY, PEY electron and photon scrubbing on the same sample.
In parallel to those activities we are developing and testing an home made designed Low Energy detector to be operated in the DAΦNE ring to directly measure the actual energy of the electrons forming the cloud, and inserting some of our newly determined imput parameters in the symulation codes, in order to identify their final impact to e-cloud phenomena.
After the first experimental observations compatible with the presence of the electron cloud effect in the DAΦNE positron ring, a systematic study has been performed regarding the electron cloud build-up. To assess the effects of the electron cloud, simulations of the cloud build-up were carried out using ECLOUD [4)] and compared with POSINST [5)]. Modifications to the secondary emission model (SEY), build up for various filling patterns and different wiggler magnetic field models have been analyzed. Simulation results show the expected dependence of the build-up on the SEY key parameters δ_{max} and δ_0, negligible dependence of the build-up on the magnetic field model, and a build-up variation with bunch filling pattern that is compatible with experimental observations [6)].
Multi-bunch and single-bunch instability simulations are being prepared to understand the nature of the instability.

2 List of Conference Talks in 2007

1. R. Cimino "Importance of realistic surface related properties as imput to e-cloud simulations". Presented at the Linear Collider Workshop ILC2007 Hamburg, Germany, May 30 to June 3, 2007.

2. M. Commisso, P. Barone, A. Bonanno, R. Cimino, M. Minniti, A. Oliva, P. Riccardi, F. Xu. 'Angular Dependence of Secondary Electron Emission from Cu Surface Induced by low energy Electron Bombardment'; Presented at the IVC-17/ICSS-13 Sweeden 2007

3. T. Demma, S. Petracca, G. Rumolo, F. Zimmermann, "Maps for Electron Cloud in LHC Dipoles", presented at ECL2 Workshop, CERN, Geneva (CH), 1-2 March 2007.

4. T. Demma, "Electron Cloud Studies at DAΦNE", presented at 2007 ILC Damping Rings Mini-Workshop, KEK, Tsukuba (JP), 18-20 December 2007.

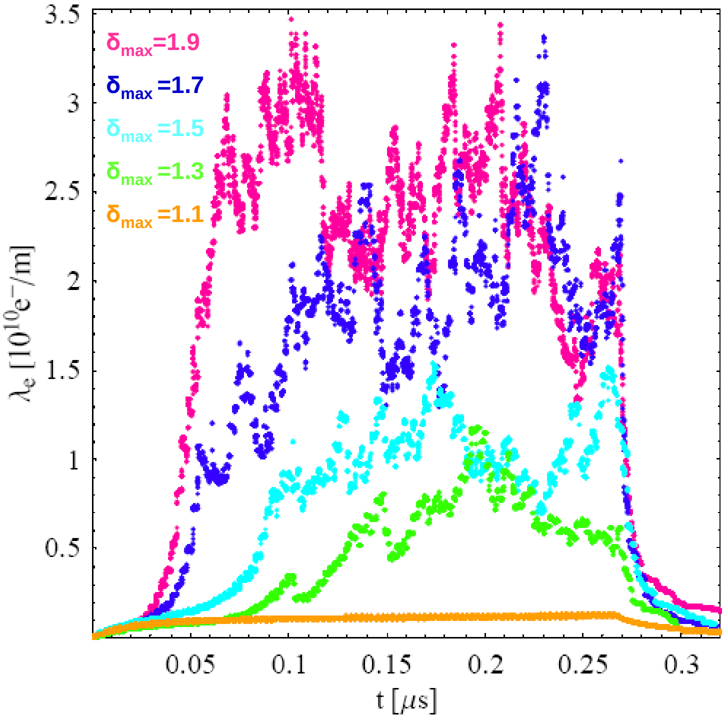

Figure 1: Time evolution of the electron line density for several values of the SEY peak value δ_{max}, as obtained from ECLOUD. The cases shown correspond to the passage through the DAΦNE wiggler of 100 successive bunches with a bunch spacing of 0.8 m and a bunch intensity of $N = 2.1 \cdot 10^{10}$ positrons, followed by 20 empty bunches.

References

1. 'Angular Dependence of Secondary Electron Emission from Cu Surface Induced by low energy Electron Bombardment'; M. Comisso, P. Barone, A. Bonanno, R. Cimino, M. Minniti, A. Oliva, P. Riccardi, F. Xu. Journal of Physics:Cenference series 100 (2008) 092013.

2. 'Can low energy electrons affect high energy physics accelerator?'; R. Cimino et al Phys. Rev. Lett 93, 14801 (2004)

3. 'DAΦNE- Light Laboratory and Activity", A. Balerna et al. This annual report.

4. F. Zimmermann, CERN, LHC-Project.Report-95, 1997.

5. M.A. Furman and M.T.F. Pivi, Phys. Rev. ST Accel. Beams **5**, 124404 (2002).

6. A. Drago et Al., in Proceeding of 2005 Particle Accelerator Conference, Knoxville, Tennessee, p. 1841.

PRESS-MAG-O

M. Cestelli Guidi, G. Della Ventura, D. Di Castro, D. Di Gioacchino (Resp.),
A. Marcelli, A. Mottana, M. Piccinini, P. Postorino

1 Purposes and *PRESS-MAG-O* Activity

PRESS-MAG-O experiment, one of the 2005 highlights of the INFN Vth Committee, is devoted to the investigation of new materials and new phenomena in condensed matter under extreme conditions. The proposal is based on the R&D of an apparatus that will allow performing ac magnetic measurements and magneto-optic experiments on samples under high pressure and high DC magnetic field in a wide temperature range. The device has been designed to perform experiments using SINBAD, the brilliant IR synchrotron radiation beam line operational at Frascati. A large collaboration is involved in this proposal joining the 'LNF-INFN magneto-dynamic' group, the SINBAD team, the 'High-pressure Raman Spectroscopy group' of the Department of Physics of "La Sapienza" University and the Department of Geological Science of the Roma Tre University.

In the third year of the project the main activities of the PRESS-MAG-O collaboration can be summarized as: **a)** the assembly and the delivery to the L.N.F. (September 2007) of the four access ports cryostat, with 8 Tesla superconducting magnet; **b)** the construction and the delivery in L.N.F. (November 2007) of the 'sample insert' for both IR experiments and ac susceptibility measurements inside a high pressure diamond anvil cell (DAC); **c)** the construction and the delivery in L.N.F. (december 2007) of the SQUID-magnetometer system and its electronics.

2 Cryostat

PRESS-MAG-O experiment is based on 'cold finger static cryostat' for concurrent magneto-optic and magneto-dynamic measurements. In September, the cryostat (see figure 1) successfully passed the vacuum test (figure 2), and test performed at the LNF allowed to reach a pressure has been 10^{-5} mBar range in a few hours. The next test related to the temperature cooling procedure are in progress. In this test two shields of the cryostat will be cool down in cold nitrogen gas while third inner shield will be cool down cold vapor of liquid helium and the magnet chamber with liquid helium.

3 PRESS-MAG-O insert

PRESS-MAG-O insert is formed by three main sections: **1)** the $x - y - z - \Theta$ micrometric positioning system (figure 3 panel A1 and A2) to make possible the external alignment of the DAC to the IR beam of the synchrotron radiation beamline with a micrometer resolution. On the bottom of this section is located the DAC , the slots for the ac exiting slpit coils around it and the gradiometer chip assembly with slider to set in the place the gradiometer between the diamond anvils near the gasket (figure 3 panel B1). A miniaturized pick-up coil glued on Si chip shown in figure 3 (panel B2); **2)** the tubular fixed insert component around the moving $x - y - z - \Theta$ element allow cooling of the insert by a cold finger. The fixed insert upper-part is showed in figure 4 (panel A1) while the fixed bottom-section is showed in figure 4 (panel A2). Here a 'Nb_3Sn SQUID magnetic cylinder shield' is placed (figure 4 panel B1) with inside the SQUID system (figure 4 panel B2). All will be inserted in the cryostat cold finger and the thermal contact between $x-y-z-\Theta$ moving sample-holder and the fixed part is guaranteed by Cu-Be springs; **3)** the load-lock system (figure 5) to move the total 'PRESS-MAG-O insert' is installed on the placed top of the cryostat and separated by a HV gate valve.

Figure 1: *Photograph of the PRESS-MAG-O cryostat chamber hosting during the vacuum test.*

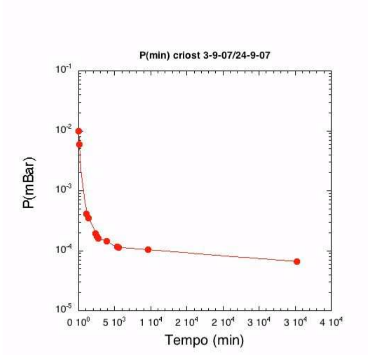

Figure 2: *Representative plot of the vacuum reached by cryostat during the first test.*

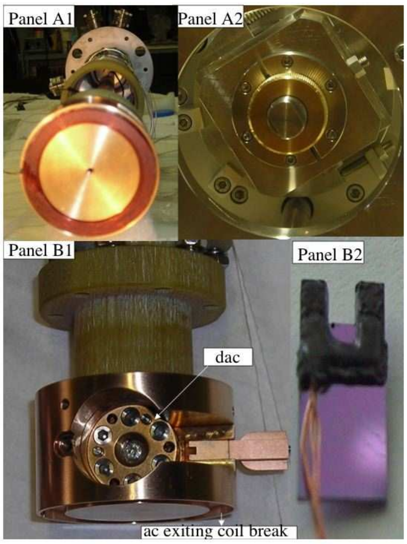

Figure 3: *the $x-y-z-\Theta$ moving insert (panel A1), the $x-y-z-\Theta$ top view (panel A2), the sample-holder with the break and slots for exciting split coils, gradiometer chip assembly (panel B1) and the pick-up coil glued on Si chip (panel B2).*

Figure 4: *The cylindrical fixed upper-part (panel A1), the cylindrical fixed bottom-part (panel A2), the SQUID system flange with magnetic Nb_3Sn screen (panel B1) and SQUID holder (panel B2);.*

Figure 5: *the load-lock system with the HV gate valve.*

4 Outline of the foreseen 2008 activity

PRESS-MAG-O planned tests will concern: 1) the temperature cooling procedure of the cryostat, the procedure is based on the cooling of two shields of the cryostat with cold nitrogen gas while the third inner shield will be cool down by cold vapor of liquid helium and the magnet chamber with liquid helium; 2) after will start the magnetic tests of the super-conducting magnet inside the cryostat and the procedure of switch on and off of the field; 3) during 2008 will be completed the design of the optical components necessary to focus the IR radiation inside the DAC on the sample holder. The manufacturer of these customized reflecting optical systems will be then identified with an international tender; 4) in the cryostat, the PRESS-MAG-O insert cabled with ac exciting coil, SQUID gradiometer and thermometers will do the magnetic test, using sample with magnetic properties well known; 5) first optical experiments with PRESS-MAG-O insert using Raman tests. 6) first tests of magneto-optic experiments at the SINBAD beamline are foreseen before the end of the year if dedicated beam time will be assigned to the experiment.

References

1. D. Di Gioacchino, P. Tripodi, A. Marcelli, M. Cestelli Guidi, M. Piccinini, P. Postorino, D. Di Castro, "PRESS-MAG-O: a new facility to probe materials and phenomena under extreme conditions", Contribution presented at the SMEC2007 Conference (Miami Beach, USA) April 15-20, 2007, in press on J. Phys. Chem. Solids.

SALAF

D. Alesini (Art. 2222), R. Boni (D.T.), A. Gallo (P.T.), F. Marcellini (T.),
M. Migliorati (R.U.)A. Mostacci (R.U.), B. Spataro (D.T.) (Resp.),
L. Ficcadenti (Art. 2222)

1 Aim of the experiment

The aim of SALAF experiment is related to the design, realization and measurements of a compact standing wave accelerating structure operating at 11.424 GHz to be used for linearizing the longitudinal space phase in the Frascati coherent light source (SPARC) [1].Two different structures have been described in the 2006 activity report, the first one is a 9-cell cavity operating on a π standing wave mode, and the second one is a bi-periodic accelerating section operating on the $\pi/2$ standing wave mode. A copper prototype for both the structures has been built and has been successfully characterized at room temperature. Additional studies, as the thermal stress of the accelerating structures, couplers design methodology, brazing and electroforming procedures for high gradient RF technology (using Cu, Mo, Cu-Zr materials and so on), have been also carried out. As a first result, we decided to make a compact π standing wave copper section to be installed on the SPARC Linac and it will be tested with high peak power at the Stanford Linear Accelerator Center (SLAC).

In addition, a memorandum of understanding between Accelerator Technology Research Department (ATR) at SLAC and the National Institute of Nuclear Physics of Italy (INFN) has been signed in order to start an intense and detailed activity on the following topics:

1. X-Band accelerator design for optimized RF parameters;
2. System integration and components design for X-Band pulsed compression system;
3. Mechanical design and fabrication technologies;
4. High gradient RF technology, including experimental tests at SLAC facilities for INFN fabricated structures and components.

2 2007 Activity

2.1 Thermal analysis studies

The electromagnetic characterization at room temperature of a compact standing wave accelerating structure, consisting of 9 cells and operating on π mode at a frequency f = 11.424 GHz, has been completed. Cooling is necessary because in standard operating conditions the power dissipated on the walls of a 9 cells structure is 300 Watts.

To get additional and detailed thermal information on the behavior of the accelerating section as a function of the copper temperature, the SALAF group at Frascati laboratory realized a brazed copper five cells prototype working on π mode at a frequency f = 11.424 GHz and carried out a thermal experiment too [2]. In order to obtain a structure with good electromagnetic behavior, particular care must be taken for the joining of the cells, and brazing procedure has been realized using a vacuum clean oven. The material used for the realization of the accelerating structure prototype is OF Cu. The structure is obtained by joining together single cells using vacuum brazing technique. The vacuum inside the oven is realized by means of a dry piston pump and a turbo molecular pump. The brazing pressure is in the mbar range and the brazing alloy used is eutectic Ag/Cu 0.6 mm wire whose melting point is 780°C. The experimental set up is shown in Fig.1. There are two K-thermocouples, one inside the iris and the other one on the outer surface of the structure near the hole of insertion of the former one, in order to measure transverse ΔT between iris and external surface of the copper. Two K-thermocouples are applied on the water inlet-outlet, in order to measure the power flux.

Figure 1: *Thermal tests of the cavity prototype.*

By introducing a thermal shield, in order to minimize the power dissipated in air by convection, at equilibrium we expect that the electrical power supplied by the heater is entirely dissipated by the water. We have performed several experiments at different power levels and by varying the inlet temperature of the water at constant flux. The equilibrium copper temperature is recorded in order to measure ΔT between iris and external surface of the structure. The temperature of the iris has been acquired by means of a system controlled by Labview software.

By means of a water cooling system made with four copper tubes, parallel to the axis, in contact with the outer surface, connected in serial mode, the external temperature can be put under control. The maximum inner temperature will be obviously on the iris.

The equilibrium temperature as well as the temperature distribution have to be known since they can modify the cells dimensions and therefore the resonant frequency. In order to simulate the RF power a heater has been inserted on the axis of a 5 cells structure. The heating rod diameter is 6 mm and it can reach up to 700 °C at maximum power. Its electrical power can be regulated between 0 W and 300 W and it is transferred to the structure both by convection and radiation. A thermal shield has been mounted outside the structure in order to minimize power dissipated in air by convection. Then, a multi-physics finite-element code [3] has allowed to verify the good agreement between the experimental results and the numerical ones [4].

2.2 Input couplers design

The procedure to design couplers for traveling wave (TW) structures with a 3D electromagnetic code in frequency domain has been proposed [5]. Simple equivalent circuit models of TW structures with input and output couplers and related properties have been studied. An example of coupler design of $2/3\pi$ X band section has been also illustrated in [5].

2.3 Electroforming activity

Electroforming is a galvanotechnical procedure able to reproduce a structure through the deposition of a metal (usually Copper) on a core (usually Aluminum) that is chemically eliminated at the end of the process [6].

The idea is to apply this process to the construction of a 11.424 GHz multicell linear RF accelerating structures, taking into consideration that this process is already in use for RADAR high frequency components, as wave-guides. The basic point is that the Al core will reproduce exactly the requested inner volume of the multicell structure both as shape and as finishing. The activity of the group was dedicated to explore the way to obtain the lowest roughness of the inner surface of the cells. An Ra = $0.2 \div 0.3$ μm is routinely reached (sufficient to start the work with RF), starting from an almost specular finishing of the core surface. The NaOH treatment, necessary to remove the Al core, gives a mat Cu surface and a roughness slightly worse. In addition this process leaves the Cu surface rather dark and with a not uniform aspect. Surely the surface roughness is considered the best parameter to predict the behavior of the accelerating structure when a high RF power is present. Anyway the presence of colored spots could create problems, for example increasing field emission and secondary electrons emission. This study is made in accordance and in a continuous collaboration with the Company specialized in Electroforming technique, GALVAIR.

The first idea was to study if the Silicon content of the Al alloy (type 6082) used for the core could have a role on the quality of the surface, because Si is not eliminated by the NaOH treatment and therefore could remain on the Cu surface. Many tests with Al alloys at low Si content showed that the dark color can not be related to the quantity of Si in the Al alloys.

A second idea was to protect Cu from the NaOH action depositing on the core firstly a thin layer of a metal able to support the NaOH treatment.

The deposition of a few micron of Silver on the core gives an increase of the quality of the Cu surface but again the Ag surface is slightly altered by NaOH.

A third idea was to deposit a layer of Gold on the core, before Cu deposition, because NaOH can not chemically react with Au. Unfortunately in our case Gold cannot be deposited on Al through an Electrolytic process. Anyway there are other procedures to obtain an Au layer, the simplest one could be the deposition by Sputtering. Just this way will be followed in the future, considering that the group has recently received a Sputtering System. Therefore the Al core will be simply covered with a sputtered Au layer, before sending it to GALVAIR for the Cu deposition.

Finally a very simple way to obtain a brilliant Cu surface is to treat it with an acid etching. This is a typical chemical procedure: there are in commerce many products able to give a shiny and brilliant Cu surface and therefore we are in contact with the GALVAIR in order to prepare some tests.

2.3.1 Cu-Mo Electroforming

Brazing of RF multicell structures continued and was developed on the base of the same procedure and design already described in the LNF 05/22 (IR) report.

This activity improved very much as soon as the new, high performance, vacuum oven was installed at Frascati and put into operation at the end of 2006 year.

The use of the Molybdenum to make the irises of the accelerating structure seems to guarantee much higher RF fields. Anyway the presence of another metal along the structure creates some difficulties that we are going to cope with.

It is not easy to obtain a good finishing of Mo, especially after a high temperature thermal cycle, as it happens during brazing.

The GALVAIR Company, that usually makes for us the accelerating structures, specialized in high precision machining, has obtained good levels of roughness (Ra = $0.3 \div 0.4$ μm). It has obtained these results using diamond tools specially prepared for this work. The Molybdenum used for these tests did not undergo any temperature treatment before machining. This work will be completed as soon as possible with tests on thermally treated Mo.

This is a point to take into consideration when preparing brazed structures. Details on this process are given in [7]. A 5 cells structure with Mo irises has been prepared in collaboration with GALVAIR. The key point is that GALVAIR is able to prepare the Mo surface for Cu deposition with a chemical treatment, thus obtaining a very reliable contact. On this base some Mo discs have been prepared with the irises already machined. Then these discs have been sent to GALVAIR for the activation of the external surface. Finally they have been mounted together with the Al cylinders (that represent the cells) in order to obtain the whole structure of the core, ready to be covered with Copper. This Electroforming procedure does not require obviously thermal treatments of Molybdenum; this means that irises can be prepared with a very good level of finishing. In Fig.2 we show the 5 cells the Mo/Cu accelerating structure with coupling tube cut into two halves in order to see the inner shape and in Fig.3 there is the whole section ready for making the first RF tests at room temperature.

2.3.2 Coupler Electroforming

One of the cells of an Electroforming structure will have a more complicated geometry due to the presence of a window and a coupler for the connection to the external wave-guide. The core of one cell has been prepared by Electro-erosion with a shape that contains the RF connection. In Fig.4 we show the Cu coupler cross section, in Fig.5 the Cu Electroformed coupler and in Fig.6 the Al core that represents the coupler ready to be Electroformed.

2.4 Cu/Mo Brazing activity

The Molybdenum seems to be very promising when used for the irises of the multicell structures because it guarantees the possibility to work at higher RF fields. For this reason an activity on

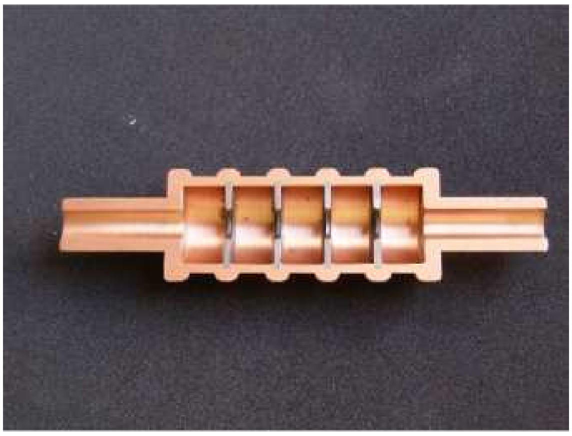

Figure 2: *The Mo/Cu Electroformed structure cross section for RF tests.*

Figure 3: *The Mo/Cu Electroformed structure for RF tests.*

Mo-Cu brazing started recently in order to study this kind of joint [7]. In Fig.7 the first brazing test using Cu-Mo materials is shown.

3 Conclusions and future work

The activities of the SALAF group on the design, realization and electromagnetic characterization at room temperature of compact linear accelerating sections, have been successfully completed. Many graduation thesis have been developed on the linear accelerator activity. The behavior of sections working at 11.424 GHz has been investigated in detail with simulations and by comparing the results with dedicated measurements carried out at the University of Rome "La Sapienza". The final π standing wave linear accelerating structure to be installed on the SPARC Linac is ready to be brazed. According to the signed memorandum of understanding between INFN and SLAC, the tests with high peak power have to be performed on 2008 at SLAC. In addition there is

Figure 4: *The Electroformed Cu - Coupler cross section.*

Figure 5: *The Cu Electroformed coupler.*

also in progress a collaboration between SLAC and INFN on dedicated linear structures by using different materials (Mo, Cu/Zr, and so on) for a research on high gradient accelerating fields and related technologies.

Moreover, in order to increase the performance of the SPS machine operation with higher beam intensity for the LHC luminosity upgrade, a strong collaboration with the Cern is continuing on measurements and estimations of the longitudinal and transverse coupling impedance [8].

Finally, the SALAF group has received formal request of collaboration from other research institutions like PSI (Zurich) ed Elettra (Trieste) for the study and development of innovative devices at higher frequency, like the RF linear accelerating structures and the RF deflectors.

Figure 6: *The Al core of the coupler ready to be Electroformed.*

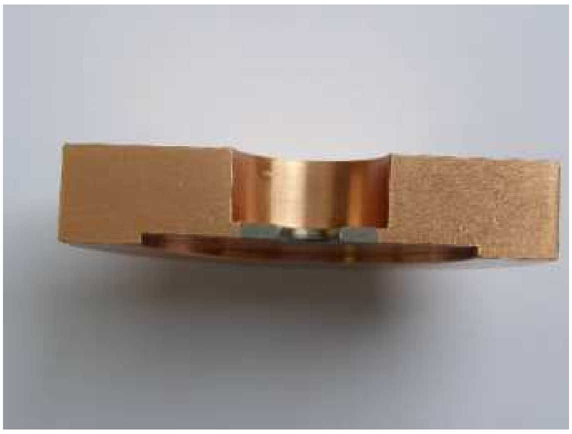

Figure 7: *Copper cell with iris in Mo after machining.*

References

1. Technical Design Report for the SPARC Advanced Photo-Injector, Technical Report, LNF-INFN, ROMA 2003;

2. B. Spataro et al., "Thermal measurements on RF 11.424 GHz accelerating structure", SPARC-RF-06/003, 29/09/2006;

3. ANSYS is a trademark of SAS Inc., (www.ansys.com);

4. B. Spataro et al., "X-band RF structure thermal analysis and tests", NIM A 578 (2007) 55-64;

5. D. Alesini, B. Spataro, et. al., "Design of input couplers for travelling wave structures", NIM A 580 (2007) 1176-1183;

6. B. Spataro et al.,"Electroforming procedures applied to the construction of 11.424 GHz linear accelerating structures: status report", SPARC-RF-07/003, May 3, 2007;
7. B. Spataro et al.,"Status report on SALAF technical activity on vacuum brazing on X-band linear accelerating structures and RF deflector of the SPARC project at Frascati Laboratories", SPARC-RF-07/004, June 11, 2007.
8. CERN AB/ABP Group : private communication

6 – Accelerator Physics

DAΦNE

The DAΦNE Team
D. Alesini, S. Bettoni, M.E. Biagini, C. Biscari, R. Boni, M. Boscolo, B. Buonomo, A. Clozza, G. Delle Monache, T. Demma, E. Di Pasquale, G. Di Pirro, A. Drago, L. Falbo, A. Gallo, A Ghigo, S. Guiducci, M. Incurvati, P. Iorio, C. Ligi, F. Marcellini, C. Marchetti, G. Mazzitelli, C. Milardi, L Pellegrino, M. Preger, L. Quintieri, P. Raimondi, R. Ricci, U. Rotundo, C. Sanelli, M. Serio, F. Sgamma, B. Spataro, A. Stecchi, A. Stella, S. Tommasini, C. Vaccarezza, M. Vescovi, M. Zobov

The DAΦNE Technical Staff
G. Baldini, P. Baldini, A. Battisti, A. Beatrici, M. Belli, B. Bolli, L. Cacciotti, A. Camiletti, G. Ceccarelli, R. Ceccarelli, A. Cecchinelli, S. Ceravolo, R. Clementi, O. Coiro, S. De Biase, I. De Cesaris, M. De Giorgi, N. De Sanctis, R. Di Raddo, M. Di Virgilio, A. Donkerlo, G. Ermini, G. Fontana, U. Frasacco, C. Fusco, F. Galletti, E. Gaspari, M. Giabbai, O. Giacinti, E. Grossi, F. Iungo, R. Lanzi, V. Lollo, V. Luppino, M. Marchetti, C. Marini, M. Martinelli, A. Mazzenga, C. Mencarelli, M. Monteduro, A. Palleschi, M. Paris, E. Passarelli, V. Pavan, S. Pella, D. Pellegrini, R. Pieri, G. Piermarini, S. Quaglia, F. Ronci, M. Rondinelli, F. Rubeo, M. Sardone, M. Scampati, G. Sensolini, R. Sorchetti, A. Sorgi, M. Sperati, A. Sprecacenere, P. Tiseo, R. Tonus, T. Tranquilli, M. Troiani, V. Valtriani, R. Zarlenga, A. Zolla

1 Introduction

DAΦNE is an "electron-positron meson factory" operating at Frascati since 1997. Factories are storage ring colliders designed to work at the energies of the meson resonances, where the production cross section peaks, to deliver a high rate of events to high resolution experiments. The collider luminosity (the number of events per unit time of the reaction under investigation divided by its cross section weighted by the acceptance of the detector) is very high, about two orders of magnitude larger than that obtained at the same energy in colliders of the previous generation. One of the key-points to get a substantial luminosity increase is the use of separated vacuum chambers for the two beams merging only in the interaction regions (IRs). When sharing the same ring the two N-bunch trains cross in 2N points and the maximum obtained luminosity is limited by the electromagnetic beam-beam interaction. The unwanted effects of this interaction can be reduced with a very strong focussing (called "low-β") at each of the crossing points, obtained by means of quadrupole doublets or triplets. At the same time these magnetic structures take up much room and excite chromatic aberrations which must be corrected elsewhere in the ring. A large number of bunches can be stored only with twice the number of low-β points and due to the compactness of the DAΦNE machine only two of these regions can be realized, and therefore only a single electron bunch and a single positron one could be stored in a single ring.

This limitation does not hold for the double ring option, consisting in two separate rings crossing at two low-β points. The number of bunches that can be stored in such a collider is limited only by the geometry of the IR's.

DAΦNE is an accelerator complex consisting of a double-ring collider, a linear accelerator (LINAC), an intermediate damping ring to make injection easier and faster and 180 m of transfer lines connecting these machines. The beam accelerated by the Linac can also be switched into a laboratory called "BEAM Test Facility (BTF)", for dedicated experiments and calibration of detectors. The accelerator complex has been designed to fit into the existing ADONE buildings (ADONE was the 3 GeV center of mass electron-positron collider in operation at LNF from 1969 to 1993); the complex is shown schematically in Fig. 1.

In the DAΦNE collider the two beam trajectories cross at the interaction point (IP) with an horizontal angle that has been recently increased from ≈30 mrad to ≈50 mrad. A positron bunch leaving the IP after crossing an electron one will reach the following electron bunch at a distance of half the longitudinal separation between bunches from the IP. Due to the horizontal angle between the trajectories of the two beams, the distance in the horizontal direction between the two bunches is equal to the horizontal angle times half the longitudinal distance between the bunches in each beam. The beam-beam interaction can be harmful to the beam stability even if the distance in the horizontal direction between bunches of opposite charge is of the order of few bunch widths at points where the β function is high and this sets a lower limit on the bunch longitudinal separation and therefore on the number of bunches which can be stored in the collider. However, the "crabbed waist" collision scheme recently implemented in the machine alleviates this problem, as it will be exhaustively explained in the following of this report. By design the minimum bunch separation at DAΦNE has been set to ≈ 80 cm, and therefore the maximum number of bunches that can be stored in each ring is 120. This number determines the frequency of the radiofrequency cavity which replaces at each turn the energy lost in synchrotron radiation, which must be 120 times the ring revolution frequency. The luminosity of the collider can therefore be up to 120 times larger than that obtainable in a single ring with the same size and optical functions.

Crossing at an angle could in principle be a limitation to the maximum single bunch luminosity. In order to make the beam-beam interaction less sensitive to this parameter and similar to the case of single ring colliders where the bunches cross head-on, the shape of the bunches at the IP is made very flat (typical ranges of r.m.s. sizes are $15 \div 30$ mm in the longitudinal direction, $0.2 \div 1.5$ mm in the horizontal and $2.5 \div 10$ μm in the vertical one).

The double ring scheme with many bunches has also some relevant challanges: the total current in the ring reaches extremely high values (5 A in the DAΦNE design, $\approx$ 2 A in the DAΦNE operation so far) and the high power emitted as synchrotron radiation ($\approx$ 50 kW) needs to be absorbed by a complicated structure of vacuum chambers and pumping systems in order to reach the very low residual gas pressure levels necessary to avoid beam loss. In addition, the number of possible oscillation modes of the beam increases with the number of bunches, calling for sophisticated bunch-to-bunch feedback systems.

The double annular structure of the DAΦNE collider as it is now after the recent modifications to implement the crabbed waist scheme is shown schematically in Fig. 2.

Both rings lay in the same horizontal plane and each one consists of a long external arc and a short internal one. Starting from the IP the two beams share the same vacuum chamber while traveling in a common permanent magnet defocusing quadrupole (QD) which increase the

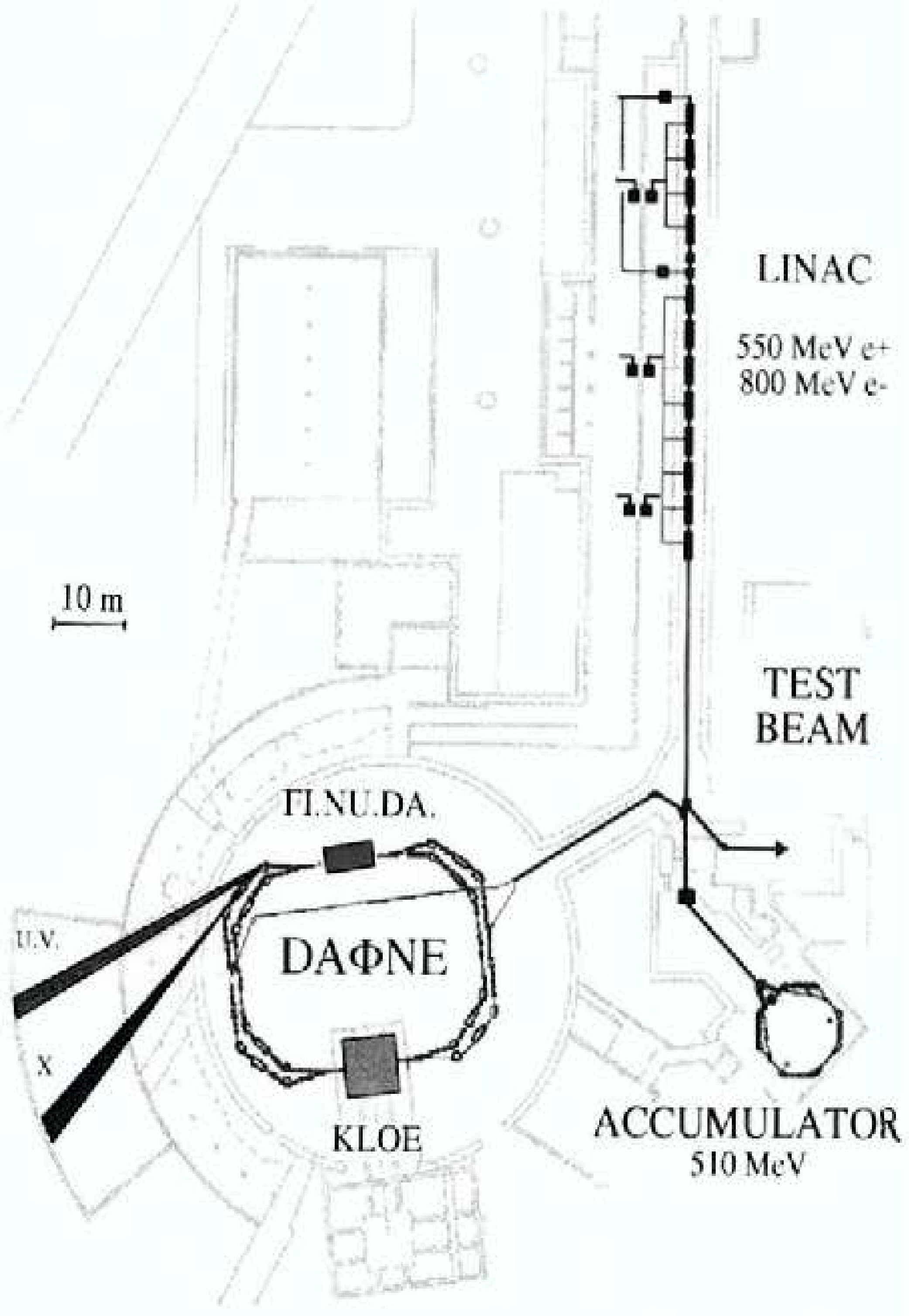

Figure 1: *The layout of the DAΦNE accelerator complex inside its buildings.*

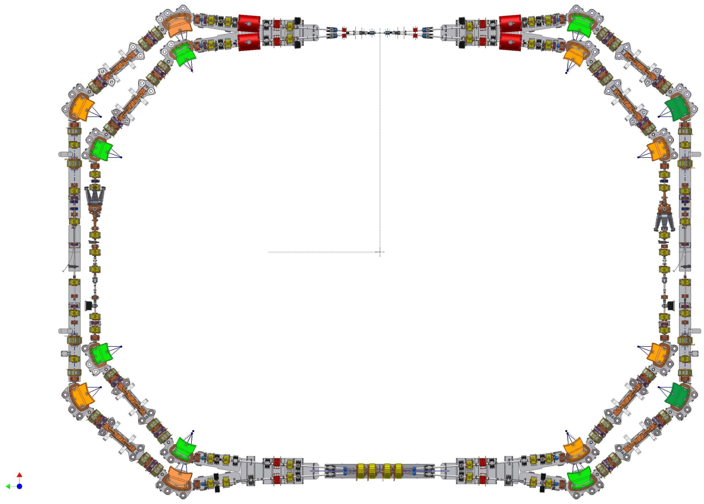

Figure 2: *The DAΦNE Main Rings.*

divergence of the two beam trajectories to $\approx$ 75 *mrad*. Shortly after the QD, at a distance of $\approx$ 82 *cm* from the IP, the common vacuum chamber splits in two separated ones connected to the vacuum chambers of the long and short arcs. Two individual permanent magnet quadrupoles (QFs) are placed just after the chamber separation. Together with the previous QD they constitute the low-β doublets focusing the beams in the IP. The long and short arcs consist of two "almost achromatic" bends (deflecting the beam by $\approx$ 85.4 *degrees* in the short arc and $\approx$ 94.6 *degrees* in the long one) similar to those frequently used in synchrotron radiation sources, with a long straight section in between. Each bend consists of two dipoles, three quadrupoles, two sextupoles and a wiggler. This structure is used for the first time in an electron-positron collider and it has been designed for the particular requirements of DAΦNE: the amount of synchrotron radiation power emitted in the wigglers is the same as in the bending magnets and the wigglers can be used to change the transverse size of the beams. The increase of emitted power doubles the damping rates for betatron and synchrotron oscillations, thus making the beam dynamics more stable, while the possibility of changing the beam sizes makes the beam-beam interaction parameters more flexible.

The straight section in the long arc houses the kickers used to store into the rings the bunches coming from the injection system, while in the short straight arc there are the radiofrequency cavity and the equipment for the feedback systems which are used to damp longitudinal and transverse instabilities.

The most delicate part of the whole structure are the IR's, which have been deeply modified during 2007 to implement the novel "crabbed waist" collision scheme as reported in details in the following of this paper. Before the last major modifications, the IRs have undergone many others readjustments during the years to optimize the performances of the machine while operating for different detectors. In principle the collider could host two experiments in parallel, but only one at a time has been installed so far. Three detectors have taken data until 2007, namely KLOE, DEAR and FINUDA, while SIDDHARTA, a renewed version of the DEAR detector, will operate and take data during 2008. KLOE has been in place on the first IP from 1999 to 2006, while DEAR and FINUDA have alternatively run on the second one. The detectors of KLOE and FINUDA are surrounded by large superconducting solenoid magnets for the momentum analysis of the decay particles and their magnetic fields represent a strong perturbation on the beam dynamics. This perturbation tends to induce an effect called "beam coupling", consisting in the transfer of the betatron oscillations from the horizontal plane to the vertical one. If the coupling is not properly corrected, it would give a significant increase of the vertical beam size and a corresponding reduction of luminosity. For this reason two superconducting solenoid magnets placed on both sides of the detector with half its field integral and of opposite direction have been turned on while running KLOE and FINUDA in such a way that the overall field integral in the IR's vanishes. However, this was not sufficient to obtain full compensation of the beam coupling induced by the main solenoids. In the case of KLOE the low-β at the IP was originally designed with two quadrupole triplets. Due to the flat shape of the beam at the IP, the low-β is realized only in the vertical plane. The quadrupoles cannot be of the conventional electromagnetic type for two reasons: the first is that the iron of the joke would degrade the flatness of the magnetic field in the detector and the second is that the overall transverse size of a conventional quadrupole is at least twice its useful aperture. Therefore quadrupoles realized with permanent magnets have been built, which exhibit an excellent field quality, very small transverse size and are fully transparent to external fields. The region of space around the IP occupied by machine elements, which is unavailable for the detection of decaying particles by the experiment consists in two cones with the vertex at the IP and a half aperture of only 9 degrees. In order to obtain a good compensation of the above mentioned coupling effects induced by the KLOE and FINUDA solenoids, the quadrupoles have been rotated around their longitudinal axis (by angles between 10 and 20 degrees in the KLOE case) and have been provided with actuators to finely adjust their rotation.

The structure of the FINUDA IR is quite similar to the KLOE one. Since its superconducting solenoid magnet has half the length (but twice the field) of the KLOE one, the low-β focusing at the IP was obtained by means of two permanent magnet quadrupole doublets inside the detector and completed with two other conventional doublets outside.

The DEAR experiment, which was installed on the IR opposite to KLOE, took data during the years 2002-2003. It does not need magnetic field and therefore only conventional quadrupoles were used for the low-β. FINUDA rolled-in at DEAR's place in the second half of 2003 and took data until spring 2004. It was then removed from IP2 in order to run the KLOE experiment with only one low-β section at IP1, and rolled-in back in 2006 for a second data taking run ended in June 2007. After that the detector has been rolled-out again, and presently there are no detectors installed in IR2. The two chambers are vertically separated so that the two beams do not suffer from parasitic interactions in the whole IR2.

Two synchrotron radiation lines, one from a bending dipole and the other from the wiggler are routinely operated by the DAΦNE-LIGHT group in a parasitic mode, providing to users radiation from the infrared to soft x-rays.

The vacuum chambers of the arcs have been designed to stand the nominal level of radiation power emitted by the beams (up to 50 KW per ring). They consist of 10 m long aluminum structures built in a single piece: its cross section exhibits a central region around the beam and two external ones, called the antechambers, connected to the central one by means of a narrow slot. In this way the synchrotron radiation hits the vacuum chamber walls far from the beam and the desorbed gas particles can be easily pumped away. The chambers contain water cooled copper absorbers placed where the radiation flux is maximum: each absorber has a sputter ion pump below and a titanium sublimation pump above.

The single cell copper radiofrequency cavities, one in each ring, resonate at 368 MHz with a maximum accelerating voltage larger than 250 KV. Particular care has been taken in damping the high order modes (HOMs) which could induce longitudinal and transverse instabilities in the multibunch structure of the beams. This has been obtained by means of external waveguides strongly coupled to the cavity HOM fields and terminated on 50 Ω loads to dissipate the energy delivered to the HOMs by the beams. Sophisticated longitudinal and transverse feedback systems have, however, been built to damp the residual coupled-bunch instabilities and reach beam currents up to 2 A in operation. These systems are based on digital signal processing techniques, and act individually on each bunch.

The correct superposition of the beams at the IP is of course critical for the luminosity of the ring. For this reason, 46 beam position monitors are available in each ring and 31 small dipoles can be used to steer the beam and correct orbit distortions caused by alignment errors or current errors in the magnetic elements by means of dedicated software algorithms implemented in the Control System of the collider. Additional beam diagnostics are two synchrotron radiation outputs, from which the transverse and longitudinal size of the beam can be measured, total beam current monitors and strip-line pickups used to measure the charge of each bunch.

In a low energy electron-positron collider, such as DAΦNE, the lifetime of the stored current is mainly limited by the Touschek effect, namely the particle loss due to the scattering of the particles inside the bunches. In the present typical operating conditions the Touschek lifetime is of the order of 1000 s. It is therefore necessary to have a powerful injection system, capable of refilling the beam without dumping the already stored one. In addition, flexibility of operation requires that any bunch pattern can be stored among the 120 available buckets. The injection system of DAΦNE is therefore designed to deliver a large rate of particles in a single bunch at the working energy of the collider.

It consists of a linear accelerator (LINAC, see Fig. 1) with a total accelerating voltage of 800 MV. In the positron mode, electrons are accelerated to $\approx\ 250\ MeV$ before hitting a tungsten target (called positron converter) where positrons are generated by bremsstrahlung and pair production with an efficiency of ≈1%. The positrons exit from the target with an energy of few MeV and are then accelerated by the second section of the LINAC to their final energy of $\approx\ 0.51\ GeV$. The positrons are then driven along a transfer line and injected into a small storage ring, called Accumulator, at frequency of 50 Hz. Up to 15 positron pulses are stacked into a single bucket of the Accumulator, then injection stops and the bunch damps down to its equilibrium beam size and energy spread, which are much smaller than the LINAC ones. Damping takes $\approx\ 0.1\ s$ and then the beam is extracted from the Accumulator and injected into the positron main ring at an overall repetition rate of 2 Hz. A powerful and flexible timing system allows the storage of any desired bunch pattern in the collider. In the electron mode, a magnetic chicane deviates the particle trajectory around the positron converter and electrons are directly accelerated to 0.51 GeV and injected into the Accumulator in the opposite direction with respect to positron operation. They are then extracted like in the positron case and injected into the electron main ring through the second transfer line.

The Accumulator ring has been introduced in the accelerator complex to increase the injection efficiency, especially for the positrons that are produced in the LINAC at 50 Hz rate in 10 ns pulses with a charge of $\approx$ 0.5 nC. Since the design charge of the main ring at the maximum luminosity is $\approx 1.5\ \mu C$ and the longitudinal acceptance of the main rings is only 2 ns, the number of 50 Hz pulses necessary to fill the ring is of the order of 10^4. In order to avoid saturation it is therefore necessary that at each injection pulse a fraction smaller than 10^{-4} of the already stored beam is lost, and this is not easy to achieve. The Accumulator instead works with a lower frequency RF cavity and therefore with a larger longitudinal acceptance. In this way the full charge coming from the LINAC can be stored in a single RF bucket. In a complete injection cycle, that has a duration of 500 ms, up to 15 LINAC pulse can be stored in a single Accumulator RF bucket, and after being damped to the ring equilibrium emittances and energy spread, the whole stacked charge can be stored into a single RF bucket of the main ring. In this way the nominal sigle bunch charge can be stored with only one pulse from the Accumulator, reducing to 120 the number of injection pulses (at 2 Hz) into each main ring. As an additional benefit, the transverse beam size and energy spread of the beam coming from the Accumulator are at least one order of magnitude smaller than those of the LINAC beam, and this strongly reduces the aperture requirements of the main ring and, as a consequence, the overall cost of the collider.

2 Summary of Year 2006 activity

In March 2006 the KLOE experiment completed its data taking. The total integrated luminosity between May 2004 and November 2005 at the Φ resonance energy of 1020 MeV was 2 fb^{-1} with a maximum peak luminosity of $1.53 \cdot 10^{32}\ cm^{-2}s^{-1}$ and a maximum integrated luminosity per day of $\approx 10\ pb^{-1}$. Between November 2005 and March 2006, according to the KLOE experiment requirements, the accelerator has been set up for runs at different energies (between 1000 and 1030 MeV). The total integrated luminosity at these different energies has been $\approx 300\ pb^{-1}$. The evolution of the DAΦNE peak and daily integrated luminosity since April 2004 is shown in Fig. 3 and Fig. 4. The last bins with lower integrated luminosity correspond to the off-energy operation.

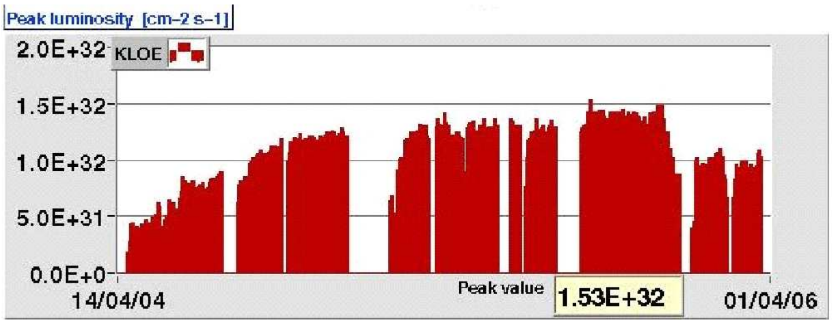

Figure 3: *DAΦNE peak luminosity evolution since April 2004 (KLOE run).*

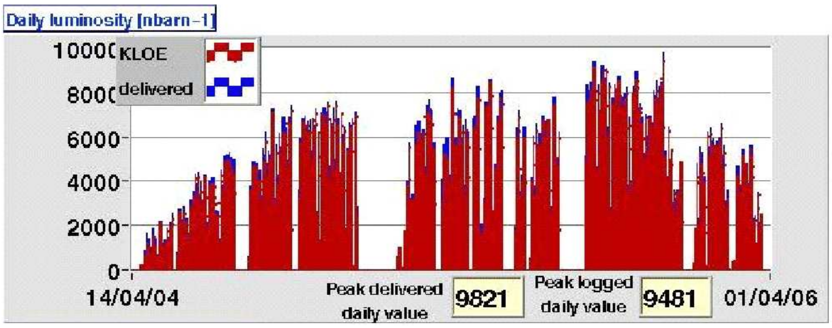

Figure 4: *Daily integrated luminosity during the KLOE run. It exhibits a steady improvement and its maximum value of* 10 pb^{-1} *per day has been obtained in November 2005. The last bins with lower integrated luminosity correspond to the off energy operation.*

In the last two weeks of March 2006 dedicated runs for machine studies have been done. All machine studies were aimed at improving DAΦNE performance for the next FINUDA run and at defining design criteria for an upgraded machine.

After that machine operation has been stopped for a six-months shutdown (from April to September 2006) dedicated to the following activities:

- the KLOE detector has been removed from the collider and parked in the KLOE hall. At the same time its interaction region (IR) has been replaced with a straight section equipped with electromagnetic quadrupoles. With this new section the collider had only one low beta point at the FINUDA IR with smooth optical functions in the other one, allowing for a more efficient separation of the two beams;
- maintenance of the LINAC, cooling, vacuum, RF and control systems, magnet power supplies, cryogenic and electric plants. In particular all the spigots (inlet of water cooling to the coils, ≈ 150 in each wiggler), which were the main source of downtime due to magnet faults, have been replaced with new ones of improved design.
- removal of the ion clearing electrodes (ICEs) in the e^- ring wigglers with a dedicated positioning and cutting system (Fig. 5). This operation has been done in order to reduce the e^- ring beam coupling impedance, thus increasing the current thresholds of vertical beam blow up due to microwave instability and of the quadrupole instability limiting the longitudinal feedback performances;
- installation of Wires for beam-beam long range compensation (BBLR) in IR2 following the successful tests done during the KLOE data taking;
- upgrade of the feedback system with the implementation of a third generation digital system;
- upgrade of the control system with new CS servers, implementation of new front-end processors (Pentium/Linux), extension of the CS Ethernet network in the LINAC area, BTF experimental hall, Damping Ring area, DAΦNE hall;

- roll-in of the FINUDA Experiment.

Figure 5: *ICE removed from e- wigglers.*

DAΦNE operation for FINUDA restarted in October 2006 with the goal of delivering $1fb^{-1}$ integrated luminosity within May 2007.

First collisions started on November 2006; then, with a continuous optimization involving mainly the main ring optics and the feedback systems, before the end of year 2006 the peak luminosity has reached $\approx 1.0 \cdot 10^{32} cm^{-2}s^{-1}$ with a maximum daily integrated luminosity of $\approx$ 5 pb^{-1}. Also the background level has been progressively reduced and, in December 2006, the rates were better than those obtained during the previous FINUDA run ($L_{peak} \approx 0.6 \cdot 10^{32} cm^{-2}s^{-1}$ and $\int_{day} L \approx 4\ pb^{-1}$). It is important to remark that, after the new startup with the FINUDA experiment:

- vacuum recovered in few weeks;
- all the upgrades done have been put in operation with benefits in machine performances, diagnostics and uptime.

3 Year 2007 activites: end of the second FINUDA run

The commissioning of the machine for the FINUDA run started with the compensation of the betatron coupling by rotating the permanent quadrupoles inside the detector solenoid, reaching an optimal value of $\approx 0.3\%$.

Commissioning also included, as usual, ring optics tuning, closed orbit optimization and feedback systems setup. The bare beam orbit (i.e. the expected orbit with all the dipole correctors turned off) in both ring has been drastically reduced by beam based alignment involving the FINUDA detector solenoid. The ring optics for the collision at FINUDA has been designed in order to have a beam emittance $\epsilon_x = 0.34\ \mu m$ and low beta parameters at IP2 $\beta_x^* = \ 2\ m$ and $\beta_y^* = \ 0.019\, m$. The vertical betatron function at IP1 has been tuned in order to trade off between an efficient beam-beam separation and the need to keep under control the blow-up due to beam-beam long range interaction; for this reason the value of β_y^{IP1} after two months of operation has been halved and set to $11m$. Beam-beam simulations, showing the beam-beam blow-up dependence on parasitic crossings for a given beam-beam separation, have been useful in this optimization process.

To reduce the total wall-plug power of the machine the wiggler current has been reduced by $\approx 25\%$. This gives $\approx 5\%$ field reduction and allows to save $\approx 1MW$ of total wall-plug power with respect to the last KLOE run, corresponding to $\approx 100\ kEuro/month$ at 2007 prices. Besides, the reduced wiggler field produces a negligible effect on the damping times, improves the ring energy acceptance, reduces the non linear terms contribution in the tune shift on energy dependence and is compatible with the operation of the x-ray beam line being the critical energy and the photon flux reduced only by $\approx 5\%$ and $\approx 10\%$ respectively.

During the luminosity adiabatic tuning the main ring working points (asymmetric at DAΦNE) have been progressively moved toward the integer $\nu^-_{x,y} = 5.086, 4.156- > 5.076, 4.140$, $\nu^+_{x,y} = 5.109, 4.192- > 5.096, 4.168$ to reduce the beam transverse size growth driven by the beam-beam interaction at high current, confirmed by experimental evidence and theoretical simulation.

The ICEs in the e^- ring wiggler chambers were removed since they were responsible for a factor 2 higher beam coupling impedance measured in the DAΦNE e^- ring with respect to the e^+ one ($Z/n = 1.1\Omega$ and $Z/n = 0.54\Omega$ respectively). This difference produced several observed detrimental effects on the e^- ring beam dynamics and collider luminosity as well. The e^- bunch length was 30% longer than the e^+ one causing a geometric luminosity reduction due to the hourglass effect. For such a longer bunch synchro-betatron beam-beam resonances, due to the collision scheme based on crossing angle, were more harmful. Single bunch instabilities, mainly longitudinal quadrupole oscillations driven by the beam coupling impedance, appeared at lower bunch current in the e^- ring. Transverse beam size blow-up, mainly in the vertical plane, has been observed beyond the microwave instability threshold. Beam measurements taken during commissioning confirmed that the e^- beam dynamics, after ICEs removal,is almost comparable to that of the e^+ beam. The e^- bunch length is $25 \div 30\%$ shorter (see Fig. 6) and there is no evidence of quadrupole instability threshold neither vertical beam blow-up at the operating bunch current ($\approx 15mA$).

Since the first phase of the FINUDA run commissioning the e^+ beam showed a threshold in the maximum storable current due to a fast horizontal instability depending on the current and on the beam fill pattern, compatible with an e-cloud driven instability. The phenomenon had been observed even during KLOE data-taking with 1.4 A current threshold in collision. During FINUDA operation the threshold seemed to be much more harmful. Starting from $\approx 0.4\ A$ the limit progressively increased by improving the injection procedure and the feedback systems. Injection optimization was aimed at reducing the oscillation amplitude of the stored beam by moving the e^+ orbit closer to the injection septum, reducing strength and length (150 ns to 90 ns) of the injection kicker pulse, and tuning the phase advance between the injection kickers, by means of the newly installed BPMs with turn by turn orbit measurement capability. The new feedback systems are based on a digital signal processing relying on a programmable gate array. They showed enhanced diagnostics and remotization capabilities, could manage any betatron and synchrotron tune, did not require specific phase advance between pick-ups and kickers, and were much less sensitive to the injection oscillation transients. The new hardware has been implemented progressively for the two rings transverse feedbacks, giving a relevant contribution to the transverse beam dynamics control and to the enhancement of the e^+ maximum storable current.

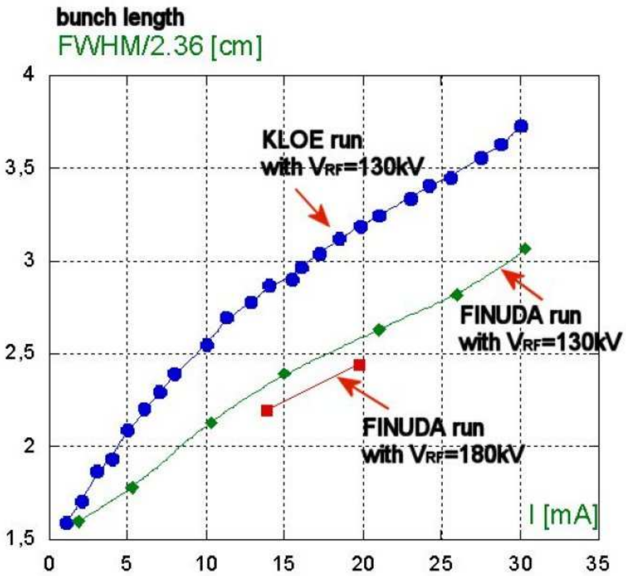

Figure 6: *Bunch length measurement before and after the ICE removal.*

Since the first two months of operation the luminosity has been significantly higher than during the previous 2003÷2004 FINUDA run, as shown in Tab. 1. The peak luminosity measured by the FINUDA detector has been almost doubled; correspondingly the maximum monthly integrated luminosity has been increased by a factor ≈ 3. This large gain is a direct consequence of the several implemented upgrades. The daily and total integrated luminosities since October 2006 are shown in Fig. 7.

An improvement can be noticed even with respect to the last KLOE run, with a peak luminosity increased by few percent, althogh the low beta parameters have not been pushed to the lowest possible values, due to the short time available for machine studies and tuning. Moreover, this result has been obtained by putting in collision lower currents and less bunches. This gain can

Table 1: DAΦNE luminosity performances and low-β parameters during the last runs.

	FINUDA Oct 03÷Mar 04	KLOE May 04÷Nov 05	FINUDA Nov 06÷Jun 07
L_{peak} $[cm^{-2}s^{-1}]$	0.85	1.53	1.6
$L_{\int day}^{MAX}$ $[pb^{-1}]$	3.9	9.8	9.4
$L_{\int month}^{MAX}$ $[pb^{-1}]$	65	209	226
$I_{coll}^{-\ MAX}$ $[A]$	1.1	1.4	1.5
$I_{coll}^{+\ MAX}$ $[A]$	1.0	1.2	1.1
$n_{bunches}$	100	111	106
$L_{\int logged}$ $[fb^{-1}]$	0.192	2.0	0.966
β_x^* $[m]$	2.33	1.5	2.0
β_y^* $[m]$	0.024	0.018	0.019
ϵ_x $[10^{-6}\ m \cdot rad]$	0.34	0.34	0.34
κ [%]	0.3	0.3	0.3

be ascribed to the higher geometric luminosity due to the ICEs removal. A $\approx 8\%$ gain in terms of maximum monthly integrated luminosity has been also obtained due to the higher collider uptime ($> 80\%$), to the subsystems maintenance and upgrade performed in the 2006 shutdown, and to the longer beam lifetimes obtained from the wires for BBLR compensation installed in both interaction regions. The background rate seen by the FINUDA detector has been progressively reduced, by tuning the collider optics and adjusting the collimators, and made lower with respect to the 2003-2004 FINUDA run. Due to the higher luminosity and uptime and to the lower background the delivered luminosity and the statistical sample acquired by FINUDA have been 5 and 7 times larger with respect to the previous run in approximately the same data-taking time. Moreover these results have been obtained with $\approx 30\%$ reduction in the wall-plug power.

4 Year 2007 activites: the crabbed waist collision scheme and its application to DAΦNE

In high luminosity colliders with standard collision schemes the key requirements to increase the luminosity are: the very small vertical beta function β_y at the IP, the high beam intensity I, the small vertical emittance ϵ_y and the large horizontal beam size σ_x and horizontal emittance ϵ_x required to minimize beam-beam effects. However, β_y can not be smaller than the bunch length σ_z without incurring in the hour-glass effect and it is very difficult to shorten the bunch in a high current ring without exciting instabilities. Moreover, high current implies high beam power losses, beam instabilities and a remarkable enhancement of the wall-plug power.

In the recently proposed Crabbed Waist (CW) scheme of beam-beam collisions a substantial luminosity increase can be achieved without bunch length reduction and with moderate beam currents. In this novel approach the hour-glass effect is avoided by shortening the length of the two-beams overlap spot by means of an increase of the crossing angle and a reduction of the horizontal beam size at the IP, as sketched in Fig. 8. The potential luminosity improvements have pushed several accelerator teams to study and consider the implementation of this scheme

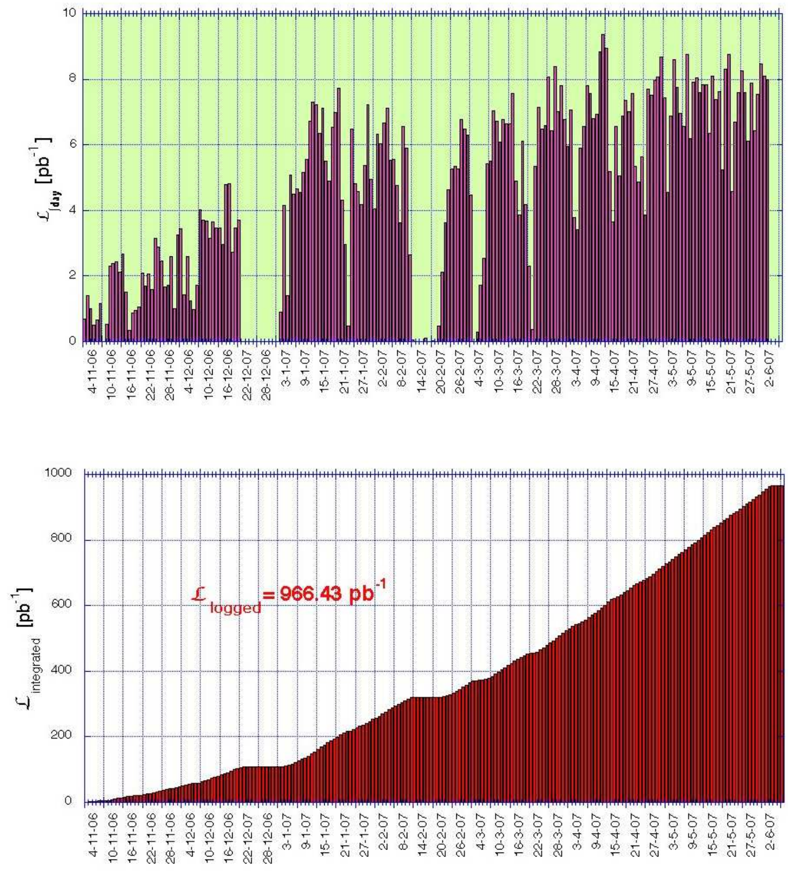

Figure 7: *Daily and total integrated luminosity during the 2006 FINUDA run.*

on their machines. In particular, the upgrade of DAΦNE is aimed at increasing its luminosity up to 10^{33} $cm^{-2}s^{-1}$ to be compared with $1.6 \cdot 10^{32}$ $cm^{-2}s^{-1}$ obtained during the last DAΦNE run for the FINUDA experiment. Besides, the physics and the accelerator communities are discussing a new project of a Super B-factory with luminosity as high as $10^{36} cm^{-2}s^{-1}$, i.e. by about two orders of magnitude higher with respect to that achieved at the existing B-factories at SLAC and KEK. The decision on the Super B-factory construction will depend much on the results of the CW collision tests at DAΦNE. The first crabbed waist collisions have been obtained recently at the beginning of 2008, during the SIDDHARTA experiment run.

In addition to preventing the hour glass effect, the Crabbed Waist scheme of beam-beam collisions combines several other potentially advantageous ideas. The first one is large Piwinski angle. For collisions under a crossing angle θ the luminosity L and the horizontal ξ_x and vertical ξ_y tune shifts scale as:

$$L \propto \frac{N\xi_y}{\beta_y} \propto \frac{1}{\sqrt{\beta_y}} \tag{1}$$

$$\xi_y \propto \frac{N\sqrt{\beta_y}}{\sigma_z\theta}; \tag{2}$$

$$\xi_x \propto \frac{N}{(\sigma_z\theta)^2} \tag{3}$$

The Piwinski angle ϕ is a collision parameter defined as:

$$\phi = \frac{\sigma_z}{\sigma_x}\tan\left(\frac{\theta}{2}\right) \approx \frac{\sigma_z}{\sigma_x}\frac{\theta}{2} \tag{4}$$

with N being the number of particles per bunch. Here we consider the case of flat beams, small horizontal crossing angle $\theta << 1$ and large Piwinski angle $\phi >> 1$.

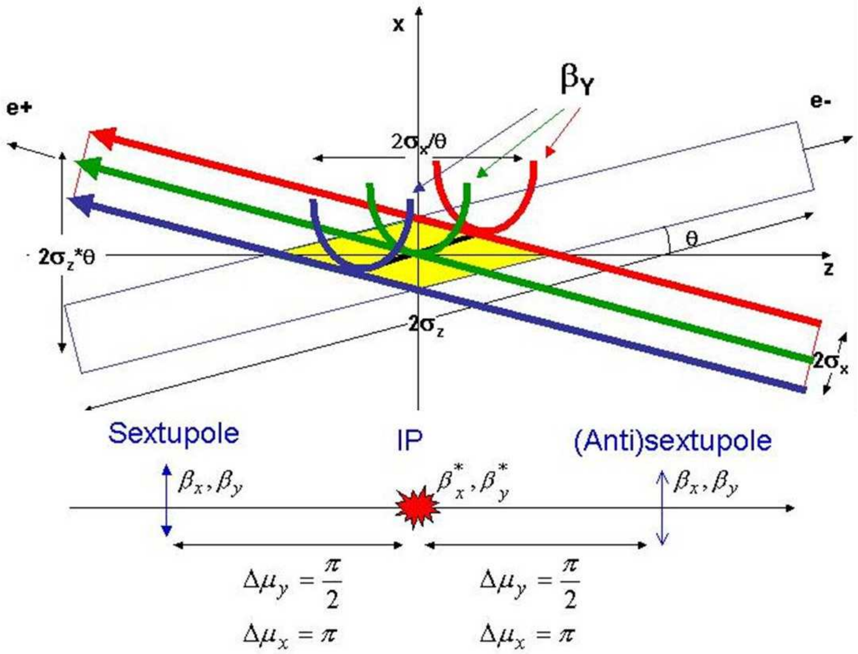

Figure 8: *Crab waist scheme*

In the CW scheme described here, the Piwinski angle is increased by decreasing the horizontal beam size and increasing the crossing angle. In such a case, if it were possible to increase N proportionally to $\sigma_z\theta$, the vertical tune shift ξ_y would remain constant, while the luminosity would grow proportionally to $\sigma_z\theta$. Moreover, the horizontal tune shift ξ_x would drop like $1/\sigma_z\theta$. However, the most important effect is that the length of the overlap area of the colliding bunches is reduced, as it is proportional to σ_x/θ(see Fig. 8). Then, the vertical beta function β_y can be made comparable to the overlap area size (i.e. much smaller than the bunch length):

$$\beta_y \approx \sigma_x/\theta << \sigma_z \tag{5}$$

We get several advantages in this case:

- Small spot size at the IP, i.e. higher luminosity L.
- Reduction of the vertical tune shift ξ_y.
- Suppression of synchrobetatron resonances.

There are also additional advantages in such a collision scheme: there is no need to decrease the bunch length to increase the luminosity as proposed in standard upgrade plans for B- and Φ-factories. This will certainly help solving the problems of HOM heating, coherent synchrotron radiation of short bunches, excessive power consumption etc. Moreover, parasitic collisions (PC) become negligible since with higher crossing angle and smaller horizontal beam size the beam separation at the PC is large in terms of σ_x. However, large Piwinski angle itself introduces new beam-beam resonances which may strongly limit the maximum achievable tune shifts. At this point the crabbed waist transformation enters the game boosting the luminosity, mainly because of the suppression of betatron (and synchro-betatron) resonances arising (in collisions without CW) through the vertical motion modulation by the horizontal oscillations. The CW vertical beta function rotation is provided by sextupole magnets placed on both sides of the IP in phase with the IP in the horizontal plane and at $\pi/2$ in the vertical one (see Fig. 8). A numerical example of the resonance suppression is shown in Fig. 9.

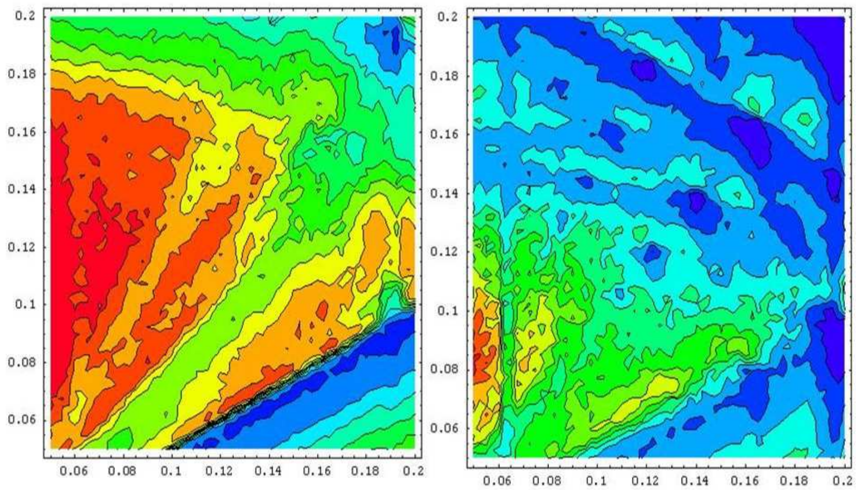

Figure 9: *Luminosity tune scan (ν_x and ν_y from 0.05 to 0.20). CW sextupoles on (left), CW sextupoles off (right). Chromatic scale is from blue (low luminosities) to red (high lumonosities)*

In order to estimate the achievable luminosity in DAΦNE with the crabbed waist scheme and to investigate distribution tails arising from beam-beam collisions, which may affect the beam lifetime, simulations with the code LIFETRAC have been performed. The beam parameters used for the simulations are summarized in Tab. 2. For comparison, the parameters used during the last DAΦNE run with the KLOE detector (2005-2006) are also shown. As discussed above, in order to realize the crabbed waist scheme in DAΦNE, the Piwinski angle ϕ should be increased and the beam collision area reduced: this is achieved by increasing the crossing angle θ by a factor 1.5

Table 2: Beam parameters for KLOE (2006) and SIDDHARTA (2008) runs.

PARAMETERS	KLOE Run	SIDDHARTA Run
$L\ [cm^{-2}s^{-1}]$	$1.5 \cdot 10^{32}$	$> 10^{33}$
$N_{bunches}$	110	110
$N_{part}/bunch$	$2.65 \cdot 10^{10}$	$2.65 \cdot 10^{10}$
$I_{bunch}\ [mA]$	13	13
$\epsilon_x\ [10^{-9}\ m \cdot rad]$	300	200
$\epsilon_y\ [10^{-9}\ m \cdot rad]$	1.5	1
$\sigma_x\ [\mu m]$	700	200
$\sigma_y\ [\mu m]$	$15\ (blow-up)$	2.4
$\sigma_z\ [mm]$	25	20
$\beta_x^*\ [m]$	1.5	0.2
$\beta_y^*\ [mm]$	18	6
$\theta\ [mrad]$	2×16	2×25

and reducing the horizontal beam size σ_x. In this scheme the horizontal emittance ϵ_x is reduced by a factor 1.5, and the horizontal beta function β_x lowered from 1.5 to 0.2 m. Since the beam collision length decreases proportionally to σ_x/θ, the vertical beta function β_y can be also reduced by a factor 3, from $1.8cm$ to $0.6cm$. All other parameters are similar to those already achieved at DAΦNE.

Using the parameters of Tab. 2 and taking into account the finite crossing angle and the hourglass effect, a luminosity in excess of $1.0 \cdot 10^{33} cm^{-2}s^{-1}$ is predicted with the beam current values already achieved during the KLOE run, which corresponds to an improvement of a factor of ≈ 6 with respect to the highest value ever measured at DAΦNE of $1.6 \cdot 10^{32} cm^{-2}s^{-1}$. The only parameter that seems to be critical for a low energy machine is the high vertical tune shift: $\xi_y = 0.08$, to be compared with the value of 0.03 so far obtained at DAΦNE. In order to check whether these tune shifts (and the luminosity) are achievable luminosity tune scan simulations have been performed. Fig. 9 shows 2D luminosity contour plots in the tune plane for the crabbed waist collisions with the crabbing sextupoles on (left) and off (right), for comparison.

The color scale of the plot goes from blue (low luminosities) to red (high luminosities). For each plot 10 contour lines between the maximum and minimum luminosities are drawn. The two plots of Fig. 9 show that the area of the high luminosity region is much wider when crabbing sextupoles are turned on in the simulations, while many betatron resonances appear when they are turned off. The absolute luminosity values are higher in the crabbed waist collisions: a peak luminosity of $L_{max} = 2.97 \cdot 10^{33} cm^{-2}s^{-1}$ is foreseen against $L_{max} = 1.74 \cdot 10^{33} cm^{-2}s^{-1}$ in the case without CW. It should be noted that the worst luminosity value obtained with CW ($L_{min} = 2.5 \cdot 10^{32} cm^{-2}s^{-1}$) is still higher than the present luminosity record at DAΦNE. Without CW the lowest luminosity value drops by an order of magnitude, down to $L_{min} = 2.71 \cdot 10^{31} cm^{-2}s^{-1}$.

5 Year 2007 activites: DAΦNE upgrade installation and machine restart for the SIDDHARTA run

In order to exploit the potentiality of the novel crabbed waist collision scheme to increase the luminosity and to perform the first experimental test of the new approach which is of great interest for the whole accelerator physics community, during the 2007 shutdown DAΦNE has been upgraded to incorporate the new IRs before the start of the SIDDHARTA run. Other machine parts not directly related to the new collision scheme, such as injection kickers and shielded bellows, have been also upgraded or renewed.

The general layout of DAΦNE upgrade has been already shown in Fig. 2, while drawings of the upgraded (top) and old (bottom) IR1 are reported in Fig. 10.

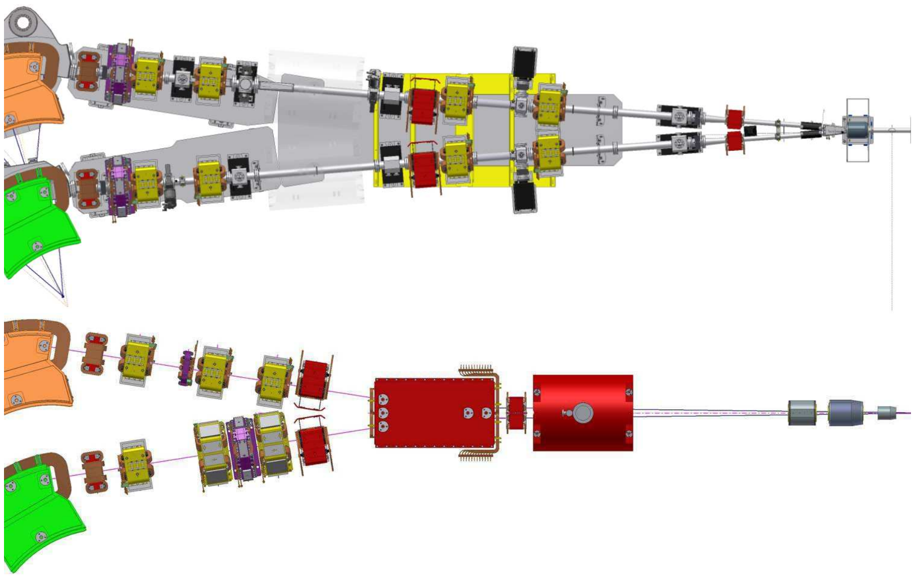

Figure 10: *DAΦNE IR1 after (top) and before (bottom) the crab waist upgrade*

The need to have a very small β_y (6 mm) and a large crossing angle (25 $mrad$ per beam) requires two new IR geometries. Due to the large crossing angle there is no more need for the splitter dipoles that have been in use at DAΦNE before, so they have been removed. The splitter removal implies a circumference reduction by $\approx 10^{-3}$. The three RF systems operating at DAΦNE (two on the main rings and one on the accumulator ring) need to be operated at correspondingly higher frequencies. The DAΦNE main ring and accumulator RF cavities are equipped with tuning plungers capable of covering the required frequency shift. On top of that, experimental tests performed at the end of the FINUDA run just before the shutdown have demonstrated the possibility of running the accumulator ring on a $\approx 10^{-3}$ shorter closed orbit without mechanical layout modifications. Therefore, machine operation with shorter orbits is transparent.

Defocusing and focusing (QD, QF) quadrupoles on both sides of the interaction point (IP) have been placed to obtain the required low-β structure. Further trajectory separation is pro-

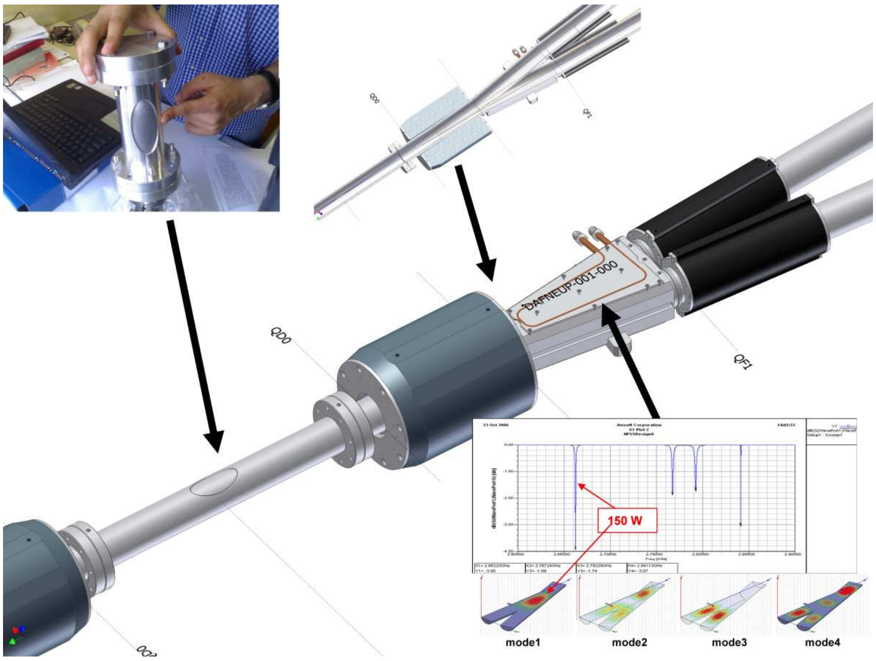

Figure 11: *IP1 chamber close-up view*

vided by two small dipole correctors upstream and downstream the quadrupole doublets, while other three quadrupoles are used to match the betatron functions in the arcs. The low-β section quadrupoles near the IP are of permanent magnet (PM) type. The QDs are located near the IP where the beams share a common vacuum chamber, while the QFs are positioned where the chambers are splitted and each one acts on a single beam. Therefore a total of two QDs and four QFs is required to get the two doublets around IP1. The characteristics of the permanent quadrupole magnets are given in Tab. 3. A close-up of the near IP1 region is shown in Fig. 11.

Four corrector dipoles provide a deflection of 9.5 $mrad$ to match the inlet and outlet arc chamber flanges. Sextupoles for the crab waist are placed at 9.3 m from the IP1. Bending dipoles facing the IRs have been rotated and their field adjusted according to Tab. 4. They have been powered with independent supplies to match these requirements. Solenoid compensator magnets have not been installed for the SIDDHARTA experiment because there is no detector solenoid at the IP; anyway, the new layout allows to reinstall the solenoid compensators for future KLOE and FINUDA runs.

Most vacuum chambers and pumps have been reused. For the SIDDHARTA experiment a new aluminium alloy (AL6082T6) chamber with two thin windows (0.3 mm 0.02 thickness) in the top and bottom sides has been designed and built (see Fig. 11). In the Y-chamber junctions, the regions where the two separate ring pipes merge in the common vacuum chamber near the IP, e.m. simulations have shown the presence of trapped modes, which add resonant contributions to the beam coupling impedance. In the worst possible scenario, that occurs when a beam spectrum line at a frequency equal to a multiple to the bunch repetition rate is in full coupling, the joule loss does not exceed 200 W. To keep this effect under control, the Y-chambers have been equipped

Table 3: low-β PM quadrupoles specifications.

Designation	QD	QF
Quantity	2	4
Minimum clear inner radius (mm)	33	30
PM inner radius (mm)	34	30.5
Maximum outer radius (mm)	100	45
Magnetic length (mm)	230	240
REM physical length (mm)	230	240
Maximum mechanical length (mm)	240	250
Nominal gradient (T/m)	29.2	12.6
Integrated gradient (T)	6.7	3.0
Good field region radius (mm)	20	20
Integrated field quality —dB/B—	$5.00E-04$	5.00E-04
REM stabilization temperature (C)	150	150
Magnet material type	$SmCo2:17$	$SmCo2:17$
Magnet construction	2 *halves*	2 *halves*

Table 4: Bending Dipoles Adjustment.

Dipole name	Rotation angle (deg)	Bending radius(mm)
Sector Long	$+2.19$	1528.11
Sector Short	-2.19	1269.76

with cooling pipes as shown in Fig. 11. This additional cooling circuit allows both to remove the beam induced HOM heating and, if necessary, to reduce it by detuning the mode frequencies with respect to the dangerous beam spectrum lines. Horizontal collimators are placed at 8 m from the IP.

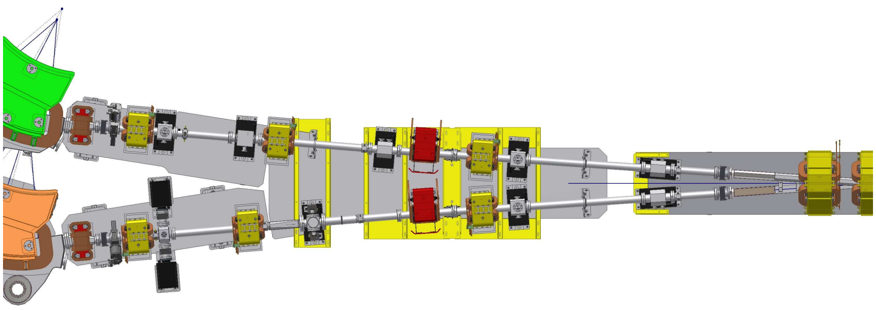

Figure 12: *Layout of the renewed IR2*

Similar modifications were made in the second interaction region (IR2), where the beams will not experience a lowβ insertion and will be vertically separated in order to avoid parasitic collisions. A layout of half IR2 is presented in Fig. 12, while the original layout before the recent modifications was very similar to the old IR1 section shown in Fig. 10. There are not sextupoles for crab waist in the IR2 magnet layout, and three large aperture electromagnetic quadrupoles replacing the permanent magnet quadrupole doublets located in the IR1. A new design of the central IR2 beam pipe, where the two beams are vertically separated, is shown in Fig. 13. The two vacuum chambers are completely separated and their cross section has an half moon profile.

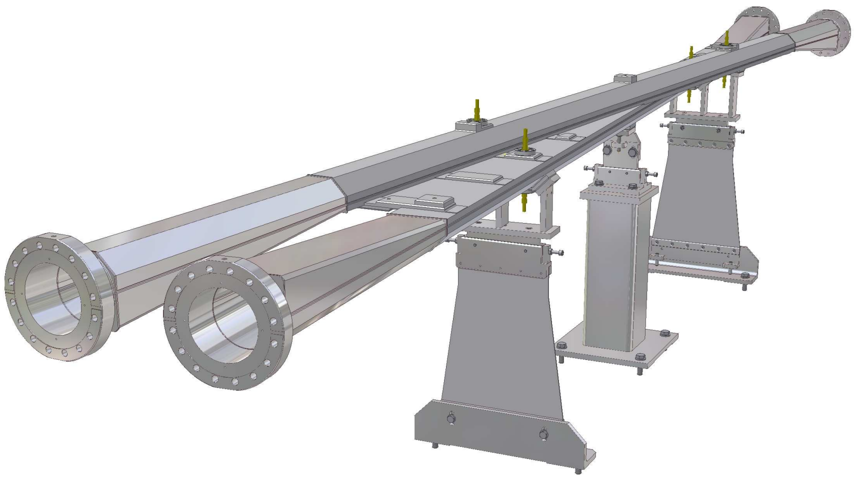

Figure 13: *New IR2 beam pipe for vertically separated beams*

In order to keep the beam coupling impedance low, the total number of bellows has been reduced to the minimum strictly needed to compensate the thermal strain and mechanical misalignment. In each crossing region only 4 bellows per beam are used. The technology of copper-beryllium strips has been adopted optimizing the cost and the shielding performance. The working axial stroke is 7 mm and the radial offset 3 mm. A section view of the bellows is shown in Fig. 14.

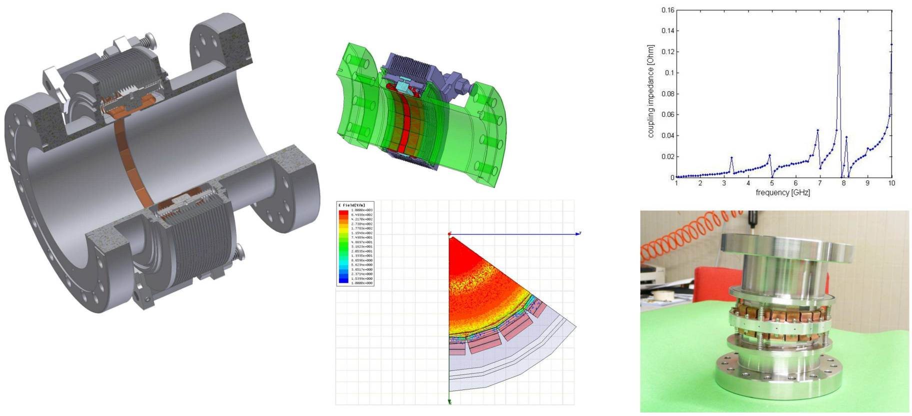

Figure 14: *New shielded bellows*

New injection kickers have been designed, built and installed. The design is based on a tapered strip inside a rectangular vacuum chamber cross section (see Fig. 15), in order to simultaneously:

- improve the deflecting field quality obtaining a uniform horizontal deflection as a function of the horizontal coordinate;
- reduce the beam coupling impedance by means of the tapered transition between the beam pipe and the kicker structure;
- have a uniform beam pipe cross section between the dipole region and the kickers region. This also reduces the total beam coupling impedance of the machine;
- obtain a better matching between the generator and the kicker structure at high frequency. This can avoid multiple reflections of the deflecting pulse in the kicker structure that can perturb the stored bunches. Moreover it allows extracting all the power released to the HOM of the structure by the beam.
- obtain a short pulse ($\approx 6\ ns$) by driving the stripline kickers with novel HV fast pulsers which are now available on the market.

Special 50 kV feed-throughs have been integrated in the device after being successfully tested on the bench.

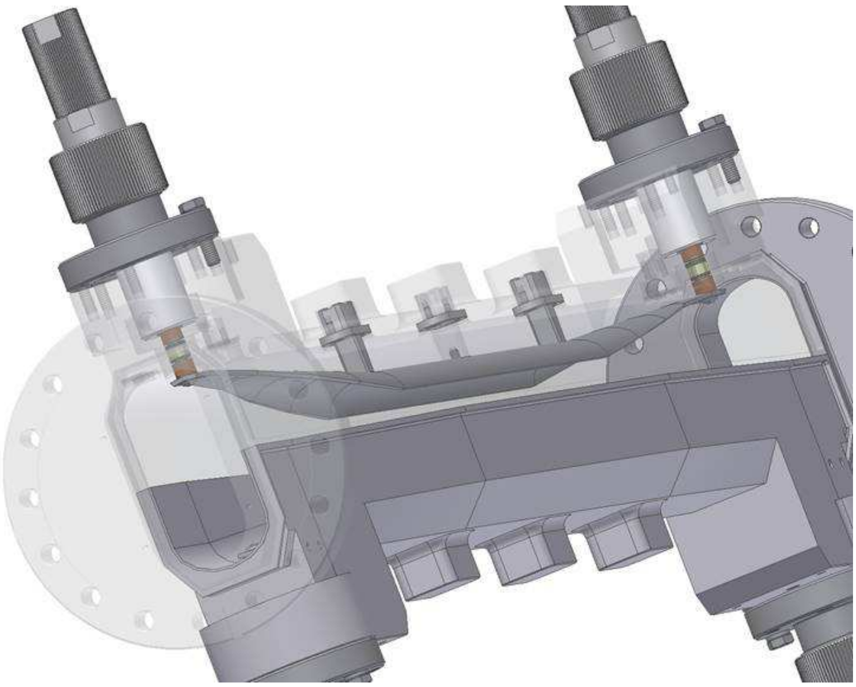

Figure 15: *New stripline based injection kickers*

A 3D CAD image of the DAΦNE IR1 equipped with the SIDDHARTA detector is shown in Fig. 16. The machine luminosity monitor is composed by three different devices: small angle Bhabha tile calorimeter subdivided into 20 sectors (30 *degrees* each) made of alternating lead and scintillating tiles, covering a vertical acceptance between 17.5 and 27 *degrees*; a GEM tracker placed in front of the tile calorimeters for redundant measurements of Bhabha events and background rejection; two single bremsstrahlung gamma detectors.

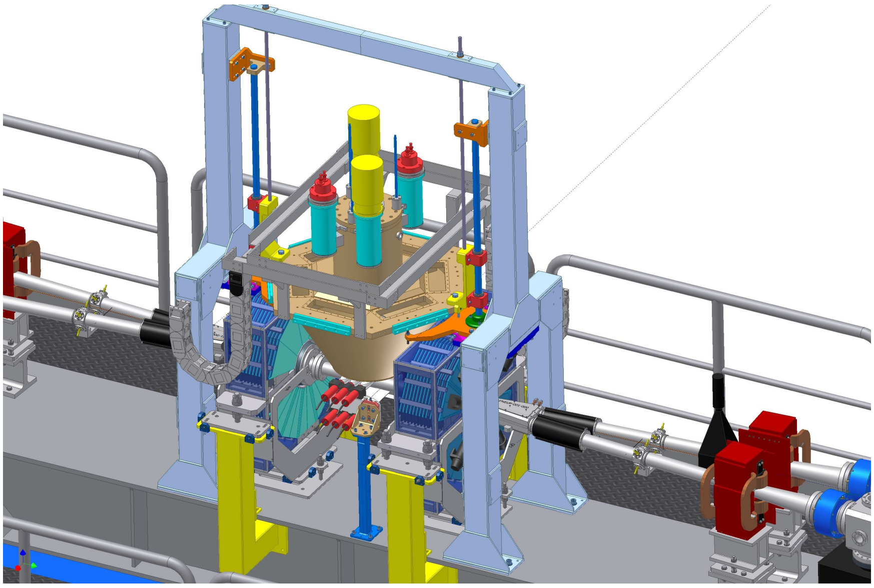

Figure 16: *DAΦNE IR1 equipped with the SIDDHARTA detector: CAD view.*

6 Present Status and Future Plans

The upgraded machine commissioning started in November 2007. At the end of the year the ring vacuum was almost recovered, the beams were stored in the upgraded rings, all the sub-systems (injection, RF, feedback and diagnostics, ...) went rapidly to regime operation.

The first collisions in the crabbed waist scheme have been obtained in February 2008, with the first experimental confirmation of the potentiality of the new configuration in terms of specific luminosity growth and reduction of the beam-beam disruption effects. However, the machine operation is still limited by other effects such as positron beam instabilities, short lifetimes of both beams, vacuum in e^- RF cavity, detector background, and presently the DAΦNE team is working on all these aspects the to get close to the SIDDHARTA run expected performances.

Meanwhile, proposals of KLOE and FINUDA future runs to exploit the crabbed waist luminosity increase are in preparation, and decisions are expected before the end of the present SIDDHARTA run.

7 Publications

1. C. Milardi, D. Alesini, S. Bettoni, M.E. Biagini, C. Biscari, R. Boni, M. Boscolo, B. Buonomo, A. Clozza, G. Delle Monache, T. Demma, E. Di Pasquale, G. Di Pirro, A. Drago, A. Gallo, A. Ghigo, S. Guiducci, P. Iorio, C. Ligi, F. Marcellini, C. Marchetti, G. Mazzitelli, L. Pellegrino, M. Preger, L. Quintieri, P. Raimondi, R. Ricci, U. Rotundo, C. Sanelli, M. Serio, F. Sgamma, B. Spataro, A. Stecchi, A. Stella, S. Tomassini, C. Vaccarezza, M. Zobov (INFN/LNF, Frascati, Italy); E. Levichev, S. Nikitin, P. Piminov, D. Shatilov (BINP, Novosibirsk, Russia); J. Fox, D. Teytelman (SLAC, Menlo Park, CA, USA): "DAΦNE Setup and Performances During the Second FINUDA Run", Proceedings of PAC07, Albuquerque, New Mexico, USA p.1457.

2. S. Bettoni, S. Guiducci, M.A. Preger, P. Raimondi, C. Sanelli (LNF/INFN, Frascati, Italy): "Reduction of the Non-Linearities in the DAΦNE Main Rings Wigglers", Proceedings of PAC07, Albuquerque, New Mexico, USA p.1463.

3. M. E. Biagini, D. Alesini, D. Babusci, S. Bettoni, R. Boni, M. Boscolo, F. Bossi, B. Buonomo, A. Clozza, G. Delle Monache, T. Demma, G. Di Pirro, A. Drago, A. Gallo, S. Guiducci, C. Ligi, F. Marcellini, G. Mazzitelli, C. Milardi, F. Murtas, L. Pellegrino, M. Preger, L. Quintieri, P. Raimondi, R. Ricci, U. Rotundo, C. Sanelli, G. Sensolini, M. Serio, F. Sgamma, B. Spataro, A. Stecchi, A. Stella, S. Tomassini, C. Vaccarezza, M. Zobov (INFN/LNF, Frascati, Italy); K. Ohmi (KEK, Ibaraki, Japan); I. Koop, E. Levichev, P. Piminov, D. Shatilov, V. Smaluk (BINP, Novosibirsk, Russia): "DAΦNE Φ-Factory Upgrade for Siddharta Run", Proceedings of PAC07, Albuquerque, New Mexico, USA p.66.

4. P. Raimondi, M. Zobov (INFN/LNF, Frascati, Italy); D. Shatilov (BINP, Novosibirsk, Russia): "Beam-Beam Simulations for Particle Factories with Crabbed Waist"', Proceedings of PAC07, Albuquerque, New Mexico, USA p.1469.

5. M.E. Biagini, P. Raimondi, M. Zobov (LNF/INFN, Frascati, Italy); K. Ohmi, Y.Funakoshi (KEK, Tsukuba, Japan): "'Beam-beam Effects in Crab Crossing and Crab Waist Schemes", Proceedings of PAC07, Albuquerque, New Mexico, USA p.1493.

6. S. Tomassini, D. Alesini, A. Beatrici, A. Clozza, E. Di Pasquale, M. Esposito, G. Fontana, F. Marcellini, G. Mazzitelli, M. Paris, P. Raimondi, G. Sensolini, C. Sanelli, F. Sgamma, M. Troiani, M. Zobov, A. Zolla (INFN/LNF, Frascati, Italy):"DAΦNE Upgrade: A New Magnetic and Mechanical Layout", Proceedings of PAC07, Albuquerque, New Mexico, USA p.1466.

7. F. Marcellini (LNF/INFN, Frascati, Italy): "Design and E. M. Analysis of the New DAΦNE Interaction Region", Proceedings of PAC07, Albuquerque, New Mexico, USA p. 3988.

8. M. Boscolo, M. Biagini, S. Guiducci, P. Raimondi (INFN/LNF, Frascati, Italy): "Touschek Background and Beam Lifetime Studies for the DAΦNE Upgrade", Proceedings of PAC07, Albuquerque, New Mexico, USA p.1454.

9. P. Raimondi, M. Zobov (LNF/INFN, ITALY); E. Levichev, P. Piminov (BINP, Novosibirsk, Russia): "Beam-Beam Issues for Colliding Schemes with Large Piwinski Angle and Crabbed Waist", LNF-07-3(IR), 29/01/2007.

10. P. Raimondi, M. Zobov (LNF/INFN, Italy); D. Shatilov (BINP, Novosibirsk, Russia): "Dynamic Aperture Optimization for the DAΦNE Upgrade", LNF-07-15(IR), 05/07/2007.

The DAΦNE Beam Test Facitily (BTF)

The BTF Staff: B. Buonomo (Art.23), G. Mazzitelli (Resp.), L. Quintieri (Art.23), P. Valente

The DAΦNE Operation Staff: G. Baldini, A. Beatrici, M. Belli, B. Bolli, G. Ceccarelli, R. Ceccarelli, A. Cecchinelli, S. Ceravolo, R. Clementi, O. Coiro, S. De Biase, M. De Giorgi, N. De Sanctis, M. Di Virgilio, G. Ermini, G. Fontana, C. Fusco, O. Giacinti, E. Grossi, F. Iungo, C. Marini, M. Martinelli, C. Mencarelli, E. Passarelli, V. Pavan, D. Pellegrini, R. Pieri, G. Piermarini, S. Quaglia, M. Sardone, M. Scampati, G. Sensolini, A. Sorgi, M. Sperati, A. Sprecacenere, R. Tonus, T. Tranquilli, M. Troiani, R. Zarlenga

The DAΦNE Technical Staff: R. U. Frasacco, F. Galletti, V. Lollo, A. Mazzenga, C. Mencarelli
The LNF Technical Staff: R.Sorchetti

1 Description of the DAΦNE BTF 2007 Activities

During 2007, national and international (mainly european) users have requested to the DAΦNE Beam Test Facility an overall beam time of about 225 days. In order to satisfy the different requirements of the hosted experiments, the BTF facility provided electrons, positrons and photons in a variable range of energy (25-750 MeV) and intensity (from single particle up to 10^{10} particles per pulse), always assuring a good beam quality[1] and an high duty cycle. In fact, thanks to the new pulsed dipole magnet, installed during 2006, the beam run time of BTF has became quite independent from the DAΦNE operation status, increasing the BTF duty cycle up to 90%.

2 2007 User Experiences

The experiments that have used the DAΦNE BTF during 2007 had mainly the objective of calibration, setup and response characterization of high energy detectors. Among all the test-beam and experiments hosted in 2007, in the following ones the BTF team has given a direct contribution:

LUMI: The Frascati e+e- collider DAΦNE , running at $\sqrt{s} = 1.02$ GeV is testing the crabbed waist scheme [1)], aiming to reach a large improvement of the specific and integrated luminosity of the accelerator. In order to have a reliable, fast and accurate measurement of the absolute luminosity a number of dedicated detectors have been designed, built, tested, calibrated and put into operation. In particular, three different monitors have been realized:

1. A couple of [back-to-back] medium-angle Bhabha calorimeters, realized with trapezoidal-shaped tiles, lead and scintillator read by WLS fibers subdivided in 10+10 ϕ sectors, covering $18° \leq \theta \leq 27°$; this detector has been optimised for detection of Bhabha events, maximising the rate [for providing fast feedback on luminosity during machine studies] and at the same time for enabling the measurement of the absolute luminosity with an uncertainty at the level of 10%. At the same time, the calorimeters have been designed in order to be positioned around the last low-β quadrupoles without interfering with the experimental setup mounted at the interaction point.
2. A couple of [back-to-back] Bhabha trackers covering the same angular range as the calorimeter, made of two semi-annular halves triple-GEM detectors, with a 4x16 pads

[1] The tipical beam spot size is of the order of σ=2 mm (both in x and y coordinates), 1% momentum resolution, with divergence that can be kept as small as 5 mrad.

readout each; the main purpose of this tracking device is to help in rejecting non-Bhabha events and in providing a better definition of the acceptance, thus reducing the systematic uncertainty due to the steep dependence of the Bhabha cross-section on the polar angle.

3. Two Bremsstrahlung proportional counters realized by four $PbWO_4$ crystals at small angle ($\sim$1.7 mrad), one on the electron and one on the positron beam-line. Even though these counters will suffer of high background levels due to gas- Bremsstrahlung photons and in general particles escaping the beam pipe, they are very useful since the counting rate is very high, while keeping a good relationship with the luminosity. They are then very useful during luminosity optimisation thanks to the very fast feedback.

In order to characterize the response of the calorimetric detectors and to calibrate and equalize the energy response of each of the 20 sectors, a campaign of data taking with a test electron beam at the Frascati Beam-Test Facility has been performed. Among the numerous measurements the most relevant tests were done checking:

1. the response of the calorimeter sectors at different impact points, both along the readout fiber coordinate and at different distance from the readout fibers;
2. the response of each sector as a function of the photomultipliers supply voltage;
3. the linearity with respect to the energy of impinging electrons;
4. the energy resolution as a function of the energy of impinging electrons;
5. the response to cosmic ray muons [minimum ionising particles];

In order to design and optimise the detectors, and to precisely estimate the acceptance of the detectors, so allowing the absolute luminosity measurement, a detailed Monte Carlo simulation has been developed, using the CERN Geant3 libraries, simulating:

- the full detector setup, including the three kind of modules and taking into account the response of the detectors at the digitisation stage;
- the beam line around the interaction region, including the effect of the magnetic fields inside the low-β permanent quadropoles;
- the presence of particles from the beams due to the Touscheck effect, thus inducing background to the signal;
- the signal cross-section, calculated in the appropriate angular and energy range according to the BHWIDE generator, of Bhabha, radiative Bhabha and $\gamma\gamma$ events.
- the effect of the discrimator thresholds and of the trigger logic on the determination of the luminosity from the acquired event rate.

The data acquisition system, capable of a several tens of kHz rate and capable of measuring the dead time with good accuracy, is based upon the KLOE experiment DAQ and acquires both the analog signal, fed into a charge ADC in order to measure the spectrum for each calorimeter sector, and the digitised one; fed into a TDC and a scaler for rate measurement. Into the TDC the digital signals from the pads of the GEM tracker are also acquired. The offline analysis of the acquired events allows to perform a number of essential checks like: the trigger efficiency, the topology of the acquired events, the threshold profile, the intercalibration of the sectors, the uniformity of the response, etc.

During the first phase of the DAFNE run the systems have been commissioned and started to provide a first estimate of the luminosity. Further studies are under way in order to reach the target accuracy on the absolute luminosity determination.

P326: The studies of the P326 group have been mainly on the choice of the layout of the "large angle veto" photon counters of the future $K^+ \rightarrow \pi^+\nu\bar{\nu}$ experiment. Those ring-shaped counters will guarantee an hermetic coverage [up to 50 mrad] for those photons escaping the acceptance of the main detector [the liquid-Kripton calorimeter]. The requirement of very good photon detection efficiency [$1 - 10^{-4}$ below 1 GeV] on one side and the need of having a cost-effective and practical system [from the point of view of design, building, installation, calibration and data-taking] has reduced the choice to three possibilities:

- Segmented rings, realized with trapezoidal sectors of lead/scintillator sandwiches; readout by wavelenght-shiftingfibers fed to green-sensitive photomultipliers;
- Partially overlapped half-rings [actually C-shaped to avoid dead areas], built with the "spaghetti"calorimeter techinique: thin lead foils with grooves, alternated to scintillating fibers layers; light-guides and blue-sensitive photomultipliers readout;
- Rings of several layers of lead-glass crystals, radially disposed in circular coronae and slightly staggered in order to avoid cracks: 5 layers should guarantee that at least 3 lead-glass crystals are hit by a photon with an incidence angle up to 50 mrad. Those crystals would be re-used from the barrel of the electromagnetic calorimeter of the OPAL experiment.In order to test all these three technologies, different prototypes have been tested with electrons and photons at the BTF:
- A 2/16 of a ring veto, built with the lead/scintillator tiles technique [built in Fermilab, USA by the former CKM collaboration];
- a C-shaped 'spaghetti" calorimeter, built by the LNF/Roma/Pisa P-326 groupsreadout at both sides by two 3x6 matrices of light-guides/photomultipliers.
- refurbished lead-glass crystals from the OPAL calorimeter.

The different tests, carried out using an ad-hoc tagging system for the incoming particles, indeed showed that a detection inefficiency at the level of [or better than] 10^{-4} for electrons of 200 MeV, 350 MeV and 500 MeV can be achieved for all the considered solutions. At the same time, measurement have been carried out in order to estimate the energy resolution [in the range of 10-15%/sqrt(E[GeV])] and time resolution [better than the required 1 ns].

Rap: The aim of the experiment RAP is to measure the longitudinal vibrations of cylindrical test masses, when electrons provided by the DAΦNE Beam Test Facility impinge on them and to investigate if the mechanism of the particle energy loss conversion into mechanical energy depends on the conduction state of the bar. During 2007 measurement campaign in BTF, data for the superconducting aluminum bar down to 540 mK have been collected. This has been possible thanks to the $^3He - ^4He$ dilution refrigerator installed inside the Rap cryostat. The experimental results confirmed that the amplitude of the longitudinal oscillation depends on the conduction state of the material. Furthermore as predicted, there is a trend to a raising of the bar oscillation amplitude in superconducting state going down in temperature. A not explained quite complicated structure of the amplitude near the transition temperature has been observed.

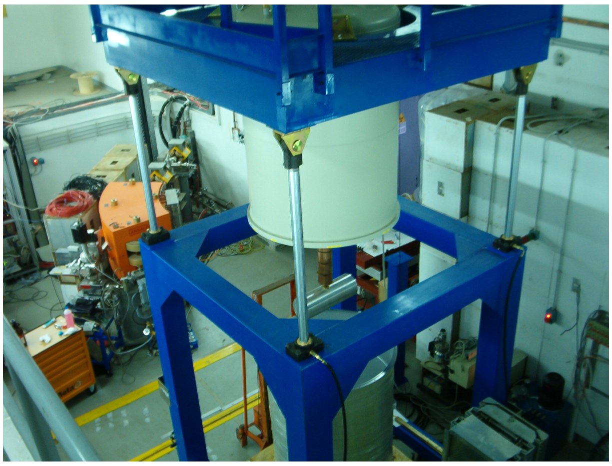

Figure 1: RAP Installation in BTF during 2007 data taking

3 Installation of a Radiation Shield around the BTF Target

At the DAΦNE BTF the reduction of the particle multiplicity is achieved in the following way: first the LINAC beam is intercepted by a (variable depth) copper target in order to degrade the beam energy, then the outcoming particles are energy selected by means of a bending magnet and slit system. The degrader target is shaped in such a way that three different radiation lengths (1.7, 2 and 2.3 X_0 respectively) can be selected by inserting it at different depths into the beam-pipe.

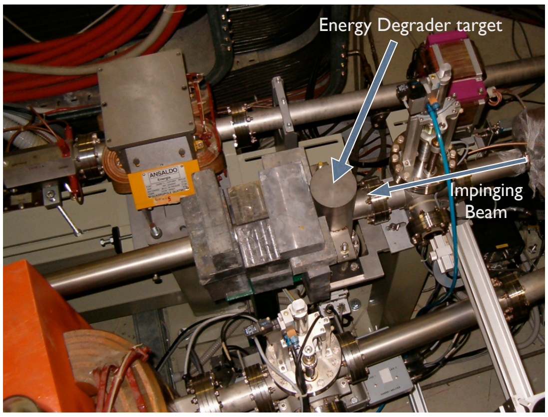

Figure 2: *Energy Degrader Target collocation on the BTF transfer line*

Figure 3: *BTF copper target: in this picture it is completely kept away from the beam pipe*

Because of the interaction of the impinging e^+/e^- beam in the copper target, this one becomes a source of secondary radiation: gamma rays, secondary electrons and positrons (essentially bremsstrtrahlung and pair production, Compton scattering and ionization) as well as hadrons produced by electromagnetic cascade such as neutrons, pions, protons (mainly due to photonuclear reactions).

3.1 Radiation Source Term Calculation

The estimation of the secondary particles produced in the BTF copper target has been obtained by the Monte Carlo FLUKA code [2], considering the following beam data: the particles impinging on the target are electrons having energy equal to 0.510 MeV (nominal DAΦNE energy), momentum spread equal to 0.0051 GeV/c, divergence equal to 1 mrad, beam width in transversal direction equal to 0.2355 cm.

In figure 4 the histogram gives the overall number of secondaries produced per unit beam particle in the BTF target. The corresponding energy spectra is reported in terms of particle fluence per unit energy and unit particle in figure 5.

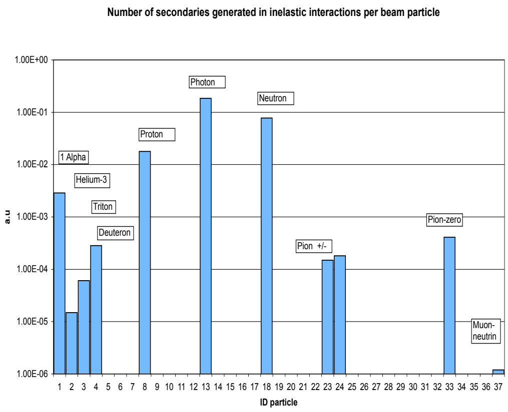

Figure 4: *Number of secondaries produced per beam particle*

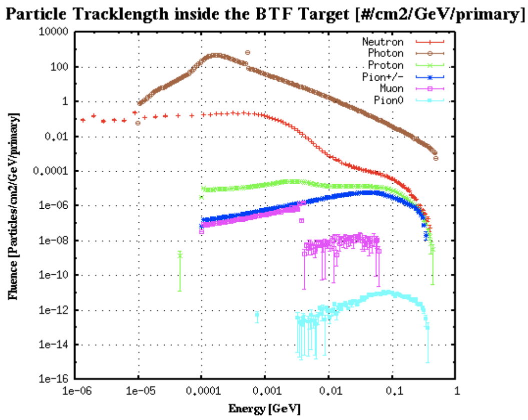

Figure 5: *Energy spectra of secondaries produced in the BTF Target*

In the BTF target case, the energy loss by ionization can be neglected with respect to the radiative energy loss (Bremsstrahlung). The energy spectrum of the radiated photons ranges from zero to the energy of the incident electrons and the number of photons in a given energy interval is approximately inversely proportional to the photon energy. As we expected for, the calculated bremsstrahlung spectra are noticeably more energetic (i.e "harder") at forward angles (see figure 6) respect to the other directions.

Neutron production is expected to occur in any material irradiated by electrons in which bremsstrahlung photons above the material-dependent threshold are produced. This threshold varies from 10 to 19 MeV for light nuclei and 4 to 6 MeV for heavy nuclei.The mechanisms of neutron production are only briefly recalled here: Giant Photonuclear Resonance neutrons (the most important source of neutron emission up to approximatively 30 MeV), Quasi-Deuteron neutrons (dominating at energies above the giant resonance), neutrons associated with the production of other particle (neutrons produced by secondary interactions of pions for example). For both Giant Resonance and Quasi-Deuteron process the directionality of the incident electron or photon is lost so that these emissions are isotropic (see figure 9).

As it is shown in figure 8, for energy less than 150 MeV the spectrum is described as a Maxwellian distribution with average energy around 1 MeV. Approaching the higher energies, the Quasi-Deuteron effect adds a tail of higher-energy neutrons to the Giant-Resonance spectrum. The slope becomes steeper as the incident electron energy is approached.

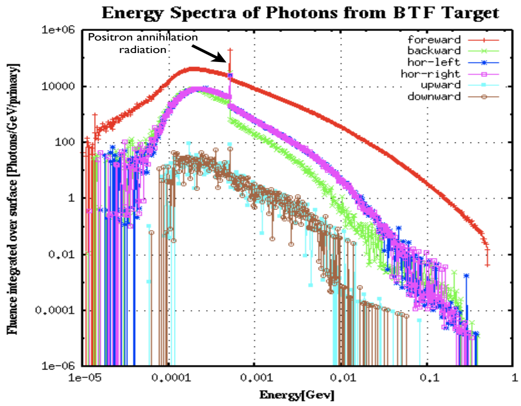

Figure 6: *Spectra of bremsstrahlung photons emerging in various direction from the BTF copper target irradiated by normally incident monoenergetic electron beams.The arrow indicates the abundant positron annihilation radiation at 0.511 MeV*

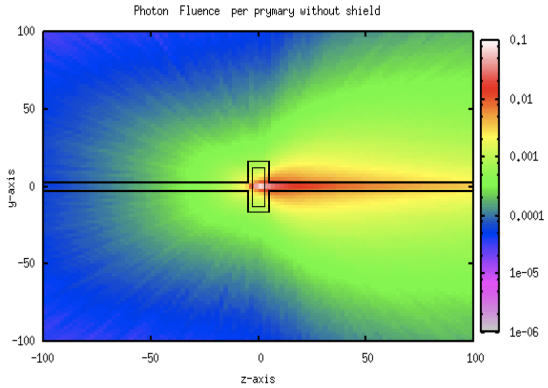

Figure 7: *Spacial distribution of photon fluence from BTF target (The unit on the plot is Photon/cm^2/primary). The beam is travelling on z axis (from left to right for the reader), whereas the y axis is the vertical one.*

3.2 BTF Target Shield Description

The necessity of shielding the energy degrader target of the DAΦNE BTF comes essentially from two exigencies:

1. To reduce the radiation damage of electronic and mechanical instrumentation located just around the BTF target
2. To reduce the background arriving in the BTF hall, where the experiment devices and appartus are placed for data taking

Concerning the second point it is important to stress that the shield around the target is not enough by itself alone to assure a low radiation background in the BTF hall, because the higher energy photon radiation is entering the beam-pipe mainly in the forward direction, so that it is necessary to intercept the radiation in a well suitable point along the transfer line. The complete BTF transfer line simulation by a Geant4 based application (BDSIM [3]) is still under development. At the end of this study we should be able to evaluate the background all around the transfer line, and consequently to determine where to locate other shields and how thick they have to be. Anyway the BTF shield is the starting point needed to guarantee a reduction of background in the BTF hall in the frame of a complete multiple step shielding design.

The limited room available around the target has been the more stringent boundary condition that we had to take into account in the shield design, in addition to the difficulty of acces in the area in which the target is placed, due to the concentration of many structural and instrumentations apparatus. The shield is composed of layers of different materials in order to create a modular structure that can be easily mounted and moved away around the target, once the support basement has been installed. The major difficulty during the installation was, in fact, mounting the stainless steel plate and columns to support the shield (se figure 10). The technicians of the accelerator division showed a great ability in moving very heavy plates (each one having a mass of about 40 kg), since they couldn't use any load displacer device, during the installation (ended on March 28).

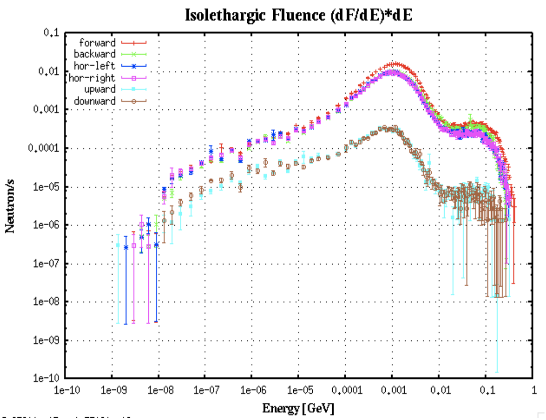

Figure 8: *Spectra of neutrons emerging in various direction from the BTF copper target irradiated by normally inicident monoenergetic electron beams*

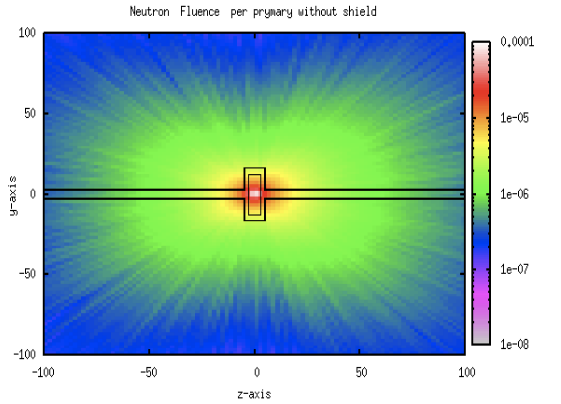

Figure 9: *Spacial distribution of neutron fluence from BTF target (Neutron/cm^2/primary). The beam is travelling on z axis (from left to right for the reader), whereas the y axis is the vertical one.*

The shield has been designed in order to reduce as much as possible[2], mainly, gamma and neutron fluxes coming from the BTF target, so that appropriate materials have been chosen according the following criteria:

1. High Z heavy materials are suitable for gamma rays shielding.
2. Hydrogenous material are needed for neutron moderation and to attenuate "fast" neutrons.
3. Boron planner sheets are chosen for thermal neutron capture (by means of the $^{10}B(n,\alpha)^7Li$ reaction with cross section for room temperature thermal neutrons of 3837 barns).

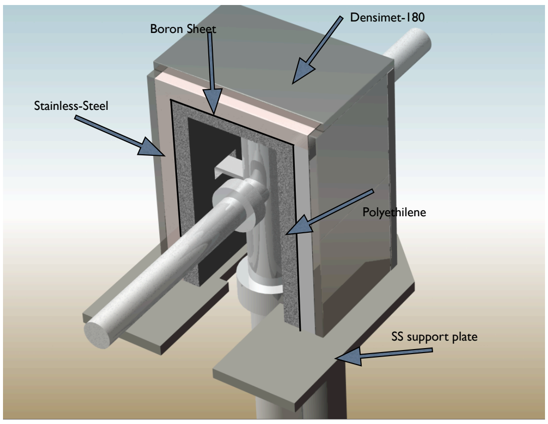

Figure 10: *BTF Target Shield Design: chosen materials (back view)*

Figure 11: *Target Shield installation (frontal view)*

[2] At least a reduction factor 50 in the neutron and photon fluence

As high Z heavy element a special Tungsten alloy, Densimet-180, has been chosen for the BTF target shield. In table 4 the main characteristics of this material are reported. This choice came from an accurate evaluation of the ratio benefits/coast of using Densimet-180 with respect to an alternative machined lead shield.

The Densimet-180 alloy is only little bit lighter than pure Tungsten (18.0 vs 19 g cm^{-3}) , but in spite it offers the main advantage that is as well machinable as a steel. The densimet layer is the external one (see figure 10) and has a thickness of 25 mm.

Densimet-180 Alloy			
Chemical Composition[%]		Nominal Density [g cm^{-3}]	Modulus of elasticity [GPa]
W	Rest		
90	Ni, Fe	18.0	380.

Polyethilene,$(CH_2)_n$ has been chosen as hydrogenous material. It is very effective for neutron shielding because of its hydrogen content (14% by weight) and its density (0.92 g cm^{-3}). The polyethilene layer consitues the inner layer and has a thickness of 40 mm.

Stainless steel is a relatively high density materials (7.8 g cm^{-3}), that thanks to its low cost is an attractive shielding material for gamma rays. Furthermore, iron (the main component of ss) is relatively good for slowing down fast neutrons by inelastic scattering and is a good absorber of thermal neutrons. The knowledge of the elemental composition is important about radioactivation estimation and it has been considered in the FLUKA calculation .

The stainless steel layer in the BTF shield has the double role of shielding material and structural leading structure, being rigidly bolted to the horizontal support plate. The steel layer has a thickness of 35 mm. The inner layer of polyethylene and the outer one of densimet are tighten with screws on the steel layer. Nowadays the polyethylene layer and boron sheets are not yet installed: this will be done soon after having received these materials (foreseen by end of April 2008).

The expected reduction of the photon and neutron are shown in figure 12 and 13 respectively, reported in terms of the fluence in a solid angle of $\pi/2$ around the beam axis in forward direction. The cut at higher energies in the plot of gamma ray spectra is due to the fact that after the target the more energetic gammas escape inside the beam pipe.

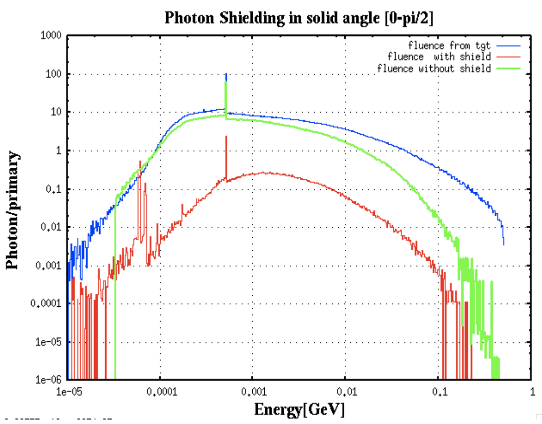

Figure 12: *Photon Shielding*

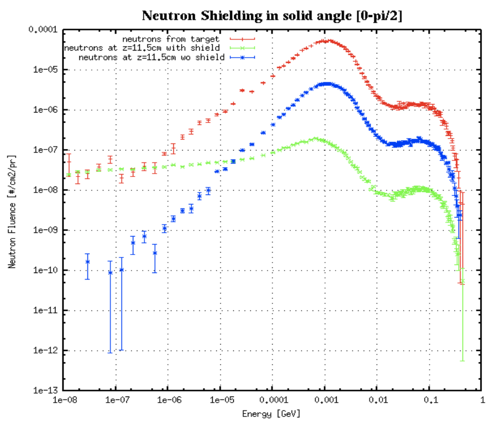

Figure 13: *Neutron Shielding*

Measurements of the doses due to gamma rays and neutron in a range of 1-2 m around the shielding are going to be taken during the next BTF runs, allocating 7 dosemeters for gamma rays

(Calcium Fluoride thermoluminescence detectors) and 7 particle detectors (Cr-39 detectors) based fast neutron plastic dosemeters, sensitive in the 0.1 - 20 MeV energy interval. These experimental value will be compared with the predictions in order to validate the FLUKA model used for the estimation

4 Feasibility Study of a Neutron Source at the DAΦNE BTF Facility

Since the old safety limit of 10^3 e^-/s (or e^+/s) as maximum admissible beam in BTF has been removed by the National Regulatory Authority, it is now possible to bring in BTF hall up to 10^{10} e^- /s. This has encouraged to advance in the study of feasibility of neutron source in BTF. Just to briefly remind what already described in the annual report of DAΦNE BTF 2005, neutrons in BTF can be produced by photo-absorption of continuous bremsstrahlung photons generated when high energy electrons (or positrons) impinge on a suitable target. Above a certain energy (typically 100 MeV) of the beam electrons (or positrons), the neutron yield from photo-absorption becomes quite proportional to the incident power, regardless the energy of the incident particles.

In collaboration with the LNF FISA department, some calculations have been made for choosing the best material in terms of yield of neutrons produced per electron or positron impacting on a "infinitely" thick target[3].

According to the work made from Swanson [4)] at SLAC concerning the neutron photoproduction in electron accelerators, as preliminary calculations with FLUKA we chose as target material the following high Z materials : lead (rad.length 6.37 g cm^{-2}), tantalum (rad.length 6.82 g cm^{-2}) and tungsten (rad.length 6.72 g cm^{-2}). For sake of semplicity, just as starting point, the geometry of the target has been assumed to be spherical with a radius $R \simeq 10X_0$. In figure 14 and 15 the spatial fluence and the energy spectrum for neutrons coming out from the lead target have been reported. Similar results are obtained for the tungsten and tantalum case, even if a little difference in the energy spectrum has been found as shown in figure 16[4].

The main goal of these calculations was, in fact, to validate the Fluka predictions on the basis of Swanson semi empirical correlations that represent an important reference in this field.

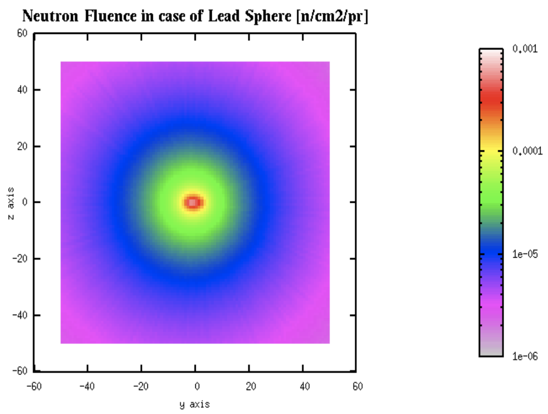

Figure 14: *Isotropic Neutron Fluence of photo-neutrons on a Lead spherical target*

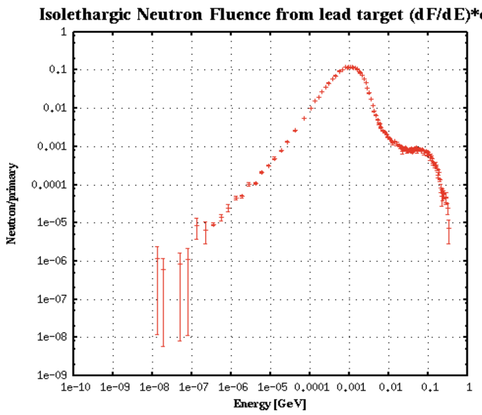

Figure 15: *Energy Spectrum of of photo-neutrons on a Lead spherical target*

[3]Thickness ≥10 radiation length X_0

[4]As expected the mean energy is lower in tungsten and tantalum target than in lead, due to a better moderation for higher density material

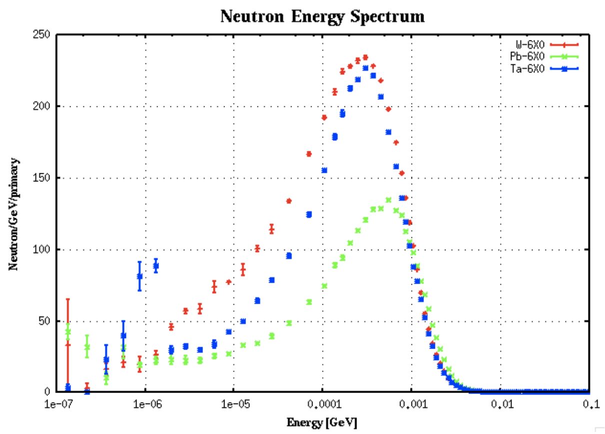

Figure 16: *Energy spectra of photoneutron produced in lead, tungsten and tantalum Target*

Neutron Yield ($10^{12} neutrons\ \ s^{-1}\ kW^{-1}$) for thick target and 510 MeV electrons

Target Material	Swanson semiempirical correlations [4]	Fluka predictions
Lead	1.98	2.08
Tantalum	2.13	2.45
Tungsten	2.4	2.7

The good agreement between Swanson estimations and Fluka predictions make us confident to have a reliable tool to estimate the neutron source term.

5 Diagnostic Tool Upgrade

During the 2007 shoutdown in order to reduce the electromagnetic field induced on the vacuum chamber by the fast dipole, we have installed ceramic gap to decoupled the vacuum chamber of the diplole to the transfer line of the BTF, hodoscope and dafne injection. To improve the diagnostic system of the facility, a new fluorescent screen (YAG:CE) has been mounted on the BTF transfer line.

6 Future Plans and Conclusion

The DAΦNE Beam Test Facility is continuing showing very good performance, both from the point of view of operation reliability and the flexibility needed in order to cope with very different experimental needs. Diagnostics, data acquisition system, and tools available for experiments are continuously improving. Concerning the background reduction in experimental hall the first stage of a multiple shielding system has been mounted (just around the BTF target). In this frame a complete study, supported by Monte Carlo simulations, of all the background around the BTF transfer line is still in progress. Contemporarily we are making advances in the study of feasibility of a neutron source in BTF, accomplishing the first step concerning the geometry and material definition of the target for the photoneutron production.

References

1. D. Alesini et al.“*Dafne Upgrade for Siddharta Run*”, G-68, 28/11/2006

2. A. Fasso et al.“*a multi-particle transport code*”,CERN-2005-10 (2005), INFN/TC-05/11, SLAC-R-773

3. I. Algapov et al.“*The BDSIM Toolkit*”,EUROTeV-Report-2006-014-1

4. W.P. Swanson “*Calculation of Neutron Yields Released by Electrons Incident on Selected Materials*”, SLAC-PUB-2042 November 1977

DAΦNE-Light Laboratory and Activity

A. Balerna (Resp.), P. Calvani (Ass.), R. Cimino, M. Cestelli Guidi (Art. 23), M. Commisso (Ass. Ric.) A. Frani (Tecn.), A. Grilli (Tecn.), A. Nucara (Ass.), E. Pace (Ass.), M. Piccinini (Ass. Ric.), M. Pietropaoli (Art. 15), A. Raco (Tecn.), V. Sciarra (Tecn.), F. Tombolini (Ass. Ric), V. Tullio (Tecn.), G. Viviani (Art. 15).

1 Summary

During 2007 the main experimental activities were related to the organization and improvement of the existing soft X-ray and IR beamlines, to the reorganization of the UV beamline but also to the realization of two new XUV beamlines. On the IR and soft X-ray beamlines, new experiments were performed by Italian and European users in parasitic mode, during FINUDA runs, but also using dedicated days for some specific experiments from January 2007 up to the end of May 2007 when the DAΦNE shutdown started. In particular, 14 EU teams within the Integrated Infrastructure Initiative for Transnational Access to Research Infrastructure (TARI) and 10 Italian teams with the submission of their scientific proposals to the Synchrotron Radiation Scientific Committee got access to the synchrotron radiation facilities.

The synchrotron infrared beamline (SINBAD) was equipped, in November 2007, with a focal plane array (FPA) detector. This detector was set on the IR Bruker microscope Hyperion 3000 of one of the two IR end stations and now a great reduction of measurements acquisition time can be achieved in moving from a point to a matrix of points mapping (Fig. 1).

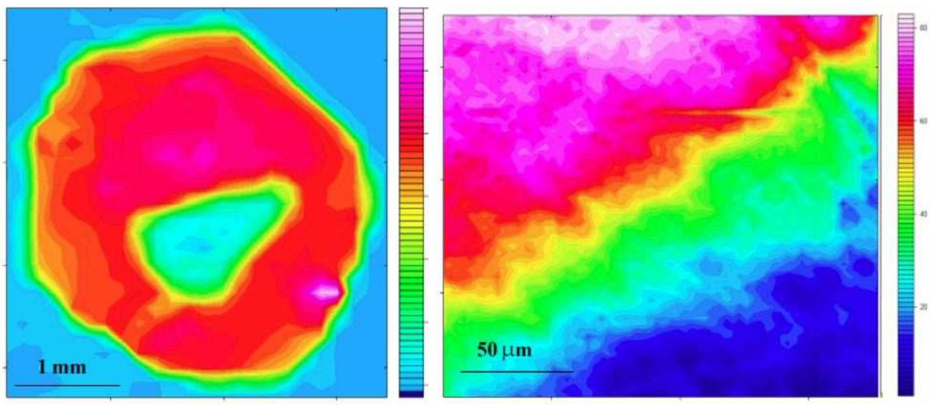

Figure 1: Left: H_2O distribution in a crystal of leucite. Right: image taken with a focal plane array detector and a Bruker Hyperion 3000 microscope, it shows the detailed H_2O content profile across the core-rim boundary with a spatial resolution of 5μm.

The soft X-ray beamline was improved with a silicon drift (SDD) detector for X-ray measurements in fluorescence mode and with a cryostat for sample conditioning. Concerning the x-ray beam definition and alignment, other improvements were also performed . The UV branch-line was equipped with a clean room to accept large mirrors for space applications as required by a Vth Committee experiment named SOURCE or Synchrotron Optical Ultraviolet Radiation for Calibration Experiments and it was decided to let it become a general purpose facility as the other beamlines. Concerning the new XUV beamlines after the preparation of the new laboratory that

will host the optics and the experimental end-stations, their construction started and the first optical UHV chamber was mounted near one of the bending magnets of DAΦNE. Among the many initiatives of 2007 mention should be given to the organization of a meeting with the responsible of the IA-SFS (Integrating Activity on Synchrotron and Free electron laser Science) that is a program for research cooperation involving laboratories and institutions throughout Europe, corresponding to the world largest network of synchrotron and FEL facilities, in order to be involved in this initiative in the European seventh framework program (FP7) starting from 2009. Mention should also be given to the partecipation of the DAΦNE Light scientific staff to the organization in June 2007 at the Frascati National Laboratory of the workshop *From Synchrotron to FEL radiation: new opportunities for science in Frascati* which has seen the presence of more than 100 scientists.

2 Activity

2.1 SINBAD - IR beamline

SINBAD is the Synchrotron Infrared Beamline At DAΦNE, which was opened to users in 2002. Synchrotron radiation, extracted from a bending magnet of the DAΦNE electron beam and collected within a solid angle of HxV = 18x45 mrad^2 by a gold mirror, is transferred to a first focus, where the image of the source is demagnified by an ellipsoidal mirror and is finally transmitted as a parallel wave towards the wedged diamond window located at the entrance slit of the interferometer, where it is focussed by a toroidal mirror. The beamline is equipped with two experimental stations. The first one is a made of a Bruker Equinox 55 interferometer which was installed in 2006 and modified to work in vacuum up to 10^{-5} mbar. One of its exit ports hosts the Bruker Hyperion 3000 microscope, working both in transmission and reflection mode and operating in the near- mid- and far-IR ranges down to about 200 cm^{-1}. The second end station is another Equinox 55 interferometer, owned by the University of Rome *La Sapienza* and is actually working with conventional sources but it will be connected to the beamline in 2008. At that point both interferometers will be able to use, alternatively, synchrotron radiation as source for the IR experiments. At the end of 2007 the IR microscope has been equipped with a 64x64-element focal plane array detector, which allows performing high-resolution imaging in the wavelength range of 900-5500 cm^{-1}. Both interferometers have also been equipped with accessories for performing attenuated total reflection and diffuse reflectance measurements and with a cell for transmittance measurements on liquid samples. In addition, a complete system for high-pressure experiments, made of a diamond anvil cell, has been acquired and will be installed in 2008.

In 2007 experiments with synchrotron radiation could be performed only from January to May in parasitic mode during FINUDA runs and with six dedicated days for specific experiments. The scientific activity at SINBAD was associated to experiments performed by Italian teams that submitted scientific proposals approved by the LNF Synchrotron Radiation Scientific Committee and by European scientists who got access within the EU framework of TARI I3 program. In 2007 about 14 experimental teams were hosted and 185 experimental days were assigned. The EU funded research projects at SINBAD were nine while the Italian ones were five and included the participation of graduates and PhD students who had access to the IR beamline performing experiments together with the SINBAD staff; almost all of the teams re-applied to continue their researches in 2008. Measurements at SINBAD were performed also within the framework of the 5^{th} INFN Committee experiment called *3+L* to test high speed infrared detectors to be used for DAΦNE beams diagnostics. Some of the 2007 scientific highlights achieved with the experimental activity are here summarized:

1. *SR-based FT-IR microspectroscopy for the high spatial resolution analysis of tumour blood vessels extracellular matrix.* The aim of the project was to provide novel diagnostic tools for

detecting the volume limits of cerebral cancers, notably for small volume tumors such as low-grade gliomas (1-5 mm^3). As a molecular probe of tissue composition, FTIR imaging may favourably help histopathology in detecting and diagnosing diseases. The high brilliance of IR synchrotron radiation is the unique resource to obtain high quality spectra (with high S/N ratio) suitable for sophisticated data treatment methods (notably spectral curve fitting) at a spatial resolution of 10 μm or better. The first results demonstrated that tumor blood vessels exhibit abnormal composition due to their unusual proliferating rate during angiogenesis.

2. *FTIR analysis on micro archaeological residues.* FTIR analysis was carried out in order to identify micro-residues of the worked material on selected archaeological tools coming from Italian, Ukrainian and Siberian sites, in the frame of an international cooperation supported by Wenner-Gren grant. The nature of archaeological micro-residues has been inferred comparing micro-residues sampled on the surface of experimental tools used in different activities: butchering, skin tanning, piercing and sewing leather, hunting activities, carving bone and antler and shell objects, etc. Samples of raw material (fleshy tissues, ivory, bone, tendons, antler, shell, leather, etc.) were also analyzed as a reference. The data obtained supported and integrated the qualitative observation previously performed by use-wear analysis in reflecting light optical microscopy (by stereo and metallographic microscopes). As an example, the spectra (Fig. 2) allowed to identify micro-residues of adipocere (salt of palmitic stearic and myristic acids) due to the transformation of subcutis of fresh hide after death confirming the use of the tools in skin treatment suggested by the use-wear analysis.

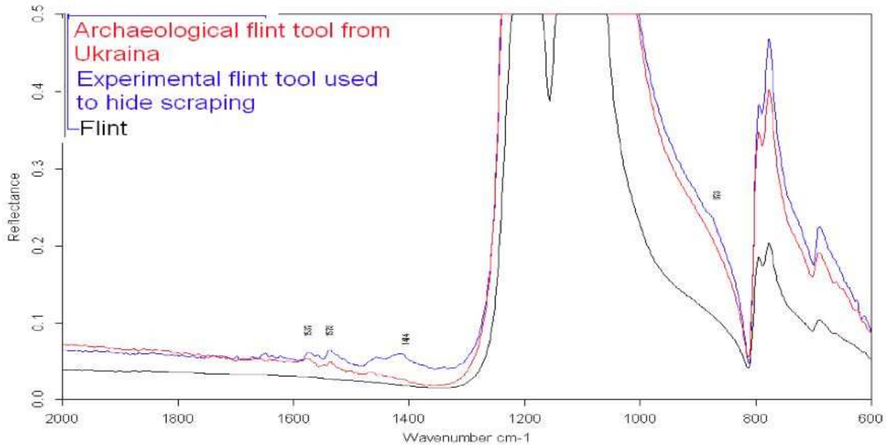

Figure 2: Comparison between pure flint, archaeological flint tool and experimental flint tool used for hide scraping. The doublet at 1537 and 1573 cm^{-1} are assigned to adipocere. The experimental tools shows traces of calcite (bands at 1414 and 873 cm^{-1}).

3. *Ironporphyrin aggregates investigated by IR.* Depending on the environment, iron porphyrins form dimers or oligomers through -oxo bridges (Fe-O-Fe). The aim of this work was to define the type of bounding in porphyrins aggregates, the way of aggregation and to perform an oligomer characterization. The expected type of bonds are: C-H, C-N, C=O, CHO and Fe-O-Fe groups. Analyzed samples were: ProtoporphyrinIX, Fe-protoporphyrinIX-chloride and its complexes, containing the μ-oxo dimmers (synthesized according to a modified Adler&Fleischer procedure). The analysis was performed in both mid- and far-IR ranges

in the temperature range of 30-200K. The FTIR spectra of the porphyrin (organic macrocycle, containing 76 atoms) reveals a very complex structure. It has been confirmed that the insertion of the metal ion into the center of the porphyrin ring and the aggregation process influence the distant porphyrin organic bands (e.g. pyrrole NH, CH_2 , C=C). It has been also indicated the characteristic behaviour of the Fe-N and Fe-O-Fe modes. In the temperature dependent spectra, broadening and shifting of the Fe-N (350 cm^{-1}) and Fe-O-Fe (840 cm^{-1}) modes was observed. The additional information on the local dynamical states of iron in the investigated samples were obtained from the temperature dependences of the Mssbauer and EXAFS spectra, but the FTIR data gave a very important contribution to the complex analysis.

4. *Infrared imaging/mapping of H_2O and CO_2 in volcanic minerals.* The analysis of volatile traces such as H_2O and CO_2 in volcanic minerals may provide significant constraints on the genesis and evolution of magmatic systems. The analysis of water using FTIR spectrometry is a relatively routine technique, however still few data exist on the H_2O content and distribution in nominally-anhydrous minerals from volcanic environments. On the other side, the spectroscopic analysis of CO_2 in geological materials is still a challenge and so far widely used only for glasses or fluid inclusions, while only few attempts have been done for minerals. The FTIR imaging showed all samples (from several occurrences in central Italy), and particularly the nominally anhydrous leucite and hauyne, to contain systematically significant water (2.7 wt%) and CO_2 (0.4 wt%). In addition, the data showed that the distribution of these volatile species is not homogeneous; in particular, the leucite crystals (Fig. 1) show an anhydrous core and a water-rich rim, pointing to an increase of the water fugacity during the evolution of the magmatic system. FTIR spectroscopy shows to be extremely valuable for monitoring the evolution of magmatic systems and it is a very promising tool to derive geothermometric information from mineral compositions.

2.2 DXR1 - Soft X-ray Beamline

The DAΦNE soft X-ray beamline, DXR-1, is mainly dedicated to soft X-ray absorption spectroscopy. The X-ray source of this beamline is one of the 6-poles equivalent planar wiggler devices installed on the DAΦNE electron ring (0.51 GeV) for the vertical beam compaction. The 6 wiggler poles and the high storage ring current (higher then 1 Ampere) give a useful X-ray flux for measurements well beyond ten times the critical energy. The useful soft X-ray energy range in 2007 was 900 eV - 3000eV where the lower limit is given by the Beryl crystals used in the double-crystal monochromator and the higher limit is given by the wiggler working conditions. At the end of 2007 many important elements like:

1. SDD detector
2. a double wire beam monitor to control the X-ray beam dimension and position (see figure 3)
3. remotely controlled output slits
4. new motorized support for the experimental chamber
5. He cryostat for sample cooling

were installed on the beamline but their tests will be performed in 2008 when DAΦNE will start working again. The scientific activity at the soft X-ray beamline included the use of 13 dedicated beam time days distributed between 5 experiments performed by Italian teams and 5 by European scientists that achieved the access within TARI program. In the first five months of 2007 about

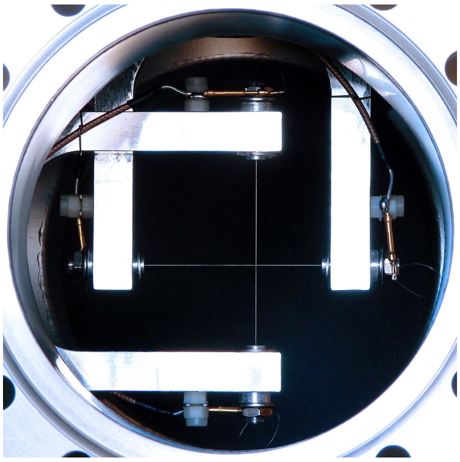

Figure 3: Internal view of the double wire soft X-ray beam monitor.

10 experimental groups were hosted at the soft X-ray beamline. The EU funded experimental runs related to the feasibility of the experimental proposal, accounted for a total of 5 experimental weeks with 9 dedicated beamtime days.

Several Italian scientists coming from different Italian Universities or related to INFN Vth Committee experiments used the beamline with dedicated and parasitic beamtime for about 8 weeks (4 dedicated days). In parasitic mode X-ray absorbtion measurements have been performed on in treated and untreated leaves at the Mg K-edge (A. Reale MIDIX INFN - Vth Committee) and tests (2 weeks parasitic beamtime) have been performed to control the performances as x-ray detectors of diamond based detectors (proposal by E. Pace and A. DeSio from University of Firenze). Beamtime was also given (1 week with 1 dedicated day) to make studies on biological samples at the S and Cl K-edges and at the L_3 edge of Ru (proposal by T. Congiu-Castellano and I. Ascone, University 'La Sapienza' Rome) and at the S K-edge (1 week with 1 dedicated day) on liquid crystals used as nanoparticles templates (V. Turco-Liveri, A. Martorana and A. Longo, CNR and UNiverssity of Palermo). The LNF staff performed some tests at the Na K edge to control the Beryl crystals performances.

Some of the 2007 scientific highlights achieved by the performed experimental activities are here summarized:

1. *X-ray absorption studies of adducts of gold and ruthenium anticancer metallo-drugs with a serum protein.* Due to the clinical success of platinum-based anticancer drugs, much attention has been focused on similar metal complexes of potential use in cancer treatment. Specifically, a great attention has been given to ruthenium and gold complexes that seem to be very promising. The mechanisms through which the metal complexes produce their biological and pharmacological effects are still largely unexplored and it seems that gold and ruthenium complexes act on different targets, most likely on protein targets. Measurements have been performed at the Sulfur K- edge on Bovine Serum Albumin (BSA) proteins which have interacted with ruthenium(III) and gold(III) metallo-drugs

2. *Near-edge X-ray Absorption spectroscopic investigations: Fe doped CoS_2. (TARI 56)* Conventional electronics are based on the transport of charges. Attempts to use other fundamental properties of an electron, e.g. its spin, have given rise to a new, rapidly evolving field, known as spintronics. Spintronics or spin-based electronics also known as magnetoelectronics is an

emergent technology which exploits the quantum spin states of electrons. The electron spin itself is manifested as a two state magnetic energy system. The structural investigation was performed around the S K-edge of Fe doped CoS_2 samples, which are well known materials for spintronics. The study of the S K edge gives information on the electronic structural changes induced in t he local environment of S by a substitutional doping of 3d transition metal ion , Fe, in polycrystalline and nanocrystalline materials of $Co_{(1-x)}Fe_xS_2$ achieved as a solid solution of CoS_2 and FeS_2.

2.3 DXR2 -UV branch Line

In 2005 the UV branch line was dedicated to the experimental proposal submitted by E. Pace of the University of Florence named SOURCE (Synchrotron Optical Ultraviolet Radiation for Calibration Experiments). The main objective of the SOURCE experiment was setting up an apparatus addressing the simulation of UV tracks in the atmosphere, induced by Ultra High Energy Cosmic Rays (UHECR). This experiment was motivated by the large experiments already existing as AUGER and mainly by the future space experiments. The UV tracks can be obtained using a specific apparatus producing these transient phenomena starting from the UV synchrotron radiation (SR) available at the DXR2 branch line of the DAΦNE-L laboratories. This radiation source

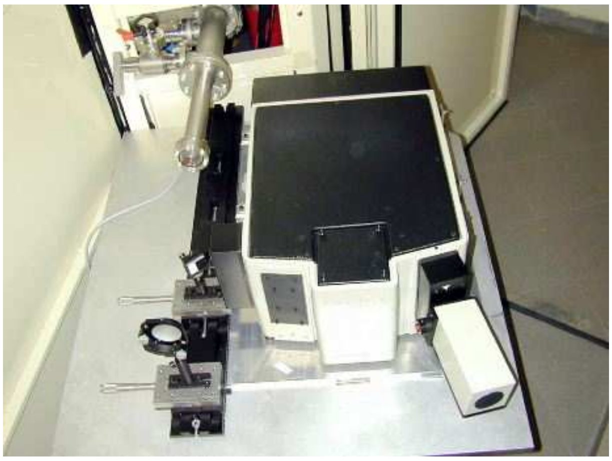

Figure 4: DXR2 UV-VIS monochromator and optical system that will be used for the UV-VIS channel of the facility.

is very appealing for such experiment because of its spectral and temporal features: a continuous spectrum in the 300-400 nm range is available, extended to the red portion to simulate backgrounds and time resolution of 2.7 ns can be achieved , thus providing the 10 ns resolution required by UHECR experiments. In addition, the radiation flux of 10^9 photons/s can be easily achieved taking into account all the optical system losses. This 3-years experiment, involving 3 experimental groups from Florence Section (INFN-FI, the coordinator), Frascati National Laboratories (LNF) and Legnaro National Laboratories (LNL), was funded by the 5^{th} INFN Committee. Unfortunately, the LNF Group left the experiment after the first year. The continuation of the experiment was attempted by reconfiguring the LNF participation in order to make the experiment and to achieve the objectives of the project, but in May 2007 it was decided to close SOURCE experiment at the end of 2007. At the same time it was also decided to let the DXR2 branch line become a general purpose facility since the UV synchrotron radiation can be used for several applications in physics, astronomy, astro-particle, biology, and geology as well as in the medical and technological fields. In any case the calibration and characterization measurements for space experiments will still remain one of the top priorities of the DXR2 facility. Therefore, a collaboration including people from LNF, INFN-FI, the University of Florence and the National Institute for Applied Optics (INOA) started working on setting up the new facility together with a 10000-class clean room for UV-VIS applications in the range 120-650 nm (2-10 eV). The design of the facility is based on three different apparatuses taking SR from the DXR-2 beam line alternatively: the first apparatus will make UV-VIS monochromatic measurements available in the 200-650 nm range (Fig.4) ,the second apparatus will be used for VUV monochromatic measurements in the 120-250 nm range, and the third apparatus will be used for wide band UV-VIS measurements in the 200-650 nm range by using filters. This third apparatus will be used in case of measuring the performance of large optics or focal plane array detectors. The radiation will be passed through the wave band selecting filter and an optical fiber to an inverted Cassegrain telescope providing collimated beams of 20 cm or 40 cm diameter. The energy range will partially cover the low-energy spectral region of the XUV line that will be soon available and this is an advantage because it will allow tests and measurements in a very wide spectral range through cross-calibration of the two lines in the common spectral range. The activity related to the design and fabrication of the 10000-class clean room was started in June 2007. The UV-VIS new area includes the old hutch at the end of the branch line and the adjacent the clean room. The clean room has been completed during the summer and certified in September 2007 as class 1000 (Figure 5). Its dimensions are suitable to

Figure 5: Inside the clean room. The SR beam will arrive in this area from an aperture close to the black spot on the wall

house large optical systems, that means up to 4 m diameter. The hutch will contain the UV-VIS monochromator and the main optical system to distribute the beam among the three lines and the conventional sources that will be discussed later. The last months of 2007 were devoted to the design of the new UV-VIS lines. In particular, it was decided to start from the instrumentation already available i.e. a spherical mirror collecting and focussing the emerging radiation from the line onto a folding mirror and then onto the entrance slit of a monochromator. This first channel should be operational from March 2008. The design of the whole instrumentation was started in October 2007 in order to send the SR beam not only to the UV-VIS monochromator, but also inside the clean room to provide radiation both to the VUV monochromator and to the wide-band channel. The design was commissioned to INOA and developed in a tight collaboration. The final design includes the previous optical system adding a spherical mirror placed on the back of the folding mirror of the UV-VIS channel that sends, when placed in the correct position, the SR into a 2-meter-long arm at the end of which a VUV vacuum monochromator is positioned. A vacuum experimental chamber has been designed and ordered for fabrication to be positioned at the exit slit of the VUV monochromator. To improve the operational time of the facility it was decided to include also two different conventional sources that will be operated when SR is lacking. A 500 W Hg-Xe lamp will be put in proximity of the entrance window of the SR branch line and the emitted radiation will be collimated and inserted in the line through a plano-convex quartz lens and a flat mirror that have been designed and fabricated by INOA. This lamp will provide radiation in the 180-700 nm spectral range and therefore will substitute SR in the UV-VIS and the wide-band channel. The other lamp is a 150 W deuterium lamp emitting radiation in the 120-400 nm range owing to its magnesium-fluoride exit window. This lamp will be arranged nearby the entrance slit of the VUV monochromator. In particular, it has been designed a small vacuum chamber housing a mirror that is normally off-line, but it can be inserted in order to send radiation from the deuterium lamp to the monochromator entrance slit or SR from the vacuum line to an optical fiber bringing light to the wide-band channel arranged on an optical bench. The two lamps have been ordered to Hamamatsu Photonics and they are already available and tested. The experimental chamber, the VUV monochromator, the optics and the optical bench have been ordered during December 2007 at the end of the design phase and will be availble in 2008.

2.4 New XUV beamlines

In 2007, the construction of the new XUV beamlines has started, based both on the detailed plans approved by the Synchrotron Radiation Scientific Committee and on the available resources. The

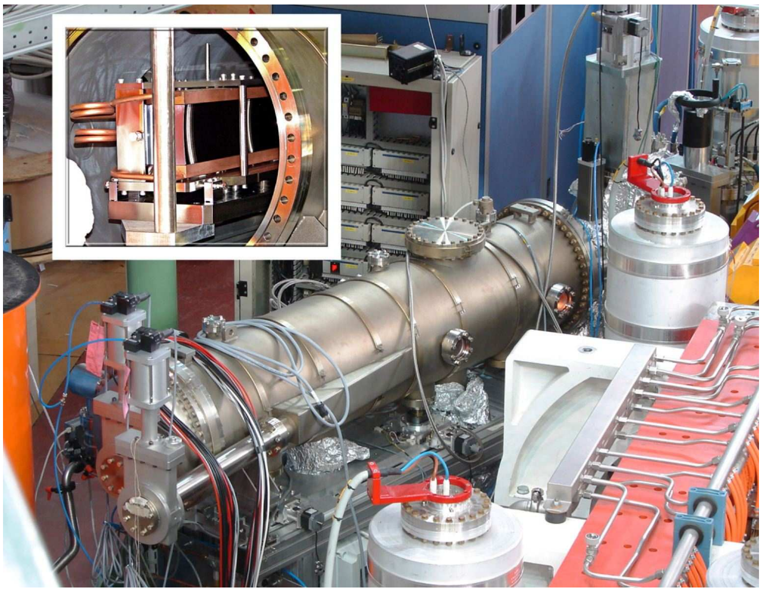

Figure 6: New XUV beamlines optical UHV chamber aligned and connected to DAΦNE: in the top left inset the collimating mirrors are shown.

two bending magnet (BM) beamlines will cover the energy range from 5 eV to 1000 eV, their optical project has been done and covers an High energy beamline (XUV-H from 60 eV to1000 eV) and a Low energy beamline (XUV-L from 5 eV to 150 eV). As suggested by the Scientific Committee priority was given to the construction of the XUV-H beamline (whose energy range covers the one expected from the FEL-SPARX project, in construction in the Tor Vergata University Campus) keeping the option of inserting the second beamline in the future. For this reason, in 2007, the UHV chamber hosting the first optical elements, which will collimate the emitted radiation into a parallel beam entering an existing laboratory has been installed, aligned and is ready for the first tests with the beam. In figure 6 there is a view of the UHV chamber placed in its position in the DAΦNE storage ring building and of the optically prepared mirror surfaces (in the inset) in their working positions, collecting about 9 mrad of the light emitted horizontally. During 2007, the group V experiment, SOURCE, made available a spherical grating monochromator (SGM) with movable exit slits able to deliver monochromatic light between 35 and 200 eV. This monochromator was rotated by 90^o to be optimally used on the XUV-L collimated beam and all the elements for a simplified high flux, low energy beamline, have been purchased so it will be installed in mid 2008 and finally commissioned for the beginning of 2009 in order to be open to users. Fig. 7 shows the optical design of the XUV-L beamline. LT1 (310 x 40 mm^2) is a toroidal mirror set at 2355 mm from the BM light source centre, working in sagittal configuration at 7.5^o of grazing incidence angle and accepting, horizontally, 17.3 mrad and, vertically, 16.6 mrad of the total solid angle emitted by the stored electrons. This mirror must collimate the diverging beam to a close to parallel beam entering into the laboratory. LT2 is a toroidal mirror (271 x 22 mm^2), working again in sagittal configuration, collecting the previously collimated radiation and focusing it vertically, in the laboratory frame, onto the entrance slit of the following SGM monochromator and horizontally onto its exit slits. The SGM monochromator is equipped with a holographic

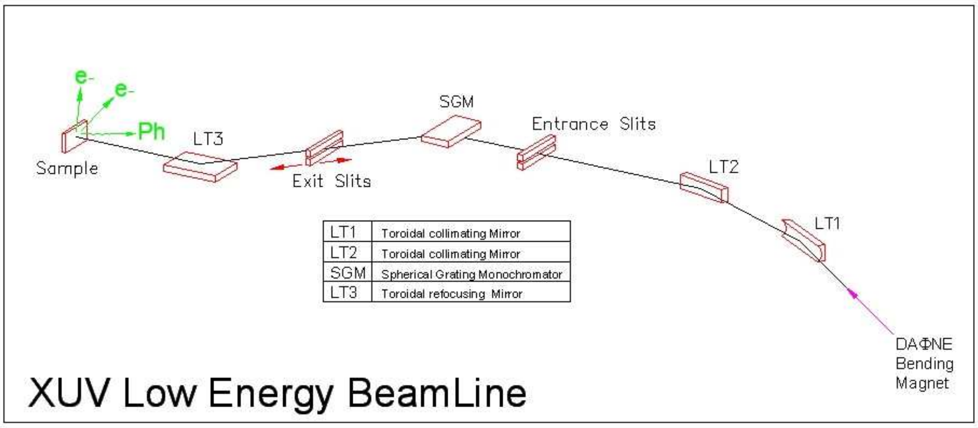

Figure 7: Schematic view of the XUV-L optical layout.

spherical grating, working at a constant included angle of 20^o and with a groove density N = 900 l/mm, optimised to monochromatize light between 35 and 200 eV. The rotation of the grating and the movement of the movable exit slit in the direction of the diffracted beam are related in order to fully compensate resolution losses typical of a spherical grating and optimaze flux and resolution. The spherical grating, working in tangential configuration, can only vertically focus, onto the exit slit ,the beam passing through its entrance slit while has no effect on the beam sagittal focus. In this way with the described optical elements,at the movable exit slit, the beam will be focused in both directions. LT3 is the last refocusing optical element (25 x 8 mm^2), which operates in tangential configuration. It deflects the beam that moves again parallel to the laboratory floor and can focus the exit slits spot in to an image, magnified close to 1:2, at the sample position. At the sample position the focussed beam will be about (0.2 x 0.8) mm^2 . The performances of this beamline have been computed and will need careful testing and experimental verification.

References

1. G. Della Ventura, F. Bellatreccia, G.C. Parodi, F. Camara, M. Piccinini, Single-crystal FTIR and X-ray study of vishnevite, ideally $[Na_6(SO_4)]$ $[Na_2(H_2O)_2][Si_6Al_6O_{24}]$, American Mineralogist **92**, 713 (2007)

2. I. Bolesta, S. Velgosh, Yu. Datsiuk, I. Karbovnyk, V. Lesivtsiv, T. Kulay, A.I. Popov, S. Bellucci, M. Cestelli Guidi, A. Marcelli, M. Piccinini, Optical, infrared and electron-microscopy studies of $(Cdi)_n$ metallic clusters in layered CdI_2 crystals, Radiation Measurements **42**, 851 (2007)

3. A. Bocci, A. Marcelli, E. Pace, A. Drago, M. Piccinini, M. Cestelli Guidi, A. De Sio, D. Sali, P. Morini, J. Piotrowski, Fast infrared detectors for beam diagnostics with synchrotron radiation, Nuclear Instruments and Methods in Physics Research A **580**,190 (2007)

4. L. Malfatti, T. Kidchob, P. Falcaro, S. Costacurta, M. Piccinini, M. Cestelli Guidi, A. Marcelli, A. Corrias, M.F. Casula, H. Amenitsch, P. Innocenzi, Highly ordered self-assembled mesostructured membranes: porous structure and pore surface coverage, Microporous and Mesoporous Materials **103**, 113 (2007)

5. B.V. Robouch, A. Marcelli, M. Cestelli Guidi, A. Kisiel, E.M. Sheregii, J. Polit, J. Cebulski, M. Piccinini, A. Mycielski, V.I. Ivanov-Omskii, E. Sciesinska, J. Sciesinski, E. Burattini, Statistical model analysis of local structure of quaternary sphalerite crystals, Low Temperature Physics **33**, 214 (2007)

6. J. Generosi, M. Piccinini, A. Marcelli, S. Belardinelli, D. Pozzi, A. Congiu Castellano, Characterization of solid supported lipoplexes by FTIR microspectroscopy, Infrared Physics and Technology **50**, 14 (2007)

7. C. Paluszkiewicz, W.M. Kwiatek, A. Banas, A. Kisiel, A. Marcelli, M. Piccinini, SR-FTIR spectroscopic preliminary findings of non-cancerous, cancerous and hyperplastic human prostate tissues, Vibrational Spectroscopy **43**, 237-242 (2007)

8. A. Leon, A. Balerna, G. Cinque, C. Frommen and M. Fichtner, Al K Edge XANES Measurements in $NaAlH_4$ Doped with TiCl $_3$by Ball Milling, J. Phys. Chem. C **111**, 3795 (2007)

9. L. Reale, J. Kaiser, A. Reale, A. Lai, F. Flora, A. Balerna, G. Cinque, M. Fanelli, F. Ruggieri, A. Faenov, T. Pikuz, A. Tucci, A. Poma, P. Zuppella, M. Lika, R. Malina, Mapping the intake of different elements in vegetal tissues by dual-energy X-ray imaging at DAΦNE synchrotron light source, Microscopy Research and Technique **71**, 179 (2007)

10. A. Soldatov, G. Yalovega, G. Smolentsev, A. Kravtsova, D. Lamoen, C. Balasubramanian, A. Marcelli, G. Cinque, S. Bellucci, ALN nanoparticles XANES analysis: Local atomic and electronic structure, Nuclear Instruments and Methods in Physics Research A **575**,85 (2007)

GILDA
General Purpose Italian Beamline for Diffraction and Absorption at ESRF

A. Balerna, A. Grilli (Tecn.), S. Mobilio (Resp.), A. Raco (Tecn.),
V. Sciarra (Tecn.), V. Tullio (Tecn.)

1 Introduction

GILDA (General Purpose Italian BeamLine for Diffraction and Absorption), is the Italian CRG beamline, built to provide the Italian scientific community with an easy access to the European Synchrotron Radiation Facility to perform experiments with a high energy and brilliance X-ray photon beam. GILDA was proposed, designed, constructed and commissioned by a collaboration between LNF and a large number of University groups; it is operative since autumn 1994. Today GILDA is funded by the Italian public research Institutes: Consiglio Nazionale delle Ricerche (CNR) and Istituto Nazionale di Fisica Nucleare (INFN). Experimental stations for X-ray Absorption Spectroscopy, Anomalous X-ray Scattering and X-ray Diffraction (XRD) are present on the GILDA beamline.
The LNF group is involved in the technical maintenance and update of the beamline, with particular emphasis to the electronic and software controls of all the instrumentation and to the apparatus for X-ray diffraction.

2 Summary of the Activity on the GILDA beamline during 2006

The main technical activity during 2006 were: the installation of a new He cryostat; the migration of the beamline control system from Microware OS9 to LINUX for the optical hutch; the modification of the second mirror support to recover the possibility to expose both the mirror coatings to the X-ray beam; the development of an oscillating total yield detector.
4000 hours of the 5300 delivered by ESRF were used for user's experiments; a total of 49 experiments were performed, 36 of Italian users and 13 of European users.
Among the relevant studies performed, we mention the study on the Iron oxidation, interfacial expansion and buckling at the Fe/NiO(001) interface; the study of Er site in Er-implanted Si nanoclusters embedded in SiO_2; the study on the Sub-nanometric metallic Au clusters as Er^{3+} sensitizer in silica; the study on the Negative Thermal Expansion of Au nanocluster.

3 Activity on the GILDA beamline during 2007

During 2007 many technical works were performed on the instrumentation both to keep the very good beamline efficiency and to upgrade its characteristics. Namely:
1) A new Linux based VME was installed in the Absorption hutch; now all the equipment are completely controlled and the macro allows experiments to run automatically for several days.
2) EXAFS spectra with very high signal/noise ratio were recorded on very small 200 μ-thick optical fibers; to get such spectra the beam was focussed vertically through the cylindrically bent second mirror, and horizontally by selecting a single rib of the second crystal. It was necessary to move the sample during the spectra, in order to compensate the small horizontal shift of the beam position.
3) Two new coupled segments were installed on the existing EXAFS chamber, to perform XAS experiments in grazing incidence geometry: the first segment is a high-precision vertical movement, coupled with a second segment for the sample rotation with the rotation axis in the horizontal plane, perpendicular to the incoming x-ray beam. By tuning the incidence angle, the beam footprint size

on the sample can be finely adjusted: this is of paramount interest when measuring XAS spectra in fluorescence mode from thin surface layers because the fluorescence signal from the layer can be largely enhanced (improving the overall signal-to-noise ratio). This permits to carry out XAS investigations at grazing incidence with the full beam and avoiding the time consuming alignment procedures of the ReflEXAFS chamber
4) A software package for on-the-fly XAS data analysis was developed, installed and commissioned. The software reads the experimental file during the acquisition and performs an automated data analysis. Once launched the program reads the experimental file each x seconds (where x can be set by the user) and give information on the edge step, energy position, noise estimation. Further, the program performs the extraction of the EXAFS signal following a standard procedure: pre-edge background removal, polynomial subtraction of the post-edge region and Fourier transform of the EXAFS signal. Each step of this procedure is plotted on a graphic window. The program is very useful to follow the behavior of experiments, in particular for estimating the quality of the recorded spectra and to have a first view of the EXAFS results.
5)A liquid nitrogen cryostat was successfully installed for recording diffraction spectra from samples in capillaries at low temperature.
6) The use of beamline mirrors for X-ray diffraction experiments was tested with very good results. The major advantages in using the mirrors are the achievement of a small vertical spot size and the harmonic rejection; this allows to tune the monochromator at the top of the rocking curve, so increasing the flux on the sample. A very high resolution set-up is achieved by coupling the vertical focusing with the horizontal focusing, made by choosing a single rib of the monochromator crystal; in this way a very small spot (0.1×0.1 mm^2) on the sample is achieved.
7) The use of Imaging Plate detector for full Debye scattering analysis, via the radial distribution functions formalism, has been tested with encouraging results. Actually some problems are still to be fully understood, in particular the effect of the polarization, of the detector efficiency at high energy, of some geometrical parameters and of the distortions to to the detector reader.

4 Beamtime use during 2007 and scientific outcomes

During 2007 ESRF delivered beam for about 5300 hours; about 4000 hours were used for user's experiments,the remaining for in-house research, beamline improvements, maintenance and alignment. Totally 45 experiments were performed, 33 of Italian users and 12 of European users. Studies and results to be mentioned are the followings:

1. *Indium Doping in Barium Cerate: the Relation between Local Symmetry and the Formation and Mobility of Protonic Defects*
   The solid solution series $Ba(In,Ce)O_{3-d}$ has been investigated with respect to structure, formation, and mobility of protonic defects. Compared to the limited solubility of Y_2O_3 in $BaCeO_3$ and $BaZrO_3$, the complete solubility of In_2O_3 is suggested to reflect a relation between absolute hardness of the dopant and the ease of insertion into the hosting lattices. Extended X-ray absorption fine structure (EXAFS) was used to probe the local environment of In^{3+} in barium cerate: in the surroundings of the dopant, the orthorhombic structure is strongly modified, resulting in an increase of local symmetry. The InO_6 octahedra are very regular, and there is no indication for any defect clustering. This is suggested to be the main reason for the low entropy of formation of protonic defects by water dissolution. The mobility of such defects is slightly lower than in Y-doped $BaCeO_3$, but at high dopant levels the high local symmetry allows for formation of very high concentrations of protonic defects. This leads to high proton conductivities, which makes In^{3+} an attractive dopant for $BaCeO_3$-based proton conductors.

2. *Diamond detector for synchrotron X-ray detection applications*

The development of X-ray detectors with better characteristics in term of efficiency, resolving power and speed is a challenging task of interest for many scientific and practical applications. The exiasiting semiconductor technologies allow to design clever detector configuration; diamond, due to its unique physical and electrical characteristics, it is one of the most appealing material in this field. Due to its strong chemical bonds, wide bandgap and high carrier mobility diamond based detectors guarantee radiation hardness, low dark currents (¡1 pA), visible blindness, fast response and high signal to noise ratio. Measurements planned and carried out at the Italian X-ray beamline Gilda at the European Synchrotron Radiation Facility at Grenoble are addressed to study diamond photoconductors, based on different quality of synthetic diamond, as X-ray detectors. Since the measurements on detectors are not standard for synchrotron beamlines, an accurate set up of the experiment was preliminarily developped. Then the detection performances of some diamond based photoconductor, illuminated with radiation in the 5 KeV 20 KeV spectral range, have been measured. By using the Micro Focused Beam configuration available at the Gilda beamline the photoconductive properties of detectors have been studied. Some maps of the photoresponse of diamond detectors have been carried out. The experiments have evidenced that diamond detectors have promising characteristics. They have stable response under long exposures, fast raise and fall times, and good signal to noise ratio. Good linearity of the response has been measured with an impinging flux variation of two orders of magnitude. The detector was tested also for a standard application. Extended X-ray absorption fine structure (EXAFS) spectroscopy measurements were performed on a standard metal iron foil at the Fe K edge ($E_0 = 7112$ eV) in transmission geometry. The X-ray intensity transmitted through the sample was measured both with a photoconductive diamond device and with a ionization chamber (IC). The measured EXAFS spectra and the further data analysis has evidenced the similarity between the two spectra and a comparable signal to noise ratio.

3. *Fe implantation in InGaP alloys*
   It has been recently shown that Fe implantation can induce the conversion of n^+- doped GaInP epilayers into semi-insulating material with a reduced damage rate thanks to a high temperature implantation procedure. In fact, in InP-based materials Fe is a very efficient electron trap, due to the near-midgap deep acceptor level, $Fe^{2+/3+}$, located at E_V +0.74eV, but little is known about its activation and thermal evolution after implantation in ternary III-V alloys, aspects which are closely related to the local structure of Fe. In order to shed light on this issue we have performed XAFS investigations at the Fe K-edge of the atomic environment of Fe impurities introduced by high temperature ion implantation in GaInP layers grown by Metal-Organic Vapour Phase Epitaxy. Implantation was performed at 190keV to produce a shallow high resistivity layer. Complementary characterizations were performed by proton-induced X-ray emission in channeling geometry and electrical measurements. In the as-implanted samples, Fe was found to be four-fold coordinated, indicating a substitutional site; compared to the previously studied case of Fe in InP (Cesca et al, Phys. Rev. B 68 224113 (2003)) an increased thermal stability was found, with a reduced tendency to form Fe-P precipitates. Finally, no effect related to the n-doping has been pointed out.

4. *The binding sites of Zn: a proton transfer inhibitor in respiratory enzymes*
   A study of the site of Zn as a functional inhibitor in selected respiratory enzymeswas performed. Binding of Zn^{2+} has been shown previously to inhibit the ubiquinol cytochrome c oxidoreductase (cyt bc1 complex). X-ray diffraction data in Zn-treated crystals of the avian cyt bc1 complex identified two binding sites, located close to the catalytic Qo site of the enzyme. One of them (Zn01) might interfere with the egress of protons from the Qo site to the aqueous phase. Using Zn K-edge XAFS we report on the local structure of Zn^{2+}

bound stoichiometrically to non crystallized cyt bc1 complexes. We performed a comparative XAFS study by examining the avian, the bovine and the bacterial enzymes. A large number of putative clusters, built by combining information from first-shell analysis and metalloprotein databases, were fitted to the experimental spectra by using ab initio simulations. This procedure led us to identify the binding clusters with high levels of confidence. In both the avian and bovine enzyme a tetrahedral ligand cluster formed by two His, one Lys and one carboxylic residue was found, and this ligand attribution fit the crystallographic Zn01 location of the avian enzyme. In the chicken enzyme the ligands were the His121, His268, Lys270 and Asp253 residues, and in the homologous bovine enzyme they were the His 121, His267, Lys269 and Asp254 residues. Zn^{2+} bound to the bacterial cyt bc1 complex exhibited quite different spectral features, consistent with a coordination number of six. The best fitting octahedral cluster was formed by one His, two carboxylic acids, one Gln or Asn residue and two water molecules. Interestingly, by aligning the crystallographic structures of the bacterial and avian enzyme, this group of residues was found located in the region homologous to that of the Zn01 site. This cluster included the His276, Asp278, Glu295 and Asn279 residues of the cyt b subunit. The conserved location of the Zn^{2+} binding sites at the entrance of the putative proton release pathways, and the presence of His residues point out to a common mechanism of inhibition. As previously shown for the photosynthetic bacterial reaction center, zinc would compete with protons for binding to the His residues, thus impairing their function as proton donor/acceptors. In a second investigation, we have reported EXAFS analysis of Zn binding site(s) in bovine-heart cytochrome c oxidase and characterization of the inhibitory effect of internal zinc on respiratory activity and proton pumping of the liposome reconstituted oxidase. EXAFS indentifies tetrahedral coordination site(s) for Zn^{2+} with two N-histidine imidazoles, one N-histidine imidazol or N-lysine and one O-COOH (glutamate or aspartate), possibly located at the entry site of the proton conducting D pathway in the oxidase and involved in inhibition of the oxygen reduction catalysis and proton pumping by internally trapped zinc. Finally, we have applied Zn K-edge EXAFS to investigate the local structure of the bound zinc ion and to identify the nature of the coordinating residues in bovine NADH-Q oxidoreductase (complex I). The EXAFS spectrum is consistent with a structured zinc binding site. By combining information from first-shell analysis and from metalloprotein data bases putative binding clusters have been built and fitted to the experimental spectrum using ab initio simulations. The best fitting binding cluster is formed by 2 histidine and 2 cysteine residues arranged in a tetrahedral geometry.

5. *Magnetic systems exhibiting exchange bias*
   We have studied the relation between structure and magnetic properties in Ni/NiO nanogranular samples exhibiting exchange bias; samples have been prepared by mechanical milling and partial hydrogen reduction of NiO; the Ni weight fraction varied between 4% and 69 %.The results indicate that both in the as-milled NiO powder and in the hydrogenated samples, the NiO phase is composed of nanocrystallites (having a mean size of $\sim$ 20 nm, structurally and magnetically ordered) and of highly disordered regions. The samples with low Ni content (up to 15%) can be modeled as a collection of Ni nanoparticles (mean size of $\sim$ 10 nm) dispersed in the NiO phase; with increasing the Ni content, the Ni nanoparticles slightly increase in size and tend to arrange in agglomerates. In the Ni/NiO samples, the exchange field depends on the Ni amount, being maximum ($\sim$ 600 Oe), at T = 5 K, in the sample with 15% Ni. However, exchange bias is observed also in the as-milled NiO powder, despite the absence of metallic Ni. In all the samples, the exchange bias effect vanishes at $\tilde{2}00$ K. We propose a mechanism for the phenomenon based on the key role of the disordered NiO component, showing a glassy magnetic character. The exchange bias effect is originated by the exchange interaction between the Ni ferromagnetic moments and the spins of the disor-

dered NiO component (in the as-milled NiO powder, the existence of ferromagnetic moments has been connected to chemical inhomogeneities of the NiO phase). The thermal dependence of the exchange bias effect reflects the variation of the anisotropy of the NiO disordered component with temperature.

6. *Effect of the Er-Si interatomic distance on the Er^{3+} luminescence in silicon-rich silicon oxide thin films*
   The photoluminescence intensity of Er-doped silicon monoxide thin films obtained by co-evaporation of silicon monoxide and Er was studied for different deposition and annealing atmosphere compositions. All samples exhibit a luminescence peak at 1.54 μ due to the radiative de-excitation of Er^{3+}. Theluminescence intensity is highest when nitrogen atoms are incorporated in the layer during deposition. Extended x-ray absorption fine structure spectroscopy evidences that the local order around the erbium ion is modified in the presence of nitrogen. In particular, the shorter the Er-Si interatomic distance is, the higher the Er^{3+} luminescence intensity is.

7. *Depth resolved study of impurity sites in low energy ion implanted As in Si*
   An extended x-ray absorption fine structure investigation in depth-resolved mode allows us to identify the different sites of the arsenic along its concentration profile in shallow junctions, obtained by low energy arsenic implantation of silicon. In the deeper part of the sample, arsenic mainly occupies substitutional sites and vacancyarsenic complexes are evidenced, whereas in the region close to the surface a mixed phase of arsenic aggregates and arsenic impurities is present. First principles calculations supporting the observations are presented.

8. *Thermal negative expansion*
   Studies on materials showing the interesting phenomenon of the negative thermal expansion continued during 2008. In particular the analysis and interpretation of EXAFS data on CuCl, affected by rather strong NTE below 100 K, have been completed. A quantitative analysis of the first coordination shell, performed by the cumulant method, reveals that the nearest-neighbor Cu-Cl interatomic distance undergoes a strong positive expansion, contrasting with the much weaker negative expansion of the crystallographic distance between average atomic positions below 100 K. The anisotropy of relative thermal vibrations, monitored by the ratio between perpendicular and parallel mean square relative displacements, is considerably high, while the diffraction thermal factors are isotropic. The relative perpendicular vibrations measured by EXAFS are related to the tension mechanism and to the transverse acoustic modes, which are considered responsible for negative thermal expansion in zincblende structures.

9. *Decorated pottery study: analysis of pigments by X-ray absorbance spectroscopy measurements*
   Characterization of pigments on decorated pottery fragments has been fully carried out by nondestructive x-ray absorbance spectroscopy. The samples were a series of pottery shards excavated from the archeological site of Caltagirone (Sicily, Italy), a well-known ceramic production center. Aesthetical criteria and morphological observations allowed us to attribute the samples to quite different historical periods, starting from the 18th century B.C. up to the 16th century A.D. An extensive time interval led us to suppose that different materials and techniques were used for the production of the ceramic paste and also for the preparation of pigments. XAS measurements were performed at the Cu and Fe K-edges. The analysis was carried out both in the near-edge (x-ray absorption near-edge spectroscopy, XANES) and in the extended (extended x-ray absorption fine structure, EXAFS) region. From the results, we observed Fe oxides as the main pigmenting agents in the most ancient fragment, while in

the other ceramic shards, besides Fe oxides, copper oxides were also found. Oxidation states and local environments of the atoms present were characterized.

10. *Arsenic uptake by gypsum and calcite: Modeling and probing by neutron and x-ray scattering* Uptaking of contaminants by solid phases is relevant to many issues in environmental science as this process can remove them from solutions and retard their transport into the hydrosphere. Here we report on two structural studies performed on As-doped gypsum ($CaSO_4$ $2H_2O$) and calcite ($CaCO_3$), using neutron (D20-ILL) and X-ray (ID11-ESRF) diffraction data and EXAFS (BM8-ESRF). The aim of this study is to determine whether As gets into the bulk of gypsum and calcite structures or is simply adsorbed on the surface. Different mechanisms of substitution are used as hypotheses. The combined Rietveld analysis of neutron and X-ray diffraction data shows an expansion of the unit cell volume proportional to the As concentration within the samples. DFT-based simulations confirm the increase of the unit cell volume proportional to the amount of carbonate or sulphate groups substituted. Interpolation of the experimental Rietveld data allows us to distinguish As substituted within the structure from that adsorbed on the surface of both minerals. Results obtained by EXAFS analysis from calcite samples show good agreement with the hypothesis of replacement of As into the C crystallographic site.

5 2008 - GILDA Forseen Activity

During the 2008 the activity foresees the followings: 1) A special sample holder will be mounted on the equipment installed in 2007 for grazing incidence XAS: it is expected to allow cooling down the sample at low temperature ($\sim$ 150 K). 2) the completion of the migration of the operating system of the beamline from Microware OS9 to LINUX, particular for the diffraction hutch and for those controls of the absorption hutch that are still under a OS9 VME system 3) the conceptual study and preliminary design of the beamline implementation needed for the foreseen updates of the ESRF storage ring; 4) the end of the commissioning and the beginning of the operating phase of the magneto-sputtering cluster source.

References

1. F. Giannici, A. Longo, F. Deganello, A. Balerna, A. S. Arico and A. Martorana, Solid State Ionics **178**, 587 (2007).

2. F. Giannici, A. Longo, A. Balerna, K-D. Kreuer and A. Martorana, Chem. Mater. **19**, 5714 (2007).

NTA CLIC
CLIC TEST FACILITY 3

D. Alesini, C. Biscari , B. Buonomo, M. Castellano, A. Ghigo (Resp.), F.Marcellini,
M.A. Preger, M. Serio, A. Stella, C. Vicario

1 Introduction

The feasibility study of the Compact Linear Collider is the main goal of the CLIC Test Facility (CTF3) project. The two beam acceleration scheme with acceleration gradient of 100MeV/m is provided by high power 12 GHz radio-frequency generated by a powerful electron drive beam. An international collaboration participates to the construction of the CTF3 accelerators and the INFN Frascati Laboratory (LNF) has realized the two rings of the drive beam recombination system. The first ring named Delay Loop, realized under LNF fully responsibility has been installed in 2005 in the existing building at CERN that hosted the LEP preinjector and commissioned in 2006. The Memorandum of Understanding of the accelerated CTF3 program foresees the participation of INFN in the realization of the Combiner Ring vacuum chamber. The second ring (Combiner Ring) has been realized by the collaboration and INFN was in charge of the construction of the RF deflectors, the vacuum chambers and diagnostics. The ring has been installed in 2006 and completed in 2007. The commissioning continued during the year 2007.

2 LNF Group Contribution in year 2007

In CTF3 collaboration the INFN, after the Delay Loop realization, decided to contribute also to the Combiner Ring. The Layout of the machine was managed by CERN and INFN Frascati laboratories take full responsability of the optical design, the wiggler magnet and the vacuum chamber realization, including RF deflectors and beam diagnostics. In 2006 all the components of the vacuum chamber have been realized by Italian firms, vacuum tested then shipped to CERN in pure nitrogen overpressure. The installation continued sharing the time with the Delay Loop commissioning and it has been completed in the winter shutdown until March 2007. The commissioning of the Combiner Ring started after the winter shut down; following measurements have been performed: - Optical parameters of the ring with magnetic injection - Injection efficiency with RF deflectors - Beam trajectory and its correction - recombination efficiency of the train of bunches With short bunch trains and low current the multiturn in the machine and the recombination of four bunch trains were proved, but increasing the current coming from the linac a vertical beam instability appeared in the ring. Many measurements have been devoted to understand where is the source of the instability. A vertical mode 50 MHz apart from the 3 GHz resonant frequency seems to be stored in the RF deflectors. INFN decided to study and realize two new RF deflectors with special loops inserted in the cavities to extract the parasitic dangerous mode. In the meantime a new optics less sensitive to the vertical oscillation has been studied.

3 Foreseen activity of the LNF group during year 2008

The foreseen activities for the year 2008 include the study and realization of the two new RF deflectors, the commissioning of the combiner ring, in particular the commissioning of new beam optic and the participation to the CLIC Test Facility scientific program.

4 References

http://accelconf.web.cern.ch/AccelConf/e08/papers/mopp011.pdf
http://accelconf.web.cern.ch/AccelConf/e08/papers/mopp010.pdf
http://accelconf.web.cern.ch/AccelConf/e08/papers/wepp125.pdf
http://accelconf.web.cern.ch/AccelConf/e08/papers/thyg02.pdf

NTA-DISCORAP

G. Celentano (Ass.), A. Della Corte (Ass.), U. Gambardella (Resp.)

1 Purposes of the project

The *DISCORAP* (DIpoli Super COnduttori RApidamente Pulsati) program comes out from the new requirement of developing fast ramped superconducting dipoles for the SIS 300 of the FAIR accelerator complex at GSI, Darmstadt, Germany. The four years program includes the development of a fully working bent dipole 3.8 m long in its horizontal cryostat. The dipole peak field is 4.5 tesla with ramping rate of 1 tesla/sec [1]. Among other requirements it has to keep dissipations at reasonable levels as well as to generate low harmonic contents. A suitable wire must be developed to withstand these requirements. Three INFN sections are involved: Genova (group leader), Milano LASA, and LNF, in cooperation with Ansaldo Superconduttori Genova, Italy, and LUVATA Italy, Fornaci di Barga (LU).

2 The Frascati group activity

The Frascati group, made of *LNF* and *ENEA* Frascati researchers, in 2007 took care of wire characterizations, analyzing NbTi superconducting wires for low losses applications previously developed in the framework of other projects. Though the NbTi alloy is well known, the production of μ-size filaments is not yet well developed and may suffer of many problems: filament sausaging and/or breaks, proximity effect between Nb filaments when the distance between filaments becomes comparable to the coherence length, etc..We have performed magnetization measurements, being this characterization fast and easy, to extract information on the intrinsic magnetization losses, the critical current density, filament size, paramagnetic impurities, and filament coupling. In addition as the low losses NbTi requires extremely narrowed filaments, in the range 2-4 μ, we also performed morphological SEM as well as compositional analysis on wires.

In Figure 1 it is shown the M(H) curve for sample IGC944 (left side), a NbTi wire with a 2.6 μm filament size manufactured by Intermagnetic, designed for the SSC project. The presence of the CuMn is evidenced by the relevant paramagnetic signal superimposed to the usual magnetization signal. On the right side of the figure 1 it is shown the virgin magnetization for the same wire as

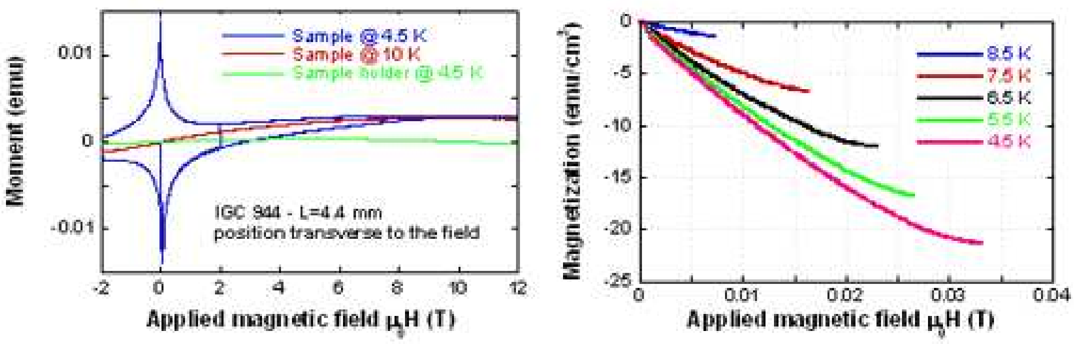

Figure 1: *M(H) cycle for IGC944 wire (left); low field virgin magnetization for IGC944 (right).*

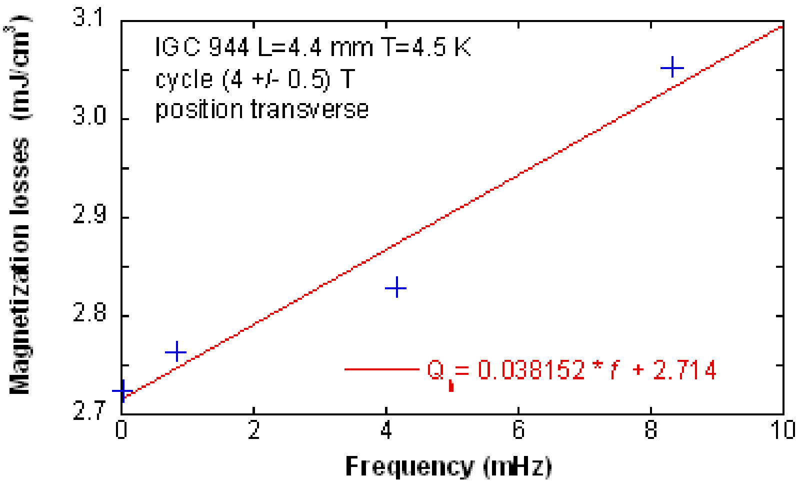

Figure 2: *Magnetization losses as a function of the ramp rate.*

a function of the temperature. In this measure we analyzed the Nb shielded volume (assuming a Meissner state) and the effect of the field penetration into the superconducting filaments.

The eddy current losses Q_h could be derived with eq. 1 when there is a steady variation of B in a time T_m which is long compared to the wire characteristic time τ. Under these hypotheses:

$$Q_h = \frac{B_m^2}{2\mu_0}\frac{8\tau}{T_m} \tag{1}$$

where B_m is the maximum value of the ramping magnetic field. Being magnetization losses independent of the frequency, the eddy currents losses are responsible for the increase of the total losses. From the slope of the curve $Q_h - vs - f$ the wire characteristic time τ can be computed as well as the wire transverse resistivity ρ_{et}. We are setting up a method to derive these features from VSM measurements. In Figure 2 it is shown a measure of losses computed in a cycle $[4 \pm 0.5]$ T performed with different ramp rates, ranging from 0.3 mHz to 8.3 mHz. Actually an increase of the cycle loss with the increasing frequency is found. The uncertainity of the slope is however large, but results are encouraging. An hardware upgrade of the VSM power supply is needed to increase the maximum ramp rate available.

The LNF group will continue this activity also in the next year, as the wire specifically developed within the DISCORAP project, and already ordered to LUVATA, will became available. In addition a new task will be started, according to the project schedule, which foresee the design of the horizontal cryostat for the dipole. The project will be completed by the end of 2009 when the dipole in its horizontal cryostat will be delivered to GSI for final tests.

References

1. P. Fabbricatore, M. Greco, C. Ferdeghini, C. Bernini, U. Gambardella, G. Celentano, A. Devred, "Low Field Instabilities in Nb3Sn Multifilamentary Wires: a Possible Role of Un-reacted Nb", Superconducting Science and Technology **20**, L34 (2007)

2. Michela Greco, Cristina Bernini, Pasquale Fabbricatore, Carlo Ferdeghini, Umberto Gambardella, "Investigation of Magnetization Behavior of Nb_3Sn Wires for the Next European Dipole (NED) activity", IEEE Transaction on Magnetics, **17**, 2722 (2007)

NTA ILC

D. Alesini, S. Bettoni (Art. 23), M. E. Biagini, R. Boni, R. Cimino,
T. Demma (Art. 23), G. Di Pirro, A. Ghigo, S. Guiducci (Resp.), F. Marcellini,
S. Pella (Tecn.), P. Raimondi, G. Sensolini (Tecn.), C. Vaccarezza

1 Introduction

After the unanimous choice of the superconducting radio frequency technology for the International Linear Collider (ILC) the INFN has contributed to the project design and R&D with a qualified participation to the GDE (Global Design Effort). The INFN ILC activity is focused on the superconducting accelerator technology and on the Damping Rings (DR). The groups participating in the collaboration are: LNF, LNL, Milano (LASA), Pisa, Roma Tor Vergata. The INFN groups actively contributed to the preparation of the "Reference Design Report" (RDR) [1] with the cost estimate, presented to the international community at the 9th ACFA ILC Physics & Detector Workshop & ILC GDE Meeting (IHEP, Beijing 4-7 February 2007).

The LNF activity is focused on damping rings and consists of DR studies and simulations and on the realization of prototypes of some critical elements. The possibility of making experimental observations at DAΦNE offers a great opportunity to test simulation studies and prototypes. The DR activity is fully integrated at the European level with the coordination of the DR work package of the EUROTeV design study and at the global level, in the GDE, with the responsibility of the DR Area System Leader.

On 5-7 March 2007 the international scientific meeting dedicated to the DR "LCDR07 - Damping Rings R&D Workshop" has been organized at LNF, with a consistent participation of the DAΦNE team to the program and discussions [2], showing the strong synergy between DAΦNE and the ILC DR.

2 Year 2007 Activities

The most critical DR elements are the injection and extraction kickers. In fact the rise and fall times of the kickers pulse determine the minimum bunch distance in the rings. In the RDR, with a 6.4 km DR circumference, to store the 2700–5400 bunches needed to get the design luminosity the required bunch distance is 6–3 ns respectively. The realization of fast kickers with pulse rise/fall times shorter than 3 ns is one of the very high priority issues in the GDE R&D plan. In 2006 at LNF has been realized the design of stripline kickers with very short pulse satisfying the requirements of high intensity, good field uniformity and low beam impedance [3]. Laboratory tests on a prototype have been performed in 2007 and the design of a vacuum feedtrough with the proper impedance and capable to sustain the high voltage needed (up to 50 kV) has been developed at LNF [4, 5]. The kickers have been built and installed in both DAΦNE rings during 2007 shutdown and are continuously operating for the injection [6]. The effect of wiggler magnets on beam dynamics is one of the main DR research themes since it requires a long wiggler section (200 m with 1.6 T peak field) in order to increase radiation damping. In 2006 has been studied, in collaboration with CERN, the possibility to modify the pole shape of the DAΦNE wigglers in order to reduce the harmful nonlinear components of the field on the beam trajectory. The work of modeling and optimization of the wiggler field continued in 2007 and produced an optimized solution achieved by simply shifting the poles with respect to the magnet axis [7]. The field modeling has been performed also for the study of a permanent magnet wiggler for the ILC DR [8] The e-cloud instability is the most crucial DR beam dynamics issue since it could produce a limitation of the maximum stored current or a growth of the vertical beam emittance for the positron DR. Studies on the e-cloud instability in the DAΦNE positron ring, and in particular in the wigglers, are in progress. Simulation studies have been performed during 2007 to understand the dependency of the instability on the various machine parameters [9]. Electron detectors will be installed on the DAΦNE rings to measure energy and distribution of the cloud electrons in a section of the vacuum chamber [10]. They are presently under test. For the RDR the LNF group has prepared the layout and cost estimate for the RF system, one of the main technical systems based on superconducting cavities, and for the digital fast feedback systems based on DAΦNE high current experience.

3 Plans for Year 2008

The next phase of the ILC Global Design Effort should produce a technical design of the ILC in sufficient detail that project approval from all involved governments can be sought in a timescale when LHC results justify the project. In this phase the INFN activity will continue both on superconducting RF and on damping rings. The new fast kickers are operating on DAΦNE: the time pulse shape of the fast pulsers and the field uniformity will be tested with beam soon. A new ultra fast kicker, with pulse duration suitable for the 3 ns bunch distance, is being designed and will be built [5].

A collaboration with KEK is being defined in order to use this kicker for the extraction of the ILC-like beam at ATF2, the beam delivery international test facility. Electron cloud detectors will be installed in DAΦNE, and the comparison between simulation studies and experimental observations will continue. The R&D on fast feedback systems will continue with special attention to the effect of the feedback on the vertical beam emittance.

4 Publications

1. N. Phinney et al., "International Linear Collider Reference Design Report", August 07, ILC-REPORT-2007-001, LNF - 07 / 9(NT).
2. S. Bettoni, M. Biagini, A. Drago, C. Milardi, M. Preger, "ILCDR07 Damping Rings R&D Workshop", INFN-LNF, Frascati, March 5-7, (2007). https://wiki.lepp.cornell.edu/ilc/bin/view/Public/DampingRings/FrascatiWorkshopTalks
3. D. Alesini, S. Guiducci, F. Marcellini, P. Raimondi, "Design and Tests of New Fast Kickers for the DAΦNE Collider and the ILC Damping Rings", Proc. of EPAC06, Edimburgh, Scotland, 1502, (2006.)
4. F. Marcellini, "Kickers for Injection and Extraction in Damping, Combiner and Storage Rings", Proc. of APAC 2007 RRCAT, Indore, India, 539, (2007).
5. D. Alesini, "Update on Kickers R&D at LNF", LCWS 2007/ILC 2007, DESY, Hamburg, 30 May - 2 June, (2007) http://lcws07.desy.de/
6. D. Alesini, "Kicker Studies at LNF", Presented at the 2007 ILC Damping Rings Mini-Workshop 18-20 December, 2007 KEK, Tsukuba, Japan, (2007). https://wiki.lepp.cornell.edu/ilc/bin/view/Public/DampingRings/KEKWorkshopTalks
7. S. Bettoni, S. Guiducci et al. "Reduction of the Non-Linearities in the DAΦNE Main Rings Wigglers", Proc. of PAC07, Albuquerque, New Mexico, 1463, (2007) and EUROTeV-Report-2007-051, (2007).
8. A. Babayan , M. Preger, "Large Aperture Permanent Magnet Wiggler for the ILC Damping Rings", EUROTeV-Report-2007-004, (2007).
9. T. Demma, "Electron Cloud Studies at DAΦNE", Pres.at 2007 ILC Damping Rings Mini-Workshop 18-20 December, 2007 KEK, Tsukuba, Japan, (2007)
10. R. Cimino, "Importance of realistic surface related properties as input to e-cloud simulations", LCWS 2007/ILC 2007, DESY, Hamburg, 30 May - 2 June, (2007).

PLASMON-X

C. Benedetti, V. Lucarini, P. Londrillo, S. Rambaldi, A. Sgattoni, G. Servizi, G. Turchetti, F. Zanlungo **Sez. INFN Bologna**
R. Bonifacio, M. Castellano, A. Clozza, L. Cultrera, G. Di Pirro, A. Drago, M. Esposito, M. Ferrario, D. Filippetto, A. Gallo, G. Gatti, P. Gaudio, A. Ghigo, A. La Monaca, M. Migliorati, D. Nanni, E. Pace, L. Palumbo, M. Richetta, C. Sanelli, F. Tazzioli, A. Tenore, F. Terra, S. Tomassini, C. Vaccarezza, C. Vicario - **Lab. Naz. di Frascati**
L. Calabretta, C. Cavallaro, L. Giuffrida, R. Miracoli, L. Torrisi - **Lab. Naz. del Sud**
A. L. Bacci, F. Broggi, M.M.Cola, G. D'angelo, C De Martinis, A. Fazzi, A. S. Giulini Castiglioni, C. Maroli, M. Passoni, V. Petrillo, N. Piovella, A. Pola, R. Pozzoli, M. Rome', A. R. Rossi, L. Serafini, P. Tomassini - **Sez. INFN Milano**
A. Galassi, D. Batani, G. Lucchini, R. Jafer, R. Redaelli, R. Benocci, T. Desai - **Sez. INFN Milano Bicocca**
U. De Angelis, S. De Nicola, R. Fedele, G. Fiore, C. Stornaiolo - **Sez. INFN Napoli**
S. Betti, C.A. Cecchetti, A. Giulietti, D. Giulietti, A.Gamucci, L.A. Gizzi, P. Koester, L. Labate, T. Levato, A. Macchi, M. Vaselli **Sez. INFN & CNR Pisa**

1 Aim of the experiment

The two main goals of the PLASMON-X project are the development of an innovative, high-gradient, laser-driven acceleration technique and the set up of a tuneable, hard X/γ-ray source, based upon Thomson Scattering (TS) of optical photons by energetic electrons. The laser driven acceleration will be investigated both in the self-injection scheme based upon the Laser Wake Field Acceleration (LWFA) and in the external injection scheme, using the electron bunches generated by the SPARC linac. Both experiments require very high power, ultra-short laser pulses in combination with very bright and short electron bunches.

Our programme follows the impressive progress in the field of laser-driven acceleration that has been achieved in the very recent years thanks to the advent of the ultra-short pulse lasers based upon the Chirped Pulse Amplification (CPA) technique [3]. In fact, CPA has allowed few joules, femtosecond pulses to be produced and used at a repetition rate of 10 Hz. Recently, very encouraging results have been achieved concerning the energy and the quality of the electron bunches produced by LWFA [4, 5, 6, 7]. Electrons with energies above 100 MeV and with an high degree of monochromaticity have been experimentally obtained and reproduced in many laboratories worldwide, while in some cases electron top energies above 1 GeV have been reached [8]. These experiments strongly suggest the possibility of setting up a prototype of a fully optical electron accelerator, provided that both laser and plasma performances are experimentally controlled with an high accuracy. With such an apparatus one would be also capable of accelerating externally generated electron bunches which, once produced by a suitable source, could be injected into a laser-generated plasma, where they could experience an high gradient accelerating field capable of significantly increasing their energy. In our case, the external source of electron bunches will be either a conventional Radio-Frequency (RF) accelerator or a laser-plasma injector, i.e. a second laser-driven electron accelerator. In view of this, the recent PLASMON-X project activity has also been devoted to performing basic experiments [9, 10, 11, 12, 13] aimed at investigating the possibility of adopting a laser-driven accelerator also as an electron photo-injector.

2 Group activity: experimental

2.1 Laser set up

During 2007, the lased design was completed and construction of the system started at Amplitude Technologies (Fr). The image of Figure 1 shows the front-end of the laser assembled at the Amplitude factory. The FLAME laser is a CPA system that will deliver < 20 fs, 800 nm, up to 300 TW, laser pulses with a 10 Hz repetition rate. The system features a high, sub-ns contrast ratio ($> 10^{10}$) and has a fully remotely controlled operation mode. In view of the above discussed requirements for prototyping of a laser-based electron photo-injector, the laser system will provide shot by shot monitoring of both temporal and spatial properties of the laser pulse. Spatial characterization will be performed both in the near and in the far field, using an equivalent plane monitor. Temporal characterization will be performed using two kinds of diagnostics. The first one will operate on a multiple-shot base while the second will operate in a single-shot regime. The multiple-shot diagnostics will offer the advantage of a better performance in view of a fine tuning of the laser parameters during setup. A third order autocorrelator will instead be used to monitor the contrast ratio. Also an interferometric second order autocorrelator will be set up to monitor the oscillator behaviour. The shot by shot performance of the laser system will be monitored using a second order single-shot autocorrelator.

Figure 1: *Front end of the FLAME laser system assembled for testing at the factory. The front end includes the advanced system for contrast enhancement and DAZZLER-MAZZLER combination for bandwidth and pulse duration optimisation.*

As anticipated above, synchronisation of the FLAME laser system with the LINAC will be required. In the existing set-up, the CPA laser driving the LINAC photoinjector is already synchronized with an external radiofrequency by changing dynamically the length of the oscillator cavity. The final result is a jitter between the radiofrequency and the laser pulse of less than 1 ps. This jitter is still much higher than that required in the case of acceleration of externally injected electrons. This issue is presently under investigation within the Comm.V project named FAST (Femtosecond Active Sync and Timing) and a preliminary characterisation of the sub-picosecond jitter of the LINAC bunches has already been carried out. Based on this characterisation, a dedicated synchronization system is being studied which is based upon an electro-optics approach [25].

2.2 The FLAME Laboratory

During 2007, the design of the basic layout of the FLAME installation at LNF that will allow execution of the PLASMON-X scientific programme was completed and the construction of the building was carried out. Figure 2 shows the top and side view of the FLAME laboratory with the layout of the laser and of the laser beam transport line up to the bunker connection conduits.

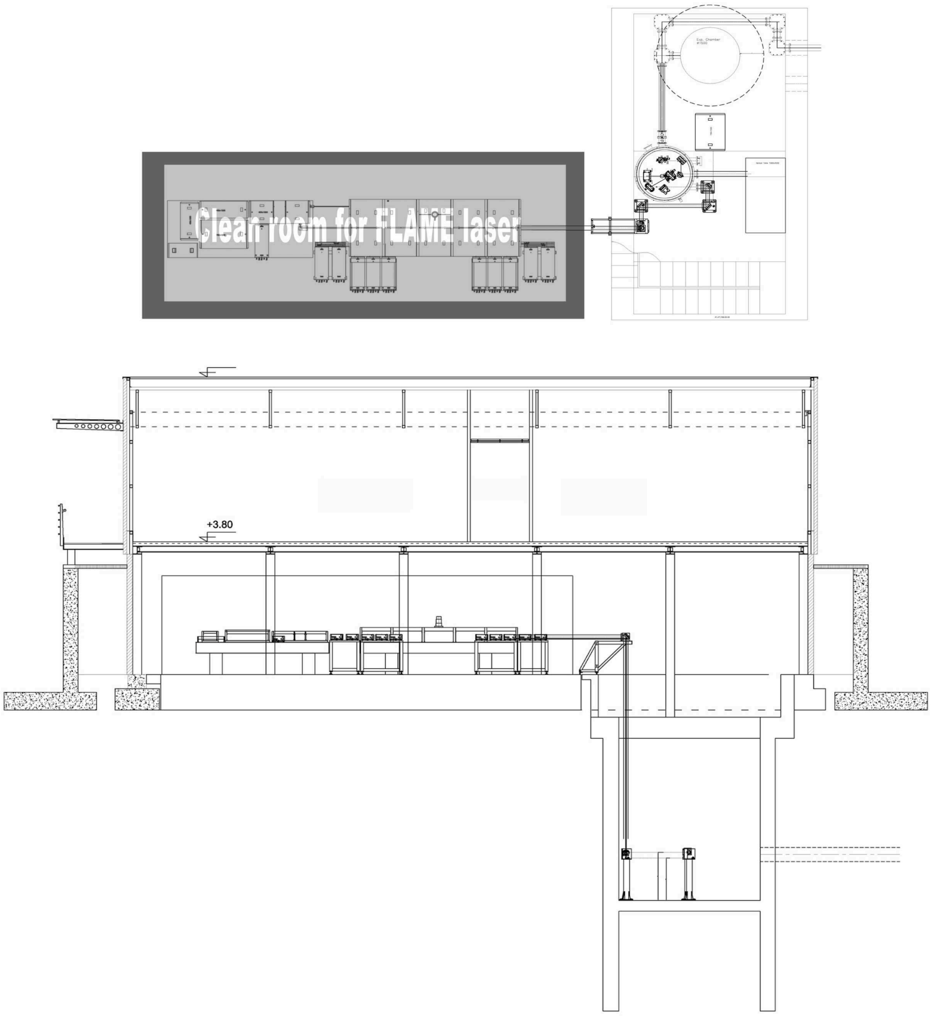

Figure 2: *Up (on top) and side (on bottom) view of the FLAME laboratory with the layout of the laser and of the laser beam transport line up to the bunker connection conduits.*

The 10 Hz, 300 TW TiSa laser system and the 10 Hz, 150 MeV SPARC [1, 2] linear accelerator are now well into the construction phase and additional R&D on ultra-fast electron-photon synchronization is being planned. The set of experiments identified for the first phase of operation of the installation include laser-driven acceleration of self-injected as well as externally injected electron bunches, TS aimed at the production of tunable, hard X-rays for bio-medical applications. All these experiments have now been under extensive modelling and test experiments are already in progress at collaborating small-scale laboratories. A significant part of the Plasmon-X experimental activity has in fact been carried out at LASERLAB laser facilities, including CLF at RAL (UK) and SLIC at CEA-Saclay. In addition, an intense R&D activity on laser driven acceleration was carried out in collaboration with the INFN section of Pisa at the CNR-IPCF laboratory in Pisa, where a moderate laser power installation exists. Here we briefly describe the main streams on which group activity has been prevalently focused in 2007, and summarize recent results on the modelling of the experiments.

2.3 Laser-driven acceleration: the precursor experiment

The laser-driven electron acceleration experiment which has been set up at the CNR (IPCF) Laboratory in Pisa, in collaboration with Sez. Pisa INFN, during 2007 and early 2008 is based upon a Ti:Sa laser system generating a main pulse of 67 fs duration FWHM at the repetition rate of 10 Hz. Within the PLASMON-X activity, a fraction (10 %) of the existing 67 fs laser pulse was further amplified by a 6-pass amplifier pumped by a frequency doubled Nd:YAG laser delivering 1 J pulses pumping a 2-cm diameter TiSa crystal. The output is further expanded to a 33 mm diameter beam and compressed by a two-grating compressor placed under vacuum. The pulse is compressed to a minimum pulse duration of 67 fs and is then transported under vacuum into the target chamber via two beam steering, motorised turning mirrors, placed in two separate small vacuum chambers. A diagram of the back-end of the laser system, showing a top view of the vacuum compressor and the beam steering mirrors is shown in Figure 3.

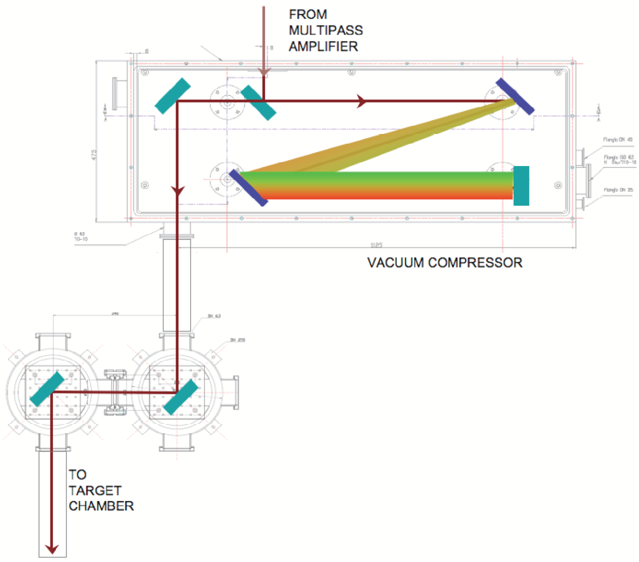

Figure 3: *Schematic layout of the last components of the laser system, including the vacuum compressor and the beam steering mirrors.*

The temporal and spatial properties of the femtosecond pulses have been characterised in detail using custom developed second-order autocorrelator. The contrast of the laser pulse, i.e. the ratio between the peak power and the low intensity pedestal originating both from prepulses and from amplified spontaneous emission (ASE) was measured with a third-order cross-correlator (SEQUOIA). According to the characteristion measurements, the FWHM focal spot on target using an f/6 numerical aperture is approx. 10 μm. Considering the pulse length of 67 fs and an energy of 120 mJ we find that the peak intensity on the target can exceed 10^{18} W/cm^2 required for laser-plasma acceleration.

3 Group activity: theoretical modelling

In this section we describe the theoretical activity which has been developed concerning the production and acceleration of high quality electron beams. The key parameters here are energy gain and energy spread, and various ways of reducing the energy spread are being investigated.

3.1 Self injection in Laser Wake Field

In the scheme proposed in [21], the production of high-quality electron beams in the LWFA regime is achieved via activation of a controlled longitudinal non-linear wave-breaking. The latter is induced by a suitably chosen electron density profile characterized by a downward step-like feature along the laser propagation direction. The initial plasma density profile consists of a smooth rising edge and of a first plateau where an high amplitude plasma wave is excited. Next, a density downramp makes a transition to a second, lower density plateau. According to both 1D analytical results and 2.5D numerical simulations, a partial break of the wave crests at the transition (downramp) capable of injecting electrons with the appropriate phase with the plasma wave excited in the second plateau (accelerating region) might occur. As the plasma density decreases in the direction of the pulse propagation, the wave number increases with time. This results in a decrease of the phase velocity and in a breaking of the wave at the interface between the two uniform density regions, even if the wave initial amplitude is below the nonlinear wave-breaking threshold. As a result of the wave breaking which occurs at the interface between the two density regions, fast electrons from the wave crest are trapped by the wave and accelerated into the lower density region where the wake field remains regular. PIC simulations indeed show that this approach successfully generates mono-energetic electron bunches [22]. Figure 4 (left) shows the energy spectrum of the electrons produced by such an acceleration scheme as obtained by PIC simulations [22].

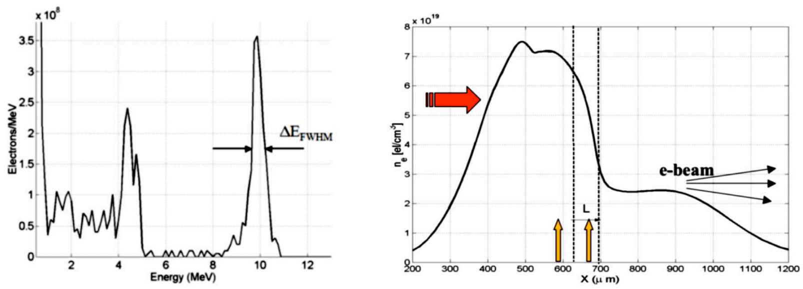

Figure 4: *Energy spectrum (left) of the accelerated electrons in a pre-formed plasma with a sharp density depletion (shown on right). The spectrum is obtained with 2-dimensional hydrodynamic simulations of laser explosion of a two-foil target as shown by the yellow arrows. The red arrow indicates the direction of propagation of the laser pulse.*

In the simulations, the electron density profile consisted of a smooth vacuum-plasma transition followed by a first density plateau ($n_e = 2.1 \times 10^{19}$ cm^{-3}). Then, an abrupt density decrease on a scale length of $L = 60$ μm leads to a second density plateau ($n_e = 1.1 \times 10^{19}$ cm^{-3}), as shown in Figure 4 (right). In the simulation, the laser pulse is 1 μm wavelength and has a Gaussian envelope (waist $w = 20$ μm, time duration $\tau_{\rm FWHM} = 17$ fs) with an intensity of $I = 2.5 \times 10^{18}$ W/cm^2. From the plot of Figure 4 (left) we can see that the electrons with energy above 7 MeV represent a bunch of $N_e \approx 10^8$ particles with energy $E \approx 10MeV$ and energy spread of less than 5 %, while the transverse and longitudinal spatial bunch extent are 1 μm and 0.5 μm, respectively.

3.2 External bunch quality control: compression

A scheme similar with the one in the preceeding section (see [21]) can be adopted to tackle the issue of bunch compression in plasmas when dealing with external injection. Compression schemes are at presently investigated because they might allow the matching conditions of LWFA to be matched at higher electron densities. In the scheme described in [21], the electron bunch is set to propagate initially in a low density plasma so that its length is much smaller than the plasma wavelength and its velocity smaller than the phase velocity of the wave. The bunch is injected close to the node of the plasma wave where the transverse forces are focusing. The gradient of the longitudinal force induces a longitudinal bunch compression, which forces particles to accumulate close to the trapping point. Figure 5 shows the results of a numerical simulation carried out using a 2D-cylindrical fluid code for the cold plasma in the quasi-static approximation. The code includes fully relativistic, nonlinear, space-charge and beam-loading effects and uses an optimised mesh size depending on the local pulse waist and plasma density. In the code, a 10 pC, 10 MeV electron bunch with a 60 μm full longitudinal size is injected in the node of the plasma wave generated by a 50 fs laser pulse in a plasma with a density of 5×10^{16} cm^{-3}.

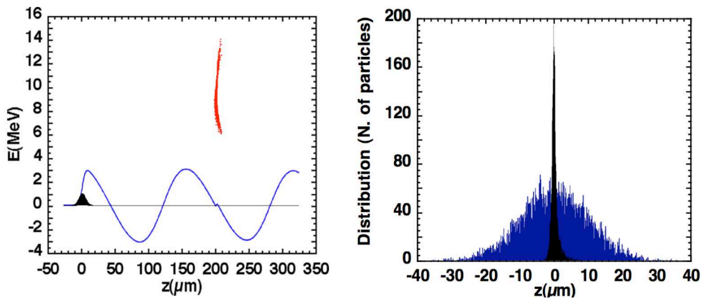

Figure 5: *Numerical simulation of bunch compression in an electron plasma wave. (left) The electron bunch after compression around the node of the longitudinal field of the electron plasma wave. (right) Comparison between the initial longitudinal bunch distribution and the same distribution after compression.*

The plots of Figure 5 clearly show the effectiveness of this bunch compression scheme. In particular, in the case presented an electron bunch with an initial 60 μm full size (10 μm rms) has been compressed by a factor of roughly 10 down to a 7 μm full size (1 μm rms). These parameters set the conditions for the second accelerating stage, whose modelling is at present in progress. Here we point out that with a bunch length after compression such as the one obtained in the simulations presented, the accelerating stage can take place even with a moderately high plasma density of the order of $1 - 5 \times 10^{17}$ cm^{-3}, which corresponds to an accelerating plasma wave wavelength shorter than 100 μm. This would allow the electrons to gain 1 GeV of energy on a spatial scale of 10 cm, while keeping the final energy spread down to a few percent, It is also worth to note that in order to accomplish to such a task one would need, in the case of a 50 μm waist size pulse, to guide the laser radiation over roughly 10 Rayleigh lengths, possibly with additional control of the phase velocity of the accelerating wave (via channel tapering). and represents a significant progress of the external injection scheme originally planned which required a plasma density well below 10^{17} cm^{-3}.

3.3 Thomson scattering source modelling

The PLASMON-X approach to Thomson scattering includes a configuration based upon the use of the LINAC-produced electron bunches, and a more advanced configuration based upon the use of electron bunches generated by LWFA. Ultrashort, intense laser pulses offer unique opportunities to activate novel regimes of X-ray generation processes [14]. TS from free electrons is a purely electro-dynamic process in which each particle radiates while interacting with an electromagnetic wave.

The first configuration has been investigated and modelled in several different operating modes, including the High-Flux-Moderate-Monochromaticity (HFM2) mode and the Short and Monochromatic (SM) operating mode. A detailed description of these two regimes, which can be found in [23], was obtained with the aid of a Monte Carlo code named Thomson Scattering Simulation Tools, $(TS)^2$ [24], which accounts for the actual focusing of the laser beam with the possibility of implementing propagation up to multiple Rayleigh length via pulse guiding. The code also includes full treatment for non-linear effects (multi-photon absorption), an accurate description of the electron bunch emittance effects and non-perfect pulse-bunch overlapping. In the second configuration, LWFA-generated electron bunches with controlled injection are used as an alternative to conventional LINAC-accelerated electron bunches. As already discussed above, injection by longitudinal nonlinear breaking of the wave at a density downramp is one of the most promising way of achieving e-beams having both low energy spread and low transverse emittance. Simulations of the LWFA process were performed with a fully self-consistent Particle-In-Cell (PIC) code in the 2.5D (3D in the fields, 2D in the coordinates) configuration. A full description of the numerical design of this configuration is reported in [23]. Here we summarise the final result obtained for the expected performances of the FLAME laser system.

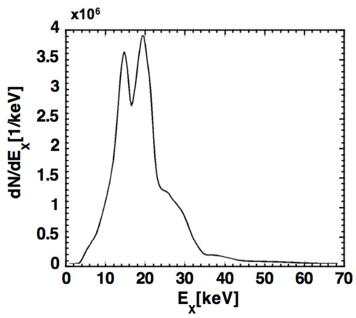

Figure 6: *Spectrum of the TS radiation of the ultra-short source in the case of a normalized acceptance angle of 0.5 deg.*

The numerical results therefore show that the head-on collision of the 20 pC e-bunch with a 5J, 5ps laser pulse focused with a 15μm waist might produce a 1 fs-long X-ray pulse with mean energy 20 keV at the fundamental frequency, an energy spread of 25% rms and with a total flux of 10^8 photons/shot (i.e. photons/s @10Hz). The duration of the scattered radiation is thus remarkably small (less than 1 fs). This result, still under further validation with a fully 3D configuration, therefore strongly suggests the possibility of achieving an ultra-short, hard X-ray source.

4 Conclusions

The PLASMON-X experiment will make use of complex hardware consisting of the most advanced LINAC technology and the most powerful. high repetition rate laser system ever built. The aim is to demonstrate the possibility of achieving an high quality acceleration of externally injected bunches, together with the generation of tunable hard X-ray radiation. At the same time, the most recent progress in the control of laser driven acceleration opens the way to complementary, all-optical schemes for X-ray generation that offer the opportunity of unique performances in terms of ultra-short pulse duration. The construction of the required infrastructure, namely the FLAME laboratory is under construction. Parallel to this, theoretical and numerical modelling is being carried out to further validate experimental parameters and to study even more advanced schemes.

References

1. D. Alesini et al., Proceedings of EPAC 2006, Edinburgh, Scotland, p. 2439.
2. D. Alesini et al., NIM-A **507**, 345 (2003).
3. D. Strickland and G. Mourou, Opt. Comm. **56**, 219 (1985).
4. T. Katsouleas, Nature **431**, 515 (2004).
5. S.P.D. Mangles *et al.*, Nature **431**, 535 (2004).
6. C.G.R. Geddes *et al.*, Nature **431**, 538 (2004).
7. J. Faure *et al.*, Nature **431**, 541 (2004).
8. W. Leemans *et al.*, Nature Physics **2**, 696 (2006).
9. L.A. Gizzi *et al.*, Phys. Rev. E **74** 036403 (2006).
10. A. Giulietti *et al.*, Phys. Plasmas **13**, 093103 (2006).
11. A. Gamucci *et al.*, Appl. Phys. B **85**, 611 (2006) .
12. T. Hosokai *et al.*, Phys. Rev. E **73**, 036407 (2006) .
13. S. Kar *et al.*, New J. Phys. **9**, 402 (2007).
14. L.A. Gizzi *et al.*, Plasma Phys. Contr. Fus. **49**, B211 (2007).
15. R.H. Milburn, Phys. Rev. Lett. **10** 75 (1963).
16. C. Bemporad *et al.*, Phys. Rev. **138**, 1546 (1965).
17. W. P. Leemans *et al.*, Phys. Rev. Lett. **67** 1434 (1991).
18. P. Tomassini *et al.*, IPCF-CNR Internal Report (2002).
19. P. Tomassini *et al.*, Phys. Plasmas **10**, 917 (2003).
20. L. Labate *et al.*, Nucl. Instr. And Meth. A **495**, 148 (2002).
21. S. V. Bulanov *et al.*, Phys. Rev. E **58** 5, R5257.
22. P. Tomassini *et al.*, Phys. Rev. ST-AB **6** 121301 (2003).
23. P. Tomassini *et al.*, Proc. of the LPAW 2007, IEEE TRANS. ON PLASMA SCI. (2007), in press.
24. P. Tomassini *et al.*, Appl Phys B DOI:10.1007/S00340-005-1757-X (2005).
25. A. L. Cavalieri *et al.*, Phys. Rev. Lett. **94**, 114801 (2005).

THE SUPERB ACCELERATOR PROJECT

S. Bettoni, M.E. Biagini (Resp.), R. Boni, M. Boscolo, A. Drago,
S. Guiducci, G. Mazzitelli, M. Preger, P. Raimondi, G. Sensolini,
S. Tommasini, C. Vaccarezza, M. Zobov

1 Introduction

The PEP-II at SLAC, and KEKB at Tsukuba, asymmetric B-Factories [1, 2] have successfully produced unprecedented luminosities, above 10^{34} cm^2 s^{-1}, taking our understanding of accelerator physics and engineering demands of asymmetric e$^+e^-$ colliders to a new parameter regime. This very high luminosity, coupled with the innovation of continuous injection and the high efficiency of the accelerators and detectors, as allowed each of these machines to produce 800 fb^{-1} or more. With the much larger data sample made possible by a Super B-Factory, qualitatively new studies will be possible. These studies will provide a uniquely important source of information about the details of the New Physics uncovered at hadron colliders in the coming decade. As a nascent international enterprise, SuperB aimed at the construction of a very high luminosity (10^{36} cm^2 s^{-1} at least) asymmetric e$^+e^-$ Flavour Factory, with possible location at the campus of the University of Rome Tor Vergata, near the INFN National Laboratory of Frascati.

Attempts to design a Super B-Factory date to 2001. The initial approach at SLAC and KEK had much in common: they were extrapolations of the very successful B Factory designs, with increased bunch charge, more bunches, somewhat reduced β^*_γ values, and crab cavities to correct for the crossing angle at the Interaction Point. These proposed designs reached luminosities of 5 to 7 x 10^{35} cm^2 s^{-1} but had wall plug power of the order of 100 MW. This daunting power consumption was a motivation to adapt linear collider concepts from SLC and ILC to the regime of high luminosity storage ring colliders. The new SuperB design is based on a novel collision scheme, the "large Piwinski angle and crab waist". This scheme will be firstly tested at the upgraded DAΦNE Φ-Factory in Frascati. Details on the scheme features and principles can be found in [3]. The low emittance design adopted can reach the desired luminosity regime with beam currents and wall plug power comparable to those in the present B-Factories. Since Fall 2005, when the first international study group was settled, 5 Workshops and 2 accelerator "retreats" have taken place in order to focus on the accelerator and detector designs and on physics motivations. In order to evaluate the proposal, an International Review Committee (IRC) has been established in 2007, formed by 8 international experts and chaired by J. Dainton (Daresbury, UK). In November 2007 an IRC meeting was organized at LNF for the presentation of the various aspects of the proposal. The IRC will meet again in spring 2008 to discuss the results of the DAΦNE upgrade with "crab waist" scheme and future developments of machine and detector. In case of positive results, the IRC will then issue its statement of endorsement, which will be essential in view of the presentation to the CERN Strategy Group before any formal approval and funding model definition. In case of success, a Technical Design Report (TDR) will be then needed on the time scale of 2 years to proceed with construction. In the following section the work performed at LNF on the design of the accelerator will be briefly described. This activity has been funded by the INFN NTA commission for 30 keuro in 2007 for LNF.

2 Year 2007 activity

In 2007 the main activity has been devoted to the Conceptual Design Report (CDR), which was published in March [4]. The CDR contains three sections dedicated to the Physics, Detector and Accelerator, for a total of 480 pages. As many as 320 scientists from 85 Institutions, spread in 15 countries, have signed the CDR. In particular, a big contribution to the accelerator design, about 200 pages, came from machine experts from LNF (Italy), SLAC (US), KEKB (Japan) and BINP (Russia). A group of 25 international accelerator experts, coordinated by the LNF team, has contributed to the CDR. For the accelerator design the CDR covers most of the main topics, such as: optics, beam-beam simulations, backgrounds, beam dynamics, instabilities, machine errors, feedbacks, as well as RF, vacuum, magnets and injection systems. A chapter is dedicated to the longitudinal polarization scheme, particularly appealing for some of the physics topics. The lattice design is based on the reuse of all PEP-II magnetic elements, RF and vacuum. The overall length will be about 1.8 Km. The two asymmetric energy rings (4 x 7 GeV) will be crossing at a horizontal angle of 50 mrad and have ultra low-emittances, similar to those of the ILC Damping Rings. Beam currents will be of the order of just 2 A per beam, a number close to the achieved currents in the present B-Factories. After the CDR completion, the work on the lattice design has continued in order to decrease power consumption and costs, optimize the crab waist compensation by sextupoles and the Final Focus design. The updated lattice presents better characteristics, and for Phase I operation it will not be necessary the insertion of wigglers to reach the emittances and damping times needed. This work has been presented and discussed in an accelerator retreat at SLAC, with PEP-II and LNF experts, which approved it as the baseline lattice. Background studies have continued after the CDR, in synergy with the detector experts, in order to optimize the collimators set for backgrounds reduction and the design of the Final Focus, in particular a new, optimized design of the first QD0 quadrupole has been studied. Fig. 1 shows the layout of one ring, with close-up of one arc cell and of the Final Focus.

The work on the accelerator design will continue in 2008 in order to study the insertion of the polarization scheme into the lattice and study other beam dynamics issues in view of the TDR. A Workshop dedicated to the accelerator will take place in Novosibirsk (Russia) on April 14-17 2008, while a general SuperB project Workshop will be organized on Elba island on May 31- June 3 2008.

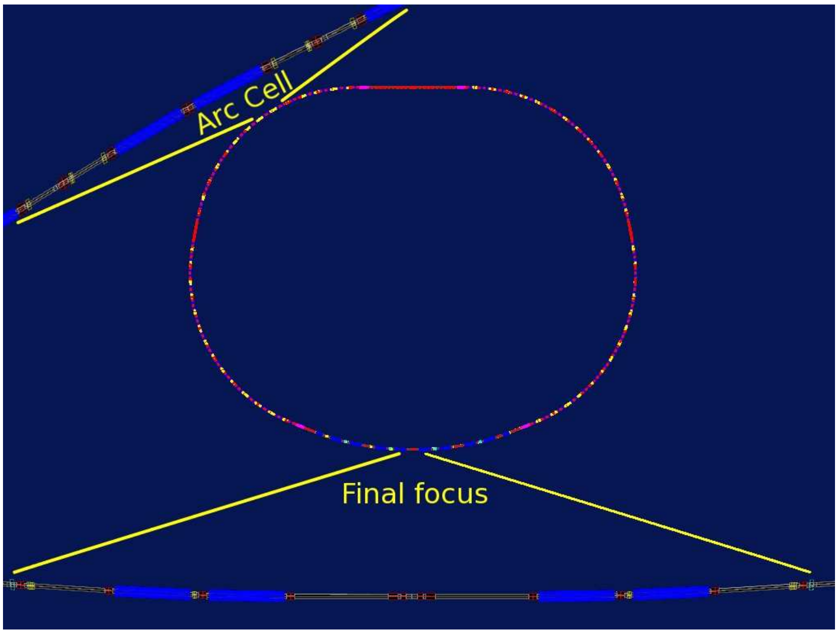

Figure 1: The layout of one ring with close up of Final Focus and one arc cell.

3 Publications in 2007

1. "SuperB Conceptual Design Report", INFN/AE-07/2, SLACR-856, LAL 07-15, March 2007.

2. Y. Cai, S. Ecklund, A. Fisher, S. Heifets, A. Novokhatski, M. Pivi, J. Seeman, A. Seryi, M. Sullivan, U. Wienands (SLAC), M. Biagini, S. Guiducci, P. Raimondi, M. Zobov (INFN-LNF), I. Koop, D. Shatilov (BINP), "Super-B factory using low emittance storage rings and large crossing angle", Proc. of Particle Accelerators Conference, Albuquerque, June 2007.

3. K. Ohmi, Y. Funakoshi (KEK), M.E. Biagini, P. Raimondi, M. Zobov (INFN/LNF), "Beam-beam effects in crab crossing and crab waist schemes", Proc. of Particle Accelerators Conference, Albuquerque, June 2007.

4. Y. Ohnishi (KEK), M.E. Biagini, P. Raimondi (INFN/LNF), A. Wolski (Liverpool University), Y. Cai, J. Seeman, M. K. Sullivan, U. Wienands (SLAC), "Low emittance lattice and final focus design for a SuperB project" Proc. of Particle Accelerators Conference, Albuquerque, June 2007.

5. M. Sullivan, J. Seeman, U. Wienands (SLAC), M.E. Biagini, P. Raimondi (INFN/LNF) "Interaction region design for a Super-B factory", Proc. of Particle Accelerators Conference, Albuquerque, June 2007.

6. P. Raimondi (INFN/LNF) "New developments in Super B-factories", Proc. of Particle Accelerators Conference, Albuquerque, June 2007.

7. M.E. Biagini (INFN/LNF) for the SuperB Team, "The SuperB Factory project", European Physics Society Conference, Manchester, July 2007
8. M.E. Biagini (INFN/LNF) for the SuperB Team, "The SuperB Factory project", CARE-HHH-APD Mini-Workshop IR'07 "Interaction Regions for the LHC Upgrade, DAΦNE and SuperB", LNF, November 2007

4 References

1 J. Seeman et al, "PEP-II at 1.2x10^{34} cm^2 s^{-1} Luminosity", Proc. of Particle Accelerators Conference, Albuquerque, June 2007.

2 K. Oide et al, "Compensation of the Crossing Angle with Crab Cavities at KEKB", Proc. of Particle Accelerators Conference, Albuquerque, June 2007.

3 P. Raimondi, D. Shatilov, M. Zobov, "Beam-beam issues for colliding schemes with large Piwinski angle and crabbed waist", LNF-07/003 (IR), January 2007.

4 "SuperB Conceptual Design Report", INFN/AE-07/2, SLACR-856, LAL 07-15, arXiv:0709.0451 [hep-ex] March 2007.

NTA TTF

L. Cacciotti (Tecn), M. Castellano (Resp), E. Chiadroni, A. Clozza,
G. Di Pirro, R. Sorchetti (Tecn.)

1 Introduction

The TESLA Test Facility (TTF) is an international effort, based at Desy (Hamburg), aiming at the development of the technologies required for a Superconducting e+e- Linear Collider. High gradient superconducting RF cavities, with their high power coupling and tuning device, and low cost cryostats were the main goal of the project, but also the production of a high power, long pulse electron beam from a RF gun was required. This involved the development of new photocathode, an adequate laser source and new beam diagnostics. In addition to prove the possibility of producing and accelerating the kind of beam required for the future superconducting Lineal Collider, TTF has also demonstrated that this beam was of enough good quality to be successfully used for the production of UV coherent radiation with the Self Amplified Spontaneous Emission (SASE) Free Electron Laser process. TTF is now transformed in FLASH (Free-electron LASer in Hamburg), becoming a test bench not only for the Linear Collider, but also for the European X-ray FEL Facility. INFN contribution comes from LNF, LNL, Sezione di Milano and Sezione di Roma 2.

2 Activities in the year 2007

At the beginning of 2007 we could use a good number of machine development shifts to improve the results for the experiment on Optical Diffraction Radiation from a rectangular slit. Due to the slightly higher energy and a better beam transport, we could confirm that ODR was really capable of giving quantitative information both on beam size and beam divergence. The background produced by synchrotron radiation and by beam losses was again the main difficulty of the measurement. A long machine shutdown in summer allowed the installation of the last accelerating module, and before the end of the year the FLASH energy reached the design value of 1 GeV. During the shutdown we inserted a screen supported by the same holder few centimeters in front of the ODR slit. The screen has a rectangular cut larger than the slit and centered on it. This screen will be our last resource to avoid the synchrotron radiation background. In 2007 a very small maintenance of the OTR system was required.

3 Publications

1. E. Chiadroni, M. Castellano, A. Cianchi, K. Honkavaara, G. Kube, V. Merlo, F. Stella, Non-Intercepting Electron Beam Transverse Diagnostics with Optical Diffraction Radiation at the DESY FLASH Facility Proceeding PAC07 3982, (2007).

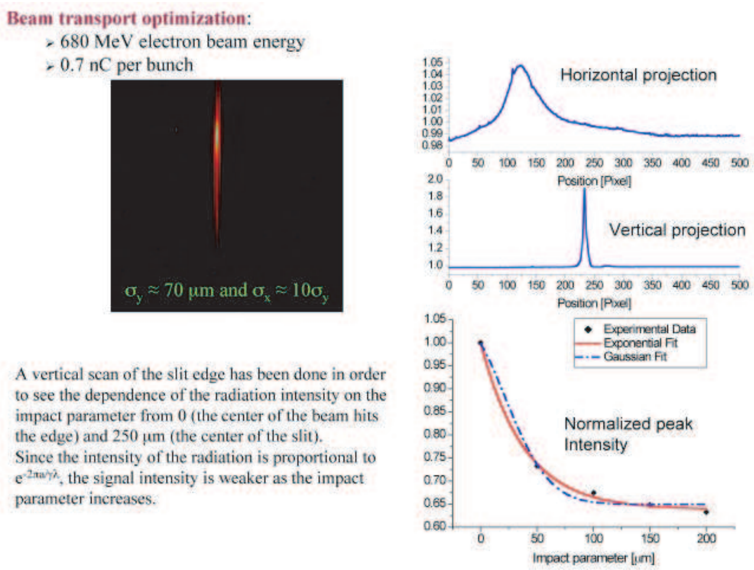

Figure 1: Image and projections of the beam used for the experiment, together with the analysis of the image tail.

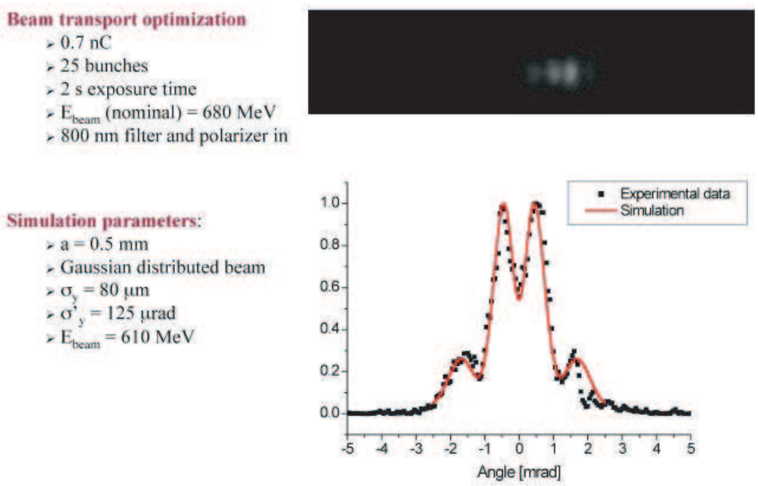

Figure 2: ODR image and its profile compared with simulations.

SPARC

D. Alesini, M. Bellaveglia, S. Bertolucci, R. Boni, M. Boscolo, M. Castellano, A. Clozza, L. Cultrera, G. Di Pirro, A. Drago, A. Esposito, M. Ferrario, L. Ficcadenti, D. Filippetto, V. Fusco, G. Gatti, A. Gallo, A. Ghigo, M. Incurvati, C. Ligi, F. Marcellini, M. Migliorati, A. Mostacci, L. Palumbo, L. Pellegrino, M. Preger, R. Ricci, C. Sanelli, M. Serio, F. Sgamma, B. Spataro, A. Stecchi, A. Stella, F. Tazzioli, S. Tomassini, C. Vaccarezza, M. Vescovi, C. Vicario **(INFN/LNF);**

F. Alessandria, A. Bacci, I. Boscolo, F. Broggi, S.Cialdi, C. De Martinis, D. Giove, C. Maroli, M. Mauri, V. Petrillo, M. Romè, A. R. Rossi, L. Serafini **(INFN/Milano);**

D. Levi, M. Mattioli, P. Musumeci, G. Medici, D. Pelliccia, M. Petrarca **(INFN/Roma1);**

L. Catani, E. Chiadroni, A. Cianchi, E. Gabrielli, S. Tazzari **(INFN/Roma2) ;**

A. Perrone **(INFN/Lecce);**

F. Ciocci, G. Dattoli, A. Dipace, A. Doria, G.P. Gallerano, L. Giannessi, E. Giovenale, G. Messina, P.L. Ottaviani, S. Pagnutti, L. Picardi, M. Quattromini, A. Renieri, G. Ronci, C. Ronsivalle, M. Rosetti, E. Sabia, M. Sassi, A. Torre, A. Zucchini **(ENEA/FIS);**

J. Rosenzweig, G. Travish, S. Reiche **(UCLA);**

1 Aim of the experiment

The aim of the SPARC project is to promote an R&D activity oriented to the development of a high brightness photoinjector to drive SASE-FEL experiments. It has been proposed by a collaboration among ENEA-INFN-CNR-Università di Roma Tor Vergata-INFM-ST and funded by the Italian Government and INFN.

The main goals of the SPARC project are:

- the generation of a high brightness electron beam able to drive a Self Amplified Spontaneous Emission Free Electron Laser (SASE FEL) experiment in the green visible light, Seeding and Higher Harmonics Generation,
- the development of an ultra-brilliant beam photo-injector needed for the future SASE FEL-based X-ray sources, as for the recently funded 1 GeV 10 nm FEL project SPARX whose SPARC is become its test facility.

The SPARC injector will allow also investigations into the physics of ultra-short beams, plasma wave-based acceleration, and production of X-ray Compton back-scattering as reported in the PLASMON activity section.

2 Group activity in 2007

2.1 Data analysis

The operation of the e-meter (the movable emittance measuring instrument fully illustrated in the last year report) was terminated at the beginning of December 2006, and soon after that a systematic analysis of the data was started. Three different algorithms were implemented, differing mainly in how the background subtraction was performed. The results were extremely consistent and have been published in international journals (see the List of Publications).

Qualities of our measurements and the accurate analysis have established a new standard in the evaluation of photo injector properties and the relative beam dynamics.

2.2 Linac installation

Soon after the e-meter disassembling, the installation of the whole linac took place, starting from the accelerating sections. Then the transport line to the undulators was completed, and the undulators themselves aligned on the reference beam line.

The bypass and diagnostics channel was installed as last element. The installation progression is documented in Figs. 1 and 2.

Figure 1: *The installation of the whole linac and of the undulators.*

In the framework of an international collaboration, partially funded by the European Community through the VI PQ, an experiment to demonstrate the potentialities of using SPARC as an amplifier of an external radiation seed is ready to be performed. A fraction of the signal from the Ti:Sa oscillator used for the generation of the electron beam is amplified by a dedicated amplifier

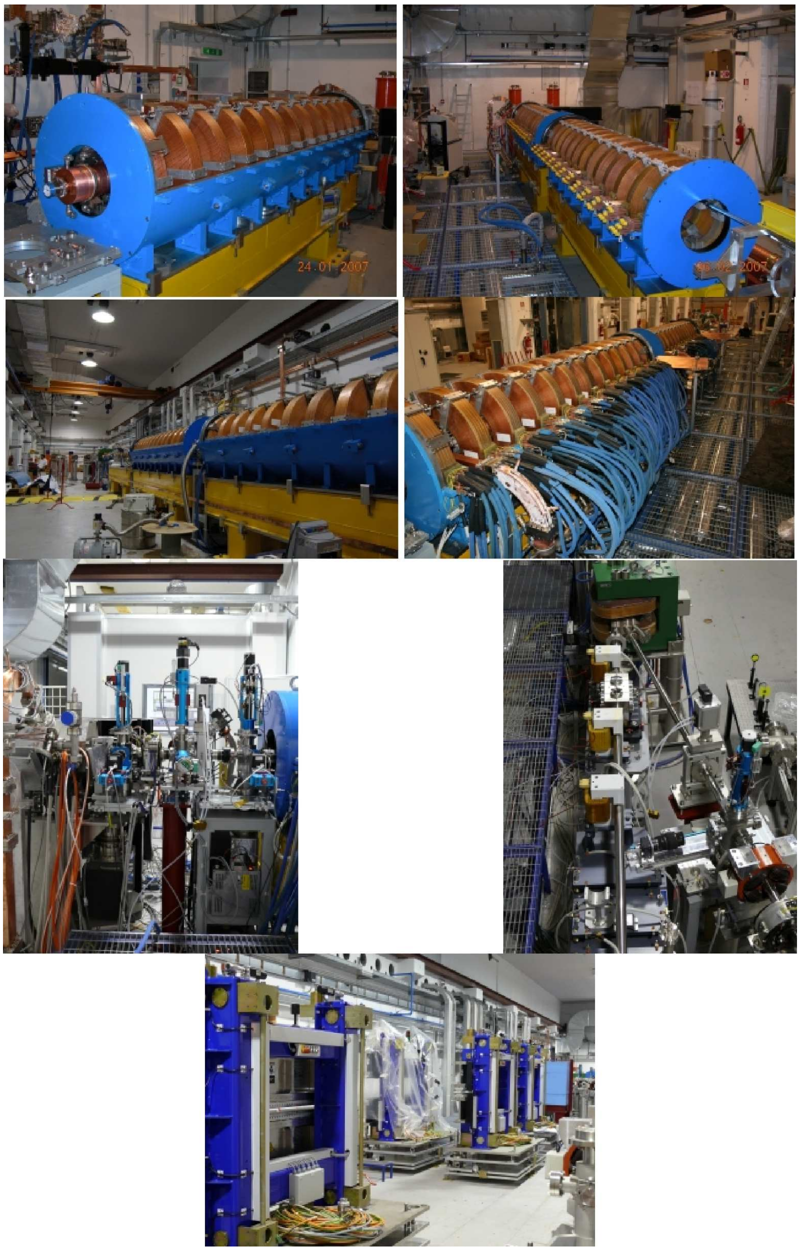

Figure 2: *The installation of the whole linac and of the undulators.*

maintaining the temporal synchronization with the electron beam itself, and is used for producing high order harmonics radiation in gas. These harmonics are inserted together with the electrons inside the undulators, providing the seed that is amplified.

The laser amplifier and the chamber for the production of the harmonics have been installed and commissioned.

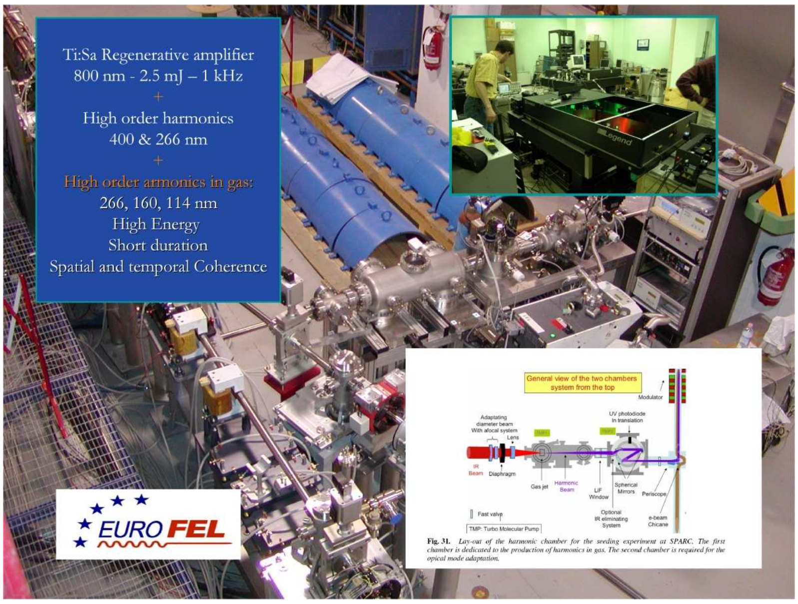

Figure 3: *The chamber for the production of laser high order harmonics installed and commissioned.*

2.3 RF conditioning

After the installation of the accelerating cavities was completed, together with waveguides, cooling and ancillary systems, their conditioning was started, limited in time by the necessity of human presence in the accelerator hall for the installation of beam lines, diagnostics and undulators.

At the end of the year about 100 hours of high power operation were accumulated and multimegawatt power levels have been reached. The RF conditioning is however still in progress and will take some time to achieve the nominal design values.

At the moment the total energy that a beam could obtain is about 140-150 MeV, very near to the nominal minimum value.

Fig. 4 shows the waveforms of the RF pulses at different positions of the RF system.

2.4 First beam

In July 2007 we received the final prescriptions from the Security Agencies, and for the end of the year all the prescriptions were satisfied. We are now waiting for the permission of operation.

In the meantime, during the RF conditioning, we observed that the dark current extracted from the gun cathode by field emission could be easily transported through the accelerator, even if with non optimized phases between the accelerating sections, as shown in Fig. 6. This is an indication of a rather good alignment of all the elements, and allowed us to verify the operation of part of the transport optics, as beam steerings, and of the beam diagnostics, as fluorescent screens, camera, beam position and current monitors.

2.5 Beam dynamics

Along with the hardware installation and commissioning, the theoretical study of possible experiments with special electron bunch structures was continued.

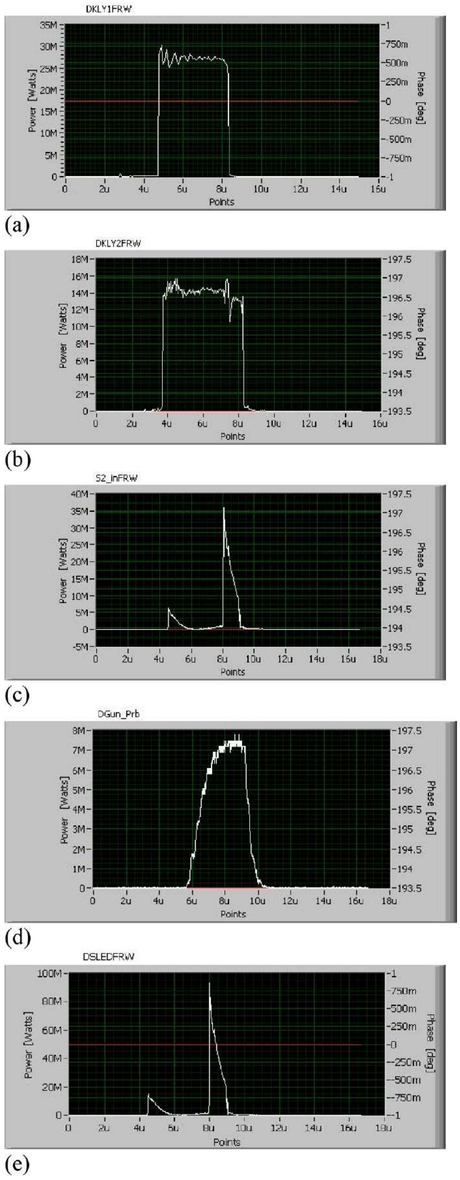

Figure 4: *RF waveforms at different positions of the system: (a) Klystron#1 output RF Pulse, (b) RF Gun Input Pulse, (c) Klystron#2 output RF Pulse, (d) SLED output RF pulse, (e) Acc. section#2 Input RF Pulse.*

In particular, the possibility of producing a single short pulse, as short as the cooperation length in the FEL SASE process, starting with a very low charge bunch, has been investigated. In this way a single spike would be present in the frequency spectrum.

Generated by a 300 fs laser pulse, a 1 pC electron bunch is compressed through velocity bunching and magnetic compression to a final length of 30 fs (10 μm) at 2 GeV.

The GENESIS simulation of the SASE radiation spectrum produced in a SPARC-like undu-

Figure 5: *Sparc Hall Installation of the waveguides.*

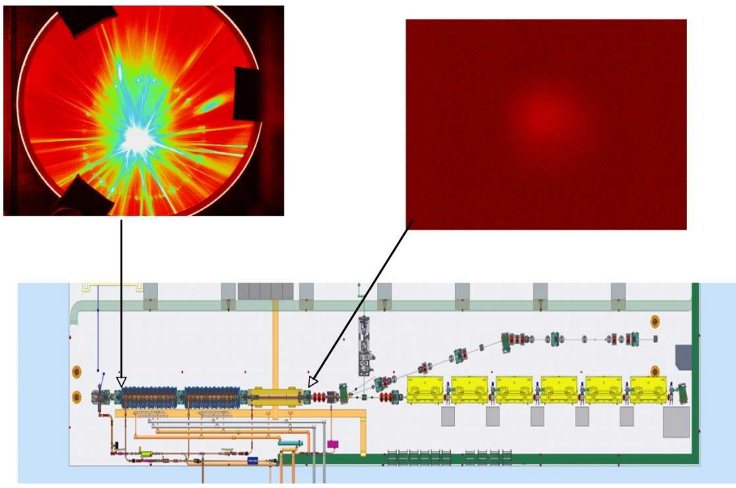

Figure 6: *Dark current from the gun transported through the linac.*

lator is shown in Fig. 7.

A second bunch structure that was investigated is the so-called "comb-like bunch", in which

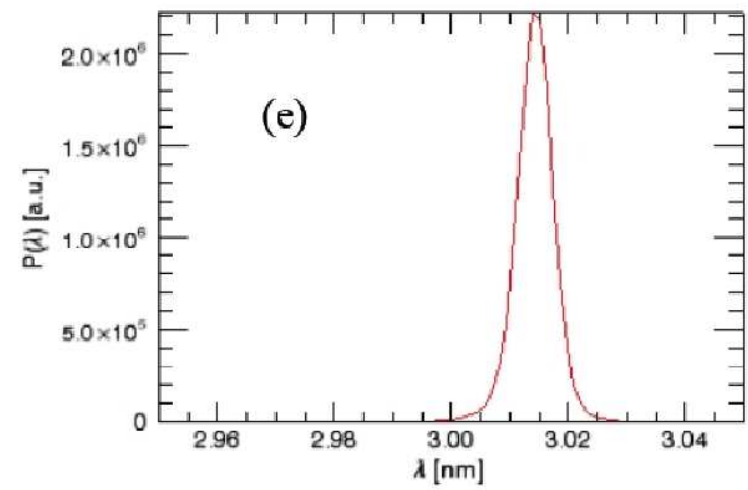

Figure 7: *Power spectrum at undulator exit.*

a charge modulation at the THz frequency level is obtained at the final energy before the passage through the undulator.

A train of femtoseconds laser pulses produces an electron bunch composed by a succession of high charge density disks. In this configuration the electrons in each disk experience a large longitudinal space charge field with a linear correlation along the bunch. As the micro-bunches travel along the gun and the downstream drift they expand longitudinally, loosing the spatial modulation, but the work done by the space charge force produces an energy modulated electron beam with a saw tooth profile of the energy modulation with $\Delta E < 0.4$ MeV. This energy modulated electron beam can be transformed again into a density modulated electron beam in a magnetic or rf compressor device.

Simulations of comb beams having both sinusoidal and Gaussian waveforms and different number of pulses ($2 \leq N \leq 10$) have been modeled with PARMELA code. The intent is to determine the beam characteristics in term of spatial shape, energy and density modulation. Some example of these simulations is shown in Fig. 8.

The comb bunch structure can be source of intense coherent THz radiation that can be used as diagnostics for the modulation process itself or extracted for scientific users. A collaboration group is evaluating the potentiality of this radiation and the instruments required for its use.

References

1. M. Ferrario et al. "Direct Measurement of the Double Emittance Minimum in the Beam Dynamics of the Sparc High-Brightness Photoinjector", Physical Review Letters, 99, 234801 (2007)

2. A. Cianchi et al. "Advanced measurements at the SPARC photoinjector" Proc. of DIPAC2007, Venezia (2007)

3. A. Cianchi, C. Ronsivalle, L. Giannessi, M. Quattromini, M. Castellano, D. Filippetto, "Accurate emittance calculation from phase space analysis", SPARC/EBD-07/003

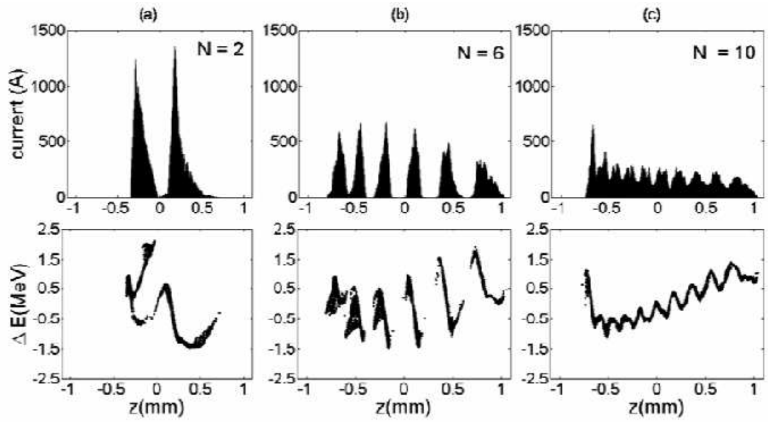

Figure 8: *The intensity modulated electron comb beam at the end of the accelerator for the three cases: (a) N = 2, (b) N= 6 and (c) N = 10.*

4. G. Di Pirro, F.Anelli, M. Bellaveglia, D. Filippetto, S.Fioravanti, E. Pace, L. Catani, A. Cianchi, "SPARC control system", Proc. of ICALEPS 2007, pag214-216, Knoxville (Texas, USA)

5. E. Pace, S. Fioravanti, A. Cianchi, "SPARCBOOK, a new electronic logbook", proc of ICALEPS 2007, pag638-640, Knoxville (Texas, USA)

6. C. Vaccarezza et al. "Status of the SPARX project", Proc. of PAC07, pag 1001-1003, Albuquerque (New Mexico, USA)

7. C. Ronsivalle, L. Giannessi, M. Quattromini, A. Bacci, A.R. Rossi, L. Serafini, M. Boscolo, E. Chiadroni, M. Ferrario, D. Filippetto, V. Fusco, G. Gatti, M. Migliorati, A. Mostacci, C. Vaccarezza, C. Vicario, A. Cianchi, M. Petrarca, "COMPARISON BETWEEN SPARC E-METER MEASUREMENTS AND SIMULATIONS", Proc. of PAC07, pag 986-988, Albuquerque (New Mexico, USA)

8. D. Alesini et al. "Experimental result with the SPARC Emittance-meter", Proc. of PAC07, pag 80-82, Albuquerque (New Mexico, USA)

9. A. Bacci, C. Maroli, V. Petrillo, A. Rossi, L. Serafini: "Analysis of Inhomogeneities Effects on the Photocathode Using Retar", BD-07/001

10. M. Boscolo, M. Ferrario, C. Vaccarezza, I. Boscolo, F. Castelli, S. Cialdi: "Generation of Short THz Bunch Trains in a RF Photoinjector", BD-07/002, 04/2007

11. I. Boscolo, M. Boscolo, S. Cialdi, M. Ferrario, V. Petrillo: "Laser Comb m-Workshop", BD-07/003, 14/05/2007

12. J. Rosenzweig, G. Andonian, M. Dunning, A. Fukusawa, E. Hemsing, P. Musumeci, B. O'Shea, C. Pellegrini, S. Reiche, L. Faillace, A. Marinelli, L. Palumbo, D. Alesini, M. Ferrario, M. Boscolo, B. Spataro, C. Vaccarezza, V. Petrillo, L. Giannessi, C. Ronsivalle: "Generation of Ultra-Short, High Brightness Electron Beams for Single Spike SASE FEL Operation", BD-07/004, 10/10/2007

13. M. Castellano, E. Chiadroni: "Coherent Emission from an Electron Bunch with a Comb Structure", BD-07/005, 15/11/2007

14. M. Boscolo, M. Ferrario, I. Boscolo, F. Castelli, S. Cialdi, V. Petrillo, R. Bonifacio, L. Palumbo, L. Serafini: "Single Spike Operation in SPARC SASE-FEL", BD-07/006, 12/2007

15. D. Filippetto, P. Musumeci: "Trace Space Reconstruction Data Analysis", EBD-07/001, 02/01/2007

16. D. Filippetto: "A Robust Algorithm for Beam Emittance and Trace Space Evolution Reconstruction", EBD-07/002, 14/06/2007

17. A. Bacci: "A Genetic Code Able to Compute the Emittance Value of a Real Beam by a Multiple Ellipse Slice Analysis of the Transversal Phase-Space Image", EBD-07/004, 24/07/2007

18. A. Rossi: "NoLFiPS: Non Linear Fit of Phase Spaces", EBD-07/005, 06/09/2007

19. A. Mostacci, M. Boscolo, A. Cianchi, E. Chiadroni, M. Migliorati, D. Filippetto, C. Ronsivalle: "Selected Data from the First Emittance Measurements at the SPARC Photoinjector", EBD-07/006, 08/11/2007

20. V. Fusco, M. Ferrario, C. Ronsivalle: "Spatial Correlation for Laser Beam Quality Evaluation", EBD-07/007, 27/11/2007

21. C. Vicario, M. Petrarca, S. Cialdi, P. Musumeci: "High-power Third-harmonic Flat Laser Pulse Generation", LS-07/001, 23/05/2007

22. C. Vicario, M. Petrarca, S. Cialdi, P. Musumeci: "Simplified Scheme for UV Time Pulse Shaping", LS-07/002, 23/05/2007

23. B. Bolli, S. Ceravolo, M. Esposito, P. Iorio, F. Iungo, M. Paris, C. Sanelli, F. Sardone, F. Sgamma, M. Troiani, G. Bazzano, I. De Cesaris : "Mechanical and Magnetic Qualification of the Focusing Solenoids for SPARC", ME-07/001, 02/03/2007

24. D. Alesini, A. Gallo, B. Spataro, A. Marinelli, L. Palumbo: "Design of Input Couplers for Traveling Wave Structures", RF-07/001, 22/01/2007

25. L. Quintieri, F. Tazzioli: "Electromagnetic-Thermal Analysis of an x-band Linac Structure by Finite Element Simulations", RF-07/002, 15/01/2007

26. S. Bini, P. Chimenti, V. Chimenti, R. Di Raddo, V. Lollo, B. Spataro, F. Tazzioli: "Electroforming Procedures Applied to the Construction of 11.4 GHz Linear Accelerating Structures: Status Report on SALAF Activity", RF-07/003, 29/05/2007

27. S. Bini, A. Clozza, P. Chimenti, V. Chimenti, R. Di Raddo, V. Lollo, F. Tazzioli: "Status Report on SALAF Technical Activity on Vacuum Brazing on X-band Linear Accelerating Structures and RF Deflector of the SPARC Project at Frascati Laboratories", RF-07/004, 11/06/2007

LNF Publications

YEAR 2007 FRASCATI PUBLICATIONS

Available at www.lnf.infn.it

1 – Frascati Physics Series

Volume XLIII –Special Issue
Neutral Kaon Interferometry at A Phi-Factory: from Quantum Mechanics to Quantum Gravity
Ed.: A. Di Domenico
Frascati, March 24th 2006
ISBN—978—88–86409–50–8

Volume XLIV– Special Issue
Les Rencontres de Physique de la Vallée d'Aoste –
Results and Perspectives in Particle Physics
Ed.: M. Greco
La Thuile, Aosta Valley, February 28, 2 March 5, 2007
ISBN—978—88–86409–49–4

Volume XLV *Frontier Science–Science with the New Generation*
High Energy Gamma-ray Experiments
Eds.: A. Lionetto, A. Morselli
Villa Mondragone, Monteporzio, Italy June 18 -20, 2007
ISBN—978—88–86409–54–0

Volume XLVI
XII International Conference on Hadron Spectroscopy
Eds.: L. Benussi, M. Bertani, S. Bianco, C. Bloise, R. de Sangro, P. de Simone,
P. di Nezza, P. Giannotti, S. Giovanella, M.P. Lombardo, S. Pacetti
Laboratori Nazionali di Frascati, October 713, 2007
ISBN—97–88–86409–55–1

2 – Frascati Physics Series – Italian Collection

Collana: Scienza Aperta Vol. I (2006) - ComunicareFisica2005
Atti 1 Convegno "Comunicare Fisica e altre Scienze",
Frascati 24-27 Ottobre 2005
Eds: Franco L. Fabbri, Piero Patteri
ISBN— 88-86-409-48-6

3 – LNF Frascati Reports

LNF–07/01(IR)
D. Alesini, B. Spataro, L. Ficcadenti, A. Mostacci, L. Palumbo, A. Bacci, R. Parodi
A Biperiodic X-Band Cavity for SPARC

LNF–07/02(NT)
S. Bartalucci, V. Angelov, K. Drozdowicz, D. Dworakc, G. Tracz
MoonLIGHT-R:
Moon Laser Instrumentation for General Relativity High-Accuracy Tests–
An ASI study for a robotic mission on the Moon

LNF–07/03(NT)
S. Bartalucci, V. Angelov, K. Drozdowicz, D. Dworakc, G. Tracz
Conceptual Design of an Intense Neutron Source for Time-of-Flight Measurements

LNF–07/04(IR)
Carlo Ligi, Sam Masa Vinko
The RAP Cryogenics

LNF–07/05(NT)
S. Bartalucci, V. Angelov, K. Drozdowicz, D. Dworakc, G. Tracz
Conceptual Design of an Intense Neutron Source for Time-of-Flight Measurements

LNF–07/06(NT)
G. Pancheri and R. Godbole and A. Grau and Y.N. Srivastava
Total Cross-Section at LHC from Minijets and Soft Gluon Resummation in the Infrared Region

LNF–07/07(IR)
A Candela, G. Felici, F. Terranova
Experimental study of the (K^+, K^0) *interactions on* ^7Li *close to threshold*

LNF–07/08(IR)
R. Vittori, A. Boni, C. Cantone, S. DellAgnello, G.O. Delle Monache, M. Garattini, N. Intaglietta, C. Lops, M. Martini, C. Prosperi, G. Bellettini, R. Tauraso
ETRUSCO: Extra Terrestrial Ranging to Unified Satellite COnstellations

LNF–07/09(NT)
Eds. Nan Phinney (SLAC), Nick Walker (DESY), and Nobu Toge (KEK)
International Linear Collider Reference Design Report 2007

LNF–07/10(P)
The FINUDA Collaboration:
M. Agnello, G. Beer, L. Benussi, M. Bertani, H.C. Bhang, S. Bianco, G. Bonomi, E. Botta, M. Bregant, T. Bressani, S. Bufalino, L. Busso, D. Calvo, P. Camerini, M. Caponero, P. Cerello, B. Dalena, F. De Mori, G. D'Erasmo, D. Di Santo, D. Elia, F. L. Fabbri, D. Faso, A. Feliciello,

A. Filippi, V. Filippini, R. Fini, M.E. Fiore, H. Fujioka, P. Gianotti, N. Grion, O. Hartmann, H.B. Kang, A. Krasnoperov, V. Lenti, V. Lucherini, V. Manzari, S. Marcello, T. Maruta, N. Mirfakhrai, O. Morra, T. Nagae, A. Olin, H. Outa, E. Pace, M. Pallotta, M. Palomba, A. Pantaleo, A. Panzarasa, V. Paticchio, S. Piano, F. Pompili, R. Rui, G. Simonetti, H. So, V. Tereschenko, S. Tomassini, R. Toyoda, R. Wheadon, A. Zenoni
Experimental study of the (K^+, K^0) *interactions on* ^7Li *close to threshold*
Accepted by Physics Letters B

LNF–07/11(NT)
V. Chimenti, L. Palumbo, B. Spataro, L. Quintieri, F. Tazzioli
Experimental study of the (K^+, K^0) *interactions on* ^7Li *close to threshold*

LNF–07/12(NT)
Marco Cordelli, Roberto Habel, Agnese Martini, Luciano Trasatti
NERONE: First Results

LNF–07/13(IR)
AA.VV
2006 Annual Report

LNF–07/14(IR)
G. Giordano and G. Pizzella
Searching for Triple Coincidences among the Resonant Gravitational Wave Detectors AURIGA, EXPLORER and NAUTILUS in the year 2005: A Study on the Coincidence Window A Biperiodic X-Band Cavity for SPARC

LNF–07/15(IR)
Eugene Levichev, Pavel Piminov, Pantaleo Raimondi, Mikhail Zobov
Dynamic Aperture Optimization for the DAΦNE Upgrade

LNF–07/16(P)
Gian Paolo Murtas
Distributions of the Signals from Gravitational Antennas Versus Nautilus Local Sidereal Hours (NALSH) and Correlations Between the Signals and X-Ray Signatures in Close Binary Systems and SGR
Presented at the Multifrequency Behaviour of High Energy Cosmic Source
May 28^{th}–June 2^{nd} 2007, Vulcano, Italy

LNF–07/17(Thesis)
Student: Alessandro Lucantoni
Thesis Advisor: Prof. A. Paolozzi
Co-Thesis Advisor: Dott. S. DellAgnello
Optical Characterization of Lares Cube Corner Reflectors

LNF–07/18(IR)
V. Andreassi, G. Cappuccio, F. Celani1, P. Di Biagio, V. Di Stefano, F. Falcioni, F. Fontana,

L. Gamberale, D. Garbelli, D. Hampai, M. Marchesini, P. Marini, A. Marmigi, A. Mancini, U. Mastromatteo, M. Nakamura, E. Purchi, P. Quercia, E. Righi, P.G. Sona, A. Spallone, F. Todarello, G. Trenta
High Temperature Deuterium Absorption in Palladium Nano-Particles
Invited Paper at ICCF13, June 24-July 2 2007, Sochi (Russia).
Preprint submitted for pubblication on 'Condensed Matter Nuclear Science'; World Scientific, 2007

LNF–07/19(IR)
F. Bossi, F. Anulli, D. Babusci, R. Baldini, G. Bencivenni, M. Beretta, S. Bertolucci, C. Bloise, P. Campana, G. Capon, P. Ciambrone, E. Dané, E. De Lucia, P. De Simone, D. Domenici, G. Felici, E. Iarocci, J. Lee Franzini, M. Martini, F. Mescia, S. Miscetti, S. Müeller, F. Murtas, L. Pancheri, M. Palutan, V. Patera,M. Poli Lener, P. Santangelo, B. Sciascia, A. Sciubba, G. Venanzoni, R. Versaci, R. Beck, B. Borasoy, A. Nikolaev, R. Nissler, M. Unverzagt, G. De Robertis, O. Erriquez, F. Loddo, A. Ranieri, E. Czerwinski, P. Moskal, J. Zdebik, V. Babkin, V. Golovatyuk, I. Tyapkin, P. Beltrame, A. Denig, W. Kluge, D. Leone, S. A. Bulychjov, V. V. Kulikov, M. A. Martemianov, M. A. Matsyuk, C. Bini, V. Bocci, G. De Zorzi, A. Di Domenico, P. Franzini, P. Gauzzi, E. Pasqualucci, M. Testa, A. D'Angelo, R. Di Salvo, A. Fantini, R. Messi, D. Moricciani, P. Branchini, F. Ceradini, B. Di Micco, E. Graziani, F. Nguyen, A. Passeri, L. Tortora, A. Go, L. Kurdadze, D. Mchedlishvili, M. Tabidze, H. Calén, K. Fransson, B. Hóistad, T. Johansson, A. Kupsc, P. Marciniewski, J. Zloman
A Proposal for the Roll-in of the KLOE-2 Detector

LNF–07/20(IR)
D. Alesini, B. Spataro, L. Ficcadenti, A. Mostacci, L. Palumbo, A. Bacci, R. Parodi
A Biperiodic X-Band Cavity for SPARC

LNF–07/21(IR)
D. Alesini, R. Boni, M. Calvetti, V. Chimenti, A. Clozza, A. Gallo, L.Pellegrino, R. Ricci, C. Sanelli, B. Spataro, F. Tazzioli, C. Vaccarezza
Proposal for a Set up of an Rf Power Hall For X-Band Accelerating Structures Testing at LNF

LNF–07/23(IR)
A. Babaev, S.B. Dabagov
On Possibility of Spin Manifestation in Channeling Radiation

LNF–07/24(IR)
P. Buehler, M. Cargnelli, A. Hirtl, T. Ishiwatari, P. Kienle, J. Marton, E. Widmann, J. Zmeskal, M. Faber, A. Ivanov, A. Hussein, F. Nichitiu, D. Gill, G. Beer, A. Olin, B. Borasoy, R. Nissler, U. Raha, A. Rusetsky, H. Orth, A. Gillitzer, V.E. Lyubovitskij, N. Hermann, L. Fabietti, B. Ketzer, R. Kreken, S. Neubert, S. Paul, K. Suzuki, W. Weise, Q. Weitzel, S. Choudhoury, J. Esmaieli, S.Z. Kalantari, M. Raiesi, S. Bartalucci, M. Bazzi, M. Catitti, C. Curceanu, A. d'Uffizi, C. Guaraldo, M. Iiescu, P. Levi Sandri, M.P. Lombardo, D. Pietreanu, A. Romero Vidal, S. Scordo, D. Sirghi, F. Sirghi, L. Sperandio, O. Vazquez Doce, F. Ghio, B. Girolami, L. Bombelli, C. Fiorini, T. Frizzi, A. Longoni, L. Ludhova, G. Violini, P. Gensini, R. Casalbuoni, M. Di Toro, A. Dote', Y. Akaishi, T. Yamazaki, S. Wycech, P. Hawranek, S. Kistryn, A. Magiera, J. Smyrski, A. Wronska, A.M. Bragadireanu, T. Ponta, T. Preda, A. Tudorache, V. Tudorache, M. Calin, A. Jipa, I. Lazanu,

A.E. Astratyan, V.V. Barmin, V. Baru, L. Bogdanova, V.S. Borisov, G.V. Davidenko, A. Dolgolenko, V. Grishina, L. Kondratyuk, A. Krotenkova, M.A. Kubantsev, A. Kudryavtsev, I.F. Larin, V.A. Matveev, V.A. Shebanov, N.N. Shishov, L.I. Sokolov, V. Tarasov, G.K. Tumanov, E. Turdakina, O.V. Bulenkov, B.A. Chernysev, Yu.B. Gurov, S.V. Lapushkin, A.K. Ponosov, D.A. Romanov, F.M. Sergeev, R.R. Shafigullin, P. Aslanyan, A. Galoyan, V. Uzhinsky, V.V. Burov, V.S. Richvitsky, S.H. Connell, R. Lemmer, J.-P. Egger, L. Schaller, S. Popescu, L. Tauscher, B. Lauss
AMADEUS Phase-1: Physics, Setup and Roll-in Proposal

LNF–07/25(IR)
G. Modestino and G. Pizzella
EXPLORER and NAUTILUS Correlation for Damped Sinusoid Signals

LNF–07/26(P)
A. Donini, E. Fernandez-Martinez, P. Migliozzi, S. Rigolin, L. Scotto Lavina, M. Selvi, T. Tabarelli de Fatis, F. Terranova
Neutrino Hierarchy from CP-Blind Observables with High Density Magnetized Detectors
Accepted for publication in JHEP

LNF–07/27(P)
A. Donini, M. Maltoni, D. Meloni, P. Migliozzi, F. Terranova
Sterile Neutrinos at the CNGS
Accepted for publication in JHEP

LNF–07/28(IR)
Camillo Lo Surdo
Alcune Riflessioni Generali sulle Teorie Fisico-Matematiche

4 – INFN Reports

INFN/AE–07/1
Simone Riggi, Rossella Caruso, Antonio Insolia, Mario Scuderi
A Neural Network Approach to High Energy Cosmic Rays Mass Identification

INFN/AE–07/2
M. Bona, J. Garra Tic'o, , E. Graug'es Pous, P. Colangelo, F. De Fazio, A. Palano, M. Manghisoni, V. Re, G. Traversi, G. Eigen, M. Venturini, N. Soni, M. Bruschi, S. De Castro, P. Faccioli, A. Gabrielli, B. Giacobbe, N. Semprini Cesari, R. Spighi, M. Villa, A. Zoccoli, C. Hearty, J. Mc Kenna, A. Soni, A. Khan, A.Y. Barniakov, M.Y. Barniakov, V.E. Blinov, V.P. Druzhinin, V.B. Golubev, S.A. Kononov, I.A. Koop, E.A. Kravchenko, E.B. Levichev, S.A. Nikitin, A.P. Onuchin, P.A. Piminov, S.I. Serednyakov, D.N. Shatilov, Y.M. Shatunov, Y.I. Skovpen, E.P. Solodov, C.-H. Cheng, B. Echenard, F. Fang, D.G. Hitlin, F.C. Porter, T.N. Pham, R. Fleischer, G.F. Giudice, T. Hurth, M. Mangano, G. Mancinelli, B.T. Meadows, A.J. Schwartz, M.D. Sokoloff, A. Soffer, C.D. Beard, T. Haas, R. Mankel, G. Hiller, P. Ball, M. Pappagallo, M.R. Pennington, W. Gradl, S. Playfer, A. Abada, D. Becirevic, S. Descotes-Genon, O. P'ene, D. Andreotti, M. Andreotti, D. Bettoni, C. Bozzi, R. Calabrese, A. Cecchi, G. Cibinetto, P. Franchini, E. Luppi, M. Negrini, A. Petrella, L. Piemontese, E. Prencipe, V. Santoro, G. Stancari, F. Anulli, R. Baldini-Ferroli, M.E. Biagini, M. Boscolo, A. Calcaterra, A. Drago, G. Finocchiaro, S. Guiducci, G. Isidori, S. Pacetti, P. Patteri, I.M. Peruzzi, M. Piccolo, M.A. Preger, P. Raimondi, M. Rama, C. Vaccarezza, A. Zallo, M. Zobov, R. de Sangro, A. Buzzo, M. Lo Vetere, M. Macr'i, M.R. Monge, S. Passaggio, C. Patrignani, E. Robutti, S. Tosi, J. Matias, W. Panduro Vazquez, F. Borzumati, V. Eyges, S.A. Prell, T.K. Pedlar, S. Korpar, R. Pestotnik, M. Stariv c, M. Neubert, A.G. Denig, U. Nierste, T. Agoh, K. Ohmi, Y. Ohnishi, J.R. Fry, C. Touramanis, A. Wolski, B. Golob, P. Krivzan, H. Flaecher, A.J. Bevan, F. Di Lodovico, K.A. George, R. Barlow, G. Lafferty, A. Jawahery, D.A. Roberts, G. Simi, P.M. Patel, S.H. Robertson, A. Lazzaro, F. Palombo, A. Kaidalov, A.J. Buras, C. Tarantino, G. Buchalla, A.I. Sanda, , G. D'Ambrosio, G. Ricciardi, I. Bigi, C.P. Jessop, J.M. LoseccoK. Honscheid, N. Arnaud, R. Chehab, Y. Fedala, F. Polci, P. Roudeau, V. Sordini, V. Soskov, A. Stocchi, A. Variola, A. Vivoli, G. Wormser, F. Zomer, A. Bertolin, R. Brugnera, N. Gagliardi, A. Gaz, M. Margoni, M. Morandin, M. Posocco, M. Rotondo, F. Simonetto, R. Stroili, G.R. Bonneaud, V. Lombardo, G. Calderini, L. Ratti, V. Speziali, M. Biasini, R. Covarelli, E. Manoni, L. Servoli, C. Angelini, G. Batignani, S. Bettarini, F. Bosi, M. Carpinelli, R. Cenci, A. Cervelli, M. Dell'Orso, F. Forti, P. Giannetti, M. Giorgi, A. Lusiani, G. Marchiori, M. Massa, M.A. Mazur, F. Morsani, N. Neri, E. Paoloni, F. Raffaelli, G. Rizzo, J. Walsh, V. Braun, A. Lenz, G.S. Adams, I.Z. Danko, E. Baracchini, F. Bellini, G. Cavoto, A. D'Orazio, D. Del Re, E. Di Marco, R. Faccini, F. Ferrarotto, M. Gaspero, P. Jackson, G. Martinelli, M.A. Mazzoni, S. Morganti, G. Piredda, F. Renga, L. Silvestrini, C. Voena, L. Catani, A. Di Ciaccio, R. Messi, E. Santovetti, A. Satta, M. Ciuchini, V. Lubicz, F.F. Wilson, R. Godang, X. Chen, H. Liu, W. Park, M. Purohit, A. Trivedi, R.M. White, J.R. Wilson, M.T. Allen, D. Aston, R. Bartoldus, S.J. Brodsky, Y. Cai, J. Coleman, M.R. Convery, S. DeBarger, J.C. Dingfelder, G.P. Dubois-Felsmann, S. Ecklund, A.S. Fisher, G. Haller, S.A. Heifets, J. Kaminski, M.H. Kelsey, M.L. Kocian, D.W.G.S. Leith, N. Li, S. Luitz, V. Luth, D. MacFarlane, R. Messner, D.R. Muller, Y. Nosochkov, A. Novokhatski, M. Pivi, B.N. Ratcliff, A. Roodman, J. Schwiening, J. Seeman, A. Snyder, M. Sullivan, J. Va'Vra, U. Wienands, W. Wisniewski, H. Stoeck, H.-Y. Cheng, H.-N. Li, Y.-Y. Keum, M. Gronau, Y. Grossman,F. Bianchi, D. Gamba, P. Gambino, F. Marchetto,

E. Menichetti, R. Mussa, M. Pelliccioni, G.F. Dalla Betta, M. Bomben, L. Bosisio, C. Cartaro, L. Lanceri, L. Vitale, V. Azzolini, J. Bernabeu, N. Lopez-March, F. Martinez-Vidal, D.A. Milanes, A. Oyanguren, P. Paradisi, A. Pich, M.A. Sanchis-Lozano, R. Kowalewski, J.M. Roney, J. Back, T.J. Gershon, P.F. Harrison, T.E. Latham, G.B. Mohanty, A.A. Petrov, M. Pierini,
SuperB, a High-Luminosity Heavy Flavour Factory: Conceptual Design Repor

INFN/BE–07/1
Andrea Bersani, Renzo Parodi, Andrea Pastorino
Solenoid Magnet and Flux Return for the $P\overline{P}$ Detector

INFN/CCR–07/1
Alessandro Tirel
Tecnologia iSCSI Prime Esperienze

INFN/CCR–07/2
Domenico Diacono, Sabino Caló
High Availability a Basso Costo
Workshop CCRWS06 Otranto (LE)

INFN/CCR–07/3
Giuseppe Sava, Rosanna Catania, Emidio Giorgio, Gianluca Passaro, Gianni Mario Ricciardi
General Computation and Grid TIER2 Toward LHC

INFN/CCR–07/4
Marco Bencivenni
Ottimizzazioni del Protocollo TCP per Connessioni LHCOPN a 10 GB/S

INFN/CCR–07/5
Alberto Guerra
Temp Sentry: Un Sistema di Rilevazione Dati Ambientali

INFN/CCR–07/6
Giacinto Donvito, Vincenzo Spinoso
dCache, Storm/GPFS and DPM: Performance Tests, SRM Compliance, Advanced Configurations

INFN/CCR–07/7
Nunzio Amanzi, Silvia Arezzini, Enrico M.V. Fasanelli, Gian Piero Siroli, Giulia Vita Finzi
Nota su Windows Vista

INFN/CCR–07/8
Riccardo Veraldi
XEN e i Benefici della Virtualizzazione HVM

INFN/CCR–07/9
Michele Michelotto
Confronto di Prestazioni di Applicazioni Hep con Benchmark Sintetici

INFN/CCR–07/10
Michele Michelotto
Confronto di Prestazioni di Applicazioni Hep con Benchmark Sintetici

INFN/CCR–07/11
Michele Michelotto
Costi e Prestazioni dei Worker Node per il Calcolo LHC

Glossary

Glossary

These are the acronyms used in each status report to describe personnel qualifications other than Staff Physicist:

Art 15	Term Contract (Technician)
Art. 23	Term Contract (Scientist)
Ass.	Associated Scientist
Ass. Ric.	Research Associate
Bors.	Fellowship holder
Bors. PD	PostDoc Fellow
Bors. UE	European Community Fellow
Dott.	Graduate Student
Laur.	Undergraduate Student
Loc. Coor.	Local Coordinator
Osp.	Guest Scientist
Perfez.	PostLaurea Student
Resp.	Local Spokesperson
Resp. Naz.	National Spokesperson
Specializ.	PostLaurea Student
Tecn.	Technician